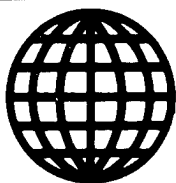


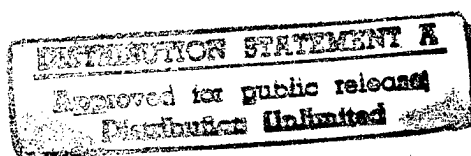
JPRS-JST-90-002

5 JANUARY 1990



**FOREIGN  
BROADCAST  
INFORMATION  
SERVICE**

# ***JPRS Report***



# **Science & Technology**

***Japan***

MECHANISM OF SUPERCONDUCTIVITY

REPRODUCED BY  
U.S. DEPARTMENT OF COMMERCE  
NATIONAL TECHNICAL INFORMATION SERVICE  
SPRINGFIELD, VA. 22161

**DTIC QUALITY INSPECTED 3**

22161

NTIS  
ATTN: PROCESS 103  
5285 PORT ROYAL RD  
SPRINGFIELD, VA

22161  
45

19980128 193

JPRS-JST-90-002

5 JANUARY 1990

## SCIENCE & TECHNOLOGY

### JAPAN

## MECHANISM OF SUPERCONDUCTIVITY

[Papers presented as the "first year report on Mechanism of Superconductivity", Science Research on Priority Areas No 031 sponsored by the Ministry of Education, Science and Culture]

43060709 Tokyo RESEARCH REPORT ON MECHANISM OF SUPERCONDUCTIVITY  
in English Mar 89 pp 1-307

## CONTENTS

### Part I. Oxide Superconductors ; Experiments

Photoemission Study of High - $T_c$ Superconductors and Related Compounds	
..... A. Fujimori	1
Synchrotron - Radiation Photoemission Study of Single Crystal $\text{Bi}_2\text{Sr}_2\text{CaCu}_2\text{O}_8$	
..... T. Takahashi, H. Matsuyama, H. Katayama-Yoshida and Y. Okabe	4
Low - Energy Electron Energy Loss Spectroscopy on High - $T_c$ Superconductors	
..... A. Ando, K. Saiki and A. Koma	7
Optical Absorption in $(\text{La}_{1-x}\text{Sr}_x)_2\text{CuO}_4$ Single Crystal Thin Films	
..... M. Suzuki	10
Transmission Spectra of Crystal Film Bi-Sr-Ca-Cu-O in the Range 3 to 500 $\text{cm}^{-1}$	
..... K. Nagasaka, M. Sato, T. Shibayama and K. Ishida	13
Universality of Infrared Anomaly in $(\text{La}_{1-x}\text{M}_x)_2(\text{Cu}_{1-y}\text{N}_y)\text{O}_4$ :	
M = Ca, Sr, Ba ; N = Ni, Zn .....	K. Ohbayashi, H. Tsukamoto,
H. Yamashita, A. Fukumoto, Y. Utunomiya, N. Ogita, K. Kojima and M. Udagawa	17
Raman Studies of Magnons, Phonons, and Electronic States in High $T_c$ Superconductors	
..... S. Sugai	21

Cu NQR/NMR Studies of $\text{YBa}_2\text{Cu}_3\text{O}_y$ ( $6.0 \leq y \leq 6.98$ )	H. Yasuoka	25
Study of High $T_c$ Oxide Superconductor by NMR and Other Measurements	Y. Kitaoka, K. Ishida, K. Fujiwara, T. Kondo, Y. Kohori, H. Shibai, K. Asayama, Y. Oda, H. Toyoda, H. Fujita and N. Kawaji	31
Cu-NQR and Low Temperature Heat Capacity of $\text{La}_{2-x}\text{Sr}_x\text{CuO}_4$	K. Kumagai, Y. Nakamura, H. Nakajima, M. Muro-oka and N. Wada	38
Proton NMR in Hydrogen-doped Superconductor $\text{YBa}_2\text{Cu}_3\text{O}_{7-\delta}\text{H}_x$	H. Niki, T. Suzuki, S. Tomiyoshi, H. Hentona M. Omori, T. Kajitani, T. Kamiyama and R. Igei	43
$\mu\text{SR}$ Study of Oxide-Superconductors	N. Nishida	47
Neutron Magnetic Scattering from Superconducting $\text{La}_{2-x}\text{Sr}_x\text{CuO}_4$ --- Status Report for 1988 ---	Y. Endoh, R.J. Birgeneau, Y. Hidaka, K. Kakurai, M.A. Kastner, K. Kitazawa, H. Kojima, M. Matsuda, T. Murakami, G. Shirane, I. Tanaka, T.M. Thurston and K. Yamada	52
Mössbauer Study on Fe-Sitting Site and Origin of Magnetic Order in $\text{YBa}_2(\text{Cu}_{0.95}\text{Fe}_{0.05})_3\text{O}_{7-\delta}$	T. Tamaki, M. Nishizawa and A. Ito	56
$^{57}\text{Fe}$ Mössbauer Study of $\text{YBa}_2\text{Cu}_3\text{O}_{7-x}$	T. Shinjo and S. Nasu	59
Broadening of Superconducting Transition under Magnetic Field in $(\text{La}_{1-x}\text{Sr}_x)_2\text{CuO}_4$ Single Crystal	K. Kitazawa, S. Kambe, A. Fukuoka, I. Tanaka and H. Kojima	62
Growth and Superconducting Properties of Single-Crystal $\text{Bi}_2\text{Sr}_2\text{CaCu}_2\text{O}_8$	Y. Koike, T. Nakanomyo, N. Kobayashi and T. Fukase	65
Thermally Activated Behavior in $\text{YBa}_2\text{Cu}_3\text{O}_z$ and $\text{Bi}_2(\text{Sr}, \text{Ca})_3\text{Cu}_2\text{O}_z$ Films	N. Kobayashi, H. Iwasaki, H. Kawabe, K. Watanabe, H. Yamane, H. Kurosawa, H. Masumoto, T. Hirai and Y. Muto	69
Transport Studies on Superconducting and Normal Metallic La-Sr-Cu Oxides	Y. Iye, T. Tamegai, N. Tanahashi C. Murayama, N. Mori and S. Yomo	73
Investigation of Transport Properties of Bi-Sr-Ca-Cu-O Superconductors	K. Oto, K. Murase and S. Takaoka	79
Variation of $T_c$ with Hole Concentration in $\text{YBa}_2\text{Cu}_3\text{O}_{7-\delta}$ -Type Superconductors: Hall Measurement and Chemical Analysis in $\text{Ln}_{1+x}\text{Ba}_{2-x}\text{Cu}_3\text{O}_{7-\delta}$ ( $\text{Ln} = \text{La}, \text{Nd}, \text{Sm}$ and $\text{Eu}$ )	K. Takita, H. Akinaga, H. Katoh, K. Masuda, H. Asano, T. Mochiku, Y. Takeda and M. Takano	82

Low Temperature Specific Heat and Anisotropic Electrical Transport Properties of Single Crystal $\text{Bi}_{2.2}\text{Sr}_{1.8}\text{CaCu}_2\text{O}_y$ .....	K. Yamaya, N. Ono, T. Honma, T. Haga, Y. Abe, F. Minami and S. Takekawa	85
Study of High-Temperature Superconductors in the La-Sr-Cu-O and Bi-Sr-Ca-Cu-O Systems .....	R. Yoshizaki and I. Nakai	88
Magnetic Susceptibility and Magnetization of Superconducting Oxides .....	K. Okuda and S. Noguchi	93
Electron Tunneling Study on High- $T_c$ Superconductors .....	T. Ekino and J. Akimitsu	97
Thermal Conductivity of $\text{LnBa}_2\text{Cu}_3\text{O}_{7-y}$ ( $\text{Ln} = \text{Y}$ and $\text{Gd}$ ), $\text{YBa}_2\text{Cu}_3\text{O}_{6+x}$ and $\text{Bi}_{0.7}\text{Pb}_{0.3}\text{CaSrCu}_{1.5}\text{O}_x$ .....	K. Mori, K. Noto, M. Sasakawa, Y. Ishikawa, K. Sato and Y. Muto	100
Ultrasonic Studies of High $T_c$ Superconductors .....	S. Mase, Y. Horie and T. Fukami	103
High Pressure Effect on the Critical Temperature of $\text{YBa}_2(\text{Cu}_{1-x}\text{Ga}_x)_3\text{O}_{7-y}$ .....	S. Yomo, L. Gao, Y. Y. Xue, R. L. Meng, P. H. Hor and C. W. Chu	106
Effects of Oxygen Stoichiometry and Oxygen Ordering in $\text{Ba}_2\text{YCu}_3\text{O}_y$ ( $6 \leq y \leq 7$ ) .....	Y. Nakazawa and M. Ishikawa	109
Broad Experimental Studies on High- $T_c$ Oxides .....	M. Sato, M. Sera, M. Onoda, S. Shamoto, S. Kondoh, K. Fukuda, Y. Ando and S. Yamagata	112
Magnetic and Superconducting Properties of $\text{RBa}_2\text{Cu}_3-x\text{M}_x\text{O}_y$ ( $R = \text{Y}, \text{Nd}, \text{Gd}, \text{Dy}$ and $\text{Er}$ ; $M = \text{Ni}$ and $\text{Zn}$ ) .....	K. Sekizawa and Y. Takano	120
High $T_c$ Superconducting Properties in Ln-(Ba,M)-Cu-O Ceramics and Bi-Sr-Ca-Cu-O Thin Films .....	Y. Saito, T. Noji, Y. Hayashi, Y. Fujino, T. Oikawa, A. Hattori, K. Furuse and M. Masuzawa	123
Electrical, Magnetic and Structural Properties of $\text{Ba}_2\text{LnCu}_3\text{O}_{7-8}$ Compounds .....	S. Ohshima, S. Seino, S. Ichino, K. Aizawa and K. Okuyama	126
Critical Current Density and Its Hysteresis in Magnetic Field for Ba-Y-Cu-O Films Prepared by a Sputtering Technique .....	H. Morita, K. Watanabe, Y. Murakami, Y. Koyanagi, K. Noto, H. Fujimori and Y. Muto	129
Discovery of Electron-Doped Superconducting Cuprates: $\text{Ln}_{2-x}\text{Ce}_x\text{CuO}_{4-y}$ ( $\text{Ln} = \text{Pr}, \text{Nd}$ and $\text{Sm}$ ) .....	Y. Tokura, H. Takagi and S. Uchida	132
Superconductivity of the Nd-Ce-Sr-Cu-O System .....	E. Takayama-Muromachi	136
New Preparations of $\text{YBa}_2\text{Cu}_3\text{O}_y$ and $\text{YBa}_2(\text{Cu}_{1-x}\text{Fe}_x)_3\text{O}_y$ by Utilizing High Purity Inert Gases ( $\text{N}_2, \text{Ar}$ ) .....	K. Kosuge, Y. Ueda and S. Katuyama	142



Synthesis and Superconducting Properties of High $T_c$ Complex Copper Oxides with Double and Single Thallium Layers .....	M. Kikuchi, S. Nakajima, T. Kajitani, T. Suzuki, N. Kobayashi, H. Iwasaki and Y. Syono	145
The Effect of Oxygen Concentration on the $T_c$ in the Bi-Sr-Ca-Cu-O System .....	Y. Ishizawa	152
Synthesis of $\text{Bi}_2\text{Sr}_2\text{CuO}_x$ and $\text{A}_2\text{CuO}_4$ Type Superconducting Ceramics .....	N. Ohashi, Y. Teramoto, T. Taniguchi, H. Ikawa and O. Fukunaga	155
Material Syntheses of Layered Oxides Related with $\text{Bi}_4\text{Ti}_3\text{O}_{12}$ Family Ferroelectrics .....	M. Takashige, F. Shimizu, H. Suzuki and S. Sawada	158
Ultrahigh - Pressure Study of High $T_c$ Oxides .....	H. Aoki, M. Kumazawa, K. Kurita, S. Kobayashi, S. Ikehata, A. Nakamura, S. Katsumoto, F. Komori, T. Fujii, T. Ishii, K. Kinoshita and T. Yamada	161
High - $T_c$ Superconductors Produced by Oxidation of Melt-spun Bi-Sr-Ca-Cu-Au (Ag) Alloy Ribbons .....	A. Inoue, K. Matsuzaki, H. Toribuchi and T. Masumoto	164
Low Temperature Formation of Bi (Pb)-Sr-Ca-Cu-O Thin Films by a Successive Deposition Method with Excimer Laser .....	T. Kawai, M. Kanai and S. Kawai	168
$\text{Ba}_{1-x}\text{K}_x\text{BiO}_3$ Thin Film Preparation with ECR Ion Beam Oxidation, and Their Properties .....	T. Murakami, Y. Enomoto and K. Moriwaki	171
Preparation and Characterization of High Temperature Oxide Superconductor Films .....	Y. Maruyama, Y. Kawai, T. Terui and T. Inabe	174
Single Crystal Growth of Superconducting Oxides and Related Compounds by the Flux and Floating Zone Methods .....	T. Shishido, N. Toyota, K. Ukei, D. Shindo, T. Sasaki, Y. Saito, S. Hosoya, H. Iwasaki, T. Kajitani, H. Yamauchi and T. Fukuda	177
Growth of Superconducting $\text{La}_{2-x}\text{Sr}_x\text{CuO}_4$ Single Crystals .....	H. Kojima and I. Tanaka	180
Crystal Growth and Properties of Superconducting Oxides and Related Compounds .....	H. Takei, H. Takeya, F. Sakai, T. Kitazawa, M. Koike and J. Akimoto	183
An Approach to the Growth of $\text{YBa}_2\text{Cu}_3\text{O}_{7-x}$ Single Crystals by the Flux Method .....	K. Watanabe	186
Low - Temperature Crystalline Structure of $(\text{La}_{1-x}\text{Ba}_x)_2\text{CuO}_{4-\delta}$ .....	T. Suzuki and T. Fujita	190
Neutron Diffraction Studies on Crystal Structures of Oxide Superconductors .....	H. Asano	193
Electron Microscopic Studies of High - $T_c$ Superconductors .....	K. Hiraga, D. Shindo, T. Oku and M. Hirabayashi	196
High Resolution Observation of Grain Boundaries in Oxide Superconductors .....	Y. Takahashi, M. Mori and Y. Ishida	198
High - Resolution Electron Microscopy In-Situ Observation of a Transformation Interface between Tetragonal and Orthorhombic Phases in $\text{YBa}_2\text{Cu}_3\text{O}_{7-x}$ .....	K. Sasaki, K. Kuroda and H. Saka	201

## Part II. Mechanisms of Superconductivity ; Theory

Electronic Band Structure of $\text{La}_2\text{NiO}_4$	K. Takegahara and T. Kasuya	207
Implications of Band - Structure Calculations for High - $T_c$ Related Oxides		
- Extra Hole Doping -	K.T. Park and K. Terakura	210
Multiplet Structure of Cu 2p - XPS in $\text{La}_2\text{CuO}_4$ and CuO	K. Okada and A. Kotani	213
Dispersive Electronic States near the Fermi Level in High $T_c$ Superconductors	Y. Kuramoto and T. Watanabe	219
The Madelung Energy in Oxide Superconductors	J. Kondo and S. Nagai	222
Superconductivity in $\text{BaPb}_{1-x}\text{Bi}_x\text{O}_3$ and $\text{Ba}_x\text{K}_{1-x}\text{BiO}_3$	M. Shirai, N. Suzuki and K. Motizuki	225
Researches on High $T_c$ Superconductivity in Our Group	M. Tachiki	229
To Understand Electronic Properties of High Temperature Superconductors		
-- On the Basis of Fermi Liquid Theory --	K. Yamada and H. Kohno	233
Superconductivity by Intra - Layer and Inter - Layer Cooper Pairing and Investigation of Plasmon Mechanism for a Two - Dimensional Superconductors	M. Inoue, T. Takemori and K. Ohtaka	236
Theory of Strongly Correlated Electrons	Y. Nagaoka	239
Magnetic Correlations in Strongly Correlated Electron Systems	T. Saso	242
Anisotropic Superconductivity in Strongly Correlated Systems : Auxiliary - Particle Formulation	F.J. Ohkawa	245
Small - Cluster Studies on Holes in Two - Dimensional $\text{CuO}_2$ Systems	H. Shiba and M. Ogata	248
Numerical Analysis on Magnetic Mechanism of Superconductivity in Two - Band Models	M. Imada, Y. Hatsugai and N. Nagaosa	251
Pseudospin Formalism of Superconductivity in Strong Correlation	S. Nakajima, M. Hasegawa and N. Baba	257
Electron - Superconductor and the Model Hamiltonian for High $T_c$ Cu - Oxides	H. Fukuyama and H. Matsukawa	260
Theoretical Study of Holes in Quantum Magnetic Insulators	S. Maekawa	263
Superexchange Interaction Constant in p - d Mixing Model	Y. Isawa	266
Holon Local Density of States of 2D RVB Quantum Spin Liquid	Y. Takahashi and P. Lederer	269
On Three Dimensional Gauge Theory	N. Imai, K. Ishikawa, N. Kimura, T. Matsuyama and I. Tanaka	272

### Part III. Organic Superconductors

Possible Relation between the Superstructure and Superconducting Critical Temperatures in the Organic Superconductor $\beta$ - (BEDT - TTF) <sub>2</sub> I <sub>3</sub>	S. Kagoshima, Y. Nogami, M. Hasumi, H. Anzai, M. Tokumoto, G. Saito and N. Mori	275
Crystal Growth and Superconductivity of Mixed Crystals of $\beta$ - (BEDT - TTF) <sub>2</sub> Trihalides	H. Anzai, M. Tokumoto, K. Takahashi, K. Murata, N. Kinoshita, H. Bando and T. Ishiguro	280
Anomalous Magnetotransport Phenomena in $\theta$ - (BEDT - TTF) <sub>2</sub> I <sub>3</sub>	K. Kajita, Y. Nishio, T. Takahashi, W. Sasaki, R. Kato, H. Kobayashi, A. Kobayashi and Y. Iye	283
Superconductivity in $\kappa$ - (BEDT - TTF) <sub>2</sub> Cu (NCS) <sub>2</sub>	G. Saito, H. Urayama, H. Yamochi and K. Oshima	286
Anomalous NMR Relaxation in the Organic Superconductor (BEDT - TTF) <sub>2</sub> Cu(NCS) <sub>2</sub>	T. Takahashi	289
Thermoelectric Power of Organic Superconductors. Calculation on the Basis of the Tight-Binding Theory	T. Mori and H. Inokuchi	292
Structural Characteristics of BEDT - TTF Superconductors and a New Type of Molecular Metal with Coordination Structure	H. Kobayashi, R. Kato and A. Kobayashi	293
Coexistence of a Magnetic Order and Metallic Conduction in an Organic System, (DMDCNQI) <sub>2</sub> Cu	T. Mori, S. Bandow, K. Imaeda, H. Inokuchi, A. Kobayashi, R. Kato and H. Kobayashi	296
Magnetic Behavior and Resonating Valence Bond State in Organic Free Radicals	K. Takeda, H. Deguchi, T. Hoshiko, K. Takahashi, K. Konishi, T. Idogaki, N. Uryû and J. Yamauchi	298
Crystal Structures of DMET Organic Superconductors	I. Ikemoto, K. Kikuchi and K. Saito	301

A. Fujimori

Department of Physics, University of Tokyo, Hongo, Bunkyo-ku, Tokyo 113, Japan

We have studied the electronic structure of superconducting and insulating Cu oxide systems by photoemission spectroscopy with particular emphasis on the electronic states near the Fermi level. The results suggest that they are split-off oxygen p states, formed possibly through hybridization with Cu  $d^8$  states, and cannot be due to a Kondo-type resonance and resulting renormalized band states.

Photoemission studies have established that the Cu d electrons in high- $T_C$  superconductors are highly correlated and that doped holes enter oxygen sites rather than Cu sites [1]. However, the nature of the electronic states in the vicinity of the Fermi level ( $E_F$ ), which are directly involved in Cooper pairing, is not yet obvious. Firstly, it is important to identify the location and symmetry of doped oxygen holes. Secondly, the formation process of the Fermi-liquid states from the hybridized Cu d-oxygen p bands with strong electron correlation has to be clarified. In order to elucidate these problems, we have performed detailed photoemission studies of superconducting as well as insulating Cu-oxide systems combined with cluster model analyses.

The valence-band photoemission spectra of  $\text{La}_{2-x}\text{Sr}_x\text{CuO}_4$  or  $\text{YBa}_2\text{Cu}_3\text{O}_y$  can be well reproduced by cluster model calculations as shown in Fig. 1, and thereby one can determine the parameters of the model, namely, Cu d-d correlation  $U$ , p-d charge-transfer energy  $\Delta$ , and p-d transfer integral  $T$  [2]. However, the symmetry of the lowest binding energy feature,  $^1A_1$  or  $^3B_1$ , depends on the energy difference  $\Delta\epsilon_p$  between the oxygen p orbitals in the  $\text{CuO}_2$  planes and those in the BaO (LaO) planes. In the  $^1A_1$  state the doped hole enters p $\sigma$  orbitals in the  $\text{CuO}_2$  plane and forms a local singlet with the Cu  $d^9$  spin, whereas in the  $^3B_1$  state it enters both

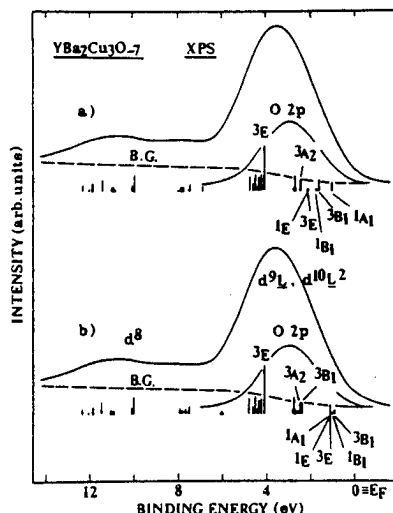


Fig. 1. Calculated valence-band x-ray photoemission spectra of  $\text{YBa}_2\text{Cu}_3\text{O}_{0.7}$  with  $U = 7$  eV,  $\Delta = 1.2$  eV, and  $T = 2.3$  eV. (a)  $\Delta\epsilon_p = 0.7$  eV, (b)  $\Delta\epsilon_p = 1.7$  eV.

the  $\text{CuO}_2$  and  $\text{BaO}$  ( $\text{LaO}$ ) planes and forms a triplet state.

Although the density of states (DOS) near  $E_F$  of oxide superconductors observed by photoemission spectroscopy is quite low, one observes clear Fermi edges for sufficiently doped materials, particularly for  $\text{Bi}_2(\text{Sr,Ca})_3\text{Cu}_2\text{O}_{8+y}$ . Further, recent angle-resolved photoemission studies [3] have revealed the existence of dispersive states crossing  $E_F$  in this low DOS region. As Fermi-liquid states in high- $T_C$  superconductors have been discussed in analogy with the renormalized  $f$  bands in heavy-Fermion systems resulting from Kondo resonances [4], it is important to see whether the states near  $E_F$  observed by photoemission spectroscopy are due to

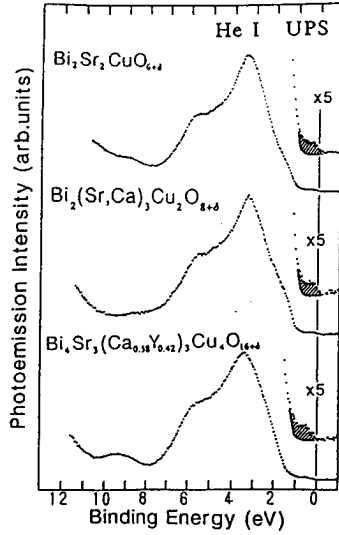


Fig. 2. Photoemission spectra of superconducting  $\text{Bi}_2\text{Sr}_2\text{CuO}_{6+y}$  (one- $\text{CuO}_2$ -layer) and  $\text{Bi}_2(\text{Sr,Ca})_3\text{Cu}_2\text{O}_{8+y}$  (two- $\text{CuO}_2$ -layer) and insulating  $\text{Bi}_4\text{Sr}_3(\text{Ca}_{0.58}\text{Y}_{0.42})_3\text{Cu}_4\text{O}_{16+y}$  (two- $\text{CuO}_2$ -layer). Shaded areas represent split-off oxygen states.

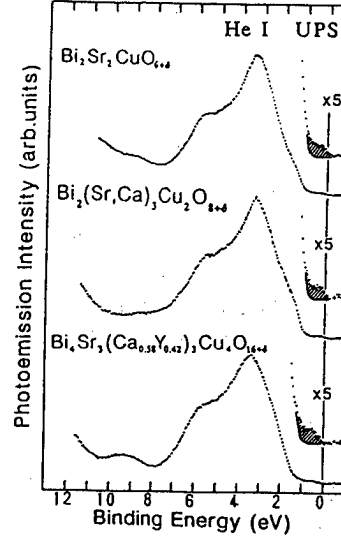


Fig. 3. Photoemission spectra of  $\text{Sr}_2\text{CuO}_2\text{Cl}_2$ . The 21.2 eV spectrum is dominated by Cl 3p-derived emission whereas the 40.8 eV spectrum by O 2p-derived emission.

such heavy-electron states. Figure 2 shows photoemission spectra of  $\text{Bi}_2(\text{Sr,Ca})_3\text{Cu}_2\text{O}_{8+y}$  and of the corresponding insulator  $\text{Bi}_4\text{Sr}_3(\text{Ca}_{0.58}\text{Y}_{0.42})_3\text{Cu}_4\text{O}_{16+y}$  [5,6]. Both spectra are virtually identical, particularly for the weak emission feature near  $E_F$ , except for the slight shift of the whole spectrum to higher binding energy in going from the metal to the insulator and the concomitant disappearance of the DOS at  $E_F$ . This observation clearly indicates that the states near  $E_F$  are split-off oxygen p states and cannot be due to a Kondo resonance and resulting heavy-electron band states.

In order to further demonstrate the existence of split-off oxygen states in insulators, we present in Fig. 3 the spectra of  $\text{Sr}_2\text{CuO}_2\text{Cl}_2$  which is a  $\text{K}_2\text{NiF}_4$ -type insulator consisting of  $\text{CuO}_2$  and  $\text{SrCl}$  planes [6]. Because the 21.2 eV spectrum is dominated by Cl 3p-derived emission and the 40.8 eV spectrum by O 2p-derived emission, we may conclude that this compound also shows split-off oxygen p states above the top of the main O 2p band. In this case, one can unambiguously assign these states to  $1A_1$  since it is always the lowest energy p-hole state when there are no apex oxygens [2]. Thus it is tempting to assign the split-off oxygen states of the Bi compounds to the same local singlets formed within the  $\text{CuO}_2$  planes. However, one cannot exclude at present the possibility that these split-off states are derived from the Bi-O planes. (Note that the oxygen K-edge absorption has identified the direction of oxygen p-

hole orbitals and not their location [7].) Indeed, analyses of the valence-band x-ray photoemission spectra suggest  $1A_1$  to be shifted away from  $E_F$  compared to the other Cu oxides and significant contributions of Bi-derived states near  $E_F$  [5]. Further studies are necessary to determine the location of doped holes in high- $T_C$  superconductors.

I would like to thank collaborations with many people, particularly E. Takayama-Muromachi, S. Takekawa, T. Takahashi, H. Katayama-Yoshida, M. Sato, Y. Tokura, H. Eisaki, and S. Uchida.

#### References

- [1] A. Fujimori, E. Takayama-Muromachi, Y. Uchida, and B. Okai: Phys. Rev. B 35 (1987) 8814; Solid State Commun. 63 (1987) 857.
- [2] A. Fujimori: Phys. Rev. B 39 (1989) 793.
- [3] T. Takahashi, H. Matsuyama, H. Katayama-Yoshida, Y. Okabe, S. Hosoya, K. Seki, H. Fujimori, M. Sato and H. Inokuchi : Nature 334 (1988) 691; F. Minami, T. Kimura, and S. Takekawa: Phys. Rev. B (submitted).
- [4] K. Miyake, T. Matsuura, K. Sano, and Y. Nagaoka: Physica B 148 (1987) 381.
- [5] A. Fujimori, S. Takekawa, E. Takayama-Muromachi, Y. Uchida, A. Ono, T. Takahashi, Y. Okabe, and H. Katayama-Yoshida: Phys. Rev. B 39 (in press).
- [6] A. Fujimori, Y. Tokura, H. Eisaki, H. Takagi, S. Uchida, and M. Sato: Phys. Rev. B (submitted).
- [7] N. Nücker, H. Romberg, X. X. Xi, J. Fink, B. Gegenheimer, and Z. X. Xiao: Phys. Rev. B (in press).

# Synchrotron-Radiation Photoemission Study of Single Crystal $\text{Bi}_2\text{Sr}_2\text{CaCu}_2\text{O}_8$

T. Takahashi, H. Matsuyama, H. Katayama-Yoshida, and Y. Okabe

Department of Physics, Tohoku University, Sendai 980, Japan

Angle-resolved and resonant photoemission measurements with synchrotron radiation have been performed on single crystal  $\text{Bi}_2\text{Sr}_2\text{CaCu}_2\text{O}_8$ . Two dispersive bands intersecting the Fermi level midway between the  $\Gamma$  point and the Brillouin-zone boundary were observed. The other bands in the higher-binding-energy region are almost dispersionless in contrast to the band structure calculation. The Fermi-edge peak exhibits a pronounced enhancement at the photon energy of O 2s core threshold, indicating a dominant O 2p nature of the Fermi-edge states. The experimental results indicate the existence of the Fermi-liquid states with dominant O 2p nature in the high- $T_c$  superconductor.

The mechanism of high- $T_c$  superconductivity has not been well established although numerous experimental and theoretical studies have been done. It is certain that understanding the electronic structure is the first step to establish the high- $T_c$  mechanism. In this report, we present a comprehensive result of our synchrotron-radiation photoemission study [1,2] on single crystal  $\text{Bi}_2\text{Sr}_2\text{CaCu}_2\text{O}_8$ . We have performed two types of photoemission measurements, one is an angle-resolved photoemission to determine the valence-band structure and the other is a resonant photoemission to study the atomic-orbital nature of the energy bands in the vicinity of the Fermi level.

A single crystal of  $\text{Bi}_2\text{Sr}_2\text{CaCu}_2\text{O}_8$ , typically  $5 \times 5 \times 0.5 \text{ mm}^3$ , was grown with KCl flux method. The single-crystallinity was confirmed by an x-ray diffraction. A magnetic-susceptibility measurement showed that this crystal becomes superconductive at 85 K. Photoemission measurement was performed with an angle-resolved photoemission spectrometer at the UVSOR, Institute for Molecular Science (IMS), Japan. The crystal was cleaved in-situ along the ab plane and kept at room temperature. We checked a possible degradation of the sample surface by measuring a standard spectrum several times throughout the measurements and found no detectable change. The angular and energy resolutions were  $2^\circ$  and 0.2 eV, respectively.

Figure 1 shows angle-resolved photoemission spectra measured in the high-symmetry direction  $\Gamma X$ , together with the band structure of  $\text{Bi}_2\text{Sr}_2\text{CaCu}_2\text{O}_8$  determined from the photoemission measurements. Experimental results obtained with  $\hbar\omega = 40 \text{ eV}$  and for another high-symmetry direction  $\Gamma M$  are also included in the figure. Several band structure calculations of  $\text{Bi}_2\text{Sr}_2\text{CaCu}_2\text{O}_8$ , which are essentially the same, are available and one of them [3] is shown in Fig. 1 for comparison. As shown in Fig. 1, band A intersects the Fermi level at the points about  $\Gamma X/3$  and  $\Gamma M/2$  from the  $\Gamma$  point for the  $\Gamma X$  and  $\Gamma M$  directions, respectively. Band B obviously crosses the Fermi level just midway between the  $\Gamma$  and X points while it slightly touches the the

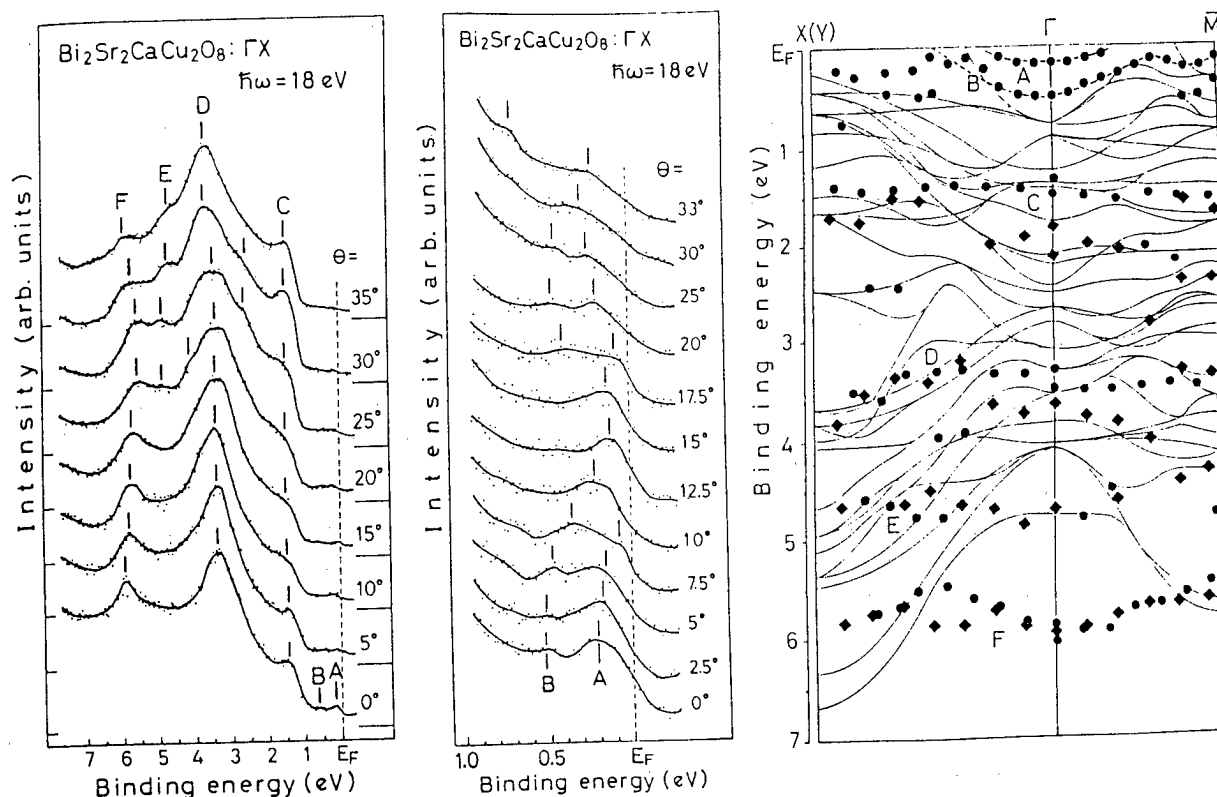


Fig. 1 Angle-resolved photoemission spectra of  $\text{Bi}_2\text{Sr}_2\text{CaCu}_2\text{O}_8$  measured in the high symmetry direction  $\Gamma\text{X}$  for the valence band (left) and for the vicinity of the Fermi level (middle), together with the experimental band structure derived from the present photoemission experiment (right) compared with the band structure calculation (thin solid lines).

Fermi level in the  $\Gamma\bar{\text{M}}$  direction. The other experimental bands except for band F show no remarkable energy dispersion. Band F has a noticeable upward dispersion in the vicinity of the  $\Gamma$  point and reaches the  $\bar{\text{M}}$  point without changing the dispersing direction while in the  $\Gamma\text{X}$  direction it turns downward midway between the  $\Gamma$  and  $\text{X}$  points.

In Fig. 1, we find an overall disagreement between the experiment and the calculation, which has been naturally expected from the reported displacement by 1-2 eV between the angle-integrated photoemission spectrum for the valence band and the calculated one-electron density of states. However, an experimental band in the vicinity of the Fermi level shows a fairly good agreement with one of the calculated bands; band B may be correlated with the calculated antibonding band of the Cu 3d and O 2p orbitals which is located at 0.7 eV at the  $\Gamma$  point and intersects the Fermi level midway between the  $\Gamma$  and  $\text{X}$  points. This is surprising because it has been generally believed that the strong electron correlation fully destroys the one-electron band structure. The observed agreement implies that the one-electron approximation may be qualitatively correct at least in the vicinity of the Fermi level. However, we cannot find a counterpart of band A in the band structure calculation when we correlate band B to the theoretical Cu3d-O2p antibonding state.



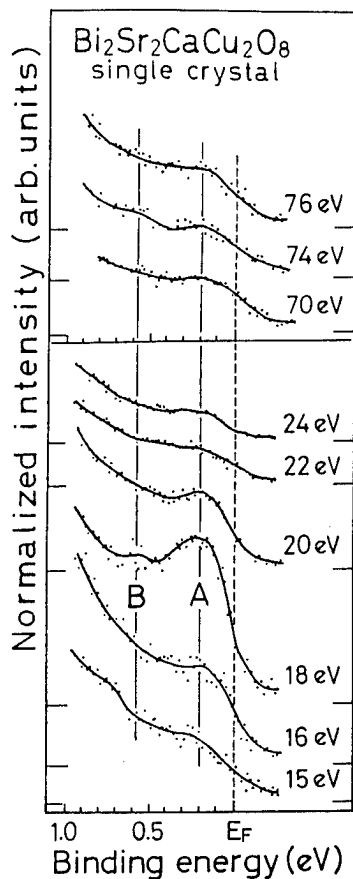


Fig. 2 Photoemission spectra in the vicinity of the Fermi level measured at the photon energies near the O 2s (lower) and Cu 3p (upper) core thresholds.

Figure 2 shows photoemission spectra in the vicinity of the Fermi level taken at several photon energies near the O 2s and Cu 3p core thresholds. We should remark the pronounced enhancement of the Fermi-edge peak (band A) at the photon energy near the O 2s core threshold (18 eV) and its almost no change when passing the Cu 3p core threshold (74 eV). The observed resonance gives a direct evidence for the dominant O 2p nature in the electronic states at the Fermi level. This presents a sharp contrast to the prediction from the band structure calculation where the Fermi-edge state is a heavily hybridized Cu3d-O2p antibonding state. Thus, the observed coincidence in the dispersive feature between band B and the calculated Cu3d-O2p antibonding state cannot necessarily be served as an indication of the validity of the one-electron approximation. The validity of the one-electron approximation should be discussed by viewing the whole valence band structure. In the higher-binding energy region, on the other hand, all the experimentally observed bands except for band F are almost dispersionless in contrast to the highly dispersive feature of the calculated bands. As for band F, the direction of energy dispersion is just opposite to that of the calculated Cu3d-O2p bonding states, suggesting a substantial renormalization by the strong electron correlation in the high-binding-energy region.

All these experimental results described above clearly provide a direct experimental evidence for that the electronic structure of  $\text{Bi}_2\text{Sr}_2\text{CaCu}_2\text{O}_8$

consists mainly of the two parts; the Fermi-liquid states in the vicinity of the Fermi level and localized states with strong electron correlation in the higher-binding-energy region. The superconductivity could be driven by Cooper-pairing of the O 2p holes in the Fermi-liquid states through the spin or charge fluctuation.

**Acknowledgements**—We thank Dr. S. Hosoya (Tohoku University), Prof. K. Seki (Hiroshima University), Dr. H. Fujimoto, Prof. M. Sato, and Prof. H. Inokuchi (IMS) for their kind collaborations.

#### References

- 1) T. Takahashi, H. Matsuyama, H. Katayama-Yoshida, Y. Okabe, S. Hosoya, K. Seki, H. Fujimoto, M. Sato, and H. Inokuchi, *Nature* 334, 691 (1988).
- 2) T. Takahashi, H. Matsuyama, H. Katayama-Yoshida, Y. Okabe, S. Hosoya, K. Seki, H. Fujimoto, M. Sato, and H. Inokuchi, *Phys. Rev. B* (submitted).
- 3) S. Massidda, J. Yu, and A.J. Freeman, *Physics C* 52, 251 (1988).

Atsushi ANDO, Koichiro SAIKI and Atsushi KOMA

Department of Chemistry, The University of Tokyo  
Bunkyo-ku, Tokyo 113, Japan

Electronic structures of ortho- and tetra- $\text{YBa}_2\text{Cu}_3\text{O}_y$  and  $\text{Bi}_2\text{Sr}_2\text{Ca}_{n-1}\text{Cu}_n\text{O}_{2n+4+x}$  ( $n=1,2$ ) have been investigated by low-energy electron energy loss spectroscopy. Loss peaks due to inter-band transitions, plasmon excitation and core electron excitations have been observed. It has been found from the observed spectra that the electronic structures of ortho- and tetra- $\text{YBa}_2\text{Cu}_3\text{O}_y$ , and those of  $\text{Bi}_2\text{Sr}_2\text{CuO}_{6+x}$  and  $\text{Bi}_2\text{Sr}_2\text{CaCu}_2\text{O}_{8+x}$  resemble to each other, respectively, except for the energy regions below and above the Fermi levels by a few eV.

The electronic structure of various high- $T_c$  superconductors have been investigated by using such electron spectroscopies as photoemission [1,2] and inverse photoemission [3,4]. The former has mainly gives informations on the filled electronic states including core levels, whereas the latter yields the informations on the empty electronic states above the Fermi level ( $E_F$ ). Here we will report the electronic structures of orthorhombic  $\text{YBa}_2\text{Cu}_3\text{O}_{7-y}$  (abbreviated as ortho-YBCO hereafter), tetragonal  $\text{YBa}_2\text{Cu}_3\text{O}_6$  (abbreviated as tetra-YBCO hereafter),  $\text{Bi}_2\text{Sr}_2\text{CaCu}_2\text{O}_{8+x}$  (abbreviated as BSCCO hereafter) and  $\text{Bi}_2\text{Sr}_2\text{CuO}_{6+x}$  (abbreviated as BSCO hereafter), which were measured by low-energy electron energy loss spectroscopy (LEELS). LEELS gives informations on both filled and empty electronic states, and can reveal several types of excitations over a wide energy region with a single apparatus.

The specimens of ortho- and tetra-YBCO were made by sintering. The tetra-YBCO sample was obtained

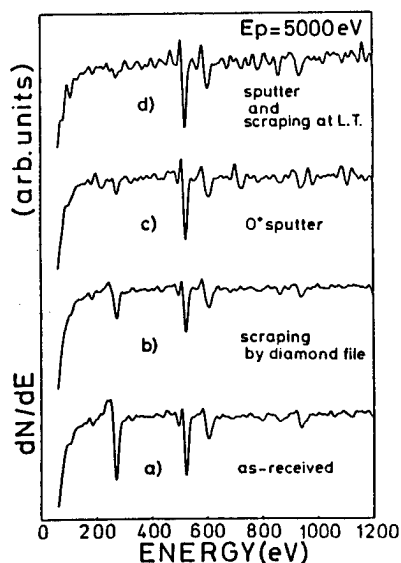


Fig. 1. Auger spectra of a sintered specimen of ortho-YBCO after various cleaning procedures.

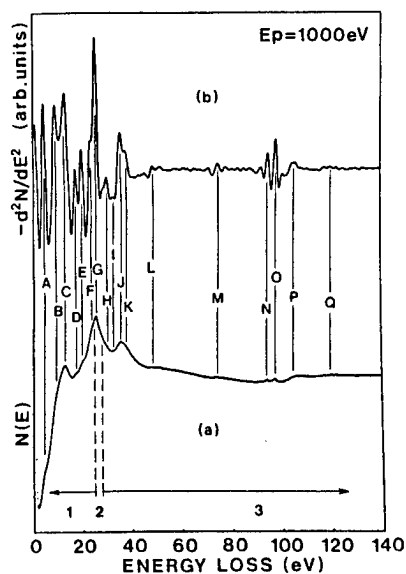


Fig. 2. LEELS spectra of ortho-YBCO.

by quenching from 950 °C. The crystal structures were checked by X-ray diffraction. The specimens of BSCCO and BSCO were single-crystalline ones made by the flux method. Prior to the measurement of LEELS spectra of sintered YBCO samples, we measured AES spectra to determine an effective method to clean the specimen surface. We tried the following three methods: (i) scraping by a diamond file, (ii)  $O^+$  sputtering ( $1 \times 10^{-3}$  Pa, 30 min), (iii) scraping by a diamond file after sputtering. Fig. 1(a) shows the AES spectrum of an as-sintered specimen surface. The intensity of the carbon peak was as large as that of the oxygen peak. This carbon peak intensity decreased after the specimen was scraped by a diamond file but still remained at about two thirds of that of the oxygen peak (Fig. 1(b)). The carbon peak intensity further decreased when the specimen was sputtered by  $O^+$  ions (Fig. 1(c)). Although  $O^+$  sputtering was performed to suppress the expected oxygen deficiency in the surface region, no significant difference was observed in the oxygen AES signal when  $Ar^+$  ions were used as sputtering species instead of  $O^+$  ions. Thus, sputtering seems to be effective for the cleaning of YBCO specimen surfaces. Since an amorphous layer is usually formed in the surface portion by sputtering, we scraped the surface region with a diamond file after sputtering had been carried out, and a clean surface could be obtained as is seen in Fig. 1(d).

It was found from Q-mass measurements that the partial pressure of oxygen increased by about one order of magnitude in the  $10^{-8}$  Pa range when the sintered ortho-YBCO sample was irradiated by the electron beam at room temperature (RT). This means that oxygen is very easily desorbed from the ortho-YBCO specimen surface by electron irradiation. Nevertheless, the oxygen signal in the AES spectra did not change greatly during prolonged electron irradiation. Therefore, the diffusion rate of oxygen in the sintered specimen is very high at RT and the oxygen deficient sites in the surface region are rapidly filled to realize an equilibrium of surface oxygen concentration. The electron-induced oxygen desorption, on the other hand, was not observed when the specimen was cooled to 170 K. Therefore, the LEELS spectra for ortho-YBCO were measured at 170 K. In the cases of tetra-YBCO, BSCCO and BSCO, the oxygen desorption induced by electron irradiation was much less, and the LEELS spectra were measured at RT.

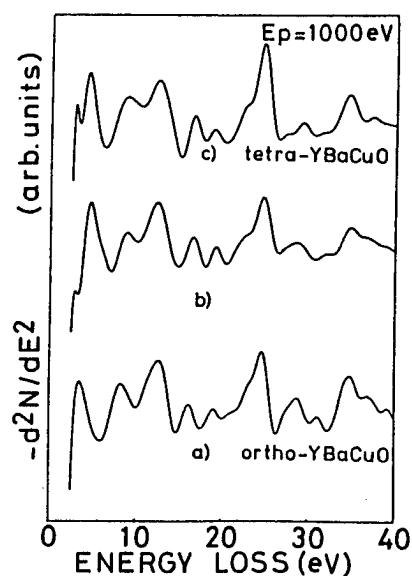


Fig. 3. LEELS spectra of ortho-YBCO (a), e-beam irradiated ortho-YBCO (b) and tetra-YBCO.

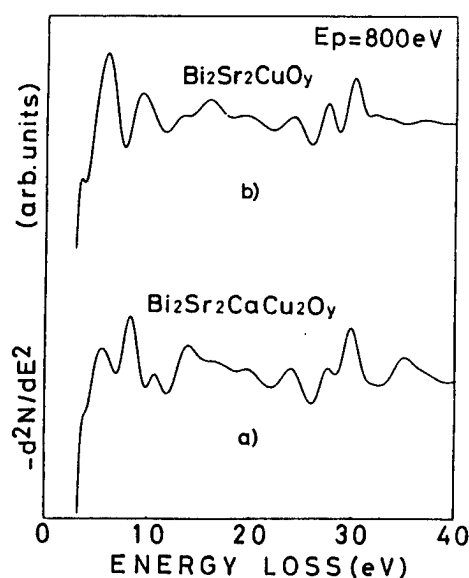


Fig. 4. LEELS spectra of BSCCO (a) and BSCO (b).

Figure 2 shows the overall LEELS spectrum of ortho-YBCO and its second derivative in the energy region of 0 - 140 eV. The incident electron energy was 1000 eV. The detailed assignment of the observed peaks are shown elsewhere [1], but brief description will be given in the followings. In the energy region of 0 - 40 eV, the peaks observed are derived from interband transitions, plasmon excitation and shallow core electron excitations. The most prominent peak in the spectra is peak G originating from the volume plasmon excitation. The peaks A through F can be assigned to result from interband transitions from valence band states to a common high-density portion of the first conduction band which is located up to 2 - 4.7 eV above  $E_F$ . The peaks N and O arise from electronic transitions from the Ba ( $4d_{5/2}$ ) and Ba ( $4d_{3/2}$ ) core levels to the same final state in the first conduction band, respectively. Peak P is assigned to result from the electronic transition from the Ba ( $4d$ ) core level to the second conduction band. From the separation between peak P and peaks N and O, the second conduction band is located at about 10 eV above the lowest conduction band.

The LEELS spectra of tetra-YBCO are compared in Fig. 3 with that of ortho-YBCO. As is seen in the figure, the spectra are almost the same and the difference is only seen in the lowest loss energy region. This indicates that the oxygen deficiency in tetra-YBCO affects only the electronic states near the Fermi level. In this connection, the loss spectrum of tetra-YBCO in the Ba( $4d$ ) core electron excitation region is almost the same as that of ortho-YBCO. It shows that the conduction band structure is almost same between tetra- and ortho-YBCO. Then it is concluded that the difference in the electronic structures of ortho- and tetra-YBCO lies only in the top portion of the valence band formed mainly from  $O(2p)$  orbitals.

The surface region of ortho-YBCO changes with the prolonged electron irradiation. The loss spectrum of ortho-YBCO after 1.5 C electron irradiation is shown in Fig. 4(b), which agrees well with that of tetra-YBCO shown in (c). This means the surface of ortho-YBCO changes into tetra-YBCO by electron irradiation, which seems to arise from the easy electron-induced desorption of oxygen atoms in the linear chains in ortho-YBCO.

Fig. 4 shows the second derivative LEELS spectra of a cleaved faces of BSCCO and BSCO. The single-crystalline samples were air-cleaved just before loading into the UHV chamber. The sample surfaces were cleaned by heating at 400 °C under the vacuum of  $1 \times 10^{-8}$  Pa. The cleanliness was checked by AES before the LEELS measurement. Although LEELS spectra were measured with several incident electron energies from 100 eV to 1600 eV, there were no significant differences in all the spectra. These results indicate that all the observed peaks are derived from bulk origins. As is seen in the figure, the LEELS spectra of the two samples resemble to each other except for the low loss energy region, indicating that those materials have similar electronic structures. The difference between them are mainly seen in the loss energy region below 10 eV. Thus the insertion of a Ca layer mainly changes the electronic structures above and below Fermi levels by a few eV.

The authors thank Prof. S. Uchida for giving them single-crystalline samples of BSCCO and BSCO.

## References

- [1] R.L. Kurtz, R.L. Stockbauer, D. Mueller, A. Shih, L.E. Toth, M. Osofsky and S.A. Wolf: Phys. Rev. B 35 (1987) 8818.
- [2] S. Kohiki, T. Wada, S. Kawashima, H. Takagi, S. Uchida and S. Tanaka: Phys. Rev. B 38 (1988) 8868.
- [3] T.J. Wagener, Y. Gao, J.H. Weaver, A.J. Arko, B. Flandermeyer and D.W. Capone II: Phys. Rev. B 36 (1987) 3899.
- [4] J.A. Yarmoff, D.R. Clarke, W. Drube, U.O. Karlsson, A. Taleb-Ibrahimi and F.J. Himpsel: Phys. Rev. B 36 (1987) 3967.
- [5] A. Ando, K. Saiki, K. Ueno and A. Koma: Jpn. J. Appl. Phys. 27 (1988) L304.

# Optical Absorption in $(\text{La}_{1-x}\text{Sr}_x)_2\text{CuO}_4$ Single Crystal Thin Films

Minoru Suzuki

NTT Opto-Electronics Laboratories, 162 Tokai, Ibaraki 319-11, Japan

An experimental study on optical absorption is described for  $(\text{La}_{1-x}\text{Sr}_x)_2\text{CuO}_4$  ( $x = 0 \sim 0.18$ ) single crystal thin films. The optical transmission spectrum has the fundamental absorption corresponding to the energy gap of about 2 eV and an anomalous absorption band centered at  $0.85 \mu\text{m}$ . This absorption, the intensity of which increases with Sr doping, implies the development of the density of states within the gap of  $\text{La}_2\text{CuO}_4$ . With Sr doping, the density of states forms a band about 1 eV wide and about 1 eV above the original valence band. This emerging density of states within the gap is totally at variance with the conventional rigid band model, and shows correlation with the  $x$  dependence of  $T_c$ .

## I. INTRODUCTION AND SUMMARY

To shed light on the mechanism of high  $T_c$  superconductivity, probably arising from a non-phonon origin, in the series of cuprates, it is of primary importance to make clear the electronic structure of these materials. Experimentally, insight into the electronic structure is obtained by means of, *e.g.*, electron energy loss spectroscopy (EELS), x-ray photoemission spectroscopy (XPS) or optical spectroscopy. Recent experimental studies<sup>1,2</sup> using the former two methods revealed that the electronic states at the Fermi level come from O 2p states, providing evidence that conducting carriers are holes at oxygen sites in nature. Optical spectroscopy, on the other hand, also provides important information about the band structure near the Fermi level. For most of the high  $T_c$  oxides, appropriate doping changes the systems from an insulator of the charge transfer type to a metal. This change is usually accompanied by a systematic change in the electronic structure, to which the optical absorption spectroscopy is most sensitive. This report describes an optical absorption study<sup>3</sup> in the  $(\text{La}_{1-x}\text{Sr}_x)_2\text{CuO}_4$  system, the material widely viewed as the prototype for understanding high  $T_c$  superconductivity.

From the systematic measurements of optical reflectance and transmittance, it is found that Sr doping induces the development of electronic density of states, which come basically from O 2p states, within the energy gap of the host compound  $\text{La}_2\text{CuO}_4$ . With further doping, this density of states forms a band about 1 eV wide. This change in the density of states is totally at variance with the conventional rigid band model, and shows clear correlation with the  $x$  dependence of  $T_c$ .

## II. EXPERIMENT

As is usually the case for transition metal oxides, absorption coefficient of the high  $T_c$  cuprates is considerably large, so that optical transmission measurements need thin films. The specimens used are single crystalline  $(\text{La}_{1-x}\text{Sr}_x)_2\text{CuO}_4$  films ( $x = 0 \sim 0.18$ ) epitaxially grown by rf magnetron sputtering on (100) face  $\text{SrTiO}_3$  substrates with the c-axis perpendicu-

lar to the film surface, so that the electric field of radiation is parallel to the CuO plane. Film thickness, measured with a stylus profilometer, is from 3000 to 4000 Å. Films were annealed after deposition in air for 8 h in order to minimize oxygen vacancies. Optical transmission and reflectance spectra were measured at room temperature with a monochromator in the wavelength range from 0.4 to  $4.5 \mu\text{m}$ . The reflectivity was calibrated with an evaporated silver thin film.

## III. RESULTS AND DISCUSSION

Temperature dependence of resistivity  $\rho(T)$  is shown in Fig. 1 as a function of  $x$ . With increasing  $x$ , temperature dependence becomes more metallic and  $\rho$  decreases systematically. The  $\rho$  values are much lower than those of sintered polycrystals, reflecting single crystal quality. Superconductivity was observed for  $0.05 \leq x \leq 0.15$  with the highest  $T_c$  of 29 K at  $x = 0.075$ . Although  $\rho$  becomes lowest for  $x = 0.18$  among the specimens, no sign of superconductivity was observed above 4.2 K. For  $x = 0.05$ ,  $\rho(T)$  is metallic over the entire temperature range measured, and the absence of upturn, as often observed for sintered specimens with the same  $x$  or below 0.05, indicates that the amount of oxygen vacancies is sufficiently reduced.

Room temperature reflectance spectra for these films are shown in Fig. 2. The results are basically the same as observed by Tajima *et al.*<sup>4</sup> except for being larger in magnitude because of the surface flatness, the form of a thin film, and the total alignment of the CuO planes within the specimens. In the shorter than  $1.4 \mu\text{m}$  wavelength range, a structure with an oscillator strength centered at around  $1 \mu\text{m}$  is clearly seen, reflecting an electronic structure inherent in this material. This structure corresponds to an interband transition, which appears clearer in the transmission spectra. It should be noted that this structure was also observed in the optical reflectance measurements on sintered polycrystals.<sup>4,5</sup>

The solid lines in Fig. 2 are the Drude fits to the experimental results using the formula,

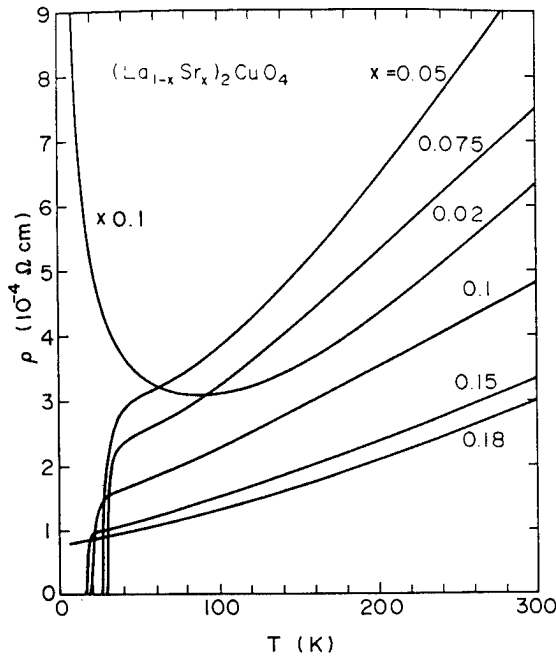


Fig. 1. Temperature dependence of resistivity along the CuO plane for the  $(\text{La}_{1-x}\text{Sr}_x)_2\text{CuO}_4$  (001) epitaxial thin films with  $x$  from 0.02 to 0.18.

$$\epsilon(\omega) = \epsilon_{\infty} \left( 1 - \frac{\omega_p^2}{\omega^2 + i\gamma\omega} \right).$$

As clearly seen, the fits are reasonably good for the wavelength range longer than  $1.5 \mu\text{m}$ . The values of the plasma frequency  $\omega_p$  obtained by this fitting is basically the same as those by Tajima *et al.*<sup>5</sup> The optical scattering time ( $\tau = \gamma^{-1}$ ) increases with  $x$  up to  $1.3 \times 10^{-14}$  s at  $x = 0.18$ , which is consistent with the systematic change in the electrical properties from an insulator to a metal.

In contrast to the modest change in reflectance spectrum with  $x$ , however, the transmittance spectrum shows a dramatic change, as clearly seen in Fig. 3. The most prominent change is the development of an absorption peak centered at  $0.85 \mu\text{m}$ . For  $x = 0$ , where the LSCO system is a semiconductor, the spectrum shows only an absorption edge corresponding to an energy gap of about 2 eV. With the systematic doping with Sr, in addition to the decrease in transmittance in the infrared region ( $\lambda > 2 \mu\text{m}$ ), transmittance at  $0.85 \mu\text{m}$  decreases nearly proportionally to Sr concentration. The former absorption probably corresponds to the intraband transitions involving free carriers generated by doping, while the latter indicates an interband electronic transition which is not immediately evident within the electronic structure of  $\text{La}_2\text{CuO}_4$ . This is quite unusual when taking into account a transmission spectrum of an ordinary oxide superconductor, say  $\text{BaPb}_{1-x}\text{Bi}_x\text{O}_3$ , where the transmission spectrum shows only the fundamental absorption edge and the absorption in near-infrared due to intraband electronic transitions.

Figure 4 shows absorption coefficient  $\alpha(\hbar\omega)$  for the same  $x$  values, calculated from reflectance  $R(\hbar\omega)$  and transmit-

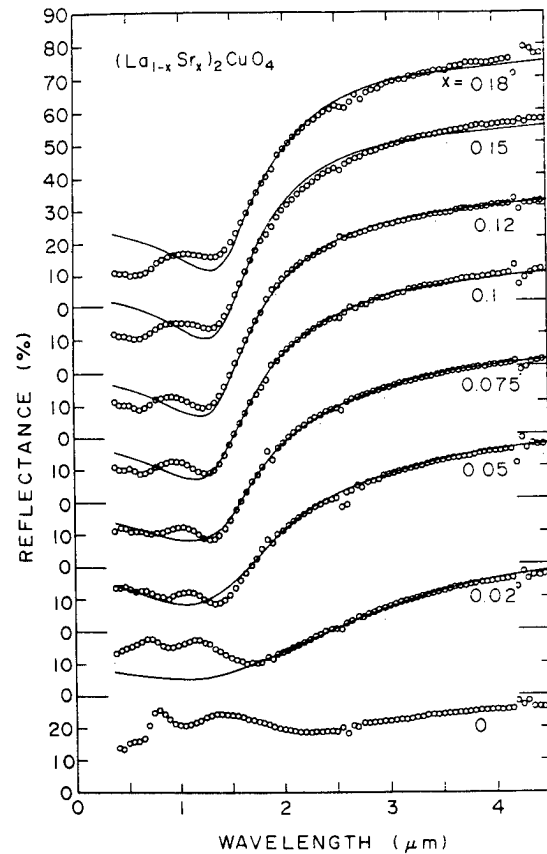


Fig. 2. Reflectance spectra for the  $(\text{La}_{1-x}\text{Sr}_x)_2\text{CuO}_4$  (001) epitaxial thin films with  $x$  from 0 to 0.18. Solid lines are Drude fits.

tance  $T(\hbar\omega)$  values using the approximate formula,  $T = (1 - R)e^{-\alpha d}$ . Approximately,  $\alpha$  is proportional to the joint density of states (JDOS)  $N(E)N(E - \hbar\omega)$ , and reflects the structure of the density of states (DOS) near the Fermi level  $E_F$ . If it is assumed that there is no particular structure in the upper Hubbard band (the final states of the electronic transition), then  $\alpha$  roughly reflects the DOS structure below  $E_F$ , i.e., the valence band structure. Bearing this in mind, it is evident that Sr doping induces the development of DOS in the energy gap of the original semiconductor  $\text{La}_2\text{CuO}_4$ . Furthermore, the DOS increases in proportion to  $x$ , forming a band about 1 eV wide in the superconducting  $x$  range. This behavior is totally at variance with the conventional oxide superconductors, indicating that the rigid band model is ineffective in explaining the electronic structure of the  $(\text{La}_{1-x}\text{Sr}_x)_2\text{CuO}_4$  system.

Optical absorption is proportional to the frequency dependent conductivity  $\sigma(\omega)$ , and the present result is compared with the  $\sigma(\omega)$  spectrum obtained from reflectance data using Kramers-Kronig analysis. The small maximum corresponding to the absorption peak at 0.85 eV is recognized in  $\sigma(\omega)$  obtained, e.g., by Herr *et al.*<sup>6</sup> or by Etemad *et al.*,<sup>7</sup> although its origin or its  $x$  dependence is not shown clearly. Also in the EELS measurements, Nücker *et al.*<sup>2</sup> observed a maximum just below  $E_F$ , which is compared to the spectrum in Fig. 4.

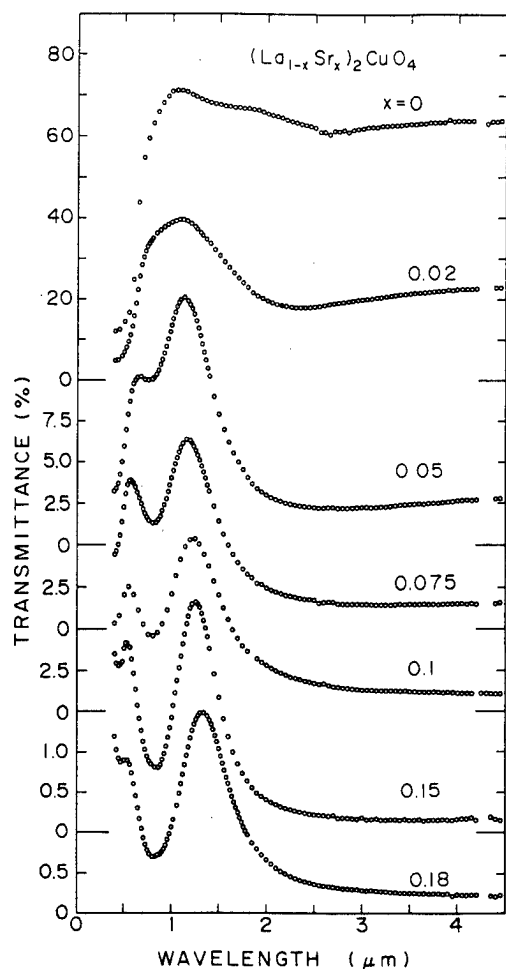


Fig. 3. Optical transmittance spectra for the  $(\text{La}_{1-x}\text{Sr}_x)_2\text{CuO}_4$  (001) epitaxial films with  $x$  from 0 to 0.18.

The systematic change in  $\alpha(\hbar\omega)$  in Fig. 4 provides useful information about the band structure. For  $x = 0$ , there is an upper Hubbard band and a band basically coming from O 2p states, and in between a gap of the charge transfer type about 2 eV wide. Doping with Sr moves  $E_F$  to the level in the DOS which emerges by doping, not in the original valence band. In a low  $x$  region, the DOS at  $E_F$  is low and basically composed of localized states. This is consistent with the experimental result that the electric conduction for  $x \leq 0.02$  is well expressed by the two-dimensional variable range hopping conduction. At a higher doping rate, the DOS forms a band about 1 eV wide and the  $E_F$  lies within it, giving rise to metallic conduction with hole carriers. With the further doping, it seems probable that  $E_F$  almost reaches the midband, as reflected by the  $x$  dependence of Hall coefficient.

In relation to superconductivity in this system, the development of DOS within the gap has definite correlation with the  $x$  dependence of  $T_c$ . If this absorption band may have close relevance to the occurrence of high  $T_c$  superconductivity, understanding the mechanism of the DOS development within

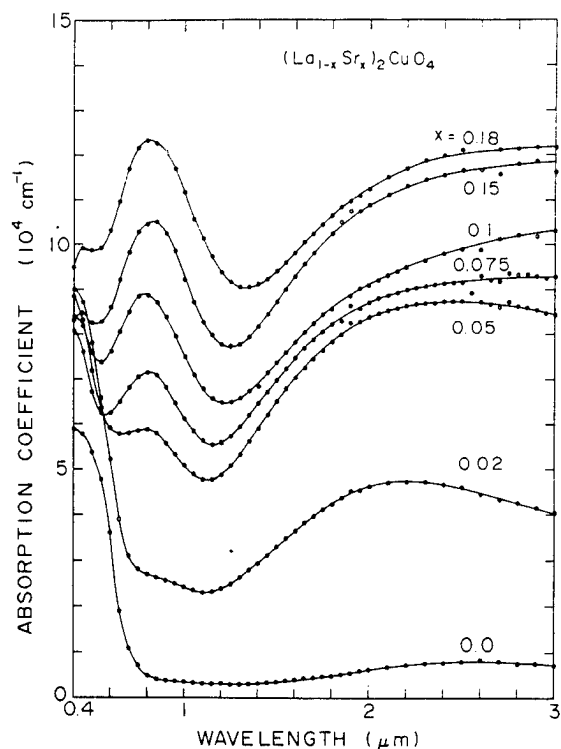


Fig. 4. Optical absorption coefficient  $\alpha(\hbar\omega)$  for the  $(\text{La}_{1-x}\text{Sr}_x)_2\text{CuO}_4$  (001) epitaxial thin films with  $x$  from 0 to 0.18.

the gap might be crucial.

The author would like to acknowledge useful discussions with Profs. S. Uchida and S. Tajima at the University of Tokyo, and valuable comments by Prof. H. Fukuyama at the University of Tokyo and Prof. M. Tachiki at Tohoku University. He is also obliged to his colleagues at NTT Laboratories for discussions and encouragement.

## REFERENCES

1. A. Fujimori, E. Takayama-Muromachi, Y. Uchida, and B. Okai, *Phys. Rev. B* **35**, 8814 (1987); A. Fujimori, E. Takayama-Muromachi, Y. Uchida, *Solid State Commun.* **63**, 857 (1987).
2. N. Nücker, J. Fink, J. C. Fuggle, P. J. Duhram, and W. M. Temmerman, *Phys. Rev. B* **37**, 5158 (1988).
3. M. Suzuki, *Phys. Rev. B* **39**, No. 4 (1989).
4. S. Tajima, T. Nakahashi, S. Uchida, and S. Tanaka, *Physica C* **156**, 90 (1988); S. Tajima, S. Uchida, S. Tanaka, S. Kanbe, K. Kitazawa, and K. Fueki, *Jpn. J. Appl. Phys.* **26**, L432 (1987).
5. J. Orenstein, G. A. Thomas, D. H. Rapkine, C. G. Bethea, B. F. Levine, R. J. Cava, E. A. Rietman, and D. W. Johnson, Jr., *Phys. Rev. B* **36**, 729 (1987).
6. S. L. Herr, K. Kamarás, C. D. Porter, M. G. Doss, D. B. Tanner, D. A. Bonn, J. E. Greedan, C. V. Stager, and T. Timusk, *Phys. Rev. B* **36**, 733 (1987).
7. S. Etamad, D. E. Aspnes, P. Barboix, G. W. Hull, M. K. Kelly, J. M. Tarascon, R. Thompson, S. L. Herr, K. Kamarás, C. D. Porter, and D. B. Tanner, *Proc. Materials Research Society*, Boston, 1987.

Transmission Spectra of Crystal Film Bi-Sr-Ca-Cu-O  
in the range 3 to 500  $\text{cm}^{-1}$

Keigo NAGASAKA, Masayuki SATO, Takasi SHIBAYAMA  
and  
Kohtaro ISHIDA

Department of Physics, Science University of Tokyo  
Kagurazaka, Shinjuku-ku, Tokyo, 162  
Department of Physics, Faculty of Science and Technology,  
Science University of Tokyo, Noda, Chiba 278

We present the transmittance in the low frequency range from 3 to 500  $\text{cm}^{-1}$  for about 5 $\mu\text{m}$  films which are cleaved from the high- $T_c$  superconductor crystal Bi-Sr-Ca-Cu-O ( $T_c=80\text{K}$ ). However, it is not certain whether the crystal films used for this experiments are superconductor or normal metal. The transmittance decreases with the frequency in the range 3 to 300  $\text{cm}^{-1}$ . The ratios of the transmittance in the superconducting state to the transmittance in the normal state (90K) for temperatures of 8 and 50K have been obtained. From these experimental results, we obtained that the absorption coefficient versus the frequency  $\omega$ ;  $\alpha=650\cdot\omega^s$  ( $s=1/3$ ) and the phonon absorptions at 60, 130, 175, 240 and 290  $\text{cm}^{-1}$ . The conduction mechanism is the variable range hopping conduction in the crystal film Bi-Sr-Ca-Cu-O.

There has been considerable attention paid to the determination of superconducting energy gap by using far infrared spectroscopy. Thomas et al.[1] present the reflectance,  $R=1$ , at low frequency and the relation between the superconducting energy gap at  $T=0\text{K}$ , and the critical temperature,  $2\Delta_0/kT_c=3-4$ , using microtwinning crystals  $\text{Ba}_2\text{YCu}_3\text{O}_7$  with  $T_c=50$  and 68 K. Recently, Timusk and Tanner collaboration group[2] measured the reflectance of crystals of  $\text{Bi}_2\text{Sr}_2\text{CaCu}_2\text{O}_8$  in the superconducting state and a sharp reflectance edge at 300  $\text{cm}^{-1}$  associated with a threshold in the real part of the optical conductivity.

To investigate the superconductivity, low frequency transmission spectroscopy is a more direct method of assessing conductivity than the wide range reflectance measurements and the Kramers and Krönig transformation of their spectra, because by transmission spectroscopy we can observe a direct interaction with the elementary excitation which plays an important role in the superconducting state. In this paper, we report the far infrared transmission measurement of crystal Bi-Sr-Ca-Cu-O in the range 3 to 500  $\text{cm}^{-1}$ .

Measurements have been made on layered (code number 1) and single (code number 2) crystal films[3]. Sample preparation and crystal structure are reported elsewhere. We prepared the thin film (code number 1) cleaving a layered crystal and the other film (code number 2) cleaving a single crystal. Their thickness is about 5 $\mu\text{m}$  and the size is about 2x2  $\text{mm}^2$ . It is not certain whether these crystal films, used for the FIR spectroscopy, are superconductor or normal metal. However, the slabs (1x2x10  $\text{mm}^3$ ) which are prepared from the same crystals always present superconductivity.



We measured the far infrared transmission spectra with the incident electric field in the metallic a-b plane of our crystal film in the range 3 to 40  $\text{cm}^{-1}$  using a lamellar grating Fourier spectrometer and in the range 15 to 500  $\text{cm}^{-1}$  using a Michelson Fourier spectrometer. In this case, there is no need to take care of the interference in the specimen films, because the thickness of 5 $\mu\text{m}$  is smaller than the wavelength in the range 30 to 3000  $\mu\text{m}$ . We find two characteristic properties in the far infrared transmission spectra of the high- $T_c$  superconducting crystal: the non-Drude transmittance with  $\omega$ , and the temperature dependence of the ratio of superconducting to normal transmittance,  $T_s/T_n$ .

Figure 1 shows the transmittance spectra for the crystal film (code number 1) below and above the critical temperature,  $T_c \sim 80\text{K}$ . However, there is no drastic change between the transmittance at 50K and that at 90K. In this case, in the range from 30 to 150  $\text{cm}^{-1}$  the transmittance decreases with the temperature. However, we cannot observe any clear change in the range 150 to 500  $\text{cm}^{-1}$ . In addition, we observe transmission spectra in the range 3 to 100  $\text{cm}^{-1}$  at 8K using the other crystal film (code number 2), as shown in the inset to Fig. 1.

The critical temperature of this superconductor is 80K. On the basis of the BCS theory the superconducting energy gap  $T=0$ ,  $2\Delta_0$ , is equal to  $3.5kT_c \sim 195\text{cm}^{-1}$ . To interpret several features of the transmission spectra shown in Fig. 1, we consider the variation of the transmittance with  $\omega$  in the range 5 to 300  $\text{cm}^{-1}$  at 8K, shown in the inset to Fig. 1. In this region, it is noted that the transmittance varies as  $1/\omega^5$  ( $s=1/3$ ) approximately. Moreover, to determine the bulk behavior of this material more clearly, we consider the ratios of superconducting transmittance at 8 and 50K to a normal transmittance at 90K above  $T_c$ . These ratios are shown in Fig. 2. In this range 30 to 150  $\text{cm}^{-1}$ ,  $T(8\text{K})/T(90\text{K})$  and  $T(50\text{K})/T(90\text{K})$  also vary as  $1/\omega^5$ , respectively. As was discussed by Mattis and Bardeen[4], the transmittance ratio  $T_s/T_n$  of an ordinary superconductor, in the anomalous limit as an increasing function of  $\omega$  in the gap region from 0 to the absorption edge  $\omega_g = 2\Delta/\hbar$ , shows a peak at  $\omega = \omega_g$ , and decreases with  $\omega$  above  $\omega_g$ [5]. The transmittance ratio which we measured behaves quite differently from Mattis and Bardeen's prediction; it is a monotonously decreasing function in the whole region of  $\omega$ , as is clearly shown in Fig. 2. The feature of our transmittance ratio suggests that the absorptive part of complex conductivity  $\sigma = \sigma_1 - i\sigma_2$  is finite even in the low frequency region  $\omega \rightarrow 0$  and is an increasing function of  $\omega$  in the whole frequency region of the measurement. Such behavior of the absorption is generally expected of gapless superconductors. Thus one possible interpretation of the transmittance features of our experiments is the assumption that our crystal Bi-Sr-Ca-Cu-O is gapless. Another possibility is that the superconductor measured has an anisotropic energy gap, and the average absorption observed in the present experiment is due to excitation propagating in various directions in the crystal films.

Next, let us discuss with the conduction mechanism in the states from 0 to  $2\Delta/\hbar$  where  $2\Delta$  is so called the superconducting energy gap at TK. The reflectance is about 90% and almost flat below 300  $\text{cm}^{-1}$ . For simplicity, neglecting the reflectance, we calculated an absorption coefficient  $-1/d \ln(I/I_0)$  where  $I_0$  is the intensity of the incident radiation,  $I$  is that passing through the crystal film and  $d$  is the thickness. This absorption coefficient versus  $\omega$  is shown in Fig. 3. From the absorption spectra in the range below 100  $\text{cm}^{-1}$ , we have the absorption coefficient;

$$\alpha = 650 \cdot \omega^5 \quad (s=1/3).$$

Subtracting the this absorption coefficient from the total absorption coefficient, we

obtain several absorption peaks with the absorption coefficient as large as  $500 \sim 1000 \text{ cm}^{-1}$ . Their frequencies are listed in Table 1, which exhibit fairly good correspondence to those of the Raman scattering spectrum[6]. Figure 4 shows  $\log \alpha$  versus  $\log \omega$ . From this relation, this spectrum represents the photon-induced hopping conduction, by which we can relate the terms of the variable range hopping from a localized state to the other states in the random potential.

In summary, we observed the following phenomena in the high- $T_c$  superconducting crystal. (1) The transmittance varies as  $1/\omega^s$  ( $s=1/3$ ) in the range 3 to  $300 \text{ cm}^{-1}$ . It is noted that the transmission is realized in the presence of simultaneous reflection and absorption in this case. (2) Ratios of superconducting to normal transmittance vary as  $1/\omega^s$  in the range from 30 to  $150 \text{ cm}^{-1}$  at temperatures of 8 and 50K. The energy gap in the quasi-particle density of states was not observed in the far infrared transmission measurement. (3) Phonon absorption was observed in the low frequency region. (4) The absorption spectra present the variable range hopping conduction. It is quite different from a Drude free-electron conduction.

It is concluded that the conduction mechanism in the crystal film Bi-Sr-Ca-Cu-O is the variable range hopping in the range 3 to  $300 \text{ cm}^{-1}$  at 8K. However, it is not certain yet whether the films used are superconductor or normal metal.

#### References

- [1] G.A.Thomas, J.Orenstein, D.H.Rapikine, M.Capizzi, A.j.Millis, R.N.Bhatt, L.F.Schneemeyer and J.V.Waszcak: Phys.Rev.Lett. **61**(1988)1313.
- [2] M.Reedyk, D.A.Bonn, J.D.Garret, J.E.Greedan, C.V.Stager, T.Timusk, K.Kamarás and D.B.Tanner: Phys.Rev. **B38**(1988)11981
- [3] M.Sato, K.Nagasaka, T.Shibayama and K.Ishida: Jpn.J.Appl.Phys. **27**(1988)L2333
- [4] D.C.Mattis and J.Bardeen: Phys.Rev. **111**(1958)412.
- [5] M.Tinkham :in Optical Properties and Electronic Structure of Metals and Alloys, ed. F.Abeles (North-Holland Publishing Company, Amsterdam, 1966).
- [6] A.Yamanaka, T.Kimura, F.Minami, K.Inoue and S.Takekawa: Jpn.J.Appl.Phys. **27**(1988)L1902

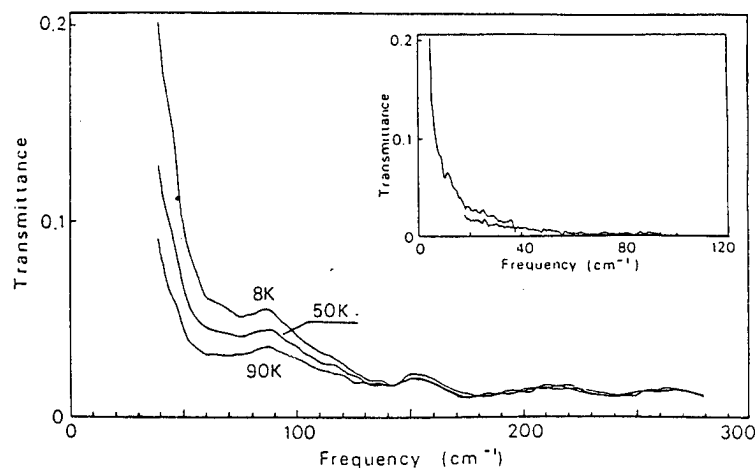


Fig.1 Measured transmittances of layered crystal film (code number 1) Bi-Sr-Ca-Cu-O at 8, 50 and 90 K. Insert: measured transmittance of single crystal film (code number 2) Bi-Sr-Ca-Cu-O at 8 K.

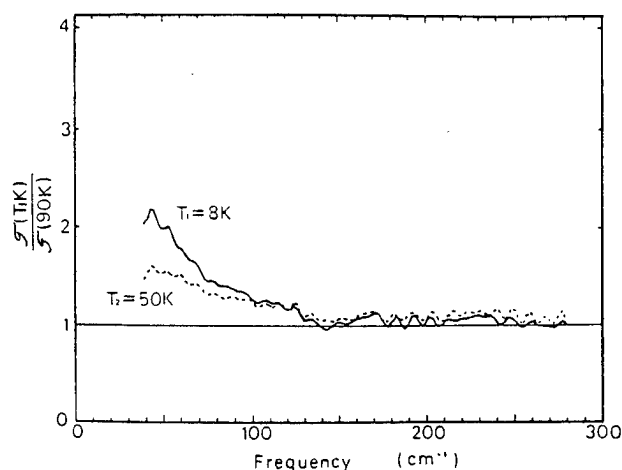


Fig.2 The measured ratios of superconducting to normal transmittance for the temperature of 8 and 50 K. The temperature of the normal state is 90 K.

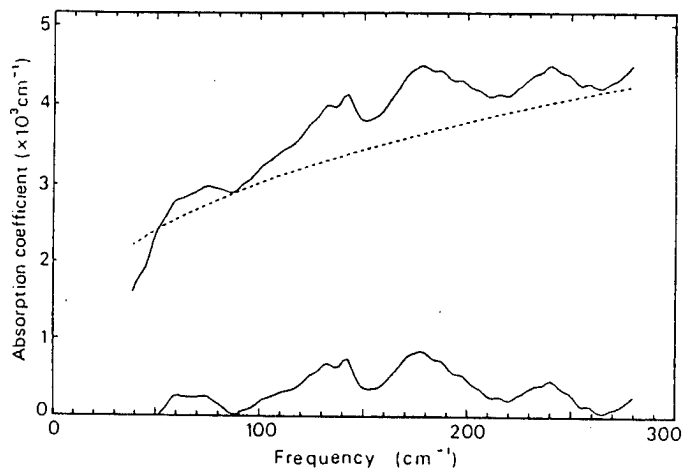


Fig.3 The measured absorption coefficient,  $-(1/d)\log(I/I_0)$  versus the frequency  $\omega$  and  $\alpha=650\cdot\omega^s$  ( $s=1/3$ ). Lower curve exhibits phonon absorption spectrum.

Table 1 Phonon frequencies observed by far infrared and Raman[6] spectroscopy.

	Frequency (cm <sup>-1</sup> )							
FIR	60	130	175	240	(290)			
Raman	-	120	175	225	295	345	470	627

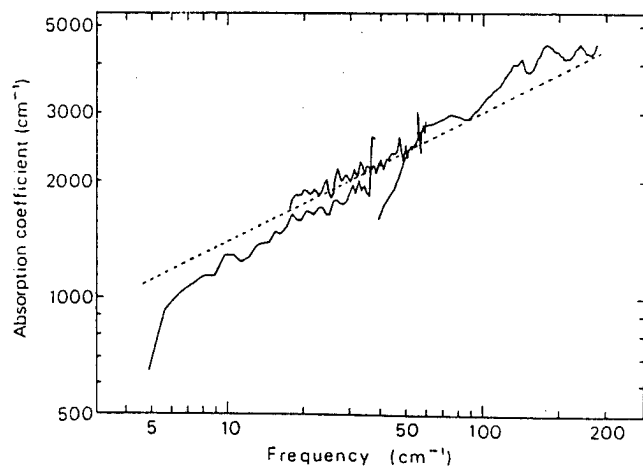


Fig.4 The absorption coefficient,  $-(1/d)\log(I/I_0)$  versus the frequency  $\omega$ . The dotted line shows  $\alpha=650\cdot\omega^s$  ( $s=1/3$ ). The line indicates the photon-induced hopping conduction.

# Universality of Infrared Anomaly in $(\text{La}_{1-x}\text{M}_x)_2(\text{Cu}_{1-y}\text{N}_y)\text{O}_4$ : $\text{M}=\text{Ca}, \text{Sr}, \text{Ba}$ ; $\text{N}=\text{Ni}, \text{Zn}$

K. Ohbayashi, H. Tsukamoto, H. Yamashita, A. Fukumoto,  
Y. Utunomiya, N. Ogita, K. Kojima and M. Udagawa

Faculty of Integrated Arts and Sciences,  
Hiroshima University, Hiroshima 730, Japan

In  $\text{La}_2\text{CuO}_4$  based high- $T_c$  superconductors, an Eu mode infrared absorption peak at about  $680\text{ cm}^{-1}$  shows an anomalous behavior that it cannot be observed for samples which exhibit superconductivity. We have found this infrared anomaly is a universal effect observed not only for  $(\text{La}_{1-x}\text{M}_x)_2\text{CuO}_4$  ( $\text{M} = \text{Ca}, \text{Sr}$  and  $\text{Ba}$ ), but also for  $(\text{La}_{1-x}\text{Sr}_x)_2(\text{Cu}_{1-y}\text{N}_y)\text{O}_4$  ( $\text{N} = \text{Ni}$  and  $\text{Zn}$ ). The anomalous mode has been assigned to be the stretching motion of Cu-O bond parallel to the direction of this bond in the ab plane.

In this report, among many interesting features that can be investigated using optical method, we note the anomaly in the infrared absorption spectrum of  $(\text{La}_{1-x}\text{M}_x)_2\text{CuO}_4$  found by our group<sup>1-4)</sup> and also others<sup>5-10)</sup>. In this system, the peak height of the infrared absorption at about  $680\text{ cm}^{-1}$  decrease with an increase of  $x$  and disappears in the concentration region of  $x \geq 0.03$ , where the system shows superconductivity. This is the infrared anomaly we note, which is closely correlated with superconductivity of this system.

The polycrystalline samples were prepared by standard ceramic techniques. As starting materials,  $\text{NiO}$ ,  $\text{CuO}$ ,  $\text{ZnO}$ ,  $\text{CaCO}_3$ ,  $\text{SrCO}_3$ ,  $\text{BaCO}_3$ , and  $\text{La}_2\text{O}_3$  were used. The purity of all these starting materials was 99.99%. Powders of starting materials were combined in appropriate proportions to prepare mixtures with desired compositions. These mixtures were pressed at about  $100\text{ kg/cm}^2$  to form cylindrical pellets of  $\approx 1.5\text{ cm}$  in diameter and  $\approx 0.5\text{ cm}$  thick. The pellets were fired in air twice with an intermediate grinding and pressing. The samples were prefired at  $860^\circ\text{C}$  for 14 hours. The second firing was done for 14 hours in the appropriate temperature between  $1100$  and  $1190^\circ\text{C}$ . We used only single phase samples confirmed by powder X-ray diffraction analysis. All infrared absorption spectra were measured at room temperature either with a JASCO model IR-810 spectrometer or a Hitachi model 270-50 infrared spectrophotometer.

Fig. 1 (a) shows how the infrared spectrum of  $(\text{La}_{1-x}\text{Sr}_x)_2\text{CuO}_4$  changes with a concentration change. Three peaks are observed in the energy region of  $250 - 800\text{ cm}^{-1}$ , which we label from the higher energy side as  $P_1$ ,  $P_2$  and  $P_3$ , respectively. Of the three peaks, the  $P_1$  peak at about  $680\text{ cm}^{-1}$  disappears as  $x$  increases and the sample becomes superconductive. The other two peaks, the  $P_2$  peak at about  $510\text{ cm}^{-1}$  and  $P_3$  peak at about  $370\text{ cm}^{-1}$ , do not show such behavior. The absorption peak  $P_1$  is allowed by the group theoretical selection rule. Thus the selective disappearance of the  $P_1$  peak is an anomalous effect. Of the four samples shown in this figure, the samples with  $x = 0.04$  and  $x = 0.06$  showed a superconductive transition. No superconductive

transition was observed for the other two samples. Thus the infrared anomaly is characteristic for superconducting samples. In fact, we observed that the  $P_1$  peak does not disappear in  $(La_{1-x}Sr_x)_2NiO_4$  ( $0 \leq x \leq 0.15$ ), which has the same  $K_2NiF_4$  type crystal structure but does not show superconductivity<sup>11</sup>).

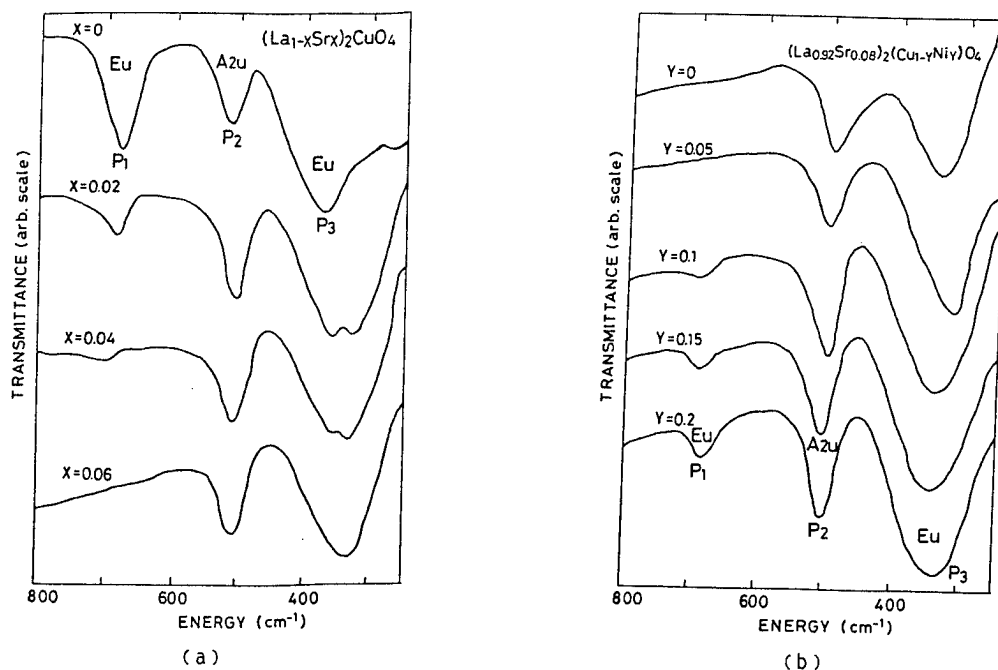
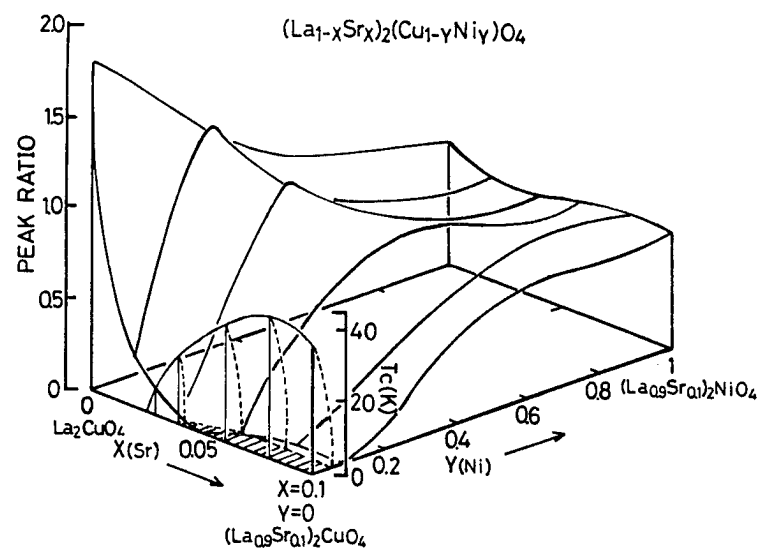


Fig. 1 Infrared absorption spectra of (a)  $(La_{1-x}Sr_x)_2CuO_4$  and (b)  $(La_{0.92}Sr_{0.08})_2(Cu_{1-y}Ni_y)O_4$ . The vertical scale shows transmittance. Curves are suitably shifted to avoid overlap.

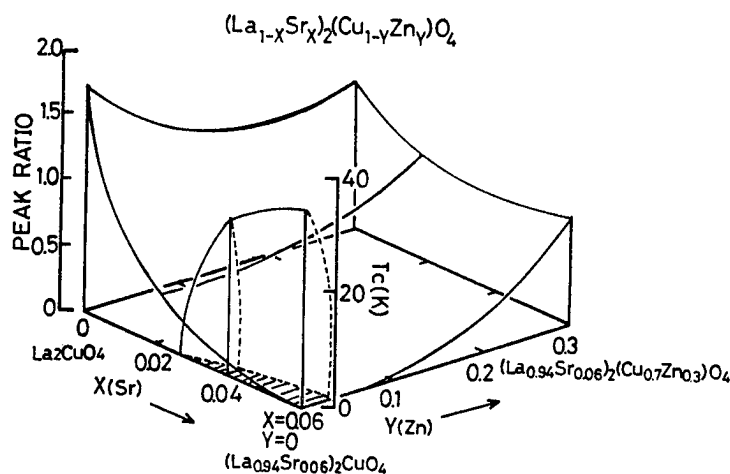
We checked whether the correlation between the infrared anomaly and the appearance of superconductivity is universal for substitution of La ions in  $La_2CuO_4$  with three different cations; Ca, Sr and Ba. And we obtained the result that the correlation is universal. To express the infrared anomaly quantitatively, we use the intensity ratio  $I(P_1)/I(P_2)$ . Superconductivity was observed only for samples which show negligibly small intensity ratio. The superconducting property of  $(La_{1-x}M_x)_2CuO_4$  can be controlled also by substitution of Cu with other cations. We checked whether the correlation of the infrared anomaly and the superconductivity is also universal for this case. We chose  $(La_{1-x}Sr_x)_2CuO_4$  system and substituted Cu with Ni and Zn ions. In Fig. 1 (b), the result for  $(La_{0.92}Sr_{0.08})_2(Cu_{1-y}Ni_y)O_4$  is shown. In the figure, superconductivity was observed for the samples with  $y=0$  and  $y=0.05$ . The other three samples were normal down to 7 K. In this case also, the peak  $P_1$  is observed only for normal samples. A more clear representation of the correlation is given if we plot the superconducting transition temperature  $T_c$  and the intensity ratio  $I(P_1)/I(P_2)$  as functions of concentration  $x$  and  $y$ . The plots are shown in Fig. 2 (a) and (b) for  $(La_{1-x}Sr_x)_2(Cu_{1-y}Ni_y)O_4$  system and  $(La_{1-x}Sr_x)_2(Cu_{1-y}Zn_y)O_4$ , respectively. Superconductivity is observed to appear where the intensity ratio  $I(P_1)/I(P_2)$  is very small and the  $P_1$  peak intensity is nearly zero, clearly demonstrating universality of the infrared anomaly.

In order to clarify why the infrared anomaly is correlated with the

superconductivity, the anomalous mode must be assigned. By the analysis of the Raman spectrum and the infrared spectrum of  $\text{La}_2\text{NiO}_4$ , we assigned all the observed optical active phonons<sup>11)</sup>. The result shows that the three modes shown in Fig. 1 are assigned as follows. The anomalous  $P_1$  peak is the the Eu mode corresponding to the stretching motion of Cu-O bond along the a or b axis, the peak  $P_2$  is the Au mode corresponding to the stretching motion of Cu-O bond in the direction of the c axis, and the peak  $P_3$  is the Eu mode corresponding to the bending motion of Cu-O bond in the ab plane.



(a)



(b)

Fig. 2 The peak height ratio  $I(P_1)/I(P_2)$  and the superconducting transition temperature  $T_c$  are plotted as functions of  $x$  and  $y$  for (a)  $(\text{La}_{1-x}\text{Sr}_x)_2(\text{Cu}_{1-y}\text{Ni}_y)\text{O}_4$  and for (b)  $(\text{La}_{1-x}\text{Sr}_x)_2(\text{Cu}_{1-y}\text{Zn}_y)\text{O}_4$ . Superconductivity is only observed in the concentration region where the intensity ratio is very small, thus demonstrating correlation between the infrared anomaly and superconductivity.

Several possibilities have been proposed to explain the infrared anomaly. And generally accepted idea is the anisotropic shielding of the electromagnetic light wave. Bassat et al. found that optical response of a single crystal of  $\text{La}_2\text{NiO}_4$  is very anisotropic<sup>12)</sup>. A plasma edge was observed when the reflectivity was measured with the polarization of the electric field of incident light wave perpendicular to the c axis. But the edge was not observed with the polarization parallel to the c axis. Thus the extinction of light wave is large in the former case compared with the latter case. Then the infrared active lattice vibration in the direction perpendicular to the c axis is harder to observe compared with the vibration in the direction parallel to the c axis because of the electric shielding by plasma oscillations. However this explanation cannot be applied to the experimental result shown in Fig. 1. In the figure, the two Eu modes are associated with lattice vibrations perpendicular to the c axis. Although the peak  $P_1$  disappears, the peak  $P_3$  does not show any tendency to become weak. Even if the concentration  $x$  increases and sample becomes metallic, the peak height of  $P_3$  does not become smaller compared with that of  $P_2$ , which is an Au mode and associated with a lattice vibration parallel to the c axis. From this result, we must conclude that the infrared anomaly occurs, selecting some particular mode from the Eu modes. At present, our interpretation is that there will be some favorable direction in the ab plane for carriers to move. A stretching lattice vibration in the direction of this carrier path will be easily shielded with carrier motion. However, the motion perpendicular to this direction will not be shielded, even if it is a motion in the ab plane.

### References

- 1) N. Ogita, K. Ohbayashi, M. Udagawa, Y. Aoki, T. Fujita: Jpn. J. Appl. Phys. **26** (1987) L415.
- 2) K. Ohbayashi, N. Ogita, M. Udagawa, Y. Aoki, Y. Maeno and T. Fujita: Jpn. J. Appl. Phys. **26** (1987) L420.
- 3) K. Ohbayashi, N. Ogita, M. Udagawa, Y. Aoki, Y. Maeno and T. Fujita: Jpn. J. Appl. Phys. **26** (1987) L423.
- 4) N. Ogita, M. Udagawa and K. Ohbayashi: Jpn. J. Appl. Phys. **26** (1987) Suppl.26-3 1005.
- 5) M. Stavola, R. J. Cava and E. A. Rietman: Phys. Rev. Lett. **58** (1987) 1571.
- 6) K. Oh-ishi, M. Kikuchi, Y. Syono, K. Hiraga and Y. Morioka: Jpn. J. Appl. Phys. **26** (1987) L484.
- 7) S. Sugai: Jpn. J. Appl. Phys. **26** (1987) L1517.
- 8) H. Sawada, Y. Saito, T. Iwazumi, R. Yoshizaki, Y. Abe and E. Matsuura: Jpn. J. Appl. Phys. **26** (1987) L426.
- 9) Y. H. Kim, A. J. Heeger, L. Acedo, G. Stucky and F. Wuld: Phys. Rev. B **36** (1987) 7252.
- 10) Z. Schlesinger, R. T. Collins, M. W. Shafer and E. M. Engler: Phys. Rev. B **36** (1987) 5275.
- 11) N. Ogita, M. Udagawa, K. Kojima and K. Ohbayashi: J. Phys. Soc. Jpn. **57** (1988) 3932.
- 12) J. M. Bassat, P. Odier and F. Gervais: Phys. Rev. B **35** (1987) 7126.

S. Sugai

Department of Physics, Faculty of Science, Osaka University,  
1-1 Machikaneyama-cho, Toyonaka 560, Japan

Magnetic and electronic excitations as well as phonons in high  $T_c$  superconductors ( $\text{La}_{1-x}\text{Sr}_x\text{CuO}_4$ ,  $\text{YBa}_2\text{Cu}_3\text{O}_{7-y}$ , and  $\text{Bi}_2\text{Sr}_2\text{Ca}_{1-x}\text{Y}_x\text{Cu}_2\text{O}_{8+y}$ ) are investigated by Raman scattering and luminescence spectroscopy. Obtained results are the location of doped holes, the exchange integral between localized spins and its modification by hole doping, specific phonon modes with strong electron-phonon interactions, and the intermediate magnetic polaronic excitations.

Many high  $T_c$  superconducting oxides have been discovered in these two years. The common features are (1) all materials include Cu atoms, (2) the itinerant carriers are holes, and (3) the crystal structures are two-dimensional composed of either  $\text{CuO}_6$  octahedra or  $\text{CuO}_5$  pyramids. Parent materials of those superconductors are charge-transfer insulators in which Coulomb interactions  $U$  between d electrons are larger than energy differences between metal d orbitals and ligand p orbitals. The superconductivity is induced by hole doping. The doped holes enter O 2p orbitals and the  $\text{Cu}^{2+}$  3d electrons behave as nearly localized  $d^9$  configurations. The localized electrons have spins 1/2, which induce antiferromagnetism in the insulating phases. Many models of high  $T_c$  superconductivity are based on magnetic interactions between the localized d electrons and the itinerant p holes. Very recently Tokura et al.[1], however, discovered electron-doped superconductors;  $\text{Ln}_{2-x}\text{Ce}_x\text{CuO}_{4-y}$  ( $\text{Ln}=\text{Pr}, \text{Nd}, \text{and Sm}$ ). It is supposed that the doped electrons enter the upper Hubbard states and the zero-spin states of  $d^{10}$  configurations are released from the superconductivity mechanisms based on the spin fluctuation, although details are not known. Finite isotope effects observed in high  $T_c$  superconductors suggest the existence of some contribution from phonon-mediated mechanisms. The coupling of phonons with spin and charge fluctuation is supposed to increase the  $T_c$ 's. This paper reports the results of Raman scattering of some hole-superconductors about magnons, phonons, and electronic states.

Semiconducting phases of  $(\text{La}_{1-x}\text{Sr}_x)_2\text{CuO}_4$ ,  $\text{YBa}_2\text{Cu}_3\text{O}_{7-y}$ , and  $\text{Bi}_2\text{Sr}_2\text{Ca}_{1-x}\text{Y}_x\text{Cu}_2\text{O}_{8+y}$  undergo antiferromagnetic states at low temperatures. With the increase of the hole concentration the antiferromagnetic transition temperatures ( $T_N$ 's) decrease and the superconducting states appear. Figure 1 shows polarized Raman spectra of  $\text{La}_2\text{CuO}_4$  with the excitation of  $\lambda_1=5145 \text{ \AA}$  at 30 K. The  $3230 \text{ cm}^{-1}$  peak in the  $(x, x)$  spectra is assigned to the 2-magnon scattering.[2, 3] The symbol  $(x, y)$  denotes that the incident light is polarized along the x axis and the scattered light along y. The 2-magnon peak is not observed in the  $(y, x)$  and the  $(z, z)$  spectra as expected from the selection rule of the 2-magnon scattering from the antiferromagnetic spin order on the 2-dimensional quasi-square lattice. The 2-magnon peak intensity does not weaken rapidly even above  $T_N$  (240 K), which indicates that the observed scattering is attributed to the spin dynamics in the 2-dimensional antiferromagnetic domain as a fluctuating state consistently with the results of neutron scattering experiments.[4] With the increase of the Sr concentration the energies and the scattering intensities decrease in relation to the decrease of the correlation length.



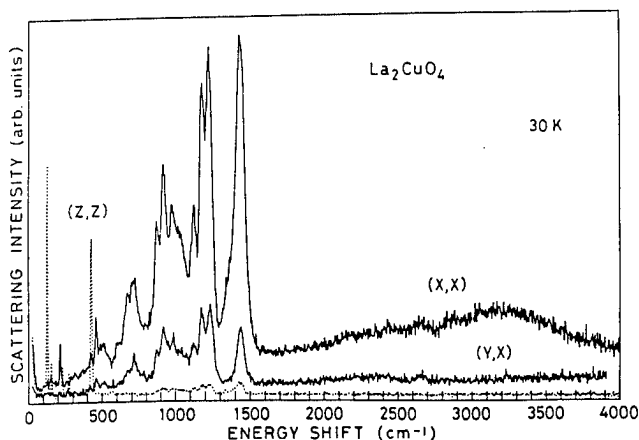


Fig.1 Polarized Raman spectra of  $\text{La}_2\text{CuO}_4$  at 30 K excited with  $\lambda_i=5145 \text{ \AA}$ .

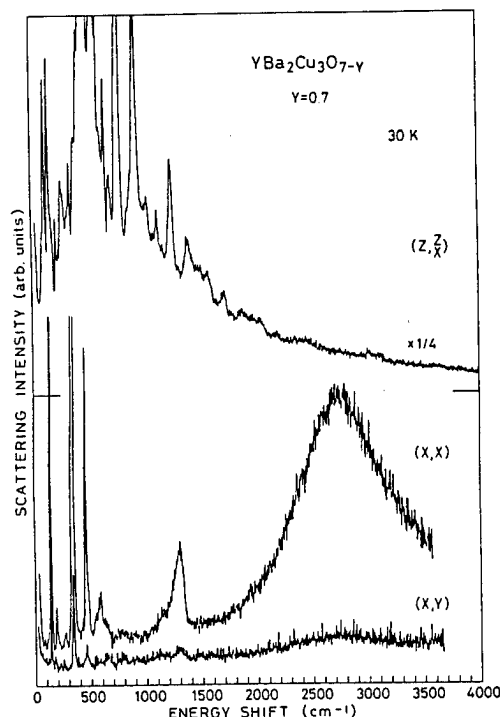


Fig.2 Polarized Raman spectra of  $\text{YBa}_2\text{Cu}_3\text{O}_{6.3}$  excited with  $\lambda_i=5145 \text{ \AA}$ .

Figure 2 shows the polarized Raman spectra of insulating  $\text{YBa}_2\text{Cu}_3\text{O}_{6.3}$  at 30 K measured with  $\lambda_i=5145 \text{ \AA}$ . [5] The 2-magnon peak is observed in the (x, x) polarization configuration at  $2740 \text{ cm}^{-1}$ . Similar 2-magnon scattering is observed at  $3080 \text{ cm}^{-1}$  in  $\text{Bi}_2\text{Sr}_2\text{Ca}_{0.5}\text{Y}_{0.5}\text{Cu}_2\text{O}_{8+y}$ . [5] The effective exchange integral  $J^* = v_{2\text{-magnon}}/2.7$  is  $1200 \text{ cm}^{-1}$  in  $\text{La}_2\text{CuO}_4$ , [2,3]  $1140$  in  $\text{Bi}_2\text{Sr}_2\text{Ca}_{1-x}\text{Y}_x\text{Cu}_2\text{O}_{8+y}$ , [5] and  $1010$  in  $\text{YBa}_2\text{Cu}_3\text{O}_{6.3}$ . [5, 6] The  $J^*$  decreases as the increase of the Cu-Cu distance. In the high hole concentration enough to induce the superconductivity no obvious 2-magnon peak is observed. However large scattering intensity ranging from low energy to over  $4000 \text{ cm}^{-1}$  is noticed. Usually no phonon peak above  $1000 \text{ cm}^{-1}$  nor single particle excitation of holes or electrons above  $100 \text{ cm}^{-1}$  is observed in oxides. Then the scattering intensity is assigned to the overdamped 2-magnons caused by the interaction with holes.

The (x, x) spectra of  $\text{La}_2\text{CuO}_4$  show abnormally large 2-phonon scattering as shown in Fig 1. This indicates that the scattering is in the resonant condition and the electron-phonon interactions of those modes are very large. The energies of the 2-phonon peaks are decomposed into sums of energies of two modes among four modes; two breathing vibrational modes ( $B_{2g}$ ) and two quadratic vibrational modes ( $B_{3g}$ ) of O atoms on the  $\text{CuO}_2$  layer. [7] The decrease of the scattering intensity with the increase of the hole concentration is the same as the 2-magnon scattering. This indicates that the magnon and the breathing phonon have some correlation and they are resonantly enhanced simultaneously via the same intermediate electronic states. The observed 2-phonon peak energies are  $1449 \text{ cm}^{-1}$  in  $\text{La}_2\text{CuO}_4$ ,  $1298 \text{ cm}^{-1}$  in  $\text{YBa}_2\text{Cu}_3\text{O}_{6.3}$ , and  $1354 \text{ cm}^{-1}$  in  $\text{Bi}_2\text{Sr}_2\text{Ca}_{0.5}\text{Y}_{0.5}\text{Cu}_2\text{O}_{8+y}$ .

The location of holes can be obtained from the anomaly of the polarized Raman spectra. In  $(\text{La}_{1-x}\text{Sr}_x)_2\text{CuO}_4$  the (z, z) spectra are simple. The 2-phonon scattering is weak and the number of peaks is the same as expected from the group theory. While in the (x, x) spectra the 2-phonon scattering is abnormally strong and unusual number of peaks appear in the 1-phonon scattering. The case of  $\text{YBa}_2\text{Cu}_3\text{O}_{7-y}$  is the contrary. The 1-phonon scattering in the (x, x) spectra is simple, while strong multi-phonon scattering is observed in the (z, z) spectra. These can be explained as follows. If holes enter the O  $2p \sigma_x, y$  orbitals on the  $\text{CuO}_2$  layers, the single particle excitation of holes is allowed in the (x, x) polarization configuration. While if holes enter the O  $2p \sigma_z$  orbitals at apexes, it is allowed in (z,

z). As a consequence of the hole-phonon interaction many phonon modes which are forbidden in themselves become active in the polarization configuration where the hole scattering is allowed. Therefore the following results are induced. Holes in  $(\text{La}_{1-x}\text{Sr}_x)_2\text{CuO}_4$  are located at O atoms on the  $\text{CuO}_2$  layers and those in  $\text{YBa}_2\text{Cu}_3\text{O}_{7-y}$  at apexes of the  $\text{CuO}_5$  pyramids. These results are consistent with experiments of polarized Cu L<sub>3</sub>-edge x-ray absorption. [8] In  $\text{Bi}_2\text{Sr}_2\text{CaCu}_2\text{O}_{8+y}$  the (x, x) spectra include much larger number of peaks than expected from group theory, and therefore the location of holes is tentatively assigned to the O atoms on the  $\text{CuO}_2$  layers, although the (z, z) spectra are not obtained yet.

In the (z, z) polarization configuration multi-phonon scattering of the  $468\text{ cm}^{-1}$  mode is dominant in  $\text{YBa}_2\text{Cu}_3\text{O}_{7-y}$  as shown in Fig. 2. This mode is the vibrational mode of O atoms at apexes of  $\text{CuO}_5$  pyramids. Figure 3 shows the hole concentration dependence of the (z, z+x) spectra. With the increase of the hole concentration new modes appear at  $444$  and  $501\text{ cm}^{-1}$  besides  $471\text{ cm}^{-1}$  ( $468\text{ cm}^{-1}$  at  $y=0.7$ ), and the original  $468\text{ cm}^{-1}$  mode disappears in the sample with sufficient O concentration. Among the new modes the  $444\text{ cm}^{-1}$  mode is assigned to the same mode as the  $454\text{ cm}^{-1}$  mode which is observed in the (x, x) spectra at  $y=0.7$ . The activity in the (z, z) polarization is attained by the relaxation of the selection rule by the hole doping. Multi-phonon scattering is observed in the  $471\text{ cm}^{-1}$  mode, but not in the  $501\text{ cm}^{-1}$  mode. The  $501\text{ cm}^{-1}$  mode is assigned to the same vibrational mode as the  $468\text{ cm}^{-1}$  mode, but the only difference is the location of a hole at the apex. The location of a hole decreases the interatomic distance between the O atom at the apex and the in-plane Cu atom and in consequence increases the interatomic force constant.

The lowest energy state of the pyramidal  $\text{CuO}_5$  cluster with a hole is a singlet  $^1\text{A}_1$  state or a triplet  $^3\text{B}_1$  state.[9] When a hole enters a  $x^2-y^2$  orbital consisting of O p  $\sigma_x$ , y orbitals, it couples with Cu d<sup>9</sup> spin antiferromagnetically and forms a singlet  $^1\text{A}_1$  state. When a hole enters a  $3z^2-r^2$  orbital consisting of O p  $\sigma_z$  and p  $\sigma_x$ , y orbitals, it couples ferromagnetically and forms a triplet  $^3\text{B}_1$  state. Cooper et al.[10] observed the symmetry dependent superconducting gap in  $\text{YBa}_2\text{Cu}_3\text{O}_{7-y}$  from Raman scattering. The  $\text{B}_{1g}$  symmetric gap is larger than the  $\text{A}_{1g}$  gap. It is supposed that the  $\text{A}_{1g}$  gap corresponds to the breaking process of the  $^3\text{B}_1$  pair into two  $^3\text{B}_1$  quasi-particles and the  $\text{B}_{1g}$  gap to the breaking of the  $^3\text{B}_1$  pair into the  $^3\text{B}_1$  and the  $^1\text{A}_1$  quasi-particles. The transition between the  $^3\text{B}_1$  and the  $^1\text{A}_1$  states couples with the  $340\text{ cm}^{-1}$   $\text{B}_{1g}$  phonon and causes the decrease of the phonon energy and the increase of the linewidth below  $T_c$ . [11]

The Raman scattering from  $(\text{La}_{1-x}\text{Sr}_x)_2\text{CuO}_4$ ,  $\text{YBa}_2\text{Cu}_3\text{O}_{7-y}$ , and  $\text{Bi}_2\text{Sr}_2\text{Ca}_{1-x}\text{Y}_x\text{Cu}_2\text{O}_{8+y}$  are under the resonant condition for the incident light in the visible region. It is obvious from the existence of the strong multi-phonon scattering and the strong dependence of the spectra on the incident wavelength. From the incident wavelength dependence, the intermediate electronic transition energy is estimated at  $18000\text{ cm}^{-1}$  ( $2.2\text{ eV}$ ) in  $\text{La}_2\text{CuO}_4$ .

At high hole concentration the 2-magnon and 2-phonon peaks disappear simultaneously and the spectra change into structureless in the energy region above  $1000\text{ cm}^{-1}$ . Such spectra, however, have strong dependence on the incident wavelength. Figure 4 shows the incident wavelength dependence of the spectra in  $\text{YBa}_2\text{Cu}_3\text{O}_{6.9}$ . The region of the energy shift below  $1300\text{ cm}^{-1}$  is Raman scattering, while the region of the higher energy shift is hot luminescence. The absolute energies of the luminescence peaks are  $18030$

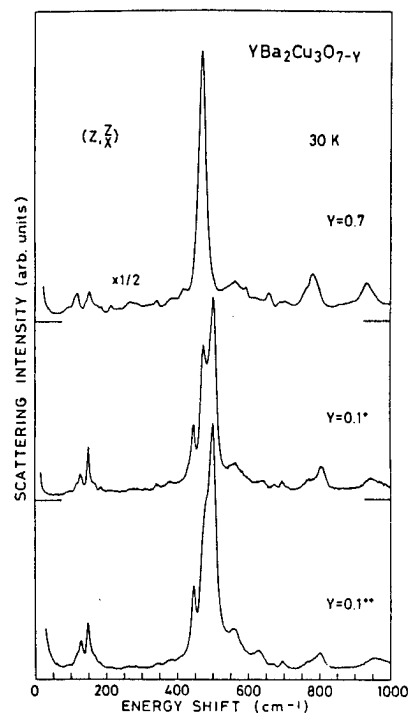


Fig.3 Hole concentration dependent Raman spectra of Semiconducting ( $y=0.7$ ) and superconducting ( $y=0.1$ ,  $T_c=92\text{ K}$ )  $\text{YBa}_2\text{Cu}_3\text{O}_{7-y}$ .

$\text{cm}^{-1}$  (2.24 eV), 18770 (2.33), and 19520 (2.42) with the excitation of  $\lambda_i=4579 \text{ \AA}$ . The similar spectra are also observed in  $(\text{La}_{0.942}\text{Sr}_{0.058})_2\text{CuO}_4$ . No structure is observed in the light reflection spectra in this energy region, which is in contrast with the case of  $\text{BaPb}_{1-x}\text{Bi}_x\text{O}_3$  in which the intermediate transition energy of the resonant scattering is directly observed in the light reflection spectra. This means that some energy relaxation occurs in the high  $T_c$  superconductors. The origin of the hot-luminescence is supposed to be magnetic polaron excitons.

Raman scattering experiments associated with resonant scattering and hot-luminescence present many important data for the explication of the high  $T_c$  superconductivity mechanism. The obtained results at present are antiferromagnetic exchange integral  $J$  from the 2-magnon scattering, assignment of the location of doped holes, the superconducting gap, the characteristic phonon modes which have strong electron-phonon interaction, and intermediate magnetic polaronic states. Raman scattering experiments suggest the correlation between the magnon and the breathing phonon mode. The symmetric properties that the different gap energy is observed between the  $A_{1g}$  and the  $B_{1g}$  symmetries in  $\text{YBa}_2\text{Cu}_3\text{O}_{7-y}$  [10] and that the phonon mode influenced most strongly by the gap generation is the  $B_{1g}$  mode suggest that the interaction between the lowest two levels  $^1A_1$  and  $^3B_1$  in the  $\text{CuO}_5$  cluster is important for the superconductivity. The transition between  $^1A_1$  and  $^3B_1$  states implies that the spin flip, the charge transfer between O sites at the  $\text{CuO}_2$  layer and the apex, and phonons contribute to the appearance of the superconductivity cooperatively.

#### Acknowledgments

The author thanks M. Sato, S. Shamoto, S. Uchida, H. Takagi, H. Takei for the supply of good single crystals. This work is supported by a Grant-in-Aid for Scientific Research on Priority Areas "Mechanism on Superconductivity" from the Ministry of Education, Science and Culture, Japan, the Iwatani Naoji Foundation's Research Grant, and the Murata Science Foundation.

#### References

1. Y.Tokura, H.Takagi, and S.Uchida: Nature (1989).
2. K.B.Lyons, P.A.Fleury, J.P.Remeika, A.S.Cooper, and T.J.Negran: Phys. Rev. **B37**, 2353 (1988)
3. S.Sugai, S.Shamoto, and M.Sato: Phys. Rev. **B38**, 6436 (1988)
4. G.Shirane, Y.Endoh, R.J.Birgeneau, M.A.Kastner, Y.Hidaka, M.Oda, M.Suzuki, and T.Murakami: Phys. Rev. Lett. **59**, 1613 (1987)
5. S.Sugai: Proceedings of the Second NEC Symposium on Fundamental Approach to New Material Phases "Mechanisms of High Temperature Superconductivity", Tokyo, 1988 (Springer-Verlag,1989).
6. K.B.Lyons, P.A.Fleury, L.F.Schneemeyer, and J.V.Waszcak: Phys. Rev. Lett. **60**, 732 (1988)
7. S.Sugai: Phys. Rev. **B39** (1989).
8. A.Bianconi, M.De Santis, A.Di Cicco, A.M.Flank, A.Fontaine, P.Lagarde, H.Katayama-Yoshida, A.Kotani, and A.Marcelli: Phys. Rev. **B38**, 7196 (1988)
9. A.Fujimori: Phys. Rev. **B39**, 793 (1989).
10. S.L.Cooper, F.Slakey, M.V.Klein, J.P.Rice, E.D.Bukowski, and D.M.Ginsberg: Phys. Rev. **B38**, 11934 (1988).
11. S.L.Cooper, M.V.Klein, B.G.Pazol, J.P.Rice, and D.M.Ginsberg: Phys. Rev. **B37**, 5920 (1988)

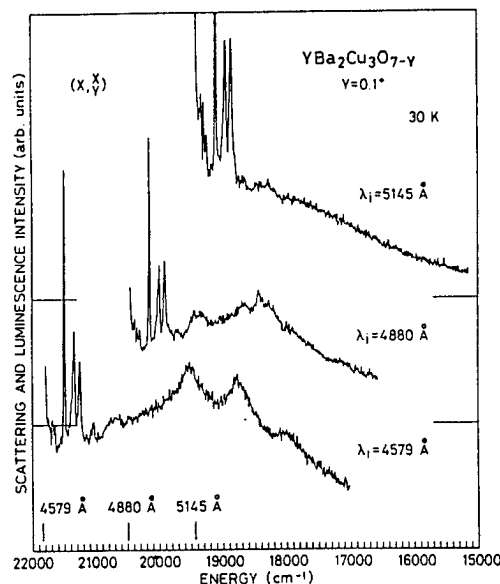


Fig.4 Incident wavelength dependence of Raman ( $\Delta\nu < 1300 \text{ cm}^{-1}$ ) and luminescence spectra in  $\text{YBa}_2\text{Cu}_3\text{O}_{6.9}$  ( $T_c=92 \text{ K}$ ).

# Cu NQR/NMR Studies of $\text{YBa}_2\text{Cu}_3\text{O}_y$ ( $6.0 \leq y \leq 6.98$ )

HIROSHI YASUOKA

Institute for Solid State Physics,  
University of Tokyo, Roppongi, Tokyo 106, JAPAN

## Abstract

The nuclear quadrupole resonance (NQR) and nuclear magnetic resonance (NMR) techniques have been utilized to characterize the local oxygen coordination of inequivalent Cu sites in  $\text{YBa}_2\text{Cu}_3\text{O}_y$  ( $6.0 \leq y \leq 6.98$ ). Essentially, four distinct NQR lines which correspond to 2, 3, 4 oxygen coordinated Cu(1) sites in the Cu-O chains and 5 oxygen coordinated Cu(2) sites in the Cu-O planes have been observed. The electric field gradient EFG which is mainly due to intra-atomic in origin depends mainly on the oxygen coordination, hence locally differentiated charged state of Cu atoms, in the Cu(1) sites. The charge differentiation is also found in the Cu(2) sites and the degree of it is found to be increased progressively with decreasing  $y$  from 6.98. An anomalous temperature dependence of Cu nuclear spin-lattice relaxation time in the Cu(2) plane sites for both  $y=9.91$  ( $T_c=91\text{K}$ ) and  $y=6.50$  ( $T_c=60\text{K}$ ) has been observed. The normal state behaviors are discussed in connection with temperature induced antiferromagnetic spin fluctuations or characteristic quasi-particle excitations.

## 1. Introduction

The existence of oxides of intermediate or mixed Cu valence with transition from metallic to either high- $T_c$  superconducting or antiferromagnetic insulating behavior adds an interesting new dimension to the problem of highly correlated electron system. Particularly, recent experimental developments in ternary and quaternary superconducting oxides, e.g.  $(\text{La}_{1-x}\text{Sr}_x)_2\text{CuO}_{4-\delta}$ ,  $\text{YBa}_2\text{Cu}_3\text{O}_{6+x}$  and  $\text{Tl}_2\text{Ba}_2\text{CaCu}_2\text{O}_{8+\delta}$ , have renewed considerable interest in the theoretical understanding of the mechanism of superconductivity. Although a number of theoretical models ranging from conventional phonon-mediated coupling to a variety of exotic mechanisms including the magnetic couplings have been explored, most of the theories are based on the unusual structural aspect of the Cu-O sublattices present in these compounds. The tetragonal  $\text{La}_{2-x}\text{Sr}_x\text{Cu}_2\text{O}_4$  structure contains square-planar  $\text{CuO}_2$  layers with weak coupling between them, while the orthorhombic  $\text{YBa}_2\text{Cu}_3\text{O}_y$  structure consists of nearly square-planar  $\text{CuO}_2$  layers (Cu(2) sites) with weakly bounded through Cu-O-Cu bonds along the c-axis to one dimensional  $\text{CuO}_3$  chains (Cu(1) sites).

The most dramatic change in the transport and magnetic properties occurs in  $\text{YBa}_2\text{Cu}_3\text{O}_y$  when the oxygen content is varied. Namely, high temperature superconducting transition of about 90 K at  $y \sim 7.0$  decreases with decreasing  $y$  toward almost non-superconducting property at  $y \sim 6.2$ . Further decreasing  $y$ , this system undergoes to an antiferromagnetic ordered state which are established by  $\mu$  SR, neutron diffraction and magnetic resonance experiments. This transition seems to be accompanied by the metal to non-metal transition in a transport sense and the orthorhombic to tetragonal transition in a crystallographic sense. It is interesting to note that the superconducting phase exists exclusively in the orthorhombic phase. With changing  $y$  from 6.0 to 7.0, it is believed that starting with empty oxygen sites in the Cu(1) basal plane at  $y=6.0$ , excess oxygen atoms randomly (in most case) fill sites between the Cu(1) atoms along the b-axes. This leads to a variation of the nominal Cu valence of the Cu(1) atoms ( $\text{Cu}^{1+}$  like valence state for  $y=6.0$  to  $\text{Cu}^{3+}$  like for  $y=7.0$ ), as well as an adjustment of the hole concentration of the Cu(2) planes. Presumably, the valence charge in the Cu atoms

is associated locally with the oxygen coordination of those atoms.

Generally, in compounds with only one valence state for the metal ions, the charge-transfer processes needed for metallic conductivity are costly in Coulomb energy. However, in compounds with several metal-ion valence states, transfer of charge between sites of different valence can be of lower energy. In spite of this process, a number of mixed-valence transition-metal oxides have been found to undergo transitions to an insulating or a superconducting state. In order to examine such processes and transitions, it is desirable to use a probe which might resolve the charge and spin distributions of the inequivalent sites from both the static and dynamical points of view. In this report, we restrict ourselves to describe our studies of the microscopic properties of  $\text{YBa}_2\text{Cu}_3\text{O}_y$ , as a typical example, by means of Cu nuclear quadrupole resonance (NQR) and Cu nuclear magnetic resonance (NMR) techniques. These techniques offer an attractive way to investigate the microscopic properties since the response of inequivalent sites can, in principle, be resolved in the nuclear-resonance spectra and the dynamical properties of those can be studied by the nuclear magnetic relaxation at respective sites. It is also true that the variations in local behavior which might be expected, such as valence change in the Cu atoms, band paramagnetism, antiferromagnetism and superconductivity, all have quite characteristic signatures in nuclear-resonance experiments.

## 2. Experimental Procedures

It is well known that a number of physical quantities of  $\text{YBa}_2\text{Cu}_3\text{O}_y$  strongly depends on the preparation procedure owing to the oxygen-nonstoichiometry and order-disorder transition. In this study,  $\text{YBa}_2\text{Cu}_3\text{O}_y$  ( $6.0 < y < 6.98$ ) with perfectly-ordered Cu(1)-O planes (oxygen atoms are fractionally and randomly occupied only along the b-axis) was prepared by cooling slowly in  $\text{O}_2$  and  $\text{N}_2$  gases. The details have been published already<sup>1)</sup>.

The nuclear resonance experiments have been performed by a spin-echo pulse sequence mode using conventional pulsed NMR spectrometers. For the frequency spectrum data taking, the super-heterodyne technique has been used for the signal detection and the amplitude of the time averaged spin-echo signal is recorded as a function of frequency at typically 0.1 MHz step. The  $T_1$  measurement has been made by observing the time evolution of the nuclear magnetization after the saturating rf comb pulsed using a coherent type pulsed gear.

## 3. Results and Discussions

### 3.1) Static Part --- Cu-NQR spectra.

The superconducting and magnetic phase diagram in  $\text{YBa}_2\text{Cu}_3\text{O}_y$  has been established by now from the neutron diffraction,  $\mu\text{SR}$  and NQR experiments. With decreasing  $y$  from 7.0, the  $T_c$  of 90 K decreases, having some plateau around 60 K, to zero at  $y \sim 6.2$  where the orthorhombic to tetragonal crystallographical transition takes place. Further decreasing  $y$ , the antiferromagnetic long range order is developed and the Neel temperature  $T_N$  reached its maximum value of about 500 K at  $y = 6.0$ . As is described in the previous section, when  $y$  is varied from 6.0 to 7.0 the excess oxygen in our sample believed to occupy fractionally and randomly at the sites in between the Cu(1) atoms along the b-axis. Then, we would expect three different oxygen coordinated Cu(1) sites which may have different valence states, hence NQR frequencies.

The full investigation for the Cu NQR and antiferromagnetic nuclear resonance (AFNR) spectra in inequivalent Cu sites has been completed and published already<sup>1)</sup>. To see clearly the dependence of each NQR frequency on the oxygen content, the peak frequency for the respective sites are plotted as a function of

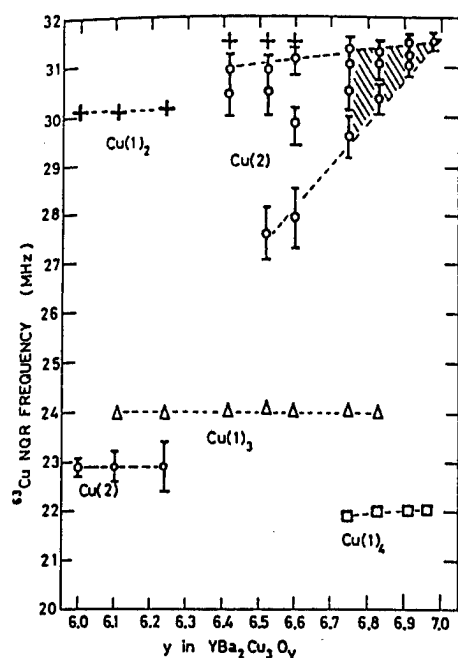


Fig. 1. Oxygen content dependence of  $^{63}\text{Cu}$  NQR frequency in  $\text{YBa}_2\text{Cu}_3\text{O}_y$  at 1.3 K. Subscripts in  $\text{Cu}(1)$  sites denote oxygen coordination number.

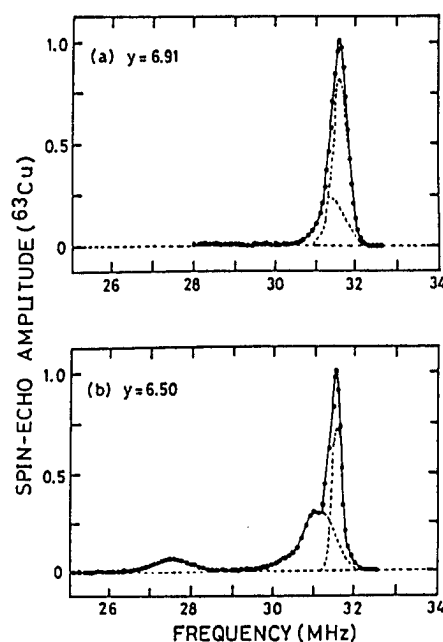


Fig. 2.  $^{63}\text{Cu}$  NQR spectra associated with the  $\text{Cu}(2)$  sites in  $\text{YBa}_2\text{Cu}_3\text{O}_{6.91}$  (a) and  $\text{YBa}_2\text{Cu}_3\text{O}_{6.50}$  (b) at 1.3 K. Note that the narrow line at 31.5 MHz in (b) is due to  $\text{Cu}(1)_2$  sites.

$y$  in  $\text{YBa}_2\text{Cu}_3\text{O}_y$  in Fig. 1. For the  $\text{Cu}(2)$  sites, we have used the decomposing procedure of the observed spectra to obtain the peak frequencies of different sites in  $\text{Cu}(2)$  planes. It is immediately apparent from Fig. 1 that the three distinct NQR frequencies for the  $\text{Cu}(1)$  sites are independent of  $y$ , except a discontinuous change was found for  $\text{Cu}(1)_2$  sites between tetragonal and orthorhombic phases.

The electric field gradient EFG is usually written as,

$$\begin{aligned} eq &= eq_{\text{ion}} + eq_{\text{el}}, \\ eq_{\text{ion}} &= eq_{\text{latt}}(1 - r_{\infty}), \end{aligned} \quad (1)$$

where  $eq_{\text{ion}}$  and  $eq_{\text{el}}$  are the ionic and electronic contributions, respectively. The ionic term may be evaluated as the contributions from charges on the surrounding lattice points,  $eq_{\text{latt}}$ , and distorted core interactions which may be accounted for in terms of the familiar Sternheimer antishielding factor  $r_{\infty}$ . A simple point charge calculation predicts about 10% change in the NQR frequencies when  $y$  is varied, that is not consistent with the experimental findings. Therefore the main source of the EFG is considered to be intra-atomic in origin and it depends only on the charged state of Cu atoms which are well differentiated by the oxygen coordination nearby. We believe that the lattice contribution to the EFG is relatively small and contributes only the line broadening. Contrary to this, the NQR frequencies for the  $\text{Cu}(2)$  sites tends to spread toward the lower frequency side. Two interesting features are noticeable: (1) The frequency for the most varying line seems to be joined eventually to that observed in AFNR at  $y=6.0$ , hence this line may come from the  $\text{Cu}(2)$  sites with two oxygen coordinated  $\text{Cu}(1)$  sites along the  $c$ -axis. (2) All the split lines seem to be collapsed to a unique line at  $y=7.0$

where we would expect the narrowest line width. From the latter fact, it is explained why the NQR for the Cu(2) sites has broader line width compared to that for the Cu(1) sites that is usually seen in many literatures for  $y \sim 6.9$ . Although the detailed assignment of the observed line is not given at present, it is nevertheless clear that the charge differentiation exists even in the Cu(2) layers and the degree of that is found to be increased with decreasing oxygen content, i.e. having more three or two oxygen coordinated Cu(1) sites. This general trend might be related to the decrease of  $T_c$  and play an important role for the understanding of the mechanism of high- $T_c$  superconductivity in this system.

### 3.2) Dynamical part --- Nuclear spin-lattice relaxation time $T_1$

It is well known that the study of nuclear spin-lattice relaxation time  $T_1$  is one of the most crucial clues to clarify the electronic structure of the high- $T_c$  oxide superconductors. Particularly, the temperature dependence of the relaxation rate  $1/T_1$  yields detailed information about the elementary excitations of the electronic spin system in both the normal and superconducting states. It is essential to understand, for example, the effect of spin-fluctuations in the normal state, and the superconducting energy gap  $\Delta$ , the density of quasi-particle excitations and coherence factor in the superconducting state. Apart from variety of such relaxation studies in deferent systems, we just focus on the discussion for the results of Cu(2) sites in  $y=6.91$  ( $T_c=92$  K) and  $y=6.50$  ( $T_c=60$  K). The  $^{63}\text{Cu}$  NQR spectra which are obtained by subtracting the  $^{65}\text{Cu}$  spectra using chi-square deconvolute procedure of the observed full spectra are shown in Fig. 2. Here we should note that the sharp line observed at 31.5 MHz for  $y=6.50$  is associated with the Cu(1)<sub>2</sub> sites which has almost three orders of magnitude slower relaxation rate compared with the other lines. The other lines including the structure observed in  $y=6.91$  are associated with the charge differentiated Cu(2) sites as described in the previous section. The temperature dependence of  $1/T_1$  for 31.5 MHz line in  $y=6.91$  and 27.7 MHz line in  $y=6.50$  has been measured and the result is shown in Fig. 3 in a linear scale.

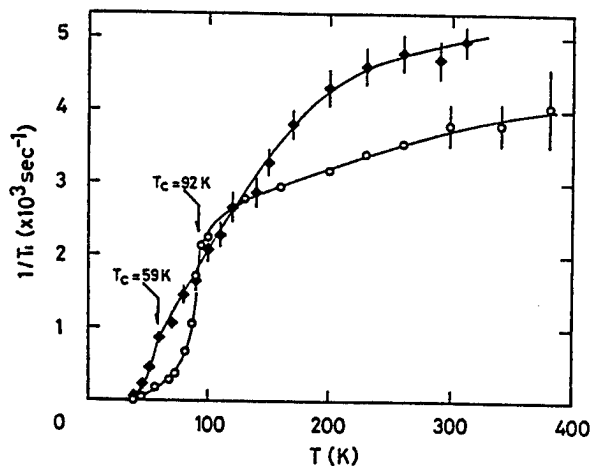


Fig. 3. Temperature dependence of  $1/T_1$  for Cu(2) sites in  $\text{YBa}_2\text{Cu}_3\text{O}_{6.91}$  (open circles : 31.5 MHz line) and  $\text{YBa}_2\text{Cu}_3\text{O}_{6.50}$  (closed diamonds : 27.7 MHz line).

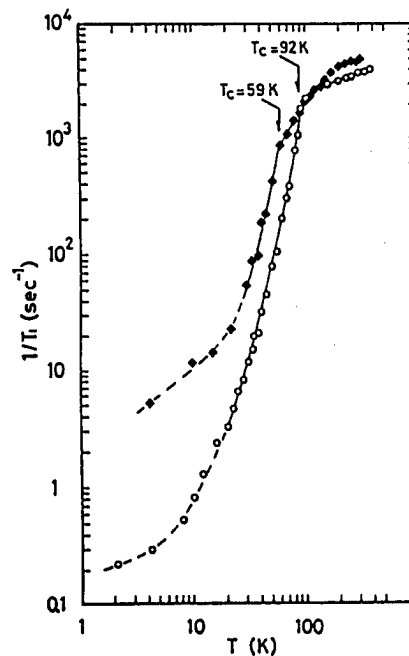


Fig. 4. Log-log plots of  $1/T_1(T)$  data shown in Fig. 3.

The most striking feature observed in the normal state is that the temperature dependence does not obey the Korringa relation ( $T_1 T = \text{constant}$ ), which is expected from the electron-hole pair excitations for the normal Fermi liquid states with a flat band structure. The origin of this anomalous temperature dependence is not clear at present. However, two speculative arguments may be made from different physical points of view. The first is the discontinuous occurrence of temperature induced antiferromagnetic spin fluctuations where the local antiferromagnetic spin fluctuations develop at a certain temperature (around 50 K for both cases) and tend to saturate at high temperatures. In this context, the high temperature behavior is described by a relation  $1/T_1 = a + bT$  and a term is considered to be due to the spin fluctuations. The second is based on the quasi-particle excitations with unusually high density of states at the Fermi surface. From the plot of  $1/T_1 T$  vs.  $T$  plots, one can see some peak in the density of states near 100 K and it drastically decreased just above  $T_c$ . This may be related to a gap formation in the quasi-particle excitation spectrum in the normal state.

In order to see the characteristic temperature dependence of  $1/T_1$  in the superconducting state, the data are replotted in a log-log scale and shown in Fig. 4. The values of  $1/T_{1s}$  (s stand for superconducting state) for both cases show a steep decrease just below  $T_c$  without any relaxation enhancement which is characteristic to BCS superconductors of s-wave pairing. For temperature below  $T_c$  an activation type excitations through the superconducting gap  $\Delta(T)$  is expected for  $1/T_1(T)$  in the s-wave superconductors. However, the experiments show a power-law like temperature dependence:  $1/T_{1s} \sim T^n$ ,  $n$  being dependent on the temperature range. Therefore, any convincing evidences for the s-wave pairing has not been observed from the  $T_1$  measurements. Although the experimental results suggest a possibility of an anisotropic pairing in these system, we have to wait to make the definite conclusion until the normal state properties have been explored.

#### 4 Concluding Remarks

Our measurements of oxygen concentration dependence of the NQR lines for inequivalent Cu sites in  $\text{YBa}_2\text{Cu}_3\text{O}_y$  show the following characteristic features.

- (1) The antiferromagnetic moments reside only on the Cu(2)-O plane sites and the direction of the moments is perpendicular to the c-axis.
- (2) The electric field gradient EFG which is mainly due to intra-atomic in origin depends only on the oxygen coordination, hence on locally differentiated charged state of the Cu atoms, in the Cu(1) chain sites.
- (3) The charge differentiation is also found in the Cu(2) plane sites and the degree of it is found to be increased progressively with decreasing  $y$  from 6.98, that might be related to the decrease of  $T_c$  with decreasing  $y$  in this system.

Anomalous temperature dependence of nuclear relaxation rate  $1/T_1$  has been observed in the Cu(2) plane sites of both 90 K superconductor  $y=6.91$  and 60 K superconductor  $y=6.50$ . In the normal state, highly enhanced  $1/T_1(T)$  is observed and we speculate that either discontinuous occurrence of temperature induced antiferromagnetic spin fluctuations or quasi-particle excitations with high density of states is the possible mechanism for this behavior. In the superconducting state, there exists no evidence for the BCS s-wave pairing in the  $1/T_1(T)$ . We could not rely on any kind of existing theory to explain those anomalous temperature dependence in both normal and superconducting states. It should be stressed that we have to have a proper microscopic theory which describes the highly correlated electronic state in the normal (metallic) phase before discussing the mechanism of the high- $T_c$  superconductivity.



### Acknowledgments

Present research has been proceeded by the collaboration with T. Shimizu, T. Imai, S. Sasaki (ISSP) and Y. Ueda and K. Kosuge (Kyoto University), and supported by Special Project Research on High Temperature Oxide Superconductors of Grant-in-Aid for Scientific Research from the Ministry of Education, Science and Culture.

### References

- 1) Y. Ueda and K. Kosuge: Physica C156 (1989) 281
- 2) H. Yasuoka, S. Sasaki, T. Imai, T. Shimizu, Y. Ueda and K. Kosuge: Phase Transitions (1989) to be published.
- 3) T. Imai, T. Shimizu, H. Yasuoka, Y. Ueda and K. Kosuge: J. Phys. Soc. Jpn. 57 (1988) 2280

## Study of High $T_c$ Oxide Superconductor by NMR and Other Measurements

### 1. NMR

Y. Kitaoka, K. Ishida, K. Fujiwara, T. Kondo, Y. Kohori\*, H. Shibai and K. Asayama

### 2. Susceptibility and Resistivity

Y. Oda, H. Toyoda, H. Fujita and N. Kawaji

Dept. of Material Physics, Faculty of Engineering Science, Osaka University, Toyonaka, Osaka 560

\*Present Address : Basic Research Laboratory, Himeji Institute of Technology, Shosha, Himeji 671-22

1. NQR signals of Cu in  $(La_{1-x}Sr_x)_2CuO_4$  and  $Bi_2Sr_2Ca_2Cu_3O_{10}$  have been observed. The behaviors of the nuclear relaxation in superconducting compounds are similar to that of Cu in  $CuO_2$  plane in  $YBa_2Cu_3O_7$ . Above  $T_c$ ,  $1/T_1$  does not follow Korringa relation, but changes more slowly. In superconducting state  $1/T_1$  decreases rapidly without BCS type enhancement. For  $x=0.15$  in La system  $1/T_1$  follows the relation of  $T_1T=const.$  The absolute value of  $1/T_1$  decreases with  $x$  although the number of holes increases. The behavior of  $T_1$  of Tl in  $Tl_2Ba_2Ca_2Cu_3O_{10}$  below  $T_c$  is also similar to Cu. NMR measurement of  $^{17}O$  has been made in field of about 3 T.  $1/T_1$  shows a slight enhancement of 1.2 ~ 1.3 just below  $T_c$ . High resolution NMR measurement suggests more than one line of  $^{17}O$  contributing to  $T_1$  observed.

2. Detailed characterizations of the substituted  $YBa_2(Cu_{1-x}M_x)_3O_{7-6}$  systems with  $M=Fe, Co, Ni, Zn$  and  $Al$  were made for ordinary air-annealed and high pressure oxygen annealed samples. The effect of the pair breaking by magnetic dopants was found to be very small in the  $T_c$ -suppression of these systems.

### 1. NMR

#### (1) NQR of Cu

##### (i) $YBa_2Cu_3O_7$

$T_1$  of Cu in  $CuO_2$  plane in  $YBa_2Cu_3O_7$  has been measured in several groups [1][2][3][4]. We assigned the two pairs of observed Cu NQR signals to respective Cu sites,  $CuO_2$  plane and  $CuO$  chain, by using  $T_1$  in  $REBa_2Cu_3O_7$  [5]. The change of  $1/T_1$  above  $T_c$  is not linear in  $T$  but slow. Antiferromagnetic spin fluctuations are considered to play an important role. In the superconducting state,  $1/T_1$  decreases rapidly without enhancement just below  $T_c$ . At low temperature the decrease of  $1/T_1$  becomes slow. In our sample the quadrupole relaxation begins to appear below about 20 K which is confirmed by comparing  $T_1$  of  $^{63}Cu$  and  $^{65}Cu$ .  $T_1$  due to magnetic interaction is separated from the observed value as shown by  $\circ$  mark in the figure.  $1/T_1$  due to magnetic interaction decreases nearly in proportion to  $T^3$ . [3]

The Knight shift of Cu decreases rapidly below  $T_c$  indicating the superconducting pairing nature to be of singlet. [3]

In order to see the behavior in normal state in much wider temperature range, we have measured  $T_1$  of Cu in  $\text{YBa}_2(\text{Cu}_{1-x}\text{Zn}_x)_3\text{O}_7$ . [6] As seen in Fig.1  $1/T_1$  for  $x=0.02$  above 100 K is almost the same as for  $x=0$ , while below 100 K down to 65 K  $1/T_1$  follows  $T_1 T = \text{const.}$  law. In the case of  $x=0.08$   $T_1$  has not single but multi components. However each component follows roughly the relation of  $T_1 T = \text{const.}$  from 100 down to about 10 K. Similar result is also observed in  $(\text{La}_{1-x}\text{Sr}_x)_2\text{CuO}_4$  system as will be discussed later. The existence of the multi components in  $T_1$  may be attributed to a distribution of spin fluctuations in the random system.  $T_1$  of Cu located close to Zn is considered to be larger than that far from Zn. These works have been carried out in collaboration with Y.Oda and T. Kohara.

For the oxygen content of 6 ~ 6.4, the magnetic moments on Cu at  $\text{CuO}_2$  plane align antiferromagnetically. Corresponding to this, the NMR signals due to Cu in  $\text{CuO}_2$  plane have been observed around 90 MHz. [7] The measurement of  $T_1$  of Cu in CuO chain site indicates a second magnetic ordering appearing below about 10 ~ 20 K for oxygen content 6.2 ~ 6.4 presumably associated with the freezing of hole motion at oxygen sites. [8] The work has been performed in collaboration with H. Takagi, H. Iwabuchi and S. Uchida in Tokyo University.

## (ii) $(\text{La}_{1-x}\text{Sr}_x)_2\text{CuO}_4$

In  $(\text{La}_{1-x}\text{Ba}_x)_2\text{CuO}_4$  system three dimensional antiferromagnetic ordering appears in the concentration range from  $x=0$  to  $x \approx 0.008$ . [9] We found a magnetically ordered state (spin glass type) still existing for  $0.008 \leq x \leq 0.025$  by observing internal field at La site [10]. With further increasing  $x$  superconductivity appears for  $0.025 \leq x \leq 0.15$ .

In order to see the change of the electronic state with  $x$  at Cu site, we have made an NQR measurement of Cu in  $(\text{La}_{1-x}\text{Sr}_x)_2\text{CuO}_4$  which has similar magnetic and superconducting properties to Ba substituted system. We have found the NQR signal of  $^{63}\text{Cu}$  and  $^{65}\text{Cu}$  at 35.3 and 33 MHz on the sample with  $x=0.075$ . [11] The change of the spectra with  $x$  is shown in Fig.2. [12]  $1/T_1$  of  $^{63}\text{Cu}$  for  $x=0.075$  is shown in Fig.1. The temperature dependence is similar to that in Y system.

For  $x=0.125$  and 0.15 the relaxation behavior is not simple but multi-exponential which is attributed to a

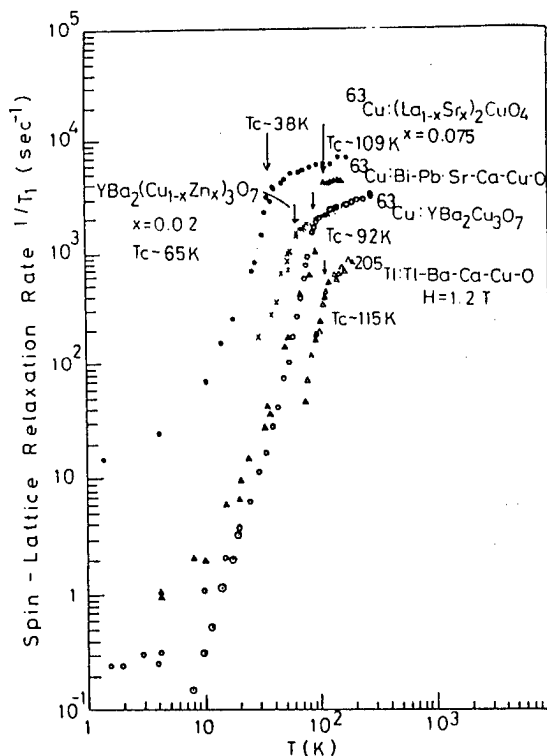


Fig. 1 Temperature dependence of  $1/T_1$  of Cu in Y(o), Zn substituted(x), La(●), Bi(▲) systems and Tl(Δ) in Tl system.

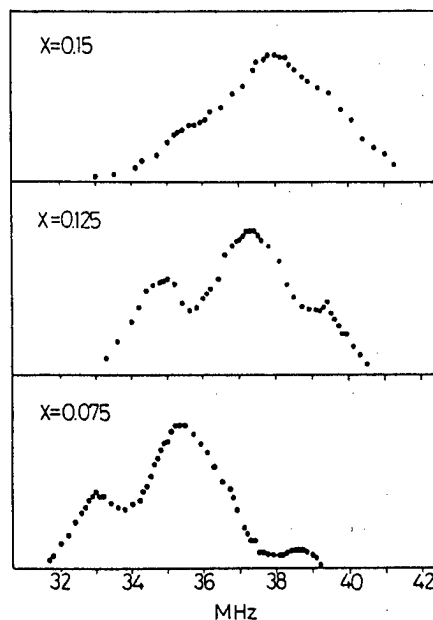


Fig. 2 Spin echo spectra of Cu in  $(\text{La}_{1-x}\text{Sr}_x)_2\text{CuO}_4$ .

distribution of the spin fluctuations on Cu associated with the random distributions of Sr and La around Cu as in the case of  $\text{YBa}_2(\text{Cu-Zn})_3\text{O}_7$  and/or the oxygen vacancies. In Fig.3 we plot  $\log(M(\infty)-M(t))$  against  $tT$ , where  $M(t)$  is the nuclear magnetization at time  $t$  after the saturating pulse, and  $T$  is the temperature. The fact that the points are distributed nearly on a line at  $T=90, 9$  and  $1.3$  K indicates that the each component of  $T_1$  follows the relation of  $T_1T=\text{const.}$  in this wide temperature range. Figure 4 shows the  $x$  dependence of  $T_1T$  value. The value of  $T_1^{-1}$  decreases with increasing  $x$  although the number of holes increases. This may be attributed to a decrease of the antiferromagnetic fluctuations that enhance  $1/T_1$  with increasing  $x$ . For  $x \sim 0.045$   $1/T_1$  of La begins to increase at low temperature indicating the system approaching to magnetically ordering state.[13]

### (iii) $(\text{Bi-Pb})_2\text{Sr}_2\text{Ca}_2\text{Cu}_3\text{O}_{10}$

Corresponding to two atomic sites of Cu we have found the NQR signal of  $^{63}\text{Cu}$  at 19.2 and 21 MHz.[14] In Fig.1 we show the relaxation behavior of  $^{63}\text{Cu}$  (21 MHz) sandwiched in CaO and SrO planes. The behavior is quite similar to that of Y system.

In all systems  $1/T_1$  decreases without enhancement just below  $T_c$  in superconducting state.  $T_1$  of Cu in normal state is considered to follow roughly the relation of  $T_1T=\text{const.}$  at low temperature and shows a saturating behavior at high temperature. This work has been carried out in collaboration with H. Sasakura et al. of University of Osaka Prefecture.

### (2) NMR of Tl in $\text{Tl}_2\text{Ba}_2\text{Ca}_2\text{Cu}_3\text{O}_{10}$

$T_1$  of Tl in  $\text{Tl}_2\text{Ba}_2\text{Ca}_2\text{Cu}_3\text{O}_{10}$  is shown in Fig.1.  $T_1^{-1}$  above  $T_c$  is proportional to  $T$ , while decreases rapidly below  $T_c$  without enhancement. The overall behavior is similar to Y in Y system. This work has been carried out in collaboration with H. Katayama-Yoshida, Y. Okabe and T. Takahashi in Tohoku University.

### (3) $^{17}\text{O}$ NMR

The photo emission[15] and X ray absorption[16] measurement indicate that the doped holes in  $\text{YBa}_2\text{Cu}_3\text{O}_7$  system are introduced mainly to oxygen site. NMR measurement of oxygen is expected to give an important

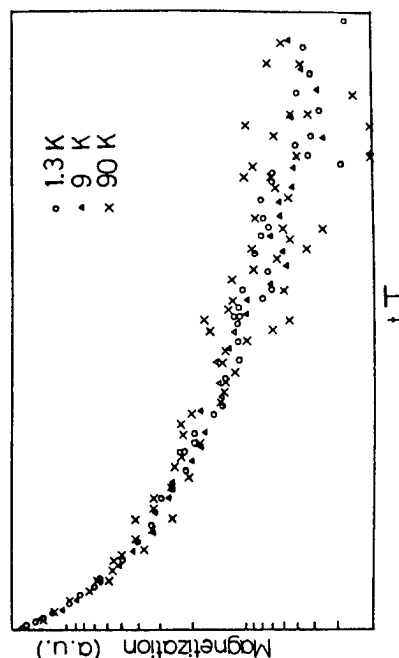


Fig. 3 Recovering behavior of nuclear magnetization (see text).

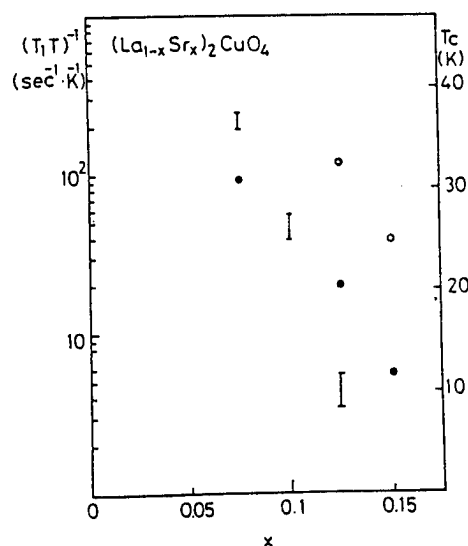


Fig. 4  $x$ -dependence of  $(T_1T)^{-1}$  in  $(\text{La}_{1-x}\text{Sr}_x)_2\text{CuO}_4$  in normal state.  $\circ$  and  $\bullet$  show the shortest and longest components of multi exponential behavior. The upper and lower end of bar indicate the on-set and off-set temperature of superconductivity obtained by resistivity measurement, respectively.

information for the investigation of the mechanism for the superconductivity.

We have made an NMR measurement of  $^{17}\text{O}$  in the samples where  $^{16}\text{O}$  is replaced partially by  $^{17}\text{O}$  at  $950^\circ\text{C}$ . [17] The spectrum is shown in Fig.5 together with those of  $\text{YBa}_2\text{Cu}_3\text{O}_{6.5}$  and  $\text{YBa}_2\text{Cu}_3\text{O}_6$ . In the measurement of  $T_1$  of central line of quadrupole split lines in field of about 3 T, the recovering behavior is not simple exponential. This behavior is analysed well with a single  $T_1$  in a initial condition where only the central line is saturated and the populations of other levels are in thermal equilibrium with  $\pm 1/2$  states. As seen in Fig.6  $T_1$  in normal state depends on the field. There appears a small peak just below  $T_c$ . The ratio  $(T_{1n}/T_{1s})$  at the peak amounts to 1.3 ~ 1.2. The appearance of an enhancement seems to suggest an s wave pairing. However this value is small compared with the usual BCS case of about 2. At low temperature  $T_1^{-1}$  decreases more slowly than those of Cu or Tl as mentioned previously. The values at the lowest temperature are almost constant in the field 1.5 ~ 3.8 T.

In order to know from which O sites the observed signal comes from, we have carried out a high resolution NMR measurement in 5 T. Fig.7(a) and (b) show the high resolution NMR spectra obtained in the samples where (a)  $^{17}\text{O}$  was exchanged at  $950^\circ\text{C}$  and (b) an annealing at  $350^\circ\text{C}$  in air was made after the exchange at  $950^\circ\text{C}$ . By comparing both figures, it is considered that there exist more than

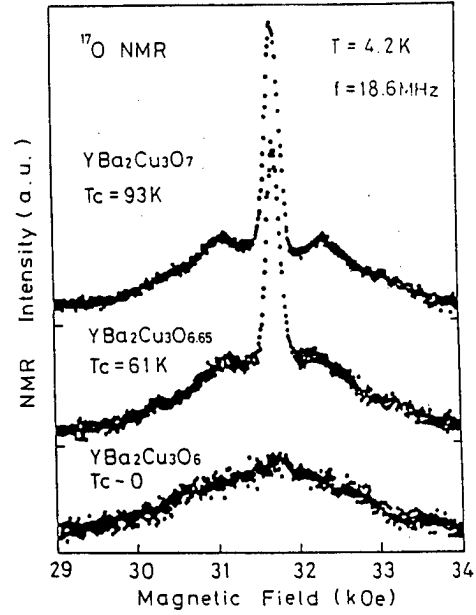


Fig. 5 NMR spectra of  $^{17}\text{O}$  in  $\text{YBa}_2\text{Cu}_3\text{O}_{7-y}$  systems.

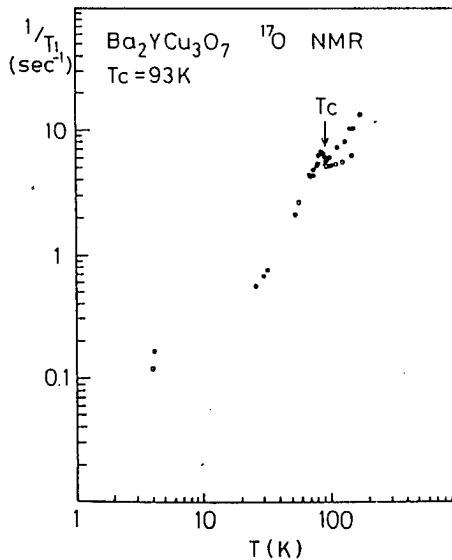


Fig. 6 Temperature dependence of  $1/T_1$  of  $^{17}\text{O}$  in the magnetic field of 3.2T (●) and 3.8T (○).

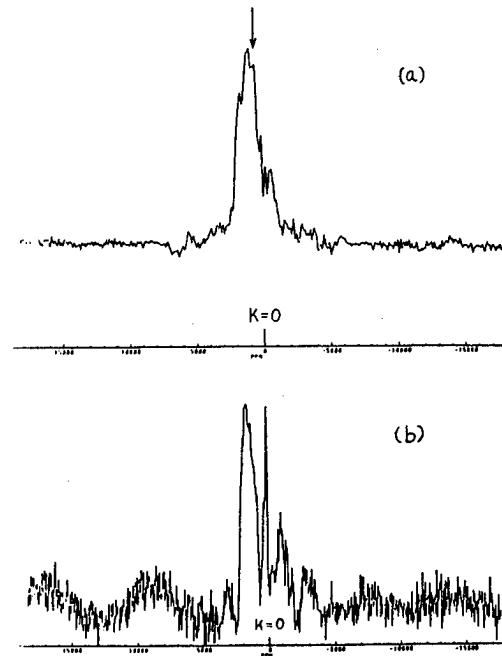


Fig. 7 High resolution NMR spectra of  $^{17}\text{O}$  in  $\text{YBa}_2\text{Cu}_3\text{O}_7$  at 300 K.

one NMR line. The part indicated by arrow in Fig.7(a) which escapes in Fig.7(b) may be attributed to the oxygen at Cu-O chain. The main signal may be attributed to  $\text{CuO}_2$  or BaO layers. Although the recovering behavior was analysed with a single  $T_1$  these signals have possibility to contribute more or less to our  $T_1$  measurement which might cause the field dependence of  $T_1$  around  $T_C$ . The parts with relatively large Knight shift may correspond to the sites where the holes are mainly introduced. In order to get a decisive conclusion, the measurement for site assignment and of the  $T_1$  at respective lines are necessary. This work is carried out in collaboration with H. Katayama-Yosida, Y. Okabe and T. Takahashi of Tohoku University and S. Takeda and H. Chihara in Osaka University.

## 2. Susceptibility and Resistivity

Detailed measurements of the superconducting transition temperature,  $T_C$ , the lattice parameters, the a.c. and d.c. susceptibilities of the  $\text{YBa}_2(\text{Cu}_{1-x}\text{M}_x)_3\text{O}_{7-\delta}$  systems have been made, where  $\text{M}=\text{Fe}, \text{Co}, \text{Ni}, \text{Zn}$  and  $\text{Al}$ . [18-22] The crystal structures of the Fe-, Co- and Al-substitutions are transformed into the tetragonal form as the result of the branching of the Cu(1)-O chains due to the different oxygen coordination of these dopants. [21] Co impurities are considered to occupy only the Cu(1) sites, Ni to occupy Cu(2). Recent Mossbauer experiment indicates that the main part of the doped Fe replaces Cu(1) with residual part replacing Cu(2) on the plane. [23]

The transition temperature,  $T_C$ , of the usual samples prepared in the air was reported to decrease roughly linearly with increasing  $x$  for all the substitutions. However, it has newly been found that  $T_C$  is dramatically enhanced by the low temperature ( $350^\circ\text{C}$ - $450^\circ\text{C}$ ) annealing in high-pressure oxygen gas ( $6$ - $12 \text{ kg/cm}^2$ ), being essentially the same as that of the undoped one up to  $x=0.035$  for Fe, Co and Al. The enhanced  $T_C$  is easily returned to the initial value of the air annealed sample, if the oxygen annealed sample is reannealed in the air at  $350^\circ\text{C}$  for 10-20 hours. In cases of  $\text{M}=\text{Zn}$  and  $\text{Ni}$ ,  $T_C$  is unchanged by the oxygen annealing. [22] These are shown in Fig.8 (a), (b) and (c). The dc magnetic susceptibilities of both the ordinary air annealed and oxygen annealed samples with Fe, Co and Ni have been measured. The magnetic moments of these substituents were found to be almost unchanged by the oxygen annealing, as shown in Fig.9. The concentrations at

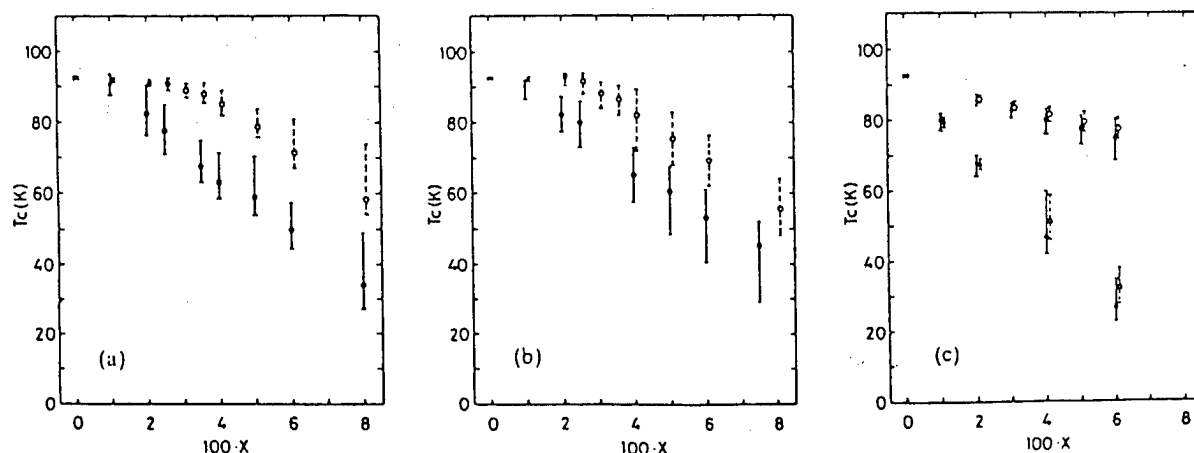


Fig. 8 Temperature dependence of  $T_C$  for both the  $\text{O}_2$ -annealed samples:  $\circ$  and dotted bars, and the air-annealed samples:  $\bullet$  and solid bars, respectively. The symbols  $\circ$  and  $\bullet$  show the midpoints, and the ends of the bars show the onset and zero resistance temperatures, respectively. The  $x$ -axis for the  $\text{O}_2$ -annealed is shifted by  $100x=0.10$  to avoid overlapping of these bars. (a): Fe substituted system, (b): Co substituted system, (c): Ni ( $\circ$  and  $\bullet$ ) and Zn ( $\triangle$  and  $\blacktriangle$ ) substituted systems.

which the crystal structures transform from the orthorhombic to the tetragonal were also unchanged by the oxygen annealing.

Concerning to the origin of the  $T_C$ -suppression in these substituted systems, there have been two speculations. The one is the pair-breaking scattering of Abrikosov and Gor'kov type by magnetic impurities.[25][26] The second is the new (unknown) mechanism which is different from the first.[27] The second is based on the fact that the  $T_C$ -suppression in the substituted material with nonmagnetic Zn were comparable with or larger than those with magnetic Fe and Co. However, the enhancement of  $T_C$  by the oxygen annealing in the present measurements shows that the observed  $T_C$ -suppression in Fe-, Co- and Al-substituted compounds, which were annealed both in air and oxygen, is not dominated by the pair breaking scattering, but dominated by "oxygen" whose coordination may be modulated. It should be noted that the  $T_C$ -suppression by the pair-breaking is proportional to the impurity concentration,  $x$ , in low concentration region.

As mentioned above, some amounts of Fe impurities replace the Cu(2). However, the  $T_C$ -suppression behaves quite similarly to the Co substitution which occupy the Cu(1) only. This fact indicates that the contribution of the pair-breaking by magnetic impurities substituting not only the Cu(1) but also the Cu(2) is very small. These results may suggest that the Cooper pairs do not run on both the Cu ions in these materials. This might be consistent with the result of the photo emission measurements where the doped holes are introduced mainly to oxygen sites.[15-16] In order to understand the mechanism of the  $T_C$ -suppression in these systems, the detailed study of the electronic state near the dopants may be necessary.

The work has been performed in collaboration with Y. Yamada, T. Kohara, H. Yamagata and S. Nasu.

#### References

- [1] W.W. Warren et al. : Phys. Rev. Lett. 59 (1987) 1860.
- [2] M. Mali et al. : Phys. Lett. A124 (1987) 112.
- [3] Y. Kitaoka et al. : J. Phys. Soc. Jpn. 57 (1988) 30, Physica C153-155 (1988) 83.
- [4] S. Imai et al. : J. Phys. Soc. Jpn. 57 (1988) 1771.
- [5] Y. Kohori et al. : J. Phys. Soc. Jpn. 57 (1988) 1568.
- [6] Y. Kohori et al. : J. Phys. Soc. Jpn. 57 (1988) 2905.
- [7] Y. Yamada et al. : J. Phys. Soc. Jpn. 57 (1988) 2663.
- M. Matsumura et al. : J. Phys. Soc. Jpn. 57 (1988) 3297.
- [8] Y. Kitaoka et al. : J. Phys. Soc. Jpn. 57 (1988) 737, Proc. ICM 88 Paris.
- [9] T. Fujita et al. : Jpn. J. Appl. Phys. 26 (1987) L368.
- [10] Y. Kitaoka et al. : J. Phys. Soc. Jpn. 56 (1987) 3024, 57 (1988) 734.
- [11] K. Ishida et al. : J. Phys. Soc. Jpn. 58 (1989) No.1.
- [12] K. Ishida et al. : submitted to J. Phys. Soc. Jpn.

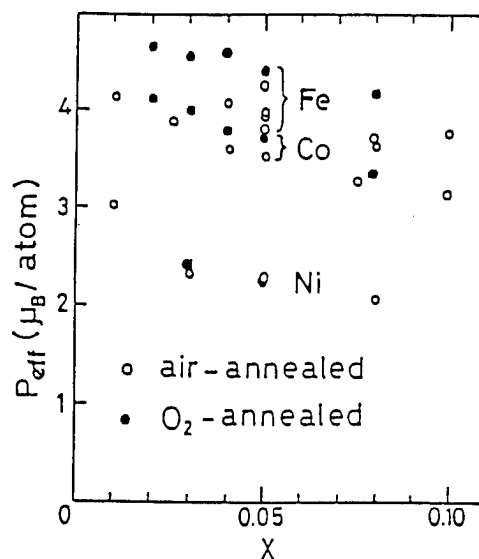


Fig. 9 Concentration dependences of effective Bohr magneton number,  $P_{eff}$ .

- [13] T. Kobayashi et al. : submitted to J. Phys. Soc. Jpn.
- [14] K. Fujiwara et al. : J. Phys. Soc. Jpn. **58** (1989) No.2.
- [15] A. Fujimori et al. : Solid State Commun. **63** (1987) 857.
- [16] A. Bianconi et al. : to be published in Phys. Rev. B.
- [17] Y. Kitaoka et al. : Proc. 2nd NEC Symposium on the Mechanism of the High Temperature Superconductivity (1988). K. Ishida et al. : J. Phys. Soc. Jpn. **57** (1988) 2897.
- [18] Y. Oda et al. : J. Phys. Soc. Jpn. **57** (1988) 1548.
- [19] Y. Oda et al. : J. Phys. Soc. Jpn. **57** (1988) 1880.
- [20] Y. Oda et al. : Jpn. J. Appl. Phys. **27** (1988) L1702.
- [21] Y. Oda et al. : Jpn. J. Appl. Phys. **26** (1987) L1660.
- [22] Y. Oda et al. : J. Phys. Soc. Jpn. **57** (1988) 4079
- [23] V. Sedykh et al. : Solid State Commun. **67** (1988) 1063.
- [24] Y. Yamada et al. : to be submitted to J. Phys. Soc. Jpn. (1989).
- [25] G. Xiao et al. : Phys. Rev. **B35** (1987) 8782.
- [26] R. Aoki et al. : Physica **C156** (1988) 405.
- [27] J.M. Tarascon et al. : Phys. Rev. **B37** (1988) 7458.



## Cu-NQR and Low Temperature Heat Capacity of $\text{La}_{2-x}\text{Sr}_x\text{CuO}_4$

K. Kumagai, Y. Nakamura, H. Nakajima, M. Muro-oka and N. Wada

Department of Physics, Faculty of Science, Hokkaido University, Sapporo 060.

The observation of  $^{63/65}\text{Cu}$ -NQR and  $^{139}\text{La}$ -NQR and the nuclear schottky anomalies of heat capacity in  $\text{La}_{2-x}\text{Sr}_x\text{CuO}_4$  reveals that the well-defined hyperfine field due to magnetic ordering of the reduced Cu moments exists in the superconducting and normal metallic regions. The nuclear spin-lattice relaxation rate,  $1/T_1$  of the Cu-spectra is suppressed apparently by the superconducting energy gap for  $0.12 \leq x \leq 0.20$ , while its temperature dependence obeys the Korringa relation for the normal region of  $x > 0.30$ .

### 1. Introduction.

The phase diagrams of high- $T_c$  superconductors of  $(\text{La},\text{M})_2\text{CuO}_4$ ,  $\text{YBa}_2\text{Cu}_3\text{O}_{7-\delta}$  and  $\text{Bi}_2\text{Sr}_2(\text{Ca}-\text{Y})\text{Cu}_2\text{O}_{8+\delta}$  resemble with each other [1]. The antiferromagnetism is situated commonly in the vicinity of superconductivity, indicating the importance of the antiferromagnetic spin fluctuations in the  $\text{CuO}_2$  planes to account for their high- $T_c$  superconductivity. The experiments such as  $^{139}\text{La}$ -NQR [2],  $\mu\text{SR}$  [3] and neutron scattering [4] have suggested that magnetic order coexists with superconductivity in the oxide superconductors. However, the observed quantities of  $\mu\text{SR}$  and neutron scattering are not sensitive to superconductivity, and does not give a decisive answer to the problem whether or not the long range magnetic order and superconductivity coexist in the same part of crystal.

In this report, we present here the observation of Cu-NQR in  $\text{La}_{2-x}\text{Sr}_x\text{CuO}_4$  system and demonstrate the coexistence of magnetic ordering and superconductivity at Cu site for  $x > 0.1$  [5]. The measurement of nuclear schottky anomalies of heat capacity indicates also the existence of static magnetic Cu-moment in the superconducting samples [6].

### 2. Experimentals.

All samples were prepared by solid-state reaction from mixed powder of  $\text{SrCO}_3$ ,  $\text{La}_2\text{O}_3$  and  $\text{CuO}$ . The details for sample preparation are reported elsewhere [2,7]. The pellets were crushed in to powder of 350mesh for NQR measurements. A conventional phase-coherent pulsed NMR apparatus was used for the NQR measurements of spectra and nuclear spin relaxation times,  $T_1$  and  $T_2$ . Search for the resonance signals has been made for frequency range between 30 to 45MHz in zero external field.

### 3. Results and discussion.

#### 3-1. Properties of Cu-NQR [5].

The spin echo signals above 30MHz are observed in zero external field for  $x > 0.12$ . In the rather complex spectra with three peaks shown in Fig. 1, the each peak frequency shifts to higher frequency side with increasing  $x$ . The observed spectra are not interpreted by the nuclear energy splitting due to only quadrupole interaction in the homogeneous samples, but are interpreted when we include internal field to the quadrupole interaction. Degenerated nuclear levels for  $I=3/2$  of Cu nuclei lead two resonance frequencies which replace the single, pure quadrupole frequency. Thus, the present NQR spectra are considered to consist with four peaks due to the signals from  $^{63}\text{Cu}$  and  $^{65}\text{Cu}$  nuclei, as shown by two sets of arrows for  $x=0.12$  in Fig. 1. The Larmor frequency,  $\nu_L$ , and quadrupole frequency,  $\nu_Q$ , are obtained by using the equation of the perturbed quadrupole interactions to the nuclear levels of  $^{63/65}\text{Cu}$ .

Hyperfine field,  $H_{hf}$ , determined from the separation of doublet is shown in Fig. 2 by the boled line, together with the results of heat capacity [6].  $H_{hf}$  decreases rapidly with increasing  $x$  from the value of 80kOe in the undoped antiferromagnetic  $\text{La}_2\text{CuO}_4$  [8]. The magnetic hyperfine field at Cu sites remains finite upto  $x=0.4$  where the system is in the normal metallic state. Assuming the hyperfine field

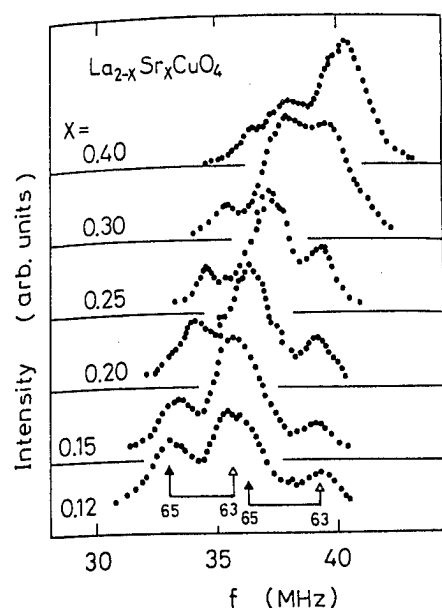


Fig. 1. Spin echo spectra of Cu in  $\text{La}_{2-x}\text{Sr}_x\text{CuO}_4$  at 1.5K.

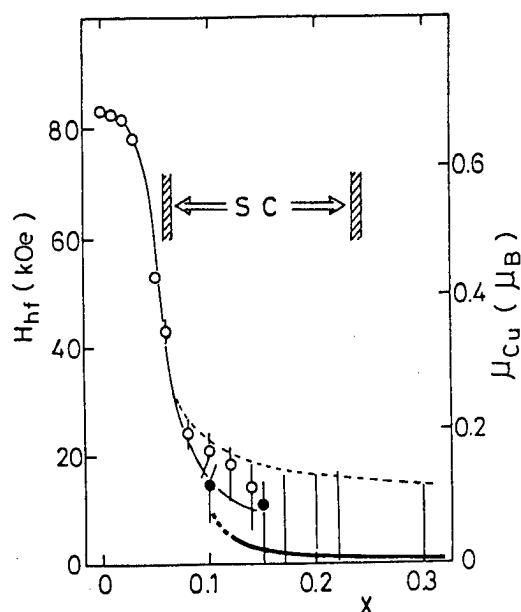


Fig. 2. Hyperfine field of Cu in  $\text{La}_{2-x}\text{Sr}_x\text{CuO}_4$  at 1.5K as a function of  $x$ .

is proportional to the magnitude of Cu moments, we deduce the extremely reduced magnetic moment per Cu atom compared to the value of  $1\mu_B$  for free  $\text{Cu}^{2+}$  atom.

The  $x$ -dependence of quadrupole resonance frequency of,  $^{63}\text{Cu}$  is shown in Fig. 3 together with the result of  $^{139}\text{La}$  obtained at 1.5K. EFG at Cu site increases monotonously with increasing of Sr-doping, while EFG of the La site decreases with  $x$ . The extrapolation value  $\nu_Q = 36\text{MHz}$  at Cu site to  $x=0$  is large compared to 32MHz obtained from the analysis of the antiferromagnetic resonance [8]. This discrepancy may be caused by the appearance of peculiar magnetic order which is accompanied with the nuclear relaxation anomalies for  $x < 0.06$  [2,7,9]. The deviation of the concentration dependence of  $^{139}\text{La}$  from the linear relation is also observed. This implies that the electronic state at O and/or Cu atoms changes between the hole-localized insulating ( $x < 0.06$ ) and hole-movable metallic state ( $x > 0.06$ ).

The nuclear spin-spin relaxation time,  $T_2$ , at the each peaks decreases rapidly with increasing  $x$ . Interestingly,  $1/T_2$  is proportional to the hyperfine field as shown in Fig. 4, indicating strongly that the main contribution to  $1/T_2$  is attributed to the Suhl-Nakamura interaction [10], ie. the indirect nuclear transition via the virtual excitation of spin waves when the system is in the magnetically ordered state. The predominant SN interactions are similarly observed in  $1/T_2$  of Cu in the magnetically ordered  $\text{YBa}_2\text{Cu}_3\text{O}_6$  [11]. This fact also support that the Cu moments order at low temperatures.

The temperature dependences of  $1/T_1$  for  $x \geq 0.25$  obeys the Korringa relation ( $T_1 T = \text{const.}$ ) which is caused by the thermal excitations of the conduction electrons. This implies that the system is metallic in nature and that the density of states of the conduction electrons at the Fermi level are sizable at the Cu site. On the contrary, in the superconducting range of  $0.12 < x < 0.2$ ,  $1/T_1$  below  $T_c$  is much suppressed as shown in Fig. 5.  $1/T_1$  of Cu at the largest peak shows a sharp decrease without any enhancement just below  $T_c$  and also decreases with power-law like behavior as decreasing temperature, as quite similar to the results in the superconducting  $\text{YBa}_2\text{Cu}_3\text{O}_7$  [12,13]. The superconductivity for  $0.06 < x < 0.22$  is confirmed by the measurements of electrical resistivity, magnetic susceptibility [14] and the heat capacity jump at  $T_c$  [6]. We emphasize here that the Cu-signals are feel the well-defined and static hyperfine field as mentioned before. Thus, the NQR results are the direct evidence for the

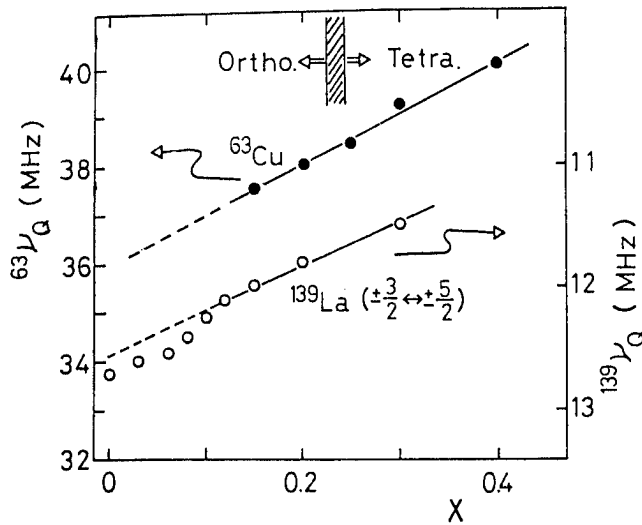


Fig. 3. Concentration dependence of the quadrupole resonance frequency  $^{63}\gamma_Q$  of  $^{63}\text{Cu}$  (●) and  $^{139}\gamma_Q$  of  $^{139}\text{La}$  (○) in  $\text{La}_{2-x}\text{Sr}_x\text{CuO}_4$ .

coexistence of superconductivity and magnetic order with very tiny moments at the same site of Cu from microscopic points of view.

### 3-2. Nuclear Schottky Anomalies of Heat Capacity [6].

The heat capacity at low temperatures down to 80mK was measured for  $0 \leq x \leq 0.30$ . Figure 6 shows  $C/T$  as a function of  $T$  for some Sr-doped samples. The upturn in  $C/T$  is evident below 200mK, indicating the high temperature tail of a nuclear schottky anomaly being to the presence of internal field and/or electrical quadrupole interaction. The low temperature part of the heat capacity is well fitted by the relation  $C = \gamma T + AT^{-2}$  i.e.  $C/T = \gamma + AT^{-3}$  as shown in Fig. 7. From this fitting, the concentration dependences of  $A$  is shown in Fig. 8. From the  $A$  and the EFG parameters obtained from Cu-NQR [5], we calculate the hyperfine field,  $H_{hf}$ , at Cu site and scaled Cu moment which are shown in Fig. 2. The magnetic moments of Cu decrease rapidly with increasing  $x$ , but survive in the superconducting state.

We obtain also the temperature linear term,  $\gamma T$ , from the low temperature range, which is shown in Fig. 8 as a function of Sr concentration together with those obtained from the best fitting to the relation of  $C/T = \gamma + AT^{-3}$  in the high temperature range between 2 and 7K [14]. The estimated value in the normal state from the jump at  $T_c$  and the BCS  $C/T_c = 1.43$  is quite comparable to those

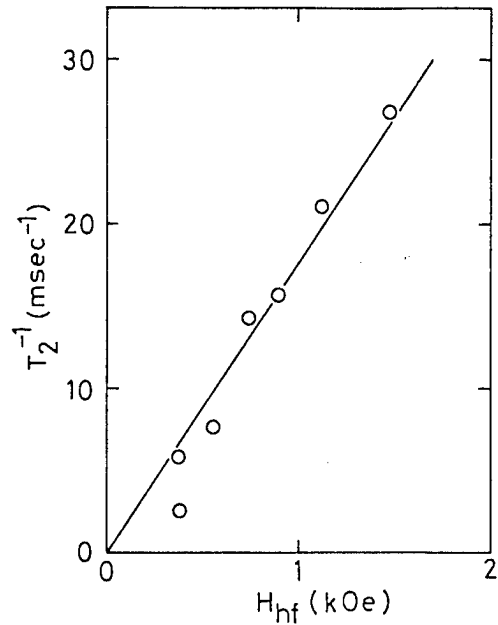


Fig. 4.  $1/T_2$  as function of the hyperfine field at Cu site.

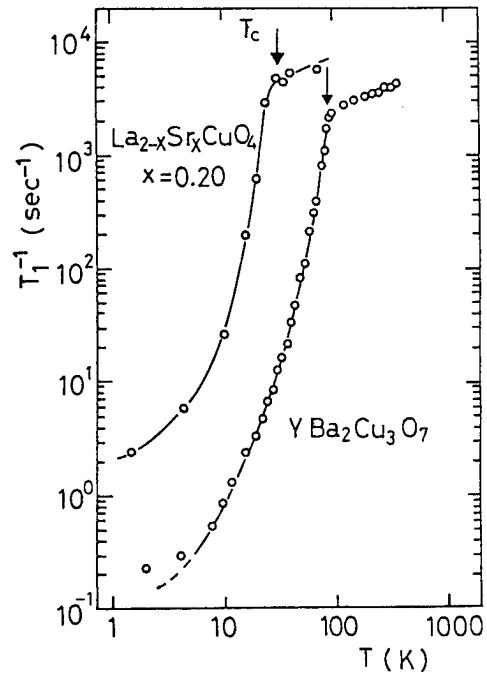


Fig. 5. Temperature dependence of nuclear spin-lattice relaxation rate,  $1/T_1$ , of  $^{63}\text{Cu}$  in the superconducting  $\text{La}_{2-x}\text{Sr}_x\text{CuO}_4$  of  $x=0.20$  ( $T_c$  is 33K, indicated by arrow). The reported result (from ref.13) of  $^{63}\text{Cu}$  in the  $\text{CuO}_2$  planes of  $\text{YBa}_2\text{Cu}_3\text{O}_7$  relation, ( $T_c=90\text{K}$ ) is also shown.

for  $x > 0.25$ . Thus, the vanishingly small  $\lambda T$  term in the superconducting state is confirmed from the independent analysis of low and high temperature range. Our conclusion is that the  $\lambda T$  term in the heat capacity due to the electronic and spin degrees of freedom is essentially reduced by the superconducting energy gap at low temperature far below  $T_c$  [7,15].

#### 4. Concluding remarks.

The observation of Cu-NQR in  $\text{La}_{2-x}\text{Sr}_x\text{CuO}_4$  and low temperature heat capacity reveals that the hyperfine field at Cu sites due to magnetic ordering of Cu moments appears in the superconducting and also the normal metallic region of  $x > 0.1$ . The gradual freezing of the Cu spins develops as decreasing temperature.

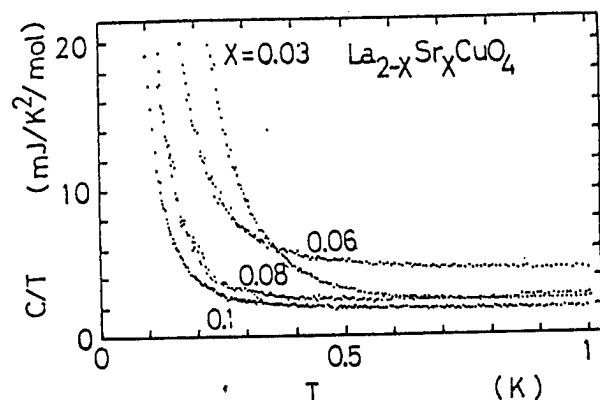


Fig. 6. Heat capacity in the low temperature range below 1K, plotted by  $C/T$  vs  $T$ .

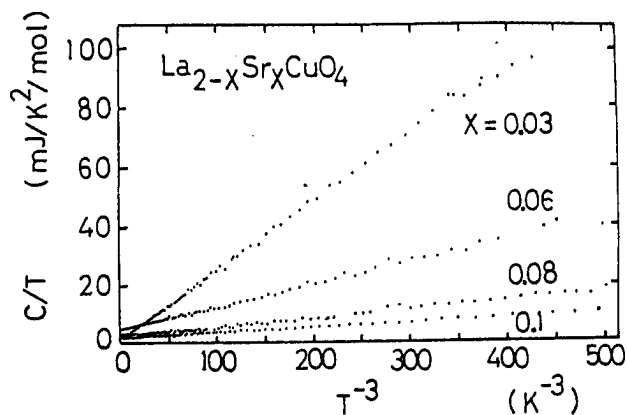


Fig. 7. Heat capacity in the low temperature range below 1K, plotted by  $C/T$  vs  $T^{-3}$ .

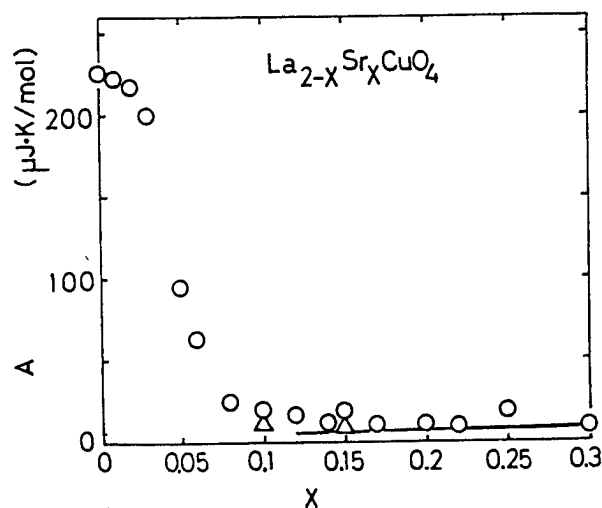


Fig. 8. Concentration dependence of the coefficient,  $A$ , of nuclear schottky anomaly in  $\text{La}_{2-x}\text{Sr}_x\text{CuO}_4$ .

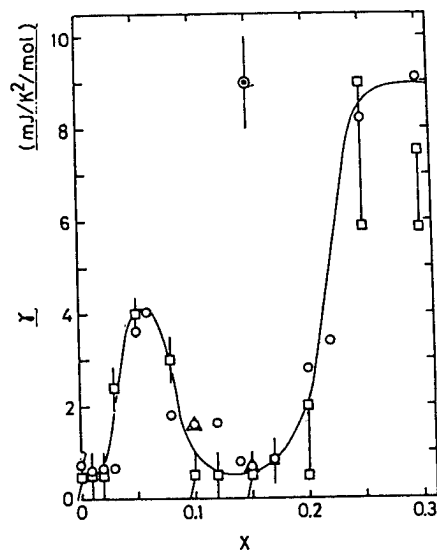


Fig. 9. Concentration dependence of the coefficient of the  $T$ -linear term of heat capacity of  $\text{La}_{2-x}\text{Sr}_x\text{CuO}_4$ . Squares ( $\square$ ) are obtained from the fitting in the high temperature range between 2 and 7K. The open circles ( $\circ$ ) are obtained from low temperatures from  $C/T$  vs  $T^{-3}$ .

The Cu moments are very reduced to be of order of  $0.05\mu_B$  even at the lowest temperature. As we have not enough information to account for the magnetic structure in the system and how the very tiny moment results from quantum effects on the strongly-correlated electron system, it should be noted that the antiferromagnetic order with tiny magnetic moments less than  $0.1\mu_B$  is currently observed in some heavy electron compounds [15,16]. In addition to this, the other important fact is that  $1/T_1$  of Cu in the heavy fermion and oxide systems shows commonly the power law of the temperature dependence,  $1/T_1 \propto T^{3-5}$  without the enhancement just below  $T_C$ , suggesting the anisotropic superconducting energy gap. Understanding of the resemblance in many magnetic and superconductive properties between the two exotic superconductors would shed further light on possible magnetic mechanism for high- $T_C$  superconductivity.

#### Acknowledgement

This work is supported in part by a Grant-in-Aid for Scientific Research on Priority Areas "Mechanism of Superconductivity" from the Ministry of Education, Science and Culture of Japan.

#### References.

- [1] T.Oashi, K.Kumagai, Y.Nakajima, T.Tomita and T.Fujita, Physica 154C (1989), to be published.
- [2] K.Kumagai, I.Watanabe, H.Aoki, Y.Nakamura, T.Kimura, Y.Nakamichi and H.Nakajima, Physica 148B (1987) 480.
- [3] H.Kitazawa, K.Katsumata, E.Torikai and K.Nagamine, Solid State Commun. 67 (1988) 119.
- [4] R.J.Birgeneau, Y.Endoh, Y.Hidaka, K.Kakurai, M.A.Kastner, T.Murakami, G.Shirane, T.R.Thurton and K.Yamada, preprint, and H.Yoshizaki, S.Mitsuda, H.Kitazawa and K.Katsumata, J. Phys. Soc. Jpn. 57 (1988) 3686.
- [5] K.Kumagai and Y.Nakamura, Physica 154C (1989), to be published.
- [6] N. Wada, K.Muro-oka, Y.Nakamura and K.Kumagai, submitted to Physica C.
- [7] I.Watanabe, K.Kumagai, Y.Nakamura, T.Kimura, Y.Nakamichi, and H.Nakajima, J. Phys. Soc. Jpn. 56 (1987) 3028.
- [8] T.Tsuda, T.Shimizu, Y.Yasuoka, K.Kishio, K.Kitazawa, J. Phys. Soc. Jpn. 57 (1988) 2908.
- [9] K.Kumagai, H.Aoki, I. Watanabe, Y. Nakamura and H. Nakajima, J. Phys. Soc. Jpn 57 (1987) 1155.
- [10] H. Suhl, Phys. Rev. 109 (1958) 606, and T. Nakamura, Progr. Theoret. Phys. 20 (1958) 542.
- [11] H.Yasuoka, T.Shimizu, Y.Ueda, and .Kosuge, J. Phys. Soc. Jpn. 57 (1988) 2659.
- [12] Y.Kitaoaka, S.Hiramatsu, T.Kondo and K.Asayama, J. Phys. Soc. Jpn. 57 (1988) 30.
- [13] T.Imai, T.Shimizu, H.Yasuoka, Y.Ueda and K.Kosuge, J. Phys. Soc. Jpn. 57 (1988) 2280.
- [14] K.Kumagai, Y.Nakamura, I.Watanabe, Y.Nakamichi and H.Nakajima, J. Mag. Mag. Mat. 76&77 (1988) to be published.
- [15] G.Aeppli, E.Bucher C.Broholm, J.K.Kjems, J.Baumann and J.Hufnagl, Phys. Rev. Lett. 60 (1988) 615.
- [16] K.Kitaoaka, H.Yamada, and K.Asayama, J. Mag. Mag. Mater., to be published.

Proton NMR in Hydrogen-doped Superconductor  $\text{YBa}_2\text{Cu}_3\text{O}_{7-\delta}\text{H}_x$

H. NIKI, T. SUZUKI<sup>\*</sup>, S. TOMIYOSHI<sup>\*\*</sup>, H. HENTONA<sup>\*\*\*</sup>, M. OMORI<sup>\*\*</sup>,  
T. KAJITANI<sup>\*\*</sup>, T. KAMIYAMA<sup>\*\*\*\*</sup> and R. IGAI

Department of Physics, Division of General Education, University of  
the Ryukyus, Nishihara, Okinawa 903-01, Japan

<sup>\*</sup>Institute of Physics, University of Tsukuba, Tsukuba, Ibaraki 305, Japan

<sup>\*\*</sup>Institute for Materials Research, Tohoku University, Sendai 980, Japan

<sup>\*\*\*</sup>Department of Physics, College of Science, University of the Ryukyus,  
Nishihara, Okinawa 903-01, Japan

<sup>\*\*\*\*</sup>Institute of Materials Science, University of Tsukuba, Tsukuba,  
Ibaraki 305, Japan

Proton NMR in  $\text{YBa}_2\text{Cu}_3\text{O}_{7-\delta}\text{H}_{0.2}$  was performed between 77 K and 300 K. The hydrogen atom is diffusing or moving in the crystal above 170 K. Below 150 K it is trapped in the O(1) or O(2) oxygen sites in Cu-O chain. In the superconducting state below  $T_c$  of 92 K, the penetration depth of the magnetic field at  $T = 0$  K was determined to be 2500 Å.

Nuclear magnetic resonance (NMR) is one of the most powerful experimental methods to investigate the superconducting properties from a microscopic point of view. Line width, relaxation time  $T_1$  and Knight shift give detailed information on penetration depth, magnetic and crystallographic states of atoms and density of states of conduction electrons at the Fermi energy. These are very important to elucidate the mechanism of superconductivity of extraordinary high- $T_c$  ceramic.

In this paper we report measurements of proton NMR in a hydrogen-doped superconductor  $\text{YBa}_2\text{Cu}_3\text{O}_{7-\delta}\text{H}_{0.2}$  [1]. The  $^1\text{H}$  nucleus is a spin 1/2 and 99.985 % abundant isotope; the absence of quadrupole interaction makes it both attractive experimentally and simple for interpretation. As shown by recent studies [2-6] a fairly large amount of hydrogen can be absorbed by the  $\text{YBa}_2\text{Cu}_3\text{O}_{7-\delta}$  system. When hydrogen concentration  $x$  for  $\text{YBa}_2\text{Cu}_3\text{O}_{7-\delta}\text{H}_x$  is less than 0.2,  $T_c$  and the volume fraction of superconducting phase are almost constant, but beyond that the volume fraction decreases abruptly [5]. This shows that, for concentration  $x < 0.2$ , the doped hydrogen atoms do not destroy superconductivity in this system. Hydrogen absorption was carried out by a gas charging method using an apparatus of Sileverts type [2]. The concentration of the hydrogen was determined to be  $x = 0.2$  from the pressure change.

The line width of an NMR spectrum was determined from peak to peak separation of an absorption derivative,  $\Delta H_{pp}$ . Figure 1 shows the temperature dependence of  $\Delta H_{pp}$  in the temperature range from 77 K to 300 K. The line width of the proton resonance spectrum is extremely narrow above 170 K due to diffusion or some other dynamical behavior of hydrogen atom with activation energy  $E_a = 50 \pm 20 \text{ kJ mol}^{-1}$ , which brings the best fit to the observed  $\Delta H_{pp}$  (see the inset in Fig. 1) [1], but it becomes broader abruptly below 170 K and keeps almost a constant value of  $\Delta H_{pp} = 2.5 \pm 0.5 \text{ Oe}$  from 150

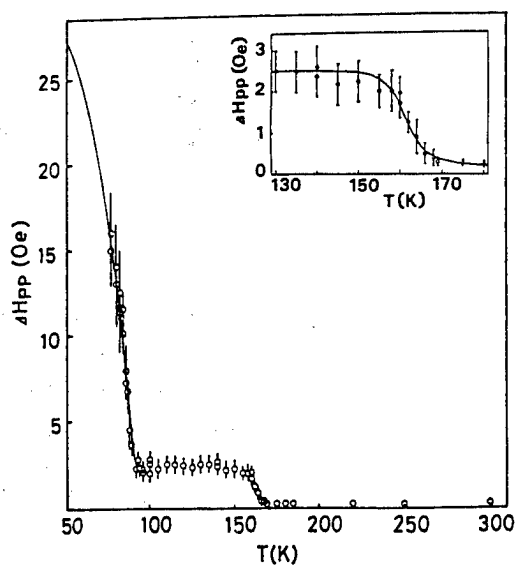


Fig. 1. Temperature dependence of peak to peak separation of the absorption derivative of  $^1\text{H}$  NMR in  $\text{YBa}_2\text{Cu}_3\text{O}_{7-\delta}\text{H}_{0.2}$ . Inset shows the blowup of temperature dependence of the line width from 130 K to 180 K. Its solid line is a curve calculated with  $E_a = 50 \text{ kJ mol}^{-1}$ .

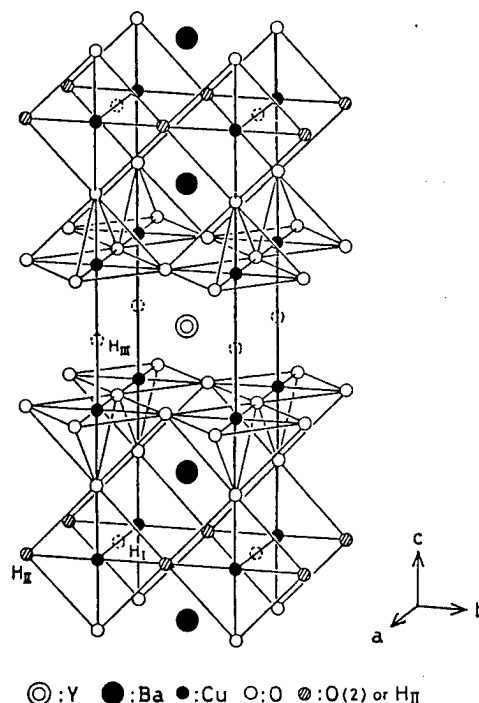


Fig. 2. Crystal structure of  $\text{YBa}_2\text{Cu}_3\text{O}_{7-\delta}$ .  $\text{H}_\text{I}$ ,  $\text{H}_\text{II}$  and  $\text{H}_\text{III}$  indicate the possible sites occupied by hydrogen atoms.  $\text{H}_\text{I}$  and  $\text{H}_\text{II}$  sites correspond to oxygen positions of vacant  $\text{O}(1)$  and occupied  $\text{O}(2)$ , respectively.

K down to  $T_c$  of 92 K. This behavior of the line width suggests that hydrogen atoms are trapped in some sites of the crystal below 150 K. Below  $T_c$  the line width increases rapidly with decreasing temperature because of distribution of magnetic field by the penetration of vortices.

We assigned the site which the hydrogen atom occupies in the temperature range from  $T_c$  to 150 K. Since  $^1\text{H}$  has no quadrupole moment, its NMR line width of  $^1\text{H}$  NMR below 150 K arises only from the nuclear magnetic dipolar interaction between  $^1\text{H}$  and other nuclei. Since the amount of doped hydrogen atoms is very small, the dipolar interaction between the  $^1\text{H}$  nuclei is neglected.

The second moment of  $^1\text{H}$ ,  $\overline{\Delta H_T^2}$ , is obtained by summing up the contribution of the dipolar interaction from each different species. Since the NMR absorption spectrum in the present experiment from  $T_c$  to 150 K exhibits the line shape of a Gaussian curve, the value of  $\Delta H_{pp}$  must be given by  $2(\overline{\Delta H_T^2})^{1/2}$ .

Three interstitial sites that accommodate hydrogen atoms can be considered in this crystal structure as shown in Fig. 2. The first site ( $\text{H}_\text{I}$ ) is the vacant  $\text{O}(1)$  site and the second one ( $\text{H}_\text{II}$ ) is the occupied  $\text{O}(2)$  site; they are on the  $\text{Cu}(1)\text{-O}$  plane sandwiched by Ba layers. The third one ( $\text{H}_\text{III}$ ) is the site surrounded by the  $2\text{Cu}(2)$  and  $4\text{Y}$  atoms. The distances between each interstitial site and other atoms are obtained by neutron diffraction in  $\text{YBa}_2\text{Cu}_3\text{O}_{7-\delta}\text{H}_{0.2}$  at 100 K [7]. Then the value of

$\Delta H_{pp}$  obtained from the calculation of the second moments are 3.17 Oe, 3.02 Oe and 4.51 Oe for  $H_I$ ,  $H_{II}$ ,  $H_{III}$  sites, respectively.

On the other hand, the value of  $\Delta H_{pp}$  obtained from this experiment is  $2.5 \pm 0.5$  Oe, which suggests within experimental accuracy that hydrogen atom occupies  $H_I$  or  $H_{II}$  sites rather than  $H_{III}$  site in  $YBa_2Cu_3O_{7-\delta}H_x$ . The experimental  $\Delta H_{pp}$  is, however, slightly smaller than the calculated ones at  $H_I$  and  $H_{II}$  sites. This suggests a possibility that either the hydrogen atoms are slightly off the center of  $H_I$  (or  $H_{II}$ ) site towards the direction normal to the line connecting Cu(1) atoms or vibrating around the center.

Fujii et al. [5] showed that in  $YBa_2Cu_3O_{7-\delta}H_x$  the lattice constant  $a$  increases with  $x$ , but on the other hand the lattice constant  $b$  decreases slightly with  $x$ , and suggested that hydrogen occupies  $H_I$  site rather than  $H_{II}$  site. But Matsunaga et al. [6] showed by neutron diffraction that the variation of lattice parameters obtained by Fujii et al. is caused by the fact that hydrogen atoms occupy the O(2) (namely  $H_{II}$ ) site so that part of oxygen atoms originally in O(2) site are pushed out to vacant O(1) site. The position of hydrogen determined from NMR is either  $H_I$  or  $H_{II}$  site, but it can not be determined exactly which position is occupied by the hydrogen atom.

Nishida et al. [8] reported in  $\mu$ SR experiment that positive muons implanted in  $YBa_2Cu_3O_{7-\delta}$  are diffusing above 200 K and that below 200 K they are trapped in a certain site feeling the nuclear magnetic dipolar field of 1.4 Oe. This value almost agrees with that of the line width of NMR spectrum when hydrogen atoms are trapped in  $H_I$  or  $H_{II}$  site. These results suggest that the muons are trapped in the same site as the hydrogen atoms in our experiment above 170 K.

In the superconducting state, the broadening of the NMR line is due to the spatial variation of magnetic field which depends on the penetration depth of vortices [9]. The second moment due to the field distribution for the square lattice of vortices is given as follows [9]:

$$\overline{\Delta H_s^2} = \frac{\phi_o^2}{16\pi^3 \lambda^4}, \quad \text{----- (1)}$$

where the  $\phi_o$  is the quantum of flux which is  $hc/2e$  and  $\lambda$  the penetration depth [10]. The temperature dependence of  $\lambda$  is given by  $\lambda = \lambda_o / (1 - t^4)^{1/2}$ , where  $\lambda_o$  is the penetration depth at  $T = 0$  and  $t$  the reduced temperature  $T/T_c$  [11].

Since, in the superconducting state, hydrogen atoms occupy the same sites as those in the normal state below 150 K, the nuclear dipolar interaction between  $^1H$  nucleus and other nuclei is the same in both states. Therefore, the line width observed in superconducting state should be a superposition of the second moments in the normal state,  $\overline{\Delta H_n^2}$ , and  $\overline{\Delta H_s^2}$  given by eq. (1). In the superconducting state, the  $\Delta H_{pp}$  becomes

$$\overline{\Delta H_{pp}^2} = 2 \left[ \frac{\phi_o^2}{16\pi^3 \lambda_o^4} (1 - t^4)^2 + \overline{\Delta H_n^2} \right]^{1/2} \quad \text{----- (2)}$$

By using 2.5 Oe for  $2(\overline{\Delta H_n^2})^{1/2}$  in the normal state below 150 K, the theoretical  $\Delta H_{pp}$  was calculated according to eq. (2). The obtained value for  $\lambda_o$  is 2500 Å which brings the best fit to the observed  $\Delta H_{pp}$  (Fig. 1): The calculated line agrees very well with the experimental values. The obtained value of the penetration depth is



comparable to that in ordinal superconductors, and almost agrees with those for  $\text{La}_{1.85}\text{Sr}_{0.15}\text{CuO}_4$ ,  $\sim 2500 \text{ \AA}$ , measured by muon spin relaxation ( $\mu\text{SR}$ ) [12,13] and  $\text{YBa}_2\text{Cu}_3\text{O}_{7-\delta}$ ,  $\sim 1500 \text{ \AA}$ , derived from Meissner effect and  $\mu\text{SR}$  [14,15].

In summary, above 170 K the hydrogen atom is diffusing or moving dynamically in the crystal with the activation energy  $E_a = 50 \pm 20 \text{ kJ mol}^{-1}$ , but below 150 K the hydrogen atom is trapped in  $\text{H}_\text{I}$  or  $\text{H}_\text{II}$  site, which is oxygen position of O(1) or O(2), respectively. The penetration depth  $\lambda_0$  at  $T = 0 \text{ K}$  was determined to be as  $2500 \text{ \AA}$ .

The behavior of hydrogen atoms resulted from the temperature dependence of spin-lattice relaxation time  $T_1$ , which we are measuring now, has been found similar to that resulted from the temperature dependence of line width in the normal state mentioned above. Also, in the superconducting state it seems that just below  $T_c$  the  $T_1$  becomes shorter and reaches minimum at  $0.93 T_c$ , and that below  $0.93 T_c$  the  $T_1$  becomes longer. Detailed investigation of  $T_1$  is now in progress.

Further investigation of hydrogen concentration dependence in  $\text{YBa}_2\text{Cu}_3\text{O}_{7-\delta}\text{H}_x$  is very important in understanding the superconductivity of ceramic superconductors.

#### References

- 1) H. Niki, T. Suzuki, S. Tomiyoshi, H. Hentona, M. Omori, T. Kajitani, T. Kamiyama and Igei: Solid State Commun. 39 (1989) (to be published).
- 2) T. Kamiyama, S. Tomiyoshi, M. Omori, H. Yamauchi, T. Kajitani, T. Matsunaga and H. Yamamoto: Physica 148 B (1987) 491.
- 3) J. J. Reilly, M. Suenaga, J. R. Johnson, P. Thompson and A. R. Moodenbaugh: Phys. Rev. B 36 (1987) 5694.
- 4) C. Y. Yang, X. Q. Yang, S. M. Heald, J. J. Reilly, T. Skotheim, A. R. Moodenbaugh and M. Suenaga: Phys. Rev. B36 (1987) 8798.
- 5) H. Fujii, H. Kawanaka, W. Ye, S. Orimo and H. Fukuba: Jpn. J. appl. Phys. 27 (1988) L 525.
- 6) T. Matunaga, T. Kajitani, T. Kamiyama, M. Omori, S. Tomiyoshi, H. Yamauchi and M. Hirabayashi: Proc. MRS Int. Meeting on Advanced Materials, Tokyo, 1988 (to be published).
- 7) T. Suzuki (private communication).
- 8) N. Nishida: Prity (Maruzen, Tokyo, 1988) Vol. 3, NO. 4, p. 54 [in Japanese].  
N. Nishida, et al.: Phys. Soc. Jpn. 57 (1988) 597.
- 9) P. Pincus, A. C. Gassard, V. Jaccarino and J. H. Wernick: Phys. Lett. 13 (1964) 21.
- 10) C. E. Gough, M. S. Colclough, E. M. Forgan, R. G. Jorgan, M. Keene, C. M. Muirhead, A. I. M. Rae, N. Thomas, J. S. Abell and S. Sutton: Nature 326 (1987) 855.
- 11) M. Tinkham: Introduction to Superconductivity (McGraw-Hill, New York, 1975).
- 12) G. Aeppli, R. J. Cava, E. J. Asaldo, J. H. Brewer, S. R. Kreitzman, G. M. Luke, D. R. Noakes and R. F. Kiefl: Phys. Rev. B 35 (1987) 7129.
- 13) W. J. Kossler, J. R. Kepton, X. H. Yu, H. E. Schone, Y. J. Uemura, A. R. Moodenbaugh, M. Suenaga and C. E. Stronach: Phys. Rev. B 35 (1987) 7133.
- 14) R. J. Cava, B. Batlogg, R. B. van Dover, D. W. Murphy, S. Sunshine, T. Siegrist, J. P. Remeika, E. A. Rietman, S. Zahurak and G. P. Espinosa: Phys. Rev. Lett. 58 (1987) 1676.
- 15) Y. J. Uemura: Prity (Maruzen, Tokyo, 1988) Vol. 3, No. 10, p. 40 [in Japanese].

# $\mu$ SR Study of Oxide-Superconductors

Nobuhiko Nishida

*Department of Physics, Tokyo Institute of Technology,  
2-12-1 Ohokayama, Meguro-ku, Tokyo 152, Japan*

We have studied magnetic properties of copper-oxide superconductors ( $\text{LnBa}_2\text{Cu}_3\text{O}_x$  ( $\text{Ln}=\text{Y}, \text{Ho}$ ),  $\text{La}_2\text{CuO}_{4-\delta}$ ,  $\text{Bi-Sr-Ca-Cu-O}$ ) by muon spin rotation or relaxation ( $\mu\text{SR}$ ) method. In this report we describe  $\mu^+\text{SR}$  studies of the  $\text{Bi}_2\text{Sr}_2\text{Y}_{1-x}\text{Ca}_x\text{Cu}_2\text{O}_y$  system by systematically changing the ratio of Y and Ca content. It was found that  $\text{Bi}_2\text{Sr}_2\text{YCu}_2\text{O}_y$  is an antiferromagnetic insulator with  $T_N$  above 300 K.  $T_N$  decreases very sharply around  $x=0.2 \sim 0.3$  and superconductivity sets in at the Ca content where the magnetic ordering disappears. The magnetic phase diagram of  $\text{Bi}_2\text{Sr}_2\text{Y}_{1-x}\text{Ca}_x\text{Cu}_2\text{O}_y$  has been obtained. It is similar to those of  $\text{YBa}_2\text{Cu}_3\text{O}_x$  or  $\text{La}_{2-x}\text{A}_x\text{CuO}_{4-\delta}$  ( $\text{A}=\text{Sr}$  or  $\text{Ba}$ ).  $\text{Bi}_2\text{Sr}_2\text{YCu}_2\text{O}_y$  is the analogue of  $\text{YBa}_2\text{Cu}_3\text{O}_6$  or  $\text{La}_2\text{CuO}_{4-\delta}$ .

## 1. INTRODUCTION

Our  $\mu\text{SR}$  studies of high- $T_c$  superconductors are briefly reviewed. We applied the muon spin rotation or relaxation method ( $\mu^+\text{SR}$ ) to magnetism studies of high- $T_c$  superconductor Y-Ba-Cu-O for the first time at the early developing stage of the sample preparation and detected some kind of magnetic ordering in Y-Ba-Cu-O ( $T_c \sim 60\text{K}$ ) samples of mixed phases [1]. In order to study the magnetism further, the  $\mu^+\text{SR}$  experiments were performed on well-characterized single-phase  $\text{YBa}_2\text{Cu}_3\text{O}_x$  samples with systematically changing the oxygen content [2,3,4]. An antiferromagnetic ordering with  $T_N \sim 300\text{K}$  was discovered for the first time in the tetragonal semiconducting phase  $\text{YBa}_2\text{Cu}_3\text{O}_{6.2}$  and around a metal-insulator transition point ( $x \sim 6.4$ ) spin glass-like behavior was observed at low temperatures [2,3]. The magnetic phase diagram of  $\text{YBa}_2\text{Cu}_3\text{O}_x$  system was obtained [3,4] as shown in Fig.1. The results were later confirmed by neutron-diffraction experiments and NMR measurements. Further  $\mu^+\text{SR}$  studies on more samples of semiconducting  $\text{YBa}_2\text{Cu}_3\text{O}_x$  ( $x=6.0 \sim 6.5$ ) gave the similar results. The magnetic phase diagram of  $\text{YBa}_2\text{Cu}_3\text{O}_x$  was found to be similar to that of  $\text{La}_{2-x}\text{A}_x\text{CuO}_{4-\delta}$  ( $\text{A}=\text{Sr}$  or  $\text{Ba}$ ). Thus, the following scheme was shown to hold in the  $\text{YBa}_2\text{Cu}_3\text{O}_x$  system as well as in  $\text{La}_{2-x}\text{A}_x\text{CuO}_{4-\delta}$  ( $\text{A}=\text{Sr}$  or  $\text{Ba}$ ); as holes are introduced into the antiferromagnetic insulator with a high Neel temperature,  $T_N$  decreases sharply and superconductivity sets in when the antiferromagnetic ordering disappears. To study how the antiferromagnetism of the parent insulator ( $\text{YBa}_2\text{Cu}_3\text{O}_6$  or  $\text{La}_2\text{CuO}_{4-\delta}$ ) will be modified as holes are introduced in it, it is important to clarify spin glass-like magnetic behavior observed around the metal-insulator transition point of the  $\text{YBa}_2\text{Cu}_3\text{O}_x$  system [3,4]. Similar spin-glass-like behavior has been reported in  $\text{La}_{2-x}\text{Sr}_x\text{CuO}_{4-\delta}$  system, too [6]. About the spin-glass-like behaviors, we need more experimental studies, paying special attentions to a uniform distribution of oxygen atoms or doping elements in the sample. The experiments are now in progress on the oxygen-vacancy ordered sample of  $\text{YBa}_2\text{Cu}_3\text{O}_{6.5}$ . In  $\text{HoBa}_2\text{Cu}_3\text{O}_{6.2}$ , we also observed an antiferromagnetic ordering of Cu moments [7]. Temperature dependences of the  $\mu^+$  hyperfine fields are similar to each other in  $\text{YBa}_2\text{Cu}_3\text{O}_{6.2}$  and

$\text{HoBa}_2\text{Cu}_3\text{O}_{6.2}$ . It was pointed out that the presence of Ho moments seems not to influence on the magnetism of  $\text{Cu}_2\text{O}$  plane [4,6] and that the magnetic phase diagram shown in Fig.1 will not be changed by substituting Y atoms by Ho atoms.

In  $\mu\text{SR}$  method, as fully polarized muons are implanted into samples and probe only the magnetic perturbations there, it is easy to detect static or quasi-static magnetic ordering and to tell what portion is magnetically ordered in the sample. Therefore,  $\mu\text{SR}$  is powerful to make a magnetic phase diagram of the copper-oxide superconductor system even at the first stage of sample preparation, when samples with a uniform oxygen distribution are not available or some impurity phases are mixed in the sample and an anomaly of magnetic susceptibility of the main phase is difficult to be observed at  $T_N$ . Such was the case in  $\text{YBa}_2\text{Cu}_3\text{O}_x$ .

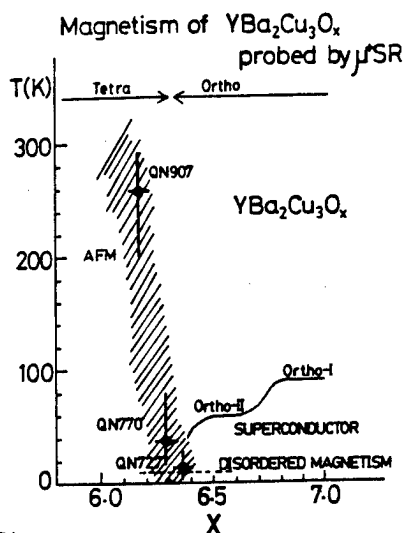


Fig. 1.

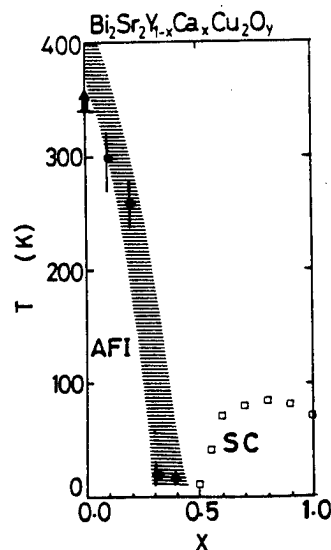


Fig. 3

In Bi(or Tl)-Sr-Ca-Cu-O, the magnetic properties have not been studied so well. Among Bi-Sr-Ca-Cu-O superconductors, for  $\text{Bi}_2\text{Sr}_2\text{CaCu}_2\text{O}_y$  (2212 compound), several groups [8,9,10] have proposed that hole concentrations can be controlled by changing the ratio of Ca atoms and Y atoms in the  $\text{Bi}_2\text{Sr}_2\text{Y}_{1-x}\text{Ca}_x\text{Cu}_2\text{O}_y$  system. The impurity phase  $\text{Y}_2\text{CuO}_5$  are always present in the sample and gives a large contribution to the magnetic susceptibility. Due to the  $\text{Y}_2\text{CuO}_5$ , magnetic studies were difficult in  $\text{Bi}_2\text{Sr}_2\text{YCu}_2\text{O}_y$ . In this paper, we report our  $\mu^+\text{SR}$  studies of  $\text{Bi}_2\text{Sr}_2\text{Y}_{1-x}\text{Ca}_x\text{Cu}_2\text{O}_y$  system.  $\text{Bi}_2\text{Sr}_2\text{YCu}_2\text{O}_y$  was found to be an antiferromagnetic insulator with a high Neel temperature [11] by  $\mu^+\text{SR}$ . And a similar magnetic phase diagram to  $\text{La}_{2-x}\text{A}_x\text{CuO}_{4-\delta}$  ( $A=\text{Sr}$  or  $\text{Ba}$ ) and  $\text{YBa}_2\text{Cu}_3\text{O}_x$  has been obtained in  $\text{Bi}_2\text{Sr}_2\text{Y}_{1-x}\text{Ca}_x\text{Cu}_2\text{O}_y$  [12]. Thus,  $\text{Bi}_2\text{Sr}_2\text{YCu}_2\text{O}_y$  will be the analogue of  $\text{La}_2\text{CuO}_{4-\delta}$  or  $\text{YBa}_2\text{Cu}_3\text{O}_6$ .

## 2. $\mu\text{SR}$ Experiments on the $\text{Bi}_2\text{Sr}_2\text{Y}_{1-x}\text{Ca}_x\text{Cu}_2\text{O}_y$ System

### 2.1 $\mu\text{SR}$ Experiments

$\mu\text{SR}$  experiments were performed at the BOOM facility, Meson Science Laboratory, University of Tokyo, located at KEK, and at TRIUMF, the meson factory of Canada. The experiments at TRIUMF were collaboration experiments of University of British Columbia, University of Tokyo and Tokyo In-

stitute of Technology. At BOOM, muon beams are polarized pulsed ones (50 ns width and 20 Hz). To observe muon spin relaxation phenomena with a long time constant ( $\sim 10 \mu\text{s}$ ) the BOOM facility was used. When a high time resolution was necessary, the  $\mu\text{SR}$  experiments were performed at TRIUMF, because muon beams are DC. Experimental details of  $\mu^+\text{SR}$  studies of copper-oxide superconductors are described in the reference [2].

## 2.2 Samples

Two sets of samples,  $\text{Bi}_2\text{Sr}_2\text{Y}_{1-x}\text{Ca}_x\text{Cu}_2\text{O}_y$ , [8,9] were prepared by solid state reactions of powders of  $\text{Bi}_2\text{O}_3$ ,  $\text{SrCO}_3$ ,  $\text{CaCO}_3$ ,  $\text{Y}_2\text{O}_3$  and  $\text{CuO}$ ; one is by the ISSIP group at U. of Tokyo [8] and the other by U. of Tsukuba group [9]. The details of preparation method are described in the references [8] and [9]. The  $\mu^+\text{SR}$  experiments gave the similar results for two sets of samples as far as the ratio of Y:Ca was same in the initial mixed powders.

## 2.3 Antiferromagnetism of $\text{Bi}_2\text{Sr}_2\text{YCu}_2\text{O}_y$

$\mu^+\text{SR}$  experiments on  $\text{Bi}_2\text{Sr}_2\text{YCu}_2\text{O}_y$  were performed in zero-external field at KEK-BOOM.  $\mu^+$  spin precessions were observed from 4.2 K up to 300 K; the precession frequency was about  $0.45 \pm 0.01$  MHz at 14 K and  $0.20 \pm 0.02$  MHz at 300 K. The observed  $\mu^+$  hyperfine fields are plotted in Fig. 2. It clearly shows that  $\text{Bi}_2\text{Sr}_2\text{YCu}_2\text{O}_y$  is antiferromagnetically ordered even at 300 K and the Neel temperature will be higher than 300 K [11]. From the longitudinal magnetic field  $\mu^+\text{SR}$  experiments at KEK-BOOM, some parts of implanted  $\mu^+$ 's were found to feel static hyperfine fields of several hundred gauss. As the muon beam at KEK-BOOM is a pulsed beam of 50 ns width, it is hard to observe fast  $\mu^+$  spin precessions or spin relaxations. Therefore, we performed  $\mu^+\text{SR}$  experiments at TRIUMF.

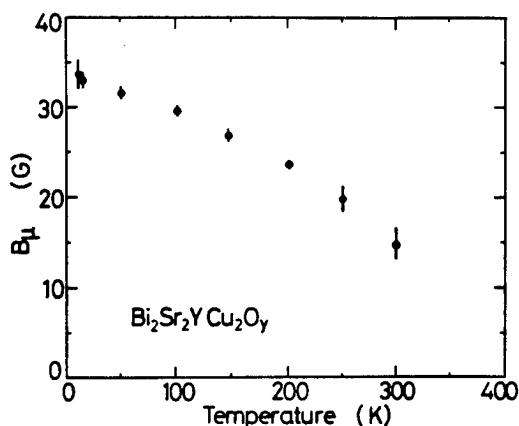


Fig. 2

In addition to 0.45 MHz,  $\mu^+$  spin precessions of 3.6 MHz and 4.4 MHz, which correspond to 266 G and 325 G, were observed. Implanted  $\mu^+$ 's are considered to occupy several sites in  $\text{Bi}_2\text{Sr}_2\text{YCu}_2\text{O}_y$  and feel different  $\mu^+$  hyperfine fields. Details will be discussed elsewhere [13].

## 2.4 Magnetic Phase Diagram of the $\text{Bi}_2\text{Sr}_2\text{Y}_{1-x}\text{Ca}_x\text{Cu}_2\text{O}_y$ System

In order to study how the above-mentioned antiferromagnetism will behave as we substitute Y atoms by Ca atoms,  $\mu^+$  spin rotation experiments were performed on  $\text{Bi}_2\text{Sr}_2\text{Y}_{1-x}\text{Ca}_x\text{Cu}_2\text{O}_y$  under the applied magnetic field of 80 G in the transversal direction to the initial  $\mu^+$  spin. When the sample are magnetically ordered,  $\mu^+$  internal magnetic fields are different from the applied magnetic field. Therefore, we are able to determine whether samples are magnetically ordered or what portions of the sample are magnetically ordered. Thus,  $T_N$  of  $\text{Bi}_2\text{Sr}_2\text{Y}_{1-x}\text{Ca}_x\text{Cu}_2\text{O}_y$  were determined and the

magnetic phase diagram of the  $\text{Bi}_2\text{Sr}_2\text{Y}_{1-x}\text{Ca}_x\text{Cu}_2\text{O}_y$  system has been obtained as in Fig.3. The antiferromagnetism of  $\text{Bi}_2\text{Sr}_2\text{YCu}_2\text{O}_y$  disappears around  $x=0.5$ , where the superconductivity sets in with increasing  $x$ . This phase diagram is similar to those of  $\text{YBa}_2\text{Cu}_3\text{O}_x$  and  $\text{La}_{2-x}\text{A}_x\text{CuO}_{4-\delta}$  ( $\text{A}=\text{Sr}$  or  $\text{Ba}$ ).

Zero-field  $\mu^+$ SR experiments were also performed on the  $\text{Bi}_2\text{Sr}_2\text{Y}_{1-x}\text{Ca}_x\text{Cu}_2\text{O}_y$  system. Three  $\mu^+$ precession frequencies were also observed in  $\text{Bi}_2\text{Sr}_2\text{Y}_{1-x}\text{Ca}_x\text{Cu}_2\text{O}_y$  at  $x=0.1, 0.2$ . At  $x=0.3$ , the  $\mu^+$ precession amplitude was damped by fast dephasing of precession due to inhomogeneity of  $\mu^+$  internal fields. In a superconducting phase of  $\text{Bi}_2\text{Sr}_2\text{CaCu}_2\text{O}_y$ , as far as  $\mu^+$  probes, neither magnetic fluctuation nor magnetic ordering of electronic origin has not been observed. It was not determined by  $\mu^+$ SR whether Cu atoms have no magnetic moments or fluctuations of Cu moments are too fast to be observed.

### 3. Future Studies

The  $\mu^+$ SR method was very powerful to detect static or quasi-static magnetic ordering in high- $T_c$ -superconductor related magnetic oxide-insulators, as successfully applied to studies of the magnetic phase diagrams of  $\text{YBa}_2\text{Cu}_3\text{O}_x$  or  $\text{Bi}_2\text{Sr}_2\text{Y}_{1-x}\text{Ca}_x\text{Cu}_2\text{O}_y$ . This sort of studies should be classified as the first stage of magnetism studies of oxide-superconductors by  $\mu$ SR. In  $\text{Bi}_2\text{Sr}_2\text{Y}_{1-x}\text{Ca}_x\text{Cu}_2\text{O}_y$ , three  $\mu^+$ precession frequencies have been observed. In  $\text{YBa}_2\text{Cu}_3\text{O}_6$ , two  $\mu^+$ precession frequencies have been detected at the present. These are able to be explained by several different sites occupied by  $\mu^+$  in oxides. From the  $\mu^+$ hyperfine field studies in  $\text{GdBa}_2\text{Cu}_3\text{O}_x$  or  $\text{YBa}_2\text{Cu}_3\text{O}_6$ , the  $\mu^+$  sites seem to be  $\mu^+$ -O bonding (analogous to OH) positions [13,14]. Now, when the locations of  $\mu^+$ 's in oxide-superconductors are determined, we should proceed to the second stage of  $\mu^+$ SR studies of oxide-superconductors; discussions about origins or temperature dependences of  $\mu^+$ hyperfine fields in  $\text{YBa}_2\text{Cu}_3\text{O}_x$  [2] or  $\text{Bi}_2\text{Sr}_2\text{Y}_{1-x}\text{Ca}_x\text{Cu}_2\text{O}_y$  [10]. The studies are now in progress. In a superconducting phase of copper-oxide superconductors,  $\mu^+$  does not detect magnetism of electronic origin. When negative muons ( $\mu^-$ 's) are used for studies of oxide-superconductor, another feature appears. As  $\mu^-$ 's are trapped by nuclei in a material and form quasi-nuclei with a large magnetic moment,  $\mu^-$ SR is able to give information about the electronic state at lattice sites, even if the nuclei are spinless and no magnetic or electric moments. To make NMR studies on oxygen sites in oxide-superconductors, oxygen isotope  $\text{O}^{17}$  which has a magnetic moment has to be substituted for oxygen atoms in high- $T_c$  superconductors. Such a procedure is not necessary for  $\mu^-$ SR.  $\mu^-$ SR studies on  $\text{La}_{2-x}\text{Sr}_x\text{CuO}_{4-\delta}$  and  $\text{YBa}_2\text{Cu}_3\text{O}_x$  are now in progress.

### acknowledgement

I thank the colleagues at KEK-BOOM and at TRIUMF. I appreciate many collaborators; S. Hikami (U. of Tokyo), M. Ishikawa, T. Takabatake, Y. Nakazawa (ISSP), T. Nakamura (TIT), Y. Hidaka, T. Murakami (NTT), Y. Ueda, K. Kosuge (U. of Kyoto). J. Akimitsu (Aoyama-Gakuin) for supplying oxide superconductor samples and making stimulating discussions.

### REFERENCES

- [1] N. Nishida, H. Miyatake, D. Shimada, S. Hikami, E. Torikai, K. Nishiyama and K. Nagamine: Jpn. J. Appl. Phys. 26 (1987) L799.

- [2] N. Nishida, H. Miyatake, D. Shimada, S. Okuma, M. Ishikawa, T. Takabatake, Y. Nakazawa, Y. Kuno, R. Keitel, J.H. Brewer, T.M. Riseman, D.Ll. Williams, Y. Watanabe, T. Yamazaki, K. Nishiyama, K. Nagamine, E.J. Ansaldò and E. Torikai, *Jpn. J. Appl. Phys.* **26** (1987) L1856.
- [3] N. Nishida, H. Miyatake, D. Shimada, S. Okuma, M. Ishikawa, T. Takabatake, Y. Nakazawa, Y. Kuno, R. Keitel, J.H. Brewer, T.M. Riseman, D.Ll. Williams, Y. Watanabe, T. Yamazaki, K. Nishiyama, K. Nagamine, E.J. Ansaldò and E. Torikai, *J. Phys. Soc. Jpn.* **57** (1988) 599.
- [4] N. Nishida, H. Miyatake, D. Shimada, S. Okuma, T. Yamazaki, Y. Watanabe, Y. Kuno, M. Ishikawa, T. Takabatake, K. Nishiyama, K. Nagamine, J.H. Brewer and S.R. Kreitzmann, *Physica C* **153-155** (1988) 761.
- [5] J.H. Brewer, E.J. Ansaldò, J.F. Carolan, A.C. Chaklader, W.N. Hardy, D.R. Harshman, M.E. Hayden, M. Ishikawa, N. Kaplan, R. Keitel, J. Kempton, R.F. Kiefl, W.J. Kossler, S.R. Kreitzman, A. Kulpa, Y. Kuno, G.M. Luke, H. Miyatake, K. Nagamine, Y. Nakazawa, N. Nishida, K. Nishiyama, S. Okuma, T.M. Riseman, G. Roehmer, R. Schleger, D. Shimada, C.E. Stronach, T. Takabatake, Y.J. Uemura, Y. Watanabe, D.Ll. Williams, T. Yamazaki and B. Yang, *Phys. Rev. Lett.* **60** (1988) 1073.
- [6] H. Kitazawa, K. Katsumata, E. Torikai and K. Nagamine, *Solid State Communications* (1988).
- [7] Y. Kuno, N. Nishida, H. Miyatake, S. Okuma, Y. Watanabe, T. Yamazaki, M. Ishikawa, T. Takabatake, Y. Nakazawa, J.H. Brewer, S. R. Kreitzman and T.M. Riseman, *Phys. Rev. B* **38** (1988) 9276.
- [8] T. Tamegai, A. Watanabe, K. Koga, I. Oguro and Y. Iye, *Jpn. J. Appl. Phys.* **27** (1988) L1074.
- [9] R. Yoshizaki, Y. Saito, Y. Abe and H. Ikeda, *Physica C* **152** (1988) 408.
- [10] Y. Ando, K. Fukuda, S. Kondoh, M. Sera, M. Onoda and M. Sato, *Solid State Communications*, submitted.
- [11] N. Nishida, H. Miyatake, S. Okuma, T. Tamegai, Y. Iye, R. Yoshizaki, K. Nishiyama and K. Nagamine, *Physica C* **156** (1988) 625.
- [12] N. Nishida, H. Miyatake, S. Okuma, R. Yoshizaki, T. Tamegai, Y. Iye, R. Kadono, J.H. Brewer, E.J. Ansaldò, W.N. Hardy, K. Nagamine and et. al., to be published (1989).
- [13] N. Nishida, to be published.
- [14] W. Dawson, K. Tibbs, S.P. Weathersby, C. Boeema and K-C. B. Chan, to be published.

# Neutron Magnetic Scattering from Superconducting $\text{La}_{2-x}\text{Sr}_x\text{CuO}_4$

--- Status report for 1988 ---

Y.Endoh<sup>1</sup>, R.J.Birgeneau<sup>5</sup>, Y.Hidaka<sup>2</sup>, K.Kakurai<sup>1</sup>,  
M.A.Kastner<sup>5</sup>, K.Kitazawa<sup>3</sup>, H.Kojima<sup>4</sup>, M.Matsuda<sup>1</sup>  
T.Murakami<sup>2</sup>, G.Shirane<sup>6</sup>, I.Tanaka<sup>4</sup>,  
T.M.Thurston<sup>5</sup> and K.Yamada<sup>1</sup>

- 1 Department of Physics, Tohoku University, Sendai 980, Japan
- 2 NTT Optoelectronics Laboratories, Tokai, Ibaraki 319-11, Japan
- 3 Department of Industrial Chemistry, University of Tokyo,  
Hongo, Bunkyo-ku, Tokyo 113, Japan
- 4 Institute of Inorganic Synthesis, Yamanashi University,  
Kofu, Yamanashi 400, Japan
- 5 Department of Physics, Massachusetts Institute of Technology,  
Cambridge, Massachusetts 02139, USA.
- 6 Physics Department, Brookhaven National Laboratory,  
Upton, New York 11973, USA.

Extensive quasielastic and inelastic neutron scattering studies have been performed on the  $\text{La}_{2-x}\text{Sr}_x\text{CuO}_4$  single crystals. We have found dramatic change in the magnetic state by Sr doping. With increasing x the Neel state is destroyed and a new incommensurate spin fluid state appears. Spin correlation length in the doped  $\text{CuO}_2$  sheets was found to be equal to the average distance of holes in the sheets, which ultimately carry the super current.

## 1 Introduction

As described in the preceding report on the special project research [1], the fundamental magnetism in pure  $\text{La}_2\text{CuO}_4$  is well described by the quantum 2 dimensional(2D) Heisenberg antiferromagnet[2]. In fact the 3D Neel state is realized due to the small interlayer exchange interactions and the anisotropic interactions generated by the orthorhombic crystal distortion[3]. The extensive experiments have been carried on the pure  $\text{La}_2\text{CuO}_4$  and then essential antiferromagnetic properties were almost completely elucidated[4]. Since the intralayer antiferromagnetic exchange interaction is very strong, we cannot thoroughly study the spin dynamics but we grasp essential evidence that the quantum effect associated  $S=1/2$  governs the spin fluctuations in this crystal. At the same time we have extended the neutron magnetic scattering studies to doped single crystals focussing on the doping effect on the spin correlations. The exact connection between these unusual 2D quantum spin fluid(QSF) state and the novel superconductivity in  $\text{CuO}_2$  lamellar compounds still remains to be elucidated at this stage.

Large single crystals have continuously been grown at NTT laboratories by using

the flux grown technique[5] and they were independently characterized in several places of our research group. Eventually the data were circulated among us to be confirmed by each member in our group. During these processes we have found very important fact that the superconducting properties are very delicate to the heat treatment. Meissner fraction with a little effect on the superconducting transition temperature( $T_c$ ) much depends on it. Although the detail will be published elsewhere, we show a temperature evolution of magnetization with respect to various heat treatments. Since the EPMA shows no appreciable change in the metallic concentration, we speculate that only oxygen concentration changes due to the fact that we could observe the weight change during each heat treatment as expected. This result indicates that the oxygen concentration is also an important parameter for the stabilization of the superconductivity in  $\text{La}_{2-x}\text{Sr}_x\text{CuO}_4$ . Furthermore the effect on the conductivity in the normal phase was found to be dominated by this heat treatment. In particular the component along the direction perpendicular to  $\text{CuO}_2$  sheets is sensitively affected by the oxygenation. In this respect a newly grown single crystal by TSFZ method [6] was supplied by Yamanashi group, which is now investigated at Brookhaven National Laboratory. This crystal contains the largest Sr concentration among such single crystals that have been afforded to the neutron scattering studies. This crystal also shows the highest  $T_c$  of 35K and a 100% shielding effect. Additionally it shows a metallic behavior in the c axis conductivity in the tetragonal phase[7], although the lower doped single crystals still show a small upturn in the resistivity along this direction with decrease of temperature. Judging from our experience to look at the resistivities from various doped crystals, we speculate that the oxygen concentrations may also dominate the superconducting properties. It is noted that the new single crystals grown by the TSFZ method may contain not only high Sr doping but also high oxygen concentration.

## 2 Spin correlations in superconducting $\text{La}_{2-x}\text{Sr}_x\text{CuO}_4$ crystals

During the last 12 months, we have concentrated in measurements of spin correlations for doped superconducting single crystals[8]. The neutron scattering experiments were mostly carried out on the triple axis spectrometers at the Brookhaven High Flux Beam Reactor. We aimed to see how the 2D QSF state observable in pure  $\text{La}_2\text{CuO}_4$  change in the superconducting crystals and also how the appearance of supercurrent may correlate to spin correlations in  $\text{CuO}_2$  sheets.

It is very important that the total magnetic scattering intensities integrated in energy with two axis scan from the incident neutron energy of  $E_0 - k_B T$  seem to be constant with respect to the different Sr coping concentration within the experimental accuracy which is not as good as more than 20%. On the other hand, the scattering profiles for superconducting crystals are significantly modified from the 2D antiferromagnetic scattering in the pure  $\text{La}_2\text{CuO}_4$ , which is sharp in Q. Firstly the two splitted peaks were observed when the scan was across the 2D Bragg ridge so called  $(h \ h-0.45 \ 0)$  scan as is shown in Fig.1. It was confirmed that the scattering is purely 2D since a strong peak appears at  $k=0.59$  for the  $(10k)$ scan, where wave vector  $k_F$  of scattered neutrons superposes the 2D Bragg ridge for the case of  $E_i=14.7\text{meV}$ . Secondly the scattering profiles are much broad and flat. Furthermore



there is essentially no temperature dependence. The instantaneous correlation function  $S(Q)$  is evidently unchanged in going from normal to the superconducting state.

Since the experiments became more and more difficult due to the facts that probably nonmagnetic background with the elastic scattering processes increases with doping concentration, it required an energy analysis method detecting solely magnetic scattering. One new technique is the filtered two - axis method where the spectrometer was set up in the triple-axis mode and all scans made twice, once detecting neutrons scattered off the PG analyzer so that energy transfer is less than spectrometer resolution of 0.5 meV energy transfer and once detecting neutrons

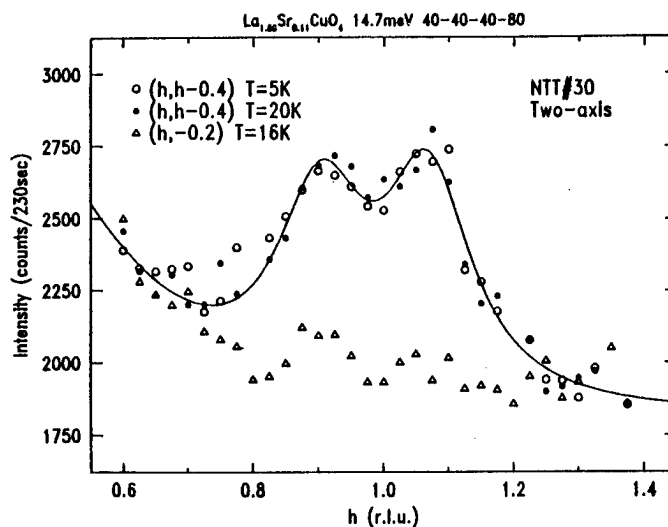


Fig.1 Two axis scan2 for  $\text{La}_{1.88}\text{Sr}_{12}\text{CuO}_4$  along  $(h\ h-0.4\ 0)$  at 5K and 20K. Background scan was made along  $(h\ -0.2\ 0)$  at 16K. Solid line is the result of the fits to two peaked 2D Lorentzian with a background.

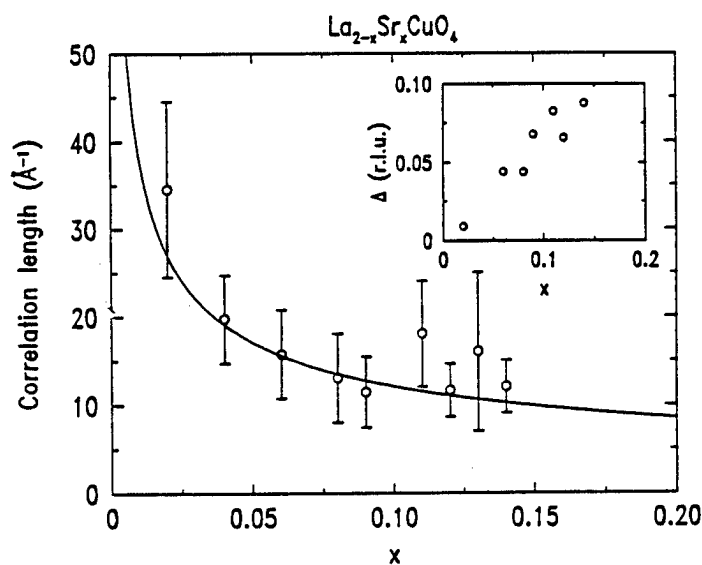


Fig.2 Instantaneous spin correlation length with respect to  $x$  in  $\text{La}_{2-x}\text{Sr}_x\text{CuO}_4$ . Lengths are deduced from the fits to two peaked Lorentzian. Solid line is the function of  $3.8/\sqrt{x}A$  representing an average separation of  $\text{O}^-$  holes.

passing straight through the analyzer[9]. The effective reflectivity of the analyzer was measured to be 78% so that by subtracting off 29% of the first scan from the second scan, one could obtain the intensity integrated over all energies with energy transfer more than 0.5meV. The two peaked structure in  $Q$  across the 2D ridge holds in both inelastic (filtered 2-axis scans) and elastic (3-axis scans) measurements, although the intensity ratios are temperature dependent. The spin fluctuations change being predominantly inelastic at 350K to dominantly quasielastic at the lowest temperature about 12K.

The data were analyzed by using a two peaked Lorentzian profile, since the two-axis scans for higher Sr doped samples clearly show that the 2D static correlations are incommensurate. The correlation lengths which are the

inverse of the intrinsic line width of the Lorentzian fall on the solid line of  $3.8/\sqrt{x}A$ , which is the average separation between the  $O^-$  holes in the  $CuO_2$  planes, suppose that all the unbalanced valencies by Sr doping are compensated by doped holes in the  $CuO_2$  site. The result clearly indicates that the holes have an extraordinarily disruptive effect on the antiferromagnetic  $Cu^{2+}$ - $Cu^{2+}$  superexchange interaction. Another interesting point is that the incommensurability for the static structure factor is approximately proportional to the inverse of the average separation of the holes. This immediately suggests that the spin correlation is drastically modified by the holes[8].

Finally the spin fluctuations in the doped superconducting crystals are found to be independent on  $Q$  perpendicular to  $Q_{2D}$ , which shows the purely 2D characters that the excitations are confined in the  $CuO_2$  planes. The inelastic scattering intensities are weakly dependent on both excitation energy and temperature, which cannot be interpreted by the Bose statistics. Since the energy range for our studies is so limited compared with the intralayer exchange energy that the statistics of magnetic excitations or detailed analysis of  $S(Q, \omega)$  remains to be elucidated in future. We have at present no appropriate theory which may account for these unusual spin correlations in both space and time. However we could conclude that the  $O^-$  holes destruct the 2D Heisenberg antiferromagnetic state spanned in  $Cu^{2+}$  lattice to modify it to the novel incommensurate spin fluid state, which should be necessary for any model of the novel superconductivity in the  $CuO_2$  lamellar compounds.

#### Acknowledgments

The research is supported by the Japanese Ministry of Education, Culture and Science under the Special Program of the Grant in Aid and Japan-U.S. Cooperative Neutron Scattering Program. The research at Brookhaven is supported by the Division of Materials Science, U.S. Department of Energy under the contract DE-AC02-76CH00016. The research at MIT is supported by the U.S. National Science Foundation under the contract no.DMR85-01856 and no.DMR84-18718.

#### References

1. Endoh Y. et al., Jpn.J.Appl.Phys. Series1 24(1988)
2. Chakravarty S., Halperin B.I., Nelson D.R., Phys.Rev.Lett.60 1057(1988)
3. Kastner M.A. et al., Phys.Rev.B38 6636(1988)
4. Endoh Y. et al., Phys.Rev.B37 7443 (1988)
5. Hidaka Y. et al., J.Cryst.Growth 85 581 (1988)
6. Tanaka I., Kojima H., Nature 337 21 (1989)
7. Kitazawa K. private communications
8. Birgeneau R.J. et al., Phys.Rev.B38 6614 (1988)
9. Birgeneau R.J. et al., Proceeding of NEC symposium (Hakone, October 1988)

# Mössbauer study on Fe-sitting site and origin of magnetic order in $\text{YBa}_2(\text{Cu}_{0.95}\text{Fe}_{0.05})_3\text{O}_{7-\delta}$

T.Tamaki, M.Nishizawa and A.Ito

Department of Physics, Faculty of Science, Ochanomizu University,  
Bunkyo-ku, Tokyo 112, Japan

Sitting sites of doped Fe's and the origin of magnetic order in  $\text{YBa}_2(\text{Cu}_{0.95}\text{Fe}_{0.05})_3\text{O}_{7-\delta}$  have been studied by comparing the Mössbauer spectra observed before and after heat-treatments at 300 °C in vacuum. From precise examination of the change in absolute intensities of the absorption lines, both of Fe's giving the quadrupole doublet D-1 and those giving D-2 (see text) are assigned to Fe's substituted for Cu's in the chain site. The heat-treated sample undergoes the magnetic transition at about 10 K which is nearly the same as the transition temperature for the as-prepared sample. On the basis of this fact, we infer that fluctuations of Cu's in the plane site play an important role for inducing the magnetic order.

Many researchers have suspected that Cu spin fluctuations take part in the origin of the superconductivity of high  $T_c$  superconductors. We have applied Mössbauer technique to Fe-doped  $\text{YBa}_2(\text{Cu}_{1-x}\text{Fe}_x)_3\text{O}_{7-\delta}$  in order to clarify connections between superconductivity and magnetism. In a previous paper [1], we have reported the following results. (1) The superconductivity is not easily destroyed by doping Fe. The superconducting transition temperature  $T_c$  decreases gradually as the Fe concentration increases. The  $x=0.085$  sample still has  $T_c$  of  $\sim 35$  K, where  $T_c$  is defined as the temperature corresponding to 50 % drop of resistivity. (2) In the samples with  $x > 0.01$ , some magnetic transition takes place at low temperatures without destroying the superconductivity. However, it has not been definitely concluded whether the superconductivity and the magnetic order coexist really concurrently or not. At present, it has been widely accepted that Cu's in the plane site (Cu2) are responsible for the superconductivity. However, the origin of the magnetic order appearing in the Fe-doped samples has not been understood well. In order to clarify this point, it is important to assign Fe-sitting sites first. The experimental results reported so far have shown that almost all Fe's replace Cu's [2]. However, there is controversy on assignment of Fe's to several, at least four, quadrupole doublets of the Mössbauer spectra at room temperature. Recently Vera Sedykh et al examined the oxygen content dependence of relative intensities of the quadrupole doublets, and they reported that Fe's contributing to major doublets D-1 and D-2 (see Fig.1) were substituted for Cu's in the chain site (Cu1) [3]. However, as the Mössbauer absorption lines are superposed upon each other, there remain some ambiguities in assignment of the line positions. Therefore, it is desirable that Fe-sitting sites are determined without decomposing the spectra into four sets of quadrupole doublet using the Lorentzian line fitting.

In this paper, we report results obtained for the  $x=0.05$  sample by comparing the Mössbauer spectra taken before and after heat treatments at 300 °C in a vacuum of  $\sim 10^{-2}$  mmHg. This is the first report that sitting sites of Fe's contributing to D-1 and D-2 are assigned from changes induced by heat treatments in absolute intensities of the absorption lines. In extracting conclusions, we take into account the following premises.

(A) By keeping the sample at 300 °C in vacuum, only oxygens around Cu1 are removed (experimental fact [4]).

(B) At such a low temperature of 300 °C, metal atoms do not change their sitting sites (assumption).

Mössbauer absorber is a thin sintered disk ( $\sim 5 \times 2 \times 0.10 \text{ mm}^3$ ) of  $\text{YBa}_2(\text{Cu}_{0.95}\text{Fe}_{0.05})_3\text{O}_{7-\delta}$  in which about 50 % of Fe's are enriched with  $^{57}\text{Fe}$ . The heat-treatment was done as follows. The sample was put in a test-tube filled with air, and it was brought in a furnace heated to 300 °C in advance. After it was kept in the furnace for a long time enough to reach equilibrium, air in the tube was pumped out to  $\sim 10^{-2} \text{ mmHg}$ . As mentioned above, we want to observe the change in absolute intensities of the absorption lines induced by the heat-treatment. Therefore, thickness of the absorber should not be changed before and after the heat-treatment. For this requirement, we repeated the Mössbauer measurement and the heat-treatment alternately by using the same disk sample. Integrating time for which the sample was kept at 300 °C in vacuum were 2 min, 10 min (2min + 8 min) and 22 min (2 min + 8 min + 12 min). Samples for resistance measurement were prepared under the same condition as that for the Mössbauer sample. It is found that the dependence of the superconducting transition temperature  $T_c$  on the heat-treatment time is rather gentle :  $T_c$  is 55.3 K for the 22 min-heat-treated sample while 65.4 K for the as-prepared sample.

In Fig.1, we show the Mössbauer spectra at room temperature of the as-prepared sample (a), and the 10 min-heat-treated sample (b), for both of which data accumulating time was 23 hours. Total

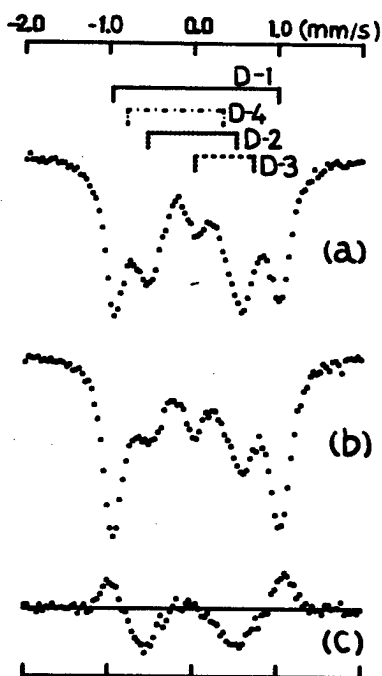


Fig. 1 Mössbauer spectra of  $\text{YBa}_2(\text{Cu}_{0.95}\text{Fe}_{0.05})_3\text{O}_{7-\delta}$  taken at room temperature before heat-treatments (a), and after heat-treatments at 300 °C in vacuum for 10 min (b). Data for each sample were accumulated for 23 hours. The positions of four quadrupole doublets are also shown at the top. (c) The difference spectra obtained by subtracting the spectra in (b) from those in (a).

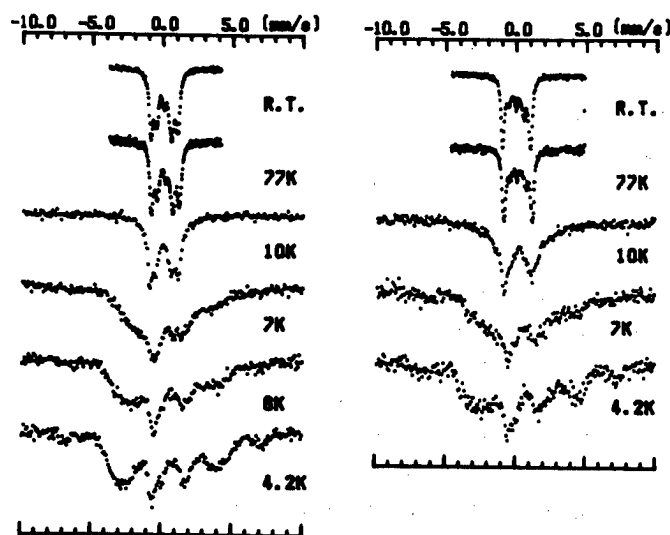


Fig. 2 Mössbauer spectra of  $\text{YBa}_2(\text{Cu}_{0.95}\text{Fe}_{0.05})_3\text{O}_{7-\delta}$  at several temperatures : (a) As-prepared sample, and (b) 22 min-heat-treated sample.

absorption area of the former is 4.1 % and that of the latter is 3.9 %. We will comment upon this fact later. As easily seen in the figure, the relative intensity of the doublet D-2 decreases while that of the doublet D-1 increases. In order to investigate the difference existing between both spectra in detail, we subtracted the spectra of the 10 min-heat-treated sample from those of the as-prepared sample. We show the result of the subtraction in Fig.1 (c). It admits of no doubt that the intensity of D-2 decreases and, on the other hand, that of D-1 increases. Taking into account the premises (A) and (B) mentioned above, this fact indicates that both of Fe's contributing to D-1 and those to D-2 are substituted for Cu1's. The fact that the intensity of D-1 increases after the heat-treatment indicates that Fe's with less oxygen coordinations give D-1. Let us look at Fig.1(c) carefully. One can find that the amount of increase of the intensity near D-1 is less than the amount of decrease of the intensity near D-2 by 35 %. This difference is consistent with the decrease of the total absorption area after the heat-treatment. It is improvable that some of Fe's are removed by the heat-treatment. Accordingly, it is natural to interpret that the Mössbauer fraction of Fe's losing a large number of coordinated oxygens becomes small.

It is generally believed that oxygens are more tightly coordinated to Fe substituted for Cu1 as compared with oxygens around Cu1 itself. If it is true, a large number of oxygens around Cu1 might be removed by the heat-treatment. Therefore, if Cu1's play an important role in forming the magnetic order at low temperatures, the heat-treatment might largely modify the magnetic property. We show in Fig.2 the temperature variations of the Mössbauer spectra of the as-prepared and the 22 min-heat-treated samples. One can see in the spectra of the latter at room temperature that the intensity of D-2 greatly decreases. This indicates that a large amount of oxygens around Cu1's are removed during the heat-treatment for 22 min. In spite of such the large decrease of oxygen content around Cu1 site, it is noticed that in the 22 min-heat-treated sample the magnetic broadening sets in around 10 K which is very close to a temperature where the magnetic broadening appears in the as-prepared sample. Therefore, the origin of the magnetic order is difficult to attribute to Cu1. Some researchers have interpreted that the doped Fe's tend to form clusters and those clusters undergo magnetic transitions at low temperatures. However, this possibility is also denied by the present work. The reason is that the magnetic transition temperature is not affected by large change of the local environment around Fe's induced by the heat-treatment. Putting all the discussion mentioned above together, we come to the conclusion that Cu's in the plane site play an important part in forming the magnetic order appearing in the Fe-doped samples. As far as we know, however, any evidence has not been reported on magnetic orders of Cu2's both in the undoped sample and the Fe-doped samples. Therefore, fluctuations of Cu2 spins are considered to play an important role for inducing the magnetic order in the Fe-doped samples. It is widely accepted that Cu2's take the leading role in inducing the superconducting transition. At present, however, it has not been known at all whether superconducting electrons behave simultaneously as magnetic electrons or not. This is one of the important questions to be solved in future.

Acknowledgment: We are deeply indebted to Professor T.Fujita for his stimulating discussion. We are also grateful to Mrs. S. Morimoto for her helpful assistance throughout this work.

#### References

- [1] T.Tamaki, T.Komai, A.Ito, Y.Maeno and T.Fujita, Solid State Commun. 65, 43 (1988).
- [2] Y.Maeno, T.Nojima, Y.Aoki, M.Kato, K.Hoshino, A.Minami and T.Fujita, Jpn. J. Appl. Phys. 26, L774 (1987).
- [3] Vera Sedykh, Saburo Nasu and Francisco E.Fujita, Solid State Commun. 67, 1063 (1988).
- [4] J.M.Tranquada, D.E.Cox, W.Kunnmann, H.Moudden, G.Shirane, M.Suenaga, P.Zolliker, D.Vaknin, S.K.Sinha, M.S.Alvarez, A.J.Jacobson and D.C.Johnston, Phys. Rev. Lett. 60, 156 (1988).

T. Shinjo and S. Nasu\*

Institute for Chemical Research, Kyoto University, Uji, Kyoto-fu 611, Japan

\*Faculty of Engineering Sciences, Osaka University, Toyonaka 560, Japan

Mössbauer spectroscopy has been applied for  $^{57}\text{Fe}$ -doped superconducting Cu-oxides and also related non-superconducting ones. It was found that Fe impurities preferentially substitute the Cu-I (chain) sites in superconducting  $\text{YBa}_2\text{Cu}_3\text{O}_7$ . If the Fe concentration is higher than a certain percent, a magnetic order is stabilized in the chain sites, coexisting with superconductivity. However, the concentration of Fe impurities in the plain sites is very small. It appears that a magnetic order and superconductivity do not coexist on a Cu atom.

Behaviors of Fe impurities in high- $T_c$  oxides are of particular interest since Fe atoms occupy the Cu sites and magnetic properties of Cu-O system are expected to be reflected in  $^{57}\text{Fe}$  Mössbauer spectra. The understanding of magnetism in Cu-oxides is crucial for the study of superconductivity.  $^{57}\text{Fe}$  Mössbauer spectroscopy is very useful to confirm the existence of magnetic order.

Concerning  $^{57}\text{Fe}$  Mössbauer studies on  $\text{YBa}_2\text{Cu}_3\text{O}_7$ , already a great number of publications have appeared. Figure 1 shows an example of spectrum for  $^{57}\text{Fe}$  in  $\text{YBa}_2\text{Cu}_3\text{O}_7$  (Fe/Cu=2% and 8%) measured at room temperature [1]. Other investigators also get similar results and the essential features of the line profile are almost the same for all the results.[2] If we assume a superposition of three doublet spectra, a fairly good fitting is obtained. The isomer shifts for the two major components are close to  $\text{Fe}^{4+}$  values but the remaining minor one is an  $\text{Fe}^{3+}$  value. As is well known, in the structure of  $\text{YBa}_2\text{Cu}_3\text{O}_7$ , there are two Cu sites, so-called "chain" (Cu-I) and "plane" Cu(II). Then, one would naively attribute two major Mössbauer components to Fe atoms in the two Cu sites. However the site assignment cannot be so straightforward. For the site assignment, it is useful to refer the results on the magnetic properties with comparing the results on non-superconducting  $\text{YBa}_2\text{Cu}_3\text{O}_6$ . Subsequently, the present authors reach the conclusion that Fe atoms preferentially occupy the chain sites [3].

Mössbauer measurements at low temperature in the presence of a strong external field are useful to check that Fe impurities possess local magnetic moments. Figure 2 shows the result for 2% Fe sample, whose superconducting  $T_c$  ( $R=0$ ) is 78K. Zero field spectrum has no significant change from that at 300K. On the other hand, by applying an external field, we obtain a magnetically-split spectrum, whose splitting is much larger than the external field. Namely each Fe ion has a paramagnetic moment in the superconducting state. The overall splitting caused by the external field of 4.5T corresponds to about 20T. Therefore the hyper fine field of Fe ion is about 25T since the sign of the hyperfine field is usually negative.

When the Fe concentration is more than 5%, a magnetic hyperfine field appears in the spectra at 4.2K, without applying any external field. In Fig. 3, the Mössbauer spectra for a sample with 8% Fe measured in the temperature range from 25K to 0.1K are shown. Apparently the spectra indicate the existence of a magnetic order and from the disappearance of the hyperfine splitting, the magnetic transition temperature,  $T_N$ , is estimated to be 15K. Very similar patterns with the present result at 4.2K were obtained by many groups but the computer fittings did not work well to deduce a unique interpretation. For the analysis of the spectrum, it is worthwhile to refer the results on non-superconducting, oxygen-deficient  $\text{YBa}_2\text{Cu}_3\text{O}_{7-x}$ .

An oxygen-deficient sample is prepared by quenching from 900°C, which does not exhibit a superconductivity but is known to be antiferromagnetic. According to neutron diffraction studies, strong antiferromagnetic couplings exist in Cu atoms in the plane sites. Figure 4 shows the Mössbauer spectra for an oxygen-deficient sample with 8% Fe, as a function of temperature. At room temperature, the major fraction is non-magnetic but another, minor fraction is observed to have a magnetic hyperfine splitting, whose valence state is  $\text{Fe}^{3+}$ . From the temperature dependence of the magnetic splitting,  $T_N$  is determined to be 420K, which agrees well with the value of  $T_N$  from neutron diffraction studies. It is natural to attribute this fraction to the Fe atoms in the plane sites. On the other hand, the major fraction shows a magnetic splitting only below about 100K. The temperature dependence of the hyperfine field for the major part also is shown in Fig. 5. This temperature dependence is unusual, deviating remarkably from a usual Brillouin-like curve. This behavior is accounted for if the exchange field at the chain sites is much weaker than that of the plane sites. This hypothesis is supported by the result from neutron diffraction study that the Cu atoms in the chain sites are almost non-magnetic. It is concluded that Fe atoms clearly reflect the magnetic behaviors of the two Cu sites in non-superconducting (antiferromagnetic)  $\text{YBa}_2\text{Cu}_3\text{O}_{7-x}$ : The Cu-O plane is strongly antiferromagnetic but the magnetic interactions in the Cu-O chain sites are relatively weak. Perhaps, the magnetic couplings in the chain sites may be enhanced by Fe impurities.

The spectrum at 4.2K for the oxygen-deficient  $\text{YBa}_2\text{Cu}_3\text{O}_{7-x}$  is a very complicated one. However if we subtract the 6-line fraction due to the plane sites from the total absorption spectrum, the resultant is obtained as shown in Fig. 4. This profile is very similar to the spectrum at 4.2K for a superconducting sample (Fig.4), whose hyperfine field is about 25T. The two patterns have practically the same profiles and resemble also with the pattern under the external field (Fig.2). From this comparison, we can attribute the absorption in the superconducting sample to the Fe atoms in the chain sites. In Fig. 3, a fraction with a larger hyperfine field also is visible but the relative amount is very smaller than that for the major fraction. It is therefore concluded that Fe impurities in  $\text{YBa}_2\text{Cu}_3\text{O}_7$  preferentially occupy the chain sites. This seems to be the reason why  $T_c$  does not drop very rapidly with the substitution of Cu sites by the magnetic Fe impurities. In the case of 8% Fe, although  $T_c$  is 34K, the magnetic transition temperature is 15K. Apparently, a magnetic order and superconductivity coexist in the same crystal. However, the present result suggests that the magnetic

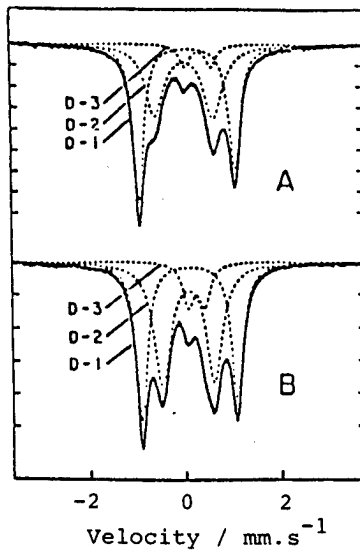


Fig.1.  $^{57}\text{Fe}$  Mössbauer spectra at 300K of Fe-doped  $\text{YBa}_2\text{Cu}_3\text{O}_7$  (Fe/Cu=2% and 8%).

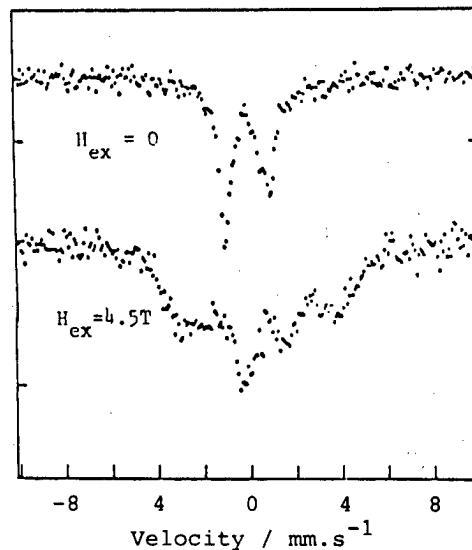


Fig.2.  $^{57}\text{Fe}$  Mössbauer spectra of Fe-doped  $\text{YBa}_2\text{Cu}_3\text{O}_7$  (Fe/Cu=2%) at 4.2K with and without an external field, 4.5T.

order is formed among Cu atoms and Fe impurities in the chain sites. The Fe concentration in the plane sites is not high enough to destroy the superconductivity. It seems probable that Cu atoms in the plane sites, involved in the superconductivity are not taking part in the magnetic order.

Mössbauer measurements on  $^{57}\text{Fe}$  and  $^{119}\text{Sn}$  impurities in  $\text{La}_2\text{CuO}_4$  and  $\text{La}(\text{Sr})_2\text{CuO}_4$  are in progress, whose results will be of interest to compare with the present results.

The authors thank to Drs. H. Kitagawa, T. Kohara, Y. Oda, K. Asayama, F. E. Fujita, T. Takabatake and M. Ishikawa.

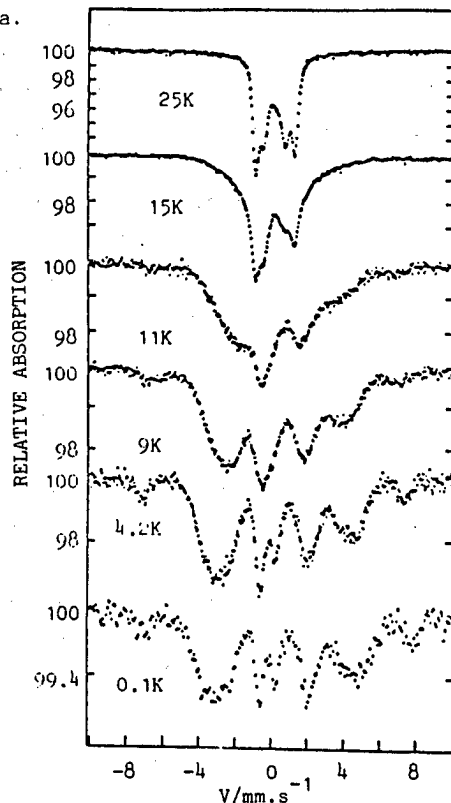


Fig.3.  $^{57}\text{Fe}$  Mössbauer spectra of Fe-doped  $\text{YBa}_2\text{Cu}_3\text{O}_7$  (Fe/Cu=8%) as a function of temperature.

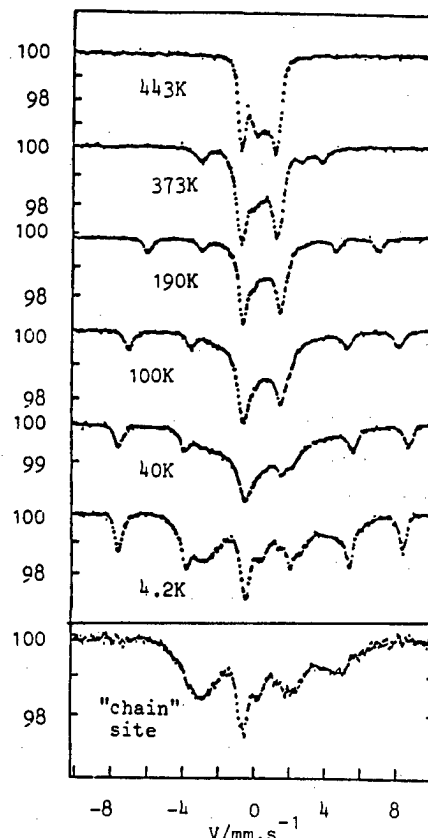


Fig.4.  $^{57}\text{Fe}$  Mössbauer spectra of an oxygen-deficient (non-superconducting) Fe-doped  $\text{YBa}_2\text{Cu}_3\text{O}_{7-x}$  as a function of temperature. The chain site spectrum is synthesized by subtracting the 6-line part from the pattern at 4.2K.

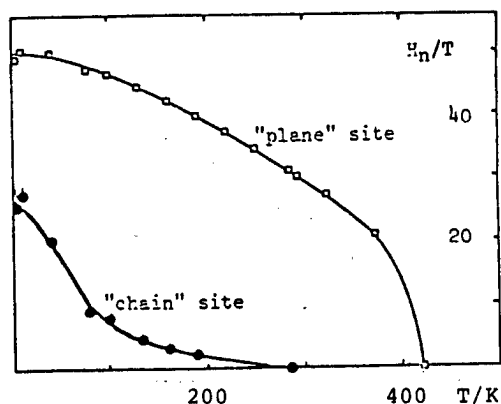


Fig.5. Temperature dependences of the two Fe hyperfine fields in an oxygen-deficient (non-superconducting)  $\text{YBa}_2\text{Cu}_3\text{O}_{7-x}$ .

#### References

- [1] S. Nasu, H. Kitagawa, Y. Oda, R. Kohara, T. Shinjo, K. Asayama and F. E. Fujita: Physica 1488 (1987) 484.
- [2] References are cited in the following review paper: T. Shinjo and S. Nasu, Proc. 2nd NEC Symp. to be published by Springer-Verlag in 1989.
- [3] T. Shinjo, S. Nasu, T. Kohara, T. Takabatake and M. Ishikawa: ICM'88 (Paris), to be published in J. de Physique.



K. Kitazawa, S. Kambe, A. Fukuoka, I. Tanaka\* and H. Kojima\*

Department of Industrial Chemistry, Faculty of Engineering, University of Tokyo

\*Institute of Inorganic Synthesis, Faculty of Engineering, Yamanashi University

Resistivity was measured parallel and perpendicular to c axis in single crystalline  $(\text{La}_{1-x}\text{Sr}_x)_2\text{CuO}_4$  ( $T_{c,\text{mid}}=37.5$  and 35K) with various configurations of current-magnetic field vs crystal orientations. The broadening of the resistive transition at the superconducting critical temperature was observed to depend only on the magnetic field vs crystal orientation but not on the magnetic field vs current orientation. This denies the flux creep mechanism to explain the significant broadening of the resistive transition commonly observed among cuprate superconductors induced under magnetic field. Involvement of superconducting fluctuation is rather suggested as the alternative mechanism.

From the early period of the studies of HTSC oxides, it has been noticed that the resistive transition is broadened significantly in these materials when a magnetic field is applied. The broadening is especially remarkable when the field is applied along the c-axis and less so perpendicular to it.<sup>1)</sup> Two mechanisms have so far been proposed. One is the so called "superconducting glass model", originally proposed by Müller and Bednorz.<sup>2,3)</sup> This assumes the presence of microscopic superconducting domains which are coupled by the Josephson junction. The size of the domains is assumed to be variable with the strength of the field. The resistivity would appear as the result of the gradual decoupling between the domains. The other is the "flux creep" model<sup>10)</sup> based on the weak pinning force exerted on vortex lines. In this model, the vortex lines are assumed to move around due to thermal activation and hence resistivity would appear even under the measurement conditions of resistivity.

Because of this phenomenon, it has been pointed out that the upper critical field  $H_{c2}$  so far reported in the cuprate superconductors should not be correct. The coherence length  $\xi$ , for instance, which has been estimated from the measurements of  $H_{c2}$ , should then be baseless also. The accurate knowledge of the extremely short  $\xi$  is one of the important clues to understand the mechanism of the HTSC. From the practical point of view, this phenomenon gives rise to a large ambiguity when to judge the value of the critical current. Small but finite resistivity is observed in most of the oxide superconductors before the major destruction of superconductivity takes place. This also seems to be related with the above stated broadening of the resistive transition. Therefore, a sound understanding of the broadening phenomenon is desired both from basic and applied research of the superconducting oxides.

The common feature of the two models proposed is that the finite resistivity appears in association with the movement of vortex lines, although the regions assigned for this motion is different; in the Josephson junction region for the superconducting glass model and in the bulk for the flux creep model. The present study, therefore, aims to examine how different the broadening is observed when the Lorentz force exerted on vortex lines is varied. Particularly, the difference in the broadening is examined when the relative orientation between the current and the magnetic field is varied. Lorentz force should be zero when the direction of the current is the same as that of magnetic field and hence the broadening should be minimized in this measurement configuration if the above described two models are to explain the phenomenon.

But, in order to conduct a precise measurement, it is essential to obtain single crystalline specimens which are sizable along c-axis because the significant broadening is observed when the magnetic field is applied in this direction.

Since a sizable and high quality single crystals of  $(\text{La}_{1-x}\text{Sr}_x)_2\text{CuO}_4$  have been grown by the TSFZ (traveling solvent floating zone) method recently by two of the authors, Tanaka and Kojima<sup>4)</sup>, we have measured the resistivity along the c-axis as well as perpendicular to it in these crystals

under magnetic field and compared the results in the various measurement configuration.

Specimens of size about  $0.2 \times 1.5 \times 5 \text{ mm}^3$  were cut out of the as grown single crystalline boule with the longer axis in the c (sample c) and in the a (sample a) direction. The resistivity was measured by the standard d.c. four probe method with epoxy-silver paste electrodes under magnetic field up to 5T. Because of the large size of the specimens both parallel and perpendicular to c axis, respectively, the resistivity could be measured unambiguously in both of the directions. No significant change was observed in the result before and after the annealing of the specimens in  $\text{O}_2$  at  $750^\circ\text{C}$  for three weeks. The resistivity did not depend upon the measurement current up to 10 mA and hence the following results were taken at the current level of 1mA.

The metal-to-semiconductor transition observed in the c-axis resistivity has been reported elsewhere.<sup>5)</sup> The resistivity-temperature curves both along a- and c-axis under various magnetic field are shown in Figs. 1 to 4. There are no significant magneto-resistance observed above  $T_c$ . The most remarkable features observed in Figs. 1 to 4 are:

- 1) The transition is broadened significantly for the configurations, (I/c, H//c) and (I//c, H//c) but not for (I/c, H/c) or (I//c, H/c).
- 2) The width of the broadening is about the same for the configurations I/c and I//c as far as the magnetic field direction is fixed relative to the crystal orientation.
- 3) The change in the  $\rho$ -T curves for H/c configuration is rather a parallel shift towards low T as H is intensified. This is similar to that observed in conventional metallic superconductors.
- 4) The absolute resistivity values are about  $10^{-4} \Omega\text{cm}$  perpendicular to c-axis while it is about  $10^{-1} \Omega\text{cm}$  in c-direction. This remarkably large anisotropy, however, dose not seem to affect the width of the broadening as stated in 2).

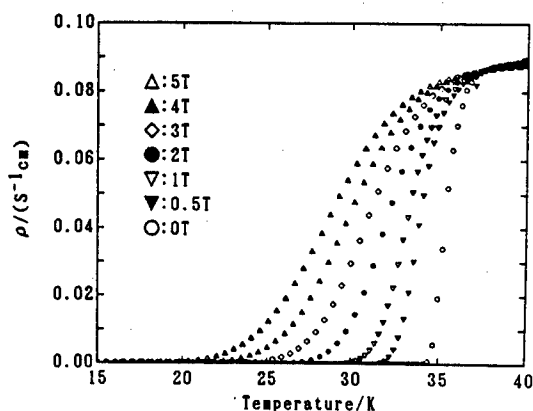


Fig. 1 Resistivity vs. temperature curves for I/c and H//c(I//H) configuration

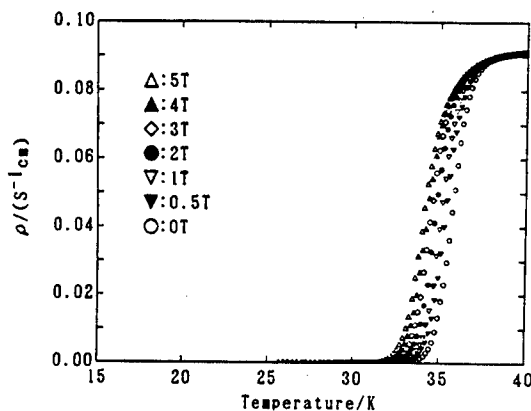


Fig. 2 Resistivity vs. temperature curves for I//c and H/c(I//H) configuration

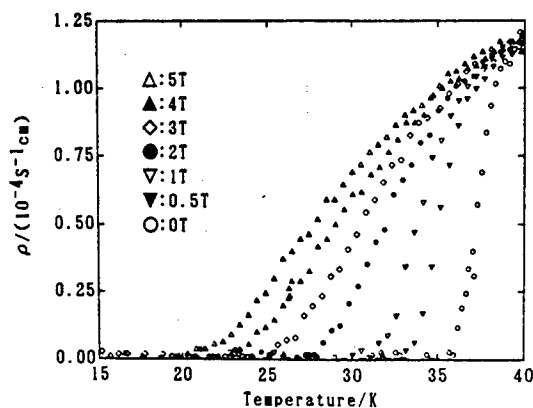


Fig. 3 Resistivity vs. temperature curves for I/c and H//c(I//H) configuration

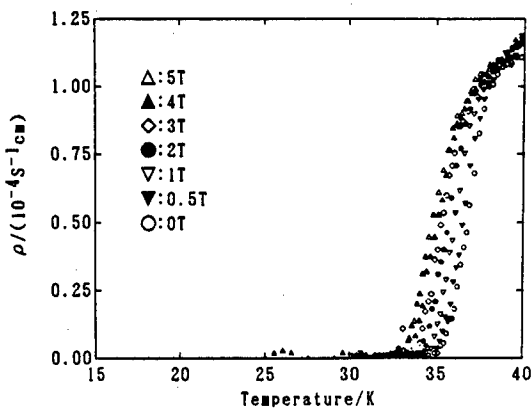


Fig. 4 Resistivity vs. temperature curves for I/c and H/c(I//H) configuration

From the above observations, we can conclude as in the following. At first, the broadening in the resistive transition is determined by the relative orientation between the magnetic field and crystal, but not by the direction of the measurement current. Namely the phenomenon is essentially the same for the configurations;  $H//I$  and  $H \perp I$ . This leads to the conclusion that Lorentz force is not involved in the broadening mechanism. Hence, the two proposed models "superconducting glass" or "flux creep" should not be able to explain the broadening of the resistive transition.

Therefore, one has to seek another model to interpret the broadening phenomenon. In this model, the vortex motion should not be the mechanism to give rise to the finite resistivity. Besides, the phenomenon is essentially determined only by the intensity and the direction of the magnetic field relative to the crystal orientation. Furthermore, the  $\rho$ - $T$  curve both along the  $c$ -axis and perpendicular to it are affected to a similar extent.

Essentially, there seems to be two different approaches to explain the origin of the broadening in the  $\rho$ - $T$  curves under magnetic field. One is to assume the energy dissipation to occur by the motion of vortex lines perpendicular to the current direction. But this approach has clearly been denied by the present study. The other conceivable approach is to assume the presence of normal as well as superconducting regions, simultaneously. The latter approach may be classified essentially into two models; the one to assume the built-in inhomogeneity in the superconducting oxide and the other to assume the appearance of the normal and superconducting regions in the homogeneous electronic system as the consequence of the thermodynamical fluctuation. The model to assume the built-in inhomogeneity cannot be completely excluded at the current moment. But the rather homogeneous flattening of the  $\rho$ - $T$  curve under a magnetic field as observed in Figs. 1 and 3 seem to be rather difficult to be successfully explained by the material inhomogeneity. The thermodynamical fluctuation model,<sup>6-9)</sup> on the other hand, seems to be quite attractive if the extremely short coherence length and the two dimensional nature of the electronic structure are taken into account. Theoretically, however, the fluctuation model has not been fully developed. Presently, the theories can only treat with the temperature regions well above the critical region and besides it is rather arbitrary to assign the mean field critical temperature for such a case as the present one in which the transition is not sharp but significantly broadened. Therefore, it does not seem to be likely that one can identify the model by the fitting of the  $\rho$ - $T$  curves to the currently available model.

In summary, making use of a sizable single crystal of  $(La_{1-x}Sr_x)_2CuO_4$ , we have been able to conduct a reliable and precise measurement of  $\rho//c$  as well as  $\rho \perp c$ . Comparing the  $\rho$ - $T$  curves under various magnetic field and in various crystal orientation, it turned out that the broadening of the resistive transition does not depend on the relative orientation between  $H$  and  $I$  but does depend solely on the crystal orientation relative to  $H$ . Consequently, we conclude that the proposed models; "superconducting glass" and "flux creep" cannot explain the broadening phenomenon in the resistive transition under magnetic field.

#### References

- 1) Y. Iye, T. Tamegai, T. Sakakibara, T. Goto, N. Miura, H. Takeya and H. Takei, *Physica*, **153-155** (1988) 26.
- 2) K. A. Muller, K. W. Blazey, J. G. Bednorz and M. Takashige, *Physica* **148B** (1987) 149.
- 3) I. Morgenstern, K. A. Müller and J. G. Bednorz, *Physica* **C153-155** (1988) 59.
- 4) I. Tanaka and H. Kojima, *Nature* (1989) in print
- 5) K. Kitazawa, K. Kambe, A. Fukuoka, M. Naito, I. Tanaka and H. Kojima, submitted to *Jpn. J. Appl. Phys.*
- 6) J. Lawrence and S. Doniach, in *Proc. 12th Int. Conf. Low Temp. Phys. Kyoto*, 1970 (Keigaku, Tokyo, 1971) p.361
- 7) D. E. Prober, M. R. Beaseley and R. E. Schwall, *Phys. Rev.* **B15** (1977) 5245
- 8) S. Hikami and A. I. Larkin, *Mod. Phys. Lett.* **B2** (1988) 693
- 9) R. Ikeda, T. Ohmi and T. Tsuneto, preprint
- 10) Y. Yeshurun and A. P. Malozemoff, *Phys. Rev. Lett.* **22**(1988)2202;  
M. Tinkham, *Phys. Rev. Lett.* **61**(1988)1658

# Growth and Superconducting Properties of Single-Crystal $\text{Bi}_2\text{Sr}_2\text{CaCu}_2\text{O}_8$

Y. Koike, T. Nakanomyo, N. Kobayashi and T. Fukase

Institute for Materials Research, Tohoku University,  
2-1-1 Katahira, Sendai 980, Japan

Single crystals of  $\text{Bi}_2\text{Sr}_2\text{CaCu}_2\text{O}_8$  have been prepared with a CuO flux method.  $T_c$  is 80.6 K and the anisotropy of  $H_{c2}$  is over 9-19. The value of  $H_{c2}^{\perp}(0)$  for  $H \perp c$ -axis is estimated to be over 270-400 T. The coherence length along the  $c$ -axis at 0 K,  $\xi_{\parallel}(0)$ , is as small as 2.1-3.6 Å, suggesting quasi-two-dimensional superconductivity. Superconducting fluctuation and flux creep are markedly observed because of the short coherence length.

Experimental studies on high- $T_c$  oxide superconductors are made using sintered samples at first, but experiments using single crystals are indispensable for definitive or detailed studies. Here, we report a simple growth method of single crystals of  $\text{Bi}_2\text{Sr}_2\text{CaCu}_2\text{O}_8$  and their superconducting properties.<sup>1)</sup>

Single crystals of  $\text{Bi}_2\text{Sr}_2\text{CaCu}_2\text{O}_8$  were grown from molten Bi-Sr-Ca-Cu-O oxide compounds using excess CuO as flux. The raw materials of  $\text{Bi}_2\text{O}_3$ ,  $\text{SrCO}_3$ ,  $\text{CaCO}_3$  and CuO powders were mixed in the molar ratio of Bi:Sr:Ca:Cu = 1:1:1:2 and pelletized, followed by firing in air between 800°C and 870°C. After pulverization, the sintered material was mixed with CuO powder in the molar ratio of  $\text{BiSrCaCu}_2\text{O}_y$ :CuO = 1:3, pelletized and heated in an alumina crucible. The heat treatment was as follows: heating to 1200°C, maintaining at 1200°C for 5 hours, cooling to 800°C at the very slow rate of -5°C/h and cooling to room temperature at a rate slower than -70°C/h. Flaky single crystals with dimensions of the order of  $1 \times 1 \times 0.1 \text{ mm}^3$  were obtained. They were easily cloven similarly to other layered compounds, but it was difficult to obtain a sizable part of the single crystal from the ingot. The composition of the single crystals was estimated from EPMA to be  $\text{Bi}_2\text{Sr}_2\text{CaCu}_2\text{O}_8$ , corresponding to the low- $T_c$  phase of the Bi-Sr-Ca-Cu-O system.

Superconducting transition of the single crystals was measured resistively by a standard dc four-point probe method with an excitation current of 0.1 mA flowing perpendicular to the  $c$ -axis (parallel to the layer plane). Electrical contacts were made using conductive silver paste. Magnetic fields up to 21 T were applied by the hybrid magnet HM-2 at HFLSM, IMR, Tohoku University. Temperature measurements were made with Pt and carbon-glass thermometers calibrated in the absence and presence of the magnetic field.

Figure 1 shows the temperature dependence of the resistivity  $\rho$  of a single-crystal sample. A sharp superconducting transition is observed. The transition temperature  $T_c$ , defined at the midpoint of the transition curve, is 80.6 K and the zero-resistance temperature is 77 K. In the high temperature region  $T$ -linear

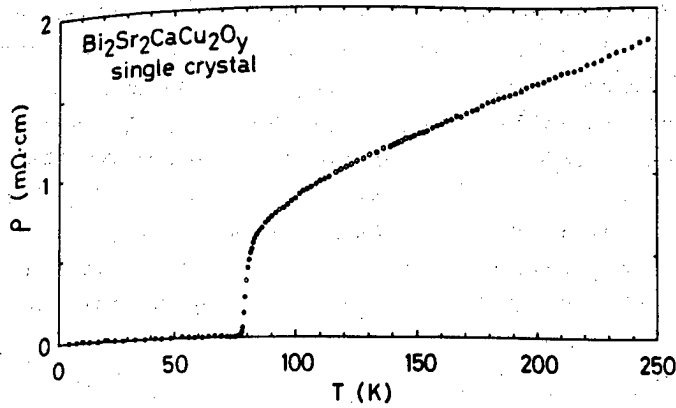


Fig. 1. Temperature dependence of the resistivity.

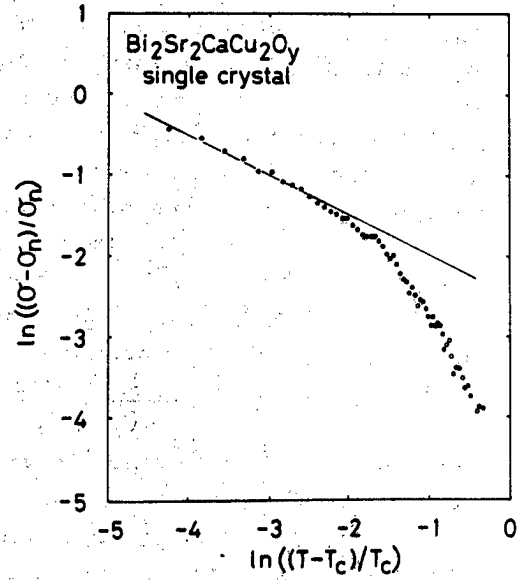


Fig. 2. Temperature dependence of the excess conductivity. The solid line is the prediction of the theory for three-dimensional systems.

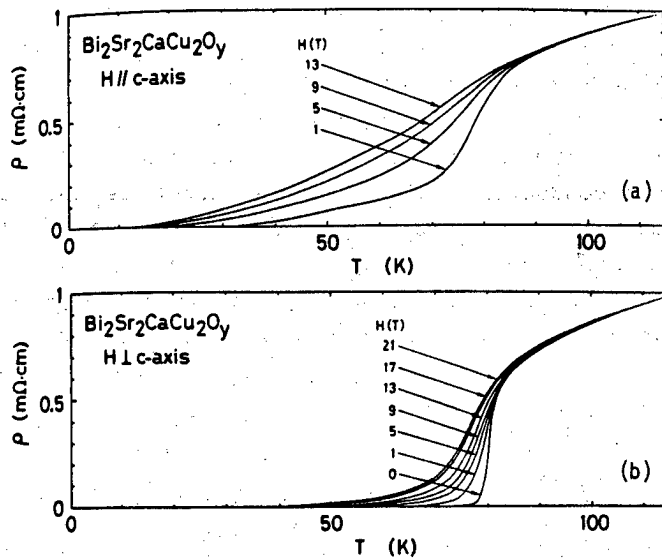


Fig. 3. Superconducting transition in various magnetic fields. (a) for  $H \parallel c$ -axis, (b) for  $H \perp c$ -axis.

Table I. Superconducting parameters of high- $T_c$  oxide superconductors.

	$\text{Bi}_2\text{Sr}_2\text{CaCu}_2\text{O}_8$	$\text{YBa}_2\text{Cu}_3\text{O}_7$ <sup>3)</sup>	$(\text{La}_{1-x}\text{Sr}_x)_2\text{CuO}_4$ <sup>4)</sup>
$T_c$	80.6 K	79 K	30 K
$-dH_{c2}^{\perp}/dT$	4.9-7.3 T/K	2.7 T/K	4 T/K
$-dH_{c2}^{\parallel}/dT$	0.39-0.55 T/K	0.52 T/K	0.3 T/K
$H_{c2}^{\perp}/H_{c2}^{\parallel}$	9-19	5.1	13
$m_{\parallel}/m_{\perp}$	80-360	26	170
$H_{c2}^{\perp}(0)$	270-400 T	40 T	83 T
$H_{c2}^{\parallel}(0)$	21-29 T	28 T	6 T
$H_p(0)$	150 T	150 T	55 T
$\xi_{\perp}(0)$	34-40 Å	35 Å	74 Å
$\xi_{\parallel}(0)$	2.1-3.6 Å	6.8 Å	5.4 Å
$s$	8.8 Å	3.3 Å	1.8 Å
$r$	0.29-0.85	22	46

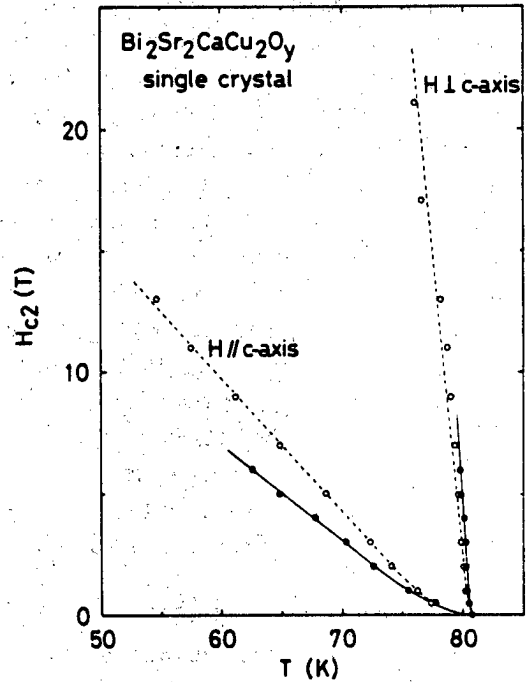


Fig. 4. Temperature dependence of the upper critical field. Open and closed circles correspond to different samples.

dependence of  $\rho$  is observed. The resistivity begins to deviate from the T-linear dependence about 150 K far from  $T_c$ . This is considered to be due to the enhancement of the superconducting fluctuation originating from the two-dimensional crystal structure and the very short coherence length. The excess conductivity over the normal conductivity  $\sigma_n$ , which is the inverse of the extrapolated value of the T-linear part of  $\rho$  in the high temperature region, is shown as a function of reduced temperature in Fig. 2. In the vicinity of  $T_c$ , the excess conductivity  $\sigma - \sigma_n$  is proportional to  $(T - T_c)^{-1/2}$ . This suggests that the superconducting fluctuation in the vicinity of  $T_c$  is three-dimensional. According to the theory by Aslamazov and Larkin<sup>2)</sup>, the excess conductivity in the three-dimensional system is given by

$$\sigma - \sigma_n = \frac{e^2}{32\hbar\xi(0)} \left( \frac{T - T_c}{T_c} \right)^{-1/2}, \quad (1)$$

where  $\xi(0)$  is the coherence length at 0 K. From eq. (1),  $\xi(0)$  of  $\text{Bi}_2\text{Sr}_2\text{CaCu}_2\text{O}_8$  is estimated to be 14 Å.

The superconducting transition in constant magnetic fields is very anisotropic, as shown in Fig. 3. The temperature dependence of the upper critical field  $H_{c2}$ , defined at the midpoint of the transition curve in various constant magnetic fields, is shown in Fig. 4. The  $H_{c2}$  vs  $T$  for  $H \parallel c$ -axis shows positive curvature near  $T_c$ . This is often observed for layered superconductors, although the reason is not yet clarified. Various parameters obtained from our measurements are shown in Table I. Those of  $\text{YBa}_2\text{Cu}_3\text{O}_7$ <sup>3)</sup> and  $(\text{La}_{1-x}\text{Sr}_x)_2\text{CuO}_4$ <sup>4)</sup> are also listed for reference. The anisotropy of  $H_{c2}$  is as large as 9-19. This is the minimum value and the anisotropy will become larger by more careful sample alignment. In any case, the anisotropy is larger than 5.1 of  $\text{YBa}_2\text{Cu}_3\text{O}_7$ . This may be reasonably understood as due to the crystallographic anisotropy, because  $\text{Bi}_2\text{Sr}_2\text{CaCu}_2\text{O}_8$  has a more two-dimensional structure where double perovskite layers are much separated by double bismuth-oxide layers. The upper critical field at 0 K,  $H_{c2}(0)$ , is roughly estimated using the relation  $H_{c2}(0) = 0.69T_c |dH_{c2}/dT|_{T_c}$  given by the Werthamer-Helfand-Hohenberg theory<sup>5)</sup> for type II superconductivity in the dirty limit. The value of  $H_{c2}^\perp(0)$  is estimated as 270-400 T for  $H \perp c$ -axis. So far as we know, this is the highest value among those of various kinds of superconductors. This value exceeds the Pauli paramagnetic limiting field  $H_p(0) = 150$  T, calculated from the equation  $H_p(0) = 1.84T_c$  where  $H_p(0)$  and  $T_c$  are in the units of T and K, respectively. The coherence lengths at 0 K,  $\xi_{||}(0)$  along the c-axis and  $\xi_\perp(0)$  perpendicular to the c-axis, are estimated as listed in Table I from the following equation<sup>6)</sup>:  $H_{c2}^\perp(0) = \phi_0/2\pi\xi_\perp^2(0)$  and  $H_{c2}^\parallel(0) = \phi_0/2\pi\xi_{||}(0)\xi_\perp(0)$ , where  $\phi_0$  is the superconducting flux quantum. The value of  $(\xi_\perp(0)\xi_{||}(0))^{1/3}$  is 13-18 Å, which is in good correspondence with  $\xi(0)$  estimated from the excess conductivity due to the superconducting fluctuation as mentioned before. The value of  $\xi_{||}(0)$  is 2.1-3.6 Å and much smaller than the spacing between perovskite layers  $s = 8.8$  Å for  $\text{Bi}_2\text{Sr}_2\text{CaCu}_2\text{O}_8$ . The parameter  $\gamma$  given by

$$\gamma = \frac{4}{\pi} \left( \frac{\xi_{||}(0)}{s/2} \right)^2, \quad (2)$$

characterizing the relative two-dimensionality of the superconductivity, is much smaller than those of  $\text{YBa}_2\text{Cu}_3\text{O}_7$  and  $(\text{La}_{1-x}\text{Sr}_x)_2\text{CuO}_4$  as listed in Table I and moreover smaller than the unity. This suggests that dimensional crossover<sup>7)</sup> from three-dimensional superconductivity to quasi-two-dimensional one may occur with decreasing temperature in this compounds. The dimensional crossover, which is characterized by the divergent increase of  $H_{c2}^\perp$ , is expected to appear at  $H_{c2}^\perp = 4.5 - 9.5$  T where  $\xi_{||}(T)$

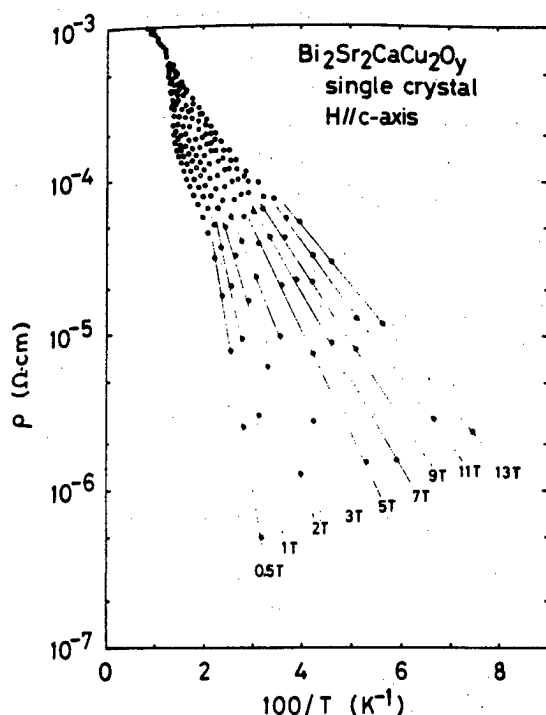


Fig. 5. Plot of  $\ln \rho$  vs  $T^{-1}$  for various magnetic fields parallel to the c-axis. The activation energy  $U_0$  is given by the slopes of the solid lines.

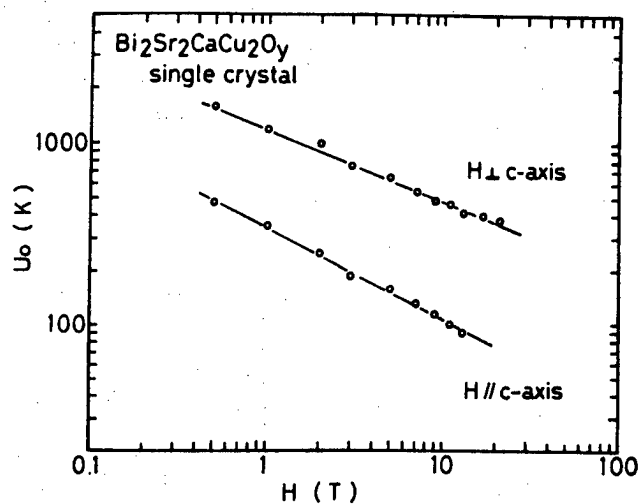


Fig. 6. Magnetic field dependence of the activation energy  $U_0$ .

$= s/\sqrt{2}$ . Unfortunately, such a symptom is not observed with our experimental accuracy. More detailed work may be necessary. It is also of great interest to measure  $H_{c2}^{\perp}$  in magnetic fields that are as high as possible and to investigate the competition between the quasi-two-dimensional superconductivity and the Pauli paramagnetic limit.

In the superconducting transition in constant magnetic fields, it is remarkable that the tail of  $\rho$  is much broader than that of single-crystal  $\text{YBa}_2\text{Cu}_3\text{O}_7$ . As shown in Fig. 5, the tail of  $\rho$  is well expressed as  $\rho = \rho_0 \exp(-U_0/T)$ , which was indicated by Palstra et al.<sup>8)</sup> Therefore, this broadness may be not due to some inhomogeneity in single crystals but due to flux creep. Magnetic field dependence of the activation energy  $U_0$  is shown in Fig. 6.  $U_0$  is roughly proportional to  $H^{-0.5}$  for  $H \parallel$  c-axis and  $H^{-0.4}$  for  $H \perp$  c-axis. It may be reasonable that flux creep is important in this superconductor, because  $U_0$  is small on account of the short coherence length and because measured temperature  $T$  is higher than that for ordinary superconductors. Detailed study is under way to obtain a better understanding.

The authors thank Professor S. Hayashi for EPMA measurements. They are also indebted to Professor Y. Muto and the staff of HFLSM for the use of the high magnetic field facilities at HFLSM, IMR, Tohoku University.

- 1) Y.Koike, T.Nakanomyo and T.Fukase, Jpn. J. Appl. Phys. **27**(1988)L841.
- 2) L.G.Aslamazov and A.I.Larkin, Phys. Lett. **26A**(1968)238.
- 3) S.Hayashi, H.Komatsu, T.Inoue, T.Ōno, K.Sasaki, Y.Koike and T.Fukase, Jpn. J. Appl. Phys. **26**(1987)L1197.
- 4) Y.Hidaka, Y.Enomoto, M.Suzuki, M.Oda and T.

- Murakami, Jpn. J. Appl. Phys. **26**(1987)L377.
- 5) N.R.Werthamer, E.Helfand and P.C.Hohenberg, Phys. Rev. **295**.
- 6) D.R.Tilley, Proc. Phys. Soc. **85**(1965)1177.
- 7) R.A.Klemm, A.Luther and M.R.Beasley, Phys. Rev. **B12**(1975)877.
- 8) T.T.M.Palstra, B.Batlogg, L.F.Schneemeyer and J.V.Waszczyk, Phys. Rev. Lett. **61**(1988)1662.

# Thermally Activated Behavior in $\text{YBa}_2\text{Cu}_3\text{O}_z$ and $\text{Bi}_2(\text{Sr,Ca})_3\text{Cu}_2\text{O}_z$ Films

N. Kobayashi, H. Iwasaki, H. Kawabe\*, K. Watanabe, H. Yamane,  
H. Kurosawa\*\*, H. Masumoto, T. Hirai and Y. Muto

Institute for Materials Research, Tohoku University  
Katahira 2-1-1, Sendai 980

\*TATSUTA Electric Wire & Cable Co., Ltd.  
Iwatacho 2-3-1, Higashi-osaka, Osaka 579

\*\*RIKEN Co. Kumagaya 810, Kumagaya 360

Electrical resistance of  $\text{YBa}_2\text{Cu}_3\text{O}_z$  and  $\text{Bi}_2(\text{Sr,Ca})_3\text{Cu}_2\text{O}_z$  CVD films in the mixed state was investigated in magnetic fields up to 25 T. Thermally activated behavior in low resistance portion was observed for both films. The activation energy is larger in  $\text{YBa}_2\text{Cu}_3\text{O}_z$  film. It also depends on the magnetic field strength and becomes smaller with increasing field. This behavior is discussed based on the flux creep model.

In high temperature superconducting oxides, following characteristic features have been observed under the magnetic fields: i) the upper critical field,  $H_{c2}$ , has a positive curvature at low fields below 10T, ii) the resistive transition is prominently broadened by applying magnetic fields, and iii) the temperature dependence of the resistance shows a thermally activated behavior at low temperature side in the resistive transition<sup>1)</sup>. These behaviors were related with the very short coherence length in high  $T_c$  oxide superconductors and tried to explain theoretically in terms of superconducting fluctuation<sup>2)</sup> or giant flux creep.<sup>3)</sup>

In this report, we describe the temperature and magnetic field dependences of the electrical resistance of chemically deposited  $\text{YBa}_2\text{Cu}_3\text{O}_z$  and  $\text{Bi}_2(\text{Sr,Ca})_3\text{Cu}_2\text{O}_z$  films in the mixed state and discuss the origin of the broadening in the resistive transition.

Preparation of the samples was described elsewhere.<sup>4,5)</sup>  $\text{YBa}_2\text{Cu}_3\text{O}_z$  and  $\text{Bi}_2(\text{Sr,Ca})_3\text{Cu}_2\text{O}_z$  films were prepared by a chemical vapor deposition (CVD) technique on  $\text{SrTiO}_3$  (100) and  $\text{MgO}$ (100) single crystal substrates, respectively. X-ray diffraction pattern indicated preferred orientation of the c-axis perpendicular to the substrates for both samples.  $\text{Bi}_2(\text{Sr,Ca})_3\text{Cu}_2\text{O}_z$  film contains a small amount of unidentified phases in addition to the main phase with  $c = 30.6\text{\AA}$  (low  $T_c$  phase), while  $\text{YBa}_2\text{Cu}_3\text{O}_z$  film is composed only by single phase with  $c = 11.67\text{\AA}$ .

The electrical resistance was measured by a usual four probe method in constant magnetic fields up to 25 T, using a hybrid magnet or a superconducting magnet. The electrical probe was attached by ultrasonic soldering or pressing indium. The resistivities of the samples used in this study are about  $1.3\text{m}\Omega\text{cm}$  and  $2.3\text{m}\Omega\text{cm}$  at room temperature for  $\text{YBa}_2\text{Cu}_3\text{O}_z$  and  $\text{Bi}_2(\text{Sr,Ca})_3\text{Cu}_2\text{O}_z$ , respectively. The temperature was measured by a carbon-glass resistance thermometer and corrections for its magnetoresistance were done.



Figure 1 shows the temperature dependence of the electrical sheet resistance for  $\text{YBa}_2\text{Cu}_3\text{O}_z$  in magnetic fields perpendicular and parallel to the c-axis. The resistive transition in zero field is rather sharp, while those in magnetic fields are pretty broad even when the magnetic field is perpendicular to the c-axis. For the fields parallel to the c-axis, the broadness in transitions is quite large. If we define the value of  $H_{c2}$  by the end point of the resistive transition, the slopes of  $H_{c2}$  near  $T_c$  are given to be  $-3.0 \text{ T/K}$  and  $-0.85 \text{ T/K}$  for the fields perpendicular and parallel to the c-axis, respectively. These results are quite similar to results for a single crystal reported by Iye et al.<sup>6)</sup>

The electrical sheet resistance for the  $\text{Bi}_2(\text{Sr,Ca})_3\text{Cu}_2\text{O}_z$  film is shown in Fig. 2. The broadness in the resistive transition becomes more significant. Particularly, in the low resistance portion, a tail of the resistance, which is slowly varying over the wide temperature range, is found for both directions of magnetic fields. Similar results have been also reported in single crystal samples.<sup>1)</sup> In this film, we cannot define  $H_{c2}$  by the end point of the resistive transition, then we define by the mid-point of the normal resistance extrapolated from above  $T_c$ . The slopes of  $H_{c2}$  near  $T_c$  are estimated to be  $-7 \text{ T/K}$  and  $-0.8 \text{ T/K}$  for the fields perpendicular and parallel to the c-axis, respectively.

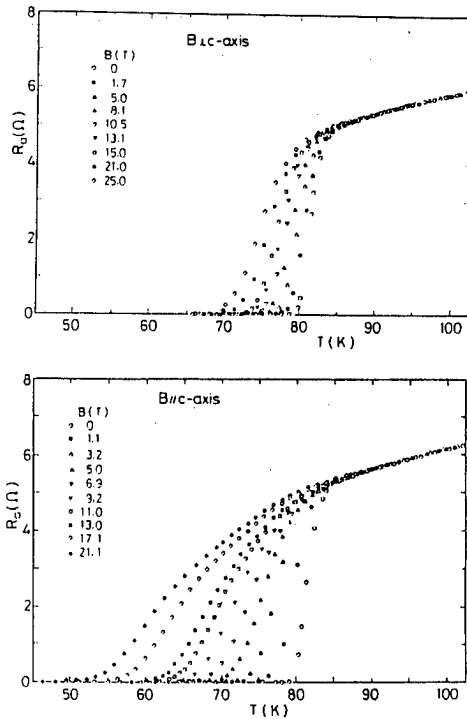


Fig. 1 Resistive transition of  $\text{YBa}_2\text{Cu}_3\text{O}_z$  in various magnetic fields

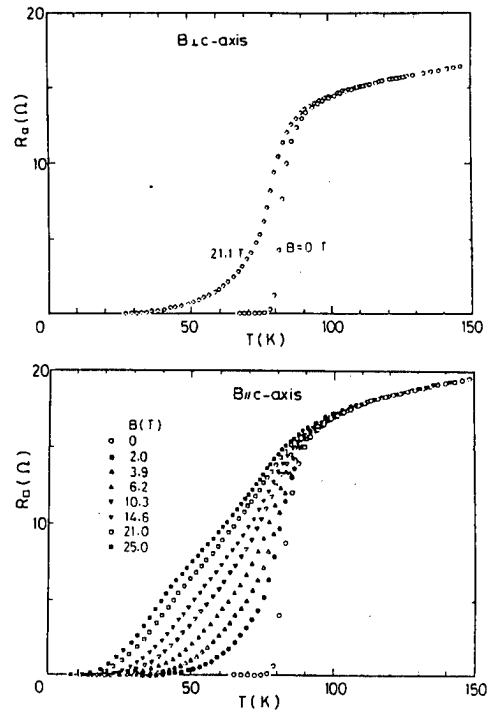


Fig. 2 Resistive transition of  $\text{Bi}_2(\text{Sr,Ca})_3\text{Cu}_2\text{O}_z$  in various magnetic fields.

The data in low resistance portion are replotted as  $\log R_\square$  versus  $T^{-1}$  in Figs. 3 [ $\text{YBa}_2\text{Cu}_3\text{O}_z$ ] and 4 [ $\text{Bi}_2(\text{Sr,Ca})_3\text{Cu}_2\text{O}_z$ ]. As can be seen in these figures, the resistance depends exponentially on  $T^{-1}$  over the wide resistance range, showing a thermally activated behavior:

$$R_\square = R_0 \exp(-U_0/kT), \quad (1)$$

where  $U_0$  is a kind of activation energy. The value of  $U_0$  is estimated from the linear portion in figures. Its value depends on the magnetic field strength. In

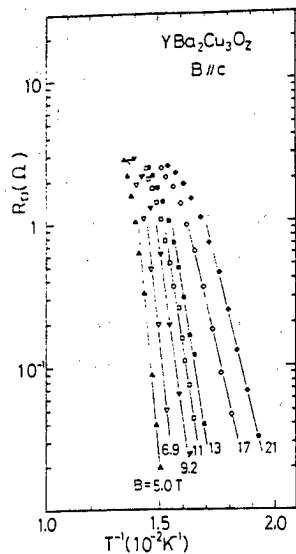


Fig. 3 Semilogarithmic plot of the resistance of  $\text{YBa}_2\text{Cu}_3\text{O}_z$  against  $1/T$ .

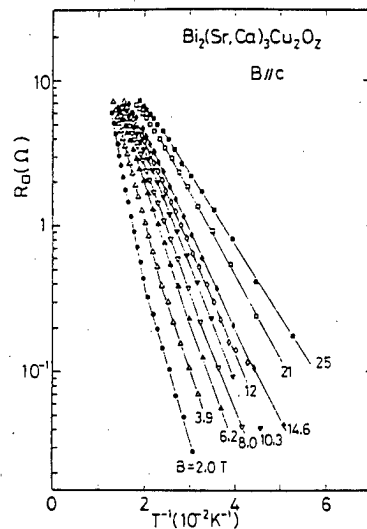


Fig. 4 Semilogarithmic plot of the resistance of  $\text{Bi}_2(\text{Sr,Ca})_3\text{Cu}_2\text{O}_z$  against  $1/T$ .

$\text{Bi}_2(\text{Sr,Ca})_3\text{Cu}_2\text{O}_z$  film, the value of  $\log R_0$  for lower fields below 8 T has two linear parts against  $T^{-1}$ , depending on the magnitude of resistance. This suggests the existence of two kinds of  $U_0$ . A similar analysis is performed on the resistance for  $\text{B}_{1c}$ -axis. The result, however, does not follow eq.(1) in our study.

Figure 5 shows the activation energy  $U_0$  as a function of the magnetic field parallel to the c-axis for both films. The dashed line represents the result for  $\text{Bi}_{2.2}\text{Sr}_{2.0}\text{Ca}_{0.8}\text{Cu}_2\text{O}_{8+\delta}$  single crystal reported by Palstra et al.<sup>1)</sup> Our result for  $\text{Bi}_2(\text{Sr,Ca})_3\text{Cu}_2\text{O}_z$  film is qualitatively agreement with their result. As can be seen in this figure, the values of  $U_0$  are expressed by a power law of  $U_0 \propto B^{-\alpha}$  with various exponent  $\alpha$ . For  $\text{YBa}_2\text{Cu}_3\text{O}_z$  film, we get a expression  $U_0 = 1.6 \times 10^4 B^{-0.77}$ . Moreover, we find two expressions for  $\text{Bi}_2(\text{Sr,Ca})_3\text{Cu}_2\text{O}_z$ , depending on the magnetic field strength:  $U_0 = 5.2 \times 10^2 B^{-0.46}$  for  $2 \leq B \leq 25\text{T}$  and  $U_0 = 2.7 \times 10^2 B^{-0.2}$  for  $B \leq 10\text{T}$ . The activation energy is much larger for  $\text{YBa}_2\text{Cu}_3\text{O}_z$  than for  $\text{Bi}_2(\text{Sr,Ca})_3\text{Cu}_2\text{O}_z$ . This may be related with the shorter coherence length in the Bi based oxide.

In a flux creep model, a flux line can thermally hop out of a potential well over

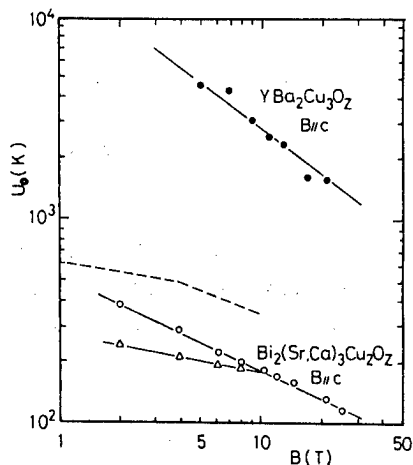


Fig. 5 Magnetic field dependence of the activation energy.

the energy barrier  $U_0$ . The hopping rate is, then, given by  $\nu = \nu_0 \exp(-U_0/kT)$ , where  $\nu_0$  is some characteristic frequency of the flux line vibration. The resistance caused by the flux creep was theoretically treated by Tinkham<sup>7)</sup> and by Dew-Hughes.<sup>8)</sup> Tinkham<sup>7)</sup> considered the resistance as arising from a phase slippage at a complicated network of channels with Josephson junctions, using a formula worked out by Ambegaokar and Halperin.<sup>9)</sup> The result is expressed in the limit of very small currents as

$$R/R_n = [I_0(\gamma_0/2)]^{-2}, \quad (2)$$

where  $\gamma_0 = U_0/kT = C[(T_c - T)/T_c]^{3/2}/2B$  and  $I_0$  is the modified Bessel function. For large values of  $\gamma_0$ ,  $R/R_n$  falls as  $\gamma_0 \exp(-\gamma_0)$ . The temperature dependence of the resistance at various magnetic fields, which are calculated from above expression with only a single fitting parameter  $C$ , was in good agreement with the experimental results for a single crystal  $\text{YBa}_2\text{Cu}_3\text{O}_z$  measured by Iye et al.<sup>6)</sup> On the other hand, when the actual current flows in the sample, a potential gradient,  $\Delta w$ , arises from a Lorentz force on the flux line. This leads a net flux jump to one direction. According to the investigation by Dew-Hughes,<sup>8)</sup> the resistivity is given by

$$\rho = [2.3\phi_0 B \nu_0 / N_p kT] \exp(-U_0/kT), \quad (3)$$

where  $N_p$  is the number density of pinning centers per unit volume. This expression means that the flux creep results in a flux flow resistivity, which is apparently linear with magnetic field and depends on the direction of the current with respect to the magnetic field.

In our experiment, the results for both transverse and longitudinal configuration of the current are almost in agreement with each other, and the resistance is roughly proportional to  $B^{1.5}$  at low field. These results indicate that the resistance is not caused by the Lorentz force assumed in the model by Dew-Hughes. Tinkham's result, which is independent of the direction of the current, qualitatively agrees with our experimental result at low temperature side. However, as can be seen in Fig.2(b), the resistive transition of  $\text{Bi}_2(\text{Sr,Ca})_3\text{Cu}_2\text{O}_z$  is more complicated than the case of  $\text{YBa}_2\text{Cu}_3\text{O}_z$ , particularly at higher magnetic fields. In the case of  $\text{Bi}_2(\text{Sr,Ca})_3\text{Cu}_2\text{O}_z$ , it seems to be difficult to explain the temperature dependence of the resistance over the wide temperature range by eq.(2). Furthermore, the magnetic field dependence of the resistance and the activation energy cannot be understood by both theoretical models.

The exponential temperature dependence of the resistance in the transition region seems to be basically understood by the flux creep model. However, theoretical models is not yet established to explain the various experimental results.

#### References

1. T. T. M. Palstra, B. Batlogg, L. F. Schneemeyer and J. V. Waszczak, Phys. Rev. Lett. 61 (1988) 1662.
2. T. Tsuneto, J. Phys. Soc. Jpn. 57 (1988) 3499.  
R. Ikeda, T. Ohmi and T. Tsuneto, preprint.
3. Y. Yeshurun and A. P. Malozemoff, Phys. Rev. Lett. 60 (1988) 2202.
4. H. Yamane, H. Masumoto, T. Hirai, H. Iwasaki, K. Watanabe, N. Kobayashi, Y. Muto and H. Kurosawa, Appl. Phys. Lett. 53 (1988) 1548.
5. H. Yamane, H. Kurosawa, T. Hirai, H. Iwasaki, N. Kobayashi and Y. Muto, Jpn. J. Appl. Phys. 27 (1988) L1495.
6. Y. Iye, T. Tamegai, H. Takeya and H. Takei, Jpn. J. Appl. Phys. 26 (1987) L1057.
7. M. Tinkham, Phys. Rev. Lett. 61 (1988) 1658.
8. D. Dew-Hughes, Cryogenics 28 (1988) 674.
9. V. Ambegaokar and B. I. Halperin, Phys. Rev. Lett. 22 (1969) 1364.

## Transport Studies on Superconducting and Normal Metallic La-Sr-Cu Oxides

Y. Iye, T. Tamegai, N. Tanahashi, C. Murayama, N. Mori and S. Yomo\*

Institute for Solid State Physics, University of Tokyo,  
7-22-1 Roppongi, Minato-ku, Tokyo 106, Japan

\* Department of Electronic and Information Technology,  
Hokkaido Tokai University, Sapporo 005, Japan

A series of La-Sr-Cu-O compounds with various chemical compositions, of which some are high temperature superconductors while others show normal metallic behavior, are studied. Pressure experiments on  $(\text{La}_{1-x}\text{Sr}_x)_2\text{CuO}_4$  have revealed that the pressure dependence of  $T_c$  is quite similar for the whole range of  $x$  in spite of the strongly  $x$ -dependent  $T_c$  itself. This suggests that a single mechanism (rather than two competing ones) governs the characteristic  $T_c$  vs.  $x$  curve of the  $(\text{La}_{1-x}\text{Sr}_x)_2\text{CuO}_4$  system. A view of high  $T_c$  copper oxides as intercalated systems is presented, and normal metallic La-Sr-Cu oxides closely related to the high  $T_c$  materials are studied in that context. Electrical transport in  $\text{La}_{1.9}\text{Sr}_{1.1}\text{Cu}_2\text{O}_{6+y}$  is dominated by disorder inevitably introduced by oxygen doping. Three dimensional compounds  $(\text{La}_{8-x}\text{Sr}_x)\text{Cu}_8\text{O}_{20-y}$  appear more like ordinary metals. Resistivity anomalies are found in the  $x=1.47$  and  $x=1.60$  compounds.

### Introduction

Despite the worldwide intensive research efforts towards its elucidation, the basic mechanism for the high temperature superconductivity in copper oxide systems has so far eluded our grasp. Given the difficulty encountered in a frontal attack on the high  $T_c$  materials, it seems a good strategy to try approaches from different angles. One useful method is to apply high pressure and see how it affects the electronic state and superconductivity of a particular material. Another is to study the electronic properties of materials with closely related structures in an attempt to extract common features. We focus in this paper on the La-Sr-Cu-O systems which occur in a variety of chemical compositions and crystal structures, some of which are high temperature superconductors and others are normal metals.

### Pressure Study on $(\text{La}_{1-x}\text{Sr}_x)_2\text{CuO}_4$

It has been known from the early stage of high  $T_c$  research that pressure causes an unusually large enhancement of  $T_c$  in  $(\text{La}_{1-x}\text{Sr}_x)_2\text{CuO}_4$ . [1,2] Also established is the fact that  $T_c$  of  $(\text{La}_{1-x}\text{Sr}_x)_2\text{CuO}_4$  has a maximum as a function of the strontium content  $x$ . [3,4] As  $x$  is increased from zero, an insulator-to-metal transition sets in at  $x \sim 0.025$  and a finite  $T_c$  appears there. The value of  $T_c$  increases with  $x$  and attains a maximum of  $\sim 40$  K at  $x \sim 0.08$  and then decreases as  $x$  is further

increased, until it vanishes at  $x \sim 0.15$ . It has been argued that the electronic state in the high  $T_c$  range of  $x$  is dominated by electron correlation, while that in the higher  $x$  region is more like an ordinary Fermi liquid. In order to gain more insight into this issue, we have carried out a systematic study of pressure effect on carrier concentration and  $T_c$  in  $(La_{1-x}Sr_x)_2CuO_4$ . Of our particular interest is the comparison between the two regions of  $x$ , in one of which  $T_c$  increases with carrier concentration, while it decreases in the other.

Figure 1 shows the pressure dependence of the Hall coefficient  $R_H$  of five samples of  $(La_{1-x}Sr_x)_2CuO_4$ . It is seen that the Hall coefficient shows virtually no change up to the highest pressure of the present work. The figure on the right side demonstrates an excellent agreement of the present data of  $R_H$  as a function of  $x$ , with those reported by Takagi et al. [4] [A small systematic upward deviation of our data from Takagi et al.'s is due to difference in temperature between our (60K) and their (80K) experiments.]

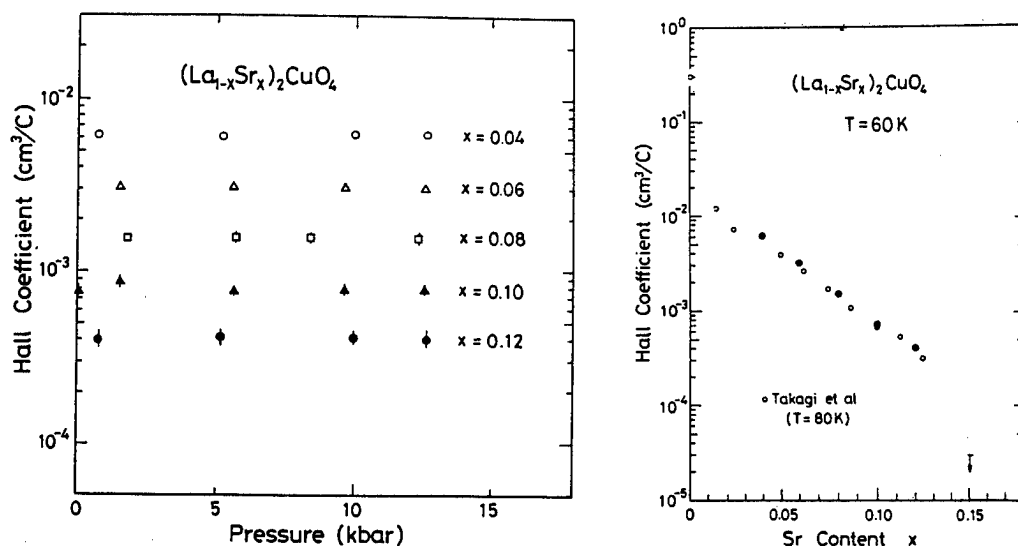


Fig. 1 The pressure dependence of the Hall coefficient for  $(La_{1-x}Sr_x)_2CuO_4$  samples with different  $x$ . The figure on the right shows the Hall coefficient as a function of  $x$ , in comparison with the data of Takagi et al. [4]

Figure 2 illustrates change in the resistively observed superconducting transition with pressure. It is commonly observed that the onset point defined as shown in the figure increases most dramatically with pressure. The pressure dependence of the midpoint is similar but smaller in magnitude. The pressure dependence of the zero resistance point is found to vary even qualitatively from sample to sample, and is probably governed by the intergrain coupling rather than more intrinsic properties. We therefore plot in Fig. 3 the onset  $T_c$  as a function of pressure. The pressure independence of the Hall coefficient shown in Fig. 1 rules out a change in the carrier concentration as an origin of this pressure induced enhancement of  $T_c$ .

A remarkable feature apparent in Fig. 3 is that the pressure coefficient  $dT_c/dp$  is almost the same for all the five samples. This means that the relative pressure coefficient  $d \log T_c / dp$  (or more fundamental quantity  $-d \log T_c / d \log V$ ) is smaller for a higher  $T_c$  material. Such trend is generally observed among the high  $T_c$  oxides [5, 6]. What we note here is that two compounds (for example  $x = 0.06$  and  $0.10$ ) having the same

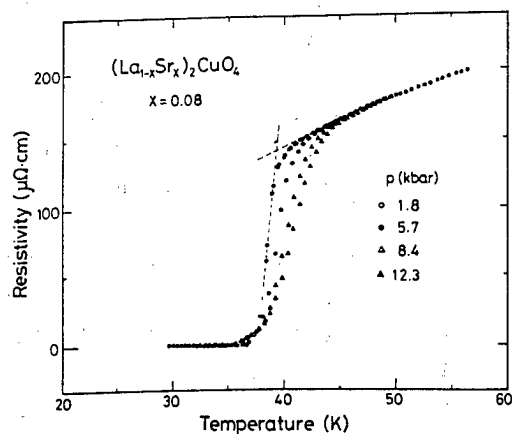


Fig. 2 Pressure dependence of the resistivity observed superconducting transition in  $(\text{La}_{1-x}\text{Sr}_x)_2\text{CuO}_4$  ( $x=0.08$ ). The definition of the  $T_C$  (onset) is indicated in the figure.

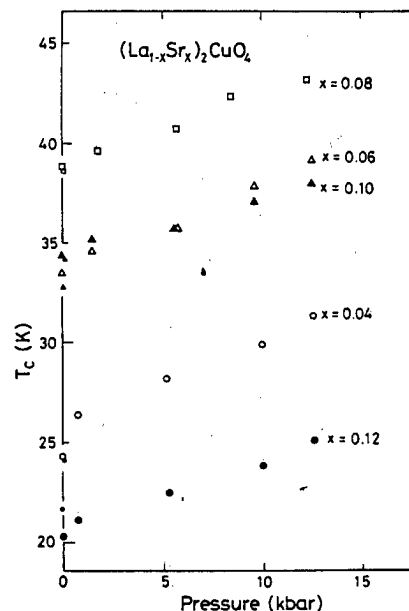


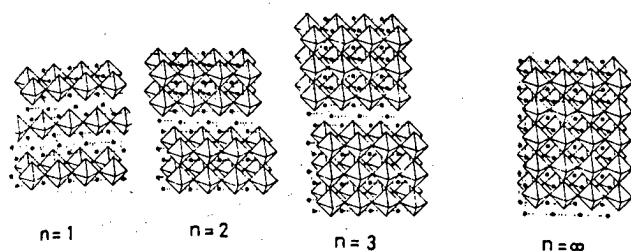
Fig. 3 Pressure dependence of  $T_C$  (onset) for  $(\text{La}_{1-x}\text{Sr}_x)_2\text{CuO}_4$ . Note that the pressure dependence is similar for all samples.

$T_C$  have very similar pressure coefficients ( $dT_C/dp$  or  $d\log T_C/dp$ ). This presents a test discriminating among theoretical models for the mechanism of high temperature superconductivity. In particular, an attempt to explain the shape of the  $T_C$  vs  $x$  curve in terms of a competition between two completely different causes, would encounter a rather serious difficulty.

In connection with the proposed magnetic mechanism for the high temperature superconductivity, it would be of great interest to investigate the pressure dependence of the exchange coupling  $J$ , by studying, for example, the two-magnon scattering under pressure, and to correlate it with the pressure dependence of  $T_C$ . We point out here that the compressibilities of  $(\text{La}_{1-x}\text{Sr}_x)_2\text{CuO}_4$  and  $\text{YBa}_2\text{Cu}_3\text{O}_{7-\delta}$  are quite comparable. [7] If the exchange coupling  $J$  is a smooth function of the interatomic distance in the present range of interest, it seems rather difficult to explain the widely different pressure dependence of  $T_C$  among the high  $T_C$  oxides, notably between  $(\text{La}_{1-x}\text{Sr}_x)_2\text{CuO}_4$  and  $\text{YBa}_2\text{Cu}_3\text{O}_{7-\delta}$ . For a theoretical model for the mechanism of high temperature superconductivity to be valid, it should successfully explain the general trend of the pressure dependence of  $T_C$ .

#### High $T_C$ Oxides Viewed as Intercalated Systems

Figure 4 illustrates basic structures of layered perovskites, which are composed of corner-sharing  $\text{CuO}_6$  octahedrons, and occur in a series of structures with different number of  $\text{CuO}$  layers,  $n$ , forming the unit. The  $n=1$  structure is the  $\text{K}_2\text{NiF}_4$  type,  $n=2$  corresponds to the  $\text{Sr}_3\text{Ti}_2\text{O}_7$  structure and  $n=\infty$  to the cubic perovskite  $\text{LaCuO}_3$ . The chemical formulae for the ideal structures illustrated in Fig. 4 are  $\text{A}_{n+1}\text{B}_n\text{O}_{3n+1}$ , where B is copper.



$A_{n+1}B_nO_{3n+1}$ —Layered Perovskite Structures

Fig. 4 Structures of layered perovskites.

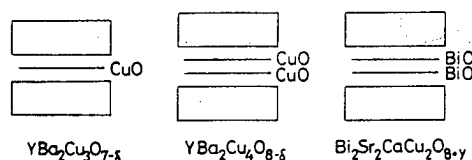
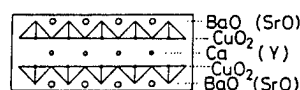
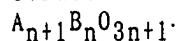
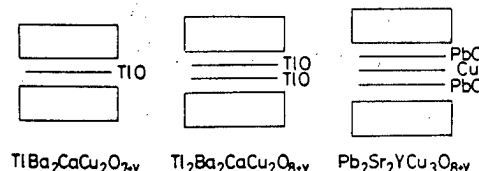


Fig. 5 Structures of the double-CuO-layer high  $T_c$  oxides viewed as intercalated systems.



The crystal structures of all the high  $T_c$  cuprates known to date can be viewed as derivatives of these basic structures. Let us see this by taking the double-CuO-layer ( $n=2$ ) compounds as an example. Figure 5 illustrates the derivation of the high  $T_c$  double CuO layer structure from the basic  $La_2Cu_2O_7$  structure. The "basic layer unit" of the high  $T_c$  cuprates is constructed in the following way:

(1) Replace the La ions in the middle plane by smaller Y (or Ca) ions.

(2) Remove oxygen ions from the middle plane, and thereby change the  $CuO_6$  octahedrons into  $CuO_5$  pyramids.

(3) Replace the La ions in the outer planes by Ba (or Sr) ions.

The layered material thus created is composed of the  $Ba(Sr)O-CuO_2-Y(Ca)-CuO_2-Ba(Sr)O$  basic units.

The high  $T_c$  materials can then be viewed as "intercalation compounds" based on the hypothetical "host materials" constructed above. Figure 5 summarizes the currently known double-CuO-layer high  $T_c$  materials viewed in this way. The intercalate layers are, CuO chain layer (for  $YBa_2Cu_3O_{7-\delta}$ ),  $Bi_2O_2$  double layer ( $Bi_2Sr_2CaCu_2O_{8+y}$ ), TlO single layer ( $TlBa_2CaCu_2O_{7+y}$ ),  $Tl_2O_2$  double layer ( $Tl_2Ba_2CaCu_2O_{8+y}$ ), and PbO-Cu-PbO layer ( $Pb_2Sr_2YCu_3O_{8+y}$ ). Similar schemes can be also drawn for the single copper layer compounds [ $(La_{1-x}Sr_x)_2CuO_4$ ,  $Bi_2Sr_2CuO_{6+y}$ ,  $Tl_2Ba_2CuO_{6+y}$ , and  $TlBa_2CuO_{5+y}$ ], and for the triple copper layer compounds [ $Bi_2Sr_2Ca_2Cu_3O_{10+y}$ ,  $Tl_2Ba_2Ca_2Cu_3O_{10+y}$ , and  $TlBa_2Ca_2Cu_3O_{9+y}$ ]. It is noteworthy that the  $T_c$ 's are in the range of 10-60 K for the single-CuO-layer compounds, 70-100 K for the double layer compounds, and 100-125 K for the triple layer compounds. Such systematics suggests that the "host layers" are principally responsible for the high temperature superconductivity. The primary role of the "intercalate layers" may be to supply carriers to the "host layers" by charge transfer without introducing disorder into the current carrying "host layers".

#### Non-Superconducting Lanthanum Cuprates

In the above context, it is interesting to study  $La_2SrCu_2O_6$  (and  $La_2CaCu_2O_6$ ) having double CuO layers but no "intercalate layers". The leftmost figure of Fig. 6 shows the structure of  $La_2SrCu_2O_6$ . Another class of materials of interest are the three dimensional compounds derived from the cubic perovskite structure. The middle and the rightmost figures of Fig. 6 are the structures of  $La_4BaCu_5O_{13-y}$  and

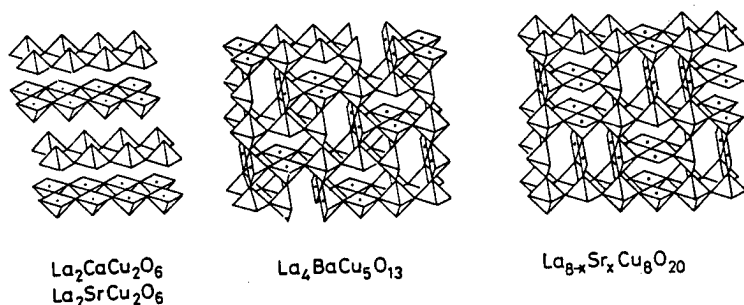


Fig. 6 Crystal structures of  $\text{La}_2\text{SrCu}_2\text{O}_6$ ,  $\text{La}_4\text{BaCu}_5\text{O}_{13-y}$  and  $\text{La}_{8-x}\text{Sr}_x\text{Cu}_8\text{O}_{20-y}$ .

$\text{La}_{8-x}\text{Sr}_x\text{Cu}_8\text{O}_{20-y}$ . The former compound had been studied by Raveau's group [8] even before the Bednorz and Mueller's discovery of high temperature superconductivity in the  $(\text{La}_{1-x}\text{Ba}_x)_2\text{CuO}_4$  system. The latter system was identified more recently by Michel et al. [9] and by Torrance et al. [10]

Figure 7 shows the temperature dependences of the resistivity and the Hall coefficient of  $\text{La}_{1.9}\text{Ca}_{1.1}\text{Cu}_2\text{O}_{6+y}$  and  $\text{La}_{1.9}\text{Sr}_{1.1}\text{Cu}_2\text{O}_{6+y}$ . The Hall coefficient is positive for these compounds. The carrier density strongly depends on  $y$ . In the case of  $\text{La}_{1.9}\text{Ca}_{1.1}\text{Cu}_2\text{O}_{6+y}$ , it is difficult to increase the oxygen content much higher than 6. The hole density is thus generally low. For the sample of Fig. 7,  $n_h \sim 5 \times 10^{20} \text{ cm}^{-3}$ . The temperature dependence of the resistivity of this sample is fitted to a variable range hopping type formula.

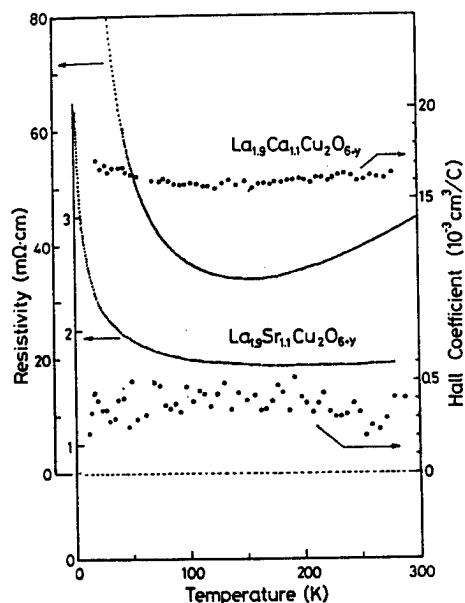


Fig. 7 Resistivity and Hall coefficient of  $\text{La}_{1.9}\text{Ca}_{1.1}\text{Cu}_2\text{O}_{6+y}$  and  $\text{La}_{1.9}\text{Sr}_{1.1}\text{Cu}_2\text{O}_{6+y}$ .

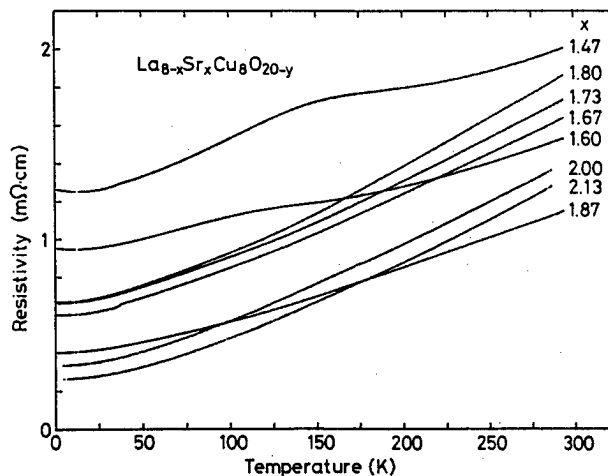


Fig. 8 Resistivities of  $\text{La}_{8-x}\text{Sr}_x\text{Cu}_8\text{O}_{20-y}$  with different values of  $x$ .

In the case of  $\text{La}_{1.9}\text{Sr}_{1.1}\text{Cu}_2\text{O}_{6+y}$ , the oxygen content can be made substantially higher than 6 by low temperature annealing. For the sample shown in Fig. 7, chemical analysis gives  $y \sim 0.25$ . The carrier concentration derived from the Hall coefficient is  $n_h \sim 1.6 \times 10^{22} \text{ cm}^{-3}$ . This is considerably larger than the chemically estimated hole concentration  $n_h \sim 4 \times 10^{21} \text{ cm}^{-3}$  and suggests that more than one type of carriers contribute to transport. The resistivity behavior is more metallic than  $\text{La}_2\text{CaCu}_2\text{O}_6$ , but shows a behavior at low temperatures which can be interpreted as the weak localiza-



tion effect. Magnetoresistance measurements at low temperature have revealed the negative magnetoresistance effect characteristic of a weakly localized system. Superconductivity is not found at temperatures higher than 0.3 K.

As seen above, the transport properties of  $\text{La}_2\text{CaCu}_2\text{O}_6$  and  $\text{La}_2\text{SrCu}_2\text{O}_6$  are strongly influenced by inherent disorder. Since these compounds have no "intercalate layers", oxygen atoms have to be doped in the Sr (or Ca) plane. Consequently, creation of charge carrier inevitably introduces disorder in the conducting layers. Whether this is the only reason for the absence of high temperature superconductivity in these compounds is not clear. But it is certainly a detrimental factor.

Figure 8 shows the temperature dependence of the resistivities of a series of  $\text{La}_{8-x}\text{Sr}_x\text{Cu}_8\text{O}_{20-y}$  samples with different x. The broad anomalies seen in the resistivity curves for  $x=1.47$  and  $1.60$  is accompanied by change in the carrier density as estimated from the Hall coefficient. It is probably associated with a certain type of Fermi surface instability such as spin density wave. Its exact nature, however, is to be elucidated by further studies. Unlike the high  $T_c$  materials, the sign of the Hall coefficient is negative. The resistivity shows a temperature dependence which look very much like an ordinary metal. The negative Hall coefficient and normal metallic resistivity behavior are also seen in the  $\text{La}_4\text{BaCu}_5\text{O}_{13-y}$  system.

The absence of high temperature superconductivity in  $\text{La}_4\text{BaCu}_5\text{O}_{13-y}$  or  $\text{La}_{8-x}\text{Sr}_x\text{Cu}_8\text{O}_{20-y}$  may be attributed to their "normal metallic" character. These compounds may be classified in a group similar to  $(\text{La}_{1-x}\text{Sr}_x)_2\text{CuO}_4$  with  $x > 0.15$ , which have "too many carriers" for high temperature superconductivity. Whether the three dimensional nature is relevant to the absence of superconductivity in these compounds should be addressed in future studies.

#### Acknowledgements

Samples of  $(\text{La}_{1-x}\text{Sr}_x)_2\text{CuO}_4$  used in the pressure experiment were kindly supplied by N. Okazaki and K. Kitazawa. This work is supported by Grant-in-Aid for Scientific Research on Priority Areas "Mechanism of Superconductivity", from the Ministry of Education, Science and Culture, Japan.

#### REFERENCES

- [1] C. W. Chu, P. H. Hor, R. L. Meng, L. Gao, Z. J. Huang and Y. Q. Wang, Phys. Rev. Lett. 58 (1987) 405.
- [2] S. Yomo, C. Murayama, H. Takahashi, N. Mori, K. Kishio, K. Kitazawa and K. Fueki, Jpn. J. Appl. Phys. 26 (1987) L603.
- [3] J. B. Torrance, Y. Tokura, A. I. Nazzari, A. Bezinge, T. C. Huang and S. S. P. Parkin, Phys. Rev. Lett. 61 (1988) 1127.
- [4] H. Takagi, Y. Tokura and S. Uchida, to appear in "Mechanisms of High-Temperature Superconductivity", ed. by H. Kamimura and A. Oshiyama (Springer, 1989).
- [5] R. Griessen, Phys. Rev. B36 (1987) 5284.
- [6] C. Murayama, N. Mori and S. Yomo, preprint.
- [7] H. Takahashi, C. Murayama, S. Yomo, N. Mori, W. Utsumi and T. Yagi, Jpn. J. Appl. Phys. 26 (1987) Suppl 26-3, p. 1109.
- [8] C. Michel and B. Raveau, Rev. Chim. Miner. 21 (1984) 407.
- [9] C. Michel, L. Er-Rakho, M. Hervieu, J. Pernetier, and B. Raveau, J. Solid State Chem. 68 (1987) 143.; C. Michel, L. Er-Rakho, and B. Raveau, J. Phys. Chem. Solids 49 (1988) 451.
- [10] J. B. Torrance, Y. Tokura, A. Nazzari, and S. S. P. Parkin, Phys. Rev. Lett. 60 (1988) 542.

K. Oto, K. Murase and S. Takaoka

Department of Physics, Faculty of Science, Osaka University  
1-1 Machikaneyama, Toyonaka, 560 Japan.

The temperature dependence of Hall coefficient and electrical resistivity have been measured in Pb-contained Bi-Sr-Ca-Cu-O superconductor system. With increasing sintering time, the 107K phase grows at the expense of the 80K phase. The Hall coefficient ( $R_H$ ) of the 107K is found to be about 4 times larger than that of the 80K phase. In the 107K phase,  $R_H$  is nearly proportional to  $1/T$ . The temperature dependence of  $R_H$  in the 80K phase is smaller than these in the 107K phase. It seems that there is an optimum "carrier concentration" ( $1/eR_H$ ) to get the maximum  $T_c$  in the 80K phase.

The high  $T_c$  superconductors of Bi-Sr-Ca-Cu-O system [1] have three different phases, that is, Bi:Sr:Ca:Cu=2:2:0:1 ( $T_c=10K$ ), 2:2:1:2(80K) and 2:2:2:3(107K). Their physical properties have been investigated by many researchers. Their crystal structures commonly include  $CuO_2$  planes, but the difference of three phases comes from the number( $N$ ) of  $CuO_2$  planes per unit cell. The phases of  $T_c = 10$ , 80, and 107K correspond to those with  $N=1, 2$ , and 3, respectively. Both the 10K and the 80K phases are easily obtained by the ordinary process, but it is difficult to synthesize the 107K single phase because its growth condition is very critical. Recently it has been reported that the 107K phase is stabilized by Pb addition and by sintering for a long time at a proper temperature [2]. In this study, we prepared the Pb-contained samples with various sintering times and investigated their electrical transport properties, that is, electrical resistivity and Hall coefficient.

The samples were prepared by solid reaction from  $Bi_2O_3$ , PbO,  $SrCO_3$ ,  $CaCO_3$ , and CuO powders of 3N grade. These powders were mixed with the cation ratio of Bi:Pb:Sr:Ca:Cu=0.7:0.3:1:1:2, and ground in an agate mortar. The mixtures were heated at 800°C for 12h in air, then reground and pressed into pellets (13mm in diameter and 1mm in thickness) at a pressure of  $7 \times 10^8$  Pa. The pellet was sintered at 845°C for 65h~260h in air, then the furnace was cooled to the room temperature. We made four samples sintered for 65, 130, 195, and 260 hours, and in this paper, they are denoted as 65H, 130H, 195H and 260H, respectively. Samples were examined by a powder X-ray diffraction method(Cu K $\alpha$ , Rigaku RAD-ROC) and the scanning electron microscopy (SEM). For transport study, samples were cut into rectangular bars (in a dimension of  $0.5 \times 1.0 \times 10mm^3$ ), and the electric contacts were made by indium soldering. The electrical resistivity was measured by a four-probe method using an AC automatic resistance bridge. The detective limit was  $0.1m\Omega$  ( $\sim 2 \times 10^{-6} \Omega \cdot cm$  in this study). We defined zero resistivity as a value less than this limit. The Hall coefficient was measured at a magnetic field 1.3T and the current was 100 mA. The temperature was stabilized within  $\pm 0.05K$  during the Hall measurement.

In Fig. 1, the powder X-ray diffraction patterns are illustrated for the samples with various sintering times. In the sample 65H, the 80K phase is dominant and a small amount of the 107K phase is detected. The peaks due to the 107K phase grow with the sintering time. Increase of relative intensity in the lowest scattering-angle peak is evident with sintering time. The impurity phase  $Ca_2PbO_4$  is detected only a little in the 65H and 130H samples, but in the long-time-sintered samples 195H and 260H, the trace of the impurity phase disappears. The SEM photographs of the samples sintered for 65 and 195h are shown in Fig. 2-a and 2-b, respectively. The sample 65H seems to be crystallized from a

melting state (Fig. 2-a). The sample 195H is well crystallized, (plate and needle like crystals) and it has a lot of chink (Fig.2-b).

In Fig. 3, the temperature dependences of the resistivity are shown for the four samples. All of these samples exhibit metallic conductivity, but values of  $T_c$  are different. In the sample 65H, a little drop of the resistivity appears at 107K and the  $T_{c0}$  (offset) is 67K. The resistivity of the sample 130H drops nearly to 50% at 107K and the  $T_{c0}$  is 78K. The resistivities of both 195H and 260H samples show almost linear temperature dependence above 130K and a sharp drop at 107K, while their  $T_{c0}$ 's are 103 and 106K, respectively.

The temperature dependences of the Hall coefficient ( $R_H$ ) are shown in Fig. 4. In this figure, the ordinate is the reciprocal of the  $R_H$ . In all samples,  $R_H$  is positive and  $1/eR_H$  is linear to temperatures. It has been reported that  $R_H$  of the 80K phase does not so depend on temperatures[3]. In this study, the temperature dependence of  $R_H$  of the sample 65H whose dominant phase is the 80K phase is found to be smaller than those of the other samples. The linearly temperature dependent  $1/eR_H$  is similar to the Y-Ba-Cu-O system[4]. The Hall coefficient is practically independent of magnetic fields below 1.3 Tesla.

It has been reported that in the Y-Ba-Cu-O system, the carrier concentration obtained from the Hall coefficient ( $P^* = 1/eR_H$ ) at about 100K agrees with the hole number measured by iodometry[5]. For the estimation of the hole number per Cu ion,  $P^*$  must be corrected by the filling factor, because the samples are sintered ceramics. In Table 1, the mass density of the samples, the filling factor calculated by the lattice parameters and the measured density, "carrier concentration"  $P^*$  at 120K, and estimated hole number per Cu ion are listed. We used the parameters of the 80K phase for the samples 65H, 130H, and the parameters of the 107K phase in the samples 195H, and 260H according to the results of the X-ray analysis. The hole number of the sample 260H, in which the 107K phase is dominant, is about 1/4 of that of the sample 65H (the 80K phase is dominant). Although the 107K phase has one more  $\text{CuO}_2$  plane than the 80K phase, both of the hole number per unit cell and per Cu ion decrease. In Fig. 5,  $T_{c0}$  (offset) vs.  $1/eR_H$  at 300K is shown. The data points for the 80K phase were obtained by partial substitution of various

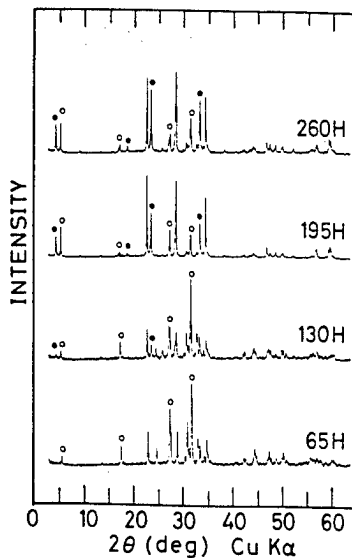


Fig.1. X-ray diffraction pattern of Pb-contained Bi-Sr-Ca-Cu-O superconductors with different sintering times. Open and closed circles correspond to peaks from 80K and 107K phases, respectively.

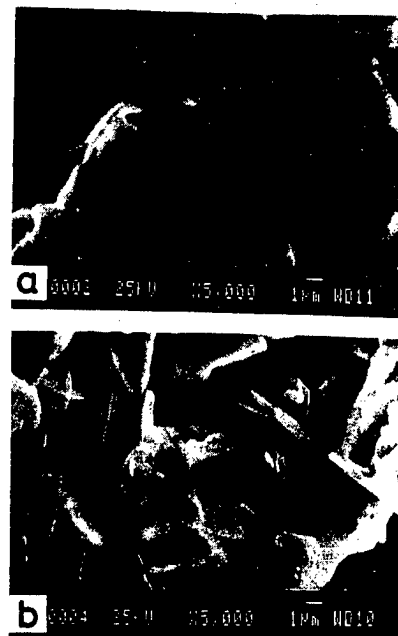


Fig.2. Typical SEM photographs of the samples (a) 65H and (b) 195H.

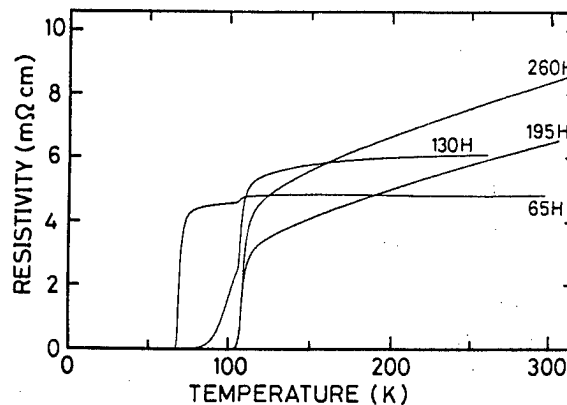


Fig.3. Temperature dependence of resistivity with various sintering times.

elements (Ag, Mg, Pb, or Sn) for Bi. The data for the 107K phase were obtained by different sintering times. In the 80K phase, it seems that there is an optimum carrier concentration obtained from  $R_H$  to show its maximum  $T_c$ , similarly to the Y-Ba-Cu-O and La-Sr-Ca-Cu-O system[6].

In summary, the Hall coefficient of the Bi-Sr-Ca-Cu-O system is positive and  $P^*(=1/eR_H)$  is linear to the temperature. Especially in the 107K phase, the temperature dependence of Hall coefficient almost satisfies  $R_H \propto 1/T$  relation, similarly to the Y-Ba-Cu-O system. The Hall coefficient of the 107K phase is about 4 times larger than that of the 80K phase. There is an optimum carrier concentration obtained from Hall coefficient ( $1/eR_H$ ) to show its maximum  $T_c$  in the 80K phase.

#### Acknowledgments

The authors are grateful to Prof. S. Ishida and Mr. M. Komura at Science University of Tokyo Yamaguchi College for the SEM analysis. The X-ray powder diffraction measurement was performed at the X-ray Diffraction Service of the Department of Chemistry, Faculty of Science, Osaka University.

#### References

- (1) H. Maeda, Y. Tanaka, M. Fukutomi and T. Asano: Jpn. J. Appl. Phys. 27 (1988) L209.
- (2) M. Takano, J. Takada, K. Oda, H. Kitaguchi, Y. Miura, Y. Ikeda, Y. Tomii and H. Mazaki: Jpn. J. Appl. Phys. 27 (1988) L1041-1043.
- (3) H. Takagi, H. Eisaki, S. Uchida, A. Maeda, S. Tajima, K. Uchinokura and S. Tanaka: Nature 332, (1988) 236-238.
- (4) T. Penney, S. von Molnar, D. Kaiser, F. Holtzberg and A.W. Kleinsasser: Phys. Rev. B38, 2918-2921 (1988).
- (5) K. Takita, H. Akinaga, H. Katoh and K. Masuda: Jpn. J. Appl. Phys. 27 (1988) L607-609.
- (6) Y. Tokura, J.B. Torrance, T.C. Huang and A.I. Nazzari: Phys. Rev. B to be published.
- (7) T. Tamegai, K. Koga, K. Suzuki, M. Ichihara, F. Sakai and Y. Iye: Jpn. J. Appl. Phys. 28 (1989) L112-115.

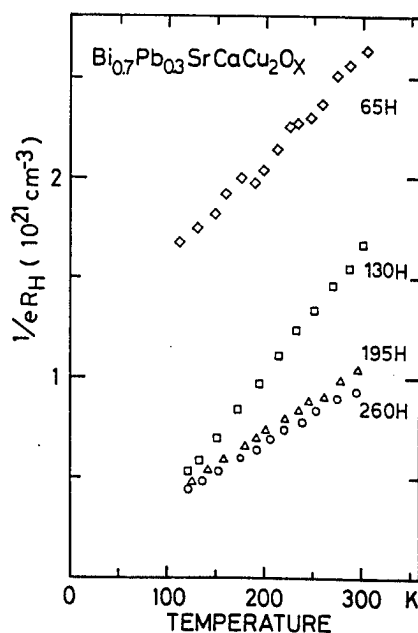


Fig.4. Temperature dependence of  $R_H$  with various sintering times.

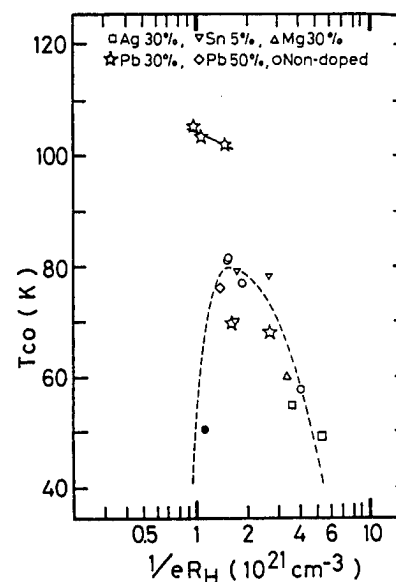


Fig.5. Plot of  $T_{c0}$  vs.  $1/eR_H$  at 300K for various samples of Bi-Sr-Ca-Cu-O system. Broken and solid lines indicate  $T_{c0}$  vs.  $1/eR_H$  of 80K and 107K phases, respectively. Closed circle is from ref.[7].

Table 1. Typical parameters of the samples.

Sample	65H	130H	195H	260H
Mass density (g/cm <sup>3</sup> )	4.97	4.42	4.02	3.91
Filling factor	0.76	0.68	0.64	0.62
$P^*(10^{20} \text{ cm}^{-3})$ at 120K	17.1	5.3	4.7	4.3
Hole number (/cell)	2.04	0.71	0.80	0.75
Hole number (/Cu ion)	0.26	0.09	0.07	0.06

Variation of  $T_c$  with Hole Concentration in  $\text{YBa}_2\text{Cu}_3\text{O}_{7-\delta}$ -Type Superconductors:  
Hall Measurement and Chemical Analysis in  $\text{Ln}_{1+x}\text{Ba}_{2-x}\text{Cu}_3\text{O}_{7-\delta}$  ( $\text{Ln} = \text{La}, \text{Nd}, \text{Sm}$  and  $\text{Eu}$ )

K. Takita, H. Akinaga, H. Katoh, K. Masuda, H. Asano,  
T. Mochiku, Y. Takeda<sup>A</sup> and M. Takano<sup>B</sup>

Institute of Materials Science, University of Tsukuba, Tsukuba-city, Ibaraki, 305

<sup>A</sup>Department of Chemistry, Faculty of Engineering, Mie University, Tsu, 514

<sup>B</sup>Institute for Chemical Research, Kyoto University, Uji, Kyoto-fu, 611

Using single phase samples of the solid solution systems  $\text{Ln}_{1+x}\text{Ba}_{2-x}\text{Cu}_3\text{O}_{7-\delta}$ , relation between  $T_c$  and the hole concentration was investigated by Hall measurement and chemical analysis. The hole concentration was found to be controlled by changing  $x$  and  $(7-\delta)$  in these systems. The plot of the superconducting  $T_c$  against hole concentration  $2P_s$  deduced from chemical analysis shows almost linear relationship between them, where  $2P_s$  is estimated based on an assumption proposed by Tokura et al. A similar plot against effective hole concentration  $P_H (=1/R_H e)$  deduced from hole coefficient just above  $T_c$  shows the same relation below 80K and deviates from linear relation above 80K. By annealing of the samples under high pressure oxygen up to 1000 atm. pressure at around 350°C, both  $T_c$  and hole concentration increase. In these samples, both of the  $2P_s$  and  $P_H$  gives almost same value and  $T_c$ - $P_H$  relation is almost linear up to  $T_c=93\text{K}$ . These facts strongly suggest that  $T_c$  of  $\text{YBa}_2\text{Cu}_3\text{O}_{7-\delta}$ -type superconductors almost linearly increases with hole concentration which can be deduced from the Hall coefficient just above  $T_c$ .

It is well known that superconducting properties of  $\text{LnBa}_2\text{Cu}_3\text{O}_{7-\delta}$  depend critically on oxygen content and the hole concentration is affected by the oxygen-doping and there exist a correlation between  $T_c$  and hole concentration[1,2]. In the present work, it is found by us that, in the solid solution systems  $\text{Ln}_{1+x}\text{Ba}_{2-x}\text{Cu}_3\text{O}_{7-\delta}$  ( $\text{Ln} = \text{La}, \text{Nd}, \text{Sm}$  and  $\text{Eu}$ ), the superconducting properties and the hole concentration can be controlled by changing  $x$  in addition to changing  $\delta$  [3,4,5,6,7]. In these systems, the trivalent Ln-element is partially substituted for divalent Ba-site and, as a result, the hole concentration of 1-2-3 phase is expected to be compensated by excess Ln. In this paper, we report the relation between  $T_c$  and the hole concentration which is determined by the Hall effect measurement and by a chemical analysis changing  $x$  and  $(7-\delta)$  in wide ranges. In order to survey the higher oxygen content region, samples of  $\text{Nd}_{1+x}\text{Ba}_{2-x}\text{Cu}_3\text{O}_{7-\delta}$  annealed in high pressure oxygen (<1000 atm.) were investigated in the experiment.

Fig.1 shows a typical result of  $x$ -dependence of  $T_c$  and lattice parameters for  $\text{Nd}_{1+x}\text{Ba}_{2-x}\text{Cu}_3\text{O}_{7-\delta}$ . In this figure, the result for the samples annealed under high pressure oxygen (600-1000atm.) at around 350°C is shown together with the result for the samples sintered under 1 atm. oxygen flow. For both cases,  $T_c$  decreases almost monotonically with increasing  $x$  in spite of the ortho-tetra structural phase transformation around  $x=0.2$  as seen in the figure. By the annealing in the high pressure oxygen,  $T_c$  increases for  $x>0.1$  as is clearly seen in the figure. These changes of  $T_c$  are interpreted as the result of hole concentration change in each samples as will be described in the following.

In Fig. 2,  $T_c$  is plotted against the effective hole concentration  $P_H$  at 100K for various systems.

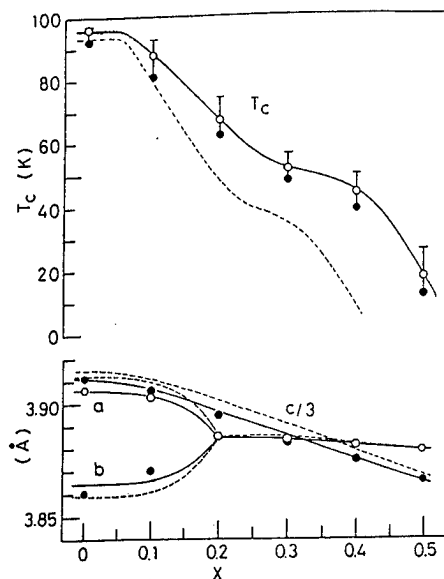


Figure 1

x-dependence of  $T_c$  and lattice parameters for  $\text{Nd}_{1+x}\text{Ba}_{2-x}\text{Cu}_3\text{O}_{7-\delta}$  annealed under high pressure oxygen. For  $T_c$ , open and closed circles represent the midpoint and zero resistance point. Horizontal bars are the onset temperature determined at 90% points. Dashed lines show the results for the samples furnace cooled under oxygen flow.

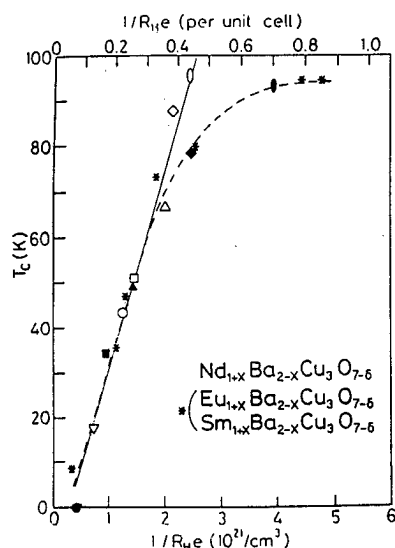


Figure 2

$T_c$  of  $\text{Nd}_{1+x}\text{Ba}_{2-x}\text{Cu}_3\text{O}_{7-\delta}$  plotted against the effective hole concentration  $P_H$  ( $=1/R_{He}$ ) deduced from Hall coefficient at 100K. Solid and open symbols represent the results before and after annealing under high pressure oxygen, respectively.

$x=0$ ; (○ ●):  $x=0.1$ ; (◇ ◆):  $x=0.2$ ; (△ ▲):  $x=0.3$ ; (□ ■):  $x=0.4$ ; (○ ●):  $x=0.5$ ; (▽ ▼)

The same plots for  $\text{Sm}_{1+x}\text{Ba}_{2-x}\text{Cu}_3\text{O}_{7-\delta}$  and  $\text{Eu}_{1+x}\text{Ba}_{2-x}\text{Cu}_3\text{O}_{7-\delta}$  are also shown by asterisc (\*) for the samples sintered by furnace cooling in oxygen flow.

$P_H$  at 100K means substantially the hole concentration just above  $T_c$ . For the samples sintered under 1 atm.,  $T_c$  shows almost linear dependence on  $P_H$  below 70K but shows a saturation above 80K as shown by dotted curves. On the contrary, it has been found that for the samples of  $\text{Nd}_{1+x}\text{Ba}_{2-x}\text{Cu}_3\text{O}_{7-\delta}$  annealed under high pressure oxygen,  $T_c$  shows almost linear relationship with  $P_H$  up to 93K as seen in Fig.2.

In Fig.3, the relation between  $T_c$  and the chemically determined hole concentrations are shown by the plots for three kinds of samples annealed under different condition.  $P$  is the average charge per [Cu-O] unit determined by an iodometric titration technique. As the unit cell has three Cu-atoms, the chemical hole concentration per unit cell is  $3P$ . According to an assumption proposed by Tokura et al.[8],  $3P$  is divided into two parts as follows

$$3P = P_c + 2P_s, \quad (1)$$

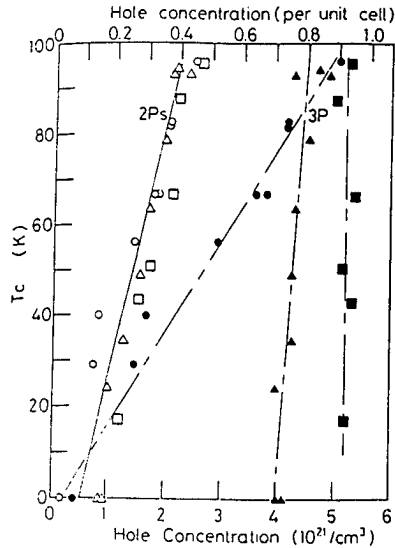


Figure 3

$T_c$  plotted against the chemically determined hole concentration  $3P$ , and the estimated hole concentration in  $\text{CuO}_2$  sheet  $2P_s$ . Solid and open symbols represent the  $T_c$ - $3P$  and  $T_c$ - $2P_s$  relations for  $\text{Nd}_{1+x}\text{Ba}_{2-x}\text{Cu}_3\text{O}_{7-\delta}$ , respectively.

Results are shown for three kinds of samples annealed under different condition. Square plots are for the samples annealed under high pressure oxygen. Triangle plots are for the samples furnace cooled under 1 atm. oxygen. Circle plots are for the samples annealed under low pressure oxygen.

where  $2P_s$  means the hole concentration in two sheets of  $\text{CuO}_2$  in the unit cell and  $P_c$  means the hole concentration within the inter-Ba plane which is chain plane in the case of orthorhombic structure. It is supposed further that  $p_c$  is trapped or localized and does not contribute to the conduction. Following after Tokura et al. and assuming a simple relation between  $P_c$  and  $(7-\delta)$  as follows,

$$P_c = (7-\delta)-6.5, \quad (2)$$

we estimated the mobile hole concentration  $2P_s$ . In spite of that  $T_c$  vs.  $3P$  relation is different for the samples which undergo different heat-treatment,  $T_c$  vs  $2P_s$  relation is almost the same as seen in Fig.3. Furthermore,  $T_c$  vs.  $2P_s$  relation shows almost the same relation of  $T_c$  vs.  $P_H$  in the case of the samples annealed under high pressure oxygen.

In conclusion, by simultaneous measurements of Hall effect and average charge of  $[\text{Cu-O}]$  unit for the same samples, it is strongly suggested that the  $T_c$  is determined solely by the hole concentration in  $\text{CuO}_2$  layers in  $\text{YBa}_2\text{Cu}_3\text{O}_{7-\delta}$ -type system. The hole concentration is determined by both of  $x$  and  $(7-\delta)$  in  $\text{Ln}_{1+x}\text{Ba}_{2-x}\text{Cu}_3\text{O}_{7-\delta}$ . Furthermore, it is suggested that  $T_c$  shows a linear dependence on the hole concentration in the region where  $T_c$  increases with hole concentration.

#### REFERENCES

- [1] Z. Z. Wang, J. Clayhold, N.P. Ong, J. M. Tarascon, L. H. Greene, W. R. McKinnon, and G. W. Hull: Phys. Rev. B36 (1987) 7222.
- [2] H. Takagi, S. Uchida, H. Iwabuchi, S. Tajima, and S. Tanaka: in Superconducting Materials, ed. S. Nakajima and H. Fukuyama: (JJAP Series 1, 1988), p.6.
- [3] K. Takita, H. Katoh, H. Akinaga, M. Nishino, T. Ishigaki, and H. Asano: Jpn. J. Appl. Phys. 27 (1988) L57.
- [4] K. Takita, H. Akinaga, H. Katoh, H. Asano, and K. Masuda: Jpn. J. Appl. Phys. 27 (1988) L67.
- [5] H. Akinaga, H. Katoh, K. Takita, H. Asano, and K. Masuda: Jpn. J. Appl. Phys. 27 (1988) L610.
- [6] K. Takita, H. Akinaga, H. Katoh, and K. Masuda: Jpn. J. Appl. Phys. 27 (1988) L607.
- [7] K. Takita, H. Akinaga, H. Katoh, and K. Masuda: Jpn. J. Appl. Phys. 27 (1988) L1676.
- [8] Y. Tokura, J. B. Torrance, T. C. Huang, and A. I. Nazzari: Phys. Rev. B38 (1988) 7156.

Low Temperature Specific Heat and Anisotropic Electrical Transport Properties  
of Single Crystal  $\text{Bi}_{2.2}\text{Sr}_{1.8}\text{CaCu}_2\text{O}_y$

K. Yamaya, N. Ono, T. Honma, T. Haga, Y. Abe,  
F. Minami\* and S. Takekawa\*\*

Department of Nuclear Engineering and \*Research Institute of  
Applied Electricity, Hokkaido University, Sapporo 060, Japan

\*\*National Institute for Research in Inorganic Materials,  
Tsukuba 305, Japan

Low temperature specific heat and electrical transport properties of single crystal  $\text{Bi}_{2.2}\text{Sr}_{1.8}\text{CaCu}_2\text{O}_y$  have been measured. No T-linear term in the specific heat has been observed within experimental accuracy. Non T-linear term in single crystal  $\text{Bi}_{2.2}\text{Sr}_{1.8}\text{CaCu}_2\text{O}_y$  is discussed and compared with results reported in polycrystalline samples and other high- $T_c$  oxides. It has been found that the resistivities in the a-b plane are anisotropic and the most conductive direction is the a-axis. From the temperature dependence of each anisotropy of the resistivity, the Hall coefficient and the mobility, it is suggested that the electrical transport of  $\text{Bi}_{2.2}\text{Sr}_{1.8}\text{CaCu}_2\text{O}_y$  are due to two types of mobile carriers.

At the present time, many high- $T_c$  oxide superconductors have been discovered. In order to investigate the mechanism of the superconductivity, it is important to identify any unconventional behaviors in both normal and superconducting states in comparison with ordinary superconductors. The occurrence of a finite T-linear term in the specific heat in the superconducting state may be one of the important features of the high- $T_c$  oxide superconductors, because such a T-linear term can be hardly explained within the framework of the BCS theory. In the normal state, the temperature dependence of the resistivity in the a-b plane exhibits a metallic behavior. However, the Hall coefficient significantly depends on temperature and its behavior is hardly explained by a simple free-electron model of one band. Therefore, it is needed to clarify electrical transport properties in the normal state in connection with the mechanism of the superconductivity.

In this paper, we report the specific heat in the superconducting state and anisotropies of the resistivities and the Hall coefficients in the a-b plane of  $\text{Bi}_{2.2}\text{Sr}_{1.8}\text{CaCu}_2\text{O}_y$ . The single crystal was grown by the floating-zone method[1]. The chemical composition determined by EPMA measurement is  $\text{Bi}_{2.2}\text{Sr}_{1.8}\text{CaCu}_2\text{O}_y$ .

#### 1. Low temperature specific heat

The typical sample size for measurement of the specific heat is 4.4mmx4.5mmx0.5mm and its weight is about 25mg. The  $T_c$  determined by the inductive method was 85K. The a-b plane of the sample was attached by a thermal compound to the opposite surface of the bolometer. The specific heat was measured by the thermal relaxation method in the temperature range from 1.3K to 10K.



In Fig. 1 is shown a plot of  $C/T$  vs.  $T^2$  in the temperature range from 1.3K to 10K. Here, the magnitude of the molar specific heat was determined by assuming that the chemical composition of oxygen,  $y$  is 8. An upturn in  $C/T$  is observed at low temperatures. The upturn in  $C/T$  has been observed in almost all high- $T_c$  oxides[2-4] and there is considerable evidence that this upturn is not an intrinsic effect but is due to the existence of the impurity phases. Thus, the impurity phases may exist even in the single crystal, although its magnitude of the upturn in  $C/T$  is quite smaller than that of polycrystalline sample. More detailed studies of identifying the impurity phases in  $\text{Bi}_2\text{Sr}_2\text{CaCu}_2\text{O}_y$  will be necessary. Because of the presence of the upturn in  $C/T$ , the task of extracting the linear relation of  $C/T = \nu + 8T^2$  from the data of  $C/T$  vs.  $T^2$  is complicated. However, in the temperature range from 3.5K to 6.5K the linear relation with  $\nu=0$  can be obtained by a least-square fit to the data. The results is represented by the solid line in Fig. 1. This result of  $\nu=0$  is consistent with those in polycrystalline samples measured by Sera et al.[4], Kumagai et al.[5], and Fisher et al.[6]. While in  $\text{LaBaCuO}$ ,  $\text{LaSrCuO}$  and  $\text{YBaCuO}$  systems[2,3,7], a finite value of  $\nu$  has been observed, but the existence of impurity phases also are confirmed in their systems[8,9]. Therefore, it is doubt whether the finite value of  $\nu$  is intrinsic. Thus, it is unsolved whether the value of  $\nu$  is finite in the high- $T_c$  oxide superconductors. It is needed to improve sample preparation techniques for obtaining more reliable information about the value of  $\nu$ .

## 2. Transport properties

The sample for measurements of the resistivity and Hall coefficient was carefully cleaved from as-grown crystal. The orientation of the crystal axis was confirmed by the X-ray diffraction(Laue method). The resistivities of the direction parallel to the a- and b-axis were measured by a dc four terminals method. The Hall coefficient was measured under the magnetic field (5T) parallel to the c-axis for the current flows parallel to the a- and b-axis.

In Fig. 2 is shown the typical temperature dependence of the resistivity of the direction parallel to the a- and b-axis,  $\rho_a$  and  $\rho_b$ . Although the magnitude of the resistivity shows the small variation from sample to sample, its typical value of  $\rho_a$  at 300K is  $0.7 \times 10^{-3}$  ohm cm and that of  $\rho_b$  is several times higher than that of  $\rho_a$ . The ratio of the resistivity,  $\rho_b/\rho_a$  is almost independent on temperature. Therefore, it is found that the most conductive direction in  $\text{Bi}_{2.2}\text{Sr}_{1.8}\text{CaCu}_2\text{O}_y$  is the a-axis, because the resistivity parallel to the c-axis has been reported to be more than an order of magnitude larger than those of  $\rho_a$  or  $\rho_b$ [10]. However, this result is inconsistent with the result measured by Martin et al.[10] with the Montgomery method, in which the most conductive direction is the b-axis. This discrepancy may be partly caused by the uncertainty on the Montgomery method.

In Fig. 3 is shown the temperature dependence of the Hall coefficient,  $R_{Ha}(I//a, H//c)$  and  $R_{Hb}(I//b, H//c)$ . The sign of both Hall coefficients is positive.  $R_{Ha}$  and  $R_{Hb}$  increase as temperature decreases and their maxima are observed at 115K and 140K, respectively. The temperature dependence of the Hall coefficients is hardly explained in terms of a simple free-electron model.

The temperature dependence of the mobility determined by the resistivity and the Hall coefficient is shown in Fig. 4. The mobility of the direction parallel to the a-axis,  $\mu_a$  increases as temperature decreases. While the mobility parallel to the b-axis,  $\mu_b$  has a maximum at near 125K and decreases with decreasing temperature below the temperature corresponding to the maximum of  $\mu_b$ . Thus, the anisotropy of the the

mobility,  $\mu_a/\mu_b$  significantly depends on temperature. On the other hand, the anisotropy of the resistivity is independent on temperature, as mentioned above. The different temperature dependence of these anisotropies suggests that the mobile carriers in  $\text{Bi}_{2.2}\text{Sr}_{1.8}\text{CaCu}_2\text{O}_y$  are necessary for two types of at least. More detailed studies of the temperature dependence of the electric transport properties are being carried out.

#### References

- [1] S.Takekawa, H.Nozaiki, A.Umezono, K.Kosuda and M.Kobayashi, to be published in J. Crystal Growth.
- [2] N.E.Phillips, R.A.Fisher, S.E.Lacy, C.Marcent, J.A.Olsen, W.K.Han and A.M.Stacy, Jpn. J. Appl. Phys. 26 (suppl. 26-3)1115.
- [3] M.Ishikawa, Y.Nakazawa, T.Takabatake, A.Kishi, R.Kato and A.Malsono, Solid State Commun. 66 (1988) 201.
- [4] M.Sera, S.Kondoh, F.Fukuda and M.Sato, Solid State Commun. 66(1988)1101.
- [5] K.Kumagai and Y.Nakamura, Physica C, 152(1988)286.
- [6] R.A.Fisher, S.Kim, S.E.Lacy, N.E.Phillips, D.E.Morris, A.G.Markez, J.Y.Wei and D.S.Ginley, Phys. Rev. B38(1988)11942.
- [7] Y.Maeno, Y.Aoki, H.Kamimura, J.Sakurai and T.Fujita, Jpn. J. Appl. Phys. 26(1987) L402.
- [8] R.Kuentzler, Y.Dossmann, S.Vilminot and S.el Hadigui, Solid State Commun. 65(1988)1529.
- [9] T.Sasaki, O.Nakatsu, N.Kobayashi, A.Tokiwa, M.Kikuchi, A.Liu, K.Hiraga, Y.Syono and Y.Nuto, to be published in Physica C.
- [10] S.Martin, A.T.Flory, R.M.Fleming, L.F.Schneemeyer and J.V.Waszcak, Phys. Rev. Letter, 66 (1988) 2194.

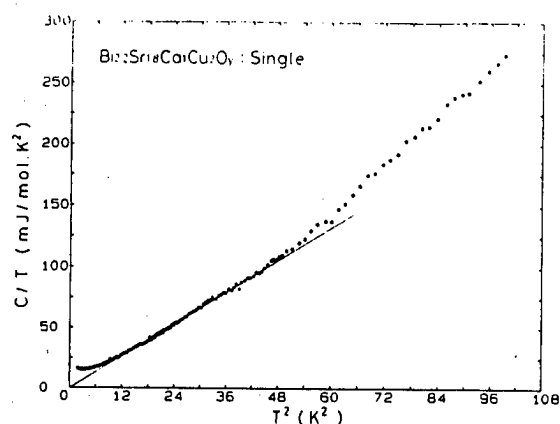


Fig. 1 C/T vs.  $T^2$ .

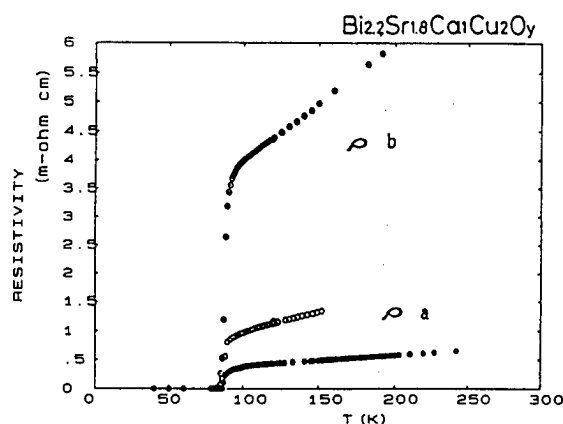


Fig. 2 Resistivities along the a and b axes vs. temperature.

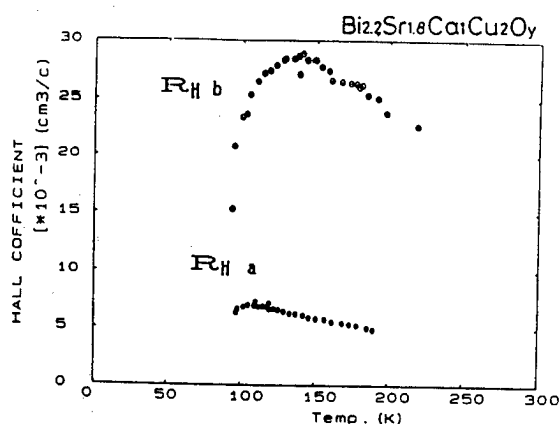


Fig. 3 Hall coefficients along the a and b axes vs. temperature.

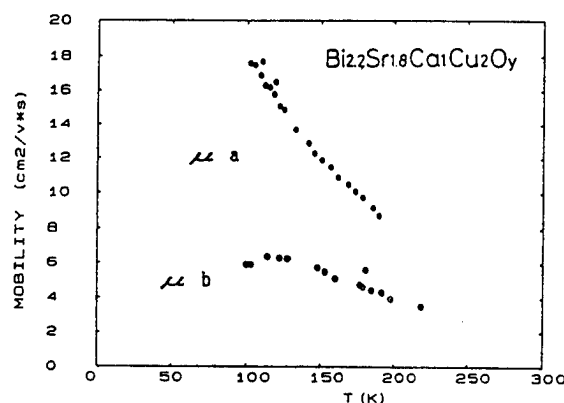


Fig. 4 Mobilities along the a and b axes vs. temperature.

R. Yoshizaki and I. Nakai<sup>†</sup>

Institute of Applied Physics, University of Tsukuba, Tsukuba, Ibaraki 305, Japan

<sup>†</sup>Department of Chemistry, University of Tsukuba, Tsukuba, Ibaraki 305, Japan

Magnetic susceptibility measurement observed in  $\text{La}_2\text{CuO}_{4-y}$  up to 1200 K elucidated that the apical oxygen atoms played an important role in the two-dimensional spin correlation. Nonmetal-to-superconductor transition was investigated for high-quality  $(\text{La}_{1-x}\text{Sr}_x)_2\text{CuO}_{4-y}$  samples prepared from a hot-press technique in the range of  $x$  from 0 to 0.075. Average structures of the 221 and 232 phases of the Bi-Sr-Ca-Cu-O system were determined from the single crystal X-ray diffraction analyses. Nonmetal-to-superconductor transition was also investigated in the 232-phase Bi-compounds by replacing Ca by Y atoms.

### 1. The La-Sr-Cu-O System

Three-dimensional antiferromagnetic spin ordering disappears at the Neel temperature  $T_N$ . Above  $T_N$  the two-dimensional spin correlation still remains in  $\text{La}_2\text{CuO}_{4-y}$  as suggested in the magnetic susceptibility measurement [1] and indicated in the neutron scattering measurement [2]. So we have measured the magnetic susceptibility of  $\text{La}_2\text{CuO}_{4-y}$  up to 1200 K by employing a magnetic balance method in order to get direct information about the two-dimensional spin correlation.

The results [3] are shown in Fig. 1 for the experiments carried out in the two kinds of environment; (a) low pressure oxygen gas and (b) helium exchange gas. In oxygen atmosphere, the magnetic susceptibility  $\chi$  gradually increases up to 1200 K even for a Sr doped sample ( $x=0.005$ ). This result means that the exchange interaction constant  $J$  is more than 1200 K in  $\text{La}_2\text{CuO}_{4-y}$  [4]. In low pressure helium gas, on the other hand, abrupt reduction of the magnetic susceptibility is observed at 1100 K in the heating process and the susceptibility restores at 950K in the cooling process. This thermal hysteresis is caused by the desorption and adsorption of oxygen atoms as seen from the weight change of the sample shown in the upper part of Fig. 1(b). The difference of the total oxygen atoms in the sample after the thermal cycle can be seen by the shift of the tail of the antiferromagnetic peak around room temperature.

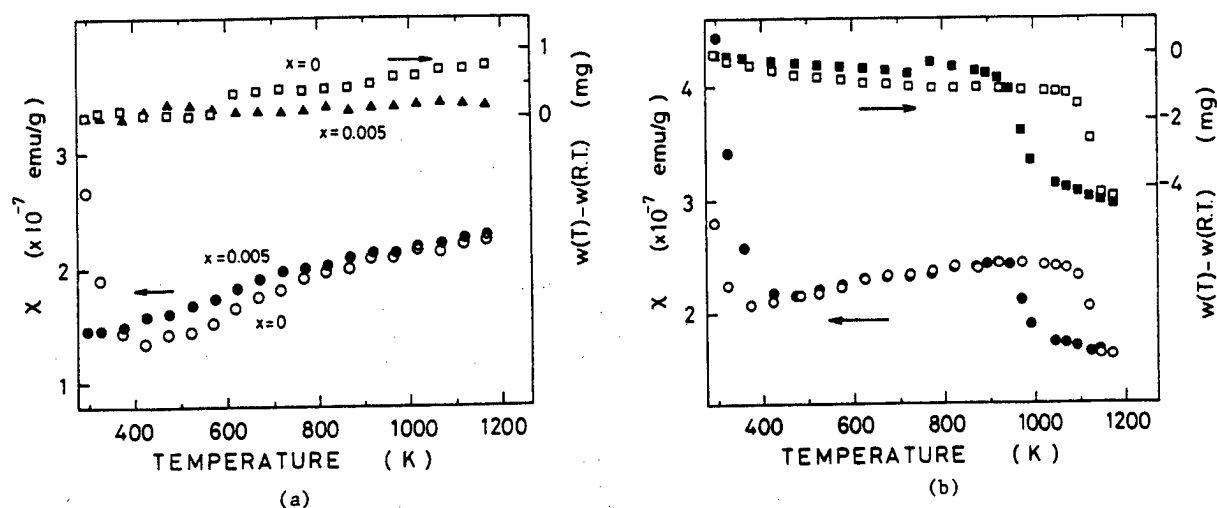


Fig. 1 Magnetic susceptibilities of  $(\text{La}_{1-x}\text{Sr}_x)_2\text{CuO}_{4-y}$  at high temperatures: (a) measured in low pressure oxygen gas in heating process,  $\circ$  for  $x=0$  and  $\bullet$  for  $x=0.005$ ; (b) in He exchange gas for  $\text{La}_2\text{CuO}_{4-y}$ ,  $\circ$  obtained in the first heating and  $\bullet$  in the succeeding cooling process. The corresponding weight change is shown by  $\square$  in heating and by  $\blacksquare$  in cooling proces. The initial weight of all samples is 1 gram.

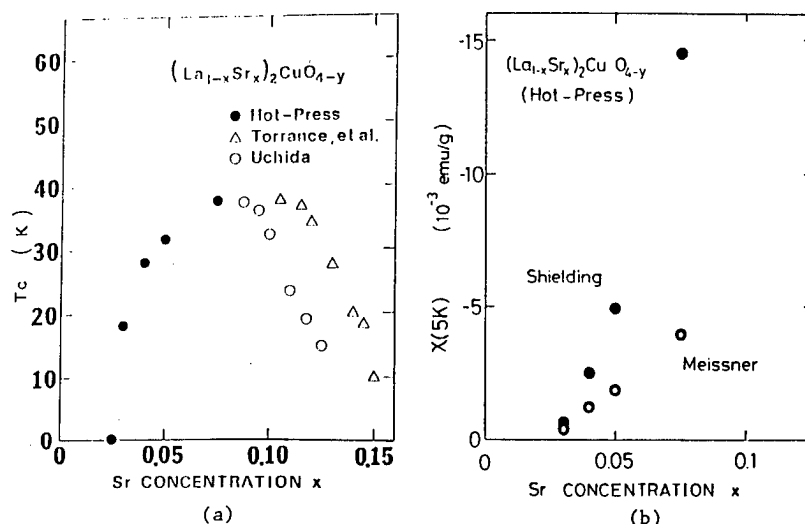


Fig. 2 (a) Dependence of  $T_c$  of  $(La_{1-x}Sr_x)_2CuO_{4-y}$  on  $x$  for the samples prepared by a hot-press method. (b) The magnetic susceptibilities at 5 K representing the shielding volume and the Meissner fraction of the samples are plotted as a function of  $x$ .

The diamagnetic susceptibility of the core levels in  $La_2CuO_{4-y}$  is estimated to be about  $-3.2 \times 10^{-7}$  emu/g. Then the susceptibility change at 1100 K is more than 10% of paramagnetic susceptibility of the valence electron system, even though only 2% oxygen atoms, estimated from the weight loss, are desorbed. The deficiency of oxygen atoms in this compound starts from the apical oxygens of the octahedron, which would not contribute directly to the two-dimensional spin correlation. But the desorption of the oxygen atoms must leave electrons in the system. These electrons will compensate holes in the system and then enters probably into  $(3d)^9$  states. Thus it is suggested that the electron doping in this system causes the destruction of spin correlation.

By means of hot-press technique, we can provide sintered  $(La_{1-x}Sr_x)_2CuO_{4-y}$  samples with large grain size of the order of 0.1-1 mm [5]. In such a sample the effect of the grain boundaries to the electrical and magnetic susceptibility properties is believed to be less compared with the sintered samples at ambient pressure in which the grain size is normally of the order of 10  $\mu m$ . The really doped content of Sr is confirmed by EPMA for  $x=0.075$  sample; there is  $90 \pm 2\%$  of the nominal content  $x$  and the homogeneity is better than 1%. We have measured the electrical resistivity by four probe method and the magnetic susceptibility by a SQUID magnetometer in the temperature range of 5-300K.

The superconducting transition temperature  $T_c$  and the magnitude of the diamagnetic susceptibilities at 5 K are plotted in Fig. 2 (a) and (b), respectively [6-8]. It is noted that the samples with  $x$  less than 0.04 have the inflection in the resistivity-temperature curve and the localization effect remains strongly in  $-T$  curve. In this range of  $x$ , the fractional volume of the superconductivity is still small and the  $T_c$  changes abruptly as increasing  $x$ . In the range of  $x \geq 0.04$ , on the other hand, the bulk superconductivity is achieved and  $T_c$  depends on  $x$  rather moderately. It is found in Fig. 2(b) that both the shielding volume and the Meissner fraction depend almost linearly on  $x$  and they converge to zero at  $x=0.025$  where the nonmetal-superconductor transition occurs. Preparation of the samples with higher Meissner fraction and higher  $x$  are now in progress.

## II. The Bi-Sr-Ca-Cu-O System

### (1) Structure [9]

We have carried out X-ray single crystal structure analyses of the 221 phase  $(Bi_2(Sr,Ca)_2CuO_x)$  with  $T_c=7-22$  K) and 232 phase  $(Bi_2(Sr,Ca)_3Cu_2O_x)$ ,  $T_c \approx 80$  K) with anisotropic temperature factors which were introduced to obtain more detailed images of the average structures. Single crystals used in this

Table I Summary of experimental conditions for the structural analyses of the 221 and 232 phases.

	221 phase	232 phase
formula	$Bi_2Sr_{1.9}Ca_{0.1}CuO_8$	$Bi_2Sr_{1.7}Ca_{1.3}Cu_2O_8$
dimensions(mm)	$0.29 \times 0.07 \times 0.02$	$0.16 \times 0.07 \times 0.01$
crystal system	orthorhombic	orthorhombic
space group	Bbmb(No.66-Ccmm)	Bbmb(No.66-Ccmm)
cell constants		
a (Å)	5.3826(8)	5.3946(8)
b	5.3761(11)	5.3895(13)
c	24.384(7)	30.649(12)
scan mode	$2\theta-\omega$	$2\theta-\omega$
$2\theta$ range	$3-70^\circ$	$3-70^\circ$
$\mu$ (cm $^{-1}$ )	570.8	506.5
absorption correction	ACACA	ACACA
total reflections	854	1086
independent reflections	282( $>3\sigma$ )	354( $>3\sigma$ )
R	0.109	0.069
$R_w$	0.108	0.064

Table II Interatomic distances (Å) in the 221 and 232 phases.

221 phase			232 phase		
Bi	- 02	1.95	Bi	- 03	2.04
	- 03	2.18		- 04	2.13
		2.78			2.79
		2.91			2.91
		3.03			3.02
Sr/Ca	- 01	2.42(3)	Sr/Ca	- 01	2.45(3)
		2.67(4)		- 02	2.71(3)
	- 02	2.53		- 03	2.45
		2.84			2.81
		3.14			3.14
Cu	- 01	1.912(6)	Ca/Bi	- 01	2.65(3)
	- 02	2.58		- 02	2.37(3)
			Cu	- 01	1.915(8)
				- 02	1.921(9)
				- 03	2.46

Table III A comparison of models reported for the average structure of the 232 phase.

	present study	Subramanian	Sunshine	Tarascon	Bordet	Kajitani
space group	B b m b (C c c m)	A m a a (C c c m)	F m m m	I 4 / m m m	B b m m (C m c m)	F m m m
a (Å)	5.395(1)	5.399(2)	5.414(2)	3.814(3)	5.401(2)	5.39(8)
b	5.390(1)	5.414(1)	5.418(2)	(a)	5.401(2)	5.39(8)
c	30.65(1)	30.904(16)	30.89(1)	30.52(3)	30.83(2)	30.725(9)
R	0.070	0.099	0.173	0.099		8.6(Rp)
R <sub>w</sub>	0.065	0.088	0.094	0.088	0.048	12.0(Rwp)
coordination number of Bi	6	8	6	6	6	9

study were prepared using a method reported previously [10]. Intensity data were collected by a Rigaku Rotaflex AFC-5 four-circle diffractometer using graphite-monochromatized MoK radiation. Crystal data and experimental conditions for intensity data collection are summarized in Table I. Initial structure models obtained by a direct method using the MULTAN80 program were further developed by Fourier synthesis and a full-matrix least-squares refinement using the RFINE2 program. The atomic scattering factors for neutral atoms were taken from Cromer and Mann [11], and the anomalous dispersion factors from International Tables for X-ray crystallography [12].

Average crystal structures of the 221 and 232 phase including the assumed oxygen atoms (O3, O4) are shown in Fig. 3 (a) and (b), respectively. Selected bond distances are listed in Table II. The two phases have similar structures and their differences result from the number of perovskite units sandwiched by the two Bi-O double-layers. The oxygen atoms of the Bi layer are projecting from the Bi-Bi plane in both structures. Structural features of the models previously reported for the 232 phase [13-17] are compared with ours in Table III. The positions of the metal atoms are basically equivalent in these 5 models. As can be seen from Table III, however, their space groups and the coordination of the Bi atom with the oxygen atoms are clearly different. The space group of the present structure model agrees with the one reported by Subramanian et al. [13]. However, the coordination of the Bi atom found in the present study supports the models reported by Sunshine et al. [14], Tarascon et al. [15] and Bordet et al. [16].

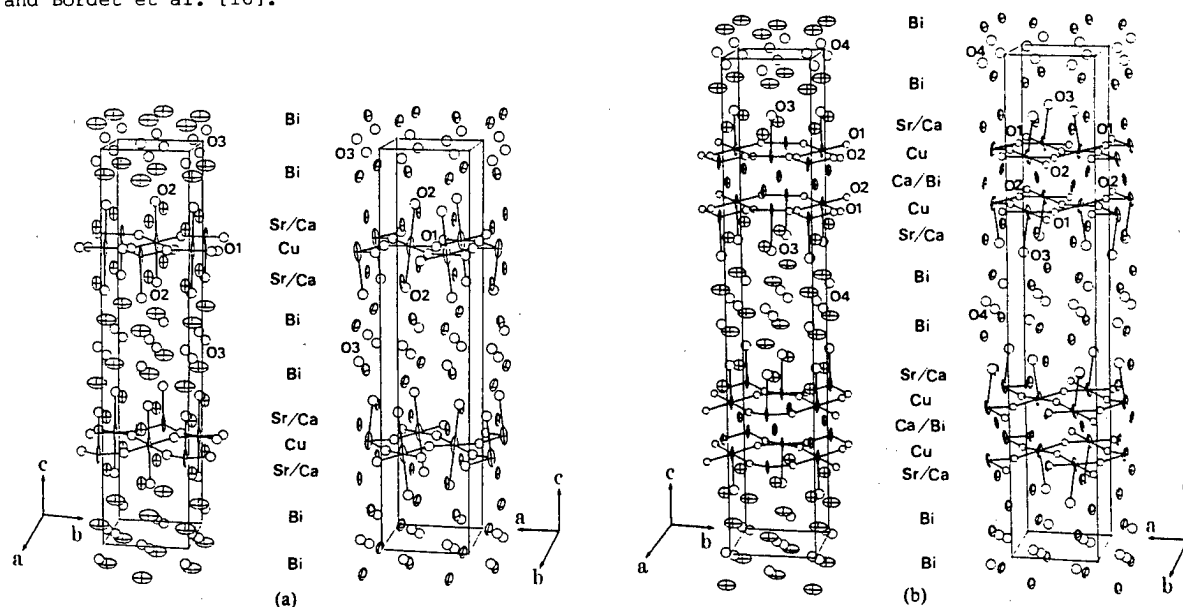


Fig. 3 Average structures of the (a) 221 and (b) 232 phases. The Cu-O bonds are only drawn.

As mentioned previously, the ellipsoids of the Bi atoms in the 221 and 232 structures are abnormally large in the bc plane (see Fig. 3) reflecting large uncertainties of the Bi positions. This is due to the existence of modulation in this plane. These observations are in good agreement with the high resolution TEM images of the bc plane, where marked modulated structure are observed (Matsui et al. [18]). We should also note that the ellipsoid of the Cu atom is abnormally small along the b-axis, but can not explain this observation.

## (2) Nonmetal-Superconductor Transition

We have measured the nonmetal-superconductor transition in the 232 phase of the  $\text{Bi}_2\text{Sr}_2\text{Ca}_{1-x}\text{Y}_x\text{Cu}_2\text{O}_y$  system by reducing holes by means of replacing Ca atom by Y atom [19]. The appropriate amount of oxides are well-mixed and calcined at 800 °C for 12 h. The sintering is performed for a pelletized sample in the following fire program; raising temperature up to the just melting temperature of the surface in a short time, lowering temperature to the range of 875-960 °C (depending on x) and keeping there for 50-70 h. In the first high-temperature process, the impurity phase  $\text{Y}_2\text{Cu}_2\text{O}_5$  is to be eliminated and the crystal quality becomes better in the second process. The impurity phase is checked for the Y-rich samples so that the magnetic susceptibility peak at 13 K is much less than  $10^{-6}$  emu/g. The lattice parameters are plotted as a function of x in Fig. 4. In  $0 \leq x \leq 0.03$  the structure is pseudotetragonal and orthorhombic in  $x \geq 0.04$ .

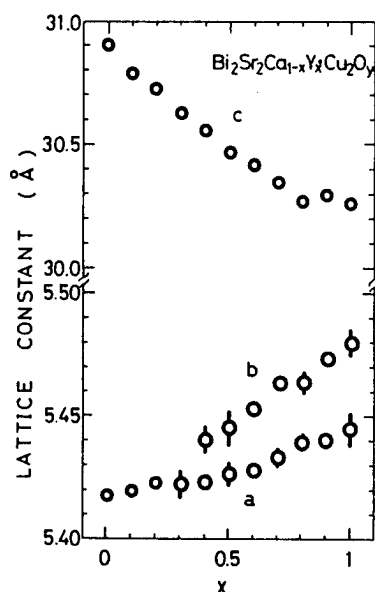


Fig. 4 The lattice constants of  $\text{Bi}_2\text{Sr}_2\text{Ca}_{1-x}\text{Y}_x\text{Cu}_2\text{O}_y$  with varying x.

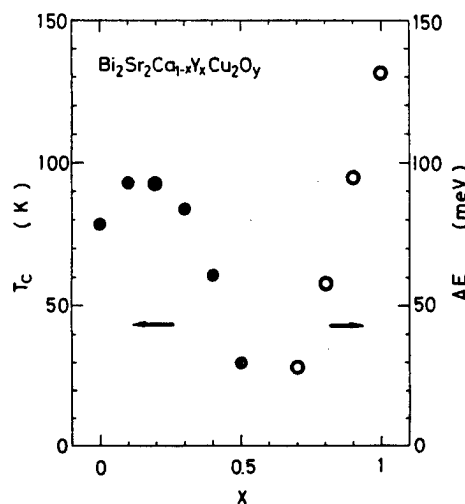


Fig. 5 Dependence of  $T_c$  (●) and the activation energy (○) on x in  $\text{Bi}_2\text{Sr}_2\text{Ca}_{1-x}\text{Y}_x\text{Cu}_2\text{O}_y$ .

The results of the low temperature magnetic susceptibility indicate that the bulk superconductivity is achieved up to  $x=0.04$ . For  $x \geq 0.06$ , the samples are insulating and the activation energies obtained from Arrhenius plot are also shown in Fig. 5 as well as  $T_c$ . With decreasing x from 1, the activation energy tends to zero at  $x \approx 0.55$ , where the nonmetal-superconductor transition occurs in this system. It is noted that the antiferromagnetic spin ordering is observed in the insulating region by means of the muon spin resonance experiment [20]. Thus the 232 phase Bi system exhibits similar phase diagram to those of the La-Sr-Cu-O and Ba-Y-Cu-O systems for varying hole concentrations.

## Acknowledgements

The authors gratefully acknowledge stimulating discussions with M. Inoue, N. Nishida, S. Sueno, T. Kawashima, A. Ono and K. Imai. We also wish to thank H. Ikeda for technical assistance. This work has been supported by Grant-in-Aid for Scientific Research on Priority Areas "Mechanism of Superconductivity".

## References

- [1] D.C.Johnston, J.P.Stokes, D.P.Goshorn and J.T.Lewandowski, *Phys. Rev. B* **36** (1987) 4007.
- [2] G.Shirane, Y.Endoh, R.J.Birgeneau, M.A.Kastner, Y.Hidaka, M.Oda, M.Suzuki and T.Murakami, *Phys. Rev. Lett.* **59** (1987) 1613.
- [3] R.Yoshizaki, H.Sawada, E.Kita and A.Tasaki, unpublished.
- [4] K.B.Lyons, P.A.Fleury, J.P.Remeika, A.S.Cooper and T.J.Negran, *Phys. Rev. B* **37** (1988) 2353.
- [5] T.Iwazumi, R.Yoshizaki, H.Sawada, H.Uwe, T.Sakudo and E.Matsuura, *Jpn. J. Appl. Phys. Lett.* **26** (1987) L386.
- [6] M.W.Shafer, T.Penny and B.L.Olson, *Phys. Rev. B* **36** (1987) 4047.
- [7] J.B.Torrance, Y.Tokura, A.I.Nazzari, A.Bezinge, T.C.Huang and S.S.P.Parkin, *Phys. Rev. Lett.* **61** (1988) 1127.
- [8] S.Uchida, Abstract of Tokai University Intern. Workshop on The Science of Superconductivity, Tokyo 1988, p.25.
- [9] K.Imai, I.Nakai, T.Kawashima, S.Sueno and A.Ono, *Jpn. J. Appl. Phys.* **27** (1988) L1661.
- [10] A.Ono, S.Sueno and F.P.Okamura, *Jpn. J. Appl. Phys.* **27** (1988) L786.
- [11] D.T.Cromer and J.B.Mann, *Acta Cryst.* **A42** (1986) 321.
- [12] International Tables for X-ray Crystallography (Kynoch Press, Birmingham, England, 1974) Vol. IV, p. 148.
- [13] M.A.Subramanian, C.C.Torardi, J.C.Calabrese, J.Gopalakrishnan, K.J.Morrissey, T.R.Askew, R.S.Flippen, U.Chowdhry, A.W.Sleight, *Science* **239** (1988) 1015.
- [14] S.A.Sunshine, T.Siegrist, L.F.Schneemeyer, D.W.Murphy, R.J.Cava, B.Batlogg, R.B.van Dover, R.M.Fleming, S.H.Clarum, S.Nakahara, R.Farrow, J.J.Krajewski, S.M.Zahurak, J.V.Waszcak, J.H.Marshall, P.Marsh, L.W.Rupp, Jr. and W.F.Peck, *Phys. Rev. B* **38** (1988) 893.
- [15] J. M. Tarascon, Y. Le Page, P. Barboux, B. G. Bagley, L. H. Greene, W. R. Mckinnon, G. W. Hull, M. Giroud and D. M. Hwang, *Phys. Rev. B* **37** (1988) 9382.
- [16] P. Bordet, J. J. Capponi, C. Chaillout, J. Chenavas, A. W. Hewat, J. L. Hodeau, M. Marezio, J. L. Tholence, D. Tranqui, *Proc. Intern. Conf. on HTSM<sup>2</sup>S*, *Physica C* **153-155** (1988) 623.
- [17] T. Kajitani, K. Kusaba, M. Kikuchi, N. Kobayashi, Y. Syono, T. B. Williams and M. Hirabayashi, *Jpn. J. Appl. Phys.* **27** (1988) L587.
- [18] Y. Matsui, H. Maeda, Y. Tanaka and S. Horiuchi, *Jpn. J. Appl. Phys.* **27** (1988) L372.
- [19] R.Yoshizaki, Y.Saito, Y.Abe and H.Ikeda, *Physica C* **152** (1988) 408.
- [20] N.Nishida, H.Miyatake, S.Okuma, T.Tamegai, Y.Iye, R.Yoshizaki, K.Nishiyama and K.Nagamine, *Physica C* **156** (1988) 625.

Kiichi OKUDA and Satoru NOGUCHI

College of Engineering, University of Osaka Prefecture  
4-804 Mozu-Umemachi, Sakai, Osaka 591

Magnetic susceptibility of  $\text{YBa}_2\text{Cu}_3\text{O}_{7-\Delta y}$  in the normal state was investigated as a parameter of oxygen deficiency  $\Delta y$ . Temperature dependence of the susceptibility was well explained by assuming three contributions of Curie-Weiss law  $\chi_{\text{CW}} = C/(T-\theta)$ , constant paramagnetism  $\chi_0$  and the triplet spin-pair excitation from the singlet ground state as written by  $\chi_{\text{pair}} = 2N_{\text{pair}}g^2\mu_B^2/kT(3+\exp(2|J|/kT))$ . Exchange coupling constant  $J$  is estimated to be  $2J/k \approx -800$  K and it does not depend on  $\Delta y$ . Magnetization process of  $\text{R}_E\text{Ba}_2\text{Cu}_3\text{O}_{7-\delta}$  ( $\text{R}_E$ : rare-earth ions), was measured at 4.2 K under a pulsed magnetic field up to 50 T. The magnetization of  $\text{R}_E$  ions and the critical current density was estimated.

Magnetic aspect of the recently developed high- $T_c$  superconducting oxides in both the normal and superconducting states is an important subject for understanding the mechanism of the superconductivity. In the present paper we report the results of two investigations: (1) magnetic susceptibility of  $\text{YBa}_2\text{Cu}_3\text{O}_{7-\Delta y}$  in the normal state as a parameter of oxygen deficiency  $\Delta y$  and (2) magnetization process of  $\text{R}_E\text{Ba}_2\text{Cu}_3\text{O}_{7-\delta}$ ,  $\text{R}_E$  = rare-earth ions, under a pulsed magnetic field up to 50 tesla.

### 1. Magnetic Susceptibility of $\text{YBa}_2\text{Cu}_3\text{O}_{7-\Delta y}$ in the Normal State

Samples with various values of oxygen deficiency  $\Delta y$  were prepared by the following two steps; the synthesis of the starting samples of  $\text{YBa}_2\text{Cu}_3\text{O}_{7-\Delta y}$  with  $\Delta y \sim 0.1$  and the heat treatment to control the oxygen content. The first step was done by a usual solid state reaction in air. The oxygen content was determined by the chemical analysis of iodometry to be  $\text{YBa}_2\text{Cu}_3\text{O}_{6.93 \sim 6.94}$ . The second step was done by the following procedure: the sample was heated in an atmospheric pressure of He gas at a desired temperature for 20 hours and then cooled rapidly to room temperature. The relation between the heat-treatment temperature and the oxygen deficiency  $\Delta y$  in  $\text{YBa}_2\text{Cu}_3\text{O}_{7-\Delta y}$  is shown by solid circles in Fig.1, together with the data obtained by quenching in air as a reference (open circles). The critical values of  $\Delta y$  for the transformation from orthorhombic to tetragonal symmetry are 0.7 and 0.8 for air-quench and He-gas-quench methods, respectively. Superconducting transition temperature  $T_c$  and the volume fraction of superconductivity  $f_{\text{super}}$  were determined by ac-magnetic susceptibility as shown in Fig.2.

DC magnetic susceptibility was measured by a Faraday type magnetometer for the samples  $\text{YBa}_2\text{Cu}_3\text{O}_{7-\Delta y}$  with  $\Delta y = 0.1, 0.380, 0.436, 0.486$ ,

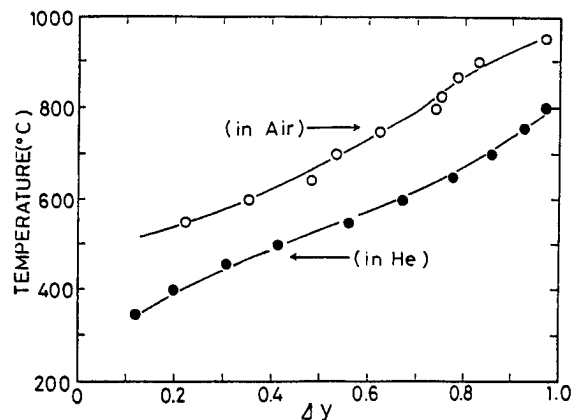


Fig.1. Heat-treatment temperature vs.  $\Delta y$ .



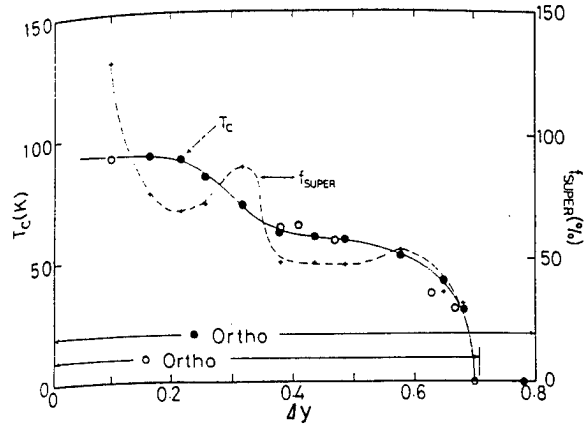


Fig. 2.  $T_c$  and volume fraction of superconductivity  $f_{\text{super}}$  as a function of  $\Delta y$ .

0.577, 0.650, 0.682, 0.770 and 0.992. The susceptibility for  $\Delta y \geq 0.380$  follows the Curie-Weiss law with the constant paramagnetic term  $\chi_0$ .  $\chi_{\text{CW}} = C/(T-\theta) + \chi_0$ , at low temperatures below about 150 K. Typical examples for  $\Delta y = 0.682$  and 0.992 are shown in Fig. 3. Broken lines are the Curie-Weiss fitting. The fitting parameters are summarized in Fig. 4. At high temperatures above  $\sim 150$  K, however, the susceptibility deviates from the Curie-Weiss law. We tried to explain the deviations by assuming the triplet spin-pair excitation from the antiferromagnetically coupled ground state given by the energy  $-2J\mathbf{S}_i\mathbf{S}_j$  where  $J$  is the exchange constant and  $\mathbf{S}_i, \mathbf{S}_j$  are the spins with the values  $|\mathbf{S}_i| = |\mathbf{S}_j| = 1/2$ . In the model the susceptibility is written as

$$\chi_{\text{pair}} = 2N_{\text{pair}}(g\mu_B)^2/kT(3 + e^{2|J|/kT}) \quad (1),$$

where  $N_{\text{pair}}$  is the number of coupled spin-pairs. The fitting to eq.(1) is shown by a broken line in Fig. 5 for the sample with  $y = 0.682$ . Good fitting was obtained for all samples. The susceptibility for  $\Delta y \sim 0.1$  was also fitted to eq.(1) with constant paramagnetism  $\chi_0$ . Thus obtained exchange constant  $-J/k$  is shown in Fig. 6 as a function of  $\Delta y$ . The exchange constant  $-J/k$  is almost constant for various oxygen deficiencies and the value was estimated to be  $-J/k \approx 400$  K. When we assumed that the temperature dependent parts of susceptibility are attributed to the  $\text{Cu}^{2+}$  ions with  $g = 2$  and  $S = 1/2$ , the numbers of isolated  $\text{Cu}^{2+}$  ions which contribute to  $\chi_{\text{CW}} = C/(T-\theta)$  and pair-coupled  $\text{Cu}^{2+}$

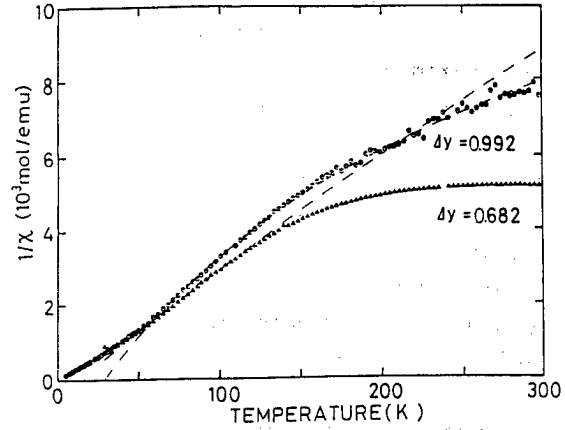


Fig. 3. DC-magnetic susceptibility for  $\Delta y = 0.682$  and 0.992 of  $\text{YBa}_2\text{Cu}_3\text{O}_{7-\Delta y}$ . Broken lines are given by Curie-Weiss fitting.

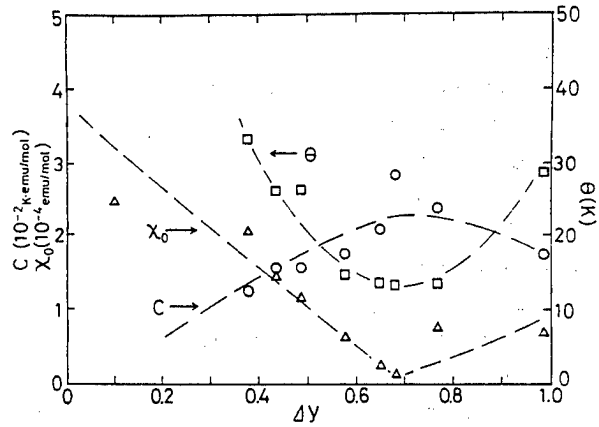


Fig. 4.  $\Delta y$ -dependence of the parameters of Curie-Weiss law.

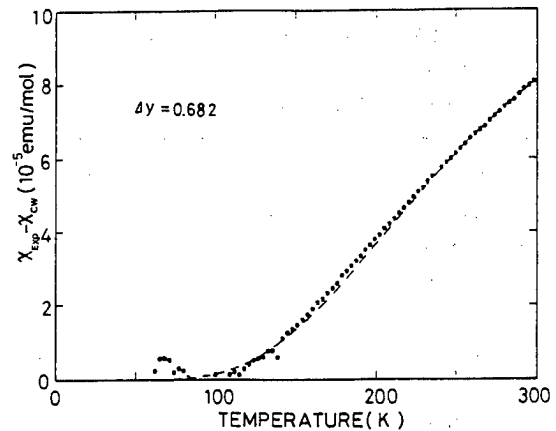


Fig. 5. Temperature dependence of the deviations of the magnetic susceptibility from the Curie-Weiss law,  $\chi_{\text{exp}} - \chi_{\text{CW}}$ . A broken line is the theoretical fitting curve given in the text by assuming the singlet-to-triplet excitation.

ions,  $N_{\text{single}}$  and  $N_{\text{pair}}$ , are obtained as a function of  $\Delta y$  in Fig.7. The numbers of  $N_{\text{single}}$  and  $N_{\text{pair}}$  have a maximum near the  $\Delta y$  corresponding to the structural transformation. It suggests that the temperature dependent terms of susceptibility,  $\chi_{\text{CW}}$  and  $\chi_{\text{pair}}$  are attributed to the  $\text{Cu}^{2+}$  ions caused by the disordering of oxygen deficiency in the Cu(1) sites on the basal plane. From the facts that the susceptibility for  $\Delta y \sim 0.1$  is well fitted to the eq.(1), however, the pair excitation may be also caused in the Cu(2)-O plane.

## 2. Magnetization and Critical Currents of $\text{R}_E\text{Ba}_2\text{Cu}_3\text{O}_{7-\delta}$

Samples of  $\text{R}_E\text{Ba}_2\text{Cu}_3\text{O}_{7-\delta}$ , where  $\text{R}_E = \text{Y, Nd, Sm, Eu, Gd, Dy, Ho, Er and Yb}$ , were prepared by a solid state reaction in air. They were checked by the X-ray diffraction. The  $T_c$  and the volume fraction of superconductivity were measured by ac-magnetic susceptibility.

The high field magnetization measurements were done for the systems  $\text{R}_E\text{Ba}_2\text{Cu}_3\text{O}_{7-\delta}$  at 4.2 K under a pulsed magnetic field up to 50 T in High Magnetic Field Laboratory of Osaka University [1]. The measurements were carried out with the standard pick-up coil system. Samples were mixed with highly purified alumina of 25~50 wt.% so as to isolate the superconducting grains. Grain size were estimated to be about 5  $\mu\text{m}$  for all samples from direct observation by microscope.

A typical example of magnetization curve at 4.2 K is shown in Fig.8 for  $\text{DyBa}_2\text{Cu}_3\text{O}_{7-\delta}$ . Magnetization due to 4f moment of  $\text{Dy}^{3+}$  and hysteresis loop which is characteristic of hard superconductor are mixed in the curve. From the hysteresis loop of magnetization curve the critical current density  $J_c$  was estimated by applying the critical-state model as follows [2,3]:

$$J_c [\text{A/cm}^2] = 160 \Delta M [\text{gauss}] / 3\pi R [\text{cm}] \quad (2),$$

where  $\Delta M$  is the difference between the magnetization for increasing and decreasing field,  $R$  the grain radius. Thus obtained results are summarized in Fig.9 for the system  $\text{R}_E\text{Ba}_2\text{Cu}_3\text{O}_{7-\delta}$ . In a low field region below 8 T,  $J_c$  is rapidly decreased with increasing field, while the  $J_c$  in a high field

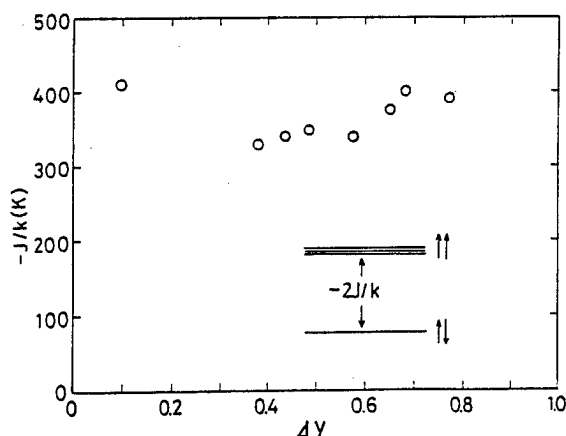


Fig.6.  $\Delta y$ -dependence of the exchange constant.

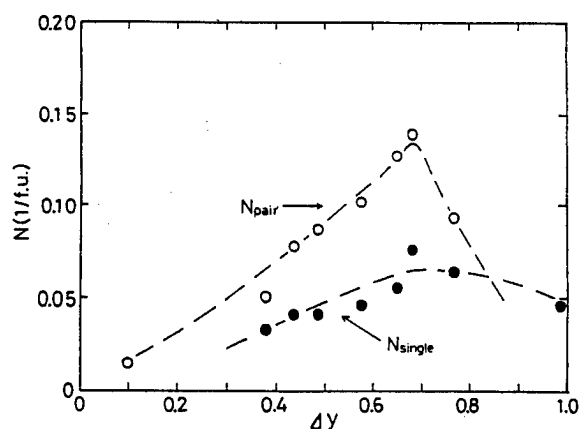


Fig.7.  $\Delta y$ -dependence of isolated spins,  $N_{\text{single}}$ , and pair-coupled spins,  $N_{\text{pair}}$ .

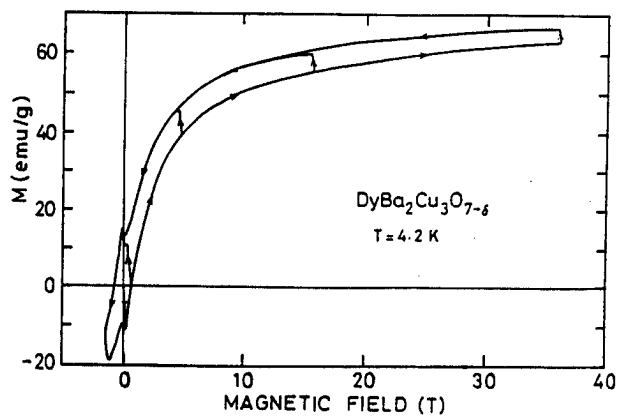


Fig.8. An example of magnetization process of  $\text{DyBa}_2\text{Cu}_3\text{O}_{7-\delta}$  at 4.2 K.

region is gradually decreased. The values of  $J_c$  at 50 T are estimated to be  $10^5 \sim 10^6$  A/cm<sup>2</sup> in the system  $R_E\text{Ba}_2\text{Cu}_3\text{O}_{7-\delta}$ .

Magnetization of rare earth ions is extracted from the experimental data by averaging the hysteresis. Results are shown in Fig.10 for the system  $R_E\text{Ba}_2\text{Cu}_3\text{O}_{7-\delta}$ . In the samples of  $R_E = \text{Gd}$ , Yb, Nd and Sm the magnetization are almost saturated and the saturation moments are 7.0, 2.1, 1.7 and 0.2  $\mu_B/R_E$ , respectively. In the samples of  $R_E = \text{Ho}$ , Dy and Er the magnetization are still increased in our experimental region. The saturation moments extrapolated to zero field are estimated to be 7.5, 7.5 and 4.8  $\mu_B/R_E$  for  $R_E = \text{Ho}$ , Dy and Er, respectively.

We find from Figs.9 and 10 that the magnitude of  $J_c$  in a high field region is correlated to the saturation moment of  $R_E\text{Ba}_2\text{Cu}_3\text{O}_{7-\delta}$  except for  $R_E = \text{Y}$  and Eu whose ground state is nonmagnetic. This correlation suggests that magnetic ions are effective to raise the critical current.

This work was supported by the Grant-in-Aid for Scientific Research on Priority Areas "Mechanism of Superconductivity".

#### References

- [1] A.Yamagishi and M.Date, in: High Field Magnetism, M.Date, ed. ( North-Holland, Amsterdam, New York, Oxford, 1982 ), p.289.
- [2] C.P.Bean, Phys. Rev. Lett. 8 (1962) 250.
- [3] J.R.Clem and V.G.Kogan, Jpn. J. Appl. Phys. 26 (1987) Suppl. 26-3 1161.

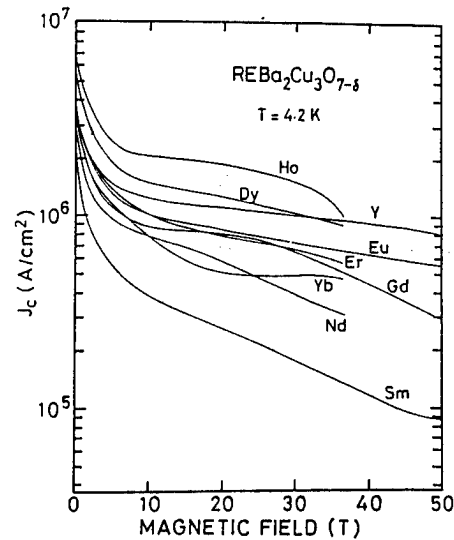


Fig.9. Field dependence of critical currents of the systems  $R_E\text{Ba}_2\text{Cu}_3\text{O}_{7-\delta}$ .

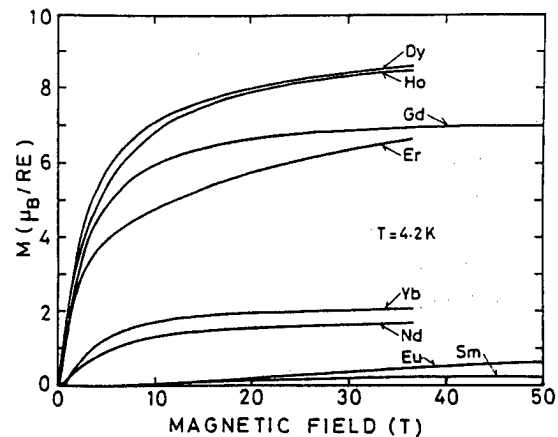


Fig.10. Magnetization of  $R_E$  ions in the systems  $R_E\text{Ba}_2\text{Cu}_3\text{O}_{7-\delta}$ .

# Electron Tunneling Study on High-Tc Superconductors

T. Ekino and J. Akimitsu

Department of Physics, Aoyama-Gakuin University

6-16-1, Chitosedai, Setagaya, Tokyo 157

We report a summary of our tunneling measurements on the series of high-Tc oxide superconductors. In the Bi-Sr-Ca-Cu-O system, the ratios  $2\Delta/kT_c = 9-11$  are obtained for the tunneling currents parallel to the  $\text{CuO}_2$  planes and gap anisotropies are  $\Delta_{//}/\Delta_{\perp} = 1.5-1.8$ .  $2\Delta/kT_c$  in Ca-absent  $\text{Bi}_2\text{Sr}_2\text{CuO}_y$  is 5.4-7.3. These values are considerably larger than those of  $\text{La}_{2-x}\text{Sr}_x\text{CuO}_4$  and  $\text{YBa}_2\text{Cu}_3\text{O}_y$  where  $2\Delta/kT_c$  are  $\sim 5$  and 3-4, respectively.

After the discovery of new oxide superconductors, extensive studies have been carried out to elucidate the mechanism of high-Tc superconductivity. Electron tunneling is one of the powerful techniques in the study of superconductivity, because it can provide the direct informations about the energy gap and the superconducting density of states. The values of gaps in the electron tunneling measurements at early stages have been widely spreaded from 3 to 10 in  $2\Delta/kT_c$ [1]. These wide spreaded values are mainly due to the sample inhomogeneities and the misunderstanding of the superconducting energy gaps. The careful sample preparations and the checks of reproducibilities converge into the  $2\Delta/kT_c = 4$  to 5.

In this paper, we report a series of tunneling measurements on the high-Tc oxide superconductors, especially focus on the values of the energy gaps. Measurements were done by the point-contact configuration with Al or Pt electrodes. The samples were polycrystals or films. To determine the  $T_c$ , the temperature dependence of energy gaps or the zero bias conductances have been measured. For the cases of La-Sr-Cu-O(LSCO), Y-Ba-Cu-O(YBCO) and Bi-Sr-Cu-O(BSCO), the tunneling barriers were often obtained from their surface insulating layers.

Fig.1 shows the temperature variation of the raw data of the  $dI/dV$  curves from the Bi-Sr-Ca-Cu-O (BSCCO)-Al tunnel junction. As seen in Fig.1, clear gap structures are observed and the  $dI/dV$  curves are symmetrical with respect to the Fermi level. This feature was rarely obtained in the cases of the LSCO and YBCO. The gap structures are smeared out at about 100K and the superconducting transition temperature  $T_c$  is determined as 104K from the temperature that the zero bias conductance  $dI/dV(0\text{mV})$  begin to reduce. Thus the electrons are tunneling mainly through the region of  $\text{Bi}_2\text{Sr}_2\text{Ca}_2\text{Cu}_3\text{O}_y$  (BSCCO2223) phase though the sample was synthesized as nominal compositions of Bi:Sr:Ca:Cu=2:2:1:2 ( $T_c=86-80\text{K}$ ). The energy gap  $2\Delta$  at  $T=52.9\text{K}$  is about 50-60meV determined from the current-voltage characteristics and the intersection of  $dI/dV$  curve with the normal state  $dI/dV=(dI/dV)_n$ . The gap values at  $T=0\text{K}$  are about 6% larger than that at  $T=52.9\text{K}$  when we employ the BCS curve for the temperature dependence of the energy gap. The ratio  $2\Delta/kT_c=6-7$  is obtained.

Fig.2 shows the temperature variation of the raw data of  $dI/dV$  curves. The polycrystal sample used here is a Pb doped BSCCO2223 phase. The sample attained the zero resistance temperature at  $T=108\text{K}$ . The  $dI/dV$  curves above  $T=58.6\text{K}$  could not be measured because the condition of tunnel junction became worse. A fine structures at  $V=\pm 35\text{mV}$  may be attributed to the gap anisotropy with respect to the  $\text{CuO}_2$  planes.  $2\Delta$  lies between 85-87meV and the transition temperature is 113-108K, so that  $2\Delta/kT_c=8.7-9.3$ . These values are considerably larger than that appeared in Fig.1. This may be due to the gap anisotropy described above and will be clarified soon later. Moreover, the observed energy gaps in BSCCO system are much larger than those of LSCO and YBCO where  $2\Delta/kT_c=5$  and 3-4, respectively. The differences among these results will be discussed later.

In Fig.3, we show the temperature dependences of the energy gaps for the both phases of BSCCO

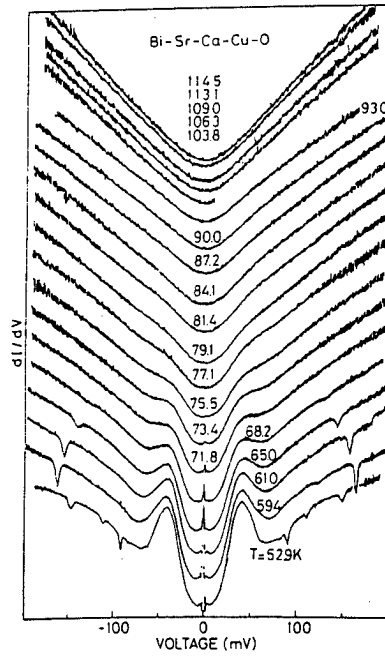


Fig.1 Temperature variation of  $dI/dV$  raw data for Bi-Sr-Ca-Cu-O.

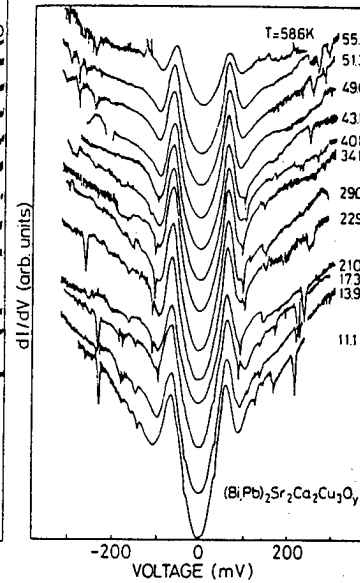


Fig.2 Temperature variation of  $dI/dV$  raw data for  $(\text{Bi,Pb})_2\text{Sr}_2\text{Ca}_2\text{Cu}_3\text{O}_y$  up to  $T=58.6\text{K}$ .

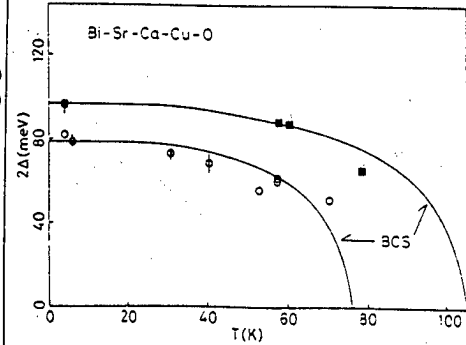


Fig.3 Temperature dependences of the energy gaps for Bi-Sr-Ca-Cu-O system. Open circles and filled squares correspond to BSCCO2212 and BSCCO2223, respectively.

polycrystals.  $2\Delta$ 's at each temperature were obtained by using the density of states proposed by Dynes et al[2] with thermal smearing. The gap values are larger than that expected from the BCS theory. However, their temperature dependences coincide with the scaled BCS curves and this trend is confirmed by ref.[3].

To clarify the gap anisotropies in the BSCCO system as predicted in the Figs.1 and 2, we have measured the energy gaps with respect to the  $\text{CuO}_2$  planes. The samples used in these measurements are the oriented films. These were kindly offered by Dr. T. Nakada of Aoyama-Gakuin University[4]. Fig.4(a) and (b) show the typical examples of the gap anisotropies with respect to the  $\text{CuO}_2$  planes for the both phases of BSCCO. It raises the question that we are actually measuring the anisotropies of the energy gaps in these samples, because the sample have to be pressed into the counter electrode or a point into the sample. However, we obtained the strong relationships between the gap values and the directions of the  $\text{CuO}_2$  planes at the interfaces of the tunnel junctions. The gap values in Fig.4(a) are  $2\Delta_{\perp}=49\text{--}54\text{meV}$ ,  $2\Delta_{\parallel}=80\text{--}88\text{meV}$ , where  $\perp$  and  $\parallel$  mean perpendicular and parallel to the  $\text{CuO}_2$  planes.  $2\Delta_{\perp}$  and  $2\Delta_{\parallel}$  agree with the gaps in Figs. 1 and 2, respectively. The ratio of gaps is  $\Delta_{\parallel}/\Delta_{\perp}=1.5\text{--}1.8$ . Since  $T_c$  is about 103K, each  $2\Delta/kT_c$  that  $2\Delta_{\parallel}/kT_c=9.0\text{--}9.9$ ,  $2\Delta_{\perp}/kT_c=5.5\text{--}6.1$ . In Fig.4(b), the gap values in  $\text{Bi}_2\text{Sr}_2\text{CaCu}_2\text{O}_y$  (BSCCO2212) phase are also obtained as  $2\Delta_{\perp}=38\text{--}40\text{meV}$ ,  $2\Delta_{\parallel}=68\text{--}70\text{meV}$ , and the anisotropy  $\Delta_{\parallel}/\Delta_{\perp}=1.7\text{--}1.8$ , agrees with that of the BSCCO2223 phase.  $2\Delta_{\perp}$  is consistent with the results in refs.[3,5,6]. These results confirm that the gap anisotropies in BSCCO systems are larger than that of LSCO and YBCO, where  $\Delta_{\parallel}/\Delta_{\perp}=1.2\text{--}1.6$ .

To elucidate the difference of the pairing natures between BSCCO and Ca-absent  $\text{Bi}_2\text{Sr}_2\text{CuO}_y$  (BSCO) which has much lower  $T_c$  (10–7K), we have also made tunneling measurements on the BSCO samples. Obtained gap values are  $2\Delta=3.0\text{--}3.5\text{meV}$  for  $T_c=6.5\text{K}$  and  $5.0\text{--}5.7\text{meV}$  for  $T_c=9\text{K}$ , so the ratios are  $2\Delta/kT_c=5.4\text{--}7.3$ . These values are much larger than that of BCS value, however the values are smaller compared to those in the Ca-contained BSCCO systems.

In Fig.5, we show the summary of our tunneling measurements on the oxide superconductors. As for

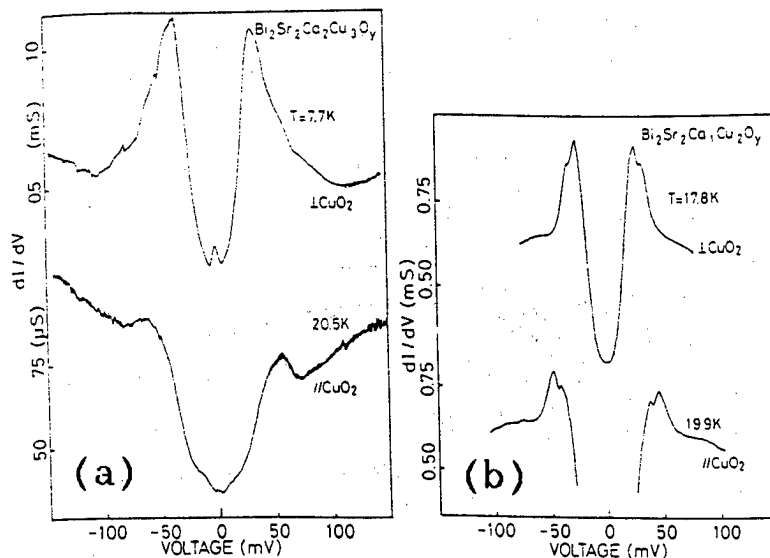


Fig.4 Gap anisotropies in (a) BSCCO2223 and (b) BSCCO2212 phases. The tunneling currents flow parallel( $//CuO_2$ ) and perpendicular( $\perp CuO_2$ ) to the  $CuO_2$  planes.

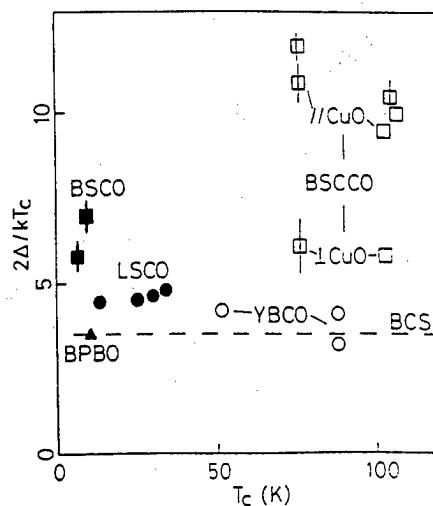


Fig.5 A summary of  $2\Delta/kT_c$  vs  $T_c$ . Data are obtained from our measurements. The abbreviation BPBO means  $BaPb_{0.78}Bi_{0.22}O_3$ .

LSCO and YBCO,  $2\Delta/kT_c$  coincide with those of another authors and these values are independent of  $T_c$ , ie, Sr concentrations or oxygen deficiencies. As seen in the figure, the  $2\Delta/kT_c$  in BSCCO and BSCO are much larger than that of YBCO(3-4) and LSCO( $\sim 5$ ), where the same  $CuO_2$  planes are crucial for the superconductivity. It is generally known that the short coherence length of high- $T_c$  oxide induces the weakening of the gap value at the interface of the tunnel junction[7]. If the pairing mechanism is same, the gap values are expected to be same, since the coherence length of YBCO and BSCCO are short and the same order of magnitude. However, one should consider that the superconductivity of surface layers of the YBCO and LSCO are much sensitive to the oxygen deficiencies than BSCCO system. Thus the weakening of gaps at the surface layers tend to occur and reduce the  $2\Delta/kT_c$  in the YBCO and LSCO systems.

In conclusion, we have observed the energy gaps of a series of high- $T_c$  oxides by the electron tunneling measurements. The ratios  $2\Delta/kT_c$  in BSCCO system are much larger than the BCS values. These fact draws a distinction between BSCCO, BSCO and YBCO, LSCO. However, these results should be carefully backed up with another experimental evidences that the electronic properties in Bi-Sr-Ca-Cu-O system are different from those of Y-Ba-Cu-O and La-Sr-Cu-O systems.

We thank Dr. T. Nakada and Prof. A. Kunioka for kindly supplying the Bi-Sr-Ca-Cu-O films.

#### References

1. K.E.Gray, M.E.Hawley, and E.R.Moog, in Novel Superconductivity, edited by S.A.Wolf and V.Z.Kresin(Plenum, New York, 1987).
2. R.C.Dynes, V.Narayanamurti, and J.P.Garno, Phys. Rev. Lett. 41, 1509(1978).
3. M.Lee, D.B.Mitzi, A.Kapitulnik, and M.R.Beasley, Phys. Rev. B39, 801(1989).
4. M.Kazusawa, K.Takahashi, T.nakada, and A.Kunioka, CPM-88-50, 101(1988).
5. Z.Shipin, T.Hongliic, C.Yinfei, Y.Yifen, and Y.Qiansheng, Solid State Commun. 67, 1179(1988).
6. S.Vieira, M.A.Ramos, M.Vallet-Regi, and J.M.Gonzalez-Calbet, Phys. Rev. B38, 9295(1988).
7. G.Deutscher, and K.A.Muller, Phys. Rev. Lett. 59, 1745(1987).

# Thermal Conductivity of $\text{LnBa}_2\text{Cu}_3\text{O}_{7-y}$ ( $\text{Ln}=\text{Y}$ and $\text{Gd}$ ), $\text{YBa}_2\text{Cu}_3\text{O}_{6+x}$ and $\text{Bi}_{0.7}\text{Pb}_{0.3}\text{CaSrCu}_{1.5}\text{O}_x$

K.Mori, K.Noto\*, M.Sasakawa\*\*, Y.Isikawa, K.Sato\*\* and Y.Muto\*

College of Liberal Arts, Toyama University, 3190 Gofuku, Toyama 930, Japan

\* Faculty of Science, Toyama University, 3190 Gofuku, Toyama 930, Japan

\*\* Institute for Materials Research, Tohoku University, 2-1-1 Katahira, Sendai 980, Japan

Temperature dependences of the thermal conductivity and electrical resistivity of  $\text{YBa}_2\text{Cu}_3\text{O}_{7-y}$ ,  $\text{GdBa}_2\text{Cu}_3\text{O}_{7-y}$  and  $\text{Bi}_{0.7}\text{Pb}_{0.3}\text{CaSrCu}_{1.5}\text{O}_x$  high- $T_c$  superconductors and  $\text{YBa}_2\text{Cu}_3\text{O}_{6+x}$  non-superconductor have been investigated in the temperature range from 1.7K to 200K. The thermal conductivity for high- $T_c$  superconductors shows a striking increase below  $T_c$ . On the other hand, for non-superconductor it shows a monotonous decrease with decreasing temperature. Therefore we ascribe the striking increase below  $T_c$  to an increase in lattice conduction due to a reduction in the scattering of phonons by holes as cooper pairs form. Magnetic field dependence of the thermal conductivity for  $\text{GdBa}_2\text{Cu}_3\text{O}_{7-y}$  has been investigated on both  $T=4.41\text{K}$  and  $1.66\text{K}$  up to  $3\text{kOe}$ , which exhibits a similar behaviour to that of the usual metallic type II superconductor.

In this report, we present the results of our thermal conductivity and electrical resistivity measurements on  $\text{YBa}_2\text{Cu}_3\text{O}_{7-y}$  ( $\text{YBCO}_{7-y}$ ),  $\text{GdBa}_2\text{Cu}_3\text{O}_{7-y}$  ( $\text{GBCO}_{7-y}$ ) and  $\text{Bi}_{0.7}\text{Pb}_{0.3}\text{CaSrCu}_{1.5}\text{O}_x$  ( $\text{BPCCSO}_x$ ) high- $T_c$  superconductors and on  $\text{YBa}_2\text{Cu}_3\text{O}_{6+x}$  ( $\text{YBCO}_{6+x}$ ) non-superconductor.

All samples were prepared by the conventional powder sintering method described in detail elsewhere (1). X-ray measurements confirm single-phase structure for  $\text{YBCO}_{7-y}$ ,  $\text{YBCO}_{6+x}$  and  $\text{GBCO}_{7-y}$ , on the other hand for (BP)CCSO<sub>x</sub> the X-ray diffraction pattern showed the lines of 2:2:2:3 phase which is the high- $T_c$  phase, and extra lines.

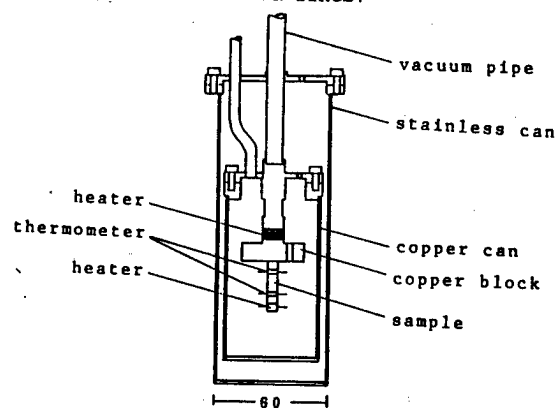


Fig.1. Double adiabatic vacuum cryostat for measurement of thermal conductivity.

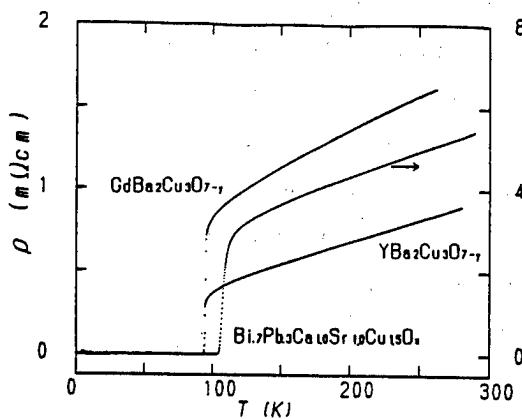


Fig.2.  $\rho$  vs.  $T$ .

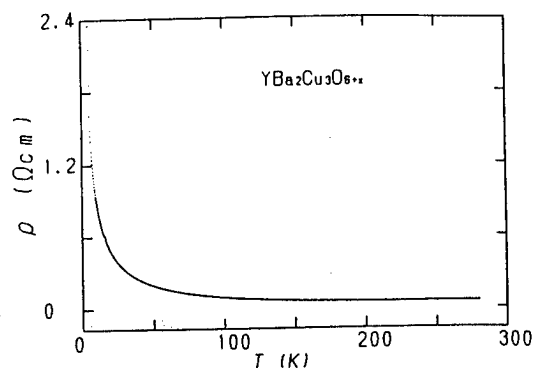


Fig.3.  $\rho$  vs.  $T$ .

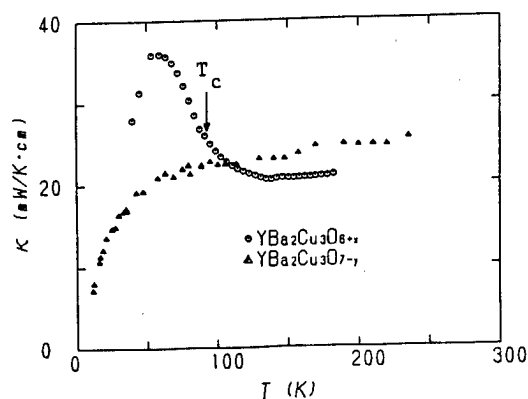


Fig.4.  $\kappa$  vs.  $T$ .

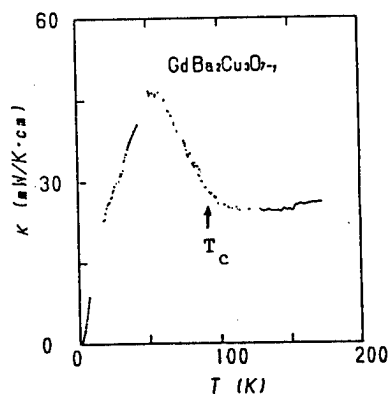


Fig.5.  $\kappa$  vs.  $T$ .

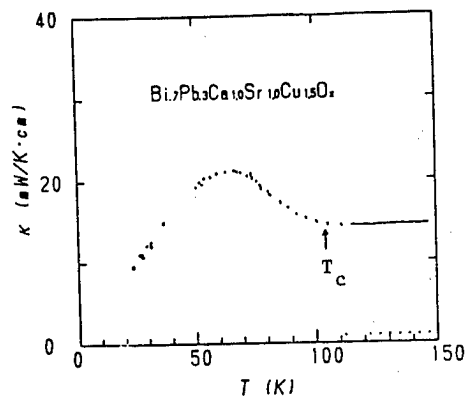


Fig.6.  $\kappa$  vs.  $T$ .

A steady heat flow method was used to measure the thermal conductivity. Detail of the measurement technique was described elsewhere [2]. A schematic sample holder cryostat is shown in Fig.1. As a thermometer, Allen-Bladley's carbon resistors below 20K and Matsushita's diodes 1S953 above 20K were used. The electrical resistivity was measured by DC method with four terminals.

Figure 1 shows results for the temperature dependences of electrical resistivity,  $\rho$  for our samples of  $\text{YBCO}_{7-y}$ ,  $\text{GBCO}_{7-y}$  and  $\text{BPCSCO}_x$ . The values of  $\rho$  decrease roughly linearly as the temperature is lowered. The values of superconducting transition temperature  $T_c$  at which  $\rho=0$  are 94.4K, 94.9K and 104K for the samples of  $\text{YBCO}_{7-y}$ ,  $\text{GBCO}_{7-y}$  and  $\text{BPCSCO}_x$ , respectively.

Figure 2 shows the temperature dependence of  $\rho$  for  $\text{YBCO}_{6-x}$ , in which the superconducting transition was not observed above 4.2K. The superconducting phase was not detected by the measurement of magnetization using a PAR model 155 vibrating sample magnetometer.

Our thermal conductivity results are shown in Figs.4-6. All samples for high- $T_c$  superconductors show the same general trend: At high temperatures, the thermal conductivity is nearly constant, but as the samples become superconducting the thermal conductivity is enhanced before reaching a peak near 50-60K for  $\text{YBCO}_{7-y}$  and  $\text{GBCO}_{7-y}$  and 65K-70K for  $\text{BPCSCO}_x$ , respectively and falling off at lower temperature.

The thermal conductivity measured experimentally is the sum of conduction due to the carriers ( $\kappa_c$ ) and due to the phonons ( $\kappa_p$ ). One can make an estimate of  $\kappa_c$  by using the Wiedemann-Franz law in



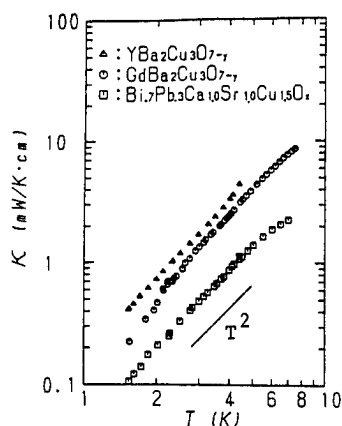


Fig. 7. log-log plots of  $\kappa$  vs.  $T$ .

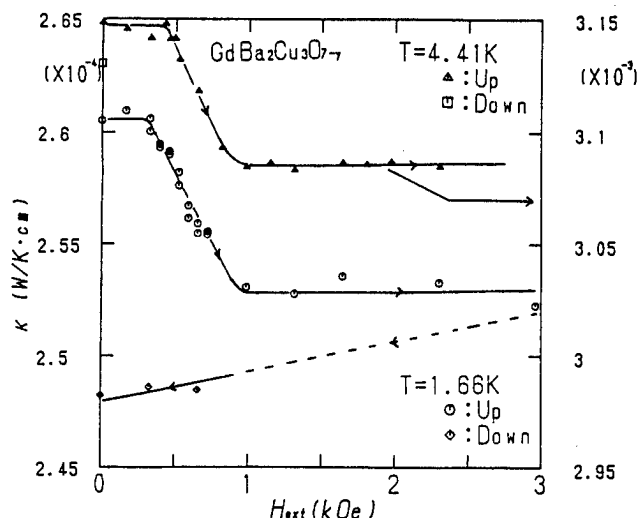


Fig. 8.  $\kappa$  vs.  $H$ .

conjunction with the electrical resistivity data,  $\rho$ ;  $L = \kappa_c \rho / T$ , where  $L = 2.45 \times 10^{-8} \text{ W}\Omega/\text{K}^2$  is the Lorenz number. If there is significant inelastic scattering of the carriers, then the effective Lorenz number always smaller than  $L$ . Thus we can obtain an upper limit to the carrier thermal conductivity by using our electrical resistivity data above the transition. It is seen immediately from Fig. 2 that close to 80% of the thermal conductivity for the samples of  $\text{YBCO}_{7-y}$  and  $\text{GBCO}_{7-y}$  and 90% for  $\text{BPCSCO}_x$  are due to the phonons. The charge carrier component of thermal conductivity normally decays as superconducting pairs form because they do not transport energy. On the other hand, since the paired carriers no longer scatter phonons, the lattice thermal conductivity  $\kappa_p$  can increase below  $T_c$ .

However, the thermal conductivity for the sample of  $\text{YBCO}_{6-x}$  does not show the peak, as seen in Fig. 5, because of the non-superconductor. In this case, the thermal conductivity is mostly dominated by the lattice contribution ( $\kappa_p$ ) because of high electrical resistivity such as a semiconductor as seen in Fig. 3. The thermal conductivity at low temperatures below 10K is shown in Fig. 7, we find that in this temperature region  $\kappa \propto T^2$ .

The magnetic field dependence of the thermal conductivity for  $\text{GBCO}_{7-y}$  up to 3kOe is shown in Fig. 8. Although the variation of the thermal conductivity in this magnetic fields range is less than 2.5%, the thermal conductivity begins to drop rapidly at  $H_{c1}$  and goes through a shallow minimum or constant. The decrease of thermal conductivity is probably due to the lattice conduction which is reduced because the lattice waves are being scattered within the normal regions. There is also the possibility of a scattering of phonons at the actual boundaries of normal-superconducting phases.

#### References

- [1] K. Mori, M. Sasakawa, Y. Isikawa, K. Kobayashi, and K. Sato, Jpn. J. Appl. Phys., Superconducting Materials (1988) 81.
- [2] K. Noto, J. Phys. Soc. Jpn., 26 (1969) 710.

S. Mase, Y. Horie and T. Fukami

Department of Physics, Kyushu University, Fukuoka 812, Japan

The temperature dependence of the sound velocities of  $\text{YBa}_2\text{Cu}_3\text{O}_{7-\delta}$  and  $(\text{La}_{1-x}\text{Sr}_x)_2\text{CuO}_4$  have been investigated in magnetic fields  $H$  up to 10 T. The superconducting transition temperature  $T_c$  has also been simultaneously measured through the a.c. susceptibility measurements. In both materials the discontinuity  $\Delta V_s$  in the  $V_s$  versus  $T$  curve has been observed at  $T \sim T_c$  under  $H = 0$ . However, the anomaly in  $V_s$  is almost independent of applied fields up to 10 T for  $\text{YBa}_2\text{Cu}_3\text{O}_{7-\delta}$ , while for  $(\text{La}_{1-x}\text{Sr}_x)_2\text{CuO}_4$  with increasing  $H$  the temperature range of the anomaly follow the decrease of  $T_c$  and the absolute magnitude of  $\Delta V_s$  decreases. The results are interpreted briefly.

## 1. Introduction

Since Bednorz and Müller found the oxide superconductor  $(\text{La}_{1-x}\text{Ba}_x)_2\text{CuO}_4$  with the superconducting transition temperature  $T_c \sim 30$  K, a great deal of studies has been made for understanding high  $T_c$  superconductors. The isotope effect,  $T_c \propto M^{-\alpha}$ , shows that  $\alpha \sim 0.22$  for  $\text{BaPb}_{1-x}\text{Bi}_x\text{O}_3$  (BPBO:  $T_c \sim 14$  K for  $x \sim 0.25$ ),  $\alpha \sim 0.17$  for  $(\text{La}_{1-x}\text{Sr}_x)_2\text{CuO}_4$  (LSCO:  $T_c \sim 40$  K for  $x \sim 0.07$ ) and  $\alpha \sim 0.05$  for  $\text{YBa}_2\text{Cu}_3\text{O}_{7-\delta}$  (YBCO:  $T_c \sim 92$  K for  $\delta \sim 0.1$ ). Thus it is found that the  $T_c$  being higher, the electron-phonon interaction seems to become less important. Based on this fact and other magnetic properties near the metal-insulator transition region of these oxide superconductors, a quite new non-phonon mechanism of high  $T_c$  superconductivity named as the RVB model was proposed by Anderson. However, the origin of the high  $T_c$  superconductivity is still not yet settled. The crystal structures of both LSCO and YBCO have the characteristic that some of a-b planes are covered with the networks of coplanar  $\text{CuO}_2$ . On the other hand, for the former the conventional BCS mechanism must be partly operative, while for the latter it is not so. Therefore, it may be worthwhile to make a comparative study of the oxides superconductors, LSCO and YBCO.

## 2. Anomalies in Sound Velocity

Let us denote the discontinuities in the compressibility, the heat capacity and the sound velocity as  $\Delta\kappa$ ,  $\Delta C_p$  and  $\Delta V_s$ , respectively. The sound velocity itself is given by  $V_s = (B/\rho)^{1/2}$ , where  $B$  is the bulk modulus and  $\rho$  is the mass density of the lattice. Using the Ehrenfest relation for  $\Delta\kappa$  and the relation  $\Delta\kappa = -\Delta B/B^2$ , the discontinuity in  $V_s(T)$  from  $V_{s+}$  at  $T > T_c$  to  $V_{s-}$  at  $T < T_c$  is written as

$$(V_{s-}^2 - V_{s+}^2)/V_{s+}^2 = -(\Delta C_p/VT_c)(\partial T_c/\partial P)^2. \quad (1)$$

Samples measured were made by the sintering method. According to eq. (1), the discontinuity in  $V_s$  is related with  $\Delta C_p$ , and  $\Delta C_p$  itself is usually considered to be caused from conduction carriers. On the other hand, the conduction carriers should be affected by applying magnetic fields, as will be manifested in the lowering of  $T_c$  with increasing field. In order to check this point, the a.c. susceptibility of the sample was simultaneously measured by a pick up coil wound on the sample. Therefore, the superconducting transition temperature  $T_c$  of the conduction system is clearly picked up. Here  $T_c$  was defined as the point of 1 % decrease of the a.c. susceptibility against the whole change of that

from 4 K to  $\sim 100$  K, since the transition becomes blunt by applying magnetic field but we must keep the same standard for determination of  $T_c$ .

In Fig. 1 we show a typical result showing an existence of an anomaly in  $V_s$  versus  $T$  curve [1]. Regarding this curve as a type of discontinuity in the  $V_s$  versus  $T$  curve, we extrapolate the upper and lower curves against  $T_c$ , we obtain  $\Delta V_s/V_s \sim -5 \times 10^{-4}$ . This magnitude of  $-\Delta V_s/V_s$  is the largest one among the results for many tested samples. The magnitudes of  $-\Delta V_s/V_s$  is distributed from  $\sim 2 \times 10^{-5}$  to  $\sim 5 \times 10^{-4}$ , but concentrate to the vicinity of

$$\Delta V_s/V_s \sim -8 \times 10^{-5}. \quad (2)$$

This magnitude is about 4 times larger than an expected value  $1.8 \times 10^{-5}$  [1]. It is to be noted that in most cases the superconductivity starts from a little lower temperature than the onset temperature of the velocity anomaly. Similar but less clear results were also observed by other investigators [2-4]. The important point to be noted is that this discontinuity type anomaly is independent of applied magnetic fields up to 10 T. On the other hand, the simultaneously measured a.c. susceptibility clearly shows the lowering of  $T_c$  ( $T_c = 92$  K at  $H = 0$  to  $T_c \sim 88$  K at  $H = 10$  T).

For  $(La_{1-x}Sr_x)_2CuO_4$  too, a rather similar type of the anomaly in the  $V_s(T)$  versus  $T$  curve near  $T_c$  was observed. However, in this case the magnitude of the discontinuity decreases with increasing the applied magnetic field as shown in Fig. 2.

Measurements of the linear expansion coefficient  $\delta$  in the vicinity of  $T_c$  were also made for a sample belonging to the same family as the one used in those of  $\Delta V_s/V_s$  mentioned above. The a.c. susceptibility of the sample was also measured so as to check the superconducting transition temperature. The result is shown in Fig. 3. The experimental result of the field dependence of the anomaly in  $\delta(T)$  also shows the field independence of the position of the anomaly.

Here too, extrapolating the  $\delta(T)$  versus  $T$  curve above and below  $T_c$ , we obtained a discontinuity

$$\Delta \delta = 8 \times 10^{-8} \quad (3)$$

at the middle of the plateau. The experimental value is the same order of magnitude as a thermodynamical expectation [1]. Kadowaki et al. [5] also observed a similar anomaly.

### 3. Discussions

As was shown in the previous section, the experimental curve showing the anomaly in the  $V_s$  versus  $T$  curve is independent of applied magnetic fields in the case of YBCO, and the experimental results of  $-\Delta V_s/V_s$  are often one order of magnitude larger than the thermodynamical expectation. These facts may be reasonably understood by interpreting the real situation of the present phenomenon. On the basis of Anderson's theory, we suppose that both the specific heat jump  $\Delta C_p$  and the present discontinuity  $\Delta V_s/V_s$  are caused by immobile valence electrons. In terms of Anderson's concept, these are caused from the spinon system. Namely, the magnetic system falls into a short-range coherent state at  $T_c^{(R)}$  which is only a little above or just the same as the superconducting transition temperature  $T_c^{(h)}$  and it might be regarded as the SR-RVB (SR: short-ranged) in [6]. Since the nearest neighbor exchange interaction energy concerned with the magnetic short-range ordering may be one order of magnitude larger than the Zeeman energy at  $H \sim 10$  T, the applied fields hardly affect the anomaly in the  $V_s$  versus  $T$  curve.

If this assumption is true, the position of the specific heat jump  $\Delta C_p/V$  associated with the spinons should also be independent of  $H$ . In truth, Fisher et al. [7] found that the observed temperature range of  $\Delta C_p/V$  is nearly independent of  $H$  up to  $H \sim 7$  T. Since the coherence length of the carriers in the high  $T_c$  superconductor,  $YBa_2Cu_3O_{7-\delta}$ , is estimated to be  $5 \sim 30$  Å from the measurements of the upper critical field  $H_{c2}$  even a short-range ordering in the magnetic system may give rise to a crucial effect on the conduction carrier system. Thus, the conduction carrier system immediately falls into the superconducting state through some attractive force. Since, however, it is pointed out that the attractive force between holons is too weak to result in  $T_c \sim 90$  K, probably some additional

attractive interaction must be invoked. Two different but closely correlated types of phase transitions,  $T_c^{(R)}$  and  $T_c^{(h)}$ , simultaneously or successively occur. Then, in the evaluation of the  $\Delta V_s/V_s$ , we should use  $(\partial T_c^{(R)}/\partial p)$  in eq. (1). We anticipate that in order to get the result of eq. (2),  $(\partial T_c^{(R)}/\partial p)$  may be 3 ~ 5 times of  $(\partial T_c^{(h)}/\partial p)$ . The field dependence of  $-\Delta V_s/V_s$  in LSCO suggests that in this material the SR-RVB state is less stable against the magnetic field. This relatively unstable SR-RVB state in LSCO may be replaced to some extent by a manifestation of the BCS nature in consistency with the larger isotope effect in LSCO than YBCO.

#### References

- [1] Y. Horie and S. Mase: Solid State Commun. 69 (1989) 535.
- [2] D. J. Bishop, A. P. Ramirez, P. L. Gammel, B. Batlogg et al.: Phys. Rev. B36 (1987) 2408.
- [3] S. Bhattacharya, M. J. Higgins, D. C. Johnston, A. J. Jacobson et al.: Phys. Rev. B37 (1988) 5901.
- [4] M. Suzuki, Y. Okuda, I. Iwasa, A. J. Ikushima, T. Takabatake et al.: Physica C153-155 (1988) 266.
- [5] K. Kadowaki, F. E. Kayzel and J. J. M. Franse: Physica C153-155 (1988) 1028.
- [6] S. Kivelson and D. S. Rokhsar: Physica C153-155, (1988) 531.
- [7] R. A. Fisher, J. E. Gordon, S. Kim, N. E. Phillips and A. M. Stacy: Physica C153-155 (1988) 1092.

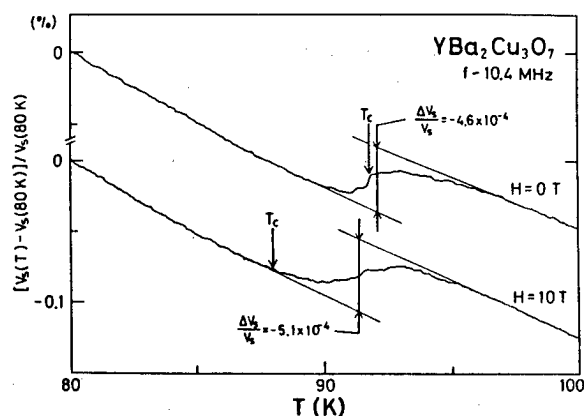


Fig. 1. Anomaly in the  $V_s$  versus  $T$  curve near  $T_c$  for YBCO under  $H = 0$  and  $H = 10$  T.

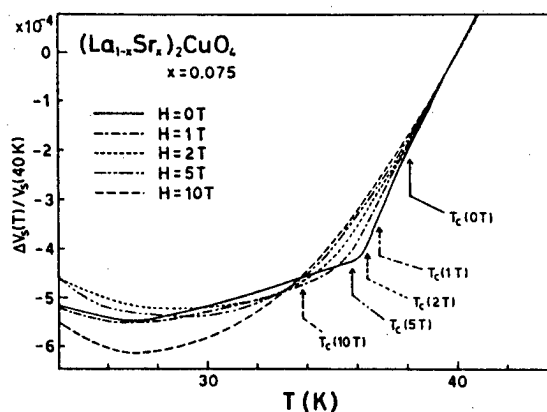


Fig. 2. Anomaly in the  $V_s$  versus  $T$  curve near  $T_c$  for LSCO under  $H = 0$  to  $H = 10$  T.

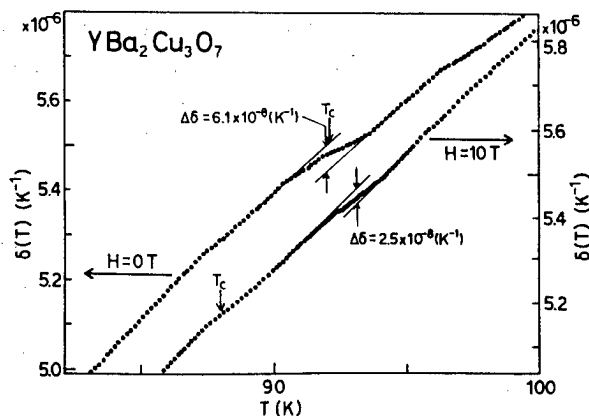


Fig. 3. Anomaly in the  $\delta$  versus  $T$  curves near  $T_c$  for YBCO under  $H = 0$  and  $H = 10$  T.

# High Pressure Effect on the Critical Temperature of $\text{YBa}_2(\text{Cu}_{1-x}\text{Ga}_x)_3\text{O}_{7-y}$

Shusuke Yomo<sup>\*,†</sup>, L. Gao<sup>†</sup>, Y.Y.Xue<sup>†</sup>, R.L.Meng<sup>†</sup>, P.H.Hor<sup>†</sup> and C.W.Chu<sup>†</sup>

\* Department of Electronic and Information Technology and Research Institute for Higher Education Programs, Hokkaido Tokai University, Minami-ku, Sapporo 005, Japan

† Department of Physics and Texas Center for Superconductivity, University of Houston, Houston, Texas 77204, U.S.A.

Pressure effect on the critical temperature of  $\text{YBa}_2(\text{Cu}_{1-x}\text{Ga}_x)_3\text{O}_{7-y}$  has been studied under hydrostatic (15 kbar) and quasihydrostatic (150 kbar) condition. The pressure effect is larger for lower  $T_c$  materials. The result is compared with other 3d-metal substitution system.

In the study of high temperature superconductivity of early stage, the large pressure effect of the critical temperature  $T_c$  [1] led with some chemical systematic relation to the discovery of a new system with  $T_c$  higher than liquid nitrogen temperature. However, the pressure effect of this  $\text{YBa}_2\text{Cu}_3\text{O}_{7-y}$  system was found to be small. To understand the difference in the pressure effect seems to be one of the important factors to clarify the origin of such a high  $T_c$  superconductivity. In this study, we have tried to find a systematic variation in the pressure effect of  $T_c$  in the  $\text{YBa}_2\text{Cu}_3\text{O}_{7-y}$  system by controlling the  $T_c$  by Ga-substitution which suppresses  $T_c$  [2]. The result is compared with high pressure results for other 3d-metal substituted systems.

The substituted compounds  $\text{YBa}_2(\text{Cu}_{1-x}\text{Ga}_x)_3\text{O}_{7-y}$  were prepared by solid state reaction in a way similar to Xiao et al. [2]. The compositions studied under pressure were  $x=0.0, 0.02, 0.04, 0.08$  and  $0.15$ . Hydrostatic pressure was generated in a clamped piston-cylinder apparatus up to 15 kbar. A clamped Bridgman-anvil apparatus was used for quasihydrostatic pressure up to 150 kbar with steatite as pressure medium. The  $T_c$  was determined by electrical resistance measurements using an ac-resistance bridge operating at 15.9 Hz.

The  $T_c$  decreased with Ga-substitution at ambient pressure from 92 K ( $x=0.0$ ) to about 60 K ( $x=0.15$ ), which is similar to Xiao et al. [2]. In the hydrostatic pressure measurements up to 15 kbar [3], the  $T_c$  increased with pressure ( $P$ ) in the present composition range and the enhancement became bigger with increasing Ga content  $x$ . Namely,  $dT_c/dP$  was about 0.1 (K/kbar) for pure  $\text{YBa}_2\text{Cu}_3\text{O}_{7-y}$  and increased with increasing  $x$  up to about 0.6 (K/kbar). Here, we took a mid-point of the resistive transition as  $T_c$ . With further increase of pressure by the Bridgman-anvil up to 150 kbar, the onset  $T_c$  tends to saturate around 100 K, as shown in Fig.1 for  $x=0.04$ . These substitutional effect and pressure effect indicates that the  $dT_c/dP$  become smaller with increasing  $T_c$  in general for the  $\text{YBa}_2\text{Cu}_3\text{O}_{7-y}$ -related oxide superconductors.

In order to examine the general tendency of the pressure effect as compared with the ambient pressure  $T_c(0)$  itself, we have plotted  $(1/T_c(0))dT_c/dP$  vs.  $T_c(0)$  in Fig.2, using the high pressure data of  $\text{YBa}_2(\text{Cu}_{1-x}\text{M}_x)_3\text{O}_{7-y}$  by various authors, where M is the

3d-metal elements: Fe, Co, Ni, Zn and Ga. It is clearly seen in this figure that there are two groups of data each of which has roughly linear correlation; a large-pressure-effect (LPE) group consists of the compounds with  $M = \text{Fe, Co and Ga}$ , and a small-pressure-effect (SPE) group consists of those with  $M = \text{Ni and Zn}$ . Since  $(1/T_c(0))dT_c/dP$  is related to the logarithmic volume derivative of  $T_c$  with a factor of compressibility ( $\kappa$ ) as  $-\kappa d\ln T_c/d\ln V$ , it is interesting to clarify the origin of the difference of the two curves in order to find the mechanism of the high-temperature superconductivity.

There are three chemical or structural factors which may distinguish the two curves in Fig.2:

- (1) The substituted metal ions in LPE group tend to have a valency of 3+ and those in SPE group 2+.
- (2) The substituted metal ions in LPE group tend to substitute Cu in chain site and those in SPE group in plane site.
- (3) The LPE group causes a change in crystal symmetry from the orthorhombic to tetragonal structure with increasing  $x$ , i.e. with decreasing  $T_c$ . The fact that tetragonal phase in these 3d-metal substituted system has large pressure effect has been pointed out previously [4].

On the other hand, Okazaki et al. [5] has recently reported that the substitution by Fe and Co reduces the number of holes and that of Ni and Zn increases the number of holes. Thus the curve of the  $T_c$  vs. number of holes ( $n_p$ ) has a maximum at around 0.5-0.6 holes/unit cell where the pure  $\text{YBa}_2\text{Cu}_3\text{O}_{7-y}$  locates as in Fig.4 in ref.6. Their results suggests a change in the band structure by Zn-substitution. Comparing with our result, the LPE group belongs to the smaller  $n_p$  side of the  $T_c$  vs.  $n_p$  curve and the SPE group belongs to larger  $n_p$  side. The difference in the pressure effect between the smaller and larger  $n_p$  region is not disagreement with their argument but is yet to be studied furthermore.

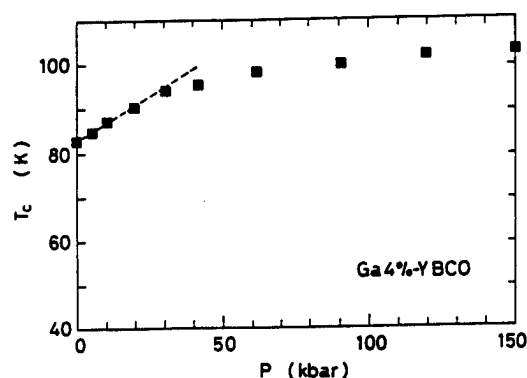


Fig.1 Pressure (P) dependence of  $T_c$  of  $x=0.04$  sample.

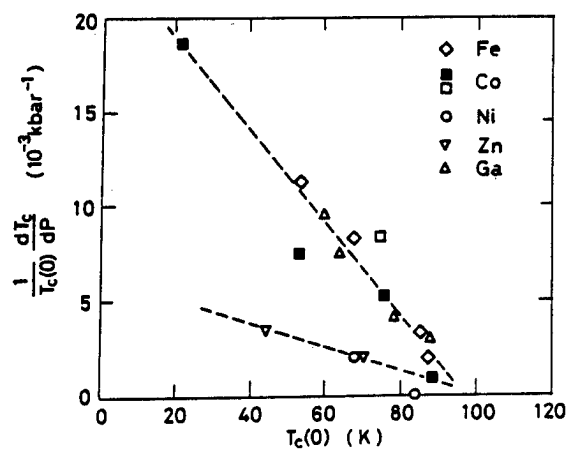


Fig.2 Normalized pressure coefficient of  $T_c$  as a function of  $T_c$  at ambient pressure. Fe, Co(open square), Ni and Zn:ref.4, Co(closed square):ref.6, Ga:this study and ref.3.

References :

- [1] C.W.Chu, P.H.Hor, R.L.Meng, L.Gao, Z.J.Huang and Y.Q.Wang, Phys. Rev. Lett. 58, 405 (1987).
- [2] G.Xiao, M.Z.Cieplak, A.Gavrin, F.H.Streiz, A.Bakhshai and C.L.Chien, Phys. Rev. Lett. 60, 1446 (1988).
- [3] L.Gao, S.Yomo, Y.Y.Xue, R.L.Meng, P.H.Hor and C.W.Chu, in preparation.
- [4] M.Kurisu, K.Kumagai, Y.Maeno and T.Fujita, Physica C152, 339 (1988).
- [5] N.Okazaki, S.Kambe, A.Kishi, N.Kanazawa, A.Ohtomo, A.Fukuoka, T.Hasegawa, K.Kishio, K.Kitazawa and K.Fueki, to be published in "Proc. of MRS Int. Meeting on Advanced Materials, Tokyo, May 30 - June 3, 1988".
- [6] C.Murayama, H.Takahashi, Y.Miyane, N.Mori, S.Yomo, J.M.Tarascon, T.Matsumoto, H.Takei and H.Takeya, in preparation.

Y. Nakazawa and M. Ishikawa

Institute for Solid State Physics, University of Tokyo,  
Roppongi, Minato-ku, Tokyo 106 Japan

By means of resistivity, magnetic susceptibility and specific heat measurements, we have studied effects of oxygen stoichiometry and oxygen ordering in an attempt to establish the equilibrium phase diagram of  $\text{Ba}_2\text{YCu}_3\text{O}_y$  for the whole range of  $6 \leq y \leq 7$ . We found that the orthorhombic phase extends down to at least  $y \approx 6.2$  and superconductivity prevails in this phase region. In the framework of this new phase diagram, results of magnetic susceptibility and resistivity are discussed.

It is generally recognized that the oxygen stoichiometry in oxide superconductors is one of the most crucial parameters for their characterization. However, details about it are not yet known at present. For example, it is not known what the optimum oxygen content in  $\text{Ba}_2\text{YCu}_3\text{O}_y$  would be and whether the proposed ordered homologous structures of  $\text{Ba}_2\text{YCu}_3\text{O}_{7-n/(2n+1)}$  [1] can be stabilized or not. We believe it very important to clarify these points for our understanding of a possible mechanism for high  $T_c$  superconductivity in these oxide superconductors. In an attempt to elucidate these questions, we undertook a careful investigation on the system of  $\text{Ba}_2\text{YCu}_3\text{O}_y$  with a new sample preparation technique and herein report the preliminary results.

Fully oxidized samples were first sintered as reported before [2] and the oxygen content was then modified to a predetermined value either by quenching from an appropriate temperature or by a getter-annealing technique. Thus prepared samples were subjected to a sufficiently long annealing in a quartz tube at low temperatures below about  $500^\circ\text{C}$ . We believe that such a low temperature annealing is very crucial to ensure the homogeneous distribution and ordering of the controlled quantity of oxygen, as revealed by marked changes in their physical properties. A chemical analysis of iodometry was done to verify the final oxygen content. The agreement was good to about 0.02/7. The lattice parameters of all samples were determined by a powder X-ray diffraction using a  $\text{Cu K}\alpha$  radiation. The results are shown as a function of the oxygen content  $y$  in Fig.1. In Fig.2 inductively determined transition temperatures  $T_c$  and the superconducting volume fraction relative to that of the ortho-I phase sample are summarized. In Fig.1 one notices that the orthorhombicity ( $a \neq b$ ) in well annealed samples seems to extend much further than the reported phase limit of about 6.4 [3,4], presumably resulting from better ordered oxygen atoms around  $\text{Cu1}$  sites. Furthermore, all the lattice parameters,  $a$ ,  $b$  and  $c/3$  vary non-linearly with  $y$  in contrast to the recent result of Ueda et al [5]. In particular, the plateau between 6.5 and 6.7 is remarkable. Also worthy of notice are plateaus on the curves of  $T_c$  and the volume fraction in the same range of  $y$ , as shown in Fig.2. These facts manifest the existence



of the so-called ortho-II phase near  $y=6.5$ [6]. We have already reported the details about this ordered phase [2] and the double-cell structure along a-axis due to the new ordering of CuO chains was confirmed by electron diffraction analysis. It is very important to note here that the superconductivity prevails in the aforementioned extended orthorhombic region, suggesting that the existence of CuO chains is essential for the superconductivity. It is also important to see how the antiferro- magnetic phase emerges in the lower concentration region. This is now investigated by neutron diffraction experiments in collaboration with Dr. Shirane's group at BNL.

In Fig.3(a)(b), the resistivity of typical samples is plotted as a function of temperature. It should be noticed in the Figures that the resistivity around room temperature systematically increases with the decreasing oxygen content and that a positive temperature coefficient is disclosed at high temperatures even for the samples of  $y=6.16$ , 6.22 and 6.32. These low oxygen well annealed samples demonstrate a variable range hopping type conduction at lower temperatures, while quenched samples showed such a localization effect in whole temperature range below 300 K[7].

The magnetic susceptibility,  $\chi$  measured with a SQUID magnetometer (BTi Model 905) in a field of 10 KOe is shown for several samples with different oxygen content in Fig.4. It can be seen that  $\chi$  of the ortho-I phase in the normal state is temperature

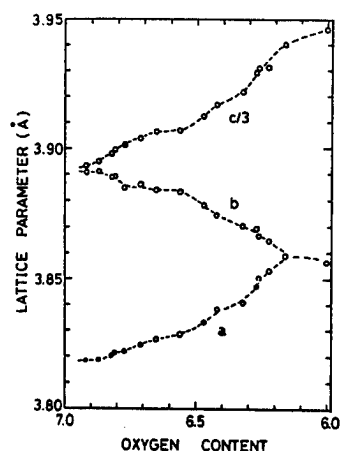


Fig. 1

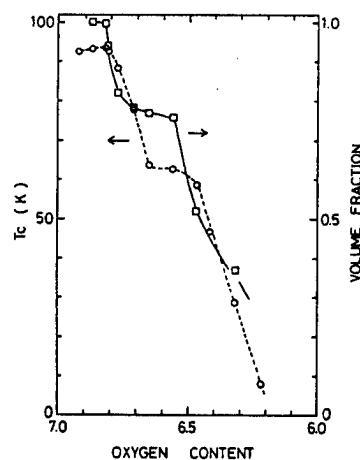


Fig. 2

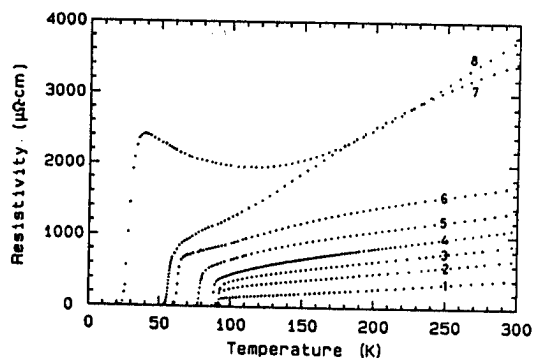


Fig. 3 (a)

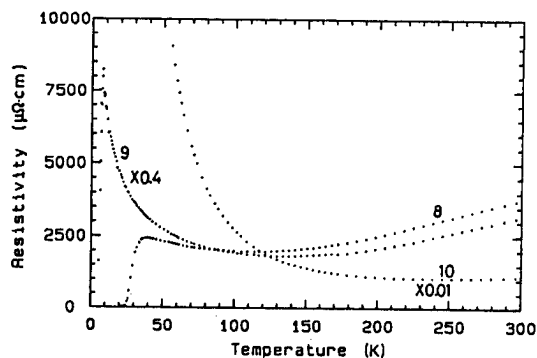


Fig. 3 (b)

- (1) 6.92 (2) 6.87 (3) 6.81 (4) 6.77 (5) 6.71  
(6) 6.65 (7) 6.47 (8) 6.32 (9) 6.22 (10) 6.16

independent, while the ortho-II phase of  $y=6.47\sim 6.56$  manifests a peculiar temperature dependence as reported before[2]. We simply note here the stronger temperature variation for the intermediate concentrations between these two phases. It may be worthwhile to briefly comment on the Curie-Weiss contribution in  $\chi$ , which apparently appears only below about  $y=6.5$  and becomes most prevalent around  $y=6.2$  and finally disappears near  $y=6.0$ . The small upturn for the sample of 6.0 may not be intrinsic but due to residual paramagnetic impurities.

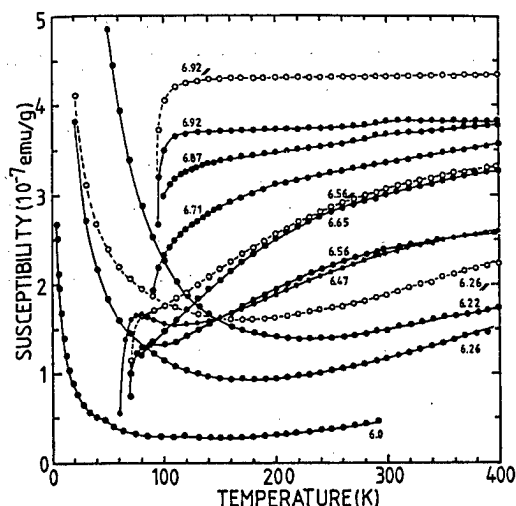


Fig. 4

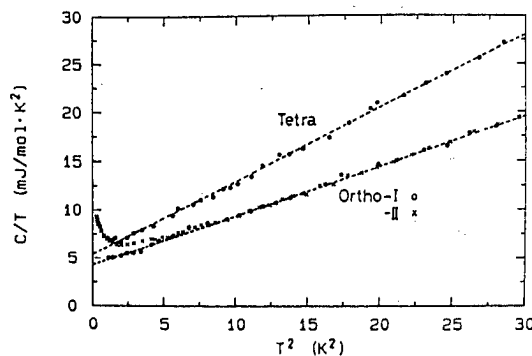


Fig. 5

In Fig.5 we present low temperature specific heat curves ( $C_p/T$  vs  $T^2$ ) for the three phases of ortho-I (6.93), -II (6.50) and tetra (6.0). It is very interesting to note here that even these well-annealed samples revealed a residual  $T$  value of about 4 mJ/mol-K<sup>2</sup>, tempting us to believe it intrinsic. We note that the jump at  $T_c$ ,  $\Delta C_p/T_c$  for annealed ortho-I samples was found to be about 58 mJ/mol-K<sup>2</sup>, as reported before [8].

Effects of oxygen ordering in  $Ba_2YCu_3O_y$  seen in various properties have been briefly reported. More detailed accounts of the present work will be published soon.

We would like to thank K. Suzuki and M. Ichihara for their electron diffraction analysis and also F. Sakai for her iodometric analysis. Technical assistance of T. Shibuya is also acknowledged.

#### References

- [1] A.G. Khachaturyan and J.W. Morris, Jr. : Phys. Rev. Letters, **61**(1988)215.
- [2] T. Takabatake, M. Ishikawa, Y. Nakazawa and K. Koga : Physica C **152**(1988)424.
- [3] R.J. Cava et al. : Physica C **153-155**(1988)560.
- [4] J.D. Jorgensen et al. : Physica C **153-155**(1988)578.
- [5] Y. Ueda and K. Kosuge : Physica C **156**(1988)281.
- [6] Y. Nakazawa, M. Ishikawa, T. Takabatake, H. Takeya, T. Shibuya, K. Terakura and F. Takei : Jpn. J. Appl. Phys. **26**(1987)L682 ; Y. Nakazawa et al. : *ibid.* **26**(1987)L796.
- [7] M. Ishikawa, T. Takabatake and Y. Nakazawa : Physica **148B**(1987)332.
- [8] M. Ishikawa, Y. Nakazawa, T. Takabatake, A. Kishi, R. Kato and A. Maesono : Solid State Commun. **66**(1988)201 and Physica C **153-155**(1988)1089.

M. Sato, M. Sera, M. Onoda, S. Shamoto, S. Kondoh\*, K. Fukuda, Y. Anodo<sup>+</sup> and S. Yamagata

Institute for Molecular Science, Myodaiji, Okazaki 444

\*Permanent address, Research & Development Division, Asahi Glass Co., LTD., Hazawa

<sup>+</sup>Permanent address, Nippon Solen, INC., Shimohasumi, Nishio 445

A brief survey of various kinds of experimental studies carried out by the present authors to clarify the physical properties of Cu oxide superconductors and (Ba,K)BiO<sub>3</sub> is presented.

## 1. Introduction

At the very early stage of the study on high- $T_c$  oxides, our experimental results suggested that the rough features of the high- $T_c$  superconductivity could still be understood by the BCS's mean field description with s-wave symmetry [1,2]. It implied that their physical behaviors did not essentially depend on the microscopic origin(s) of the electron-electron pairing force. Therefore, it seemed to be quite difficult to extract the useful clues to elucidate the mechanism of the superconductivity from a special kind of experiments and it was, we felt, quite important to carry out detailed but rather broad studies not only on their superconducting properties but also on their normal state ones. Much effort to prepare large single crystals have been made [3,4] and the obtained crystals have been used by ourselves and in collaboration with many other groups in various kinds of experiments, structural studies [5], transport studies [6], Raman scattering [7], photoemission [8], neutron scattering [9-12] and so on. For certain experiments where the oxygen number or dopant concentration had to be well controlled, powder specimens were much more suitable than crystals. For example, the low temperature specific heat was measured for Bi-Sr-Ca-Cu-O sintered pellets with very large Meissner volume fraction [13]. The result gave the first experimental evidence for the absence of the T-linear ( $\gamma T$ ) term in the low temperature electronic specific heat. Rather detailed studies on the transport and magnetic properties [14-16] and ESR [17] have also been carried out by using sintered pellets. Normal physical properties of Cu-free superconducting oxide (Ba,K)BiO<sub>3</sub> [18,19] and its oxygen isotope effect on  $T_c$  [20] have also been studied to see if both oxides with Bi and Cu have a common microscopic mechanism of high- $T_c$  superconductivity. In the field of searching for new high- $T_c$  oxides, we first found Tl-Ba-Cu-O system with  $T_c \sim 20K$  [21,22]. In the present report, a brief survey of some of these works is given. For the details, each papers should be referred.

## 2. X-Ray and Neutron Studies

The Bi-Sr-Cu-O and Tl-Ba-Cu-O systems can be considered as the members of the oxide series of  $Bi_2Sr_2Ca_{n-1}Cu_nO_y$  and  $Tl_2Ba_2Ca_{n-1}Cu_nO_y$  ( $n = 1, 2, \dots$ ), respectively, which have very high  $T_c$  values. As shown in our previous papers [22, 23], the Tl-Ba-Cu-O system has rather simple structure, although the existence of the slight long period modulation was reported for certain members of this compound series. In case of the Bi-based systems, there exist long period modulations with quite significant amplitudes, where the average structures obtained from the analyses of only the fundamental Bragg reflections may not have any meanings. In order to present the correct structural information on the series of these compounds, the X-ray four circle diffraction study was carried out [5] for the Bi-Sr-Cu-O system in which the modulation vector has an commensurate value. Fig. 1 shows the obtained

structure, where the regular lack of oxygen atoms in Bi-O layer can be seen. These oxygen defects may cause the very large shift type modulation of the atoms. The estimated chemical formula is  $\text{Bi}_{10}\text{Sr}_{10}\text{Cu}_5\text{O}_{29}$ , which indicates that one oxygen site is vacant as compared with the ideal phase of  $\text{Bi}_{10}\text{Sr}_{10}\text{Cu}_5\text{O}_{30}$ . It is monoclinic and  $a = 26.856(7)\text{\AA}$ ,  $b = 5.380(1)\text{\AA}$ ,  $c = 26.908(8)\text{\AA}$  and  $\beta = 113.55(2)^\circ$ . The holes seem to be introduced by the cation deficiency rather than the excess oxygens, which may be supported by the Sr poor atomic ratios  $\text{Bi}:\text{Sr}:\text{Cu} = 6:4:3$  determined by EPMA. Detailed analyses show that the positions  $i$  of each kind of atoms of

Bi, Sr and Cu can be described by the sinusoidal displacements,  $\vec{r}_i = \vec{r}_{0i} + \vec{u}_0 \cos(c^* \vec{r}_{0i} + \psi)$ , where  $\vec{r}_{0i}$  indicates the  $i$ -th site of each kind of atoms without the modulation and  $\psi$  is a constant. The present data gives us the essential structural features of the Bi-based series of high- $T_c$  oxides.

Neutron scattering studies were originally planned to see if the spins at the Cu sites observed in the insulating phases of high- $T_c$  oxide systems persist to the phases which exhibit superconductivity. Results on  $\text{La}_{2-x}\text{Sr}_x\text{CuO}_4$  single crystals suggested the persistence of the spins to the  $x$  region where superconductivity appears [9]. For  $\text{YBa}_2\text{Cu}_3\text{O}_{7-\delta}$ , we have prepared large ingot type crystals and at first, observed, in collaboration with BNL group, the spin wave dispersion in  $\text{YBa}_2\text{Cu}_3\text{O}_{6.2}$ , the result of which shown in Fig. 2 clearly showed that the dynamical nature of the spin system of this oxide was essentially similar to that of  $\text{La}_{2-x}\text{Sr}_x\text{CuO}_4$  [11]. For crystals with smaller  $\delta$  or with superconducting transition, we have not succeeded in observing the spin fluctuation. In case of  $\text{La}_{2-x}\text{Sr}_x\text{CuO}_4$ , Shirane and his group made use of a special measuring condition to collect the scatterings with various energy transfers and succeeded in observing the instantaneous spin correlation [24]. For the case of  $\text{YBa}_2\text{Cu}_3\text{O}_{7-\delta}$ , the existence of the large elastic contributions from small amount of impurity phases prevents us from adopting that condition used in the experiment for  $\text{La}_{2-x}\text{Sr}_x\text{CuO}_4$ , although much effort to reduce the amount of the impurities has been made. However, the possibility that the spin correlation is much weakened or does not exist in the Y-compounds with superconducting transition may not be easily excluded. We are still making much effort to prepare larger crystals with lower  $T_c$  and with less impurities, which may enable us to observe the spin fluctuations without

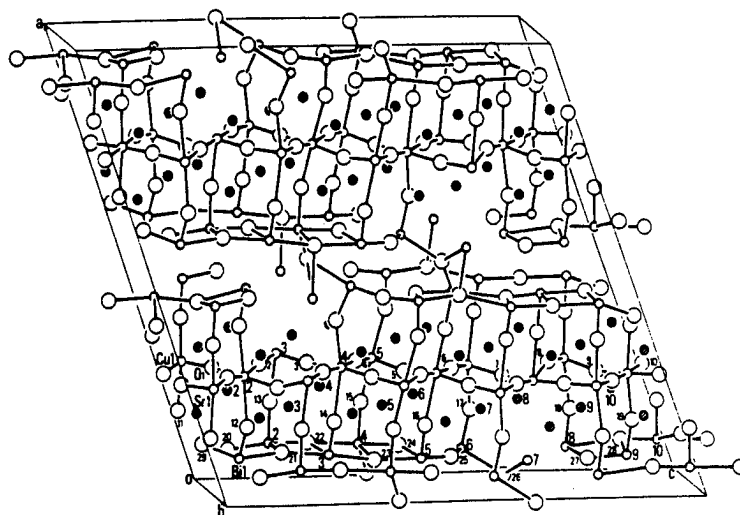


Fig. 1 Structure of  $\text{Bi}_{10}\text{Sr}_{10}\text{Cu}_5\text{O}_{29}$  obtained by X-ray four circle study.

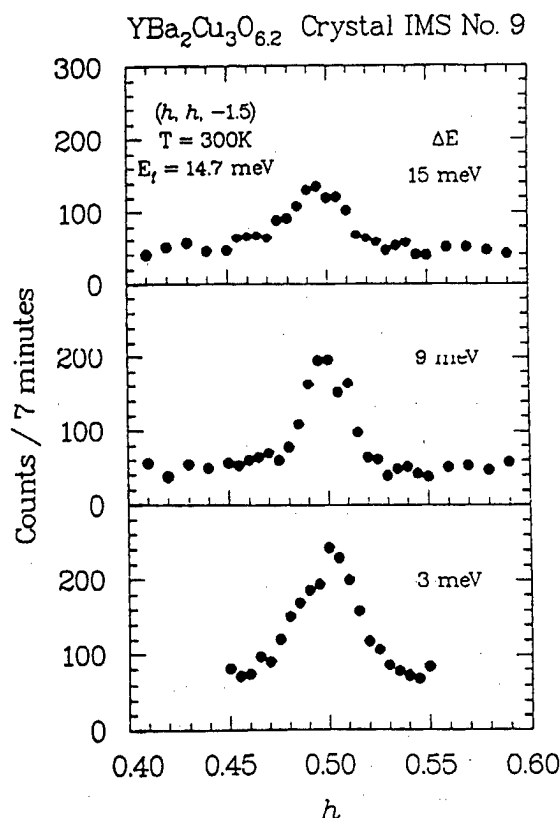


Fig. 2 Results of constant  $\Delta E$  scans across the two dimensional ridge of  $\text{YBa}_2\text{Cu}_3\text{O}_{6.2}$ . The zone center for the two dimensional spin wave is along  $(1/2, 1/2, 2)$ .

adopting the special measuring condition mentioned above. The two magnon Raman scattering observed in our  $\text{La}_{2-x}\text{Sr}_x\text{CuO}_4$  crystals with various  $x$  values exhibited the drastic  $x$  dependence [7]. This should be understood consistently with the neutron results. Finally, the spin canting in the antiferromagnetic state of  $\text{La}_2\text{CuO}_4$  was proposed by us and experimentally proved by neutron diffraction, where the expected change of the spin structure by the external magnetic field was really observed [10]. This can explain the sharp peak of the magnetic susceptibility  $\chi$  vs.  $T$  curve at  $T_N$ .

### 3. Absence of T-Linear Term in Low Temperature Specific Heat of Bi-Sr-Ca-Cu-O System

As one of the most anomalous features of the high- $T_c$  oxides, observations of the finite T-linear term ( $\gamma T$  term) in the low temperature specific heat were reported by many groups [25, 26]. Although they attracted much attention in relation to the resonating balance bond picture of the electron systems with very large correlation, there seemed to exist many experimental problems which should be overcome. For example, the oxygen deficiency in La- and Y-based oxides causes the presence of nonsuperconducting parts in the specimens. In addition, possible impurity phases may contribute to the low temperature specific heat. From this view point, Bi-Sr-Ca-Cu-O seemed to be a quite convenient system because oxygen deficiency does not easily introduced to the system. Moreover, it does not contain Ba and Y atoms which may form certain magnetic phases with very large specific heat at low temperatures. Then, we adopted this system in the specific heat measurements. Figure 3 shows the  $C/T$  vs.  $T^2$  curve of a Bi-Sr-Ca-Cu-O specimen with very large Meissner volume fraction. Although very small deviation from the linear behavior can be seen at very low temperature, it essentially indicates that there is no T-linear term in the low temperature specific heat. This was a first experimental proof of the absence of this term. Several groups reported essentially the same results as the present one later. As the origins of the finite  $\gamma T$  term observed in other high- $T_c$  oxides, large contributions of the impurity phases  $\text{BaCuO}_2$  and/or  $\text{Y}_2\text{Cu}_2\text{O}_5$  was pointed out by Kuentzler et al. [27]. For  $\text{La}_{2-x}\text{M}_x\text{CuO}_4$  ( $M = \text{Sr}$  and  $\text{Ba}$ ), besides the problems of oxygen deficiency and the existence of impurity phases, Fig. 3

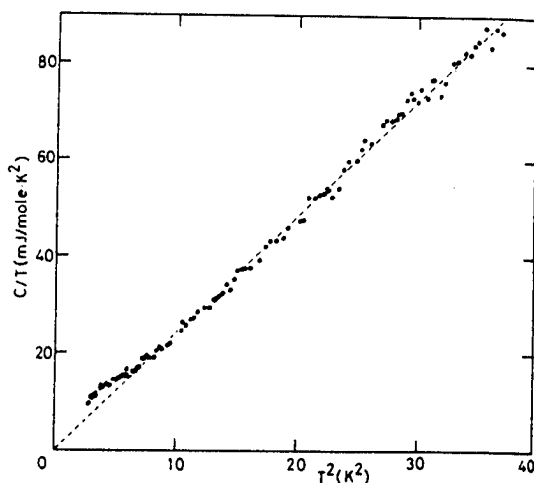


Fig. 3  $C/T$  vs.  $T^2$  of sintered pellets with a nominal composition of  $\text{Bi}_4(\text{Sr}_{0.6}\text{Ca}_{0.4})_6\text{Cu}_4\text{O}_y$  at low temperatures. Broken line indicates the relation  $C = 8T^3$  with  $\beta = 2.39$  mJ/mole  $\text{K}^4$ . Specific heat per mole was estimated for a chemical formula of  $\text{Bi}_4(\text{Sr}_{0.6}\text{Ca}_{0.4})_6\text{Cu}_4\text{O}_{16}$ .

### 4. Normal State Properties of $\text{La}_{2-x}\text{Ba}_x\text{CuO}_4$ and $\text{La}_{2-x}\text{Sr}_x\text{CuO}_4$

In the  $T_c$  vs.  $x$  curve of  $\text{La}_{2-x}\text{Ba}_x\text{CuO}_4$ , Moodenbaugh et al. [28] found the significant dip around  $x = 0.12$ . At  $x = 0.12$ ,  $T_c$  seems to vanish almost completely. In the discussion of the low temperature specific heat of  $\text{La}_{2-x}\text{Ba}_x\text{CuO}_4$ , the effect of this  $T_c$  anomaly should be taken into account. However, here we do not discuss it further but discuss what occurs there. Axe et al. [29] pointed out that the anomalous dip around  $x = 0.12$  was related to the occurrence of the structural transition: With decreasing  $T$ , transitions, high temperature tetragonal (HTT)  $\xrightarrow{T_1}$  orthorhombic (O)  $\xrightarrow{T_2}$  low temperature tetragonal (LTT), seem to take place possibly due to the successive condensations of two degenerated rotational modes of the  $\text{CuO}_6$  octahedra. Although the rotational type mode condensation is usually expected not to have much effect on the physical properties, various properties of  $\text{La}_{2-x}\text{Ba}_x\text{CuO}_4$  have been found to exhibit anomalous behaviors at  $T_1$  as shown in Figs. 4a and 4b, where the thermoelectric power  $S$  and the magnetic susceptibility  $\chi$  are shown as a function of  $T$  for various  $x$ . For  $x \approx 0.12$ ,  $S$

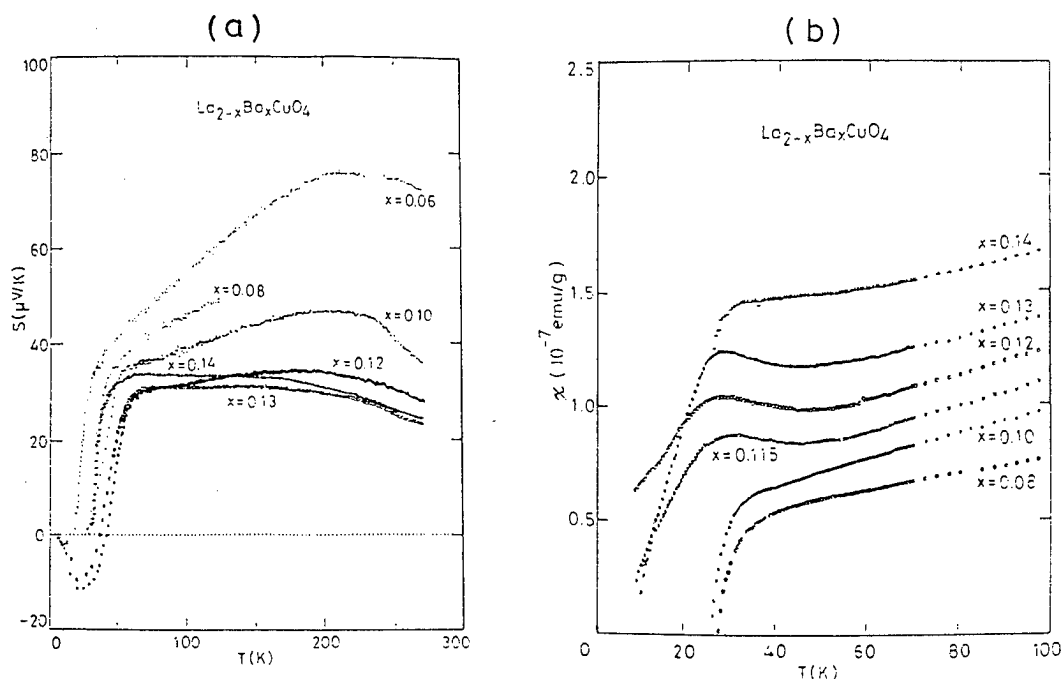


Fig. 4 a) Thermoelectric power  $S$  and b) magnetic susceptibility of  $\text{La}_{2-x}\text{Ba}_x\text{CuO}_4$  for various values of  $x$ . For the specimens with  $x \approx 0.12$ , anomalies can be seen at  $T_1 < 60$  K. Below about 30 K,  $S$  approaches zero and  $\chi$  decreases rapidly due to the partial occurrence of superconductivity.

suddenly decreases with decreasing  $T$  at  $T_1$  ( $< 60$  K), where the occurrence of the structural transition was confirmed by X-ray diffraction [29]. The Hall coefficient  $T_H$  and the resistivity  $\rho$  also exhibit anomalies at  $T_1$  [14]. However, the resistivity anomaly may not be intrinsic, because the transition to the LTT phase is the first order one and therefore formation of domains may be a cause of the resistivity anomaly. The phase diagram of  $\text{La}_{2-x}\text{Ba}_x\text{CuO}_4$  determined from the data of  $S$  is shown in Fig. 5. We have not yet succeeded in explaining why there anomalies are so significant. We just point out here that the following possibility exists: The nature of the electron system of  $\text{La}_{2-x}\text{Ba}_x\text{CuO}_4$  in LTT phase is similar to that of  $\text{La}_{2-x}\text{Ba}_x\text{CuO}_4$  in the region of  $x > 0.30$ , where the compound exhibits normal metallic behaviors without superconducting transition.

As for the normal state properties of  $\text{La}_{2-x}\text{Sr}_x\text{CuO}_4$ , Takagi et al. [31] and Oda et al. [32] observed a distinct change of the quantitative nature of  $\chi$  at  $x = 0.30$ , where  $T_c$  disappear with increasing  $x$ . Takagi et al. also found the sign change of  $R_H$  at the corresponding  $x$ . We have also found the distinct change of the qualitative natures of various properties in  $\text{La}_{2-x}\text{Sr}_x\text{CuO}_4$ . Details of the sample preparation are described in ref. 15. Figs. 6a and 6b show the  $x$ -dependence of  $S$  and  $\chi$  at fixed temperatures, which show clear change of the nature of the electron system at  $x \approx 0.30$ . Fig 7 shows the ESR line width  $\Gamma$  of Mn atoms doped to Cu sites in  $\text{La}_{2-x}\text{Sr}_x\text{CuO}_4$ . The Mn concentration is about 1 %. In the high temperature region, where the relation  $T_1 T = \text{const.}$  seems to roughly hold,  $\Gamma$  changes abruptly at the  $x$  value on the super-normal boundary of the present Mn-doped

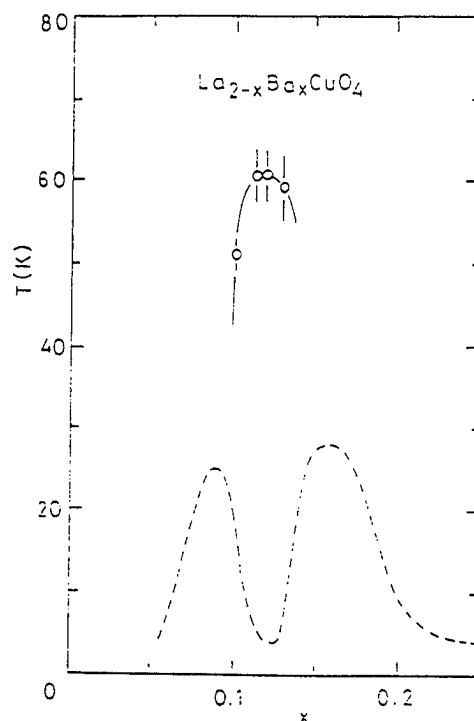


Fig. 5 Phase diagram of  $\text{La}_{2-x}\text{Ba}_x\text{CuO}_4$ . In the T-region below the solid line, the LTT phase is stable. Broken line shows  $T_c$  vs.  $x$  determined by Moodenbaugh et al.

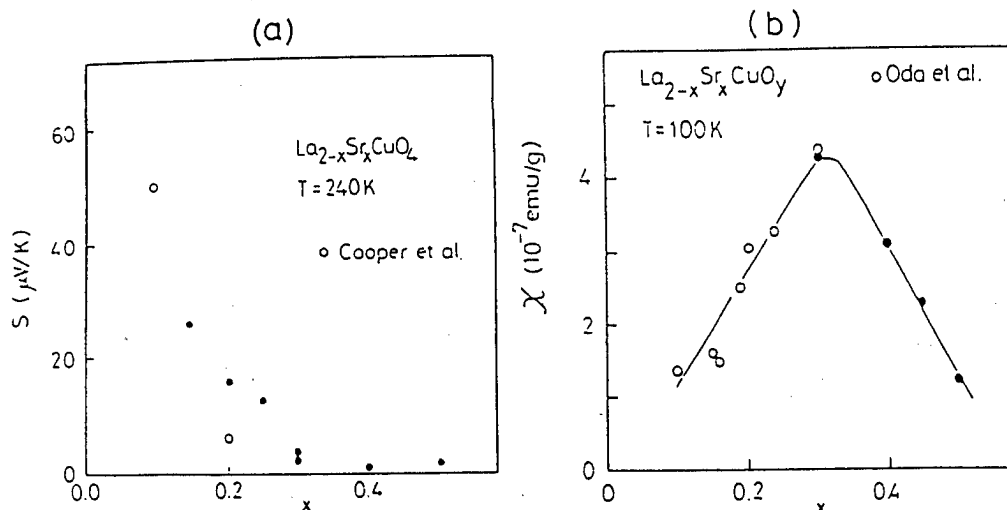


Fig. 6 Thermoelectric power  $S$  at 240 K (a) and magnetic susceptibility  $\chi$  at 100 K (b) are plotted as a function of  $x$  of  $\text{La}_{2-x}\text{Sr}_x\text{CuO}_4$ . Open circles are from refs. 32 and 33.

samples. In the  $x$  region where superconductivity does not appear, normal state properties including the temperature dependence of the resistivity [15] seem to be understood by considering the antiferromagnetically enhanced itinerant electrons, while the  $x$  region where superconductivity appears, they seem to be quite anomalous: The  $\chi$  vs.  $T$  curves have a maximum at a certain temperature, the absolute values of  $S$  are very large and  $T$ -dependence of  $S$  is also anomalous. This distinct change of the qualitative nature of the electrons may be due to the rather abrupt disappearance, at  $x \approx 0.30$  with increasing  $x$ , of the correlation gap of the band of  $\text{Cu}3d_{x-2}y_2$  orbitals. The present results seem to be consistent with the neutron result that the spins in  $\text{La}_{2-x}\text{Sr}_x\text{CuO}_4$  persist in the superconducting  $x$  region.

#### 5. Normal State Properties and Oxygen Isotope Effect of $(\text{Bi},\text{K})\text{BiO}_3$

$(\text{Ba},\text{K})\text{BiO}_3$  is a unique example of Cu-free high- $T_c$  oxides and gives us an opportunity to study on the mechanism of high- $T_c$  superconductivity from broad view points. To answer the question whether both of Cu- and Bi-oxides have a common mechanism of superconductivity, we have studied the normal state properties and the oxygen isotope effect of  $(\text{Ba},\text{K})\text{BiO}_3$ . Due to the large volatility of K atoms, much effort was necessary to prepare specimens which could be used in the present measurements [18, 34]. Our best specimens were found to have the K-concentration of about 0.25 and the zero resistivity transition temperatures are about 30 K. The magnetic susceptibility  $\chi$  was diamagnetic and the paramagnetic contribution estimated by subtracting the ion core diamagnetism is of the order of  $10^{-8}\text{ emu/g}$ , which is much smaller than those of high- $T_c$  Cu oxides [18]. The thermoelectric power  $S$  is positive but its absolute value and the temperature dependence seem to be rather normal, which has a clear contrast to those of Cu-oxide systems [19]. Figure 8 shows the temperature dependence of  $R_H$  [20]. It has a negative sign. All these data can be understood by considering the electron carriers with light effective mass or with small correlation energy, which is consistent with the fact that the charge density wave (CDW) state is stable in  $\text{BaBiO}_3$ .

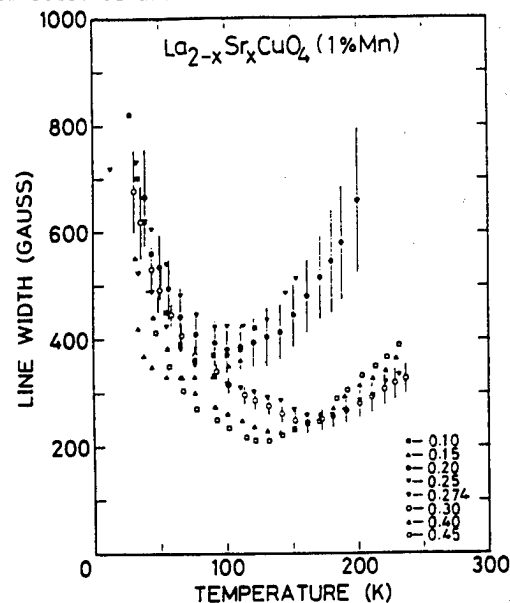


Fig. 7 Mn-ESR line widths of  $\text{La}_{2-x}\text{Sr}_x\text{CuO}_4$  for various values of  $x$ . Closed (open) symbols indicate the results for the samples with (without) superconducting transition.

and the CDW disappears as the amount of the K-doping to Ba sites increases. Then, near the metal-insulator boundary, the strong electron-phonon interaction or high- $T_c$  is expected.

Studies on the oxygen isotope effect has also been carried out by two other groups. Ballogg et al. [35] and Hinks et al. [36] obtained the value of  $\alpha = -\frac{\partial \ln T_c}{\partial \ln M} = 0.21$  and  $0.41$ , respectively. The latter authors concluded that the phonon mechanism could explain the high value of  $T_c$ , while the former groups proposed the excitonic mechanism which couples to phonons. However, it should be noted that their two step procedures in the sample preparation, the synthesis and the oxygen exchange, may easily cause the error in the estimation of the degree of exchange, because of the difficulty of preparing homogeneous samples as discussed in ref. 20. Therefore, we adopted the following synthetic processes. At first, each oxide of  $KO_2$ ,  $BaO_2$  and  $Bi_2O_3$  was synthesized by using  $^{16}O$  and  $^{18}O$  in parallel. Mixtures of these oxides with the mean oxygen isotope mass of 16, 17 and 18 were heated simultaneously in sealed Ag tubes. Fig. 9 shows the temperature dependence of the Meissner signals of three specimens, where data of each sample are normalized by the corresponding value at 7 K. Clearly,  $T_c$  depend on the oxygen isotope mass number and  $\alpha = 0.35$  is obtained. From this result, we think, it is difficult to adopt the nonphonon mechanism as Batlogg et al. did. In their discussion, they adopted the value of the Debye frequency of 150 200 K, which may be too small to get the correct result. Recently, Mochizuki and her co-workers [37] estimated the  $T_c$  value, based on the band calculation and consistently explained the observed  $T_c$  by the mechanism of the electron-phonon coupling. Their estimated  $\alpha$  is 0.27, which also seems to support the present conclusion.

Now, by the studies on normal properties and oxygen isotope effect of  $(Ba,K)BiO_3$ , we conclude that the electronic nature is quite different from that of the Cu-oxide systems with high- $T_c$  and the

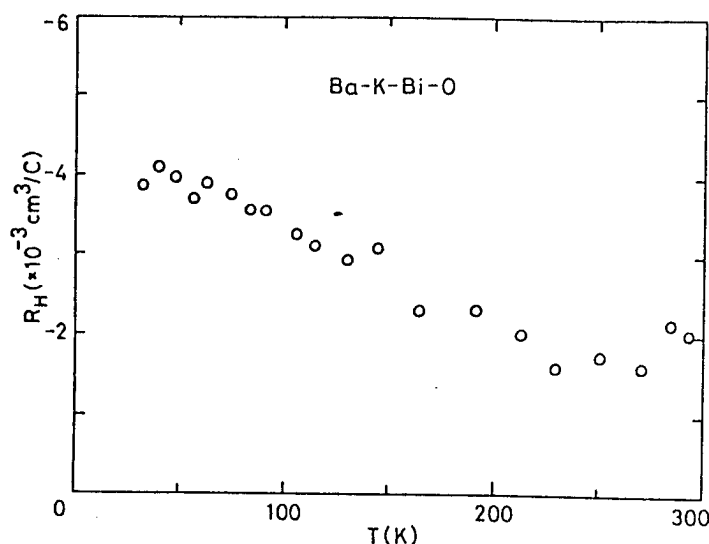


Fig. 8 Temperature dependence of Hall coefficient  $R_H$  of  $(Ba,K)BiO_3$  with the K-concentration of about 0.25.

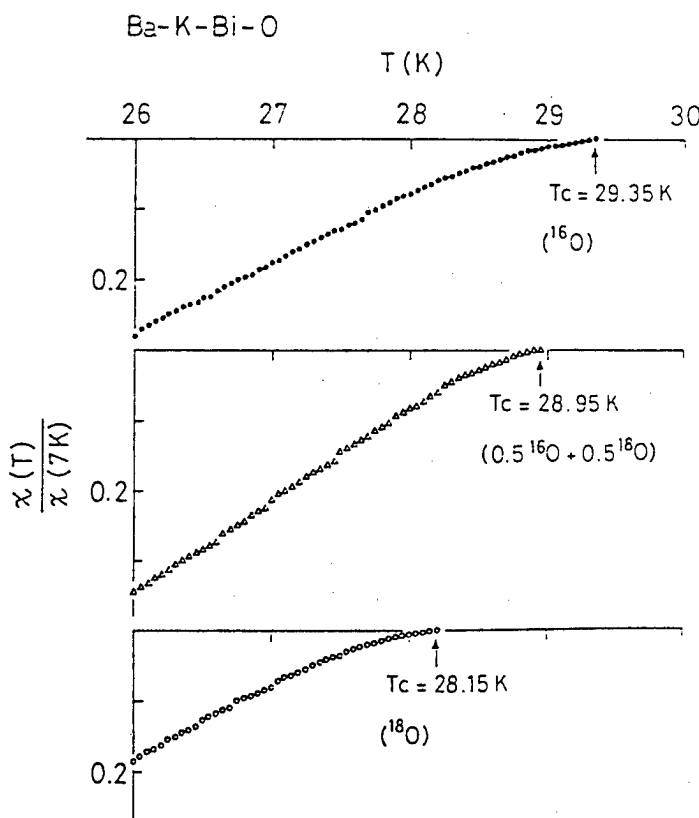


Fig. 9 Temperature dependence of the Meissner diamagnetic moments are shown for the samples with the average oxygen isotope mass of 16 (top), 17 (middle) and 18 (bottom). Data of each sample are normalized by the value at 7 K.



mechanism of the pairing force in  $(\text{Ba,K})\text{BiO}_3$  seems to be due to the electron-phonon coupling.

#### 6. Summary

We have presented results of our various kinds of studies on high- $T_c$  oxides. Because, it seems to be quite difficult, as is mentioned above, to extract direct clues of the superconducting mechanism from a special kind of experiments, detailed but rather broad studies, we believe, should be continuously carried out.

1. T. Ekino, J. Akimitsu, M. Sato and S. Hosoya: Solid State Commun. 62 (1987) 535 and S. Shamoto, M. Onoda, M. Sato and S. Hosoya: Solid State Commun. 62 (1987) 479
2. M. Sato, M. Sera, S. Shamoto, M. Onoda, S. Kondoh, K. Fukuda and Y. Ando: Proc. 2nd NEC Conf. Hakone October, 1988
3. M. Sato: Physica C 153-155 (1988) 38
4. S. Shamoto: Solid State Commun. 66 (1988) 1151
5. M. Onoda and M. Sato: Solid State Commun. 67 (1988) 799
6. M. Sera, S. Shamoto and M. Sato: Solid State Commun. 68 (1988) 649
7. S. Sugai, S. Shamoto and M. Sato: Phys. Rev. B38 (1988) 6436
8. T. Takahashi, F. Maeda, H. Katayama-Yoshida, Y. Okabe, T. Suzuki, A. Fujimori, S. Hosoya, S. Shamoto and M. Sato: Phys. Rev. B37 (1988) 9788
9. R. J. Birgeneau, D. R. Gabbe, H. P. Jenssen, M. A. Kastner, P. J. Picone, T. R. Thurston, G. Shirane, Y. Endoh, M. Sato, K. Yamada, H. Hidaka, M. Oda, Y. Enomoto, M. Suzuki and T. Murakami: Phys. Rev. B38 (1988) 6614
10. K. Fukuda, S. Shamoto, M. Sato and K. Oka: Solid State Commun. 65 (1988) 1323 and M. A. Kastner, R. J. Birgeneau, T. R. Thurston, P. J. Picone, H. P. Jenssen, D. R. Gabbe, M. Sato, K. Fukuda, S. Shamoto, Y. Endoh, Y. Yamada and G. Shirane: Phys. Rev. B38 (1988) 6636
11. M. Sato, S. Shamoto, J. M. Tranquada, G. Shirane and B. Keisner: Phys. Rev. Letters 61 (1988) 1317
12. T. R. Thuston, R. J. Birgeneau, D. R. Gabbe, H. P. Jenssen, M. A. Kastner, P. J. Picone, N. W. Preyer, J. D. Axe, P. Böni, G. Shirane, M. Sato, K. Fukuda and S. Shamoto: Phys. Rev. B in press
13. M. Sera, S. Kondoh, K. Fukuda and M. Sato: Solid State Commun. 66 (1988) 1101
14. M. Sera, Y. Ando, S. Kondoh, K. Fukuda, M. Sato, I. Watanabe, S. Nakashima and K. Kumagai: Solid State Commun. in press
15. Y. Ando, M. Sera, S. Yamagata, S. Kondoh, M. Onoda and M. Sato: Solid State Commun. submitted
16. Y. Ando, K. Fukuda, S. Kondoh, M. Sera, M. Onoda, M. Sera and M. Sato: Solid State Commun. 67 (1988) 815
17. M. Onoda and M. Sato: Solid State Commun. submitted
18. S. Kondoh, M. Sera, K. Fukuda, Y. Ando and M. Sato: Solid State Commun. 67 (1988) 879
19. M. Sera, S. Kondoh and M. Sato: Solid State Commun. 68 (1988) 647
20. S. Kondoh, M. Sera, Y. Ando and M. Sato: Physica C
21. S. Kondoh, Y. Ando, M. Onoda and M. Sato: Solid State Commun. 65 (1988) 1329
22. M. Sera, S. Kondoh, Y. Ando, K. Fukuda, S. Shamoto, M. Onoda and M. Sato: Solid State Commun. 66 (1988) 707
23. M. Onoda, S. Kondoh, K. Fukuda and M. Sato: Jpn. J. Appl. Phys. 27 (1988) L1234
24. G. Shirane, Y. Endoh, R. J. Birgeneau, M. A. Kastner, Y. Hidaka, M. Oda, M. Suzuki and T. Murakami: Phys. Rev. Letters 59 (1987) 1613
25. K. Kumagai, Y. Nakamichi, I. Watanabe, Y. Nakamura, H. Nakajima and N. Wada: Phys. Rev. Letters 60 (1988) 724
26. M. Ishikawa, T. Takabatake and Y. Nakazawa: Physica 148B (1987) 332
27. R. Kuentzler, Y. Dossmann, S. Vilminot and S. El Hadihui: Solid State Commun. 65 (1988) 1529

28. A. R. Moodenbaugh, Y. Xu, M. Suenaga, T. J. Folkerts and R. N. Shelton: Phys. Rev. B38 (1988) 4596
29. J. D. Axe, D. E. Cox, K. Mohanty, H. Moudden, A. R. Moodenbaugh, Y. Xu and T. R. Thurston: IBM J. Res. Dev.
30. J. B. Torrance, Y. Tokura, A. I. Nazzal, A. Bezing, T. C. Huang and S. S. P. Parkin: Phys. Rev. Letters 61 (1988) 1127
31. H. Takagi, Y. Tokura and S. Uchida: Proc. 2nd NEC Conf. Nakone October 1988
32. M. Oda, T. Ohguro, N. Yamada and M. Ido: preprint
33. J. E. Xoopwe, V. Alavi, L-W. Zhou, W. P. Beyermann and G. Grüner: Phys. Rev. B35
34. R. J. Cava, B. Batlogg, J. J. Krajewski, R. C. Farrow, L. W. Rupp, Jr, A. E. White, K. T. Short, W. F. Peck, Jr, T. Y. Kometani: Nature 332 (1988) 814
35. B. Batlogg, R. J. Cava, L. W. Rupp, Jr, A. M. Mjlsce, J. J. Krajewski, J. P. Remeika, W. F. Peck, Jr, A. S. Cooper and G. P. Espinosa: Phys. Rev. Letters 61 (1988) 1670
36. D. G. Hinks, D. R. Richards, B. Dabrowski, D. T. Marx, A. W. Mitchell: Nature 335 (1988) 419
37. K. Mochizuki et al., private communication

K. Sekizawa and Y. Takano

Department of Physics, College of Science and Technology, Nihon University  
Kanda-Surugadai 1-8, Chiyoda-ku, Tokyo 101, Japan

The effects of Ni and Zn substitution for Cu in  $\text{RBa}_2\text{Cu}_3\text{O}_y$  ( $\text{R} = \text{Y, Nd, Gd, Dy and Er}$ ) on the superconducting transition temperature  $T_c$  and the magnetic properties above  $T_c$  have been investigated. In heavy rare earth compounds, the effects of the substitution on magnetic properties are weak, although the decrease rate of  $T_c$  is large. In Nd compound, however, the paramagnetic Curie temperature  $\theta_p$  is large and negative ( $\sim -30$  K) and the substituent concentration dependence of  $\theta_p$  and the decrease rate of  $T_c$  are larger than those of heavy rare earth compounds.

One of the striking features of  $\text{RBa}_2\text{Cu}_3\text{O}_y$  type high- $T_c$  superconductors is that this high- $T_c$  superconductivity is not destroyed by the localized magnetic moments of the rare earth (R) ions. This is generally recognized to be due to the absence of superconducting electrons in the R ion layers. Using the magnetic moments of R ions and interaction between them, we can obtain the information about the electronic state of the R ion layers which may correlate with that of the Cu-O subsystem. In the present study, we have investigated the effect of Ni and Zn substitution for Cu in  $\text{RBa}_2\text{Cu}_3\text{O}_y$  ( $\text{R} = \text{Y, Nd, Gd, Dy and Er}$ ) on the superconducting transition temperature  $T_c$  and magnetic properties of R ions.

Samples were prepared by the solid state reaction of  $\text{R}_2\text{O}_3$ ,  $\text{BaCO}_3$ , CuO and NiO or ZnO powders. The starting materials with a ratio of  $\text{R}:\text{Ba}:\text{Cu}:\text{M}=1:2:(3-x):x$  were thoroughly mixed and calcined at  $930^\circ\text{C}$  ( $900^\circ\text{C}$  for  $\text{R}=\text{Nd}$ ). Then, they were pressed into bars and sintered at  $930^\circ\text{C}$  ( $900^\circ\text{C}$  for  $\text{R}=\text{Nd}$ ) for 10 hours in air. The sintered bars were reground and pressed into bars again, and sintered at  $930^\circ\text{C}$  ( $900^\circ\text{C}$  for  $\text{R}=\text{Nd}$ ) for 20 hours in  $\text{O}_2$  gas flow, and cooled down at the rate of  $140^\circ\text{C/h}$ . X-ray diffraction measurements showed that the samples with  $0 \leq x \leq 0.1$  were composed of the single phase with orthorhombic oxygen-deficient perovskite structure. The lattice parameters change a little bit and the ratio  $a/b$  approaches unity with increasing  $x$ . The superconducting transition temperature  $T_c$  was determined by the onset of the drop of the electrical resistivity measured by the standard four probe method. The magnetization above  $T_c$  was measured by Faraday method under the magnetic fields between 0.5 T and 0.8 T.

The superconducting transition temperature  $T_c$  exceeds 90 K for all compounds with  $x=0$  and decreases almost linearly with increasing  $x$ . The transition width is rather narrow for samples with  $x=0$  ( $1 \sim 2$  K for  $\text{R}=\text{Y, Gd, Dy and Er}$ ;  $\sim 4$  K for  $\text{R}=\text{Nd}$ ) and shows a little increase with increasing  $x$ . The decrease rate of  $T_c$  with  $x$  is nearly same in magnitude for Y, Gd, Dy and Er compounds, while that of Nd compound is large compared with those of other R compounds (Table 1). The dependence of  $T_c$  on the substituent concentration  $x$  for Nd and Er compounds are shown in Fig. 1.

The magnetic susceptibility  $\chi$  of  $\text{YBa}_2\text{Cu}_{3-x}\text{M}_x\text{O}_y$  consists of temperature independent Pauli paramagnetic part and Curie-Weiss part which increases with  $x$ . The magnetic susceptibility originated in R ions is estimated by subtracting the value of the magnetic susceptibility of corresponding Y compound (same M and same  $x$ ) from that of R compound. It shows Curie-Weiss behavior above  $T_c$  and the value of the effective magnetic moment  $\mu_{\text{eff}}$  agrees rather well with that of free  $\text{R}^{3+}$  ion in all R

Table 1. The superconducting transition temperature  $T_c$ , transition width  $\Delta T_c$  (from 10 % to 90 %) and the decrease rate of  $T_c$ ,  $(dT_c/dx) \cdot 10^{-2}$ , for  $RBa_2Cu_{3-x}M_xO_y$ .

R	M	$T_c$ (K)			$\Delta T_c$ (K)			$\frac{dT_c}{dx} \cdot 10^{-2}$
		x=0	x=0.05	x=0.10	x=0	x=0.05	x=0.10	
Y	Ni	91.9	86.8	82.9	1.1	2.5	2.5	-1.0
	Zn	91.9	72.2	54.3	1.1	1.5	2.4	-3.8
Nd	Ni	93.0	85.0	70.9	4.5	5.6	9.4	-2.0
	Zn	93.0	65.0	36.9	4.5	8.3	13.2	-5.6
Gd	Ni	93.4	86.2	84.5	2.3	3.8	5.6	-0.9
	Zn	93.4	72.5	53.6	2.3	2.9	4.6	-4.1
Dy	Ni	91.3	87.5	81.8	1.1	2.1	2.8	-1.0
	Zn	91.3	71.5	49.3	1.1	1.9	5.3	-4.1
Er	Ni	91.7	87.8	83.3	1.1	1.2	1.3	-0.8
	Zn	91.7	73.1	51.8	1.1	2.0	2.6	-3.9

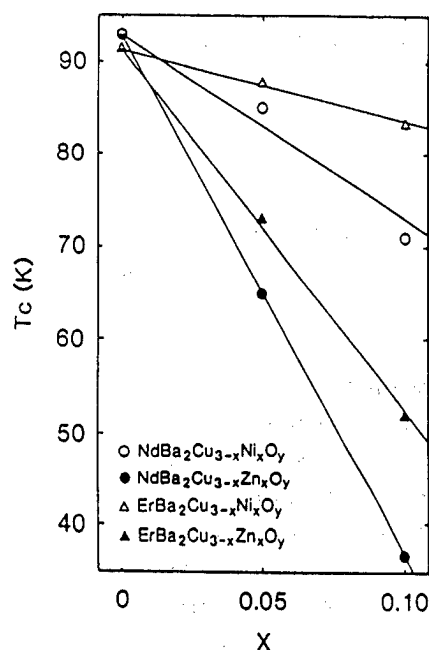


Fig. 1. The dependence of the superconducting transition temperature  $T_c$  on the substituent concentration  $x$  for Nd and Er compounds. Solid lines are guides for eye.

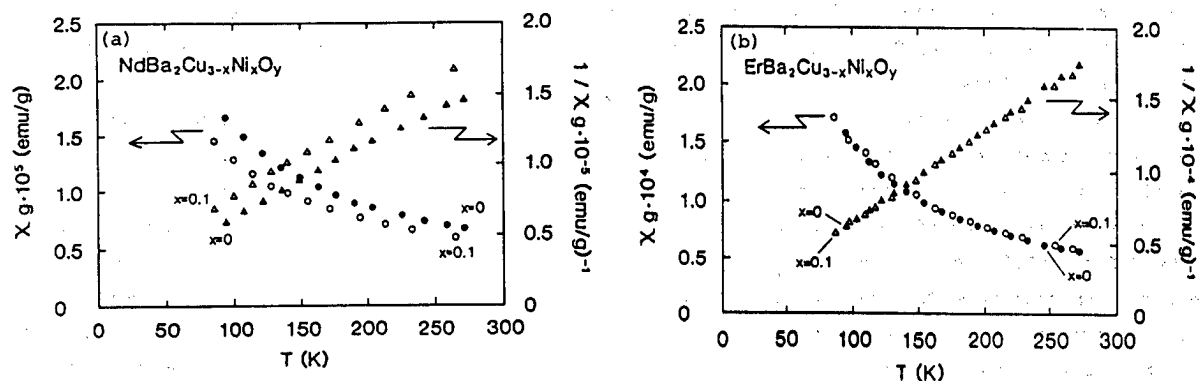


Fig. 2. The temperature dependence of the magnetic susceptibility  $\chi$  and reciprocal susceptibility in a magnetic field of 0.62 T; (a) for  $NdBa_2Cu_{3-x}Ni_xO_y$  with  $x=0$  and 0.1 and (b) for  $ErBa_2Cu_{3-x}Ni_xO_y$  with  $x=0$  and 0.1.

compounds. The temperature dependence of the magnetic susceptibility and reciprocal susceptibility of Nd ions in  $NdBa_2Cu_{3-x}Ni_xO_y$  and of Er ions in  $ErBa_2Cu_{3-x}Ni_xO_y$  for  $x=0$  and 0.1 are shown in Fig. 2 (a) and (b), respectively. The effect of the substitution on  $\theta_p$  is not pronounced for Gd, Dy and Er compounds. For Nd compound, however, the paramagnetic Curie temperature  $\theta_p$  is large and negative ( $\sim -30$  K) and its dependence on  $x$  is large. The dependence of the paramagnetic Curie temperature  $\theta_p$  on the Ni concentration  $x$  for Nd and Er compounds is shown in Fig. 3. All the magnetic data are listed in Table 2. The effect of Ni and Zn substitution for Cu on the magnetic properties of the rare earth moment is not remarkable for heavy rare earth compounds. It is noticeable that the absolute

Table 2. The paramagnetic Curie temperature  $\theta_p$  and the effective magnetic moment  $\mu_{\text{eff}}$  of R ions in  $\text{RBa}_2\text{Cu}_{3-x}\text{Ni}_x\text{O}_y$ .

R	M	$\theta_p$ (K)			$\mu_{\text{eff}}$ ( $\mu_B$ )		
		x=0	x=0.05	x=0.10	x=0	x=0.05	x=0.10
Nd	Ni	-30.7	-38.6	-43.1	3.4	3.4	3.2
	Zn	-30.7	-33.1	-22.1	3.4	3.2	3.2
Gd	Ni	5.4	2.7	4.5	7.9	7.4	7.7
	Zn	5.4	5.1	0.9	7.9	7.8	7.8
Dy	Ni	-5.2	-6.1	-6.4	10.5	10.6	10.5
	Zn	-5.2	-5.2	-7.1	10.5	10.8	10.7
Er	Ni	-5.6	-8.5	-7.9	9.3	9.6	9.4
	Zn	-5.6	-8.0	-5.8	9.3	9.5	9.5

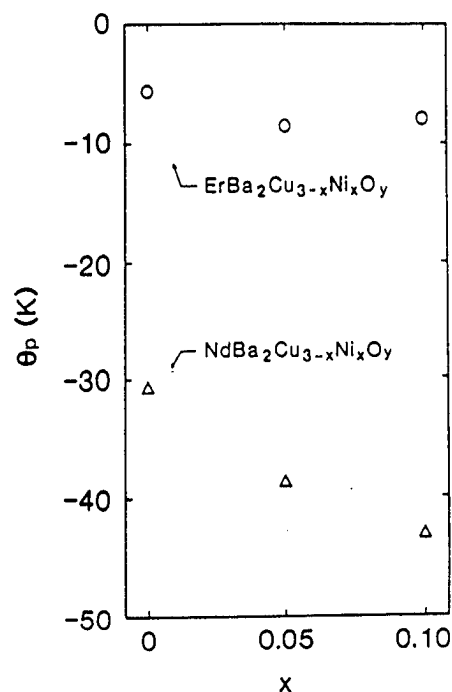


Fig. 3. The dependence of the paramagnetic Curie temperature  $\theta_p$  on Ni concentration x for Nd and Er compounds.

value of  $\theta_p$ , the change of  $\theta_p$  and the decrease rate of  $T_c$  with x of Nd compound are large compared with those of heavy rare earth compounds. These results imply that the correlation between rare earth ions and superconducting electrons in Nd compound is somewhat different from that in other rare earth compounds, although it can not be denied that the oxygen content y may differ with R. It is not so reasonable that the effective magnetic moment  $\mu_{\text{eff}}$  is close to the free ion value and the temperature dependence of the magnetic susceptibility  $\chi$  obeys Curie-Weiss law, if we take into consideration that the crystal field splitting of R ions is quite large<sup>1) - 3)</sup>.

Further investigation on the electronic state of the magnetic R ions in  $\text{RBa}_2\text{Cu}_3\text{O}_y$  is needed in order to elucidate the state of Cu-O subsystem which are considered to carry superconducting electrons.

#### References

- 1) U. Walter, S. Fahy, A. Zettl, S.G. Louie, M.L. Cohen, P. Tejedor and A.M. Stacy, Phys. Rev. B36 (1987) 8899.
- 2) A. Furrer, P. Bruesch and P. Unterhahrer, Physica C153-155 (1988) 164.
- 3) U. Walter, E. Holland-Moritz, A. Severing, A. Erle, H. Schmidt and E. Zirngiebl, Physica C153-155 (1988) 170.

# High $T_c$ Superconducting Properties in Ln-(Ba,M)-Cu-O Ceramics and Bi-Sr-Ca-Cu-O Thin Films

Y. Saito, T. Noji, Y. Hayashi, Y. Fujino, T. Oikawa, A. Hattori,  
K. Furuse and M. Masuzawa

Department of Applied Physics, Faculty of Engineering,  
Tohoku University, Sendai 980, Japan

The concentration dependence of the transition temperature  $T_c$  has been studied in  $\text{Ln}(\text{Ba}_{1-x}\text{Sr}_x)_2\text{Cu}_3\text{O}_y$  compounds.  $T_c$  showed a shallow minimum for  $0.1 < x < 0.3$  in  $\text{Ln}(\text{Ba}_{1-x}\text{Sr}_x)_2\text{Cu}_3\text{O}_7$  compounds (Ln=Nd, Sm, Gd, Dy). The  $x$  value indicating the shallow minimum was correlated with the ionic size of the rare earth ions. BiSrCaCuO superconducting films were prepared by a multilayer deposition technique using a single electron beam gun. It was found by RBS analysis that Mg impurity of MgO substrate was diffused into the films.

## 1. Introduction

It is well established by now that a series of isomorphous compounds  $\text{LnBa}_2\text{Cu}_3\text{O}_{7-y}$  (Ln=Y or rare earth ions) are oxide superconductors with  $T_c$  of about 90 K.<sup>1)</sup> In this letter, we report the effect of substitution of Ba by Sr on the superconducting properties in  $\text{Ln}(\text{Ba}_{1-x}\text{Sr}_x)_2\text{Cu}_3\text{O}_{7-y}$  with Ln=Nd, Sm, Gd, Dy, Ho and Y in order to clarify the relative difference of the rare earth ions.

On the other hand, recently, Maeda et al. discovered a new superconducting oxide Bi-Sr-Ca-Cu-O system without rare earth elements.<sup>2)</sup> The preparation of films is practically very important to utilize these materials for microelectronic devices. In this letter we report the preparation and characterization of superconducting BiSrCaCu oxide thin films (total thickness of 2000 Å) by a multilayer deposition technique using a single electron beam gun.

## 2. $\text{Ln}(\text{Ba}_{1-x}\text{Sr}_x)_2\text{Cu}_3\text{O}_{7-y}$ compounds

The bulk samples  $\text{Ln}(\text{Ba}_{1-x}\text{Sr}_x)_2\text{Cu}_3\text{O}_{7-y}$  (Ln=Nd, Sm, Gd, Dy, Ho, Y) were prepared by heating mixtures of appropriate amounts of high purity  $\text{Ln}_2\text{O}_3$ ,  $\text{BaCO}_3$  and CuO at 900°C for 5 hours in air. The calcined samples were then ground and sintered at 930-980°C for 10 hours in the flow of  $\text{O}_2$  gas. Samples were cooled to room temperature in the furnace.

The phases of all samples and the lattice parameters,  $a$ ,  $b$  and  $c$  were determined by the analysis of X-ray diffraction patterns. DC electrical resistance was measured by a four terminal technique with flowing 10 mA. Typical results on the transition temperature (onset, mid-point

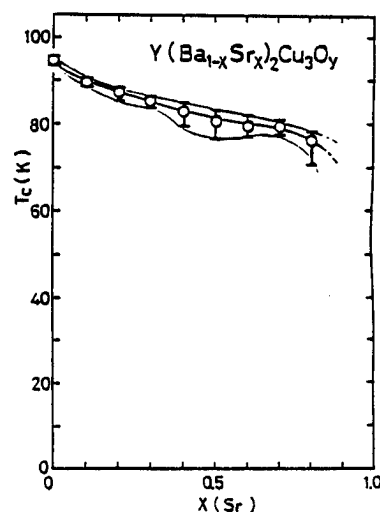


Fig.1 Superconducting transition temperature as a function of Sr concentration for  $\text{Y}(\text{Ba}_{1-x}\text{Sr}_x)_2\text{Cu}_3\text{O}_y$ .

and end-point)  $T_c$  are shown as a function of Sr concentration in cases of Y and Sm series in Figs. 1 and 2, respectively. As shown in Fig. 1,  $T_c$  in Y series decreases gradually with Sr concentration in good agreement with those widely reported.<sup>3)</sup> For Sm series (Fig. 2),  $T_c$  decreases sharply with increasing  $x$  up to  $x=0.3$ . This  $x$  value roughly corresponds to a concentration indicating the orthorhombic-tetragonal phase transition. Beyond  $x=0.3$ ,  $T_c$  increases with  $x$  and shows a plateau of about  $0.4 < x < 0.6$ . X-ray result indicates that a (1:2:3) single phase is observed up to  $x < 0.6 \sim 0.7$ . Similar results with Sm series were also obtained for another lanthanide series of Nd, Gd, Dy.

To make the experimental situation clearer, we summarize the results in Fig. 3, where the obtained  $T_c$  values are plotted as functions of both Sr concentration  $x$  and ionic size of rare earth ions. The dotted lines show the orthorhombic-tetragonal phase transition boundary, determined through X-ray diffraction study. Numerical values and solid lines in this figure indicate superconducting critical temperatures and contour lines, respectively. Figure 3 seems to indicate that the orthorhombic-tetragonal phase transition changes systematically with the ionic size of the rare earth ions. It is also interesting to note that the  $x$  value indicating the shallow minimum is correlated with the ionic size of the rare earth ions. Detailed study is needed to clarify this substitution effect.

### 3. Bi-Sr-Ca-Cu-O Thin Films

Cu, Bi and mixed  $\text{CaF}_2$  and  $\text{SrF}_2$  were used as starting materials. These materials in three-hearthers were evaporated in a vacuum of  $10^{-6}$  Torr by a single electron beam gun in the order of Cu, Bi, mixed  $\text{CaF}_2$  and  $\text{SrF}_2$  on the substrate maintained at room temperature. Single crystals of (100)MgO were used as the substrate. Films were made for single to ten deposition cycles. Total thickness was about 2000 Å. The as-deposited films were annealed in the flow of  $\text{O}_2$  gas at a temperature of 875°C for 2 hours to obtain the superconducting films. The metal compositions of the films were determined by Rutherford backscattering spectroscopy (RBS) for the as-deposited films and the same films after annealing.

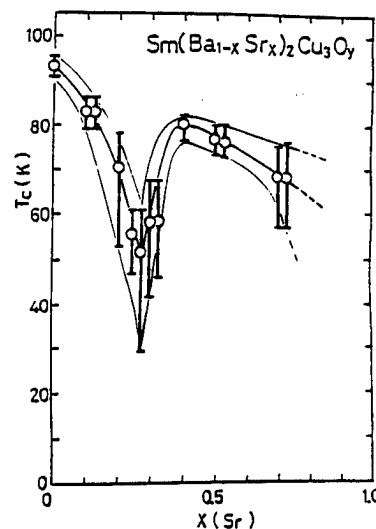


Fig. 2 Superconducting transition temperature as a function of Sr concentration for  $\text{Sm}(\text{Ba}_{1-x}\text{Sr}_x)_2\text{Cu}_3\text{O}_y$ .

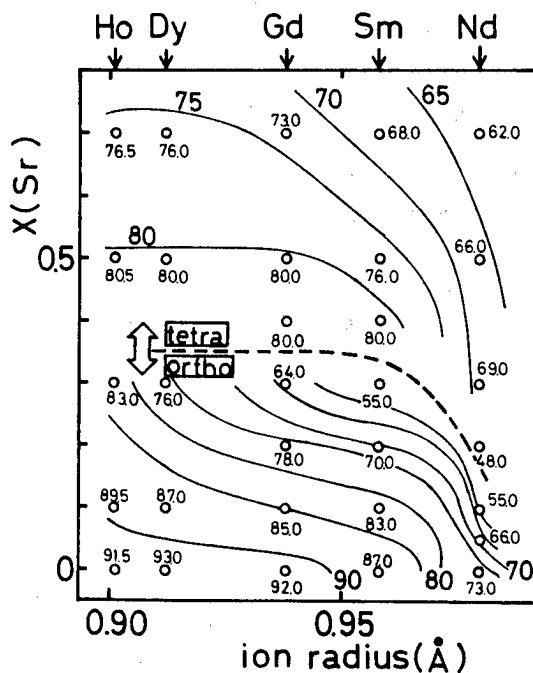


Fig. 3 Superconducting transition temperatures, Sr concentration and the ionic size of the rare earth ions.

Table 1 shows the analyzed metal compositions of the films. As shown in this table, metal composition of the films prepared by the deposition and annealing was deviated from nominal compositions.

Table 1. Film composition by RBS analysis

Cycle	nominal				as-deposited				875°C 2h annealed			
	Bi	Sr	Ca	Cu	Bi	Sr	Ca	Cu	Bi	Sr	Ca	Cu
1	1.0	1.0	1.0	2.0	1.0	1.0	1.0	2.5	0.9	1.0	0.8	1.6
3	1.0	1.0	1.0	2.0	1.0	1.0	1.0	2.3	0.9	1.0	0.9	1.8
5	1.0	1.0	1.0	2.0	1.2	1.0	1.0	2.5	1.1	1.0	1.0	1.7
10	1.0	1.0	1.0	2.0	1.0	1.0	1.0	2.6	0.8	1.0	0.9	1.8

In addition, it was found by RBS analysis that Mg was also diffused into the BiSrCaCuO films. Mg impurity seems to have influence on the superconducting properties.

Figure 4 shows the temperature dependence of the resistance in various magnetic field strength. In the absence of magnetic field, the resistance decreases almost linearly with decreasing temperature and starts to drop at about 85 K. The magnetic field gives rise to a considerable broadening of the transition. The high temperature side of the transition is only a little influenced by a magnetic field. On the other hand, the low temperature side strongly depends on the magnetic field strength and the transition is extended toward the lower temperature. Using the standard formula for dirty superconductors, the critical fields at  $T=0$  is estimated as  $H_{c2}(0) = 32$  Tesla.

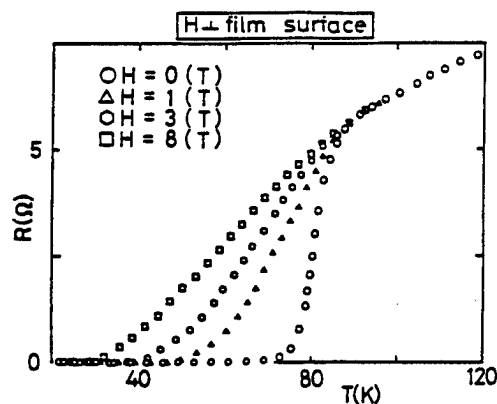


Fig.4 The temperature dependence of the resistance in various magnetic field strength in BiSrCaCuO<sub>y</sub> films.

#### References

- 1) J.M. Tarascon, L.H. Greene, B.G. Bagley, W.R. McKinnon, P. Barboux and G.W. Hull: Novel Superconductivity, ed. S.A. Wolf and V.Z. Kresin (Plenum, 1987) p.705.
- 2) H. Maeda, Y. Tanaka, M. Fukutomi and T. Asano: Jpn. J. Appl. Phys. 27 (1988) L209.
- 3) Y. Saito, T. Noji, A. Endo, N. Higuchi, K. Fujimoto, T. Oikawa, A. Hattori and K. Furuse: Jpn. J. Appl. Phys. 26 (1987) Suppl. 26-3, 1081.



# Electrical, Magnetic and Structural Properties of $\text{Ba}_2\text{LnCu}_3\text{O}_{7-\delta}$ Compounds

S. Ohshima, S. Seino, S. Ichino, K. Aizawa and K. Okuyama

Electronic Engineering, Faculty of Engineering, Yamagata University, Yonezawa 992

$\text{Ba}_2\text{LnCu}_3\text{O}_{7-\delta}$  compounds (Ln=La, Nd, Sm, Eu, Gd, Dy, Ho and Er) were prepared by a solid-state reaction. The optimum sintering temperature for obtaining a single phase of  $\text{Ba}_2\text{LnCu}_3\text{O}_{7-\delta}$  was different for each Ln element and decreased with increasing atomic number of Ln. Melting points and lattice constants of these compounds decreased monotonically with increasing atomic number of Ln. However, there was not so large difference in the  $T_c$  values of these compounds. We also found that  $T_c$  changes systematically with the Cu-O bond length.

## § 1. Introduction

After discovery of high- $T_c$  superconductivity in the Ba-Ln-Cu-O system, there has been an explosion of experimental and theoretical studies on these materials. However, the mechanism of high- $T_c$  superconductivity is not yet understood. It has been clarified so far that these compounds have  $T_c$ 's in 90 K-range and their superconducting properties are similar to each other. However, the lattice constants decrease monotonically with increasing the atomic number of Ln. In order to investigate experimentally the mechanism of high  $T_c$  superconductivity, it is important to know the correlation between the microcrystal structure and the superconducting behavior of these compounds.

It is well known that  $\text{Ba}_2\text{LnCu}_3\text{O}_{7-\delta}$  compounds have a threefold stacked perovskite structure. The position of Cu and O ions are illustrated in Fig.4. Miceli et al. reported the role of Cu(1)-O(3) bond length on the superconductivity in  $\text{Ba}_2\text{YCu}_3\text{O}_{7-x}\text{Co}_x\text{O}_{7-\delta}$  compounds. They showed that  $T_c$ 's of these compounds decreased systematically with decreasing the Cu(1)-O(3) bond length. Takita et al. reported the microcrystal structure of  $\text{Ba}_{2-x}\text{Nd}_{1+x}\text{Cu}_3\text{O}_{7-\delta}$  compounds. From the correlation between these microcrystal structure and the  $T_c$ 's, it was found that  $T_c$ 's of these compounds decreased systematically with increasing the Cu(1)-O(3) bond length.

In this report, we show the thermal, electrical, magnetic and structural properties of  $\text{Ba}_2\text{LnCu}_3\text{O}_{7-\delta}$  compounds. The reason why we have chosen these series are as follows; (1) The ionic radius of these rare earth elements can be changed from 0.88 Å to 1.18 Å. (2) The  $T_c$ 's of these compounds with these elements are higher than 90 K. We shall also discuss the correlation between Cu-O bond length and  $T_c$ 's of these compounds.

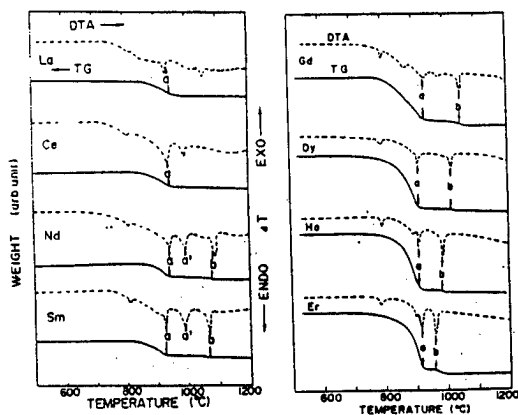


Fig.1 TG and DTA curves of mixed powder of  $\text{BaCO}_3$ ,  $\text{Ln}_2\text{O}_3$  and  $\text{CuO}$ .

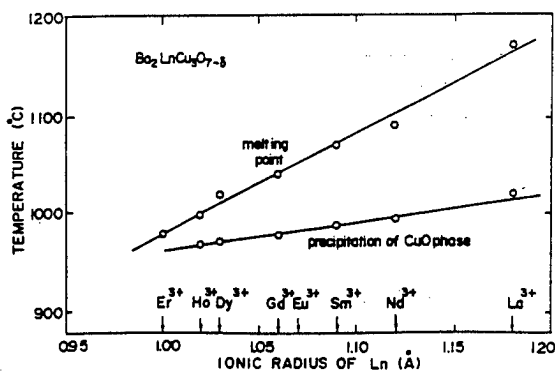


Fig.2 Melting points and precipitation temperature of  $\text{Ba}_2\text{LnCu}_3\text{O}_{7-\delta}$  compounds

## § 2. Experimental

$\text{Ba}_2\text{LnCu}_3\text{O}_{7-\delta}$  compounds (Ln=La,Nd,Sm,Eu,Gd,Dy,Ho and Er) were prepared by a solid state reaction using  $\text{BaCO}_3$ ,  $\text{Ln}_2\text{O}_3$  and CuO powders. These powders were mixed in a ball mill with the addition of methanol. The reaction temperature and melting points were determined by thermogravimetry(TG),and differential thermal analysis(DTA). Lattice constants and Cu-O bond length were determined by x-ray analysis.  $T_c$ 's were determined by electrical resistance and ac susceptibility measurements.

## § 3. Results and Discussion

For synthesis of  $\text{Ba}_2\text{LnCu}_3\text{O}_{7-\delta}$  compounds by powder sintering process, it is important to know the thermal decomposition temperature and melting points of mixed powder containing each  $\text{Ln}_2\text{O}_3$ . Figure 1 shows the TG and DTA curves of the mixed powder. From the results of TG,DTA and x-ray analysis, it was found that the peaks marked by a, a' and b are the temperatures of reaction, precipitation and melting, respectively. The reaction temperatures were almost the same. On the other hand, melting points decreased with increasing atomic number of Ln. Figure 2 presents the melting points and the precipitation temperatures of  $\text{Ba}_2\text{LnCu}_3\text{O}_{7-\delta}$  compounds. Both the temperatures increased systematically with increasing the atomic radius of Ln. Figure 3 shows the lattice constants of  $\text{Ba}_2\text{LnCu}_3\text{O}_{7-\delta}$  compounds. The lattice constant increased monotonically with increasing the atomic radius of Ln.

Recently, it was pointed out that the position of atoms supplying holes and valence value of Cu might be important to know the mechanism of high  $T_c$  superconductivity. These values may be affected by

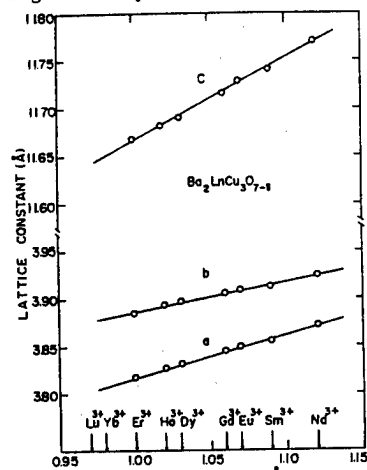


Fig.3 Lattice constants of  $\text{Ba}_2\text{LnCu}_3\text{O}_{7-\delta}$  compounds.

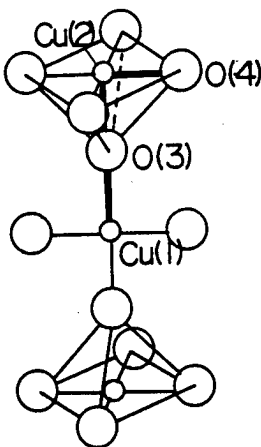


Fig.4 Schematic picture of Cu-O bond length in  $\text{Ba}_2\text{LnCu}_3\text{O}_{7-\delta}$  compound

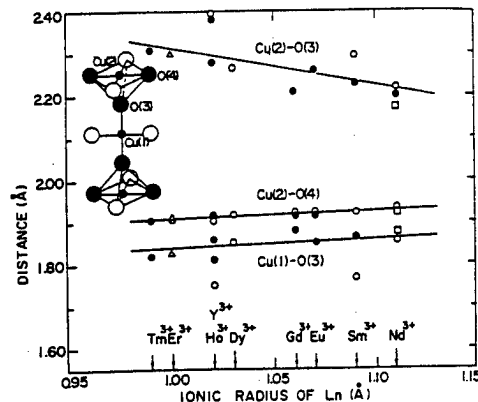


Fig.5 Cu-O bond length of  $\text{Ba}_2\text{LnCu}_3\text{O}_{7-\delta}$   
○; present data, ●;Asano et al.  
□; Takita et al, △;Ishigaki et al

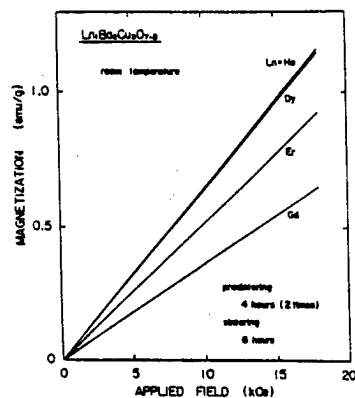


Fig.6 Magnetization curves of  $\text{Ba}_2\text{LnCu}_3\text{O}_{7-\delta}$  compounds.

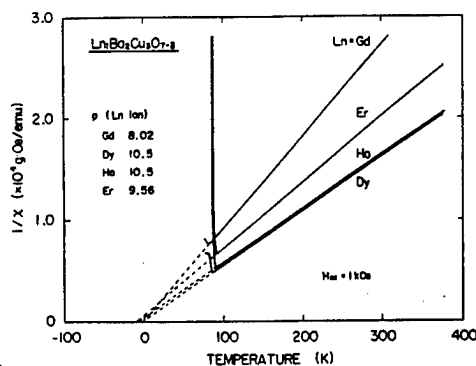


Fig.7 The reciprocal of magnetic susceptibility of  $\text{Ba}_2\text{LnCu}_3\text{O}_{7-\delta}$  compounds.

Table 1 Effective Bohr magneton of Ln in  $\text{Ba}_2\text{LnCu}_3\text{O}_{7-\delta}$  compounds  
 $\mu_{\text{eff}}(\text{e})$  and  $\mu_{\text{eff}}(\text{e})$ ; experimental  
 $\mu_{\text{eff}}(\text{t})$ ; theoretical.

	$\mu_{\text{eff}}(\text{e})$ ( $\mu_B$ )	$\mu_{\text{eff}}(\text{t})$ ( $\mu_B$ )	$\mu_{\text{eff}}(\text{e})$ ( $\mu_B$ )
Nd	3.48	—	3.82
Sm	1.97	—	0.84
Eu	3.77	3.50	—
Gd	8.03	8.02	7.94
Dy	10.50	10.50	10.63
Ho	10.58	10.50	10.63
Er	9.73	9.58	9.59

Cu-O bond length. Figure 4 shows the schematic picture of Cu-O bond. We consider the Cu(1)-O(3), Cu(2)-O(3) and Cu(2)-O(4) bond lengths, because these bond length should be important for valence value of Cu and hole concentration. Figure 5 shows the Cu-O bond length as a function of ionic radius of Ln. In this figure, the data of Asano et al. and Takita et al. are also shown. The Cu(2)-O(3) bond length decreased systematically with increasing atomic radius of Ln. However, Cu(2)-O(4) and Cu(1)-O(3) bond lengths increased slightly with increasing atomic radius of Ln.

Figure 6 shows the field dependence of the magnetization for  $\text{Ba}_2\text{LnCu}_3\text{O}_{7-\delta}$  compounds. The slope of magnetization curves was larger in order of Gd, Er, Dy and Ho. Figure 7 shows the reciprocal of magnetic susceptibility, as a function of temperature. From these data, the effective Bohr magneton for each Ln can be obtained. The value of thus obtained is listed in table 1. These results are in good agreement with  $\text{Ln}^{3+}$  free ion values calculated by van Vleck and Frank.

Figure 8 shows the  $T_c$ 's of  $\text{Ba}_2\text{LnCu}_3\text{O}_{7-\delta}$  compounds as the function of melting points. For BCS superconductor,  $T_c$  should depend on the density of state at Fermi level,  $N(0)$ . So, if these compounds behave like a BCS superconductor,  $T_c$  depend on the melting points. Because,  $N(0)$  values depend on melting points and increase with increasing the melting points. As shown in Fig. 8,  $T_c$ 's of  $\text{Ba}_2\text{LnCu}_3\text{O}_{7-\delta}$  compounds slightly increase with increasing the melting points. So it can be said that  $\text{Ba}_2\text{LnCu}_3\text{O}_{7-\delta}$  compounds behave like a BCS superconductor. Figure 9 shows a plot of  $T_c$ 's versus Cu(1)-O(3) bond length for Ba-Ln-Cu-O system. It is clear that  $T_c$ 's depend on the Cu(1)-O(3) bond length and have a maximum value around the bond length of 1.88 Å. Figure 10 shows a plot of  $T_c$ 's versus Cu(2)-O(4) bond length for Ba-Ln-Cu-O system and other oxide superconductors.  $T_c$ 's also depend on the bond length of Cu(2)-O(4) and increase with decreasing these values. It is interesting to note that the Cu(2)-O(4) bond length of high  $T_c$  oxide superconductor shows the value between that of CuO and  $\text{Cu}_2\text{O}$ . So it may be important to know the correlation between electrical properties, carrier concentration and Cu-O bond length of  $\text{CuO}_x$  ( $0.5 < x < 1.0$ ) compounds. These results will be soon carried out by us.

We have presented some results of our study on thermal, structural, magnetic and superconducting properties of  $\text{Ba}_2\text{LnCu}_3\text{O}_{7-\delta}$  compounds. It was found that  $T_c$ 's of these compounds depend on melting points and bond length of Cu(1)-O(3) and Cu(2)-O(4). However, it is not yet concluded which factor is essential on high  $T_c$  superconductivity.

#### References

- 1) W. Murphy, S. Sunshine, R. van Dover, J. Cava, B. Batlogg, M. Zahurak and F. Schneemeyer; Phys. Rev. Lett. 58 (1987) 1888
- 2) S. Ohshima and T. Wakiyama; Jpn. J. Appl. Phys. 27 (1988) 219
- 3) F. Miceli, M. Tarascon, H. Greene, P. Barboux, J. Rotella and D. Jorgensen; Phys. Rev. B 37 (1988) 5932
- 4) K. Takita, H. Katoh, H. Akinaga, M. Nishino, T. Ishigaki and H. Asano; Jpn. J. Appl. Phys. 27 (1988) L57.
- 5) H. Asano, K. Takita, H. Katoh, H. Akinaga, T. Ishigaki, M. Nishino, M. Imai and K. Masuda; Jpn. J. Appl. Phys. 26 (1987) L1410

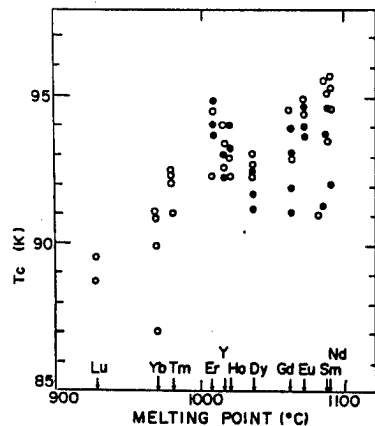


Fig. 8  $T_c$ 's of  $\text{Ba}_2\text{LnCu}_3\text{O}_{7-\delta}$  compounds as a function of melting points.

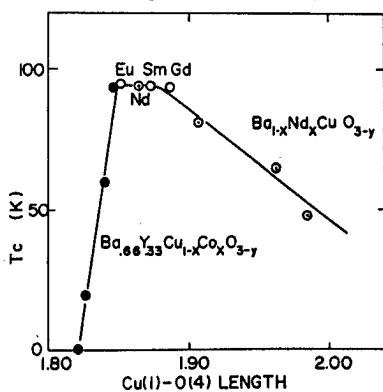


Fig. 9  $T_c$ 's of  $\text{Ba}_2\text{LnCu}_3\text{O}_{7-\delta}$  compounds as a function of Cu(1)-O(3) bond length. ○; present data, ●; Miceli et al, ◎; Takita et al.

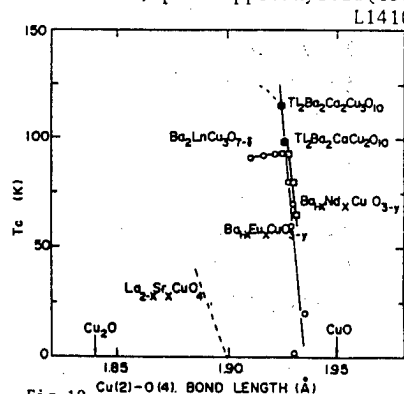


Fig. 10  $T_c$ 's of  $\text{Ba}_2\text{LnCu}_3\text{O}_{7-\delta}$  compounds as a function of Cu(2)-O(4) bond length. ○; present data, □; Takita et al, ●; Cox et al.

Critical Current Density and Its Hysteresis in Magnetic Field  
for Ba-Y-Cu-O Films Prepared by a Sputtering Technique

H. MORITA, K. WATANABE, Y. MURAKAMI, Y. KOYANAGI, K. NOTO, H. FUJIMORI and Y. MUTO

Institute for Materials Research, Tohoku University, Sendai 980, JAPAN

A considerably large transport critical current density  $J_c$  ( $1.2 \times 10^5$  A/cm<sup>2</sup> at 4.2 K and 15 T) was observed for the superconducting Ba-Y-Cu-O thin films prepared by an rf sputtering method. In association with such a large  $J_c$ , the hysteresis of  $J_c$  against applied magnetic field was smaller compared to bulk samples prepared by a solid phase reaction method. It was considered that a fairly smooth morphology of grain boundaries in the thin films improved superconducting properties.

We have previously pointed out<sup>1)</sup> that  $J_c$  of superconducting oxides shows a large hysteresis with cycles in applied field  $B$ , and this hysteresis can be observed even in high fields up to 25 T. Such a behavior is similar to the hysteresis observed in Nb and NbN thin films<sup>2)</sup>, but quite different from the so called history effect<sup>3)</sup>.

Recently, two models have been proposed for the explanation of the anomalous  $J_c$  vs.  $B$  hysteresis of the oxides. One stands on the microbridge model and attributes the hysteresis to internal screening currents of superconducting crystalline grains<sup>2,4)</sup>. The other model attributes the hysteresis to self-fields which arises from closed intragrain currents<sup>5,6)</sup>. For both models, the existence of weak links between grains play an important role, that is, the transport current is affected by the self-field or by the internal currents when it goes through the weakly linked part. From this point of view, we are interested in the recent experimental results that  $J_c$  values of Ba-Y-Cu-O thin films are remarkably large<sup>7,10)</sup>. If the above models are applicable to thin films, the hysteresis must be small and the crystalline grain morphologies must be different from those for the bulk samples.

We have, therefore, carried out the experimental investigation on the behavior of  $J_c$  vs.  $B$  hysteresis for Ba-Y-Cu-O thin films prepared by a rf sputtering technique, as well as the crystalline grain morphologies of these films.

Thin film samples of Ba-Y-Cu-O superconductors were prepared by an rf sputtering method. Sputtering for film growth was carried out in 50% Ar + 50% O<sub>2</sub> with total pressure of 3.5 mTorr. The discharge power was 70 W and the target-substrate distance was 55 mm. Films 500 nm thick were deposited on (100) SrTiO<sub>3</sub> substrates at 710 K. DC magnetic field was applied during the deposition parallel to the substrate and target surfaces. A post-deposition annealing at 1170 K for 1 h in oxygen flow followed by a slow cooling at a rate of 100 K/h was required for transformation from amorphous state to superconducting crystalline state. The bulk samples were prepared by a solid phase reaction method as described in previous paper<sup>1)</sup>.

Electrical resistance measurements were performed by a four-terminal method with a current density of 0.1 A/cm<sup>2</sup>. Critical current density  $J_c$  was measured by the same method with the criterion of about 5 V/cm. For  $J_c$  measurement, the films were cut

into a form of narrow bridge 1 mm wide and 2 mm long with current terminals 5 mm wide. The current and voltage terminals made of a low temperature solder were ultrasonically bonded to the film, and copper lead wires were soldered to these terminals with indium.

The relation between the  $J_c$ -B hysteresis and crystalline microstructure was investigated on the two characteristic film samples A and B which were deposited in a dc magnetic field of 10 and 30 Oe, respectively. Figure 1 shows the resistivity-temperature curves. The superconducting onset temperatures  $T_c^{\text{on}}$  and the zero resistivity temperatures  $T_c^{\text{off}}$  of the film samples are lower than those of the bulk sample.

Figure 2 shows the  $J_c$  vs. B curves at 4.2 K for all samples. In the case of the bulk sample,  $J_c$  drops sharply with increasing B and returns irreversibly with decreasing B, resulting in a  $J_c$  vs. B hysteresis. The magnitude of the hysteresis for the films is, however, smaller than the bulk sample. Particularly, the hysteresis of the film A is vanishingly small and the  $J_c$  shows a relatively small drop with B. In addition, it should be noted that the values of  $J_c$  for the film samples are about two order larger than that for the bulk sample. The reason for these results may be attributed to the improvement of the superconducting links around grain boundaries. To clarify this point, we have investigated the intergrain morphologies of these film and bulk samples.

Figures 3a, 3b and 3c show the SEM photographs. It is recognized that the bulk sample consists of many irregular crystalline grains and pores, while the thin films consist of rectangular grains connected smoothly each other. As seen in the film A and film B, the obscure traces of the grain boundaries and the elongated shapes of the pores seem to indicate a certain orientation of the crystal axes and a nearly complete crystallographical connection between grains. The x-ray diffraction experiments showed a preferred orientation of c-axis perpendicular to the film plane. Now, from the experimental results shown in Figs. 2 and 3, it can be said that the smaller the grain size and the better the crystallographical contact between grains, the larger the  $J_c$  and the smaller the  $J_c$  vs. B hysteresis could be. Although the theoretical investigation has not been completed yet, the above result reveals the important guide line for improving the  $J_c$  characteristics, that is, the crystallographically matched grain growth is necessary for obtaining a high  $J_c$  and a small hysteresis. Finally, a few comments should be made on the effect of magnetic field on crystalline growth. As seen in Figs. 3a and 3b, the application of magnetic field during sputtering gives rise to the regular alignment of the rectangular grains and to the grain growth. This effect is also noted as an important technique for preparing thin films with a high  $J_c$ .

The authors would like to thank the members of Cryogenic Center of Tohoku University and High Field Laboratory for Superconducting Materials for many assistances for the measurements of  $J_c$ . This work was supported by Grant-in-Aid for Scientific Research on Priority Areas "Mechanism of Superconductivity" from the Ministry of Education of Japan.

#### References

- 1) K. Noto, H. Morita, K. Watanabe, T. Murakami, Y. Koyanagi, I. Yoshii, I. Sato, H. Sugawara, N. Kobayashi, H. Fujimori and Y. Muto: Physica 148B (1987) p.239
- 2) T. Aomine and A. Yonekura: Phys. Lett. 114A (1986) p.16
- 3) H. Kupfer and W. Gey: Philos. Mag. 36 (1977) p.859

- 4) K. Watanabe, K. Noto, H. Morita, H. Fujimori, K. Mizuno, T. Aomine, B. Ni, T. Matsushita, K. Yamafuji and Y. Muto: submitted to Cryogenics (1988)
- 5) T. Matsushita, B. Ni, K. Yamafuji, K. Watanabe, K. Noto, H. Morita, H. Fujimori and Y. Muto: submitted to ISS'88 Nagoya
- 6) Evetts and B. A. Glowacki: Cryogenics 28 (1988) p.641
- 7) Y. Enomoto, T. Murakami, M. Suzuki and K. Moriwaki: Jpn. J. Appl. Phys. 26 (1987) p.L1248
- 8) S. Tanaka and H. Itozaki: Jpn. J. Appl. Phys. 27 (1988) L622
- 9) K. Watanabe, H. Yamane, H. Kurosawa, T. Hirai, N. Kobayashi, H. Iwasaki, K. Noto and Y. Muto: to be published in Appl. Phys. Lett. (1989)
- 10) J. S. Satchell, R.G. Humphreys, N.G. Chew, J.A. Edwards and M.J. Kane: Nature 334 (1988) p.331

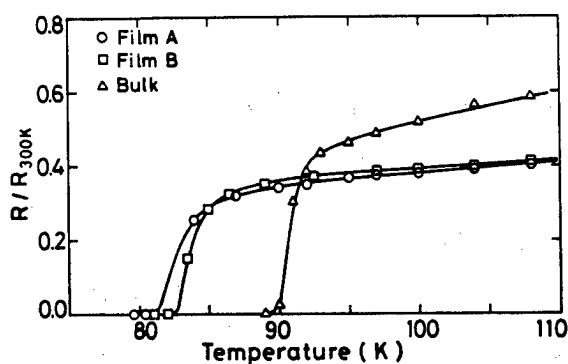


Figure 1 Temperature dependence of normalized resistance.

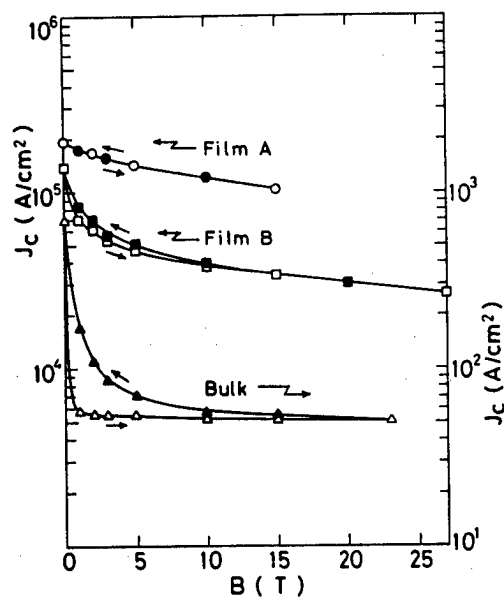
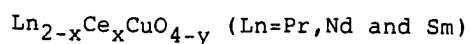


Figure 2 Magnetic field strength dependence of critical current density measured at 4.2 K.



Figure 3 Scanning electron microscope photographs.

Discovery of Electron-Doped Superconducting Cuprates:



Y. Tokura\*, H. Takagi\* and S. Uchida\*

\*Department of Physics and \*Engineering Research Institute,  
University of Tokyo, Bunkyo-ku, Tokyo 113, Japan

We have discovered that the Ce-doping and subsequent reducing procedures can give rise High  $T_c$  superconductivity with  $T_c$  up to 24K in the  $\text{Nd}_2\text{CuO}_4$ -type structure. In the new superconductors,  $\text{Ln}_{2-x}\text{Ce}_x\text{CuO}_{4-y}$  where Ln stands for Pr, Nd and Sm, the charge carriers are doped electrons, not holes, which was confirmed by the measurements of Hall coefficients as well as by the straightforward chemical analysis.

Since the discovery of high temperature superconductivity (High  $T_c$ ) in cuprate compounds by Bednorz and Müller [1], unprecedentedly extensive studies have been carried out to elucidate what is required for High  $T_c$ . There have been several families of High  $T_c$  cuprates so far discovered, all of which have a common feature: they possess the two-dimensional (2D) sheets of Cu-O pyramids or octahedra which are doped with holes. Here, we report the discovery of new electron-( not hole-)doped superconducting cuprates[2]. The new superconductors are  $\text{Ce}^{4+}$ -doped compounds,  $\text{Ln}_{2-x}\text{Ce}_x\text{CuO}_{4-y}$ , where Ln=Pr, Nd and Sm. The compounds have the  $\text{Nd}_2\text{CuO}_4$  structure [3], or the so-called T'-phase structure, as shown in Fig.1(a), which is composed of 2D sheets of Cu-O squares. This structure has no apical oxygen, in contrast to those of so far known superconducting single-layer cuprates; the T-phase structure with Cu-O octahedra (Fig.1(b)) as observed in  $\text{La}_{2-x}\text{Sr}_x\text{CuO}_4$  [1,3] (with  $T_c=40\text{K}$ ) and the T\*-phase structure with Cu-O pyramids (Fig.1(c)) in  $\text{Nd}_{2-x-z}\text{Ce}_x\text{Sr}_z\text{CuO}_4$  ( $T_c=30\text{K}$ )[4,5].

Materials were synthesized from mixture of rare-earth metal oxides ( $\text{CeO}_2$ ,  $\text{Pr}_6\text{O}_{11}$ ,  $\text{Nd}_2\text{O}_3$ ,  $\text{Sm}_2\text{O}_3$ ) and CuO. Mixed powder was first calcined at  $950^\circ\text{C}$  for 10 hours in air, then pressed into pellets, and finally sintered at  $1150^\circ\text{C}$  for 12 hours in air. The samples were quenched to room temperature in air. To produce superconductivity, procedures of annealing the Ce-doped samples under reducing condition were necessary. The samples were annealed at  $1000^\circ\text{C}$  for 10 hours in a stream of Ar/ $\text{O}_2$  gas mixture with the partial  $\text{O}_2$  pressure of  $10^{-4}\text{atm}$  and quenched to room temperature in the same atmosphere. Figure 2 shows the temperature-dependence of resistivity in  $\text{Nd}_{2-x}\text{Ce}_x\text{CuO}_{4-y}$ . Although the undoped compound  $\text{Nd}_2\text{CuO}_4$  is a typical semiconductor, the doping of  $\text{Ce}^{4+}$  ions makes the sample more conducting [5]. Remarkable decrease in resistivity was also observed in the undoped sample which was quenched from  $1150^\circ\text{C}$  in air down to room temperature to make the sample oxygen deficient ( $y\sim 0.04$ ). These observations clearly show that the doped  $\text{Ce}^{4+}$  ions and/or oxygen deficiencies

introduce mobile electrons into the compounds. According to the recent investigation [5], the T'-phase Nd-based cuprate cannot be doped with holes, whereas the T\*-phase compound  $\text{Nd}_{2-x-z}\text{Ce}_x\text{Sr}_z\text{CuO}_4$  (shown in Fig.1(c)) can be doped with holes, but not with electrons, like in the case of the T-phase structure (shown in Fig.1(b)).

Fairly low resistivity ( $<10^{-2}\text{ohmcm}$ ) in  $\text{Nd}_{2-x}\text{Ce}_x\text{CuO}_{4-y}$  was observed at the Ce-concentration of 0.15, where the sample shows semi-metallic, but not superconducting behavior. (As shown in Fig.2, the  $x=0.15$  sample shows a resistivity drop around 9K, which indicates superconductivity in tiny portion of the sample.) The bulk superconductivity in the same sample ( $x=0.15$ ) was achieved by the reducing procedure described above. The resistivity as well as the magnetization showed an onset of the superconductivity at around 24K. The concentration ( $q$ ) of introduced electrons per [Cu-O] unit, or the effective Cu valence ( $2-q$ ), was estimated by an iodometric titration technique [6], taking into consideration the reductive reaction of  $\text{Ce}^{4+}$  into  $\text{Ce}^{3+}$  during the titration process. The  $x=0.15$  sample shown in Fig.2 has the  $q$ -value of 0.20 before the reducing procedure, whereas after that the value of  $q$  in the superconducting sample is increased up to 0.28, which corresponds to the increased oxygen vacancies with  $y \sim 0.07$ . Therefore, the increase of electrons beyond a certain value of density ( $q > 0.20$ ) seems to give rise to electron-superconductivity.

Electron-type carriers in the new superconducting compound were also confirmed by measurements of the Hall coefficient. The sample  $\text{Nd}_{1.85}\text{Ce}_{0.15}\text{CuO}_{3.93}$  with  $T_c$  of 24K shows the negative Hall coefficient;  $R_H = -6.5 \times 10^{-4} \text{cm}^3/\text{C}$  at 300K and  $-2.3 \times 10^{-3} \text{cm}^3/\text{C}$  at 80K. This observation is in sharp contrast with the cases of other hole-superconducting cuprates so far known, in which positive Hall coefficients are always observed.

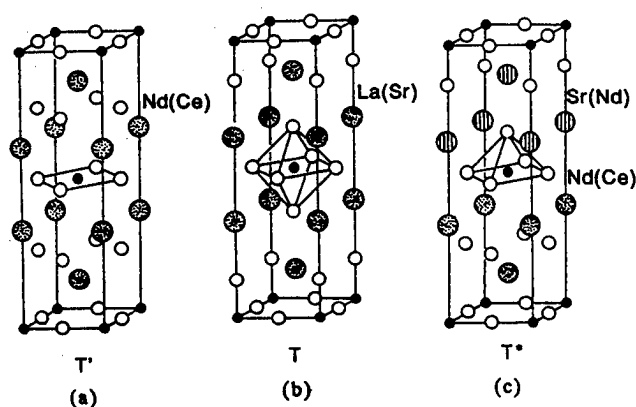


Fig.1

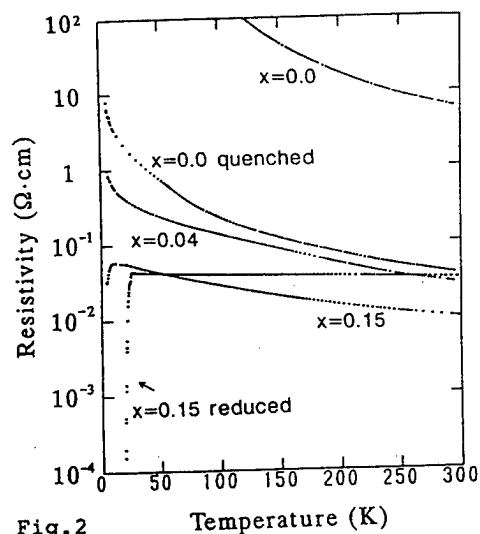


Fig.2

Fig.1: Crystal structures of (a)  $\text{Nd}_{2-x}\text{Ce}_x\text{CuO}_4$  (T'-phase), (b)  $\text{La}_{2-x}\text{Sr}_x\text{CuO}_4$  (T-phase) and (c)  $\text{Nd}_{2-x-z}\text{Ce}_x\text{Sr}_z\text{CuO}_4$  (T\*-phase).

Fig.2: Temperature-dependence of resistivity in  $\text{Nd}_{2-x}\text{Ce}_x\text{CuO}_{4-y}$ .



The X-ray diffraction pattern for this superconducting sample  $\text{Nd}_{1.85}\text{Ce}_{0.15}\text{CuO}_{3.93}$  is shown in Fig.3(a), in comparison with those of the hole-superconducting T-phase  $\text{La}_{1.85}\text{Sr}_{0.15}\text{CuO}_4$  (b) and  $\text{T}^*$ -phase  $\text{Nd}_{1.4}\text{Ce}_{0.2}\text{Sr}_{0.4}\text{CuO}_4$  (c) (see also Fig.1). The diffraction pattern (a) of  $\text{Nd}_{1.85}\text{Ce}_{0.15}\text{CuO}_{3.93}$  is essentially identical with that of the  $\text{T}'$ -phase Ce-undoped compound,  $\text{Nd}_2\text{CuO}_4$ , and all diffraction peaks discernible in the pattern (a) can be indexed with the lattice constants of the typical tetragonal  $\text{T}'$ -phase structure [3];  $a=3.95\text{\AA}$  and  $c=12.07\text{\AA}$  in the Ce-doped superconducting sample and  $a=3.93\text{\AA}$ ,  $c=12.11\text{\AA}$  in the Ce-undoped  $\text{T}'$ -phase compound. The  $\text{CuO}_4$  square in the  $\text{T}'$ -phase is appreciably expanded and its  $c$  axis is shrunk, as compared with the lattice parameters of the T- and  $\text{T}^*$ -phase structures associated with apical oxygens;  $a=3.78\text{\AA}$ ,  $c=13.2\text{\AA}$  in the T-phase (b) and  $a=3.85\text{\AA}$ ,  $c=12.5\text{\AA}$  in  $\text{T}^*$ -phase (c).

It should be emphasized that the electron-superconductivity is not restricted to the Nd-based compounds. Also in other  $\text{T}'$ -phase compounds of Pr- and Sm-based cuprates, the Ce-doping and subsequent reducing procedure, which are necessary for increasing the electron concentration beyond 0.20, could give rise to superconductivity of 20K-range. We show in Fig.4 the Meissner effects in three different samples,  $\text{Ln}_{1.85}\text{Ce}_{0.15}\text{CuO}_{4-y}$  ( $\text{Ln}=\text{Pr}, \text{Nd}$  and  $\text{Sm}$ ), which were measured by a SQUID magnetometer with applied field of 10 Oe (field-cooled). Substantial amount of Meissner signal was observed in a series of compounds. In particular, the large signal in  $\text{Nd}_{1.85}\text{Ce}_{0.15}\text{CuO}_{3.93}$  - more than 25% of the ideal value - guarantees the bulk nature of superconductivity with  $T_C=24\text{K}$ . The observed  $T_C$  is comparably high with those in the hole-superconducting single-layer cuprates;  $T_C=28\text{K}$  in the  $\text{T}^*$ -phase with Cu-O pyramids and  $T_C=40\text{K}$  in the T-phase with Cu-O octahedra.

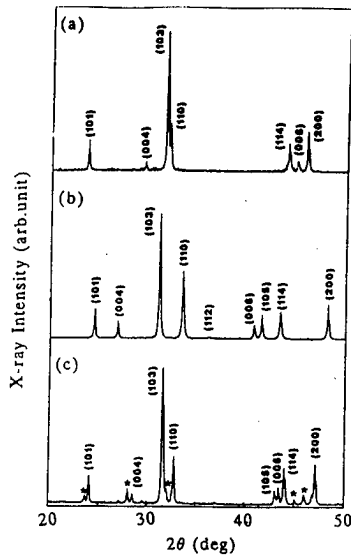


Fig.3

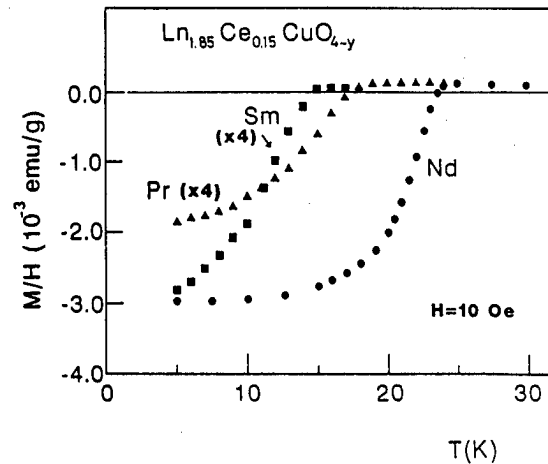


Fig.4

Fig.3: Powder X-ray diffraction patterns of (a)  $\text{Nd}_{1.85}\text{Ce}_{0.15}\text{CuO}_{4-y}$  ( $\text{T}'$ -phase), (b)  $\text{La}_{1.85}\text{Sr}_{0.15}\text{CuO}_4$  (T-phase) and (c)  $\text{Nd}_{1.4}\text{Ce}_{0.2}\text{Sr}_{0.4}\text{CuO}_{4-y}$  ( $\text{T}^*$ -phase). Asterisks (\*) indicate the peaks due to the secondary phase.

Fig.4: Meissner signals in  $\text{T}'$ -phase  $\text{Ln}_{2-x}\text{Ce}_x\text{CuO}_{4-y}$  ( $\text{Ln}=\text{Pr}, \text{Nd}$  and  $\text{Sm}$ ).

It is worth noting here that the compound  $\text{Pr}_{1.85}\text{Ce}_{0.15}\text{CuO}_{4-y}$  shown in Fig.4 is the first example of Pr-based cuprate superconductors. In hole-sustaining systems, the Pr-based cuprates, for example the  $T^*$ -phase compound  $\text{Pr}_{2-x-y}\text{Ce}_x\text{Sr}_z\text{CuO}_{4-y}$  [5], and the so-called 1-2-3 compound  $\text{PrB}_2\text{Cu}_3\text{O}_7$  [7], show neither metallic nor superconducting behavior. This has been attributed to the partial trapping of doped holes by Pr ions, or equivalently to the mixed valent nature of  $\text{Pr}^{+V}$  ions ( $3 < v < 4$ ). The appearance of superconductivity in  $\text{Pr}_{2-x}\text{Ce}_x\text{CuO}_{4-y}$  may be another evidence for the electron-nature of superconducting carriers in this  $T'$ -phase compound, because  $\text{Pr}^{3+}$  cannot be further reduced.

In conclusion, we demonstrate for the first time that electron-doping into  $\text{CuO}_2$  sheets with no apical oxygen gives rise to superconductivity with  $T_c$  up to 24K. We believe that this discovery provides a crucial test of theories for High  $T_c$  and hopefully gives a new important clue to the mystery of High  $T_c$ .

We would like to thank Messers H.Matsubara and H.Watabe for their assistance in experiments. This work was partly supported by a grant-in-aid for special distinguished research from the Ministry of Education, Science and Culture of Japan.

#### REFERENCES

- [1] Bednorz, J.G. and Müller, K.A. Z.Phys. B64, 189-194 (1986).
- [2] Tokura, Y., Takagi, H. and Uchida, S. Nature (Jan.26 1989).
- [3] Müller-Buschbaum, H. Angew.Chem.Int.Ed.Engl. 16, 674-687 (1977).
- [4] Sawa, H. et.al. Nature (in press).
- [5] Tokura, Y. et.al. submitted to Phys.Rev.B.
- [6] Nazzari, A.I. et.al. Physica, 153-156C, 1367-1368 (1988).
- [7] Kambe, S., Kishio, K., Ooba, N., Sugii, N., Kitazawa, K., and Fueki, K. Jpn.J.Appl.Phys.Suppl. 11-14 (1988).

# Superconductivity of the Nd-Ce-Sr-Cu-O system

E. Takayama-Muromachi

National Institute for Research in Inorganic Materials

1-1 Namiki, Tsukuba, Ibaraki, 305 Japan

The superconducting phase in the Nd-Ce-Sr-Cu-O system was isolated and identified. A single phase superconductor was obtained from the nominal composition  $(\text{Nd}_{0.66}\text{Ce}_{0.135}\text{Sr}_{0.205})_2\text{CuO}_y$ . From powder X-ray diffraction, electron diffraction and neutron diffraction studies, it was confirmed that the structure of the superconducting phase consists of alternative stacking of  $\text{K}_2\text{NiF}_4$ - and  $\text{T}'\text{-Nd}_2\text{CuO}_4$ -type slabs and Sr ions are concentrated in the former slabs.

Recently, a new class of superconductor was found in the Nd-Ce-Sr-Cu-O system by Akimitsu et al [1]. According to them, the superconducting phase may be described as  $(\text{Nd}_{1-x}\text{Sr}_x\text{Ce}_y)_2\text{CuO}_{4-8}$  and was suggested to have a  $\text{Nd}_2\text{CuO}_4$ - or  $\text{K}_2\text{NiF}_4$ -type structure. After their discovery, we succeeded to isolate and identify the superconducting phase and proposed a structure model which was closely related to but different from  $\text{Nd}_2\text{CuO}_4$ - or  $\text{K}_2\text{NiF}_4$ -type [2]. Neutron diffraction studies were performed and supported our structure model [3,4]. This report describes the crystal structure and the superconducting properties of the Nd-Ce-Sr-Cu oxide.

From the phase equilibrium study, it was found that at least three tetragonal phases exist in the system. The first one is a known compound,  $\text{T}'\text{-Nd}_2\text{CuO}_4$  while the second one is  $\text{Nd}_2\text{SrCu}_2\text{O}_y$  isostructural to  $\text{La}_2\text{SrCu}_2\text{O}_6$  [5]. The single phase of the third tetragonal phase (hereafter referred to as  $\text{T}''$  phase) was obtained from the nominal composition  $(\text{Nd}_{0.66}\text{Ce}_{0.135}\text{Sr}_{0.205})_2\text{CuO}_y$ . Figure 1 shows powder X-ray pattern of this phase. All peaks can be indexed by a tetragonal cell with  $a = 3.8558$  (1) and  $c = 12.487$  (1) Å. It was confirmed that this phase ( $\text{T}''$ -phase) is responsible for the superconductivity (see below).

From the composition, the lattice constants and the powder X-ray pattern, the structure of the  $\text{T}''$ -phase seems to be closely related to the  $\text{K}_2\text{NiF}_4$  or the  $\text{T}'\text{-Nd}_2\text{CuO}_4$  structure (referred simply as T- and  $\text{T}'$ -structure, respectively). Metal positions in these structures are identical and only oxygen positions are different [6]. Both belong to the space group  $\text{I4/mmm}$  and the reflections with  $h+k+l$  odd

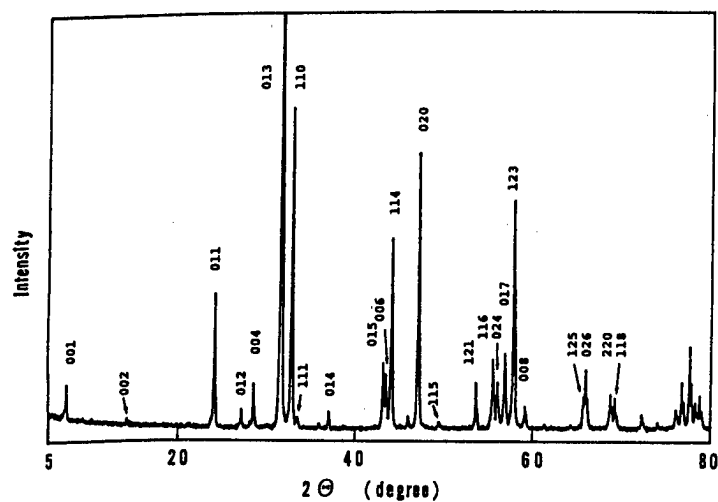


Fig.1. Powder X-ray Pattern of  $(\text{Nd}_{0.66}\text{Ce}_{0.135}\text{Sr}_{0.205})_2\text{CuO}_y$  with Cu  $K\alpha$  radiation.

Fig. 2. Lattice image of the  $T''$  phase projected along  $[100]$ . The dots indicated by A and A' correspond to Nd-Sr and Nd-Ce sites, respectively.

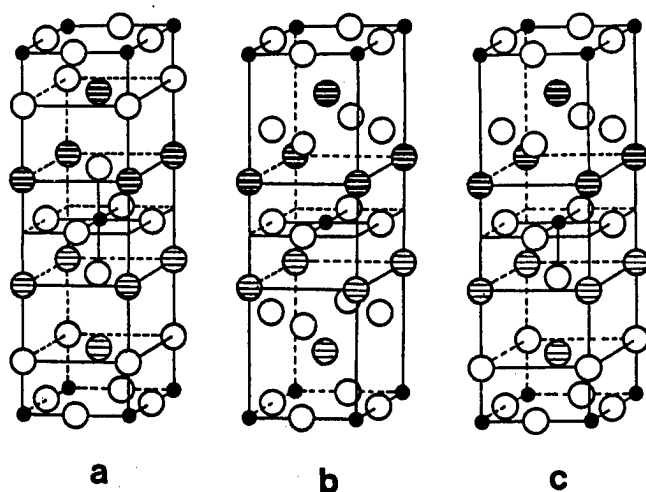
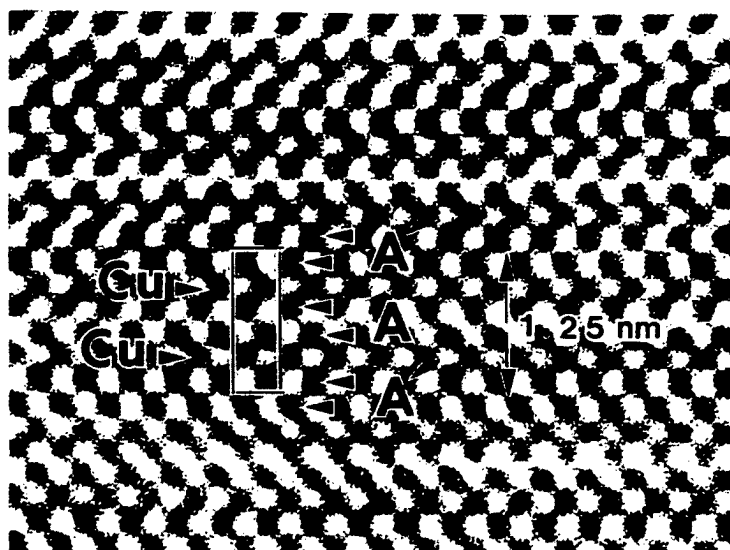


Fig. 3. Possible structure models for the  $T''$  phase; black circle : Cu site; white circle: O site; circle hatched with thin lines: Nd-Sr site; circle hatched with thick lines: Nd-Ce sites. Powder neutron studies supported the model (c).

should, therefore, be absent. In the powder X-ray pattern of the T'' phase, reflections with  $h+k+l$  odd are present, indicating that the T'' phase has a primitive lattice. These superlattice reflections are caused by ordering of cations.

Let us consider an oxide  $AA'BO_4$  with a  $K_2NiF_4$ -related structure. There are two possibilities in ordering of A and A' ions which cause the superlattice reflections, i.e., stacking sequence (along [001]) of cations is either -B-A-A-B-A'-A'- or -B-A-A'-B-A'-A-. The highest space group expected from the former is  $P4/nmm$  and  $hk0$  reflections with  $h+k$  odd being absent whereas that expected from the latter is  $P4/mmm$  without any systematic extinction. The electron diffraction patterns of the T'' phase indicated that the  $hk0$  reflections with  $h+k$  odd are systematically absent, supporting the former suggested sequence. This conclusion was confirmed by the high-resolution lattice image shown in Fig. 2. Double lines of stronger dark dots (marked A' in the image) as well as double lines of weaker dark dots (marked A) are apparent. Those pairs of lines are separated by a single line of dots corresponding to the Cu ions. The stronger dark dot indicate the metal sites occupied mainly by Nd(Ce) while weaker ones correspond to the Sr-concentrated sites. The cationic order in the T'' phase is, therefore, of the type -Cu-A-A-Cu-A'-A'- rather than -Cu-A-A'-Cu-A'-A-.

Three structure models including oxygen positions were proposed and discussed for the T'' phase; those are shown in Fig. 3. The first one is the T-type structure with the cationic order and the second one is the T'-type with the cationic order. The third one (Fig. 3(c)) consists of alternative stacking of the T- and T'-type slabs in which the Sr ions are concentrated in the former slabs and the Cu ion is coordinated by 5 oxygen ions pyramidally. The  $c/a$  ratio is a useful parameter in determining the structure type: T- or T'-type. For the Cu-containing T-type oxide,  $c/a$  is usually near 3.5 while that for the T'-type is much smaller (near 3.1). The  $c/a$  for the present T'' phase (3.24) lies between the values for the T- and T'-type structure, suggesting the last model in Fig. 3.

Powder neutron study was performed by Sawa et al. [3] to obtain definite conclusion and the results supported clearly the model (c). In their analysis, it was assumed that the Ce ions were distributed over both the T-type and T'-type slabs while Sr ions were completely concentrated in the former slab. Very recently, Izumi et al. re-examined the T'' phase by the neutron method and found that the Ce ions are concentrated in the T'-type slabs [4]. Therefore, the stacking of cations of the T''-phase can be represented as -Cu-(Nd,Sr)-(Nd,Sr)-Cu-(Nd,Ce)-(Nd,Ce)-. One point to be made here is the presence of the oxygen defects at the apex-oxygen site of  $CuO_5$

pyramid. Both neutron analysis insisted about 7% of oxygen deficiency at this site.

In Fig. 4, a-dimensions of various T'- and T-type  $A_2CuO_4$  oxides are plotted against ionic radii of A-site cations in 8-fold coordination. In the T' structure, a-dimension increases with larger A-site cation. When the A-site cation is larger than Pr, however, the T-type structure becomes more stable than the T'-type, i.e., there is a border in the size of the A-site cation which governs the structure type, T-type or T'-type. This fact suggests that the size of cation in the T'-type slab should be smaller while that in the T-type slab should be larger than the borderline value to construct the T''-type structure. Indeed, the ionic radius calculated for the mixed ion ( $Nd^{3+}_{0.73}Ce^{4+}_{0.27}$ ) which occupies the T'-type slab is smaller than the borderline value (marked by Nd-Ce in Fig. 4). On the contrary, that for the mixed ion ( $Nd^{3+}_{0.59}Sr^{2+}_{0.41}$ ) in the T-type slab is larger than it (marked by Nd-Sr). The "ideal" a-dimension for the T'-type slab, as expected from Fig. 4, approaches to the experimental a-dimension of the T'' phase by doping smaller Ce ion, which would work to diminish the size mismatch between the T'- and the T-type slab.

Figure 5 shows ac susceptibility data for some typical samples which contain the T'' phase as a major component. The  $T_c$  is very sensitive to the Nd/Ce (or Sr/Ce) ratio. The sample  $(Nd_{0.64}Ce_{0.155}Sr_{0.205})_2CuO_y$  was not superconducting at least above 4.2 K and  $T_c$  of  $(Nd_{0.65}Ce_{0.145}Sr_{0.205})_2CuO_y$  is much lower than that of  $(Nd_{0.66}Ce_{0.135}Sr_{0.205})_2CuO_y$ . It should be also noted that that superconductivity is affected by oxygen deficiency. Thermogravimetric analysis in  $O_2$  atmosphere indicated that the weight loss is very small even at 1100° C, only about 0.13 % which corresponds to  $\Delta y \sim 0.025$  in  $(Nd_{0.66}Ce_{0.135}Sr_{0.205})_2CuO_{y(max)-\Delta y}$  here  $y(max)$ , the maximum oxygen content in 1 atm  $O_2$  is close to 4. Figure 6 shows ac susceptibility data for samples quenched into liquid  $N_2$  after being equilibrated in air or in  $O_2$  at various temperatures. The sample quenched from 700° C does not indicated superconductivity above 4.2 K. In Fig. 7,  $T_c$  is plotted against the content of oxygen defects,  $\Delta y$ . The dependence of  $T_c$  on the oxygen deficiency is far more pronounced in the T'' phase than in the  $YBa_2Cu_3O_y$  system. There are two possibilities to explain this; (1) the effective hole concentration is small in the T'' phase even when it is well-oxidized and oxygen defects affect the carrier concentration substantially; (2) the apex oxygen ion in the  $CuO_5$  pyramid, which is believed to be deficient, plays some important roles in the superconductivity. Further work should be needed to decide which is the case.

This paper is based on the collaborations with Drs. Y. Matsui, Y. Uchida, F.

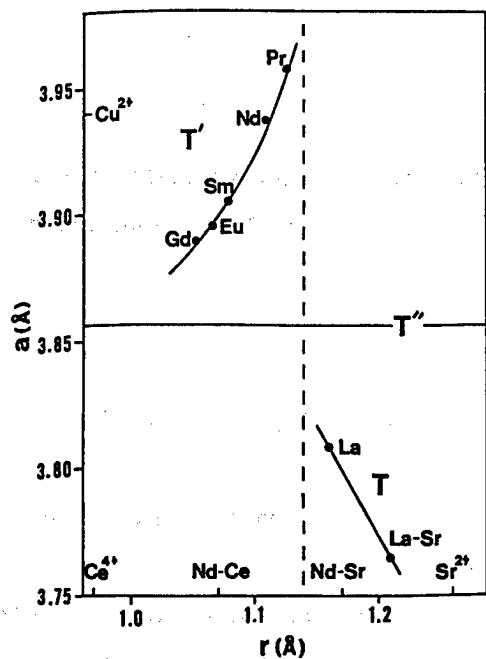


Fig. 4. Relation between a-dimensions and the ionic radii of A cations in  $A_2CuO_4$  oxides having the T- and T'-type structure.

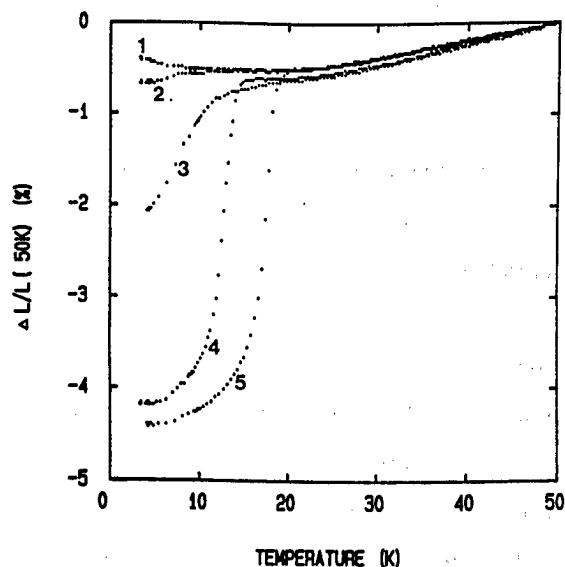


Fig. 5. AC susceptibility data. 1:  $(Nd_{0.64}Ce_{0.155}Sr_{0.205})_2CuO_y$ ; 2 and 3:  $(Nd_{0.65}Ce_{0.145}Sr_{0.205})_2CuO_y$  unannealed and annealed in  $O_2$ , respectively; 4 and 5:  $(Nd_{0.66}Ce_{0.135}Sr_{0.205})_2CuO_y$  unannealed and annealed in  $O_2$ , respectively.

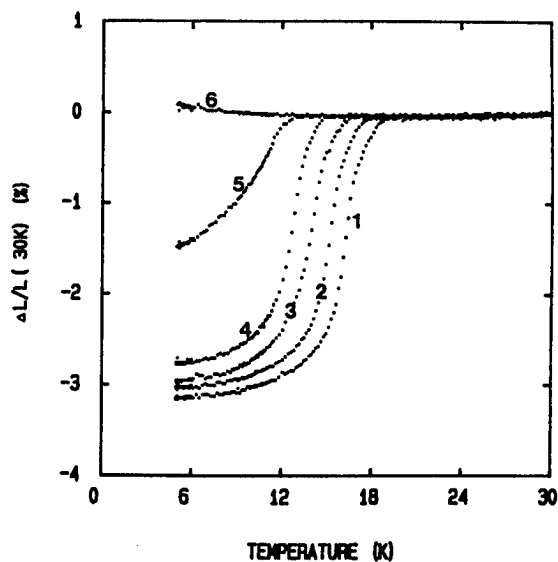


Fig. 6. AC susceptibility data for  $(Nd_{0.66}Ce_{0.135}Sr_{0.205})_2CuO_y$  quenched after being equilibrated at various temperatures in air or in  $O_2$ . 1: 400° C in  $O_2$ ; 2: 400° C in air; 3: 500° C in  $O_2$ ; 4: 500° C in air; 6: 600° C in  $O_2$ ; 7: 700° C in  $O_2$ .

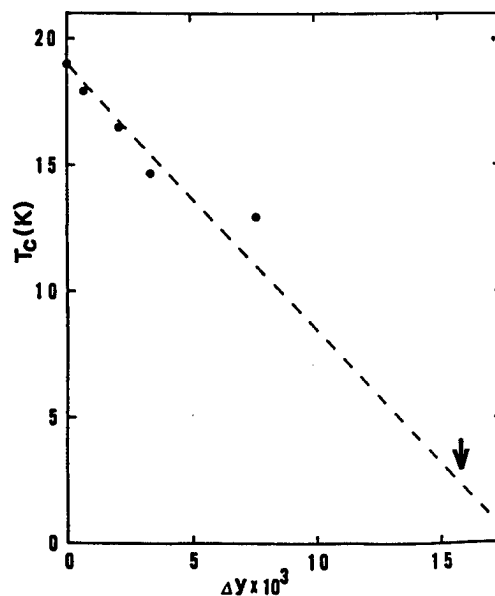


Fig. 7. Suppression of  $T_c$  in  $(Nd_{0.66}Ce_{0.135}Sr_{0.205})_2CuO_y$  by oxygen deficiency,  $\Delta y$ .

Izumi, M. Onoda and K. kato of NIRIM , Prof. J. Akimitsu of Aoyama-Gakuin Univ., Prof. H. Asano of Univ. of Tsukuba, Prof. S. Uchida of Univ. of Tokyo, and their coworkers.

#### References

- [1] J. Akimitsu, S. Suzuki, M. Watanabe and H. Sawa, Jpn. J. Appl. Phys. **27**, L1859 (1988).
- [2] E. Takayama-Muromachi, Y. Matsui, Y. Uchida, F. Izumi, M. Onoda and K. kato, Jpn. J. Appl. Phys. **27**, L2283 (1988).
- [3] H. Sawa, S. Suzuki, M. Watanabe, J. Akimitsu, H. Matsubara, H. Watabe, S. Uchida, K. Kokusho, H. Asano, F. Izumi and E. Takayama-Muromachi, Nature (in press).
- [4] F. Izumi and E. Takayama-Muromachi, A. Fujimori, T. Kamiyama, H. Asano and J. Akimitsu, to be published.
- [5] K. Takahashi, B. Okai, M. Kosuge, M. Ohta, Jpn. J. Appl. Phys. **27**, L1374 (1988).
- [6] Hk. Muller-Buschbaum and W. Wollschlager, Z. Anorg. Allg. Chem. **414**, 76 (1975).



**New Preparations of  $\text{YBa}_2\text{Cu}_3\text{O}_y$  and  $\text{YBa}_2(\text{Cu}_{1-x}\text{Fe}_x)_3\text{O}_y$  by  
utilizing high Purity inert Gases ( $\text{N}_2$ , Ar)**

K. Kosuge, Y. Ueda and S. Katuyama

Department of Chemistry, Faculty of Science, Kyoto University, Kyoto 606, Japan

$\text{YBa}_2\text{Cu}_3\text{O}_y$  (YBCO) with large variation of oxygen content  $y$  ( $6.0 < y < 6.92$ ) was prepared by reduction of fully oxidized YBCO ( $y=6.92$ ) under flowing high purity inert gases. The samples thus prepared could be regarded to be perfect ordered in the  $\text{Cu1-O}$  planes, judging from the composition ( $y$ ) dependence of the lattice parameters. The orthorhombic  $\text{YBa}_2(\text{Cu}_{1-x}\text{Fe}_x)_3\text{O}_y$  was stabilized in the composition range  $0 < x < 0.15$  by heat-treatment under high purity  $\text{N}_2$  gas followed by oxidation at low temperature.

By utilizing high purity inert gases such as  $\text{N}_2$  and Ar, we could prepare  $\text{YBa}_2\text{Cu}_3\text{O}_y$  with  $6.00 < y < 6.92$  in quasi-chemical equilibrium state and also prepare the orthorhombic  $\text{YBa}_2(\text{Cu}_{1-x}\text{Fe}_x)_3\text{O}_y$  with wider Fe concentration ranging  $0 < x < 0.15$ . We describe here the method of sample preparation of these substances, and also the chemical and physical properties of thus prepared samples, briefly.

**(1)  $\text{YBa}_2\text{Cu}_3\text{O}_y$  [4]-[12]**

It has been well established that YBCO belongs to a non-stoichiometric compound. The oxygen content  $y$  can be controlled both by temperature ( $T$ ) and oxygen partial pressure ( $\text{Po}_2$ ). Kishio et al. [1] reported the relation among  $y$ ,  $T$  and  $\text{Po}_2$ , which is very useful to obtain the YBCO samples in chemical equilibrium state. However, the popular method [2] for getting YBCO with various content of oxygen is the quenching method, i.e. quenching from various temperature at constant  $\text{Po}_2$  (0.21 atm in air or 1.0 atm). On the other hand Cava et al. [3] obtained the samples by the sample with high oxygen content by utilizing getter element such as Zr.

We have developed a new method for preparation of YBCO with various content of oxygen by utilizing high purity inert gases [5],[8]. The starting compound  $\text{YBa}_2\text{Cu}_3\text{O}_y$  was prepared by the usual ceramic method. Small disc sample of 8mm diameter and about 1mm thickness was precisely weighed, and was firstly heated in air at the rate of 10 C/min in a thermogravimetric microbalance up to 800 C and then cooled at the same rate to room temperature. In this run, the thermogravimetric analysis (TGA) traces always show a distinct change in curvature at 650 C, corresponding to the orthorhombic to tetragonal phase transition [4],[10]. Subsequently, it was heated under flowing high purity inert gas at the rate of 10 C/min up to the temperature ranging from 400-700 C, depending on the aimed values of  $y$ , and then cooled slowly at the rate of 2.5 C/min to room temperature. Figure 1 shows a typical example of TGA trace for the treatment. Oxygen content of the samples thus heat-treated was in-situ determined by measuring the weight loss at room temperature. We took the distinct change on the TGA traces at 650 C in air as a standard point of the oxygen content ( $y=6.50$ ). We could

get the samples having the composition  $6.00 < y < 6.92$ . This method is very simple, but has the following distinguishing characteristics :

- [1] the sample is prepared in quasi-chemical equilibrium state
- [2] the oxygen content is in-situ controlled by utilizing thermobalance

Figure 2 shows the  $y$  vs lattice parameters for the samples thus prepared by use of  $N_2$  gas. These curves are significantly different from those of the quenched samples. The characteristic features are as follows :

- (1) The  $a$ - and  $c$ -axes linearly increase, and the  $b$ -axis decreases, with decreasing  $y$ . The coefficient of expansion of the  $a$ -axis with oxygen loss is nearly equal to that of the  $c$ -axis.
- (2) The orthorhombic phase extends to about  $y=6.2$ , below which the samples show the tetragonal structure.

These samples have been studied from the chemical and physical point of view [5],[7]-[9],[11]. We show here the result of complex susceptibility vs temperature curves [12]. Figure 3 shows the complex susceptibility on the samples with various oxygen content, WHICH suggests a possible existence of a lower  $T_C$  phase with vacancy-ordered structure in the  $Cu1-O$  planes. We are now investigating the crystal structure originated from the vacancy-order by use of electron microscope.

## (2) $YBa_2(Cu_{1-x}Fe_x)_3O_y$ [13]-[17]

In order to search for the origin of superconductivity of YBCO, there have been published many papers on the substitution for Cu with 3d elements such as Fe, Co, Ni etc.. By utilizing high purity inert gases, we could also prepare the orthorhombic  $YBa_2(Cu_{1-x}Fe_x)_3O_y$  in the wider composition range of  $x$ . Figure.4 shows the flow chart of heat treatment for sample preparation. Figure 5 shows the  $(x)$  dependence of the lattice parameters of the samples thus prepared (Step 1-2-3), together with those of the samples Step 1 and 1-2. Mossbauer experiment has been done to get information of the distribution of Fe in  $Cu1-O$  plane and also between  $Cu1-O$  and  $Cu2-O$  planes.

Figure 1

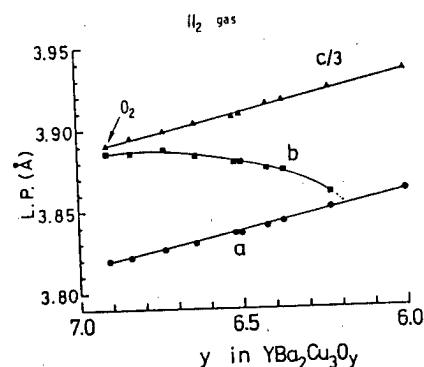


Figure 2

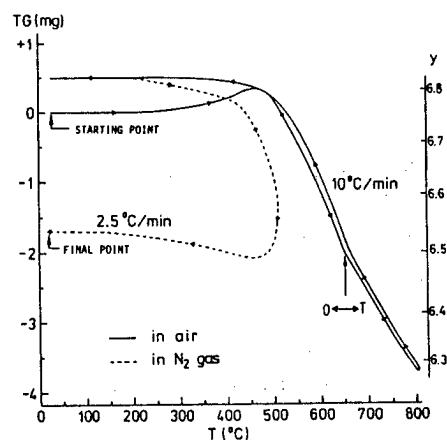


Figure 3

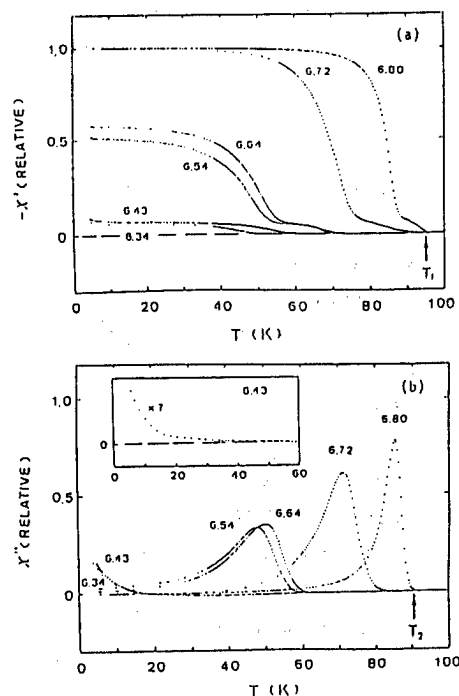


Figure 4

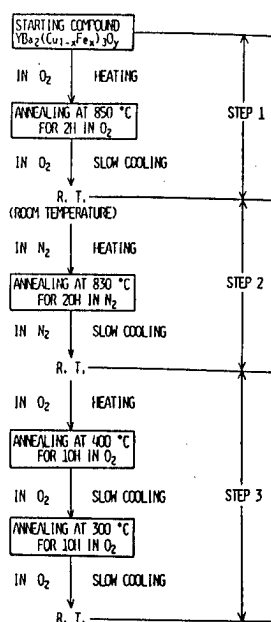
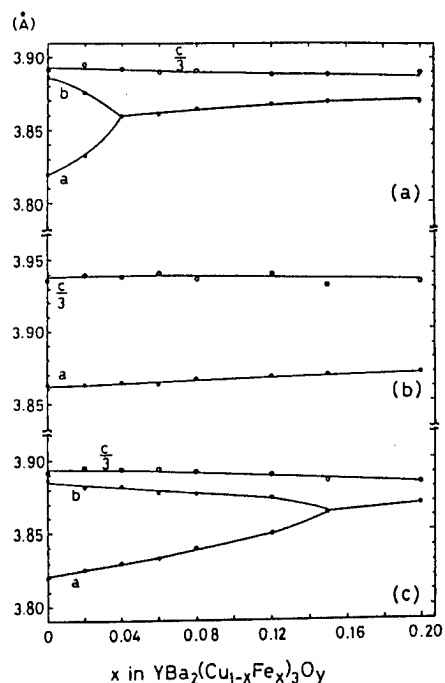


Figure 5



#### References

- [1] K.Kishio, J.Shimoyama, T.Hasegawa, K.Kitazawa and K.Fueki ; Jap. J. Appl. Phys. 26 (1987) L1228
- [2] M.Tokumoto, H.Ihara, T.Matsubara, M.Hirabayashi, N.Terada, H.Oyanagi, K.Murata and Y.Kimura ; Jap. J. Appl. Phys. 26 (1987) L1565
- [3] R.J.Cava, B.Batlog, C.H.Chen, E.A.Rietman, S.M.Zahurk and D.Werder ; Nature 329 (1987) 423
- [4] Y.Ueda, N.Kojima, M.Yoshikawa, H.Toda, A.Mitushima and K.Kosuge ; JSPM(Huntai oyobi Hunmatuyakin) 34 (1987) 636 (in Japanese)
- [5] Y.Ueda and K.Kosuge ; JSPM(Huntai oyobi Hunmatuyakin) 35 (1988) 437 (in Japanese)
- [6] H.Toda, Y.Ueda and K.Kosuge ; JSPM(Huntai oyobi Hunmatuyakin) 35 (1988) 442(in Japanese)
- [7] T.Imai, T.Shimizu, H.Yasuoka, Y.Ueda and K.Kosuge ; J. Phys. Soc. Japan 57 (1988) 2280
- [8] Y.Ueda and K.Kosuge ; Physica C 156 (1988) 281
- [9] H.Yasuoka, T.Shimizu, Y.Ueda and K.Kosuge ; J. Phys. Soc. Japan 57 (1988) 2659
- [10] Y.Ueda, A.Mitushima, H.Toda, N.Kojima, M.Yoshikawa and K.Kosuge ; Mat. Res. Bull. 23 (1988) 1409
- [11] H.Yasuoka, T.Shimizu, T.Imai, S.Sasaki, Y.Ueda and K.Kosuge ; to be published in Hyperfine Interactions
- [12] H.Toda, Y.Ueda and K.Kosuge ; to be published in JSPM(Huntai oyobi Hunmatuyakin) 36 (1989)(in Japanese)
- [13] H.Mazaki, Y.Ueda, Y.Aihara, T.Kubozoe and K.Kosuge ; to be published in Jap. J. Appl. Phys.
- [14] S.Katuyama, Y.Ueda and K.Kosuge ; to be published in JSPM(Huntai oyobi Hunmatuyakin) 36 (1989)(in Japanese)
- [15] Y.Ueda, S.Katuyama and K.Kosuge ; to be published in JSPM(Huntai oyobi Hunmatuyakin) 36 (1989)(in Japanese)
- [16] S.Katuyama, Y.Ueda and K.Kosuge ; to be published in Mat. Res. Bull.
- [17] S.Katuyama, Y.Ueda and K.Kosuge ; in preparation

Synthesis and Superconducting Properties of High  $T_c$  Complex Copper Oxides  
with Double and Single Thallium Layers

M. Kikuchi, S. Nakajima\*, T. Kajitani, T. Suzuki\*\*,  
N. Kobayashi, H. Iwasaki and Y. Syono

Institute for Materials Research, Tohoku University, Katahira, Sendai 980, Japan

\*Hachioji Research Center, CASIO, Hachioji 192, Japan

\*\*Steel Research Center, Nippon Kokan (NKK), Kawasaki 210, Japan

High  $T_c$  superconductors of  $Tl_2Ba_2Ca_{n-1}Cu_nO_{2n+4}$  ( $n=1\sim3$ ) and  $TlBa_2Ca_{n-1}Cu_nO_{2n+3}$  ( $n=2\sim5$ ) were synthesized, and their structures, chemical compositions and superconducting properties were studied by means of X-ray powder diffraction, electron probe microanalysis, transmission electron microscopy, and electrical and magnetic measurements. Superconducting critical temperatures are discussed in terms of the number of Cu layers and Cu-O bond length within the plane, and average Cu valence.

## 1. Introduction

Discovery of new superconducting oxides of Bi and Tl systems with  $T_c$  higher than 100 K<sup>1, 2)</sup> has increased expectation for the existence of other potential superconducting materials with different structures. The Bi and Tl systems have peculiar  $Bi_2O_2$  and  $Tl_2O_2$  (or  $TlO$ ) layers due to the increased covalency of Bi and Tl ions, in contrast to the previously found La series with the  $K_2NiF_4$  type structure and the Y series with the oxygen defective tripled perovskite structure, although the interposed layers of perovskite units consisting of alkaline earth metal-copper oxides are common to these high  $T_c$  oxides. In both systems, marked increase in  $T_c$  above 100 K is achieved by addition of Ca layers in which oxygen atoms are completely missing, thereby resulting in formation of Cu-O square pyramidal layers. However, there are several discrepancies between these systems. Remarkable contrast lies in that Bi ions are combined with only Sr ions in these layered systems, while Tl ions are mostly with Ba ions. Accordingly cation ordering is more complete in the Tl system for Ba and Ca combination with larger difference in ionic radii, while less complete in the Bi system for Sr and Ca combination. This situation leads to easier formation of the Tl double layered system close to the ideal composition of  $Tl_2Ba_2Ca_{n-1}Cu_nO_{2n+4}$  ( $n=1, 2$  and  $3$ )<sup>3-9)</sup>, than the more complex Bi double layered system. Furthermore, in accordance with the less covalent Tl ions, even a single Tl layer compounds of  $TlBa_2Ca_{n-1}Cu_nO_{2n+3}$  have also been synthesized which has not been known for the Bi system.

In the present work, both double and single layered compounds of the Tl system were synthesized, and examined by X-ray powder diffraction (XPD), electron probe microanalysis (EPMA), transmission electron microscopy (TEM), besides electrical and magnetic measurements for superconducting properties. Relevance of the superconducting properties to the crystal structures and chemical compositions is discussed, and special attention is paid to the origin of hole carriers responsible for high  $T_c$  superconductivity.

## 2. Experimental

Starting materials were mixture of  $Tl_2O_3$ ,  $CaO$ ,  $BaO$ ,  $CuO$ , and/or  $BaCuO_2$ . To facilitate the reaction with volatile and low melting  $Tl_2O_3$ , no carbonates which have relatively high decomposition temperatures were used. The mixture was pressed into a pellet of 10 mm diameter and 1 mm thickness, and fired at around 900°C for several minutes for double Tl layer compounds; Longer time annealing was needed to obtain single Tl layer compounds. To avoid hazardous due to toxicity of Tl, handling of powder materials was made in a glove box and heat treatment was done in a cold-trap equipped silica glass tube, in which oxygen gas was flowed at a rate of 120-150 ml/min, as shown in Fig. 1. The pellet was wrapped in a gold foil to prevent the reaction with the silica tube. Typical preparation conditions were summarized in Table 1.

Chemical composition of the sintered specimen was determined by EPMA at NKK. The diameter of the electron beam is about 3  $\mu m$ . Metallic Tl, Ba and Cu and  $CaSiO_3$  were used as standard materials.

X-ray diffraction analysis was carried out using  $CuK\alpha$  radiation. Rietveld analysis of XPD was made by using RIETAN program [10]. Oxygen parameters were fixed at those determined by du Pont group [3, 4] for single crystals, and only atomic parameters for cations were refined. No constraint was imposed on relative amount of Tl and Ca. However, no cation vacancy was taken into consideration.

Electrical resistivity measurements were done by a four probe method with a measuring current of 1 mA. Magnetization measurements were made with a vibration sample magnetometer.

## 3. Results

### 3.1 Double Tl Layer Compounds

Three kinds of compounds with different number of Cu layers ( $n=1\sim 3$ ) were successfully synthesized [7, 11, 12]. XPD patterns (Fig. 2) were almost completely indexed with tetragonal indices, indicating nearly single phase materials. Unit cell dimensions determined by least squares method

from the observed d-spacings were summarized in Table 2. Gradual contraction of a-dimension, besides increase in c-dimension, due to increasing number of Cu layers was to be noted. High resolution electron microscopy [11] confirmed the crystal structure

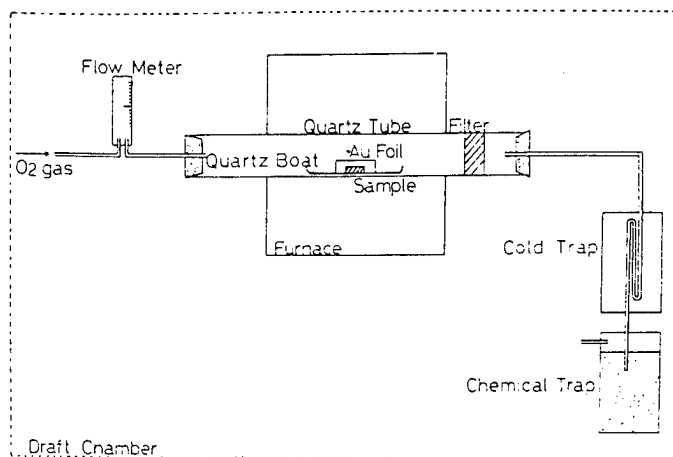


Fig. 1 Schema of reaction chamber

Table I Preparation Condition

Starting Composition	Heating Temp. (°C)	Heating Time (min)	Products
2201	890	15	2201
2212	890-910	7-30	2212
2223	910	7	2223
2212	890	600	1212
2223	890	240	1223
			1234
2223	890	360	1234
			1245
2223	890	600	1245
			1256 (EM)
			1267 (EM)
			1278 (EM)
			1289 (EM)
			12910 (EM)

EM : Identified by electron microscopy only.

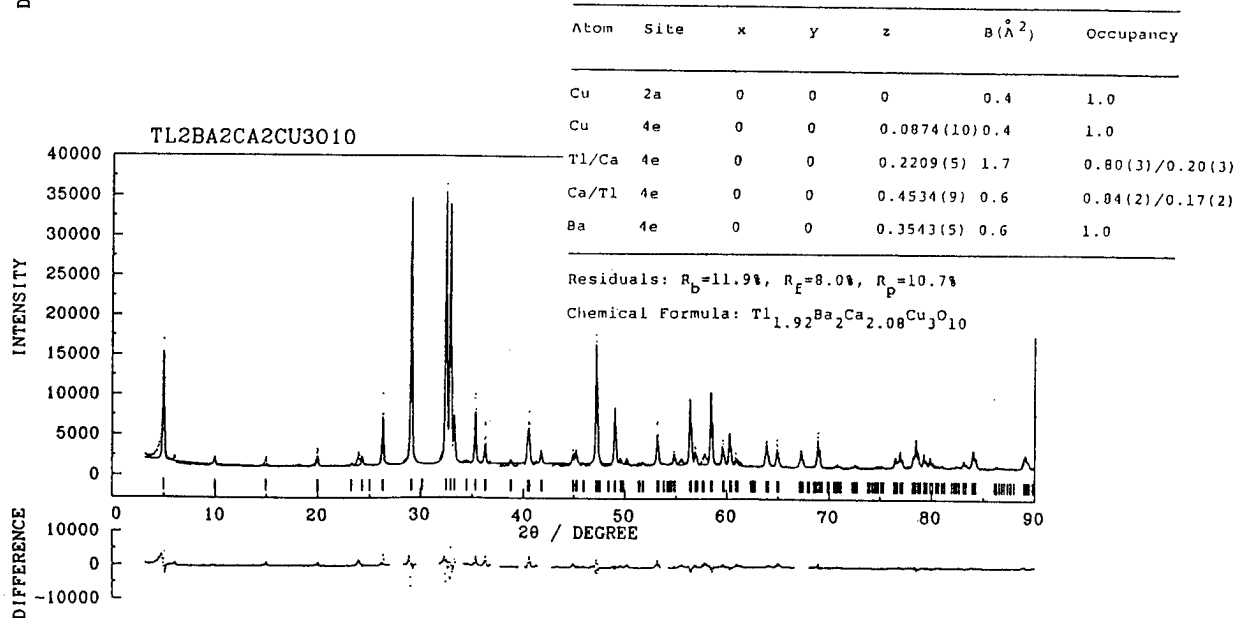
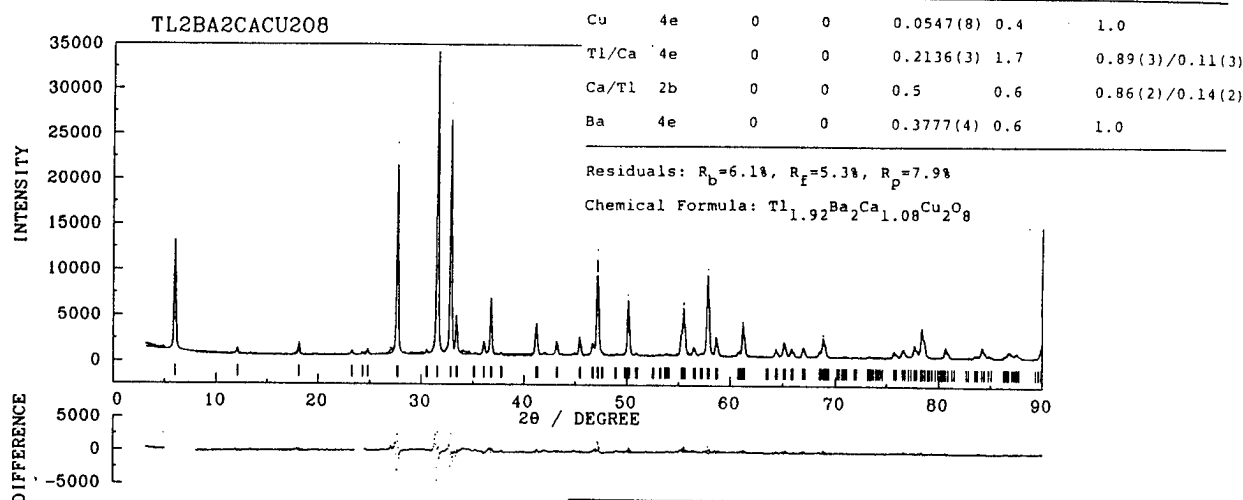
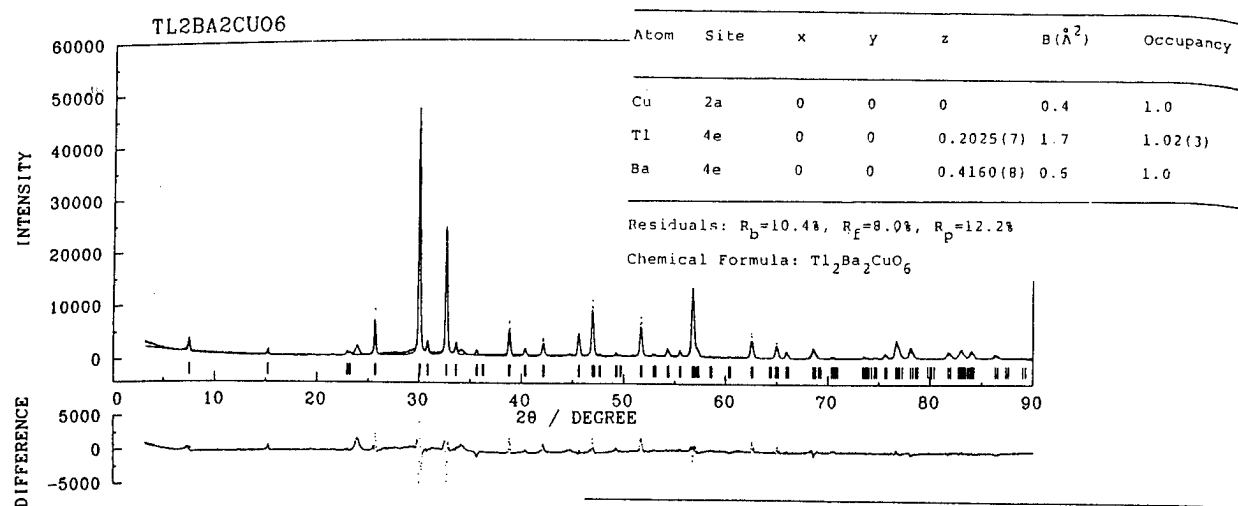


Fig. 2 Rietveld refinement profile of XPD patterns (Cu K $\alpha$ ) of double Tl layer oxides, 2201 (top), 2212 (middle) and 2223 (bottom).

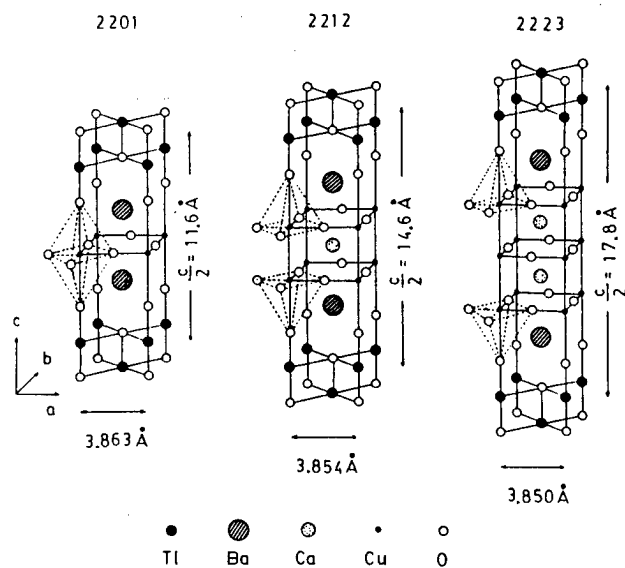


Table 2  
Summary of Unit Cell Parameters and  $T_c$

phase	a (Å)	c (Å)	T <sub>c</sub> (K)	
			end point	onset
2201	3.860	23.1	0	0
2212	3.855	29.2	98	114
2223	3.852	35.6	114	122
2234	3.853	41.9	108	114
1201	-	-	-	-
1212	3.850	12.7	-	70
1223	3.849	15.9	-	107
1234	3.844	19.1	-	122
1245	-	22(EM)	-	101
1256	-	25(EM)	-	-
1267	-	28(EM)	-	-
1278	-	31(EM)	-	-
1289	-	34(EM)	-	-

EM : electron microscopy

Fig. 3 Crystal structures of (a) double Tl layer (top) and (b) single Tl layer compounds (right). Numerals above each figure are the metal ratio with the order of Tl, Ba, Ca and Cu.

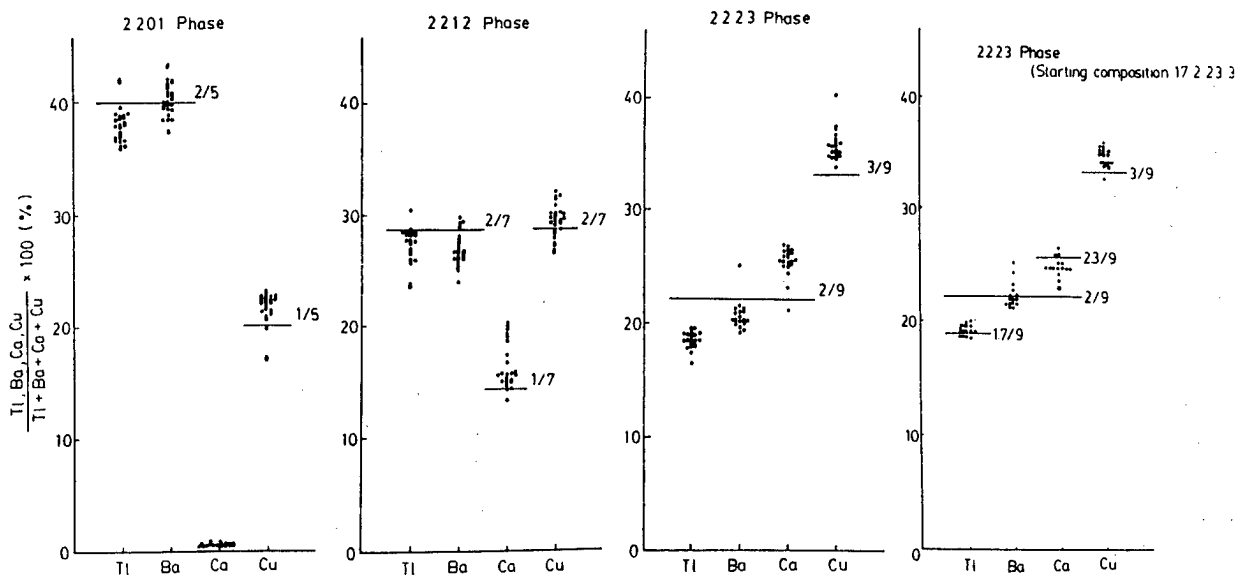
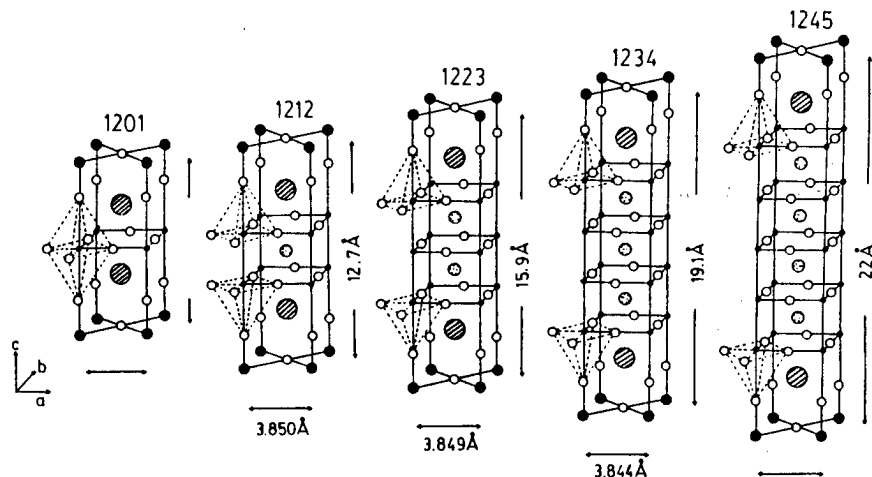


Fig. 4 EPMA results of double Tl layer compounds. Fraction shows the ideal ratio.

model proposed by du Pont group on the basis of single crystal X-ray analysis [3, 4], as shown in Fig. 3(a). Results of Rietveld refinement of measured XPD patterns were summarized in Fig. 2 [12]. Cation parameters determined were generally in good agreement with those by single crystal X-ray analysis. Partial substitution of Tl with Ca, and of Ca with Tl in a less degree, considerably reduced R factors, resulting in deficiency in Tl and enrichment in Ca as a whole.

This tendency was more enhanced with increasing number of Cu layers as confirmed by EPMA (Fig. 4). Interestingly, if the starting composition was chosen to be 1.7, 2, 2.3, 3 metal ratio, good quality product was obtained with no substantial change in the metal ratio. Partial substitution of Tl with Ca was also corroborated by computer simulation of the high resolution image of the 2223 specimen [11].

Temperature dependence of electrical resistivity and magnetization was shown in Fig. 5. No evidence for superconductivity for the as prepared 2201 specimen was observed down to 4.2 K. A sharp superconducting transition was observed at 98 K and 115 K for the 2212 and 2223 specimen respectively. Appearance of diamagnetism corresponded to  $T_c$  determined from resistivity measurements, and the value of the initial slope of magnetization curve at 4.2 K was at least above 90 volume % of the perfect diamagnetism.

### 3.2 Single Tl Layer Oxides

Synthesis of single Tl layer compounds required heat treatment for several hours, as shown in Table 1, indicating less stability than the double Tl layer compounds which were formed within a short reaction time. Although single phase materials were hardly obtainable, at least four kinds of different Cu layer compounds were identified by XPD, as tabulated in Table 2 [13]. No single Cu layer compound was synthesized yet, although structures with the

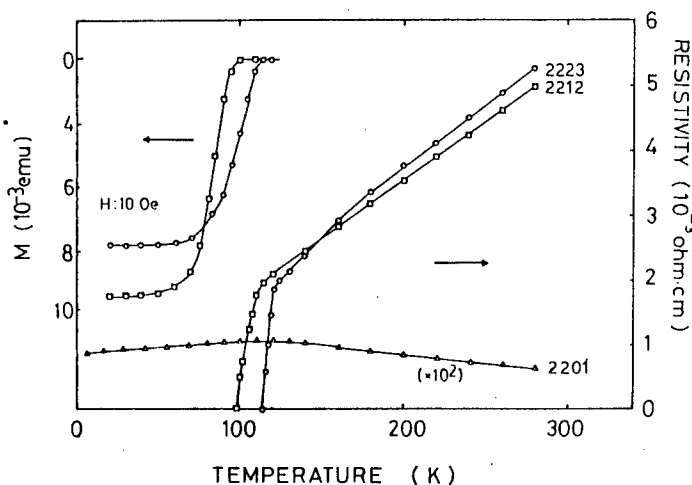


Fig. 5 Magnetization and resistivity versus temperature of double Tl layer oxides

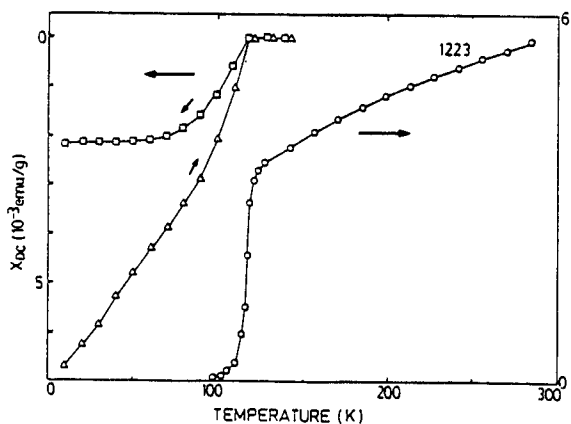
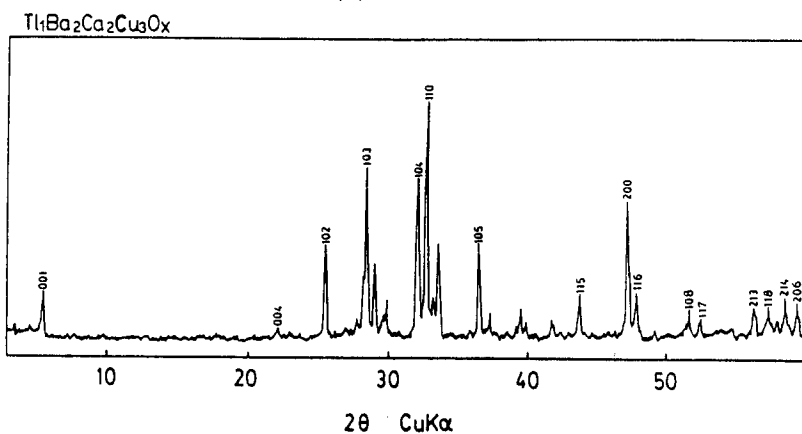


Fig. 6 DC susceptibility and resistivity vs. temperature of  $Tl_1Ba_2CaCu_2O_7$

Fig. 7 XPD pattern of 1212 specimen with tetragonal indices ↓





number of Cu layers greater than 5 were observed by high resolution electron microscopy. Measured unit cell dimensions showed similar behavior to the double Tl layered compounds with respect to the number of Cu layers. Crystal structures of single Tl layer compounds were schematically shown in Fig. 3 (b).

As a representative example, Fig. 6 shows temperature variation of resistivity and dc susceptibility of nearly single phase material of the 1212 specimen (Fig. 7).  $T_c$  estimated from resistivity and susceptibility measurements was summarized in Table 2.  $T_c$  increases with increasing number of Cu layers up to 4, but turns down for the 5 Cu layer compound.

#### 4. Discussion

High  $T_c$  Cu oxides so far discovered generally have two dimensional pyramidal Cu-O plane, which is believed to play an important role for superconductivity. In the case of double and single Tl layer compounds, these conditions are fulfilled by insertion of oxygen-defective Ca layers, similar to the Y layer in  $YBa_2Cu_3O_7$ , leading to  $T_c$  higher than 100 K in the compounds with the number of Cu layers greater than 2. Increase in  $T_c$  with the increasing number of Cu layers is also accompanied by decrease in a-dimension, suggesting importance of the Cu-O distance within the plane for  $T_c$ .

The other important factor required for achieving high  $T_c$  is sufficiently high hole concentrations, i. e. average Cu valence larger than 2 [14]. This value for 90 K superconductor of  $YBa_2Cu_3O_7$  is 2.3. However, in the case of  $Tl_2Ba_2Ca_{n-1}Cu_nO_{2n+4}$ , if the ideal composition and trivalent Tl are assumed, the average Cu valence is exactly 2, allowing no holes in Cu-O bonds. Apparently partial substitution of Tl with Ca, as proved in the present study, gives rise to hole generation to some degree, but may not be sufficient for a 120 K superconductor.

From the viewpoint of structure chemistry, it is rather surprising that  $Tl^{3+}$  ions with  $5d^{10}$  configuration form the same double layer structure as  $Bi^{3+}$  ions with  $5d^{10}6s^2$  configuration, which may explain peculiar covalently bonded layer structure, as represented by  $Bi_4Ti_3O_{12}$  type, due to their high polarizability. Hence, if partial participation of s electrons in Tl is allowed to stabilize the layer structure by charge transfer from Cu ions, thereby providing holes in Cu-O bonds, both the covalent structure and high  $T_c$  superconductor would be simultaneously explained. Evidence for such reduction in Tl ions has been obtained by observation of the chemical shift by means of X-ray photoelectron spectroscopy [15].

Noteworthy is that the situation is rather different in single Tl layer compounds. In this case, average Cu valence,  $v$ , is a function of the number of Cu layers,  $n$ , i.e.  $v = 2 + 1/n$ , and sufficient amount of holes is automatically guaranteed for the ideal composition. This suggests less covalent character of single Tl layer structure than double Tl layer one, and accordingly somewhat different electronic states in Tl ions. XPS study of single Tl layer compounds is also interesting.

#### Acknowledgements

The authors are grateful to Professors Y. Muto and M. Tachiki for invaluable discussion and warm encouragements. They also indebted to Professor K. Nagase and Ms. R. Suzuki, College of General Education, Tohoku University, for helpful cooperation.

# References

1. H. Maeda, Y. Tanaka, M. Fukutomi and T. Asano, *Jpn. J. Appl. Phys.*, 27 (1988) L209.
2. Z. Z. Sheng and A. M. Hermann, *Nature*, 332 (1988) 138.
3. M. A. Subramanian, J. C. Calabrese, C. Torardi, J. Gopalakrishnan, T. R. Askew, R. B. Flippen, K. J. Morrissey, U. Chowdhry and A. W. Sleight, *Nature*, 332 (1988) 420.
4. C. C. Torardi, M. A. Subramanian, J. C. Calabrese, J. C. Gopalakrishnan, K. J. Morrissey, T. R. Askew, R. B. Flippen, U. Chowdhry and A. W. Sleight, *Science*, 240 (1988) 631.
5. S. S. P. Parkin, V. Y. Lee, A. I. Nazzal, R. Savoy, R. Beyers and S. J. La Placa, *Phys. Rev. Lett.*, 61 (1988) 750.
6. B. Morosin, D. S. Ginley, P. F. Hlava, M. J. Carr, R. J. Baughman, J. E. Shirber, E. L. Venturini and J. F. Kwak, *Physica C*, 152 (1988) 413.
7. M. Kikuchi, N. Kobayashi, H. Iwasaki, D. Shindo, T. Oku, A. Tokiwa, T. Kajitani, K. Hiraga, Y. Syono and Y. Muto, *Jpn. J. Appl. Phys.*, 27 (1988) L1050.
8. S. Iijima, T. Ichihashi, Y. Shimakawa, T. Manako and Y. Kubo, *Jpn. J. Appl. Phys.*, 27 (1988) L837.
9. H. Ihara, R. Sugise, M. Hirabayashi, N. Terada, M. Jo, K. Hayashi, A. Negishi, M. Tokumoto, Y. Kimura and T. Shimomura, *Nature*, 334 (1988) 510.
10. F. Izumi, *J. Cryst. Soc. Jpn.*, 27 (1985) 23, in Japanese.
11. K. Hiraga, D. Shindo, M. Hirabayashi, M. Kikuchi, N. Kobayashi and Y. Syono, *Jpn. J. Appl. Phys.*, 27 (1988) L1848.
12. M. Kikuchi, T. Kajitani, T. Suzuki, S. Nakajima, K. Hiraga, N. Kobayashi, H. Iwasaki, Y. Syono and Y. Muto, *Jpn. J. Appl. Phys.*, submitted.
13. S. Nakajima et al., in preparation.
14. Y. Tokura, J. B. Torrance, T. C. Huang and A. I. Nazzal, *Phys. Rev. B*, in press.
15. T. Suzuki et al., in preparation.

# The Effect of Oxygen Concentration on the $T_c$ in the Bi-Sr-Ca-Cu-O System

Y. Ishizawa

National Institute for Research in Inorganic Materials,  
1-1 Namiki, Tsukuba, Ibaraki 305, Japan

The effect of oxygen concentration on the  $T_c$  in the low- $T_c$  phase  $(\text{Bi,Pb})_2(\text{Bi,Sr,Ca})_3\text{Cu}_2\text{O}_{8+y}$  and the high- $T_c$  phase  $\text{Bi}_{2.5}\text{Sr}_{1.9}\text{Ca}_2\text{Cu}_3\text{O}_{10+y}$  was studied by electrical resistivity and magnetic susceptibility measurements. Oxygen concentration was controlled by changing annealing conditions. It has been revealed that the  $T_c$  strongly depends on slight changes of oxygen concentration.

Since a high- $T_c$  oxide superconductor with a  $T_c$  of 80 K (low- $T_c$  phase) and 110 K (high- $T_c$  phase) was reported in the Bi-Sr-Ca-Cu-O system [1], many investigations were performed to elucidate complicated properties of this system. In this oxide superconductor, it is important to study the effect of oxygen concentration on the  $T_c$ . However, the importance of this investigation has not been fully recognized so far as in  $\text{YBa}_2\text{Cu}_3\text{O}_y$ . The oxygen concentration was controlled by two ways. One is the way of changing annealing conditions of specimens such as annealing temperatures. The other is a way of controlling the oxygen concentration by changing the Bi and Pb contents and the Sr/Ca ratio, especially in the low- $T_c$  phase. This report includes recent results on the oxygen effects of the low- $T_c$  phase and the high- $T_c$  phase.

We prepared the low- $T_c$  phase specimens with compositions  $(\text{Bi}_{2-x}\text{Pb}_x)(\text{Bi}_a\text{Sr}_b\text{Ca}_c)\text{Cu}_2\text{O}_{8+y}$  where  $x=0$  or  $0.1$ ,  $a=0$  or  $0.1$ ,  $a+b+c=3.0$ , and the high- $T_c$  phase specimen with the composition  $\text{Bi}_{2.5}\text{Sr}_{1.9}\text{Ca}_2\text{Cu}_3\text{O}_{10+y}$ . Methods of synthesis and characterisation were essentially the same as those described previously [2-6]. All samples of the low- $T_c$  specimens were quenched from annealing temperatures into liquid nitrogen temperature to change the oxygen concentration. Oxygen concentration of the high- $T_c$  specimen were controlled by changing the annealing time in vacuum at  $500^\circ\text{C}$ .

specimen	composition				
	2-x	x	a	b	c
B	1.6	0.4	0	2.0	1.0
C	1.6	1.4	0	1.6	1.4
F	1.9	0.1	0	1.6	1.4
H	1.9	0.1	0	1.4	1.6
J	1.9	0.1	0.1	1.35	1.55
K	2.0	0	0	1.4	1.6
L	1.9	0.1	0.1	1.55	1.35
M	2.0	0	0.1	1.35	1.55
N	2.0	0	0.1	1.55	1.35

Table 1. Nominal compositions of specimens represented by chemical formulae  $\text{Bi}_{2-x}\text{Pb}_x(\text{Bi}_a\text{Sr}_b\text{Ca}_c)\text{Cu}_2\text{O}_{8+y}$

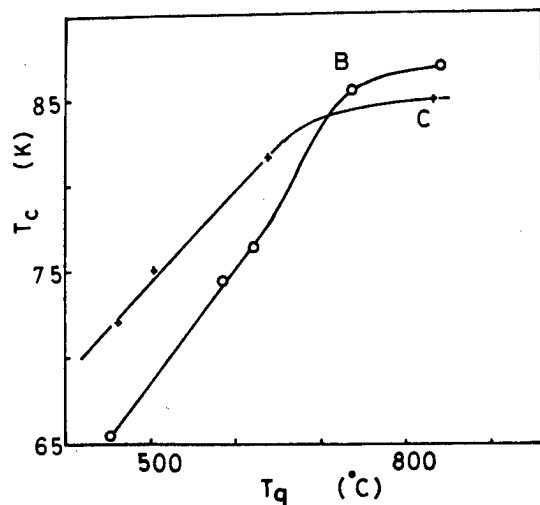


Fig. 1. Zero resistivity temperature ( $T_c$ ) as a function of quenching temperature ( $T_q$ ). B,C: specimens listed in Table 1.

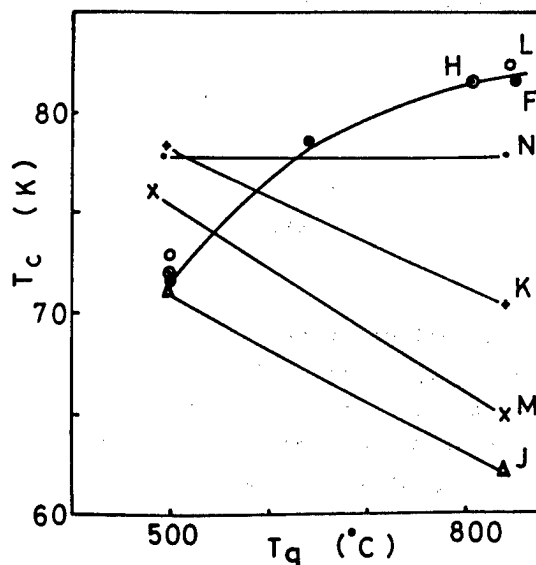


Fig. 2. Dependence of the  $T_c$  on quenching temperature ( $T_q$ ). F,H,J, K,L,M,N: specimens listed in Table 1.

The nominal compositions of the low- $T_c$  specimens studied are listed in Table 1 [6]. Specimens B and C are multiphase samples and the others are nearly single phase ones. Figure 1 shows the relationships between the zero resistivity temperature ( $T_c$ ) and quenching temperature ( $T_q$ ) for specimens B and C. The  $T_c$  decreased with decreasing quenching temperatures. We also tested the vacuum annealing effect at 500°C using a rotary pump. The  $T_c$  increased considerably by the vacuum annealing. These results indicate that the  $T_c$  decreases with increasing oxygen concentration for these Pb-containing specimens.

The relationships between the  $T_c$  and quenching temperatures of the other specimens which are nearly single phase are shown in Fig. 2. In these specimens, we selected the Sr/Ca ratio with nearly one because the  $T_c$  becomes sensitive with oxygen concentration for various cationic compositions. Taking into consideration the chemical compositions listed in Table 1, we can derive a few information from these results. The  $T_c$  was above 80 K for specimens with high Sr/Ca ratios ( $>1$ ) or Pb-containing ones when they were quenched from 800-850°C to 77 K. The  $T_c$  of these specimens was below 75 K when they were annealed at 500°C in air. However, the substitution of Bi atoms in the Ca plane depressed the  $T_c$  below 80 K as in the case of the specimen N. For specimens with low Sr/Ca ratios ( $<1$ ) or Bi-substituted ones ( $a=0.1$ ), the  $T_c$  was below 75 K when they were quenched from 800-850°C, but it was increased by low temperature annealing. However, in the case of Pb-substituted specimen H ( $x=0.1$ ), the situation was reverse. This indicates that the substitution of Pb atoms in Bi sites of the BiO layer promotes the  $T_c$  when the specimen was quenched from a high temperature.

The  $T_c$  of the specimen L increased 7 K after the vacuum annealing at 500°C. The weight loss was 0.06 %, which was close to the value for the high  $T_c$  phase superconductor. The significant change in the  $T_c$  by the vacuum annealing indicates

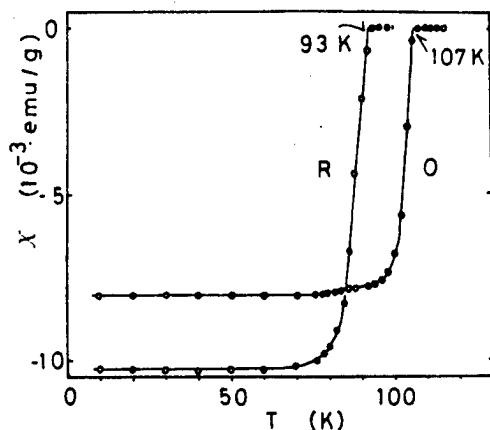


Fig. 3. Temperature dependence of magnetization of the high- $T_C$  phase specimen  $\text{Bi}_{2.5}\text{Sr}_{1.9}\text{Ca}_2\text{Cu}_3\text{O}_{10+y}$ .  
O : oxidized at 500 C in air for 25 h;  
R : reduced in vacuum at 500 C for 25 h.

a great effect of the oxygen concentration on the  $T_C$ . However, this effect differs for each specimen. That is, relationships between the  $T_C$  and  $T_q$  showed considerable variations as shown in Fig. 2. This shows that it is necessary to study the  $T_C$  among the various cationic compositions in more detail. Anyhow, it is confirmed that increase of the oxygen concentration depressed the  $T_C$  for specimens with the high Sr/Ca ratio and the high Pb content, and the reverse was observed for specimens with the low Sr/Ca ratio and the high Bi content in the temperature range above 500°C [6].

The high- $T_C$  phase specimen with the composition  $\text{Bi}_{2.5}\text{Sr}_{1.9}\text{Ca}_2\text{Cu}_3\text{O}_{10+y}$  was annealed for 25 h at 500°C in air [4]. The specimen was then reduced at 500°C in vacuum. The oxygen concentration was controlled by the annealing time. The magnetic susceptibility measurement was made in the field of 10 Oe during the cooling process using a SQUID magnetometer. Figure 3 shows the onset  $T_C$  of 107 K for the oxidized one and the 93 K for the reduced one (25 h). The zero resistivity temperature  $T_C$  was measured in several oxygen concentration. The  $T_C$  decreased with decreasing oxygen concentration (longer annealing time). After the annealing in vacuum for 25 h, the 0.044% weight loss took place. This corresponds to the loss of about 0.03 oxygen atom. This means the  $T_C$  is very sensitive to oxygen concentration.

In summary, the effect of oxygen concentration on the  $T_C$  in the low- $T_C$  phase ( $\text{Bi}_{2-x}\text{Pb}_x(\text{Bi}_a\text{Sr}_b\text{Ca}_c)\text{Cu}_2\text{O}_{8+y}$  ( $a+b+c=3$ ), and the high- $T_C$  phase  $\text{Bi}_{2.5}\text{Sr}_{1.9}\text{Ca}_2\text{Cu}_3\text{O}_{10+y}$  were studied by changing annealing conditions. The  $T_C$ 's of both phases are very sensitive to slight changes of oxygen concentration.

#### References

- [1] H. Maeda, Y. Tanaka, M. Fukutomi and T. Asano : Jpn. J. Appl. Phys. 27 (1988) L209.
- [2] A. Ono, S. Sueno and F. Okamura : Jpn. J. Appl. Phys. 27 (1988) L786.
- [3] A. Ono, K. Kosuda, S. Sueno and Y. Ishizawa : Jpn. J. Appl. Phys. 27 (1988) L1007.
- [4] A. Ono : Jpn. J. Appl. Phys. 27 (1988) L1213.
- [5] A. Ono : Jpn. J. Appl. Phys. 27 (1988) L2276.
- [6] A. Ono : Jpn. J. Appl. Phys. 28 (1989) L54.

# Synthesis of $\text{Bi}_2\text{Sr}_2\text{CuO}_x$ and $\text{A}_2\text{CuO}_4$ type Superconducting Ceramics

N. Ohashi, Y. Teramoto, T. Taniguchi, H. Ikawa and O. Fukunaga

Dept. Inorganic Materials, Tokyo Institute of Technology

2-12-1, Ookayama, Meguro-ku, Tokyo 152, Japan

Synthesis of  $\text{Bi}_2\text{Sr}_2\text{CuO}_x$  and  $\text{A}_2\text{CuO}_4$  type superconducting oxides has been studied to discuss relationship between superconductivity and crystalline phases existed in the ceramic samples. Non superconducting phase (x-phase) are coexisted with 221 superconducting phase in the Bi-Sr-Cu-O system. The x-phase appears sensitively by the change of calcination temperature and reaction time. Synthesis of the compounds  $\text{A}_2\text{CuO}_4$  has been carried out to clarify crystal phases. Some kinds of phases are coprecipitated with  $\text{Nd}_2\text{CuO}_4$ , and  $\text{La}_2\text{CuO}_4$  phase. These phases are separated with changing A ion combination. High pressure phase transformation experiments are also carried out using above samples.

## 1) Synthesis of $\text{Bi}_2\text{Sr}_2\text{CuO}_x$

Michel et al.[1] and Akimitsu et al.[2] have reported superconductivity of this compound. They started from mixture having cation ratio of Bi:Sr:Cu= 1:1:1, but structural analysis data suggested Bi:Sr:Cu= 2:2:1. We studied 221-phase synthesis using Bi:Sr:Cu=1:1:1 and 2:2:1 starting compositions. During the course of synthesis almost samples showed coexisted unknown x-phase which shown in Fig. 1. Relative amount of x-phase changed with small change of calcination temperatures of the starting compositions and subsequent sintering temperatures. We calcined samples at about 800 C and sintered about 800-880 C in air. Both 1:1:1 and 2:2:1 starting composition resulted 221-phase and x-phase mixture. Fig.1(a)-(d) shows powder X-ray diffraction charts of a typical heat treatment process starting 2:2:1 composition. This data suggested that calcination temperature and duration of the reaction effected the amount of x-phase. The amount of x-phase increased with reaction time at 800 C.

Resistivity vs. temperature curves of Fig. 2(a)-(d) corresponds each samples shown in the Fig. 1. This data showed clearly that resistivity of the sample increased with increasing amount of x-phase coexisted with 221-phase. The sample contained relatively larger amount of x-phase (sample (c)) showed small drop of the resistivity at about 10 K. This is suggesting that x-phase is predominantly distributed on the surface or outer region of the 221-phase grains in the ceramic sample.

The x-phase coexisting the 221-phase is stable to the higher temperature than the calcination temperature. Thus, when x-phase appeared in the sample, synthesis of the 221-phase become very difficult at any examined sintering temperature. The x-phase is certainly very close composition and structure to the 221-phase. We are trying to separate single x-phase and 221-phase to clear phase relation between two structures.

Conclusively, we prepared almost pure 221-phase 10 K super-conducting ceramics from corresponding starting mixture.

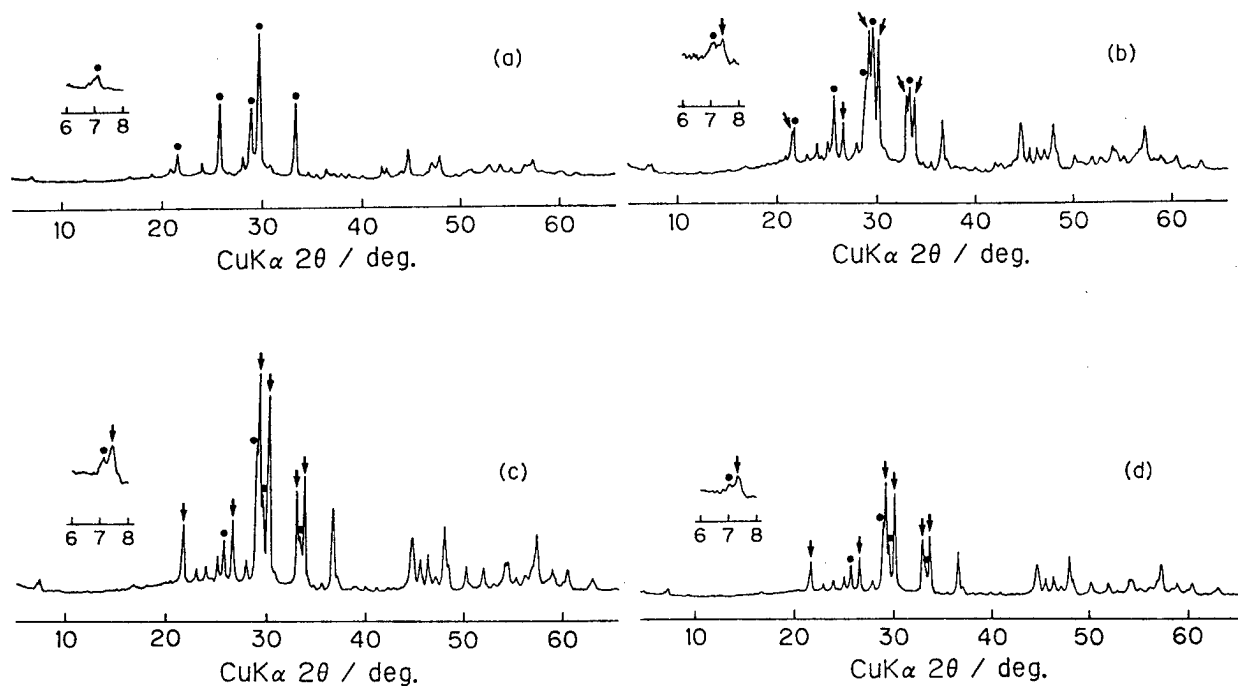


Fig. 1 X-ray powder diffraction pattern of typical heat treatment at 800 °C  
 (a) for 10h (b) for 20h (c) for 25h (d) for 30h  
 Arrows and solid circles indicate reflection of X-phase and 221 phase, respectively.

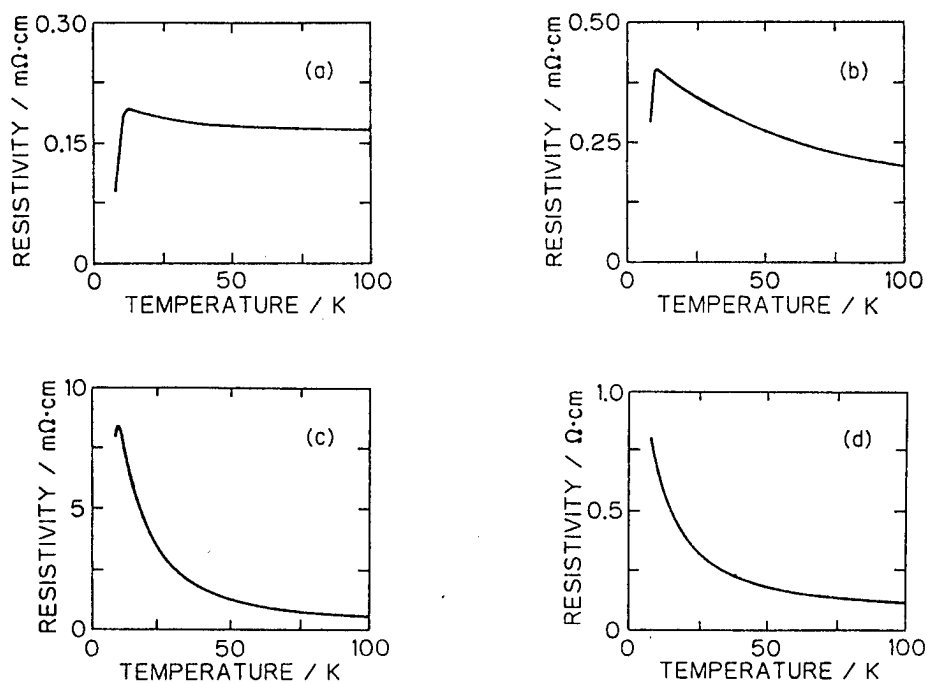


Fig. 2 Temperature dependence of electric resistivity  
 (a)-(d) corresponds to (a)-(d) in fig. 1, respectively.

## 2) Synthesis of $A_2CuO_4$ type Compounds

This series compounds become very important to understand superconductivity both hole-type and electron-type. We studied mainly Nd-Sr and La-Gd series of the A cation combinations. Synthesis was carried out through ceramic processing using constituent oxides or carbonate powder mixture and sintering in air. Although superconductivity of these compounds correlate with hole or electron control process by the selecting ions combination and process control, however, structural aspect is also important to discuss superconductivity. As shown in Fig. 3,  $Sr_2CuO_3$ ,  $K_2NiF_4$ ,  $Sr_3Ti_2O_7$ ,  $Nd_2O_3$ ,  $(Nd,Sr,Ce)_2CuO_7$  (T')[3] and  $Nd_2CuO_4$  type structures are separated with changing average ionic radius of the A cations of starting composition. In La-Gd series,  $Nd_2CuO_4$  type structure was extended to  $La_{0.5}Gd_{0.5}$  composition. Further increase of La, it became mixed phases possibly T' and  $K_2NiF_4$  type.  $(Nd,Sr,Ce)_2CuO_7$  type phase region was limited within narrow composition range near  $La_2CuO_4$  composition.

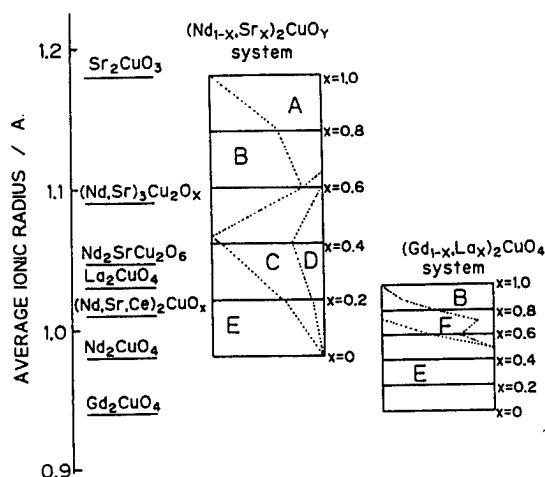


Fig. 3 Relation between average ionic radius of A cation normalized by starting composition and produced phases. Each symbol shows produced phases as follows; A;  $Sr_2CuO_3$  type, B;  $K_2NiF_4$  type, C;  $Sr_3Ti_2O_7$  type D;  $Nd_2O_3$  type, E;  $Nd_2CuO_4$  type F;  $(Nd,Sr,Ce)_2CuO_7$  type

## 3) Trial experiments on the possible high pressure phase transformation

In the  $A_2CuO_4$  series,  $Nd_2CuO_4$  to  $La_2CuO_4$  or T' type high pressure phase transformation will be possible. Because later structure is smaller lattice constant with larger constituent A site ions. In another scope, stability of x-phase of Bi-Sr-Cu-O system can be checked by high pressure experiments. Up to 7 GPa and 1000 C conditions are applied to the sample using 10 mm edge Link-type cubic anvil apparatus. Ti and Pt foil internal heater was used to prevent reduction of Cu. Results showed that no phase transformation was detected from  $Nd_2CuO_4$  to  $La_2CuO_4$  in this range. Stability of x-phase of Bi-Sr-Cu was increased with reaction time and temperature.

## References

1. C.Michel, M.Hervieu, et. al. : Z. Phys. B-condensed matter 68(1987) 422
2. J.Akimitsu, A.Yamazaki, et. al. : Jpn. J. Appl. Phys. 26(1987) L2080
3. J.Akimitsu, S.Suzuki, et. al. : Jpn. J. Appl. Phys. 27(1988) L1859



Material Syntheses of Layered Oxides  
Related with  $\text{Bi}_4\text{Ti}_3\text{O}_{12}$  Family Ferroelectrics

M. Takashige, F. Shimizu, H. Suzuki and S. Sawada

Department of Electronics, College of Science and Engineering,  
Iwaki-Meisei University  
5-5-1, Chuohdai-Iino, Iwaki-shi, Fukushima 970, Japan

Material syntheses of layered oxides have been done. Based upon crystal structures existing in ferroelectric layer-oxides as  $\text{Bi}_4\text{Ti}_3\text{O}_{12}$ , several superconducting systems were designed but  $T_c$  remained below 80K. Ferroelectric systems such as  $\text{Bi}_{4-x}\text{Tl}_x\text{Ti}_3\text{O}_{12}$  were also synthesized to investigate the possibility of Tl for the formation of layer materials as well as the superconducting systems newly appeared.

A lot of layer-oxides including Bi-ion have been known[1] which possesses a common structure with perovskite  $\text{ABO}_3$ -type layers being interposed by Bi-oxides layers. The simplest ones are those such as  $\text{M Bi}_2\text{X}_2\text{O}_9$  ( $\text{M}=\text{Ca}, \text{Sr}, \text{Ba}, \text{Pb}$ ;  $\text{X}=\text{Ta}, \text{Nb}$ ) with a single layer of  $\text{M X}_2\text{O}_7$  having one hypothetical  $\text{ABO}_3$ -cell like  $\text{M XO}_3$ , which is interposed by  $\text{Bi}_2\text{O}_2$  layers. Starting from these single-layer compounds, series of crystals with different numbers of perovskite layers are existing as listed in Table 1.

Also in the recent progress in the oxides-superconductors, this structure is forefront-research subjects in that rare-earth-free materials. One of the phases appeared in the  $\text{BiCaSrCuO}$  system[2] with  $T_c$ 's in the 80K range has a structure analogous to the double layered  $\text{Bi}_4\text{Ti}_3\text{O}_{12}$ [3]. That is the structure where the Bi-sites in the  $\text{Bi}_2\text{Ti}_3\text{O}_{10}$  layer are replaced by Cu and the Ti-sites are by Ca and Sr with 1:2, namely, the material having a formula  $\text{Bi}_2\text{CaSr}_2\text{Cu}_2\text{O}_9$ . Furthermore  $\text{Tl}_2\text{CaBa}_2\text{Cu}_3\text{O}_9$  having  $\text{Tl}_2\text{O}_2$  layers instead of  $\text{Bi}_2\text{O}_2$  is also appearing.

In this work, referring structures and compositions of ferroelectric layer-oxides, material-syntheses have been done both in the superconducting systems(1) and in ferroelectric systems(2).

#### (1) Superconducting systems[4]

Nominal compositions we synthesized are listed in Table 2, together with the reference dielectrics and our guiding principle for the replacements. All were prepared by mixing Cu-, Pb-, Bi- and rare-earth oxides and alkaline and alkaline earth carbonates in metal atom ratio. The solid-state reactions were done by the first firing at  $820 \sim 860^\circ\text{C}$  for  $\sim 10$  hours and second one at  $850^\circ\text{C}$  for  $\sim 5$  hours. No special effort such as oxygen-annealings has been adopted. Resistivity measurements were performed by the dc four-probe method with a current density of  $1 \sim 10\text{mA}/\text{cm}^2$ .

Results are demonstrated in Fig.1 (see also Tables). Within the simple heat-

Single Layered Materials	Chemical Formula of Perovskite-like Layers
(1) $M \text{ Bi}_{1-x} \text{ X}_x \text{ O}_3$ M = Ca, Sr, Ba, Pb X = Nb, Ta	$M \text{ X}_2 \text{ O}_7$
Double Layered Materials	
(2) $\text{Bi}_{1-x} \text{ Ti}_x \text{ O}_{12}$ (3) $\text{Bi}_{1-x} \text{ R}_x \text{ Ti}_3 \text{ O}_{12}$ R = La, Pr, Nd, Sm, Eu, Gd, Tb, Dy, Y, Ho, Er	$\text{Bi}_{1-x} \text{ Ti}_x \text{ O}_{10}$ $\text{Bi}_{1-x} \text{ R}_x \text{ Ti}_3 \text{ O}_{10}^*$
Triple Layered Materials	
(4) $M \text{ Bi}_{1-x} \text{ Ti}_x \text{ O}_{15}$ (5) $\text{Na}_{0.5} \text{ Bi}_{1.5} \text{ Ti}_3 \text{ O}_{15}$ (6) $\text{K}_{0.5} \text{ Bi}_{1.5} \text{ Ti}_3 \text{ O}_{15}$	$M \text{ Bi}_{1-x} \text{ Ti}_x \text{ O}_{13}$ $\text{Na}_{0.5} \text{ Bi}_{1.5} \text{ Ti}_3 \text{ O}_{13}$ $\text{K}_{0.5} \text{ Bi}_{1.5} \text{ Ti}_3 \text{ O}_{13}$
Quadruple Layered Materials	
(7) $M \text{ Bi}_2 \text{ Ti}_2 \text{ O}_{18}$	$M \text{ Bi}_2 \text{ Ti}_2 \text{ O}_{16}$

Table 1 Typical ferroelectric and related Bi-layer oxides.

Double Layered Materials	Reference Crystals
(a) $\text{Bi}_{1-x} \text{ Ca}_x \text{ Sr}_{1-x} \text{ Cu}_2 \text{ O}_{10}$ (b) $\text{Bi}_{1-x} \text{ Ca}_x \text{ Sr}_{1-x} \text{ Cu}_2 \text{ O}_{10}$ (c) $\text{Bi}_{1-x} \text{ La}_x \text{ Ca}_x \text{ Sr}_{1-x} \text{ Cu}_2 \text{ O}_{10}$ (d) $\text{Bi}_{1-x} \text{ Y}_x \text{ Ca}_x \text{ Sr}_{1-x} \text{ Cu}_2 \text{ O}_{10}$	$\text{Bi}_4 \text{ Ti}_3 \text{ O}_{12}$ $2\text{Bi} \Rightarrow 2\text{Cu}, 3\text{Ti} \Rightarrow 2\text{Sr} + \text{Ca}$ $2\text{Bi} \Rightarrow 2\text{Cu}, 3\text{Ti} \Rightarrow 1.5\text{Sr} + 1.5\text{Ca}$ $\text{Bi}_{1-x} \text{ R}_x \text{ Ti}_3 \text{ O}_{12}$ $\text{Bi}_2 \text{ O}_7$ Layer $\Rightarrow$ $\text{Bi}_{1-x} \text{ La}_x (\text{Y})_x \text{ O}_7$ Layer
Triple Layered Materials	Reference Crystals
(e) $\text{Bi}_{1-x} \text{ Ca}_x \text{ Sr}_{1-x} \text{ Cu}_2 \text{ O}_{10}$ (f) $\text{Bi}_{1-x} \text{ Ba}_x \text{ Sr}_{1-x} \text{ Cu}_2 \text{ O}_{10}$ (g) $\text{Bi}_{1-x} \text{ Ca}_x \text{ Sr}_{1-x} \text{ Cu}_2 \text{ O}_{10}$ (h) $\text{Bi}_{1-x} \text{ Ca}_x \text{ Sr}_{1-x} \text{ Cu}_2 \text{ O}_{10}$ (i) $\text{Bi}_{1-x} \text{ Pb}_x \text{ Ca}_x \text{ Sr}_{1-x} \text{ Cu}_2 \text{ O}_{10}$ (j) $\text{Bi}_{1-x} \text{ Na}_{0.5} \text{ Ca}_{1.5} \text{ Sr}_{1-x} \text{ Cu}_2 \text{ O}_{15}$ (k) $\text{Bi}_{1-x} \text{ K}_{0.5} \text{ Ca}_{1.5} \text{ Sr}_{1-x} \text{ Cu}_2 \text{ O}_{15}$	$M \text{ Bi}_4 \text{ Ti}_4 \text{ O}_{15}$ $M \Rightarrow \text{Cu}, 2\text{Bi} \Rightarrow 2\text{Cu}, 4\text{Ti} \Rightarrow 2\text{Ca} + 2\text{Sr}$ $M \Rightarrow \text{Ba}, 2\text{Bi} \Rightarrow 2\text{Cu}, 4\text{Ti} \Rightarrow 2\text{Ca} + 2\text{Sr}$ $M \Rightarrow \text{Ca}, 2\text{Bi} \Rightarrow 2\text{Cu}, 4\text{Ti} \Rightarrow 2\text{Ca} + 2\text{Sr}$ $M \Rightarrow \text{Sr}, 2\text{Bi} \Rightarrow 2\text{Cu}, 4\text{Ti} \Rightarrow 2\text{Ca} + 2\text{Sr}$ $M \Rightarrow \text{Pb}, 2\text{Bi} \Rightarrow 2\text{Cu}, 4\text{Ti} \Rightarrow 2\text{Ca} + 2\text{Sr}$ $\text{Na}(\text{K})_{0.5} \text{ Bi}_{1.5} \text{ Ti}_3 \text{ O}_{15}$ $2.5\text{Bi} \Rightarrow 2.5\text{Cu}, 4\text{Ti} \Rightarrow 2\text{Ca} + 2\text{Sr}$ $2.5\text{Bi} \Rightarrow 2.5\text{Cu}, 4\text{Ti} \Rightarrow 2\text{Ca} + 2\text{Sr}$
Quadruple Layered Materials	Reference Crystals
(l) $\text{Bi}_{1-x} \text{ Ca}_x \text{ Sr}_{1-x} \text{ Cu}_2 \text{ O}_{10}$ (m) $\text{Bi}_{1-x} \text{ Ca}_x \text{ Sr}_{1-x} \text{ Cu}_2 \text{ O}_{10}$	$M \text{ Bi}_2 \text{ Ti}_2 \text{ O}_{16}$ $2\text{H} \Rightarrow 2\text{Cu}, 2\text{Bi} \Rightarrow 2\text{Cu}, 5\text{Ti} \Rightarrow 2\text{Ca} + 3\text{Sr}$ $2\text{H} \Rightarrow 2\text{Cu}, 2\text{Bi} \Rightarrow 2\text{Cu}, 5\text{Ti} \Rightarrow 3\text{Ca} + 2\text{Sr}$

Table 2 Nominal compositions synthesized in the present work.

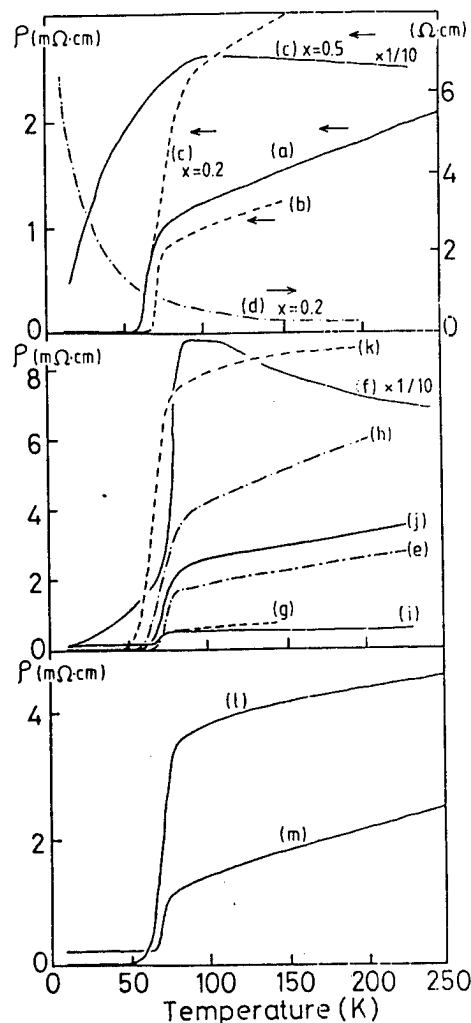


Fig.1 Temperature dependence of Resistivity  $\rho$ .

treatments of the present work it seems that the highest  $T_c$  remains below 80K and a possibility of formation of multi-layered perovskite which we intended is still open question. But we believe that the way we adopted here is one of the directions to synthesize new materials. Further optimum of preparation-condition together with those such as powder x-ray analysis are desired.

## (2) Ferroelectric systems

To the author's knowledge, no layer-oxides including Tl-ion has been known in the original  $\text{Bi}_4 \text{ Ti}_3 \text{ O}_{12}$  family. Thus one of our interests is whether  $\text{Tl}_2 \text{ O}_7$  layer is brought into this series of materials. For this purpose we attempted to synthesize systems such as  $\text{Bi}_{4-x} \text{ Tl}_x \text{ Ti}_3 \text{ O}_{12}$ .

The samples were prepared by annealing in the oxygen-gas flow at  $\sim 800^\circ \text{C}$  for  $\sim 15$  minutes after first fired stoichiometric mixtures at  $950^\circ \text{C}$  for 2 ~

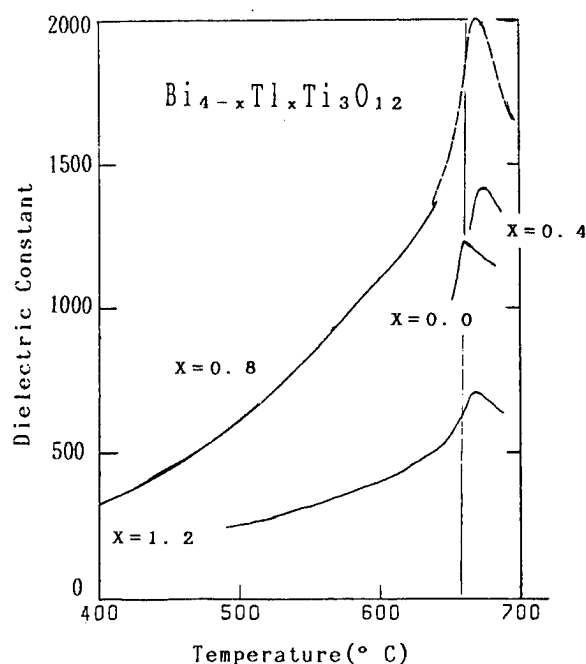


Fig.2 Temperature dependence of Dielectric Constant in the  $\text{Bi}_{4-x}\text{Tl}_x\text{Ti}_3\text{O}_{12}$ .

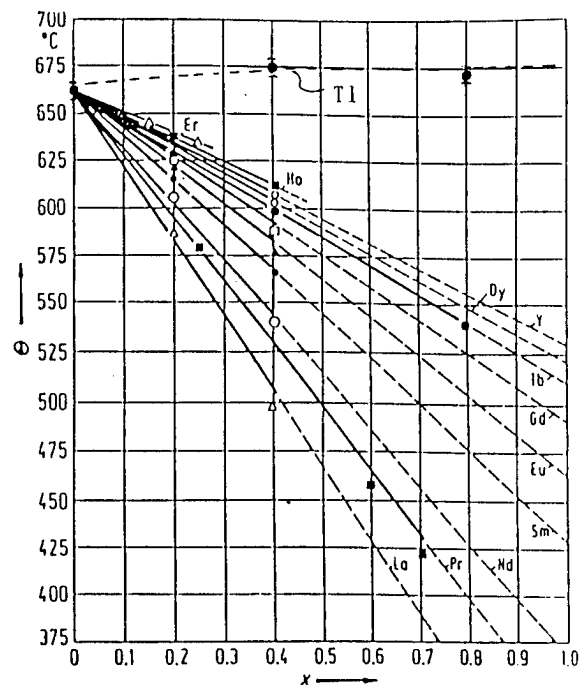


Fig.3 Curie Points  $\Theta$  vs. Composition  $x$  in the  $\text{Bi}_{4-x}\text{R}_x\text{Ti}_3\text{O}_{12}$  (after ref. [5]) and  $\text{Bi}_{4-x}\text{Tl}_x\text{Ti}_3\text{O}_{12}$  (present work).

5 hours. The x-ray powder pattern indicated that in the range  $x < 0.4$  this kind of material seems to be formed, varying ferroelectric Curie point as demonstrated in Fig.2. This is marked contrast to the old work by Wolf and Newnham[5] for the system  $\text{Bi}_{4-x}\text{R}_x\text{Ti}_3\text{O}_{12}$ , where rare-earth elements R are substituted (see Fig. 3). In that case it has known that the rare-earth substitutions are taking place into Bi sites in the perovskite layers of the original structure. Thus, the present result probably supports that the Tl ion is introducing into  $\text{Bi}_2\text{O}_2$  layers in the  $\text{Bi}_4\text{Ti}_3\text{O}_{12}$  structure, which indicates the potential ability of Tl ions for the formation of this kind of layer-oxide. However, in the samples with  $x > 0.4$ , unknown phase is existing simultaneously and the formation of the  $\text{Bi}_4\text{Ti}_3\text{O}_{12}$  structure seems to become difficult in the sample with  $x=2$ , where  $\text{Bi}_2\text{O}_2$  layer is planned to replace fully by  $\text{Tl}_2\text{O}_2$ . More detailed identification is desired in this process.

#### References

- [1] For instance, see *Landolt-Börnstein, Ferroelectrics and Related Materials*, III/16, Subvolume a Oxides (Springer 1981) and references therein.
- [2] H. Maeda, Y. Tanaka, M. Fukutomi and T. Asano, *Jpn. J. Appl. Phys.* **27** L201 (1988).
- [3] E. Takayama-Muromachi, Y. Uchida, A. Ono, F. Izumi, M. Onoda, Y. Matsui, K. Kosuda, S. Takekawa and K. Kato: *Jpn. J. Appl. Phys.* **27** L556 (1988).
- [4] M. Takashige, H. Suzuki and S. Sawada: *Ferroelectrics* (in press).
- [5] R. M. Wolf and R. E. Newnham, *J. Electrochem. Soc.* **116** 832 (1969).

## Ultrahigh-Pressure Study of High $T_c$ Oxides

H. Aoki, M. Kumazawa\*, K. Kurita\*,  
S. Kobayashi, S. Ikehata, A. Nakamura, S. Katsumoto, F. Komori,  
T. Fujii\*\*, T. Ishii<sup>+</sup>, K. Kinoshita<sup>+</sup> and T. Yamada<sup>+</sup>

Department of Physics, University of Tokyo, Hongo, Tokyo 113, Japan

\*Department of Geophysics, University of Tokyo, Yayoi, Tokyo 113, Japan

\*\*Earthquake Research Institute, University of Tokyo, Yayoi, Tokyo 113, Japan

<sup>+</sup>NTT Basic Research Laboratories, Musashino, Tokyo 180, Japan

**Abstract** Ultra-high pressure ( $\leq 13$  GPa) is applied to high  $T_c$  copper oxides ( $\text{YBa}_2\text{Cu}_3\text{O}_{7.8}$  and Bi-based cuprate) to search for possible structural phase transitions. In a relatively oxidizing atmosphere,  $T_c$  for samples quenched from the high-pressure and high temperature ( $\leq 900^\circ\text{C}$ ) treatment remains unchanged, while other conditions favouring oxygen deficiency degrade  $T_c$ . Application of high-pressure/temperature to ingredient powder mixture produces an insulating sample with peculiar magnetic property in some cases.

### 1. Introduction

The class of high- $T_c$  copper oxides first discovered by Bednorz and Muller are reminiscent of rock-forming minerals both chemically and structurally. In fact, high- $T_c$  materials all have crystal structures related to perovskite, which is a key structure for rock-forming minerals (silicates). It has been well established in geophysics that silicates such as  $\text{Mg}_2\text{SiO}_4$  undergo a series of structural phase transitions when high pressure (of the order of 20 GPa) is applied. The present study is motivated by an observation that such structural transitions can possibly be expected also for the copper oxides. Since they possess perovskite-related structures rather than perovskite itself, which is already the high-pressure form, we can expect structural flexibility under ultra-high pressure. We can also expect to fabricate new materials and structures, which is, solid state chemically, only possible under extreme conditions. The high-pressure phases tend to have higher coordination number and covalency in general, so that we can thereby probe the superconducting mechanism.

### 2. Method

The high-pressure study on the high- $T_c$  materials has been primarily focused on the *in situ* experiment[1], i.e., the change of structure and  $T_c$  during the application of pressure. By contrast, we look for new phases that are (meta)stable in normal pressure/temperature and thus can be quenched after the high pressure is turned off. As the ultra-high pressure facility, we employ the multiple-anvil high-pressure apparatus, which has been developed by Kumazawa and coworkers[2]. The multiple-anvil method (Fig.1a) has an advantage that (a)relatively large sample volumes can be accommodated and (b)well-defined high temperature can be applied. The assembly of the pressure medium and sample capsule is shown in Fig.1(b). The control parameters we have varied

include pressure ( $p \leq 20\text{GPa}$  here), temperature ( $T \leq 1350^\circ\text{C}$ ), duration of high  $p/T$  treatment, rapid or slow cooling, starting material (ceramics or ingredient powder mixture) and redox condition (including heater and capsule design).

### 3. Results

Figure 2 shows a typical result for the magnetic susceptibility for samples treated with  $p \sim 10\text{GPa}$  and  $T \sim 900^\circ\text{C}$  for 40mins. It is seen the  $T_c$  remains almost unchanged by the ultra-high pressure treatment unless the temperature during the compression is higher than  $900^\circ\text{C}$ . Thus the superconductivity in the  $\text{YBa}_2\text{Cu}_3\text{O}_{7.8}$  is resistive to high  $p/T$ , although the volume fraction of superconducting phase decreases (Fig.2b). The absence of structural or stoichiometric change in these samples has been confirmed by the x-ray diffraction and the EPMA analysis for different domains seen in the SEM image (Fig.3). In other conditions  $T_c$  is degraded or the sample becomes insulating with Curie-like susceptibility, which is considered to come from oxygen deficiency caused by the high  $p/T$  treatment. This is also the case with  $\text{Bi}_2\text{Sr}_2\text{Ca}_2\text{Cu}_3\text{O}_y$  treated with  $p = 13\text{GPa}$  and  $T = 900^\circ\text{C}$ . Within the parameter range studied here, we have not yet detected any new phase with elevated  $T_c$ .

When we start from the raw material ( $\text{Y}_2\text{O}_3 + \text{BaCO}_3 + \text{CuO}$ ), application of high  $p$  and  $T$  gives rise to an insulator with peculiar magnetic properties according to the treatment condition. A typical example (Fig.4) shows a sharp peak in magnetic susceptibility ( $\chi$ ) around  $T \sim 240\text{K}$ . This does not come from a remnant  $\text{CuO}$ , which has only a broad shoulder in  $\chi$  at Néel temperature ( $\sim 230\text{K}$ ) as shown in the figure. Some structural transition may be related to the peak, although the possibility of spin glass remains, since  $\chi$  is shown to be magnetic field dependent. Extension of the present study to higher pressures and other materials is under way.

We would like to thank Mr Y. Fujiki for collaboration in the early stage of the present study. We are indebted to Profs. K. Kitazawa and K. Kishio for providing us Bi-based samples.

[1] See, e.g., S. Yomo et al., Jpn J. Appl. Phys. **26**(1987), L603; T. Matsumoto et al., Jpn J. Appl. Phys. **27**(1988), L600.

[2] M. Kumazawa and S. Endo in Materials Science of the Earth's Interior ed. by I. Sunagawa (Tera Scientific, 1984), p.587.

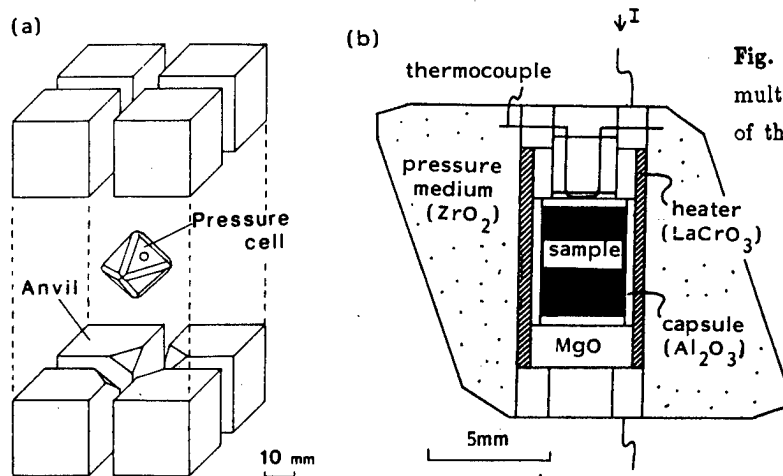
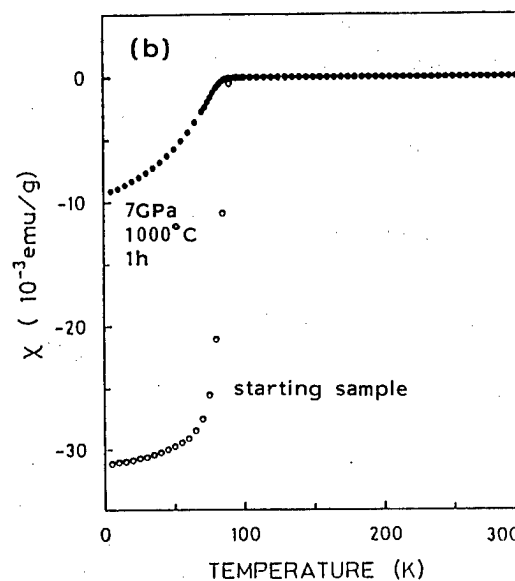
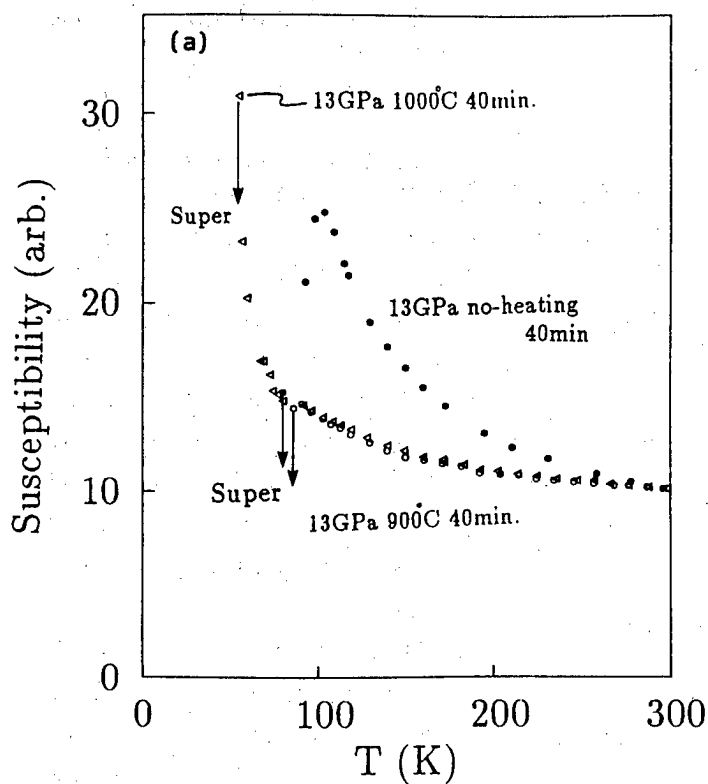
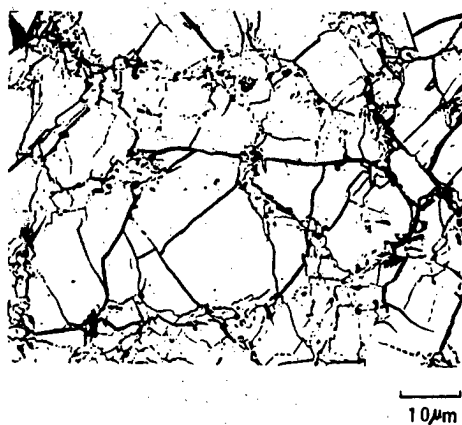


Fig. 1 (a)Pressure-generating system of multiple-anvil (MA8) type. (b)A cross section of the pressure cell.



**Fig. 2** (a) Magnetic susceptibility against temperature is shown for samples of  $\text{YBa}_2\text{Cu}_3\text{O}_{7.8}$  with various treatment conditions. (b) Meissner effect measured by SQUID for a sample before and after the high-pressure treatment.



**Fig. 3** A typical example of the SEM image of the polished surface of  $\text{YBa}_2\text{Cu}_3\text{O}_{7.8}$  treated with  $p = 7$  GPa and  $T = 1000^\circ\text{C}$  for 1h.

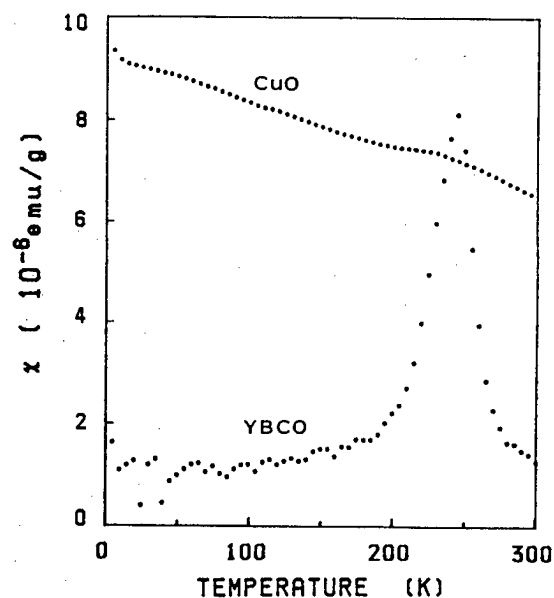


**Fig. 4** Magnetic susceptibility against temperature is shown for the sample obtained from  $(\text{Y}_2\text{O}_3 + \text{BaCO}_3 + \text{CuO})$  powder treated with  $p = 7$  GPa and  $T = 1000^\circ\text{C}$  for 30 mins with slow cooling. The susceptibility of CuO is also shown for comparison.

# High- $T_c$ Superconductors Produced by Oxidation of Melt-spun Bi-Sr-Ca-Cu-Au(Ag) Alloy Ribbons

A. Inoue, K. Matsuzaki, H. Toribuchi and T. Masumoto

Institute for Materials Research, Tohoku University,  
2-1-1, Katahira, Sendai 980, Japan

( $\text{Bi}_{1.2}\text{Sr}_{1.2}\text{Ca}_{1.2}\text{Cu}_{1.4}$ ) $_{50}\text{Au}_{50-x}\text{Ag}_x$  alloy ribbons were produced by melt spinning and had a mixed structure of fcc Au(Ag) and Bi-Sr-Ca-Cu alloy phases. Heating of the alloys in air brought about the formation of Au(Ag) and pseudo-tetragonal  $\text{BiSrCaCu}_2\text{O}_y$  with a well oriented structure. The mixed materials exhibited high  $T_c$ -superconductivity with onset at 110 K and zero resistance at 96 K combined with  $J_c$  of 540 A/cm<sup>2</sup> at 77 K and zero field. The rather high  $J_c$  value is attributable to the oriented structure developed by the present process.

Since the discovery of an  $\text{YBa}_2\text{Cu}_3\text{O}_y$  superconductor with transition temperature ( $T_c$ ) at about 90 K[1,2], similar high- $T_c$  superconductivity has been found to appear in  $\text{LnBa}_2\text{Cu}_3\text{O}_y$  (Ln=lanthanide element)[3],  $\text{BiSrCaCu}_2\text{O}_y$ [4] and  $\text{TlBaCaCuO}_y$ [5] oxides. In addition to scientific researches on clarification of the mechanism for the high- $T_c$  superconductivity of these oxides, a study on the production of the superconducting oxides with high  $J_c$  values in a form of continuous tape or wire has also attracted growing attention from an engineering point of view. The authors have reported that application of the melt-spinning technique to La-Sr-Cu[6], Yb-Ba-Cu[7] and Eu-Ba-Cu[8] alloys as well as to  $\text{LnBa}_2\text{Cu}_3\text{O}_y$ [9] oxides brings about the formation of a long ribbon with a metastable structure including an amorphous phase and subsequent oxidation in air or an oxygen atmosphere gives oxide ribbon samples exhibiting high- $T_c$  superconductivity with zero resistance in the vicinity of 90 K. We have subsequently found[10,11] that the mixture of Ag to Ln-Ba-Cu (Ln=Y, Sm, Gd or Ho) alloys brings about the formation of an alloy ribbon even in the alloy systems with large miscibility gap and the oxide ribbons produced by oxidation of the alloys exhibit a superconducting transition to zero resistance at a temperature above 77 K accompanied by significant enhancement of bending ductility. Thus, the melt-spinning technique can be regarded as a useful direct-cast method of producing a continuous oxide tape with high  $T_c$ -superconductivity. In a series of investigations on the production of a superconducting oxide tape by oxidation of a melt-spun alloy ribbon, the melt spinning and oxidation technique was also found to be applied to the formation of a continuous tape with a mixed structure of  $\text{BiSrCaCu}_2\text{O}_y$  and Au(Ag) phases in which the oxide phase has a highly oriented structure. This report describes attempts to examine the structural change of melt-spun alloy ribbons by heating in air in Bi-Sr-Ca-Cu-Au(Ag) system with an insoluble gap between Bi and Cu elements[12] and the superconductivity of the resulting oxides and to clarify the relation between the development of an oriented structure in the oxide phase and its superconducting properties.

A mixture of pure Bi, Sr, Ca, Cu, Au and Ag metals was melted in a purified and gettered argon atmosphere on a water-cooled copper mould in an arc furnace. The composition of alloys reported is assumed to be a nominal one since the loss during melting was less than about 0.8 wt%. Melt-spun ( $\text{Bi}_{1.2}\text{Sr}_{1.2}\text{Ca}_{1.2}\text{Cu}_{1.4}$ ) $_{50}\text{Au}_{50-x}\text{Ag}_x$  (wt%) alloy ribbons of about 60  $\mu\text{m}$  thickness and about 2 mm width were prepared from mixed ingots in an argon atmosphere using a single-roller melt-spinning apparatus. Subsequently, the melt-spun Bi-Sr-Ca-Cu-Au-Ag alloy ribbons were heated in air for different periods at temperatures ranging from 773 to 1153 K. The structure of the as-quenched and annealed ribbons was

examined by X-ray diffractometry with monochromated Cu K $\alpha$  and optical microscopy. In addition, changes in the structure and weight of the alloy samples upon annealing in air were examined by differential thermal and thermogravimetric analyses (DTA and TGA). Resistivity measurement was made by the four-point method in a temperature range above 77 K.

As examples, Fig. 1 shows X-ray diffraction patterns of a melt-spun  $(\text{Bi}_{1.2}\text{Sr}_{1.2}\text{Ca}_{1.2}\text{Cu}_{1.4})_{50}\text{Au}_{50}$  alloy ribbon in as-quenched (a) and annealed state in air (b). The pattern (a) indicates that the melt-spun alloy ribbon has a mixed structure of fcc Au and unidentified nonequilibrium alloy phases, since no diffraction peaks corresponding to equilibrium metals and compounds are observed. On the contrary, most of the peaks for the annealed sample can be identified as an fcc Au phase with a lattice parameter of 0.407 nm and a pseudo-tetragonal phase with lattice parameters of  $a=b=0.382$  nm and  $c=3.062$  nm, as indexed in Fig. 1 (b). The lattice parameter of Au phase is nearly the same as that (0.40704 nm)[13] of pure Au and hence no distinct dissolution of the other constituent elements into Au phase takes place even after the long time annealing at high temperatures in air. Thus, the pseudo-tetragonal  $\text{BiSrCaCu}_2\text{O}_y$  phase with the same lattice parameters as those[14,15] for the oxide obtained by the conventional powder metallurgy method is produced as one of the main phases by oxidation of the melt-spun  $(\text{Bi}_{1.2}\text{Sr}_{1.2}\text{Ca}_{1.2}\text{Cu}_{1.4})_{50}\text{Au}_{50}$  alloy ribbon in air. Furthermore, it is seen in Fig. 1 (b) that the oxide phase has a highly oriented pseudo-tetragonal structure in which the surface of the ribbon is almost perpendicular to the [001] direction.

In order to clarify the distribution of each constituent phase in the as-quenched and annealed structures, optical microscopic observation was made for the ribbon samples. Figure 2 (a) and (b) show the cross-sectional structures of  $(\text{Bi}_{1.2}\text{Sr}_{1.2}\text{Ca}_{1.2}\text{Cu}_{1.4})_{50}\text{Au}_{50}$  ribbons in as-quenched and annealed (1148Kx3.6ks, 1138Kx172.8ks and 773Kx172.8ks) states. The dark and bright areas in the optical

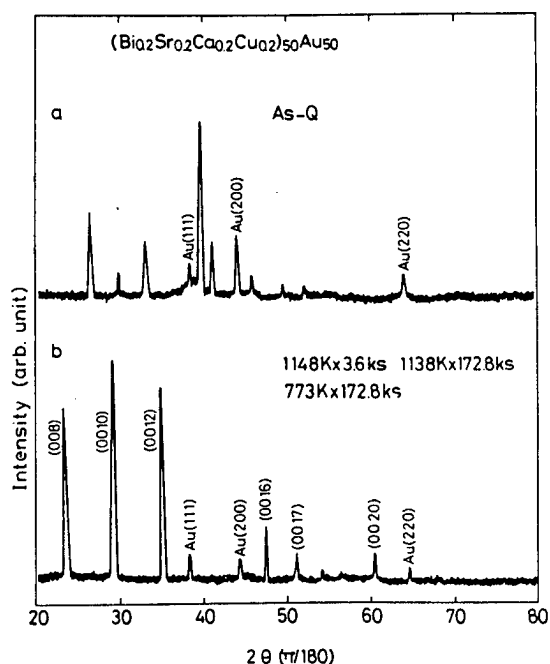


Fig. 1 X-ray diffraction patterns of a melt-spun  $(\text{Bi}_{1.2}\text{Sr}_{1.2}\text{Ca}_{1.2}\text{Cu}_{1.4})_{50}\text{Au}_{50}$  alloy ribbon. (a) as-quenched state, (b) annealed state of 1148Kx3.6ks, 1138Kx172.8ks and 773Kx172.8ks in air.

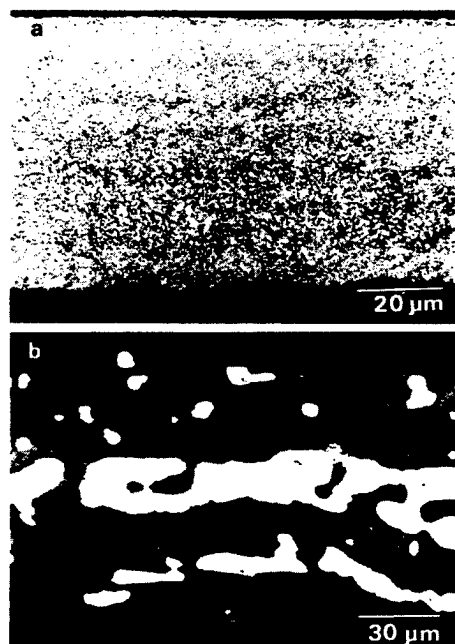


Fig. 2 Optical micrographs revealing the cross-sectional structure for a melt-spun  $(\text{Bi}_{1.2}\text{Sr}_{1.2}\text{Ca}_{1.2}\text{Cu}_{1.4})_{50}\text{Au}_{50}$  alloy ribbon. (a) as-quenched state, (b) annealed state of 1148Kx3.6ks, 1138Kx172.8ks and 773Kx172.8ks in air.



micrograph (b) correspond to  $\text{BiSrCaCu}_2\text{O}_y$  and Au phases, respectively. The as-quenched ribbon has a homogeneously mixed structure consisting of Bi-Sr-Ca-Cu alloy phase with a size of about 500 nm embedded in Au matrix. On the contrary, the annealing gives a distinctly distinguishable mixed structure in which the Au layer with a thickness of about 20  $\mu\text{m}$  lies near the central region in the ribbon sample and both the sides of the Au layer are occupied by the highly oriented oxide layers. The photograph (b) also indicates that the  $\text{BiSrCaCu}_2\text{O}_y$  phase connects continuously on a scale of about 20  $\mu\text{m}$  in thickness, revealing the steady formation of the superconducting circuit. The grain size of the Bi-Sr-Ca-Cu oxide was measured to be about 0.1  $\mu\text{m}$  from the optical micrographs of the ribbon surface. The distinct phase separation between the oxide and the Au phase as well as the development of the oriented oxide structure is probably because the annealing was made in a partially melted state of the oxide phase. The ribbon consisting of Bi-Sr-Ca-Cu oxide and Au produced by annealing in air has good flexibility and can be bent up to an angle near 180 degrees without fracture. The good flexibility is attributable to the formation of segregated Au layer in the central region of the ribbon sample. Detailed mechanism of the formation of the highly oriented structure by the present process is under investigation.

Figure 3 shows normalized electrical resistance ( $R/R_{130}$ ) as a function of temperature for the mixed materials of  $\text{BiSrCaCu}_2\text{O}_y$  and Au phases prepared by oxidation of the melt-spun  $(\text{Bi}_{1.2}\text{Sr}_{1.2}\text{Ca}_{1.2}\text{Cu}_{1.4})_{50}\text{Au}_{50-x}\text{Ag}_x$  alloy ribbons in the condition of 1148 K x 3.6 ks followed by 1138 K x 172.8 ks and then 773 K x 172.8 ks in air. With decreasing temperature, the resistance of the mixed materials with  $x=0$  and 10 wt% decreases significantly at the temperatures of 110 and 85 K and becomes zero at 81 K. Thus, the mixed materials exhibit a high- $T_c$  superconductivity with onset at 110 K and zero resistance at 81 K. It is also seen in Fig. 3 that the  $T_c$  value decreases significantly with increasing Ag content. The low  $T_c$  for the ribbons containing a larger amount of Ag is probably because the annealing temperature (773 K) at the third stage is too low to obtain an optimum superconducting property. On the basis of the result that the  $T_c$  value is strongly sensitive to annealing condition, further optimum annealing condition was searched for the  $(\text{Bi}_{1.2}\text{Sr}_{1.2}\text{Ca}_{1.2}\text{Cu}_{1.4})_{50}\text{Au}_{50}$  ribbon. As a result, a slight increase of annealing temperature was found to give an enhancement of superconductivity as shown in Fig. 4. As the temperature

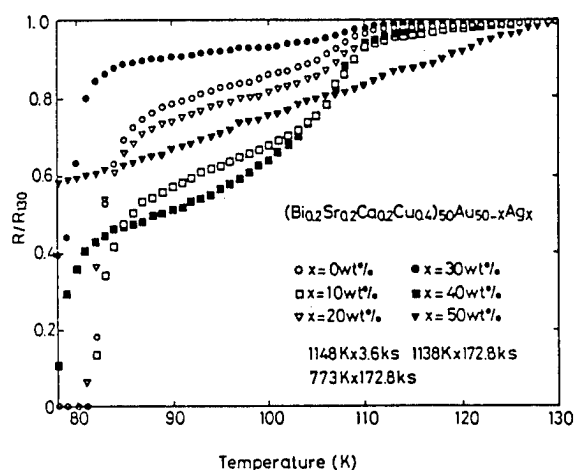


Fig. 3 Normalized electrical resistance  $R/R_{130}$  as a function of temperature for mixed materials of  $\text{BiSrCaCu}_2\text{O}_y$  and Au(Ag) prepared by annealing the melt-spun  $(\text{Bi}_{1.2}\text{Sr}_{1.2}\text{Ca}_{1.2}\text{Cu}_{1.4})_{50}\text{Au}_{50-x}\text{Ag}_x$  alloys in the condition of 1148Kx3.6ks followed by 1138Kx172.8ks and then 773Kx172.8ks in air.

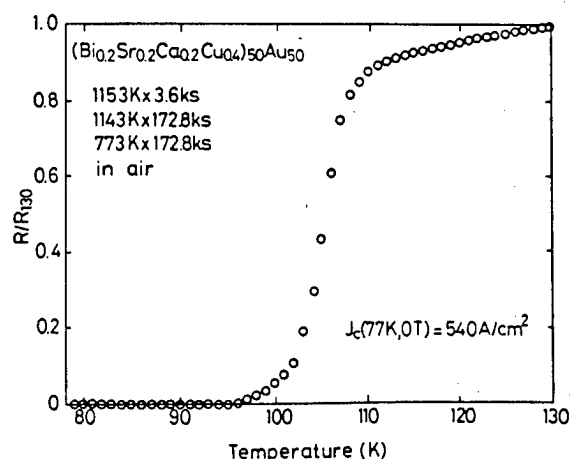


Fig. 4 Normalized electrical resistance  $R/R_{130}$  as a function of temperature for a mixed material of  $\text{BiSrCaCu}_2\text{O}_y$  and Au prepared by annealing the melt-spun  $(\text{Bi}_{1.2}\text{Sr}_{1.2}\text{Ca}_{1.2}\text{Cu}_{1.4})_{50}\text{Au}_{50}$  alloy in the condition of 1153Kx3.6ks followed by 1143Kx172.8ks and then 773Kx172.8ks in air.

decreases, the resistivity of the ribbon consisting of  $\text{BiSrCaCu}_2\text{O}_y$  and Au decreases gradually in a temperature range above 110 K, then rapidly in the vicinity of 105 K and becomes zero at 96 K. It was confirmed from the X-ray diffractometry that the increase of  $T_c$  is due to the increase of the volume fraction of the high- $T_c$  superconducting oxides[16] with lattice parameters of  $a=b=0.5396$  nm and  $c=3.7180$  nm. In addition, the critical current density of the ribbon with zero resistance at 96 K was measured to be  $540 \text{ A/cm}^2$  at 77 K in the absence of applied field. The  $J_c$  value evaluated only from the oxide phase except Au phase reaches about  $1000 \text{ A/cm}^2$ . The rather high  $J_c$  value is probably due to the formation of the highly oriented oxide phase shown in Fig. 1. Research of improving  $J_c$  value through further development of the oriented structure is in progress for the ribbon materials with the mixed structure. In any event the preparation of the mixed material consisting of oxide and Au phases by oxidation of the melt-spun alloy ribbon containing Au is notable as a simple method of producing a high- $T_c$  superconducting oxide tape with good flexibility and rather high  $J_c$  value even in the insoluble Bi-Sr-Ca-Cu alloy system.

In conclusion, the mixture of Au(Ag) into  $\text{BiSrCaCu}_2$  alloy enables us to produce a long ribbon with a mixed structure of Au(Ag) and nonequilibrium alloy phases by melt spinning even in the insoluble alloy system. The Au(Ag)-containing ribbons exhibit good flexibility and high stability against spontaneous oxidation and pulverization at room temperature in air. Subsequent annealing of the melt-spun alloy ribbon without Ag at high temperatures in air results in the mixed structure of Au and oriented  $\text{BiSrCaCu}_2\text{O}_y$  which exhibits high- $T_c$  superconductivity with onset at 110 K and zero resistance at 96 K as well as  $J_c$  of  $540 \text{ A/cm}^2$  at 77 K and zero field. The formation of segregated Au layer near the central region in the ribbon by annealing appears to play an important role in the achievement of the oriented structure and good flexibility for the superconducting ribbon. Production of a ductile superconducting tape exhibiting higher  $J_c$  values in a mixed state of oxide and Au is in progress utilizing the advantages resulting from the coexistent structure.

#### References

1. M.K. Wu, J.R. Ashburn, C.J. Torng, P.H. Hor, R.L. Meng, L. Gao, Z.J. Huang, Y.Q. Wang and C.W. Chu: Phys. Rev. Lett. 58(1987) 908.
2. S. Hikami, S. Kagoshima, S. Komiyama, J. Hirai, H. Minami and T. Masumi: Jpn. J. Appl. Phys. 26(1987) L347.
3. S. Ohshima and T. Wakiyama: Jpn. J. Appl. Phys. 26(1987) L815.
4. H. Maeda, Y. Tanaka, M. Fukutomi and T. Asano: Jpn. J. Appl. Phys. 27(1988) L209.
5. Z.Z. Sheng and A.M. Hermann: Nature 332(1988) 138.
6. K. Matsuzaki, A. Inoue, H.M. Kimura, K. Moroishi and T. Masumoto: Jpn. J. Appl. Phys. 26(1987) L334.
7. K. Matsuzaki, A. Inoue, H.M. Kimura, K. Aoki and T. Masumoto: Jpn. J. Appl. Phys. 26(1987) L1310.
8. K. Matsuzaki, A. Inoue, H.M. Kimura and T. Masumoto: Jpn. J. Appl. Phys. 26(1987) 11610.
9. K. Matsuzaki, A. Inoue, H.M. Kimura, and T. Masumoto: Jpn. J. Appl. Phys. 26(1987) L1384.
10. K. Matsuzaki, A. Inoue and T. Masumoto: Jpn. J. Appl. Phys. 27(1988) L195.
11. K. Matsuzaki, A. Inoue and T. Masumoto: Int. Meeting on Advanced Materials, Materials Research Society, Tokyo, June 1988, in press.
12. T.B. Massalski: Binary Phase Diagrams, American Society for Metals, Ohio, 1986, p.498.
13. W.B. Pearson: Handbook of Lattice Spacing and Structures of Metals and Alloys, Pergamon Press, London, 1958, p.124.
14. E.T. Muromachi, Y. Uchida, A. Ono, F. Izumi, M. Onoda, Y. Matsui, K. Kosuda, S. Takekawa and K. Kato: Jpn. J. Appl. Phys. 27(1988) L365.
15. Y. Syono, K. Hiraga, N. Kobayashi, M. Kikuchi, K. Kusuda, T. Kajitani, D. Shindo, S. Hosoya, A. Tokiwa, S. Terada and Y. Muto: Jpn. J. Appl. Phys. 27(1988) L569.
16. S. Koyama, U. Endo and T. Kawai: Jpn. J. Appl. Phys. 27(1988) L1861.

Low Temperature Formation of Bi(Pb)-Sr-Ca-Cu-O Thin Films by a  
Successive Deposition Method with Excimer Laser

Tomoji KAWAI, Masaki KANAI and Shichio KAWAI  
The Institute of Scientific and Industrial Research,  
Osaka University, Mihogaoka, Ibaraki, Osaka 567 Japan

Crystallized as-grown Bi(Pb)-Sr-Ca-Cu-O thin films are formed by laser ablation method at the substrate temperature as low as 480 °C under N<sub>2</sub>O gas flow. The as-grown thin film which has a crystal structure consisting of four or five Cu-O<sub>2</sub> layers between adjacent Bi<sub>2</sub>O<sub>2</sub> layers can be formed by combination of N<sub>2</sub>O gas flow and "successive deposition method" with excimer laser pulses.

We have prepared thin films of Bi-Sr-Ca-Cu-O (BSCCO) and Bi(Pb)-Sr-Ca-Cu-O (BPSCCO) by laser ablation[1,2] under N<sub>2</sub>O gas flow, and have succeeded in the formation of crystallized as-grown thin films at the substrate temperature as low as 480 °C. The films were prepared by a "successive deposition method" using multi-targets. The application of the successive deposition method to the controlling of the number of Cu-O<sub>2</sub> layers in the BSCCO film was tried with a multi-target magnetron sputtering method[3] at 650 °C. We have tried to control the structure of the Bi based superconducting films by the successive deposition method at lower substrate temperatures with laser ablation using activated oxygen from N<sub>2</sub>O. By this technique, we have formed as-grown Bi(Pb)-Sr-Ca-Cu-O film containing one to five Cu-O<sub>2</sub> layers at 480 °C.

The films are formed on a MgO(100) substrate using pulses of ArF excimer laser(193nm) focused on the target placed on the opposite side of the substrate. Pellets of Bi<sub>2</sub>O<sub>3</sub>, SrCuO<sub>y</sub> and CaCuO<sub>y</sub> were used as targets for BSCCO films, and those of Bi<sub>7</sub>Pb<sub>3</sub>O<sub>y</sub>, SrCuO<sub>y</sub> and CaCuO<sub>y</sub> for BPSCCO films. Film deposition was carried out successively from Bi<sub>2</sub>O<sub>3</sub> or Bi<sub>7</sub>Pb<sub>3</sub>O<sub>y</sub> for 20 sec with 7 Hz repetition rate, SrCuO<sub>y</sub> for 10sec, CaCuO<sub>y</sub> varying length of time and SrCuO<sub>y</sub> for 10 sec that consist of one cycle. The deposition time for CaCuO<sub>y</sub> was changed between 50 sec and 90 sec in order to prepare the films with different numbers of Cu-O<sub>2</sub> layers. The samples were prepared with 20 - 30 cycles to form 600 - 800 Å thickness under oxygen or N<sub>2</sub>O gas flow maintaining pressure of 10<sup>-1</sup> to 1 torr.

As-grown films of BSCCO with 700 Å thickness as obtained from 20-cycle deposition under O<sub>2</sub> atmosphere had very weak and broad X-ray diffraction peaks when the substrate temperature was 600 °C. The films formed at lower substrate temperature were amorphous. These results indicated that the crystallization of the as-grown film did not occur or hardly proceeded in those temperature regions under oxygen atmosphere. At higher substrate temperatures(>600 °C), the diffraction peaks of impurity phase attributable to Bi(Sr,Ca)O<sub>y</sub> grew and the peaks of BSCCO phase did not become larger. Therefore, a crystallized as-grown film was not obtained under these conditions. A weak and

wide diffraction peak at  $2\theta = 4^\circ - 6^\circ$  corresponding to 002 of BSCCO system, however, was shifted towards lower angles with increase in the deposition time of  $\text{CaCuO}_y$  in the cycle. This shift of the peak position indicates that the precursor of BSCCO compound was already formed in the as-grown film and the lattice constant of the c-axis of that precursor became longer with increasing of the deposition time of  $\text{CaCuO}_y$ . Therefore,  $\text{O}_2$  atmosphere during deposition is not adequate enough to form a crystallized as-grown film below 600 C, but sintering procedure at high temperature is needed.

In order to obtain crystallized as-grown films at lower temperatures and to control the number of  $\text{Cu-O}_2$  layers in the structure, much stronger oxidizing agent of  $\text{N}_2\text{O}$  was used instead of  $\text{O}_2$  gas. As the Pb doping for this system is known to facilitate the formation of high  $T_c$  phase, BPSCCO films are prepared by the same successive deposition method using  $\text{Bi}_7\text{Pb}_3\text{O}_y$ ,  $\text{SrCuO}_y$ ,  $\text{CaCuO}_y$  targets at  $520^\circ\text{C}$ . Fig.1 shows the change of the X-ray diffraction patterns of these as-grown BPSCCO films against the deposition time of  $\text{CaCuO}_y$ . These films had a thickness of 600 - 800 Å after 20 - 30 cycle deposition. The indication of the diffraction patterns in Fig.1 is that, when the deposition time of  $\text{CaCuO}_y$  was short, the film had diffraction peaks due to 80K phase(double  $\text{Cu-O}_2$  layers), its lattice constant c being 30.6 Å.(Fig.1 (a))

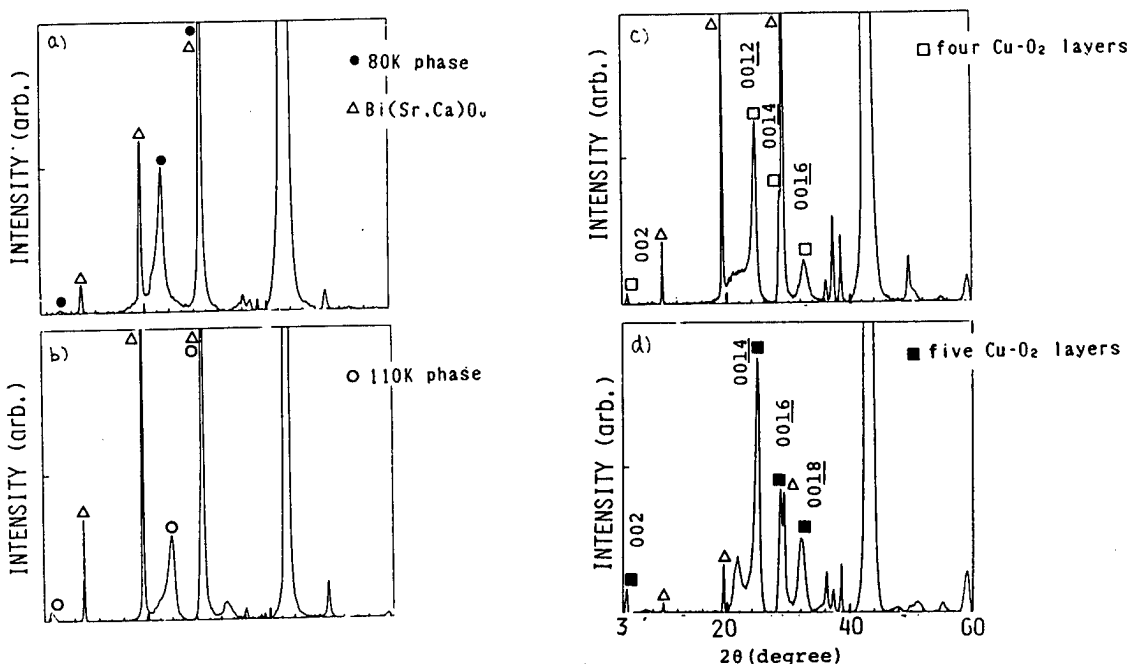


Fig.1 The change of the X-ray diffraction patterns of Bi-Pb-Sr-Ca-Cu-O as-grown films at  $520^\circ\text{C}$  under  $\text{N}_2\text{O}$  gas flow with the change of the deposition time of  $\text{CaCuO}_y$  in a cycle. The deposition time for  $\text{CaCuO}_y$  was (a) 60sec (b) 70 sec (c) 75 sec (d) 90 sec

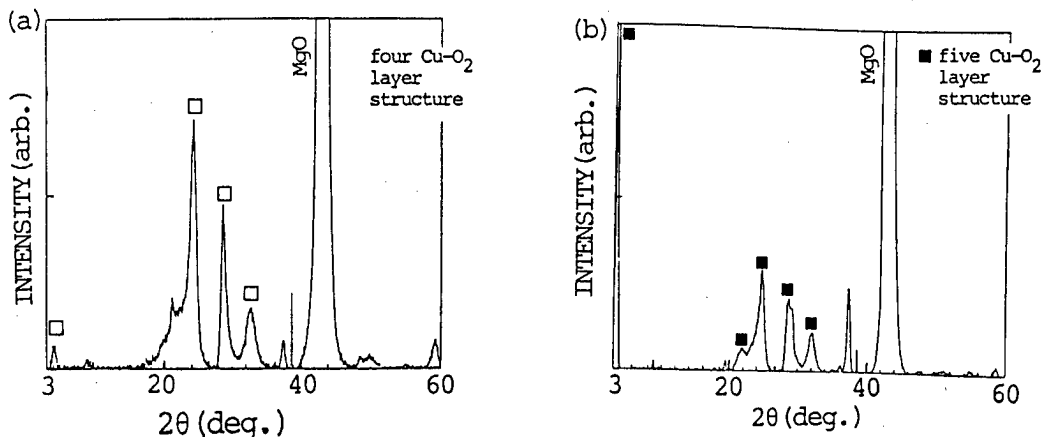


Fig.2 The X-ray diffraction patterns of Bi(Pb)-Sr-Ca-Cu-O as-grown films at 480°C.  
 (a) The lattice constant  $c$  is 43.5Å corresponding to four Cu-O<sub>2</sub> layer structure.  
 (b) The lattice constant  $c$  is 50.0Å corresponding to five Cu-O<sub>2</sub> layer structure.

As the deposition time of  $\text{CaCuO}_y$  increases, the lattice constant  $c$  becomes longer and 110K phase with triple Cu-O<sub>2</sub> layers appears whose  $c$ -axis length is 37.3Å. (Fig.1 (b)) The phase having lattice constant larger than 37Å was obtained in the region of longer deposition time of  $\text{CaCuO}_y$ . (Fig.1 (c,d)) The lattice constants  $c$  of these phases calculated on the basis of the indices shown in Fig.1 (c,d) were 43.5Å and 50.0Å. These values correspond to the lattice constant of the structures having four Cu-O<sub>2</sub> layers and five Cu-O<sub>2</sub> layers, respectively, between adjacent  $\text{Bi}_2\text{O}_2$  layers. Thus, we believe that not only one to three Cu-O<sub>2</sub> layer structures but also four and five Cu-O<sub>2</sub> layer structures with the  $c$ -axis oriented perpendicular to the substrate surface was achieved in these films. These results show that the number of Cu-O<sub>2</sub> layers even in the as-grown films made at 520 °C could be controlled. The diffraction peaks of these phases, however, shows that the films contained some impurity phase, such as  $\text{Bi}(\text{Sr,Ca})\text{O}_y$ . The film formation at lower temperatures was quite effective in reducing the impurity phase. In the X-ray diffraction pattern of the film containing 4 and 5 Cu-O<sub>2</sub> layers as prepared at substrate temperature of 480 °C (Fig.2 (a,b)), the  $\text{Bi}(\text{Sr,Ca})\text{O}_y$  was not seen though the peaks of BPSCCO became a little bit weaker.

In summary, the numbers of Cu-O<sub>2</sub> layers in Bi(Pb)-Sr-Ca-Cu-O can be controlled by successive deposition method using a laser ablation of multi-target. In BPSCCO as-grown films, the structure having large lattice constant of  $c$ -axis corresponding to four and five Cu-O<sub>2</sub> layer structure ( $c = 43\text{Å}, 50\text{Å}$ ) can be formed even at 480 °C by this method. During the laser ablation, the introduction of dinitrogen monoxide ( $\text{N}_2\text{O}$ ) gas definitely enhances the crystallization of the as-grown films, allowing the diffraction peaks of BPSCCO phase to be seen in the as-grown films even at the substrate temperature of 480 °C. We expect that  $\text{N}_2\text{O}$  gas may be effective in a film formation of other high- $T_c$  superconductors at lower temperature.

- 1) M.Kanai, T.Kawai, M.Kawai, and S.Kawai, Jpn.J.Appl.Phys. **27** (1988) L1293, **27**,2001 (1988).
- 2) H.Tabata, T.Kawai, M.Kanai, O.Murata, and S.Kawai, Jpn.J.Appl.Phys, to be published
- 3) H.Adachi, S.Kohiki, K.Setsune, T.Mithuyu, and K.Wasa, Jpn. J. Appl. Phys, **27** (1988) L1883

# Ba<sub>1-x</sub>K<sub>x</sub>BiO<sub>3</sub> THIN FILM PREPARATION WITH ECR ION BEAM OXIDATION, AND THEIR PROPERTIES

Toshiaki MURAKAMI, Youichi ENOMOTO, and Kazuyuki MORIWAKI

NTT OPTO-ELECTRONICS LABORATORIES  
TOKAI-MURA, IBARAKI-KEN 319-11, JAPAN

## ABSTRACT

Ba<sub>1-x</sub>K<sub>x</sub>BiO<sub>3</sub> thin films were epitaxially deposited on MgO substrates using an ECR-type oxygen ion source. As-grown films showed superconductivity, when substrate temperature was about 500°C and x values were 0.3 to 0.4. Lattice constants, superconductivity, and optical reflection were measured.

## INTRODUCTION

All the Cu-based high T<sub>c</sub> oxide superconductors have Cu-O layered crystal structures and many researchers attribute the high T<sub>c</sub> to those structures. Because of the layered structures, oxide superconductors have large anisotropies and very short coherence lengths along their c-axes. On the contrary, Ba<sub>1-x</sub>K<sub>x</sub>BiO<sub>3</sub> (BKBO) exhibits a maximum T<sub>c</sub> of 30 K in spite of having a cubic symmetry.<sup>(1-4)</sup> This fact brings about another possibility in the development of high T<sub>c</sub> materials. Further, the coherence length becomes isotropic and this is effective in device application.

However, the preparation of BKBO samples requires complicated processes involving sintering at a high temperature in a reduced atmosphere and a short time oxidation at a low temperature. These processes leave oxygen defects and non-uniform in K-ion distribution in the samples and such structural imperfections impair electrical properties.

This paper describes the preparation and properties of BKBO thin films using the reactive evaporation assisted by ECR ion beam oxidation. This method allows easier introduction of K ions into films together with other constituents. We succeeded in obtaining superconducting as-grown BKBO films.

## EXPERIMENTS AND RESULTS

The system involves three K-cells for metal sources and the ECR (Electron

Cyclotron Resonance) ion source, reported in our previous paper.<sup>(5)</sup> Based pressure in the vacuum chamber was reduced to

10<sup>-4</sup> Pa with a diffusion pump. The oxygen beam was bombarded onto a substrate simultaneously with three evaporated beams to form oxide films. The ECR ion beam was introduced through an outlet 10 cm in diameter and was accelerated by bias voltage of 50 V. The ion current density was monitored by Faraday cups. The maximum ion current density was 300 mA/cm<sup>2</sup> using oxygen flowing at 3 SCCM and neutralized to 50 mA/cm<sup>2</sup> with a filament heater. When the ion beam was not neutralized or the gas flow was less than the above value, as-grown films could not become superconducting. Granular metals of Ba, K and Bi were used as metal sources. Metal composition in the film was adjusted by controlling each evaporation rate. Typical preparation conditions are listed in Tables 1 and 2.

BKBO thin films were deposited on (100) MgO and (110) SrTiO<sub>3</sub> substrates at 500°C.

Table 1 Typical evaporation conditions

	deposition rate	k-cell Temp.
K	10 Å/sec	150 °C
Ba	3	650
Bi	5	500
BKBO	3 Å/sec	

Table 2 Typical oxydation conditions

Ion energy	50 eV
Ion current density	150 $\mu\text{A}/\text{cm}^2$
	(before neutralization)
	50 $\mu\text{A}/\text{cm}^2$
	(after neutralization)
Substrate temp.	500 °C

In both cases, the films grew epitaxially on the substrates. However, when the composition was about  $x = 0.2$ , cracks often arose in films. The reason is not clear at present.

The x-ray pattern of a BKBO film on (001) MgO is shown in Figure 1. Small peaks of other orientations were recognized, although the mismatch of the lattice constants is small (1.2%). In the case of  $\text{SrTiO}_3$ , no such peaks were detected in spite of a large lattice constant mismatch of 11% against the substrate, because both are of perovskite-type.

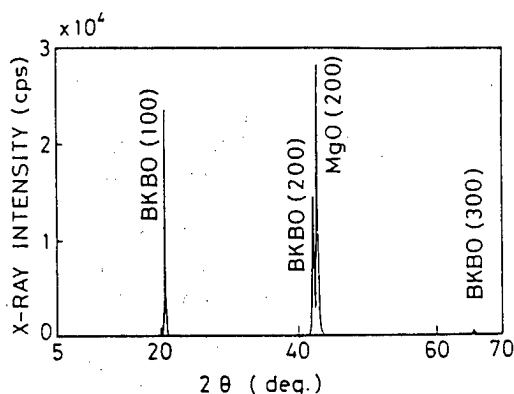


Fig.1 x-ray diffraction pattern of a BKBO film on (100) MgO.

Figure 2 shows the K/Bi dependence of the lattice constant. The lattice constant decreases with increases in K/Bi ratio below about 0.4 - similar to the result of Hinks and coworkers<sup>(3)</sup>, but it increases above 0.4. The films of  $x = 0.25$  to 0.4 became superconducting.

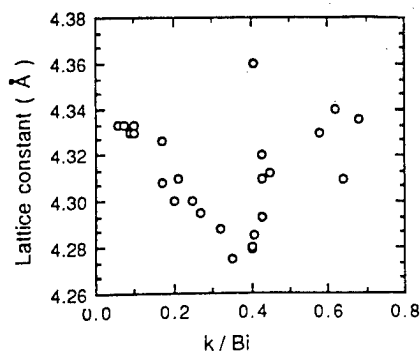


Fig.2 Lattice constant change due to K/Bi ratio.

Figure 3 indicates temperature dependences of the magnetic moment at 40 G of an as-grown film the K/Bi ratio of which is about 0.35. The sample thickness was about 500 nm and the area  $2 \times 3 \text{ mm}^2$ . The moment was somewhat reduced by annealing for two hours at 400 °C in an oxygen flow.

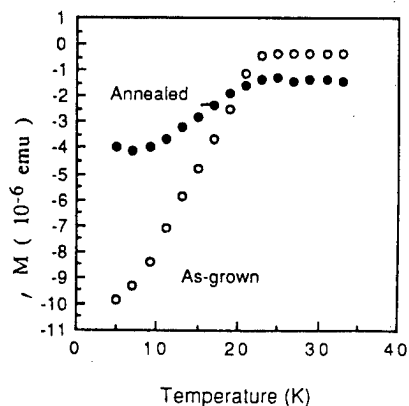


Fig.3 Temperature dependence of the magnetic moment of a BKBO film.

The K/Bi ratio is 0.35, the thickness about 500 nm, and the area  $2 \times 3 \text{ mm}^2$ .

In Fig. 4, the change in  $H_{c1}$  of the same sample as in Fig.3 is plotted against temperature, compared with the data of Batlogg and coworkers.<sup>(2)</sup> The data agree very well.

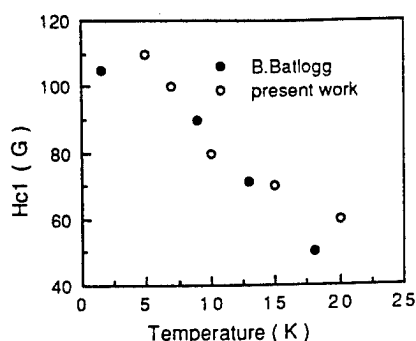


Fig.4 Temperature change of  $H_{c1}$ .  
The film is the same as that in Fig.3.

In Fig. 5, the optical reflection of a BKBO film is shown together with the data of a BPBO (by Tajima and coworkers<sup>(6)</sup>). A theoretical curve of the BKBO film was calculated using the same value as in the BPBO sample. The plasma frequency of the BKBO film is about 700 nm, while that of the BPBO sample is about 880 nm. The shorter wavelength may indicate an increase in carrier density.

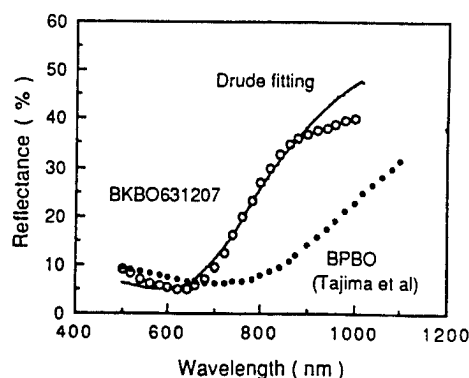


Fig.5 Optical reflectance of a BKBO film, compared with a BPBO film ( by Tajima et al )

## CONCLUSION

BKBO thin films grew epitaxially on (001) MgO and (110) SrTiO<sub>3</sub> substrates by using a reactive deposition system with an ECR-type oxygen ion source. The lattice constant agreed with the data reported, but showed an increase above  $x = 0.4$ . The superconducting properties agreed with the data reported so far. The optical reflection showed a plasma wavelength of about 700 nm. The shorter wavelength may indicate an increase in carrier density.

## ACKNOWLEDGEMENT

The authors wish to thank Y. Katayama, T. Inamura for encouragement and also to extend thanks to A. Yamaji for his helpful discussion.

## REFERENCE

1. L. F. Mattheiss, E. M. Gyorgy, and D. W. Johnson, Jr., Phys. Rev. B 37, 3745 (1988).
2. B. Batlogg, R. J. Cava, L. W. Rupp, Jr., A. M. Mulsce, J. J. Krajewski, J. P. Remeika, W. F. Peck, Jr., A. S. Cooper, and G. P. Espinosa, Phys. Rev. Lett. 61, 1670 (1988).
3. D. G. Hinks, B. Dabrowski, J. Jorgensen, A. W. Mitchell, D. R. Richards, Shiyong Pei and Donglu Shi, Nature 33, 836 (1988).
4. S. Jin, T. H. Tiefel, R. C. Sherwood, A. P. Ramirez, E. M. Gyorgy, G. W. Kammlott, and R. A. Fastnacht, Appl. Phys. Lett. 53, 1116 (1988).
5. K. Moriwaki, Y. Enomoto, S. Kubo, and T. Murakami, Jpn. J. Appl. Phys. 27, L2075 (1988).
6. S. Tajima, S. Uchida, A. Masaki, H. Takagi, K. Kitazawa and S. Tanaka, Phys. Rev. B 32, 6302 (1985).



## Preparation and Characterization of High Temperature Oxide Superconductor Films

Y. Maruyama, Y. Kawai, T. Terui, and T. Inabe

Institute for Molecular Science, Myodaiji, Okazaki, Aichi 444, Japan

Thin films of  $\text{YBa}_{2.1}\text{Cu}_{2.9}\text{O}_y$  and  $\text{Bi}_{2.3}\text{Sr}_{2.0}\text{CaCu}_{1.9}\text{O}_y$  have been prepared by RF-magnetron sputtering with using simple targets which are composed of mixed powder of each component oxide material. Both films show high c-axis orientation and superconductivity as deposited condition. A tunneling spectroscopic study has also revealed the superconducting parameters, such as gap energy,  $2\Delta$ , of both films.

Since the discovery of high- $T_c$  superconductivity of cuprate systems, a lot of studies of thin film preparation and analysis have been carried out from the view points of basic research and application. Our first motivation for this work as a basic research is to realize some new phases in thin films which are difficult or impossible to obtain in bulk specimens. Such new phases or materials could lead us to a higher  $T_c$  or different type superconductor, and also probably to a deeper understanding on the superconducting mechanisms. Thin film technique is very suitable for not only stabilization of meta-stable phases but also creation of new materials by a fine control of deposition conditions, especially in the case of multi-source evaporation. For this purpose, it is essential to prepare films without any post-heat treatment. As the first step of this line of study we have succeeded in the preparation of as-deposited superconducting films of Y-Ba-Cu-O and Bi-Sr-Ca-Cu-O systems with the use of an RF-magnetron mono-source (target) sputtering technique.

Thin films were prepared on (100)MgO and (100)SrTiO<sub>3</sub> single-crystal substrates (17 mm  $\times$  1 mm) by an RF-magnetron sputtering technique. Targets were made by mixing of the component powders ( $\text{Y}_2\text{O}_3$ (99.99%),  $\text{BaCO}_3$ (99.99%) and  $\text{CuO}$ (99.99%) for Y-Ba-Cu-O system,  $\text{Bi}_2\text{O}_3$ (99.9%),  $\text{SrCO}_3$ (99.99%),  $\text{CaCO}_3$ (99.99%) and  $\text{CuO}$ (99.99%) for Bi-Sr-Ca-Cu-O system) and then pressing into discs (100 mm  $\times$  4 mm). The distance, D, between target and substrate in the sputtering vessel was selected as 37 mm or 40 mm. The substrate was heated by a kanthal wire heater during deposition, and was cooled spontaneously in the bell-jar with oxygen atmosphere as soon as the deposition was finished. Table 1 shows the typical sputtering conditions. With a deposition of 6 hrs, thin films of about 8000 Å thick were obtained for the Y-Ba-Cu-O system and 5000 Å thick for the Bi-Sr-Ca-Cu-O system.

The crystal structures and the compositions of the films were analyzed by XRD (X-ray diffractometry) and ICP (Inductively Coupled Plasma) emission spectroscopy, respectively. Electrical resistivities were measured by a conventional four probe method. Tunneling current-voltage characteristics were observed with the use of plane-contact type cells without any insertion of insulating film between electrode (Au) and superconducting film.

### YBa<sub>2</sub>Cu<sub>3</sub>O films

Figure 1 shows the substrate temperature dependence of the elemental composition of the films. The compositions are not so sensitive to the substrate temperature in the range from 640°C to 680°C. The YBa<sub>2</sub>Cu<sub>3</sub>O<sub>y</sub> phase appeared above a substrate temperature of 640°C, and its preferential orientation of the c-axis in the film became more prominent with increasing substrate temperature (Fig. 2).

TABLE 1  
typical sputtering conditions

System	$\text{YBa}_2\text{Cu}_3\text{O}_y$	$\text{Bi}_2\text{Sr}_2\text{CaCu}_2\text{O}_y$
Target	Mixed powder of $\text{Y}_2\text{O}_3$ , $\text{BaCO}_3$ and $\text{CuO}$ (Y:Ba:Cu=1:3:10)	Mixed powder of $\text{Bi}_2\text{O}_3$ , $\text{SrCO}_3$ , $\text{CaCO}_3$ and $\text{CuO}$ (Bi:Sr:Ca:Cu=3.3:1.9:1:1.8)
Substrate	(100) $\text{SrTiO}_3$	(100) $\text{MgO}$
Sputtering gas	$\text{Ar}:\text{O}_2=1:1$	$\text{Ar}:\text{O}_2=1:1$
Gas pressure	1 Pa	1 Pa
RF-power	150 W	150 W
Substrate temperature	660-670 °C	555-565 °C
Sputtering time	6 hrs.	6 hrs.
Growth rate	1300 Å/hr.	900 Å/hr.

Superconductivity only appeared in the case of  $D = 40$  mm ( $T_c^{\text{onset}} = 89$  K,  $T_c^{\text{zero}} = 77$  K as shown in Fig. 3). The films deposited with  $D = 37$  mm did not show any superconductivity, and this may be caused by lack of oxygen in the films judging from the lattice parameters estimated from XRD ( $C_0 = 11.68$  Å and  $11.74$  Å for  $D = 40$  mm and  $37$  mm, respectively). We have tried to obtain a superconducting film in the case of  $D = 37$  mm, but it is not successful so far, even though the sputtering conditions have been changed in order to increase the contents of oxygen in the films. From the results mentioned above, it may be said that the contents of oxygen in the film are very sensitive to the distance between target and substrate.

The tunneling spectra of the film which showed superconductivity (Fig. 3) are shown in Fig. 4. From these spectra, we can roughly estimate the superconducting gap,  $2\Delta$ , to be 30 meV, which leads to about 90 K for  $T_c$  if we assume the BCS ratio,  $2\Delta/k_B T_c$ , is 3.5 - 4.0.

#### $\text{Bi}_2\text{Sr}_2\text{CaCu}_2\text{O}_y$ films

It has been said that there are two superconductive phases,  $\text{Bi}_2\text{Sr}_2\text{CaCu}_2\text{O}_y$  (low phase:  $T_c \sim 80$  K) and  $\text{Bi}_2\text{Sr}_2\text{Ca}_2\text{Cu}_3\text{O}_y$  (high phase:  $T_c \sim 120$  K), in the Bi-Sr-Ca-Cu-O system. An as-deposited low phase film was prepared by proper adjustment of the sputtering conditions (Table 1). The composition of the film was estimated to be  $\text{Bi}_{2.3}\text{Sr}_{2.0}\text{CaCu}_{1.9}\text{O}_y$  by ICP analysis. The X-ray diffraction pattern in Fig. 5 indicates that it is a highly oriented crystalline film ( $C_0 = 30.7$  Å). The critical temperature for zero resistivity was 31 K as shown in Fig. 6 (Curve A). In this system, however, a same composition film prepared under the same condition showed a different behavior in the resistivity as shown in Fig. 6, curve B. This fact means that the film is still in multi-phase structure. Tunneling characteristic curves for the films of curve B are shown in different voltage ranges (Fig. 7). We can recognize multi-gap structure in these spectra, and assign them to  $2\Delta \sim 5$  meV,  $\sim 20$  meV and  $\sim 80$  meV. The former two gaps may correspond to  $\sim 16$  K and  $\sim 70$  K, respectively. The origin of the largest one,  $\sim 80$  meV, is not yet clear.

As a trial for the stabilization of a meta- or un-stable phase, we pursued to change the relative contents of Ca in  $\text{Bi}_2\text{Sr}_2\text{Ca}_x\text{Cu}_{1+x}\text{O}_y$  phase from  $x = 1$  to 2. With increasing  $x$ , X-ray diffraction lines corresponding to  $\text{Bi}_2\text{Sr}_2\text{Ca}_2\text{Cu}_3\text{O}_y$  phase were growing. At  $x = 2$ , whole X-ray pattern, however, changed to quite different pattern. Thus, we have not yet succeeded in the fixing of the high  $T_c$ -phase of Bi-Sr-Ca-Cu-O system.

In summary, we have succeeded in the preparation of as-deposited superconducting Y-Ba-Cu-O and Bi-

Sr-Ca-Cu-O thin films by establishing the most favorable sputtering conditions. Especially, it seems to be very crucial to adjust the proper distance between target and substrate to obtain superconducting films with as-deposited condition. Electrical conductivity and tunneling current measurements have somewhat revealed the superconducting character of the prepared films.

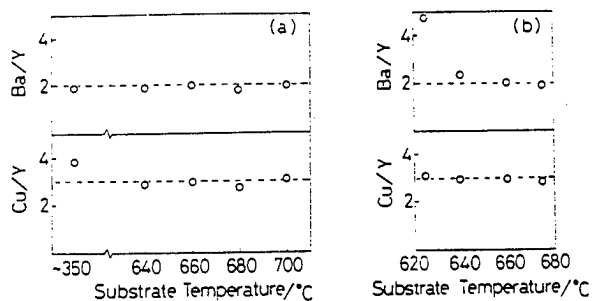


Fig. 1. Film composition-substrate temperature. (a) Y:Ba:Cu=1:2:3.5 target, D=37 mm, (b) Y:Ba:Cu=1:3:10 target, D=40 mm.

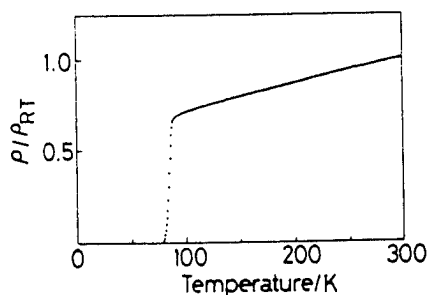


Fig. 3.  $P/P_{R.T.}$  YBa<sub>2.1</sub>Cu<sub>2.9</sub>O<sub>y</sub> as-deposited film.

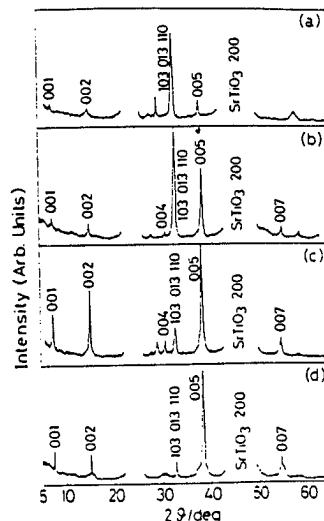


Fig. 2.

X-ray diffraction pattern of Y-Ba-Cu-O as-deposited films. (a)  $T_s=640$  C,  $D=40$  mm, (b)  $T_s=660$  C,  $D=40$  mm, (c)  $T_s=680$  C,  $D=40$  mm, (d)  $T_s=680$  C,  $D=37$  mm ( $T_s$ : substrate temperature).

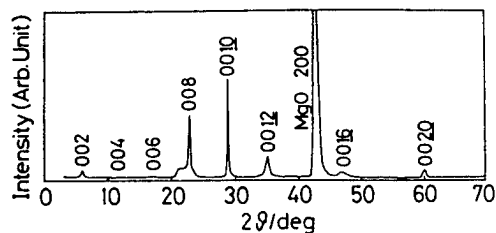


Fig. 5. X-ray diffraction pattern of Bi<sub>2.3</sub>Sr<sub>2.0</sub>CaCu<sub>1.9</sub>O<sub>y</sub> film.

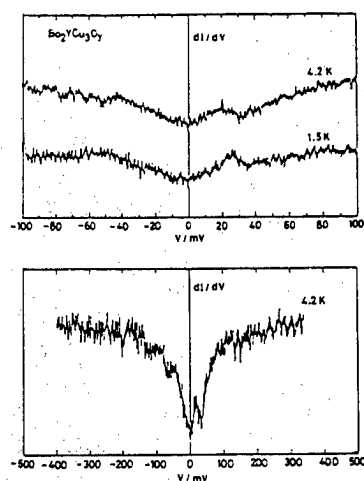


Fig. 4.

Tunneling spectra for YBa<sub>2.1</sub>Cu<sub>1.9</sub>O<sub>y</sub> film.

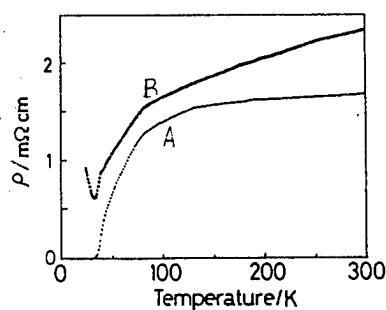


Fig. 6.

$P$  for Bi<sub>2.3</sub>Sr<sub>2.0</sub>CaCu<sub>1.9</sub>O<sub>y</sub> as-deposited film.

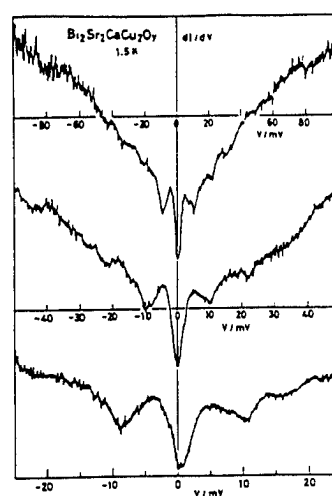


Fig. 7.

Tunneling spectra for Bi<sub>2.3</sub>Sr<sub>2.0</sub>CaCu<sub>1.9</sub>O<sub>y</sub> film.

Single crystal growth of superconducting oxides and related compounds by the flux and floating zone methods

T. Shishido, N. Toyota, K. Ukei, D. Shindo, T. Sasaki, Y. Saito  
and

S. Hosoya, H. Iwasaki, T. Kujitani, H. Yamauchi  
and  
T. Fukuda

Institute for Materials Research, Tohoku University, Katahira 2-1-1,  
Sendai, Japan

Abstract

Growth of single crystals of YBCO, BSCCO, LNBCPO were performed by the flux method using CuO and KCl as a solvent. Large single crystals of  $\text{La}_2\text{MO}_4$  ( $\text{M}=\text{Ni}, \text{Co}, \text{Cu}$ ; with and without Sr) were grown by the floating zone method, applying travelling solvent technique under the condition of controlled oxygen fugacity. The obtained crystals of BSCCO ( $\sim 3 \times 3 \times 0.03 \text{ mm}^3$ ) exhibited superconducting transition at 89 K ( $T_c$  off). New compounds LNBCPO ( $\sim 1 \times 0.3 \times 0.3 \text{ mm}^3$ ) having characteristic zig-zag chains composed of Cu, O and Pt have been found. Fundamental electrical and magnetic properties on these crystals have been investigated.

In order to elucidate the superconducting mechanism, single crystals with high quality and large dimension are essentially required. Furthermore, it is also important to crystallize the related compounds around the superconducting oxides. Almost all the copper-complex superconducting oxides known so far are regarded as incongruent melting compounds at least in air. Therefore appropriate technique such as Flux, TSFZ are employed for the growth of the single crystals. In this report we describe single crystal growth of the superconducting oxides and related compounds by the flux and floating zone methods.

1) Flux Growth

1-1 BSCCO

There have been reported that single crystals of BSCCO have been grown by the flux method using CuO or KCl as a solvent in the Bi-Sr-Ca-Cu-O system.<sup>1,2)</sup> However, the quality of the crystal seems to be not fully sufficient for some measurements. Therefore it is necessary to investigate the growth conditions in more detail. We used specially prepared solute calcined at temperatures below 500 °C as a precursor.<sup>3)</sup> The solvation of this solute to the KCl solvent proceeded very smoothly and the numerous nucleation caused by the insoluble mass was prevented. A solute was prepared from 1 mole of  $\text{Bi}(\text{NO}_3)_3 \cdot 5\text{H}_2\text{O}$  (99.9%), 1 mole of  $\text{Sr}(\text{NO}_3)_2$  (99.9%), 1 mole of  $\text{Ca}(\text{NO}_3)_2 \cdot 4\text{H}_2\text{O}$  (99% up) and 2 moles of  $\text{Cu}(\text{NO}_3)_2 \cdot 3\text{H}_2\text{O}$  (99.9%). These four reagents were dissolved in pure water and stirred to mix well each other. After water was excluded by heating, the resultant residue was heated furthermore up to 500 °C in air and kept for 20 h at that temperature in order to calcine. This low calcined material was used as a solute for the following crystal growth experiments. In a typical experiment, a 30 wt% mixture of the solute in KCl was heated to 900 °C at 300 °C h<sup>-1</sup>, kept at that temperature for 3 h, and then cooled at 5 °C h<sup>-1</sup> to 760 °C. As shown in Fig. 1, black lustering thin plates



Fig.1  $\text{Bi}_2(\text{Sr}, \text{Ca})_3\text{Cu}_2\text{O}_x$  single crystal

(maximum size  $3 \times 3 \times 0.03 \text{ mm}^3$ ) having smooth surface were typically extracted from the KCl flux. The composition of crystals was determined to be in the vicinity of  $\text{Bi}_2(\text{Sr,Ca})_3\text{Cu}_2\text{O}_x$  by an EDX analyser. Resistivity measurements by DC four points method confirmed that the crystal exhibited superconductivity at 89 K ( $T_c$  off) as shown in Fig.2.

1-2  $\text{R}_2\text{Ba}_2(\text{Cu,Pt})_2\text{O}_8$  (R=Ho, Er and Y)

New compounds in the quaternary oxide system,  $\text{Ln-Ba-Cu-Pt-O}$ , were found out. <sup>4,5,6,7</sup> Single crystals were grown using a sintered oxides  $\text{LnBa}_2\text{Cu}_3\text{O}_7$  as a solute, and  $\text{CuO}$  as a flux in a platinum crucible. Platy single crystals ( $3 \times 3 \times 0.2 \text{ mm}^3$ ) were obtained in the solidified flux: these were of  $\text{LnBa}_2\text{Cu}_3\text{O}_7$ , well established ternary oxide superconductors. On the other hand, rectangular crystals ( $1 \times 0.3 \times 0.3 \text{ mm}^3$ ) were coagulated on the bottom of the platinum crucible. Chemical analyses revealed that the crystals were of the quaternary oxides,  $\text{R}_2\text{Ba}_2(\text{Cu, Pt})_2\text{O}_8$ . The crystal system was found to be orthorhombic (space group  $\text{Pcmn}$ ). These compounds possess a characteristic one-dimensional structure, double zig-zag chains parallel to the b-axis as shown in Fig. 3. The crystal structure <sup>8</sup>, magnetic ordering <sup>9</sup>, electrical properties <sup>9</sup> on the new compounds were summarized in Table I.

## 2) Growth by the FZ method

Large single crystals of  $\text{La}_2\text{MO}_4$  (M=Ni,Co,Cu; with /without Sr) possessing  $\text{K}_2\text{NiF}_4$  structure have been grown in a lamp-image floating zone furnace under the controlled condition of oxygen fugacity. The crystal growth were performed in the flow of pure gas or gas mixture such as  $\text{Ar}$ ,  $\text{O}_2$ , air,  $\text{N}_2 + \text{O}_2$ ,  $\text{CO}_2 + \text{H}_2$ . Appropriate range of  $f\text{O}_2$  for the growth of each compounds were investigated. Cation ratio of  $\text{La}/\text{M}$  in the starting composition of nutrient rod was fixed to be 2.0 both for M=Ni and Co, while it was varied from 2.0 to 0.86 for M=Cu.

2-1  $\text{La}_{2-x}\text{Sr}_x\text{NiO}_4$  ( $0 \leq x < 1$ )

Single crystal boules with typically  $6\text{mm} \times 50 \text{ mm}$  in dimension have been grown at oxygen fugacity ranging from 1.0 to 0.01 atm as shown in Fig. 4, whereas the growth has not been succeeded in pure  $\text{Ar}$ . EPMA reveals that other phases are not included within the crystal. X-ray diffractometry shows that they crystallize in

tetragonal symmetry with slightly different axial ratios of lattice parameters  $c/a$ , depending on the growth condition of oxygen fugacity. Anisotropic susceptibility of the single crystal as a function of temperature was shown in Fig. 5. Differential thermal analyses for the pulver-

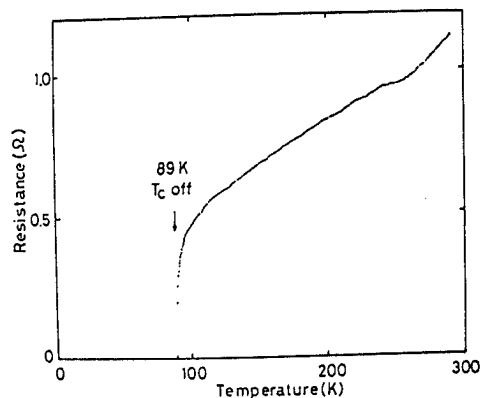


Fig.2 R vs T curve of  $\text{Bi}_2(\text{Sr, Ca})_3\text{Cu}_2\text{O}_x$

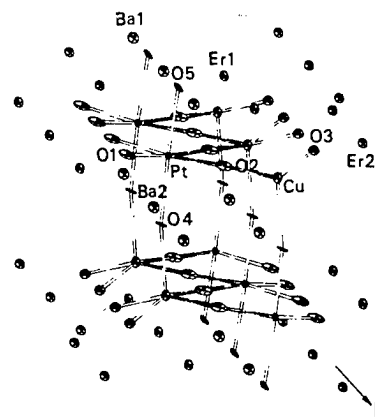


Fig.3 Projection of the structure along the b-axis on  $\text{Er}_2\text{Ba}_2(\text{Cu, Pt})_2\text{O}_8$

Table 1 Crystallographic data and physical properties of  $\text{R}_2\text{Ba}_2(\text{Cu, Pt})_2\text{O}_8$

(RE)	CS	magnetic ordering	electrical properties	Eg
Er	orthorhombic a=10.287(3) Å b=5.659(1) Å c=13.157(3) Å V=765.9 Å <sup>3</sup> Z=4 Pcmn	AF at 60K (Cu <sup>2+</sup> ) only in Hub AF (CAF) at 7K (Er <sup>3+</sup> )	Semi-con $\sigma \propto \exp(-\frac{1}{T})$ non-ohmic	~0.1ev
Ho	orthorhombic a=10.303(2) Å b=5.668(1) Å c=13.178(3) Å V=769.6(3) Å <sup>3</sup> Z=4 Pcmn	AF at 2K (Ho <sup>3+</sup> )	Semi-con $\sigma \propto \exp(-\frac{1}{T})$ non-ohmic	~0.1ev
Y	orthorhombic a=10.321(2) Å b=5.680(2) Å c=13.201(2) Å V=774 Å <sup>3</sup> Z=4 Pcmn	AF at 15K? (Cu <sup>2+</sup> ?) (poly crystal)	Semi-con $\sigma \propto \exp(-\frac{1}{T})$ non-ohmic	~0.15ev

ized single crystals in air indicated that exothermic reaction took place at 600 K. Crystals of  $\text{La}_{2-x}\text{Sr}_x\text{NiO}_4$  ( $0 < x < 1$ ) have been also obtained at  $f\text{O}_2=1$ .

## 2-2 $\text{La}_2\text{CoO}_4$

Mixed phase including  $\text{La}_2\text{CoO}_4$  crystallized at 1-0.1 atm  $f\text{O}_2$ . Single crystals with different degree of orthorhombicity, typically 6mm x 10mm have been obtained in reduced condition up to  $10^{-2}$  atm  $f\text{O}_2$ . Single crystals with tetragonal symmetry have been also obtained. Mosaicity of the crystal was estimated to be less than 0.3 for 220 reflection peak by neutron diffraction measurement (Fig. 6).

## 2-3 $\text{La}_2\text{CuO}_4\text{:Sr}$

Because of melt instability, application of ordinary TSFZ technique has not been fully valid for the La-Cu-O system, therefore searching on an optimum condition for the stable zone-pass has been aimed in this study. We have confirmed that stable zone-pass is achieved reproducibly under the condition where nutrient composition is chosen in a La/Cu ratio of 1.33~1.81, and atmospheric oxygen fugacity is held within 0.4~0.6  $f\text{O}_2$ . In such situation of the experiments, it is recognized that multi phase component enriched with  $\text{La}_2\text{O}_3$  crystallizes at an initial stage of zone-pass, however, as zone travels furthermore, composition of molten zone gradually varies toward CuO excess side and  $\text{La}_2\text{CuO}_4$  doped with Sr begins to crystallize finally. A typical boule zone-travelled under the condition is shown in Fig.7.

We wish to acknowledge Prof. J. Mydosh and his collaborators at Kamerlingh Onnes Laboratory, Drs. Y. Nishihara and K. Murata at ETL, and Drs. T. Takahashi and H. Katayama-Yoshida at Physics dept. Tohoku Univ. for their collaborations.

- 1) A. Katsui: Jpn. J. Appl. Phys. 27 (1988) L844.
- 2) T. Takahashi, H. Matsuyama, H. Katayama-Yoshida, Y. Okabe, S. Hosoya, K. Seki, H. Fujimoto, M. Sato and H. Inokuchi: Nature 334 (1988) 691.
- 3) T. Shishido, D. Shindo, K. Ukei, T. Sasaki, N. Toyota and T. Fukuda: Submitted J. C. G.
- 4) T. Shishido, T. Fukuda, N. Toyota, K. Ukei and T. Sasaki: J. C. G. 85 (1987) 599.
- 5) T. Shishido, T. Fukuda, N. Toyota, K. Ukei and T. Sasaki: Jpn. J. Association of Crystal Growth 14 (1987) 199.
- 6) T. Shishido, Y. Saito, T. Fukuda, N. Toyota, T. Sasaki, H. Iwasaki and K. Ukei: Jpn. J. Appl. Phys. 27 (1988) L1926.
- 7) K. Ukei, T. Shishido and T. Fukuda: Acta Cryst. C 44 (1988) 958
- 8) Y. Saito et al.: in preparation
- 9) N. Toyota et al.: in preparation

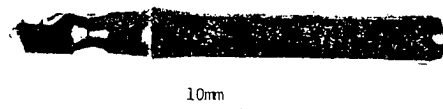


Fig.4  $\text{La}_2\text{NiO}_4$  single crystal

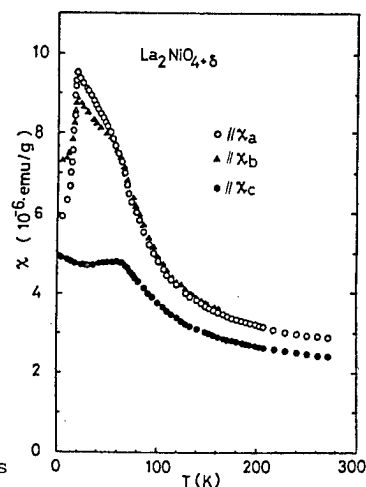


Fig.5 Anisotropy of magnetic susceptibility for  $\text{La}_2\text{NiO}_4$  grown at 0.01 atm  $f\text{O}_2$

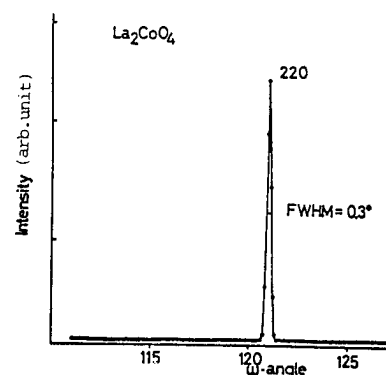


Fig.6 FWHM for 220 reflection of tetragonal  $\text{La}_2\text{CoO}_4$

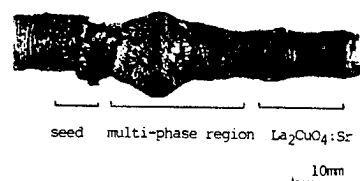


Fig.7 As grown boule of  $\text{La}_{2-x}\text{Sr}_x\text{CuO}_4$  crystal

## Growth of superconducting $\text{La}_{2-x}\text{Sr}_x\text{CuO}_4$ single crystals

H. Kojima and I. Tanaka

Institute of Inorganic Synthesis, Faculty of Engineering,  
Yamanashi University, Miyamae 7, Kofu 400, Japan

The large size of superconducting  $\text{La}_{1.88}\text{Sr}_{0.12}\text{CuO}_4$  single crystals were grown by TSFZ method. It made clear that the atmosphere was influenced the optimum growth conditions. Superconductivity of the grown crystals was confirmed from the magnetization measurement.

Since the discovery of high-temperature superconductors of the  $\text{La}_{2-x}\text{A}_x\text{CuO}_4$  type, where A is Ba or Sr, their crystal structure and properties have been actively investigated. However, the mechanism of their high-temperature superconductivity is not yet known. The physical properties of single crystals will give us much insight into this mechanism, so that it is desirable to obtain good quality and sizable single crystals of  $\text{La}_{2-x}\text{A}_x\text{CuO}_4$ .  $\text{La}_2\text{CuO}_4$  melts incongruently at 1593 K and decomposes to  $\text{La}_2\text{O}_3$  and liquid[1]. Single crystals of  $\text{La}_{2-x}\text{A}_x\text{CuO}_4$  had previously been grown by the flux method and the top-seeded solution method[2-6]. However, the crystals so grown contained inclusions of the flux and the solvent. Single crystals of optimum quality have not yet been obtained. Recently, single crystals of incongruently melting compounds such as  $\text{Y}_3\text{Fe}_5\text{O}_{12}$  have been grown by the traveling solvent floating zone (TSFZ) method described in detail elsewhere[7]. We report the growth of single crystals of  $\text{La}_{2-x}\text{Sr}_x\text{CuO}_4$  by the TSFZ method and discuss measurement of their superconductive properties.

The feed rods and solvent rods for crystal growth were prepared from  $\text{La}_2\text{O}_3$ , CuO and  $\text{SrCO}_3$  powders. Appropriate amounts of the powders were mixed in ethanol, dried and calcined at 1123 K for 12 h in air. The calcined powder was formed into a cylindrical shape of 6 mm in diameter by 50 mm in length, and pressed at a hydrostatic pressure of about 100 MPa. The rod was sintered at 1273-1473 K for 12 h in oxygen gas and then used as the feed rod and the solvent rod. The apparatus for crystal growth was an infrared heating furnace

of the double ellipsoidal type (Nichiden Machinery Ltd.) with two 1.5 kW halogen lamps as the heat source. The experimental procedure has been described in detail elsewhere[7]. The range of growth conditions employed were: growth rates of 1.0-3.0 mm/h, solvent compositions of 55-80 mol%CuO and growth atmosphere of oxygen under 0.2 MPa to prevent vaporization of copper oxide from the melt zone.

An as-grown boule of  $\text{La}_{2-x}\text{Sr}_x\text{CuO}_4$  which was grown by the TSFZ method using a solvent of 75 mol% CuO is shown in Fig. 1. The crystal is about 6 mm in diameter and 40 mm in length. An initial region of about 10 mm in length was black lusterless, and contained a two-phase mixture of  $\text{La}_2\text{O}_3$  in  $\text{La}_{2-x}\text{Sr}_x\text{CuO}_4$ . However, the remaining region black with a metallic luster was single phase  $\text{La}_{2-x}\text{Sr}_x\text{CuO}_4$ . This region exhibits two facets parallel to the growth direction. A back-reflection Laue X-ray photograph, shown in Fig.2, of the facet exhibits sharp diffraction spots and revealed a 4-fold rotation axis.

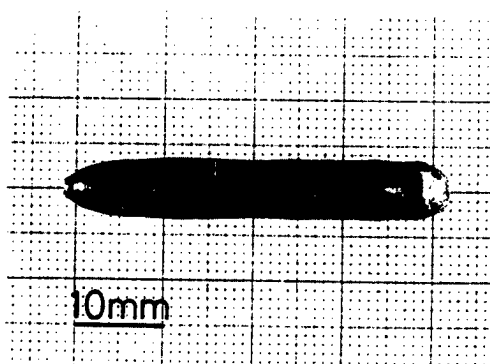


Fig.1 As-grown crystal

The crystals grown were thus identified as single crystals and the crystallographic plane of the facet was (001). Though the as-grown boules had some cracks, single crystals with a maximum size of about 6 mm diameter by 15 mm in length were obtained.

The lattice parameters of the tetragonal  $\text{La}_{2-x}\text{Sr}_x\text{CuO}_4$  crystals, which were measured by powder-XRD method with using Si powder as a standard, were  $a=3.793\pm0.003 \text{ \AA}$  and  $c=13.20\pm0.02 \text{ \AA}$ , and agreed with values obtained from the sintered  $\text{La}_{1.88}\text{Sr}_{0.12}\text{CuO}_4$  feed rod ( $a=3.792\pm0.003 \text{ \AA}$  and  $c=13.21\pm0.02 \text{ \AA}$ ). The Sr content of the  $\text{La}_{2-x}\text{Sr}_x\text{CuO}_4$  grown crystals were uniform along the radius and the length of the crystal as determined by electron probe microanalysis, and were determined to be approximately 0.12, which is lower than that of the feed material ( $x=0.15$ ).



Fig.2 The Laue pattern

Superconductivity of the grown crystals was confirmed from the result of



magnetization measurement of the  $\text{La}_{1.88}\text{Sr}_{0.12}\text{CuO}_4$  grown crystal by using a SQUID magnetometer. Upon comparing the Meissner curve with the shielding curve, the superconducting temperatures agreed well, but the magnetizations were different considerably. The superconducting transition onset temperature ( $T_{\text{Conset}}$ ) and the transition end temperature ( $T_{\text{Cend}}$ ) were 37 K and 29 K, respectively, and then  $\Delta T_c$  was 8 K. This transition was considerably sharper than the transition of sintered  $\text{La}_{2-x}\text{Sr}_x\text{CuO}_4$ , [1] and the  $\Delta T_c$  value of the grown crystals was lower than that of reported previously a  $\text{La}_{2-x}\text{Sr}_x\text{CuO}_4$  single crystal. The Meissner effect indicated that 13 % of the grown crystal was superconducting.

In conclusion, high quality large single crystals of  $\text{La}_{1.88}\text{Sr}_{0.12}\text{CuO}_4$  ( $x=0.15$ ) were grown by the TSFZ method. Crystals up to about 6 mm diameter and 15 mm length were obtained. The single crystals were superconductors with  $T_c=37\text{K}$  and  $\Delta T_c=8\text{K}$  significantly superior to values  $T_c=30\text{K}$  and  $\Delta T_c=15\text{K}$  reported previously [4]. Anisotropy of their magnetic and electrical properties will be described in elsewhere.

We wish to thank Professor K. Kitazawa of the University of Tokyo for magnetization measurements.

#### References

1. Tarascon, J. M., Greene, L. H., McKinnon, W. R., Hull, G. W. & Geballe, T. H. *Science* 235, 1373-1376(1987).
2. Freltoft, T., Fischer, J. E., Shirane, G., Moncton, D. E., Sinha, S. K., Vaknin, D., Remeika, J. P., Cooper, A. S. & Harshman, D. *Phys. Rev. B* 36, 826-828(1987).
3. Wang, H. H., Geiser, U., Thorn, R. J., Carlson, K. D., Beno, M. A., Monaghan, M. R., Allen, T. J., Proksch, R. B., Stupka, D. L., Kwok, W. K., Crabtree, G. W. & Williams, J. M. *Inorg. Chem.* 26, 1190-1192(1987).
4. Hidaka, Y., Enomoto, Y., Suzuki, M., Oda, M. & Murakami, T. *Jap. J. appl. Phys.* 26, L377-L379(1987).
5. Oka, K. & Unoki, H. *Jap. J. appl. Phys.* 26, L1590-L1592 (1987).
6. Picone, P. J., Jenssen, H. P. & Gabbe, D. R. *J. Crystal Growth* 85, 576-580(1987).
7. Kimura, S. & Shindo, I. *J. Crystal Growth* 41, 192-198(1977).

H. Takei, H. Takeya, F. Sakai, T. Kitazawa, M. Koike and J. Akimoto

Institute for Solid State Physics, The University of Tokyo, Roppongi, Minato-ku,  
Tokyo 106, Japan

The present report describes three results: (1) oriented  $\text{Bi}_2\text{Sr}_2\text{CaCu}_2\text{O}_x$  thin films are prepared on MgO substrate using the liquid-phase epitaxial (LPE) method, (2) an apparent decrease in susceptibility is observed on  $\text{La}_2\text{CuO}_4$  single crystals by a shock-compression between 50 and 70 GPa and (3) single crystals of triangular lattice antiferromagnet,  $\text{NaTiO}_2$ , are prepared in sodium-metal solution.

The object of the present study is to develop a new technique for growing single crystals of superconducting oxides and related compounds, and to clarify the physical and chemical properties of the crystals thus prepared. The experiments have been progressed along three themes and the results are summarized as follows:

(1) Liquid phase epitaxy (LPE) of Bi-Sr-Ca-Cu-O films[1]

Many studies on film-making of high- $T_c$  oxide superconductors Bi-Sr-Ca-Cu-O have been carried out. Several successes have been reported in producing films from the vapor phase. In these reports, however, no finding or discussion about epitaxial direction or mismatching problem to a substrate has been included. The present study involves trial preparation of thin films by a LPE method using flux.

Various kinds of fluxes are used for preparing films on a MgO (100) substrate. It was found that a  $\text{Bi}_2\text{Sr}_2\text{CaCu}_2\text{O}_x$  film was grown only from KCl flux. The conditions of preparation are as follows: the mole ratio  $\text{Bi}_2\text{Sr}_2\text{CaCu}_2\text{O}_x/\text{KCl}$  was 1/7, and the maximum growth temperature was about 1200°C.

The X-ray diffraction pattern of the film indicates that the major phase is  $\text{Bi}_2\text{Sr}_2\text{CaCu}_2\text{O}_x$  and the minor phase  $\text{Bi}_2\text{Sr}_2\text{CuO}_x$ . The SEM and EPMA measurements showed that the film was composed of platy grains with the size 10 - 15  $\mu\text{m}$ , and the metal composition was  $\text{Bi}:\text{Sr}:\text{Ca}:\text{Cu}=2.4:2.3:0.7:2.0$  in atom ratio. The film thickness was determined to be about 1  $\mu\text{m}$  from SEM photographs, as shown in Fig. 1. The crystallographic direction between the film and the substrate was determined by the precession method, where the photographs of the film were taken together with the substrate MgO. At first, the X-ray beam was passed perpendicularly through the film, and in the next stage, the photograph was taken after rotating the substrate plane to the horizontal position to the X-ray beam. The spots corresponding to 008, 0010, 0012 of  $\text{Bi}_2\text{Sr}_2\text{CaCu}_2\text{O}_x$  were observed in the first film, whereas only the ring pattern, which correspond to which correspond to the 200 diffraction of  $\text{Bi}_2\text{Sr}_2\text{CaCu}_2\text{O}_x$ , was detected in the next film. This fact indicates that the film was formed as a c-plane-oriented polycrystal along the (100) plane of MgO.

The packing arrangement of anions is important in the discussion of epitaxy. Based on the lattice parameters and the structure found by Tarascon et al.[2], the distance between the first nearest oxygen atoms in each layer is calculated. The misfit parameter  $f$ , defined by the equation  $f=(d_s-d_f)/d_s \times 100 (\%)$ , where  $d_s$  and  $d_f$  denote the O-O distance of the substrate and the film, respectively, at the contact

plane. It is most likely that the contact plane of  $\text{Bi}_2\text{Sr}_2\text{CaCu}_2\text{O}_x$  to  $\text{MgO}$  (100) is the (001) plane of the  $\text{CuO}$  layer, the structure of which is the same NaCl type as that of the substrate  $\text{MgO}$ . The least value of  $f$  is 10.3 % from the combination of  $\text{Mg-O}$  : 29.79 nm and  $\text{Cu-O}$  : 27.00 nm. The findings suggest that 10.3 % is too large to grow a single crystal film of  $\text{Bi}_2\text{Sr}_2\text{CaCu}_2\text{O}_x$  on  $\text{MgO}$  (100) near the equilibrium condition.

The resistivity in the as-grown state was measured by a conventional dc-four probe method (see Fig. 2). Though the onset  $T_c$  was observed at 95 K, zero resistivity was not found at above 50 K. This might be due to an incomplete dense film or the existence of the high-resistive subphase,  $\text{Bi}_2\text{Sr}_2\text{CuO}_x$ .

### (2) Shock-compression of $\text{La}_2\text{CuO}_4$ crystals

It is generally accepted that superconductivity is closely related to perfection of crystals. Shock-compression is one of the most effective treatment for reducing the perfection of crystal specimens. In the present study, we have applied the shock-compression treatment to the superconducting oxide crystals  $(\text{La}_{1-x}\text{Sr}_x)_2\text{CuO}_4$  up to 70 GPa by using propellant and two-stage light-gas guns, which was constructed by Syono group of MRI, Tohoku Univ.[3] The  $\text{CuO}$  flux method, developed by Hidaka et al.[4], were used for obtaining single crystal specimens.

Figure 3 shows a change of the lattice parameters with shock pressure. It is clear that the parameters increase with increasing pressure. This fact is contrary to the results of Takahashi et al.[5] obtained under hydrostatic pressure up to 80 Kbar, where the lattice constants of  $(\text{La},\text{Sr})_2\text{CuO}_4$  decreased with pressure increase. SEM, EPMA and X-ray measurements revealed that  $\text{La}_2\text{CuO}_4$  decomposed into three phases, expanded  $\text{La}_2\text{CuO}_4$ , perovskite phase and  $\text{La}_2\text{O}_3$  at 70 GPa. The magnetic properties were determined by measuring the ac-magnetic susceptibility. Figure 4 shows the temperature dependence of the susceptibilities as a function of shock pressure. A clear decrease in the susceptibility was observed below 30 K on the specimen shocked at 70 GPa. This decrease is thought to be due to a diamagnetic signal originated from the expanded  $\text{La}_2\text{CuO}_4$  phase. More detailed analysis is now in progress.

### (3) $\text{NaTiO}_2$ crystals from sodium-metal solutions

$\text{NaTiO}_2$  is interesting because it is composed of a typical two dimensional triangular lattice which is thought to be related to the antiferromagnetic ordering with a quantum liquid state of  $S=1/2$  [6]. Recently, Shirane et al.[7] have found out such a type of ordering in the crystals  $\text{La}_2\text{CuO}_4$  with low hole concentration.

To clarify the physical properties of this material, polycrystalline samples have been used [6], and single crystals are needed in order to obtain more precise information concerning the anisotropy in spin ordering. In the present study, we have succeeded in preparation of single crystals of  $\text{NaTiO}_2$  from the high-temperature solutions of sodium titanate powder and sodium metal. Figure 5 is a SEM photograph of the as-grown crystal indicating that it grows with a developed (001) habit. The maximum dimension is  $5 \times 5 \times 3 \text{ mm}^3$ . Figure 6 shows a transmission Laue photograph along the [001] axis. X-ray analyses using a four circle system revealed that the structure is of the layered triangle lattice. The composition was roughly estimated to be  $\text{Na}_{0.5}\text{TiO}_2$ . The static magnetic susceptibility was measured at the external field of 11.8 kOe. The preliminary result is shown in Fig. 7, where the Curie-Weiss constant ( $\times 10^{-4} \text{ emu/g}$ ) is 1.8 and 4.2, between 4.2 and 10 K, and 10 and 300 K, respectively. The former value is close to that of the powder sample[6].

We have found that  $\text{LiCuO}_2$  is also of a two dimensional triangular lattice. Further investigation of this material is needed.

### References:

- [1] H. Takeya and H. Takei, Jpn. J. Appl. Phys., in press.
- [2] J.M.Tarascon, P.Barboux, L.H.Greene, B.G.Bagley, G.W.Hull, Y.LePage and

- W.R.McKinnon, Physica C, 153-155(1988)566.
- [3] Y.Syono and T.Goto, Sci.Rep.Res.Inst.Tohoku Univ., 29A(1986)17.
- [4] Y.Hidaka, Y.Enomoto, M.Suzuki, M.Oda, A.Katsui and T.Murakami, Jpn.J.Appl. Phys., 26(1987)L726.
- [5] H.Takahashi, C.Maruyama, S.Yomo, N.Môri, K.Kishio, K.Kitazawa and K.Fueki, Jpn.J.Appl.Phys., 26(1987)L504.
- [6] K.Hirakawa, H.Kadowaki and K.Ubukoshi, J.Phys.Soc.Jpn., 54(1985)3526.
- [7] G.Shirane, Y.Endoh, R.J.Birgenau, M.A.Kastner, Y.Hidaka, M.Oda, M.Suzuki and T.Murayama, Phys.Rev.Letters, 59(1987)1613.

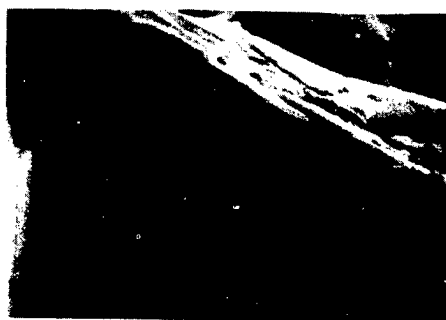


Fig.1

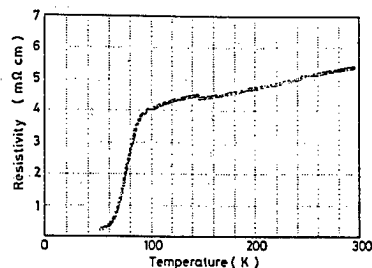


Fig.2

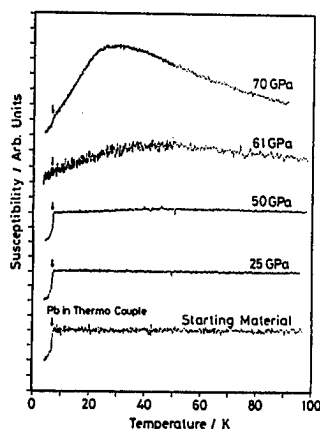


Fig.3

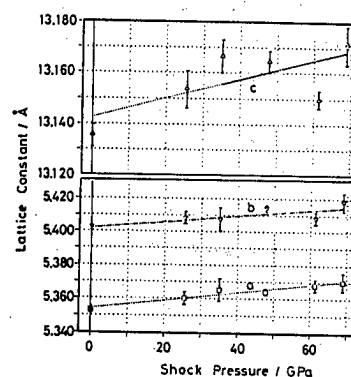


Fig.4



Fig.5

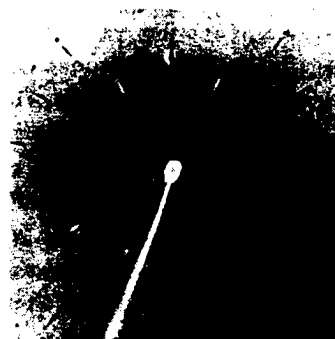


Fig.6

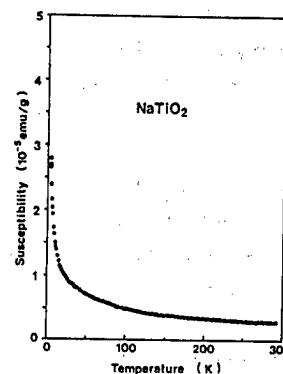


Fig.7

- Fig.1: Cross-section of Bi-Sr-Ca-Cu-O films on MgO substrate (SEM photograph).
- Fig.2: Resistivity change of the Bi-Sr-Ca-Cu-O film with temperature.
- Fig.3: Shock-induced changes in the lattice constants of La<sub>2</sub>CuO<sub>4</sub> crystals.
- Fig.4: Magnetic susceptibility of shocked La<sub>2</sub>CuO<sub>4</sub> samples below 300 K.
- Fig.5: SEM photograph of single crystal NaTiO<sub>2</sub>. The developed surface is (001).
- Fig.6: Transmission Laue photograph of NaTiO<sub>2</sub> crystal. Mo radiation was used.
- Fig.7: Dc-susceptibility of NaTiO<sub>2</sub> crystal below room temperature.

# An approach to The Growth of $\text{YBa}_2\text{Cu}_3\text{O}_{7-x}$ Single Crystals by The Flux Method

Koichi WATANABE

Department of Chemistry, Faculty of Technology  
Gunma University, Kiryu, Gunma 376 Japan

The growth of  $\text{YBa}_2\text{Cu}_3\text{O}_{7-x}$  single crystals of the superconductivity material was tried by the slow cooling technique with numerous fluxes. Chemical reagents of (Li-, Na-, K-) fluoride, chloride, carbonate, and borate,  $\text{PbO-PbF}_2$ ,  $\text{Li}_2\text{O-MoO}_3$ , Ba-carbonate, fluoride, peroxide, etc. were used as a flux. When alkali halides were used as a flux, needle-CuO of 1 mm diameter and 20 mm length was plentifully obtained. In the cases of alkali and Ba-carbonates, many and large prismatic- $\text{YBa}_4\text{Cu}_2\text{Pt}_2\text{O}_x$  single crystals which belong to hexagonal or trigonal crystal system grew at the wall of crucible. Fluxes of heavy metal compounds (Pb-, Mo-, Bi-) yielded two kind crystals of needle-CuO and irregular form  $\text{Ba}_2\text{Y}_2\text{O}_5$ .

## Introduction

Since the discovery of high-temperature superconductivity material in La-Ba-Cu-O system by Bednorz and Muller[1], all of the scientists who are working in this field are greatly motivated to the discovery and refinement of the other new materials. The most popular  $\text{YBa}_2\text{Cu}_3\text{O}_{7-x}$  "YBCO" compound in the superconductivity materials melts incongruently at about 1020 °C the green phase 2:1:1 plus liquid [2,3]. It is impossible, therefore, to grow single crystals of this compound from its stoichiometric melt under a normal pressure. Crystals must be grown at lower temperatures than the incongruent decomposition temperature. For solving this problem the high-temperature solution growth technique "flux" that reduces the crystallization temperature of solute is available. At present, however, there are no fixed rules for choosing the optimum flux for the growth of given crystal. One of the better starting points is to study informations, such as melting point, eutectic composition, and precipitated crystal phase, contained in phase diagram on the crystal that required. Another useful practice is to examine the literature for fluxes that have been successfully used for the growth of similar compounds. Many papers on the growth of YBCO single crystals by the flux method have been already published, however, all of papers is those only by the self-flux of BaO-CuO system compounds[4]. In case that the self-flux which contains common ions in both of the growing crystals and the flux is used, it is not easy to grow exactly single crystals of good quality with a fixed chemical composition and/or to separate dexterously the grown crystals from the flux.

The aim of the present study, excepting the self-flux of BaO-CuO system compounds, is to survey a suitable flux for the growth of YBCO single crystals by the flux slow cooling method and to obtain the large and good quality of YBCO compound.

## Experimental procedure

YBCO of the solute was prepared from the chemical reagents of yttrium trioxide,  $\text{Y}_2\text{O}_3$ , barium carbonate,  $\text{BaCO}_3$ , and cupric oxide, CuO. Each reagent is weighed in the atomic mole ratio of 1:2:3, and mixed mechanically in an agate mortar for 5 hr. About 2 g of powdered mixture was formed the column of  $10^\phi \times 10$  mm, and then sintered in an electric furnace at 900 °C for 50 hr. The wide variety of chemical reagents, such as alkali (Li-, Na-, K-) carbonate, fluoride, chloride, borate,  $\text{PbO-PbF}_2$ ,  $\text{Li}_2\text{O-MoO}_3$ ,

barium chloride, fluoride, peroxide, mixed copounds, etc. were used as a flux. 20 g of the mixture of the YBCO and flux, which was composed of 20:80 in weight percent, was packed in a platinum crucible of 20 cc with a lid. The crucible was embeded in alumina powder in a covered porcelain pot, and then set up in an electric furnace. Figure 1 shows an apparatus for the crystal growth. The mixture in the crucible was melt at the respective soaking temperatures of 950, 1100, or 1150 °C by the difference of the kind in flux for 30 hr. in an ambient atmosphere. Temperature range of the slow cooling was 1150 900 °C or 950 650 °C and the cooling rate was 5 °C/h. Temperature regulation of the furnace was performed by a three term electric controller(PID) with a Pt-Pt.13% Rh thermocouple. 1 g of  $B_2O_3$  was added into the flux, under certain circumstances, since it is found to diminish the number of crystal nuclei, to prevent the corrosion of platinum crucible being due to the fluoride, chloride, or carbonate compounds, and to suppress evaporation of the flux by covering with thin  $B_2O_3$  film on liquid surface.

Identification of the precipitated crystal phase was achieved by the use of the X-ray diffraction and also chemical analysis of crystals by the ICP method.

#### Results and discussion

As mentioned previously, there are no fixed rules for choosing a flux. Most simple and easy approach shall be practically tried growth of a given crystal with some representative fluxes. In the present study, thus, the most popular fluxes of  $PbO-PbF_2$ ,  $Li_2O-MoO_3$ , alkali carbonate, borate, and chloride were firstly checked. However, we could not obtain a desirable crystal. Table 1 lists some of the used fluxes and crystal phases that have been precipitated from them. The fluxes of  $PbO-PbF_2$  and  $Li_2O-MoO_3$  system produced irregular-form  $Ba_2Y_2O_5$  and the small crystals of needle-CuO, respectively. When alkali or alkaline earth carbonate was used, prismatic crystals of  $YBa_4Cu_2Pt_{2x}O_x$  "YBCPO" surrounding with large and well-developed faces grew at the wall and bottom of crucible. This crystal containning platinum of high concentration is expected to belong to hexagonal or trigonal crystal system and the size is about  $1 \times 2 \times 7 \text{ mm}^3$ . Figure 2 shows single crystals of the YBCPO. High concentration of platinum incorporated into the crystals will be to have been supplied from the crucible. In the experiment of run No. 5, so that, Ni-crucible instead of platinum crucible was used in order to suppress the growth of YBCPO crystals. Surely, the

YBCPO crystals did not grow, however, undesirable another new phases,  $Cu_2Y_2O_5$ , CuO, and  $Y_2O_3$ , appeared. An addition of the excess  $B_2O_3$  to the melt make a stable glassy-state of melt (run No. 6). The solute in the run No. 7 comprises YBCO of 15 wt% and BaO of 5 wt%. Even if the excess BaO or  $Y_2O_3$  more than the mole ratio of YBCO compound was added to the solute, as the case of run No. 7 or 8, the main product was also to be prismatic YBCPO crystals so far as carbonate flux was used. As can be seen in Table 1, using chloride, hydroxide, and peroxide compounds as a flux, the promising results were not obtained. The flux evaporation technique was utilized for the run No. 11 using an Fe-crucible with KOH flux at a constant temperature of 500 °C. Crystals obtained was to be  $Cu_2Y_2O_5$ .

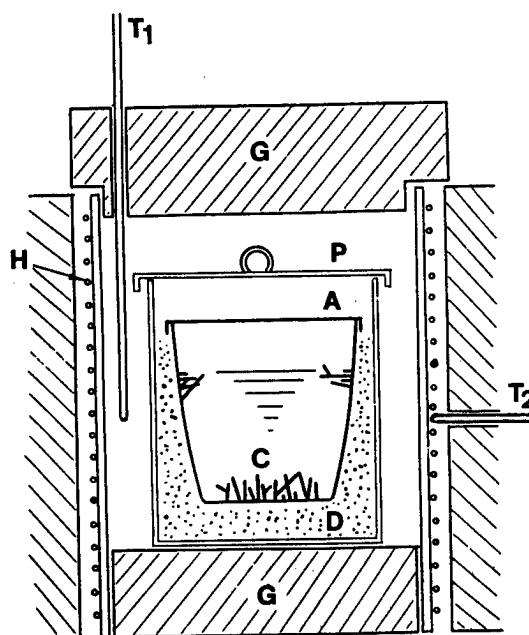


FIG. 1. APPARATUS FOR CRYSTAL GROWTH

- A; PLATINUM CRUCIBLE, P; PORCELAIN POT
- C; GROWN CRYSTALS, D;  $Al_2O_3$  POWDER
- G; FIRE BRICK, H; HEATER
- $T_1, T_2$ ; THERMOCOUPLE TUBE

Table 1.

run No.	Solute composition	Flux	Temp. range of slow cooling (°C)	Results-Products
1.	YBCO <sup>1)</sup>	PbO-PbF <sub>2</sub>	1100 ~ 800	Ba <sub>2</sub> Y <sub>2</sub> O <sub>5</sub> , unknown-phase(A)
2.	YBCO	Li <sub>2</sub> MoO <sub>4</sub>	1150 ~ 900	needle-CuO, BaMoO <sub>4</sub>
3.	YBCO	(Li-, Na-, K-) <sub>2</sub> CO <sub>3</sub>	1150 ~ 900	prismatic-YBCPO <sup>2)</sup> , unknown(B)
4.	YBCO	K <sub>2</sub> CO <sub>3</sub>	950 ~ 650	prismatic-YBCPO
*5.	YBCO	K <sub>2</sub> CO <sub>3</sub>	950 ~ 650	Cu <sub>2</sub> Y <sub>2</sub> O <sub>5</sub> , CuO, Y <sub>2</sub> O <sub>3</sub> , Ni-crucible
6.	YBCO	K <sub>2</sub> CO <sub>3</sub> (70) + K <sub>2</sub> B <sub>4</sub> O <sub>7</sub>	960 ~ 610	Y <sub>2</sub> O <sub>3</sub> , glassy, unknown(C)
7.	YBCO + BaO(4)	K <sub>2</sub> CO <sub>3</sub> (75) + K <sub>2</sub> B <sub>4</sub> O <sub>7</sub>	960 ~ 610	prismatic-YBCPO, Y <sub>2</sub> O <sub>3</sub> , unknown(D)
8.	YBCO + Y <sub>2</sub> O <sub>3</sub> (4)	K <sub>2</sub> CO <sub>3</sub> (75) + K <sub>2</sub> B <sub>4</sub> O <sub>7</sub>	960 ~ 610	prismatic-YBCPO, Y <sub>2</sub> O <sub>3</sub> , unknown(E)
9.	YBCO	KCl + B <sub>2</sub> O <sub>3</sub>	1150 ~ 900	needle-CuO, hp-BB <sup>3)</sup>
10.	YBCO	KCl + B <sub>2</sub> O <sub>3</sub>	800 ~ 500	CuCl, [CuCl·CO]·2H <sub>2</sub> O
*11.	YBCO	KOH	~ 500	hydroxide compound, Cu <sub>2</sub> Y <sub>2</sub> O <sub>5</sub> , Fe-crucible
12.	YBCO	BaO <sub>2</sub>	850 ~ 550	BaO <sub>2</sub> , Ba <sub>4</sub> Y <sub>2</sub> O <sub>7</sub>
13.	YBCO	BaCl <sub>2</sub>	1150 ~ 900	needle-CuO
14.	YBCO	BaCl <sub>2</sub>	960 ~ 610	Cu <sub>2</sub> Y <sub>2</sub> O <sub>5</sub>
15.	YBCO	KF	1150 ~ 900	needle-CuO, Cu <sub>2</sub> Y <sub>2</sub> O <sub>5</sub> , BaF <sub>2</sub>
16.	YBCO	KF	950 ~ 650	needle-CuO, BaF <sub>2</sub>
17.	YBCO	KF + B <sub>2</sub> O <sub>3</sub>	950 ~ 650	needle-CuO, BaF <sub>2</sub> , hp-BB
18.	YBCO + CuO(+5)	KF + B <sub>2</sub> O <sub>3</sub>	950 ~ 650	needle-CuO, BaF <sub>2</sub> , hp-BB
19.	YBCO + CuO(+10)	KF + B <sub>2</sub> O <sub>3</sub>	950 ~ 650	needle-CuO, BaF <sub>2</sub> , hp-BB
20.	YBCO - CuO(-5)	KF + B <sub>2</sub> O <sub>3</sub>	950 ~ 650	needle-CuO, BaF <sub>2</sub>
21.	YBCO - CuO(-10)	KF + B <sub>2</sub> O <sub>3</sub>	950 ~ 650	needle-CuO, BaF <sub>2</sub>
22.	YBCO + BaO(+5)	KF + B <sub>2</sub> O <sub>3</sub>	950 ~ 650	needle-CuO, BaF <sub>2</sub> , hp-BB
23.	YBCO + CuO(+5) + BaO(+5)	KF + B <sub>2</sub> O <sub>3</sub>	950 ~ 650	needle-CuO, BaF <sub>2</sub> , hp-BB
24.	YBCO + TiO <sub>2</sub> (1g) <sup>4)</sup>	KF + B <sub>2</sub> O <sub>3</sub>	950 ~ 650	needle-CuO, BaTiO <sub>2.95</sub> F <sub>0.03</sub>

Notice: 1) YBCO; sintered YBa<sub>2</sub>Cu<sub>3</sub>O<sub>7-x</sub>.2) prismatic-YBCPO; YBa<sub>4</sub>Cu<sub>2</sub>Pt<sub>2</sub>O<sub>x</sub> single crystal

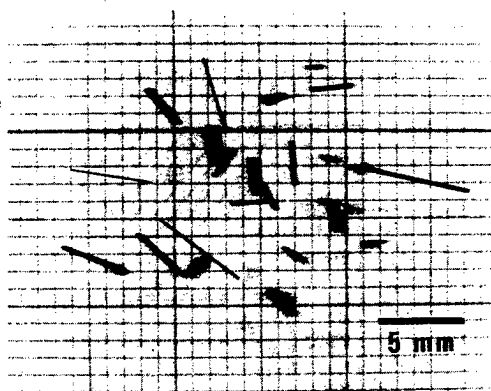
3) hp-BB; barium borate crystal of hexagonal-plate-form

4) TiO<sub>2</sub> was added as a nucleating agent.

\*) No. 11 is the evaporation method.

\*) Ni- and Fe-crucible was used in run No. 5 and 11, respectively.

Continuously, some fluxes which have been successfully used for the growth of similar compounds to YBCO were adapted in the present study[5]. For  $Y_2O_3$ -based compounds,  $PbO$ ,  $PbF_2$ ,  $B_2O_3$ ,  $KF$ , etc fluxes have been found to be useful. For  $BaO$ -based compounds, the fluxes such as  $NaCl$ ,  $KF$ ,  $PbO$ ,  $PbF_2$ ,  $Na_2CO_3$ , etc. have been often used. For  $CuO$ -based compounds it has been found that the compounds of  $KCl$ ,  $NaCl$ ,  $KF$ ,  $PbO$ ,  $PbF_2$ ,  $BaCl_2$  etc. were good fluxes.  $PbO$ - $PbF_2$  or  $KF$  compound which includes in common in the respective oxides is remarkable to be the expedient fluxes. As described already above,  $PbO$ - $PbF_2$  system flux provided the unsatisfactory results in the present study. Accordingly, the experiment by  $KF$  flux was powerfully performed. Crystals grown were, however, to be needle- $CuO$  crystals having the size of 1 mm diameter and 20 mm length, barium borate crystals of hexagonal-plate with 1~2 mm edge length, granular  $BaF_2$ , and seldom very small crystals of  $Cu_2Y_2O_5$ . Even if the chemical composition of solute changed, this result was the same. For instance, in the case of the run No. 18 the solute is composed of the YBCO of 15 wt%(3g) plus the  $CuO$  of 5 wt%(1g), however, crystals obtained were to be needle- $CuO$ , granular  $BaF_2$ , and barium borate of hexagonal-plate. The solute in run No. 21 consists of the YBCO with the deficient  $CuO$  of 10 wt%, however, crystals obtained were the same products as well as another case. The experiment of No. 24 is an example which a small quantity of  $TiO_2$  (1g) as a nucleating agent was added. In this case barium titanate compound was obtained. When alkali fluoride or chloride flux was used, needle- $CuO$  crystals grew always. This fact conjectures to ascribe to the formation of the relatively stable Ba- or Y- fluoride complex ions in the melt. Unfortunately, in the present study, we could not find out a promising flux for the growth of YBCO single crystals. Present results suggest that a more extensive and in detail search for a suitable flux will be necessary.



#### References

- [1] J. G. Bednorz and K. A. Muller, *Z. Physik* **B64** 189 (1986).
- [2] H. Takei and H. Takeya, *J. Japan Crystal Growth* **14** 3 (1987).
- [3] R. A. Laudise, L. F. Schneemeyer and R. L. Barns, *J. Crystal Growth* **85** 569 (1987).
- [4] *J. Crystal Growth "High- $T_c$  superconductors I, II"* **85** 569 (1987), **91** 249 (1988).
- [5] D. Elwell and H. J. Scheel, "Crystal Growth from High-Temperature Solutions" (Acad. press, London, 1975).



# Low-Temperature Crystalline Structure of $(\text{La}_{1-x}\text{Ba}_x)_2\text{CuO}_{4-\delta}$

Takashi Suzuki and Toshizo Fujita

Department of Physics, Hiroshima University  
Hiroshima 730, Japan

Crystal structure of  $(\text{La}_{1-x}\text{Ba}_x)_2\text{CuO}_{4-\delta}$  ( $0 \leq x \leq 0.15$ ) was extensively investigated by powder X-ray diffraction over a wide temperature range down to 4.2 K. A structural sequence of tetragonal-orthorhombic-tetragonal phases was found on cooling for the samples with concentration  $0.045 < x < 0.125$ . A new structural phase diagram is mapped in the T-x plane.

Since the discovery of superconductivity in the doped  $\text{La}_2\text{CuO}_4$  (LCO) by Bednorz and Müller,<sup>1)</sup> the LCO family has been paid a special attention to as a fundamental series of high  $T_c$  superconductors in spite of successive finding of new materials with higher  $T_c$ . In the early stage of research race on the high- $T_c$  superconductors, Fujita et al.<sup>2)</sup> reported a crystallographic, magnetic and superconductive phase diagram of the doped LCO. The crystallographic part of the work, which has been performed only above 200 K, revealed that as samples were cooled,  $(\text{La}_{1-x}\text{Ba}_x)_2\text{CuO}_{4-\delta}$  (LBCO) undergoes a structural transition from tetragonal high-temperature phase (THT) to orthorhombic mid-temperature phase (OMT), and that the transition temperature  $T_{d1}$  decreases with increasing Ba concentration  $x$ . However, several groups extended the structural studies to lower temperatures, suggesting a second transition to a monoclinic phase.<sup>3,4)</sup> Axe et al.<sup>5)</sup> repeated X-ray diffraction and neutron experiments on LBCO with  $x = 0.05$ , and confirmed the tetragonal phase (TLT) at low temperatures below 52 K, which has  $P4_2/\text{ncm}$  symmetry. Sera et al.<sup>6)</sup> paid attention to anomalies found in electrical resistivity and thermoelectric power of LBCO in a narrow region around  $x = 0.05$ , in which  $T_c$  is sharply depressed, and they claimed a close relation between these anomalies of transport properties and the structural transition.

In this paper, we report our X-ray diffraction experiments performed over a wide temperature range for  $(\text{La}_{1-x}\text{Ba}_x)_2\text{CuO}_{4-\delta}$  with  $0 \leq x \leq 0.15$ . A new phase diagram is presented for the crystal structure in the T-x plane. Relation between the structural transition and anomalous transport properties as well as depression of  $T_c$  is discussed.

Samples were prepared by following processes: reacting mixtures of  $\text{La}_2\text{O}_3$ ,  $\text{BaCO}_3$  and  $\text{CuO}$  in air at  $900^\circ\text{C}$  for 28 h, heating the pellets at  $1050^\circ\text{C}$  for 12 h and at  $1100^\circ\text{C}$  for 24 h for further reaction and sintering, annealing in air at  $500^\circ\text{C}$  for 15 h and then cooling down slowly to room temp. The second annealing was performed in oxygen initially at  $500^\circ\text{C}$  for 12 h and finally at  $400^\circ\text{C}$  for 48 h. In case of LCO, pellets were quickly cooled down to room temperature after annealing in air at  $500^\circ\text{C}$ . To remove internal strain which might be introduced by pulverizing, we annealed the powder samples finally in oxygen at  $400^\circ\text{C}$  for 1 h just before the X-ray diffraction measurements. For critical discrimination of different phases and exact determination of the lattice parameters, X-ray measurements were made with a counting tube diffractometer employing a monochromator of single-crystalline graphite for  $\text{CuK}\alpha_1$  radiation. The raw data was analyzed by smoothing and  $\text{CuK}\alpha_2$  stripping. Relative change of lattice constants was determined using [004], [103], [213] and [220] peaks of THT phase. A continuous flow cryostat (Oxford Instrument CF1108) was used for the measurements at reduced temperatures. Temperature was carefully monitored by platinum and carbon resistors. Since a first order phase transition is expected, temperature variation was controlled to be slower than 5 K per hour. The electrical resistivity and thermoelectric power were measured for sintered samples cut from the same block, from

which the samples for X-ray measurements were prepared, by using another He-cryostat.

Figure 1 illustrates part of powder X-ray diffraction pattern for the sample with  $x = 0.075$  at various temperatures. The change in spectrum suggests three phases with different symmetry: THT-OMT-TLT. Similar sequence of structural change has been already found in the layered perovskites of  $K_2NiF_4$  type with chemical formula of  $(C_nH_{2n+1}NH_3)_2MX_4$ .<sup>7)</sup> The successive transition have been studied in detail by experimental<sup>8-10)</sup> and theoretical works.<sup>11,12)</sup> The elastic anomaly, which was reported for  $La_{1.85}Ba_{0.15}CuO_4$  by Fossheim et al.,<sup>13)</sup> can be interpreted in terms of the softening of  $C_{66}$  mode, as is the case with  $(CH_3NH_3)_2FeCl_4$  (MAFC).<sup>8)</sup> In Fig. 2, the lattice constants (using the notation for the THT phase) is plotted as a function of temperature for the sample with  $x = 0.075$ . The lattice parameters at 300 K are  $a = 3.78$  Å and  $c = 13.27$  Å. The temperature dependence is quite similar to MAFC.<sup>7)</sup> As is clearly seen in the lattice constants  $a$  and  $b$ , the phase change from THT to OMT occurs gradually at  $T_{d1} \approx 210$  K whereas the change from OMT to TLT occurs discontinuously at  $T_{d2} \approx 49$  K. Hence it is suggested experimentally that the THT-OMT transition is of the second order and the OMT-THT transition is of the first order. The nature is consistent with crystallographical expectation assuming the symmetry of  $I4/mmm$  for THT,  $Cmca$  for OMT and  $P4_2/nm$  for TLT. The lattice constant  $c$  also exhibits anomalies at the transitions. The critical exponent of the order parameter can be defined as  $b-a \propto (T_{d1}-T)^{2\beta}$  for the THT-OMT transition. For our sample with  $x = 0.075$ , we obtained  $\beta = 0.33$ , which is in excellent agreement with the theoretical value of  $\beta = 1/3$  expected for the 3d-XY model.<sup>14)</sup>

The phase diagram illustrated in Fig. 3 summarizes the result of our X-ray studies on various LBCO samples with  $x = 0, 0.025, 0.045, 0.05, 0.06, 0.075, 0.09, 0.1, 0.125$  and  $0.15$ , where  $x$  denotes the nominal concentration of Ba. When temperature is very slowly reduced, the structure sequence of THT-OMT-TLT phases is found for the samples with  $0.045 < x < 0.125$ . The samples with  $x \leq 0.045$  remain in the OMT phase and the samples with  $x \geq 0.125$  remain in the THT phase at least down to 4.2 K. The transition temperature  $T_{d1}$  appears to decrease in proportion to  $x$ . Moss et al.<sup>4)</sup> reported a transition to monoclinic structure in  $La_{1.8}Ba_{0.2}CuO_4$ . From a viewpoint of group theory, such a transition is also expected for this series of oxides, as is realized in  $(CH_3NH_3)_2MnCl_4$ .<sup>7)</sup> In the present work, however, the phase with lower symmetry than orthorhombic is not detected.

It is frequently found<sup>15)</sup> that the superconducting transition temperature  $T_c$  shows an anomalous dip for the LBCO samples around  $x = 0.075$ . Axe et al.<sup>3)</sup> suggest that the superconductivity with short coherence length may be strongly depressed by structural distortion associated with the first order transition from OMT to TLT. Since the samples with  $x \leq 0.045$  in the OMT phase have a ferroelastic domain structure, the domain may produce a spin glass or disordered magnetic state<sup>16)</sup> in the Cu spin system. In this case, the magnetic properties of the samples should be analyzed carefully. Quite recently, Sera et al.<sup>6)</sup> proposed a structural phase diagram determined indirectly by inflection points in the temperature dependence of thermoelectric power. Their phase diagram does not agree so well with the present result which was determined by X-ray analysis. In order to check a possible effect due to sample dependence, we also measure the thermoelectric power of our samples with  $x = 0.075$ . As is shown for  $x = 0.075$  in Fig. 4, the result is essentially the same as that of Sera et al. The resistivity begins to increase and the thermoelectric power begins to decrease at 61 K, which was regarded as a sign of the OMT-TLT transition by Sera et al. However the transition temperature determined by the X-ray analysis is significantly lower than 61 K and the TLT phase spreads in a much wider range of  $x$  than the anomalous transport behavior is observed. For the present, we can not conclude what implication exists among the structural transition, depression of superconductivity and transport anomaly observed in LBCO. More detailed experiments are required especially on thermal and elastic properties.

#### References

1. J.G.Bednortz and K.A.Müller: Z.Phys. B64(1986)189.
2. T.Fujita, Y.Aoki, T.Maeno, J.Sakurai, H.Fukuba and H.Fujii: Jpn.J.Appl.Phys. 26(1987)L368.
3. E.F.Skelton, W.T.Elam, D.U.Gubses, V.Letourneau, M.S.Osofsky, S.B.Quadri, L.E.Toth and S.A.Walf: Phys.Rev. B36(1987)5713.

4. S.C.Moss, K.Forster, J.D.Axe, H.You, D.Hohlwein, D.E.Cox, P.H.Hor, R.L.Meng and C.W.Chu: Phys.Rev. B35(1978)7195.
5. J.D.Axe, D.E.Cox, K.Mohanty, H.Moudden, A.R.Moodenbaugh, X.Xu and T.R.Thurston: Preprint.
6. M.Sera, Y.Ando, S.Kondoh, K.Fukuba, M.Sato, I.Watanabe, S.Nakashima and K.Kumagai: Preprint.
7. For exampl, K.Knorr, I.R.Jahn and G.Hegar: Solid State Commun. 15(1974)231.
8. T.Goto, M.Yoshizawa, A.Tamaki and T.Fujimura: J.Phys. C15(1982)3041.
9. M.Yoshizawa, T.Goto and T.Fujimura: Phys.Rev. B29(1982)1499.
10. T.Suzuki, M.Yoshizawa, T.Goto, T.Yamakami, M.Takahashi and T.Fujimura: J.Phys.Soc.Jpn. 52(1983)1669.
11. A.Yoshihara, T.Suzuki and T.Fujimura: J.Phys.Soc.Jpn. 54(1985)4607.
12. J.Petzelt: J.Phys. & Chem. Solid 36(1979)1005.
13. K.Fossheim, T.Laegreid, E.Sandvold, F.Vassenden, K.A.Müller and J.G.Bednortz, Solid State Commun. 63(1987)531.
14. D.D.Betts: "Phase Transition and Critical Phenomena" ed. C.Domb and M.S.Green, Academic Press, London, 1974, Vol.3, P674.
15. A.R.Moodenbaugh, Youwen Xu, M.Suenaga, T.J.Folkerts and R.N.Skelton: Phys.Rev. B38(1988)4596.
16. K.Kumagai, I.Watanabe, H.Aoki, Y.Nakamura, T.Kimura, Y.Nakamichi and H.Nakajima: Physica 148B(1987)480.

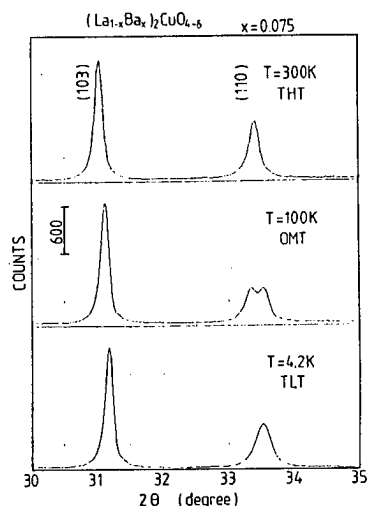


Fig. 1. Powder X-ray diffraction pattern of the sample with  $x=0.075$  at various temperatures.

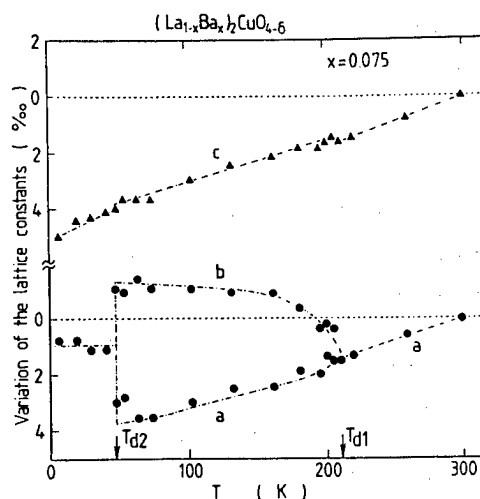


Fig. 2. Temperature dependence of the lattice constants of the sample with  $x=0.075$ .

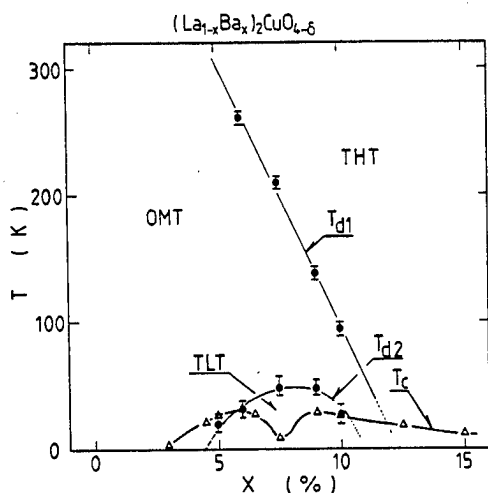


Fig. 3. Phase diagram of  $(La_{1-x}Ba_x)_2CuO_{4-δ}$ . The transition temperatures  $T_{d1}$  and  $T_{d2}$  were determined by X-ray diffraction.  $T_c$  was determined by electrical resistivity measurement.

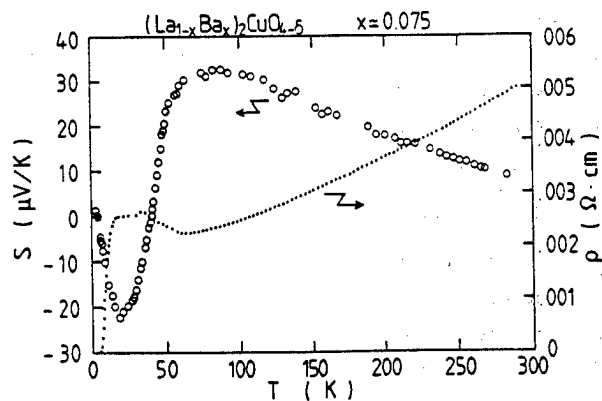


Fig. 4. Temperature dependence of thermoelectric power and electrical resistivity of the sample with  $x=0.075$ .

H. Asano

Institute of Materials Science, University of Tsukuba  
Tsukuba 305, Japan

Crystal structures of oxide superconductors  $(\text{Nd,Ce,Sr})_2\text{CuO}_{4-y}$ ,  $\text{YBa}_2\text{Cu}_{2.8}\text{Zn}_{0.2}\text{O}_{7-y}$  and  $\text{La}_{1.9}\text{Ca}_{1.1}\text{Cu}_2\text{O}_6$  have been refined by high-resolution neutron powder diffraction.  $(\text{Nd,Ce,Sr})_2\text{CuO}_{4-y}$  shows an intermediate structure between the  $\text{K}_2\text{NiF}_4$  and  $\text{Nd}_2\text{CuO}_4$  structures. In Zn-doped  $\text{YBa}_2\text{Cu}_3\text{O}_{7-y}$ , the Zn atoms occupy selectively the Cu(2) site on the  $\text{CuO}_2$  plane. Neutron diffraction of  $\text{La}_{1.9}\text{Ca}_{1.1}\text{Cu}_2\text{O}_6$  has confirmed the X-ray powder diffraction result of Nguyen et al.

### I. Crystal structure of $(\text{Nd,Ce,Sr})_2\text{CuO}_{4-y}$ [1]

Recently, a new oxide superconductor with  $T_c$  (onset) of 28K was found in the Nd-Ce-Sr-Cu-O system by Akimitsu et al. [2]. After this discovery, Takayama-Muromachi et al. [3] identified the superconducting phase to be  $(\text{Nd}_{0.66}\text{Ce}_{0.135}\text{Sr}_{0.205})_2\text{CuO}_{4-y}$  by X-ray and electron diffraction. Metal positions in this phase are identical with those of the  $\text{K}_2\text{NiF}_4$  or  $\text{Nd}_2\text{CuO}_4$  structure except the cation order of Ce and Sr. In this work, the structure of  $(\text{Nd}_{0.66}\text{Ce}_{0.135}\text{Sr}_{0.205})_2\text{CuO}_{4-y}$  was refined by neutron powder diffraction. Neutron diffraction data were taken on a high-resolution neutron powder diffractometer HRP at KEK. The observed intensity data were analyzed by the Rietveld method using a RIETAN program.

Final structure parameters based on space group  $P4/nmm$  are listed in Table I. Tetragonal lattice parameters were refined to be  $a = 3.8563(3)$  Å and  $c = 12.4843(9)$  Å. R factors were  $R_{wp} = 5.9\%$ ,  $R_p = 4.5\%$ ,  $R_I = 3.5\%$  and  $R_F = 2.7\%$ . Since the occupation factor  $g$  and the thermal parameter for site O(2) are strongly correlated, it is almost impossible to determine these parameters accurately. However, fixing  $g$  for this site at 1 gave larger R factors. Therefore, site O(2) is believed to be slightly deficient. Figure 1 shows the crystal structure of  $(\text{Nd}_{0.66}\text{Ce}_{0.135}\text{Sr}_{0.205})_2\text{CuO}_{3.93}$ . The unit cell consists of two parts; the upper part is of the  $\text{K}_2\text{NiF}_4$ -type where the (Nd,Sr) ion is coordinated to nine oxide ions, while the lower part is of the  $\text{Nd}_2\text{CuO}_4$ -type including the (Nd,Ce) ion in 8-coordination. There is only one crystallographic site for the Cu ion with a pyramidal coordination. Therefore, this compound is the first case of the Cu-based superconductor in which every Cu ion takes a pyramidal 5-coordination.

### II. Zn-location in $\text{YBa}_2\text{Cu}_{2.8}\text{Zn}_{0.2}\text{O}_{7-y}$ [4]

Substitution of foreign elements for Cu in  $\text{YBa}_2\text{Cu}_3\text{O}_{7-y}$  has generally unfavorable effect on superconductivity, but in different degree for different elements. Substitution of Zn is worthy of special attention, since anomalously large  $T_c$  suppression was reported compared with other 3d elements. Therefore, precise knowledge of the crystal structure on Zn-doped  $\text{YBa}_2\text{Cu}_3\text{O}_{7-y}$  is important for understanding the mechanism of such a large  $T_c$  depression.

The structure refinement was carried out on the basis of the orthorhombic  $\text{YBa}_2\text{Cu}_3\text{O}_{7-y}$  structure with space group  $Pmmm$ , where Zn was distributed among the 1a and 2q sites. The resulting occupation factor of Zn at the 1a site became negative. Subsequent refinements, therefore, assumed that Zn atoms

Table I. Structure parameters of

$(\text{Nd}_{0.66}\text{Ce}_{0.135}\text{Sr}_{0.205})_2\text{CuO}_{3.93}$ . Estimated standard deviations in parentheses refer to the last digit printed.

Atom	Site	x	y	z	g	B/A <sup>2</sup>
Nd,Sr	2c	0	1/2	0.3895(3)	1	0.47
Nd,Ce	2c	0	1/2	0.1038(3)	1	0.64
Cu	2c	1/2	0	0.2510(3)	1	0.48
O(1)	4f	0	0	0.2374(3)	1	1.05
O(2)	2c	1/2	0	0.4288(5)	0.93(2)	3.55
O(3)	2a	0	0	0	1	0.76

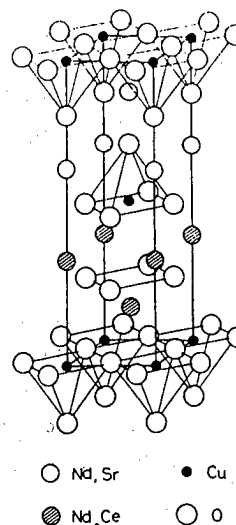


Fig. 1. Crystal structure of

$(\text{Nd}_{0.66}\text{Ce}_{0.135}\text{Sr}_{0.205})_2\text{CuO}_{3.93}$ .

share the 2q site with Cu(2) atoms in the Cu:Zn ratio of 0.9 : 0.1 and that Cu(1) atoms fully occupy the 1a site. Table II lists final structure parameters. Lattice parameters were refined to be  $a = 3.8920(2)$  Å,  $b = 3.8214(2)$  Å and  $c = 11.6829(7)$  Å. R factors were  $R_{wp} = 5.3\%$ ,  $R_p = 3.9\%$ ,  $R_I = 1.4\%$  and  $R_F = 1.0\%$ .

EXAFS measurements made on the same sample show that Zn atoms are coordinated to five oxygen atoms with four short and one long Zn-O bonds. This indicates the Zn-location on the Cu(2) site forming a  $\text{CuO}_5$  pyramid, being consistent with the neutron diffraction result. The Zn-doped compound shows a quite similar crystal structure to undoped  $\text{YBa}_2\text{Cu}_3\text{O}_{7-y}$ ; the orthorhombic distortion from the perovskite structure ( $a : b : c/3$ ) are respectively 1.018 : 1 : 1.019 and 1.017 : 1 : 1.020 for doped and undoped crystals. Moreover, occupation factors for the oxygen sites O(1) and O(2) are 0.91 and 0.03, respectively, which agree with those of the undoped crystal. In spite of the great similarity of the crystal structure,  $T_c$  of the doped sample is 40K. This large  $T_c$  suppression is due to the Zn occupancy on the Cu(2) site of the  $\text{CuO}_2$  plane which plays a crucial role in high- $T_c$  superconductivity.

### III. Structure refinement of $\text{La}_{1.9}\text{Ca}_{1.1}\text{Cu}_2\text{O}_6$ [5]

A series of superconducting oxides containing Cu has a two-dimensional  $\text{CuO}_2$  plane. Cu ions on this plane are coordinated to oxide ions octahedrally, pyramidally or square-planarly. In addition, the formal charge of Cu must be within the range of +2.1 - 2.3, which introduces an appropriate amount of  $(\text{Cu}-\text{O})^+$  holes into the  $\text{CuO}_2$  plane.  $\text{La}_{2-x}\text{A}_{1+x}\text{Cu}_2\text{O}_{6-y}$  compounds ( $x \sim 0.1$  for  $A = \text{Ca}$  and  $0 < x < 0.14$  for  $A = \text{Sr}$ ) do not show superconductivity, although they satisfy the structural condition. Since the structures of  $\text{La}_{2-x}\text{A}_{1+x}\text{Cu}_2\text{O}_{6-y}$  were investigated only by X-ray powder diffraction [6], the structure parameters, particularly of oxygen, may not be accurate. More detailed knowledge of the crystal structure is desired to understand the lack of superconductivity in these compounds. This study was

Table II. Structure parameters of

$\text{YBa}_2\text{Cu}_{2.8}\text{Zn}_{0.2}\text{O}_{6.94}$ .

Atom	Site	x	y	z	g	B/A <sup>2</sup>
Y	1h	1/2	1/2	1/2	1	0.43
Ba	2t	1/2	1/2	0.1840(3)	1	0.57
Cu(1)	1a	0	0	0	1	0.54
Cu(2)	2q	0	0	0.3543(2)	0.9	0.39
Zn	2q	0	0	0.3543(2)	0.1	0.39
O(1)	1b	1/2	0	0	0.91(1)	0.86
O(2)	1e	0	1/2	0	0.03(1)	0.86
O(3)	2q	0	0	0.1591(2)	1	0.65
O(4)	2r	0	1/2	0.3787(3)	1	0.56
O(5)	2s	1/2	0	0.3784(3)	1	0.44

undertaken to reinvestigate the crystal structure of  $\text{La}_{1.9}\text{Ca}_{1.1}\text{Cu}_2\text{O}_{6-y}$  by high-resolution neutron powder diffraction. Although the concentration of  $(\text{Cu}-\text{O})^\ddagger$  holes increases with increasing Ca content,  $\text{La}_{2-x}\text{Ca}_{1+x}\text{Cu}_2\text{O}_{6-y}$  has a limited homogeneity range at  $x \sim 0.1$ .

The structure refinement was carried out on the basis of the X-ray diffraction result of Nguyen et al. [6] with space group  $I4/mmm$ . Since the occupation factors of sites La(1), Ca(1), La(2) and Ca(2) have relations  $g_{\text{La}(1)} + g_{\text{Ca}(1)} = 1$ ,  $g_{\text{La}(1)} + 2g_{\text{La}(2)} = 1.9$  and  $g_{\text{Ca}(1)} + 2g_{\text{Ca}(2)} = 1.1$ , only  $g_{\text{La}(1)}$  was refined under the linear constraints. Preliminary refinement revealed that the lowest R factor was obtained at  $g_{\text{O}(2)} = 1$ , and this site was regarded as fully occupied in subsequent refinements. Although  $g$  of the 2b site: (0, 0, 1/2) and (1/2, 1/2, 0) was refined, occupation of this site was proved to be negligible, and the site was fixed at vacant. The resulting structure parameters are listed in Table III, and the crystal structure is shown in Fig. 2. Tetragonal lattice parameters were refined to be  $a = 3.8245(2)$  Å and  $c = 19.420(1)$  Å. R factors were  $R_{\text{wp}} = 5.5\%$ ,  $R_p = 4.0\%$ ,  $R_I = 2.0\%$  and  $R_F = 1.8\%$ . Chemical composition of the present compound is  $\text{La}_{1.9}\text{Ca}_{1.1}\text{Cu}_2\text{O}_6$ , from which formal charge of Cu is deduced to be +2.05. This value is evidently too small for the occurrence of superconductivity.

Table III. Structure parameters of  $\text{La}_{1.9}\text{Ca}_{1.1}\text{Cu}_2\text{O}_6$ .

Atom	Site	x	y	z	g	$B/\text{\AA}^2$
La(1)	2a	0	0	0	0.12(1)	0.54
Ca(1)	2a	0	0	0	0.88(1)	0.54
La(2)	4e	0	0	0.17571(7)	0.89(1)	0.56
Ca(2)	4e	0	0	0.17571(7)	0.11(1)	0.56
Cu	4e	0	0	0.41488(7)	1	0.47
O(1)	8g	0	1/2	0.08217(7)	1	0.77
O(2)	4e	0	0	0.2962(1)	1	1.55

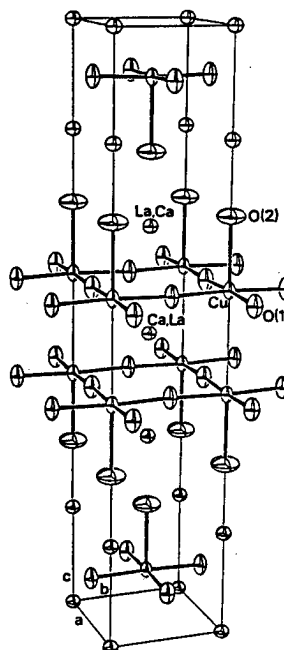


Fig. 2. Crystal structure of  $\text{La}_{1.9}\text{Ca}_{1.1}\text{Cu}_2\text{O}_6$ .

#### References

- [1] H. Sawa, S. Suzuki, M. Watanabe, J. Akimitsu, H. Matsubara, H. Watabe, S. Uchida, K. Kokusho, H. Asano, F. Izumi and E. Takayama-Muromachi: Nature, in press.
- [2] J. Akimitsu, S. Suzuki, M. Watanabe and H. Sawa: Jpn. J. Appl. Phys. **27** (1988) L1859.
- [3] E. Takayama-Muromachi, Y. Matsui, Y. Uchida, F. Izumi, M. Onoda and K. Kato: Jpn. J. Appl. Phys. **27** (1988) L2283.
- [4] H. Maeda, A. Koizumi, N. Bamba, E. Takayama-Muromachi, F. Izumi, H. Asano, K. Shimizu, H. Moriwaki, H. Maruyama, Y. Kuroda and H. Yamazaki: to be submitted to Jpn. J. Appl. Phys.
- [5] F. Izumi, E. Takayama-Muromachi, Y. Nakai and H. Asano: Physica C **157** (1989) 89.
- [6] N. Nguyen, L. Er-Rakho, C. Michel, J. Choisnet and B. Raveau: Mat. Res. Bull. **15** (1980) 891.

# Electron Microscopic Studies of High-Tc Superconductors

K. Hiraga, D. Shindo, T. Oku and M. Hirabayashi

Institute for Materials Research, Tohoku University  
2-1-1 Katahira, Sendai 980, Japan

High-resolution electron microscopy was made on high-Tc superconducting oxides of the Tl-Ba-Ca-Cu-O system with a 400 kV electron microscope having a resolution of 0.17 nm. Arrangements of oxygen atoms as well as cation atoms in  $\text{Tl}_2\text{Ba}_2\text{Ca}_n\text{Cu}_{n+1}\text{O}_{2n+6}$  ( $n=1-4$ ) and  $\text{TlBa}_2\text{Ca}_n\text{Cu}_{n+1}\text{O}_{2n+5}$  ( $n=1-6$ ) were examined from the high-resolution observations.

In our previous papers, it was found that high-resolution electron microscopic studies with a 400 kV electron microscope having a resolution of 0.17 nm give us informations about not only arrangements of cation atoms but ordered arrangements of oxygen atoms in the high-Tc superconducting oxides based on a perovskite structure. Recently many polytypes with different numbers of perovskite units between single or double Tl layers were reported in a Tl-Ba-Ca-Cu-O system. The purpose of the present work is to make high-resolution microscopy on various types of superconducting oxides in the Tl-Ba-Ca-Cu-O system.

## 1) $\text{Tl}_2\text{Ba}_2\text{Ca}_n\text{Cu}_{n+1}\text{O}_{2n+6}$ oxides

We observed high-resolution images of four types of polytypes ( $n=1-4$ ) in a series of  $\text{Tl}_2\text{Ba}_2\text{Ca}_n\text{Cu}_{n+1}\text{O}_{2n+6}$  formed with double Tl layers. An example of the observed images is shown in Fig. 1 together with a structure model. In the observed image, an arrangement of cation atoms is directly seen as that of dark spots. Darkness of the dark spots can be considered to be proportional to atomic numbers of the cation atoms in thin crystal approximation. On the other hand, although oxygen atoms located in between the cation atoms are not represented as dark spots, positions of oxygen vacancies on the Ca layers can be clearly investigated from the other bright spots corresponding to oxygen positions as brighter spots indicated by Ov. The calculated image based on the structure model represented well the observed image.

In all observations of  $\text{Tl}_2\text{Ba}_2\text{Ca}_n\text{Cu}_{n+1}\text{O}_{2n+6}$  ( $n=1-4$ ), arrangements of the cation atoms proposed by X-ray or neutron diffraction were confirmed, and oxygen sites on the Ca layers were found to be always vacant. Also we often observed ordered intergrowth formed with different polytypes. The intergrowth changes the relative contents of Tl and Ba to Ca and Cu.

## 2) $\text{TlBa}_2\text{Ca}_n\text{Cu}_{n+1}\text{O}_{2n+5}$

We observed high-resolution images of many types of structures from  $n=1$  to 8 in

the  $\text{TlBa}_2\text{Ca}_n\text{Cu}_{n+1}\text{O}_{2n+5}$  system. An example of the observations is shown in Fig. 2. The image shows the structure formed with single Tl layers. In the image, oxygen atom positions on the Ca layers can be seen as brighter spots, indicating oxygen vacancies. We observed an well ordered structure of  $n=6$  as the longest stacking sequence and also a longer sequence of  $n=8$  as intergrowth defects. The result shows the possibility for forming many polytypes from  $n=0$  to  $n=8$  with decreasing Tl and Ba contents.

The our observations with a 400 kV electron microscope show that high-resolution electron microscopy is a powerful tool for the structure analyses of the high- $T_c$  superconducting oxides, particularly for the samples including defects and some phases with other structures.

The work was supported by a Grant-in-Aid for Scientific Research on Priority Areas "Mechanism of Superconductivity."

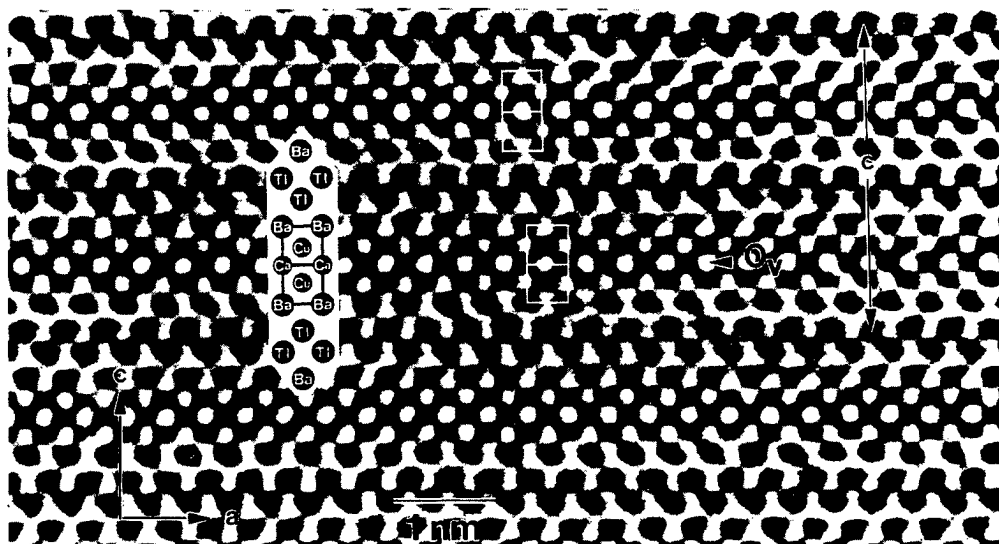


Figure 1 High-resolution image of  $\text{Tl}_2\text{Ba}_2\text{CaCu}_2\text{O}_8$

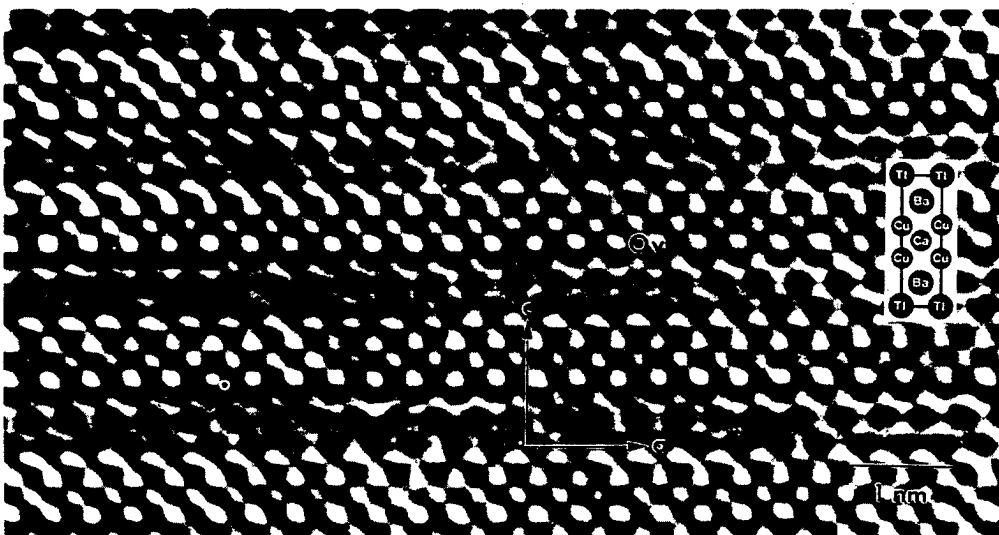


Figure 2 High-resolution image of  $\text{TlBa}_2\text{CaCu}_2\text{O}_7$



# High Resolution Observation of Grain Boundaries in Oxide Superconductors

Y. Takahashi, M. Mori and Y. Ishida

Institute of Industrial Science, University of Tokyo,  
7-22-1 Roppongi, Minato-ku, Tokyo 106, Japan

Grain boundaries in  $\text{YBa}_2\text{Cu}_3\text{O}_{7-x}$  and  $\text{Bi}_2(\text{Sr,Ca})_3\text{Cu}_2\text{O}_x$  were investigated by high resolution electron microscopy. A flat boundary parallel to a basal plane for one of neighboring grains was frequently observed in sintered specimens. In a bismuth superconductor, a  $\text{Bi}_2\text{O}_2$  layer tended to connect both the grains. A relationship between grain boundaries and a low  $J_c$  property in a polycrystalline specimen is discussed.

There are three important parameters in superconductors; critical temperature  $T_c$ , upper critical field  $H_{c2}$  and critical current  $J_c$ . The  $T_c$  is an intrinsic value of materials and it is very advantageous for practical applications that the  $T_c$  is above liquid nitrogen temperature in both  $\text{YBa}_2\text{Cu}_3\text{O}_{7-x}$  (YBCO) and Bi-Sr-Ca-Cu-O (BSCCO). The  $H_{c2}$  is also large enough at 77K. However, the third parameter  $J_c$  changes extensively by the synthesis process. Although  $J_c > 10^6 \text{A/cm}^2$  is achieved in single crystal and epitaxial thin film, it is less than  $10^4 \text{A/cm}^2$  in a sintered specimen. Some defects might be related to the large discrepancy. It is difficult to decide whether or not they act favorably as a pinning center of fluxoid, because the materials belong to type-II superconductors but coherence length is extremely short. Recently, H. Kumakura et al [1] and D.C. Larbalestier et al [2] reported a small  $J_c$  value measured by the direct resistive method as compared to that evaluated by a hysteresis of magnetization curve. They indicated a weak coupling of grains in sintered specimens.

In this report, we show a structural analysis of grain boundary (G.B.) in YBCO and BSCCO by high resolution TEM observation. The obtained results suggest a barrier effect of G.B., which are consistent with their macroscopic measurements.

The YBCO sample was prepared by a solid state reaction method using  $\text{Y}_2\text{O}_3$ ,  $\text{BaCO}_3$  and  $\text{CuO}$  in a stoichiometric composition. A transition temperature measured by four terminal method was about 90K. The BSCCO sample was prepared similarly. After mixing powders in  $\text{Bi}_2\text{Sr}_2\text{Ca}_2\text{Cu}_3\text{O}_x$  ratio, a final sintering was performed at 1123K for 14hr.

The specimen is composed of some phases. A resistivity curve showed that most of them is 70K phase, but it contained a few 110K phase.

Thin foils for TEM observation were prepared by argon ion thinning method. High resolution electron microscopy was performed by JEM-2000EX operated at 200keV.

Figure 1 and 2 show high resolution images of G.B. in YBCO. In most cases, G.B. is intimately connected to each other grains as shown in Fig. 1. It is rare that there exists a thin amorphous layer (1-2nm) [3]. On the other hand, a flat boundary is often observed in a sintered specimen. The boundary plane is parallel to a basal plane of a grain (c-plane boundary). The preferential growth during sintering may be related to a layered structure of YBCO. The boundary is often observed to be decorated by a thick amorphous layer (10nm), which is mainly caused by a G.B. fracture owing to an anisotropy of thermal expansion coefficients between a- (or b-)axis and c-axis.

A c-plane boundary is observed more frequently in BSCCO because it is also a layered structure. But a largest difference between YBCO and BSCCO is that the latter is composed of a perovskite unit and a  $\text{Bi}_2\text{O}_2$  layer. Dots in Fig. 3 indicate a position of bismuth atom, where Bi double layers



Fig. 3 High resolution image of c-plane boundary in BSCCO

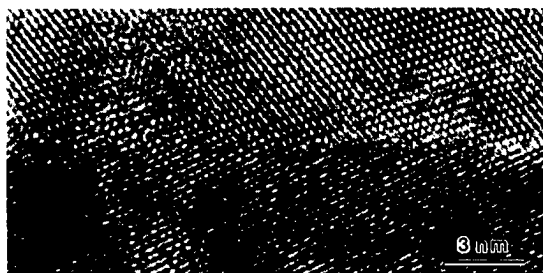


Fig.1 High resolution image of general boundary in YBCO

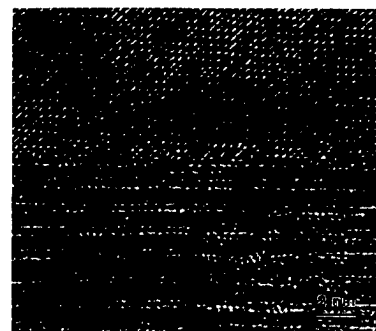


Fig. 2 High resolution image of c-plane boundary in YBCO

are found to be flat in atomic scale at G.B. Another example is shown in Fig. 4. A crystal orientation of a bottom grain is [100]. An ordered structure is seen at G.B. and the periodicity coincides to lattice parameters of BSCCO ( $5b \times c/2 = 2.7 \times 1.5\text{nm}$ ). In addition, a  $\text{Bi}_2\text{O}_2$  layer connects a neighboring grain in a facet of G.B. These preferential selectivity of  $\text{Bi}_2\text{O}_2$  layer is explained by its flexibility; two bismuth planes is widely separated by oxygen plane, then, the bonding of the layer is weak and it can accommodate an incommensurate modulation. Therefore, a  $\text{Bi}_2\text{O}_2$  layer makes G.B.

energy lower in a relaxation of G.B strain. However, a  $\text{Bi}_2\text{O}_2$  layer at G.B. is not beneficial from a view of  $J_c$  property. It is believed that a Cu-O plane in a perovskite unit plays a main role of conductivity and that a  $\text{Bi}_2\text{O}_2$  layer only separates these sheets. Thus a  $\text{Bi}_2\text{O}_2$  layer at G.B. may be compared with a S-I-S junction, where a coupling is very weak in superconductivity.

TEM observation showed that there is no obstacle at G.B., but it still acts as a barrier. Recently, D.Dimos et al [4] postulated an orientation dependence of  $J_c$  across G.B ( $J_c^{\text{gb}}$ ) using bicrystal thin films in YBCO.  $J_c^{\text{gb}}$  decreases drastically in two orders magnitude of that in a grain ( $J_c^{\text{G}}$ ). We analyzed their result again and the G.B. width as a barrier was estimated to be  $w=1.8\text{nm}$  in thickness [5]. The result explains a weak coupling at G.B because a coherent length is so small and anisotropic owing to its layered structure ( $\xi=3.1\text{nm}$  in a basal plane and  $\xi=0.51\text{nm}$  parallel to c-axis) that the reduction in the width of G.B. ( $w/\xi$ ) varies from 0.58 to 3.5. It indicates  $J_c^{\text{gb}}$  is heavily depends on a crystal orientation; a [001] tilt boundary is most advantageous since a direction of current is parallel to c-planes for both grains. On the other hand,  $J_c^{\text{gb}}$  may be almost zero when a boundary plane is c-plane for one of grains because the reduced thickness tends to be largest. As described above, the type of boundary is abundant in a sintered specimen which is also related to the low  $J_c$  in polycrystalline specimens.

In summary, G.B. in YBCO and BSCCO were examined by high resolution electron microscopy. Grains are tightly connected in atomic scale, however it is electrically weak coupling due to the short coherence length. The poor  $J_c$  at G.B. may be enhanced when a boundary is parallel to c-plane, which is abundant in a sintered specimen. Improving the connection of grains may contributes to  $J_c$  property in a polycrystalline material.

#### References

- [1] H.Kumakura, M.Uehara and T.Togano: Appl. Phys. Lett., **51**(1987),1557.
- [2] D.C.Larbalestier, M.Daeumling, P.J.Lee, T.F.Kelly, J.Seuntjens, C.Meingast, X.Cai, J.Mackinnell, R.D.Ray, R.G.Dillenburg and E.E.Hellstrom: Cryogenics, **27** (1987),411.
- [3] Y.Ishida, Y.Takahashi, M.Mori, K.Kishio, K.Kitazawa, K.Fueki and M.Kawasaki: J. Electron Microsc., **36**(1987),251.
- [4] D.Dimos, P.Chaudhari, J.Mannhart and F.K.LeGoue: Phys. Rev. Lett., **61**(1988),219.
- [5] Y.Takahashi, M.Mori and Y.Ishida: submitted to Phys. Rev. Lett.

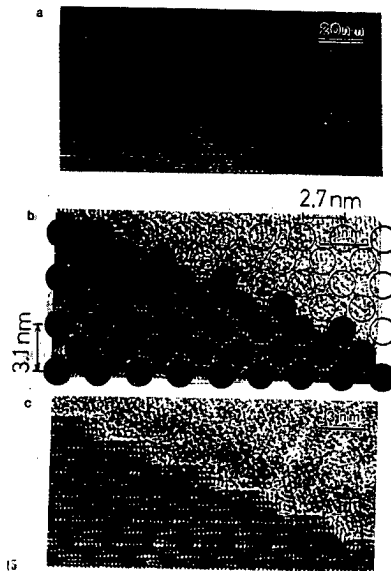


Fig. 4 Periodic boundary structure in BSCCO

High-resolution electron microscopy in-situ observation  
of a transformation interface between tetragonal  
and orthorhombic phases in  $\text{YBa}_2\text{Cu}_3\text{O}_{7-x}$

K. Sasaki, K. Kuroda, and H. Saka

Department of Metallurgy, Faculty of Engineering, Nagoya University,  
Furo-cho, Chikusa-ku, Nagoya 464-01, Japan

The phase transformation between the tetragonal and orthorhombic phases in  $\text{YBa}_2\text{Cu}_3\text{O}_{7-x}$  has been observed by in-situ high resolution electron microscopy and the structure of a transformation interface between the two phases has been determined directly from an analysis of the lattice fringes. It has been shown that the interface is fully coherent and broad over 50nm, and that the lattice cells undergo a continual transition from the tetragonal phase to the orthorhombic phase. This observation is in good agreement with a model proposed by Malis and Gleiter (1979a,b) for the ferroelectric-paraelectric transformation in  $\text{BaTiO}_3$ .

#### § 1. Introduction

A perovskite-type oxide  $\text{YBa}_2\text{Cu}_3\text{O}_{7-x}$ , which has the normal to superconducting transition temperature ( $T_c$ ) at around 90K (Cava, Batlogg, Dover, Murphy, Sunshine, Sigrist, Remeika, Rietman, Zahurak and Espinosa 1987), has two polymorphous types, i.e. orthorhombic and tetragonal phases as the high and low temperature phases, respectively, the latter showing the superconductivity below  $T_c$  (Sigrist, Sunshine, Murphy, Cava and Zahurak 1987).

The crystal structures of the tetragonal and orthorhombic phases have already been determined (Izumi, Asano, Ishigaki, Takayama, Uchida, Watanabe and Nishikawa 1987). The phase transformation between the orthorhombic and tetragonal phases is caused by ordering and disordering of oxygen vacancies (Iijima, Ichihashi, Kubo and Tabuchi 1987).

A preliminary in-situ observation by transmission electron microscopy of the phase transformation in  $\text{YBa}_2\text{Cu}_3\text{O}_{7-x}$  (Sasaki, Kuroda, Saka and Imura 1987) has shown that no distinct diffraction contrasts are associated with a transformation interface between the orthorhombic and tetragonal phases. Similar observations on the transformation interface have been made by Malis and Gleiter (1979a,b) on a ferroelectric-paraelectric transformation between a cubic phase and a tetragonal one in  $\text{BaTiO}_3$ , which also has a perovskite-type structure. They explained their observations by assuming that the transformation interface is rather broad and that the lattice cells undergo a continual transition from one phase to the other across it (Malis and Gleiter 1979a,b).

In the work which will be described in the present letter, the motion and the atomistic structure of the interface between the tetragonal and orthorhombic phases in  $\text{YBa}_2\text{Cu}_3\text{O}_{7-x}$  was observed at high resolution allowing the observation of lattice fringes by in-situ electron microscopy. The validity of the Malis and Gleiter's model was confirmed directly, and moreover, the width of the transformation interface was determined quantitatively.

## § 2. Experimental

The samples were prepared by a standard powder metallurgical method from high purity  $Y_2O_3$ ,  $BaCO_3$  and  $CuO$  powders. They were ground, pelletized, and sintered at  $1000^\circ C$  for 8hr. Specimens for electron microscopy were prepared by mechanical grinding and ion thinning. In-situ heating experiments at lower resolution level were carried out in a JEOL 200CX microscope equipped with a side-entry single-tilt heating holder at an accelerating voltage of 200kV.

In-situ high resolution electron microscopy observations of the motion of a transformation phase interface were carried out in a Hitachi H-1250ST equipped with a side-entry double-tilt holder at an accelerating voltage of 1000kV. In this case, in order to minimize the drift of a specimen due to the thermal instability, a beam-heating technique was employed, that is, the specimen was heated locally by a fine focused electron beam.

## § 3. Results and Discussion

The preliminary heating experiment in the electron microscope has shown that the phase transformation between the orthorhombic and tetragonal phases in  $YBa_2Cu_3O_{7-x}$  is accompanied by disappearance or reappearance of twins, depending on the sense of the transformation (Sasaki et al. 1987). Fig. 1(a) shows twins which are shrinking during heating under observation. The phase transformation started in the central part of the figure presumably because of beam heating of the sample. The area which does not contain the twins is identified as the tetragonal phase (in the center of Fig. 1(a)) and those which contain the twins are identified as the orthorhombic phase (in the upper and lower sides of Fig. 1(a)), as can be seen from the electron diffraction patterns taken from these areas (fig. 1(b) and (c)). Although no distinct transformation interface was observed between the tetragonal and the orthorhombic phases, a boundary along which the twins disappear (hereinafter referred to as the disappearance front (Malis and Gleiter 1979)) is considered to correspond to the interphase interfaces. The interphase interfaces between the tetragonal phase in the center and the orthorhombic phases in the upper and lower sides of Fig. 1(a) were indicated by two broken lines in this figure.

Figure 2(a) is a high resolution electron micrograph of a twin similar to those shown in fig. 1(a) but viewed end on. Again, neither localized interface nor defects such as dislocations were observed near the disappearance front, i.e., near the tip of the twin. It is evident that the transformation interface between the tetragonal and the orthorhombic phases is fully coherent.

Figures 2(b), (c) and (d) are enlarged images of the areas B, C and D, respectively, shown in Fig. 2(a). The lattice fringes in Fig. 2(b) correspond to the {100} plane of the tetragonal phase. In areas E and F in Fig. 2(d) are observed {100} and {010} lattice fringes of the orthorhombic phase. The ratio of lattice constants  $a/b$  can be calculated from the angle  $\theta$  between the fringes in the upper and lower sides of the twin boundary. In Figs. 2(b), (c) and (d), the fringes are indicated by two solid lines to show clearly the angle  $\theta$ . Figure 3(a) shows schematically the structure of a twin boundary and the relationship between the  $a/b$ -value and the angle  $\theta$ . The ratio of  $a/b$  is expressed by

$$a/b = \tan \phi \quad (1)$$

where  $\phi$  is the angle between the {010} fringe and the diagonal line of a rectangular surrounded with the {100} and the {010} fringes, and  $\theta$  is the angle

between the (010) fringes in area A and the (100) fringes in area B. The angles  $\theta$  and  $\phi$  are correlated by  $\theta + 2\phi = \pi/2$ , i.e.,  $\phi = \pi/4 - \theta/2$ . The substitution of this equation into Eq(1) gives

$$a/b = \tan (\pi/4 - \theta/2) \quad (2)$$

Figure 3(b) shows the variation of the a/b-value along the twin boundary. No sharp change in the a/b-value was observed across the transformation interface between the tetragonal and orthorhombic phases. Instead, the a/b-value decreased continuously from 0.995 in the tetragonal region to 0.985 in the orthorhombic one across the disappearance front, the width of the transition region being about 50nm. Phase transformation between the orthorhombic and the tetragonal phases is achieved by a passage of the coherent transformation interface through material.

Essentially similar model of the structure of the transformation interface (Fig.3(c)) has been assumed to explain the observed absence of the diffraction contrast associated with the phase transformation between a cubic phase and a tetragonal one in BaTiO<sub>3</sub> by Malis and Gleiter(1979). In this model the interface are divided into four regions, i.e. regions I, II, III, IV. They correspond to the tetragonal, transition, cubic with continuous lattice plane curvature and undistorted cubic phase regions. In the present case, the region I corresponds to the area of the orthorhombic phase where the a/b-value is 0.985, the region II corresponds to the area in which the a/b-value changes, and the region III corresponds to the area where the a/b-value is 0.995. In Fig.2 the area where the a/b-value of 1 (corresponding to region IV) was not observed. However, as shown in Fig.1(b), an electron diffraction pattern taken from that area which contains no twin boundary and which is far from the interphase interface between the tetragonal and orthorhombic phases showed the existence of the undistorted tetragonal phase, i.e. a/b=1. The facts suggest that the a/b-value increases gradually from 0.995 to 1 in region III over a rather wide distance (probably of the order of a few  $\mu$ m) from the interphase interface. Thus, it is not surprising that the whole area of the region III was not recorded on a single micrograph especially when taken at high magnification in order to attain high resolution. The present high resolution electron microscopy observation confirms that the structure of the transformation interface between the tetragonal and orthorhombic phases in YBa<sub>2</sub>Cu<sub>3</sub>O<sub>7-x</sub> is in good agreement with the model by Malis and Gleiter.

#### References

- Cava, R., Batlogg, B., Dover, R., Murphy, D., Sunshine, S., Siegrist, T., Remeika, J., Rietman, E., Zahurak, S. and Espinosa, G., 1987, Phys. Rev. Lett., 58, 1676.
- Iijima, S., Ichihashi, T., Kubo, Y. and Tabuchi, J., 1987, Jpn. J. Appl. Phys., 26, L1478.
- Izumi, F., Asano, H., Ishigaki, T., Takayama-Muromachi, E., Uchida, Y., Watanabe, N. and Nishikawa, T., 1987, Jpn. J. Appl. Phys., 26, L649.
- Malis, T. and Gleiter, H., 1979a, J. Appl. Phys., 50, 4920, 1979b, Ibid., 50, 4924.
- Sasaki, K., Kuroda, K., Saka, H. and Imura, T., 1987, J. Electron Microsc., 36, 232.
- Siegrist, T., Sunshine, S., Murphy, D., Cava, R. and Zahurak, S., 1987, Phys. Rev., B35, 7137.
- Yukino, K., Sato, T., Ooba, S., Ohta, M., Okamura, F. and Ono, A., 1987 Jpn. J. Appl. Phys., 26, L869.

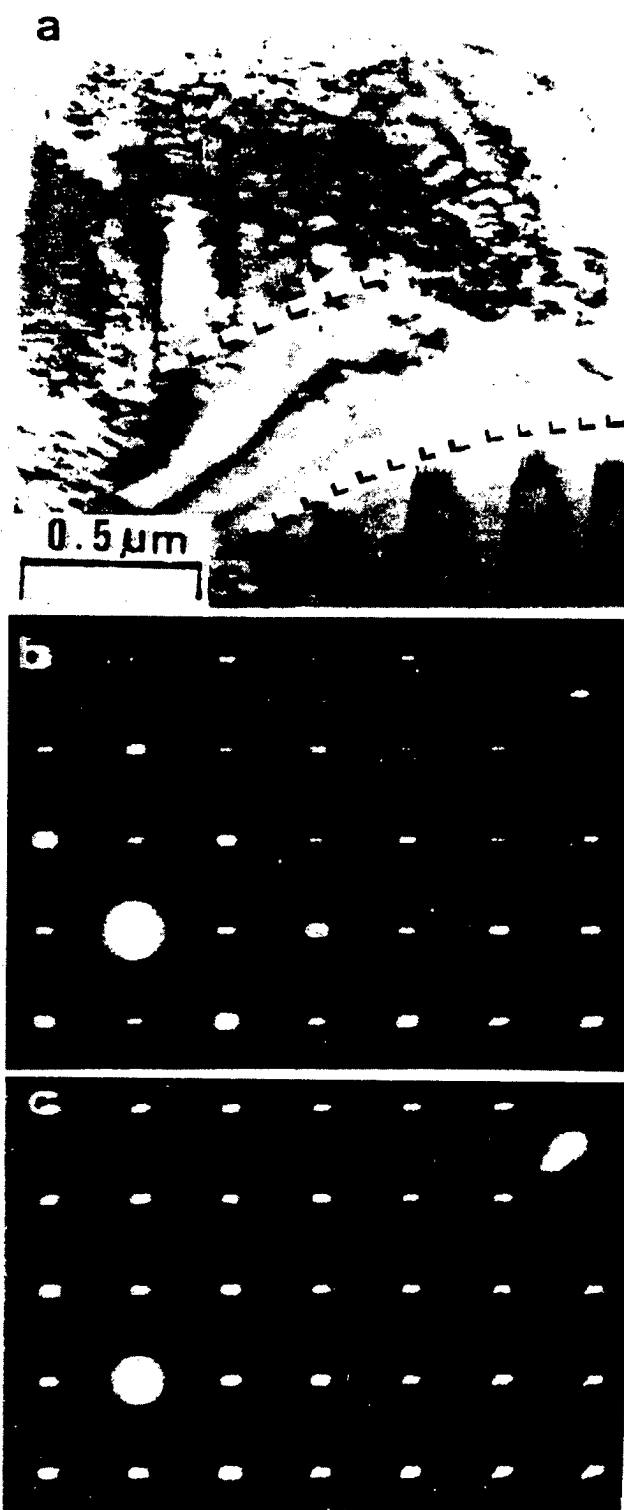


Fig. 1 TEM micrographs showing (a) twins which shrink during heating under observation and selected area diffraction patterns from the areas (b) which do not contain the twins and (c) which contain the twins. Broken lines in (a) indicate the disappearance front of the twin boundaries.

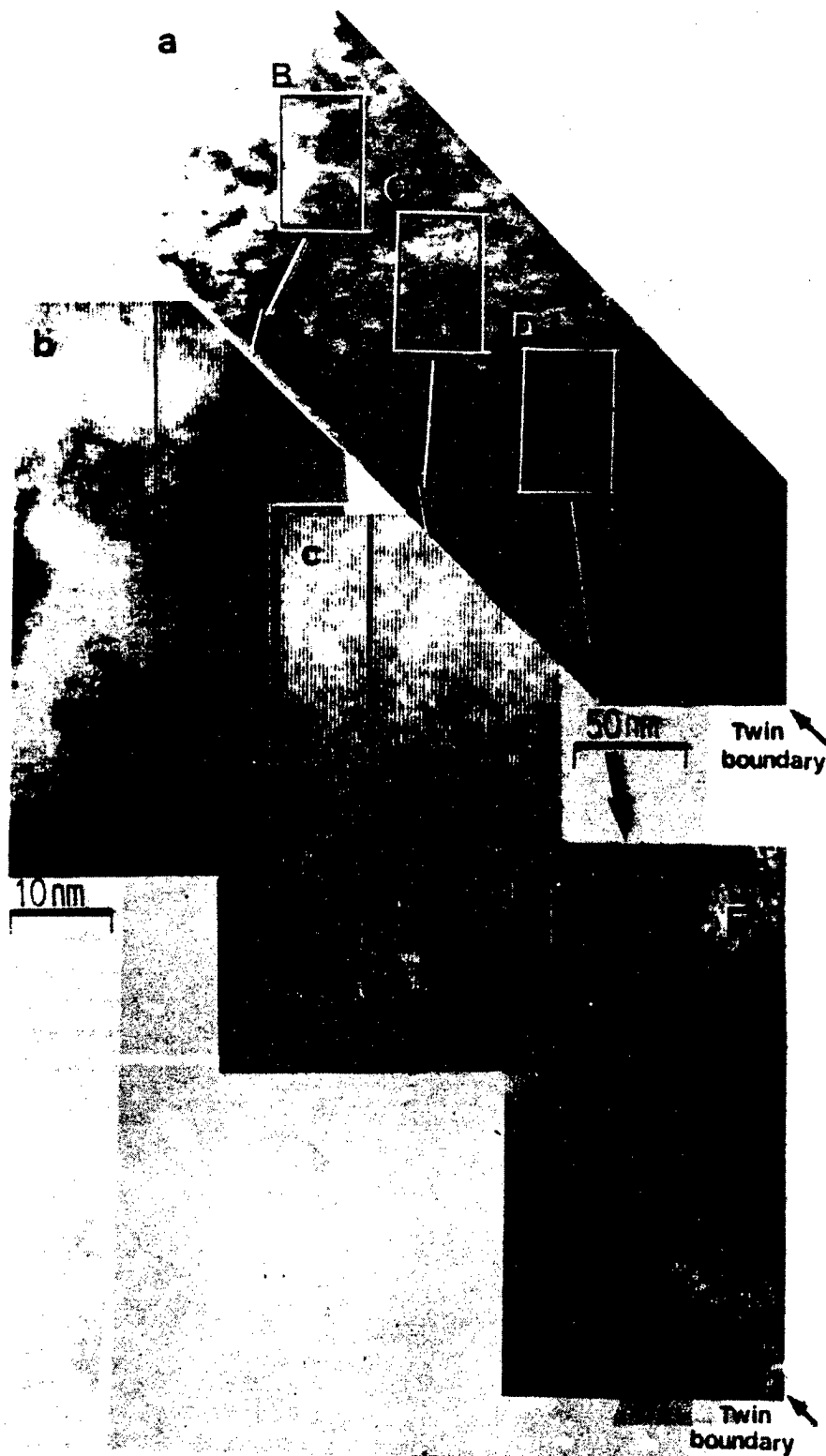


Fig. 2 High resolution electron micrographs showing a twin boundary shrinking under observation. (a) shows the overall view of the tip of the twin boundary. (b), (c) and (d) are enlarged images of the areas B, C and D in (a), respectively. Solid lines in the center of (b), (c) and (d) indicate the angle  $\theta$  between (100) fringes and (010) fringes.



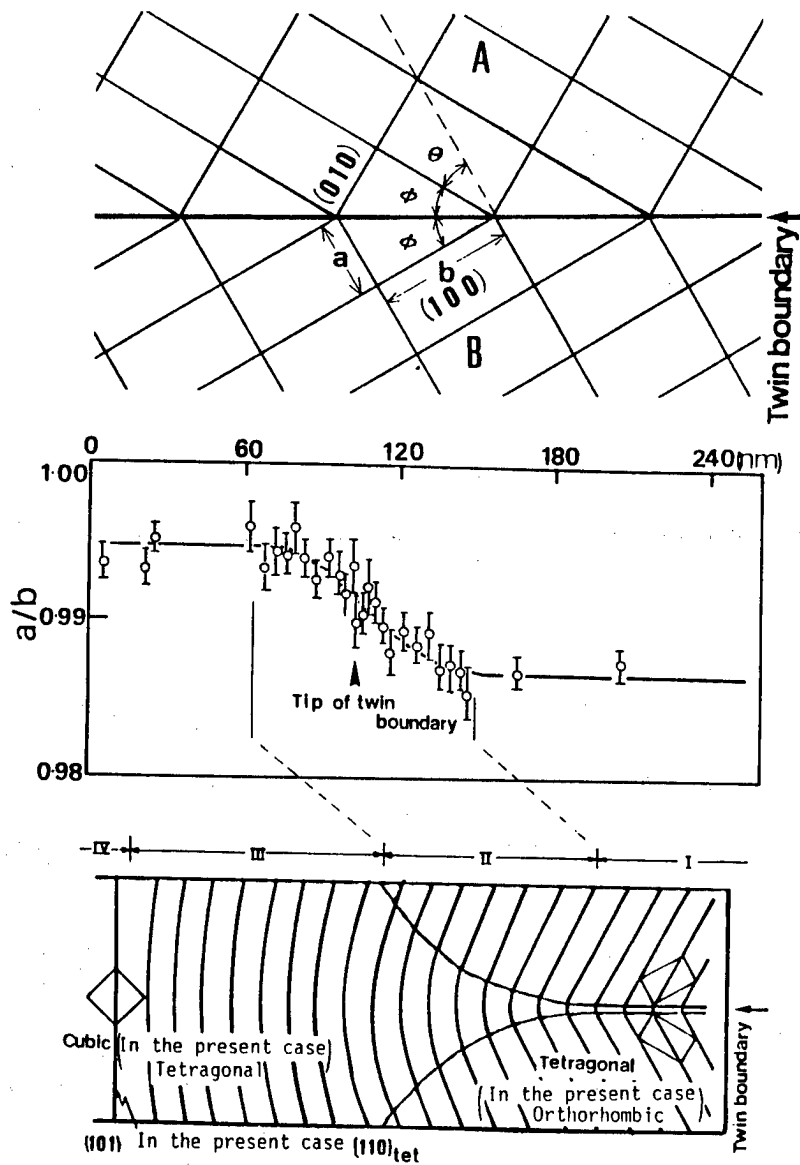


Fig. 3 (a) Schematic drawing of a twin boundary in the orthorhombic phase. (b) The variation of  $a/b$ -value along the twin boundary. The arrow indicates the tip of the twin boundary. (c) The model of the structure of the transformation interface between a cubic and a tetragonal phases in  $\text{BaTiO}_3$ , associated by Malis and Gleiter (1979 a,b).

# Electronic Band Structure of $\text{La}_2\text{NiO}_4$

Katsuhiko TAKEGAHARA and Tadao KASUYA

Department of Physics, Tohoku University, Sendai 980, Japan

The one-electron energy band structures for paramagnetic and antiferromagnetic  $\text{La}_2\text{NiO}_4$ , which is one of the isomorphous compound of  $\text{La}_2\text{CuO}_4$ , were calculated by the self-consistent APW method. The paramagnetic state with the tetragonal structure is metallic. Within the conventional local spin density approximation, the antiferromagnetic ground state is found to be unstable. By 1.5 times the exchange splitting, the stable antiferromagnetic state with the sublattice magnetization of 1.1 Bohr magneton/Ni is obtained.

$\text{La}_2\text{NiO}_4$  crystallizes in the  $\text{K}_2\text{NiF}_4$ -type structure [1]. Recent magnetic neutron scattering experiment [2] showed that the antiferromagnetic structure is identical to that for  $\text{La}_2\text{CuO}_4$  except for the direction of ordered moments and the behavior of magnetic fluctuation is similar in both compounds. For the transport properties, the resistivity increases with temperature for high temperature but is described by the simple activation type for low temperature.

In the viewpoint of band theory, this compound is also interesting. We calculated the antiferromagnetic state of  $\text{La}_2\text{CuO}_4$  with the conventional local spin density approximation (LSDA) [3]. However, we failed to obtain the stable antiferromagnetic state due to the inadequate exchange correlation potential in LSDA. There are various ways to treat this problem but we simply multiplied the exchange term so as to get the sublattice magnetization consistent with the experimental results. Then, by doubling the exchange term, we obtained the antiferromagnetic state with the sublattice magnetization of 0.4 Bohr magneton/Cu. Within the LSD approximation, the LCAO calculation [4] also failed to obtain the stable antiferromagnetic ground state but the pseudopotential [5] and LMT0 [6] calculations found the stable antiferromagnetic ground state. In this context, it is still an open question whether the ground state of  $\text{La}_2\text{CuO}_4$  within LSDA is the antiferromagnetic state. In  $\text{La}_2\text{NiO}_4$ , the Ni d component at the Fermi energy increases and thus the antiferromagnetic state is expected to be stabilized. In this report, we investigate the stability of antiferromagnetic ground state of  $\text{La}_2\text{NiO}_4$  within LSDA.

The electronic structure in a paramagnetic state is calculated on the body centered tetragonal phase [1]. The space group is  $I4/mmm$  with La in 4e site: (0,0,0.3717), Ni in 2a: (0,0,0), O1 in 4c: (0,1/2,0) and O2 in 4e: (0,0,0.1771). The lattice constants are  $a_t = 3.869$  Å and  $c_t = 12.664$  Å. The muffin-tin sphere radii are determined as following; 1.572 Å (La), 1.042 Å (Ni) and 0.893 Å (O1 and O2). The total muffin-tin spheres occupy 52 % of the unit cell volume. The local density approximation proposed by Gunnarsson and Lundqvist [7] is used. Details of the method of this self-consistent APW calculation are as described in previous paper on  $\text{La}_2\text{CuO}_4$  [8].

Figure 1 shows the energy band structure along the symmetric axes. In the figure, La 5p and O 2s bands are not shown. The average energy levels are as follows; La p at -0.6 Ry, O1 s at -1.0 Ry and O2 s at -0.8 Ry. The bands at 0.7 Ry is derived from the La 4f states mainly. Between these bands there are 17 bands which consist of the Ni d and O p states. The Fermi energy  $E_F$  is located at 0.4495 Ry.

In the  $\text{NiO}_6$  octahedron, the length of four Ni-O1 bonds on the xy-plane is 1.93 Å and that of two Ni-O2 bonds along the c axis is 2.24 Å. Note that the Cu-O1 bond length is 1.90 Å and the Cu-O2 bond length is 2.40 Å in  $\text{La}_2\text{CuO}_4$ . Two  $X_u$  states at 0.61 and 0.0 Ry are a pair of states of bonding-

antibonding Ni  $d(x^2-y^2)$  and O1 p states. The splitting of these states, 0.61 Ry, is 0.03 Ry larger than that in  $\text{La}_2\text{CuO}_4$ . The  $X_1$  state at 0.47 Ry is the antibonding state between the Ni  $d(3z^2-r^2)$  and O2 p states.

The results for the density of states are shown in Fig. 2. In  $\text{La}_2\text{CuO}_4$ , the Cu d partial density of states in the 17 bands is fairly proportional to the O1 p partial density of states. However, the Ni d states in  $\text{La}_2\text{NiO}_4$  move to higher energy side. Due to the bonding-antibonding effect between the Ni d and O1 p states, the d states have the large distribution near the Fermi energy and the O1 p states distribute at the lower energy part. The partial and total densities of states at the Fermi energy are as following; 19.97 states/Ry-F.U. (Ni d component), 2.26 (O1 p), 7.34 (O2 p) and 34.26 (total) and the corresponding specific heat coefficient is 5.93 mJ/mole-K<sup>2</sup>. This value is a little bit smaller than that of metallic Ni (7.02 mJ/mole-K<sup>2</sup>).

For the calculation on the antiferromagnetic state, the up-spin and down-spin sites of Ni atoms are treated as the non-equivalent site and thus the unit cell volume is twice as large as that of paramagnetic case. The spin structure of antiferromagnetic state is the same as the result observed by the neutron diffraction study [2]. The crystal structure used in the calculation is the base centered orthorhombic Cmmm with La1 in 4i site: (0,0.3717,0), La2 in 4j: (0,0.8717,1/2), Ni1 in 2a: (0,0,0), Ni2 in 2c: (1/2,0,1/2), O1 in 8o: (1/4,0,1/4), O2 in 4i: (0,0.1771,0) and O3 in 4j: (0,0.6771,1/2). The lattice constants are  $a_0 = c_0 = 2^{1/2}a_t$  and  $b_0 = c_t$ . The definition of muffin-tin radius is the same as that of paramagnetic case.

The starting crystal charge density is obtained by superposition of self-consistent charge densities for neutral atoms in which the Ni atom is the spin-polarized state; the electron configuration of Ni1 is ...3d<sup>5</sup>4s<sup>1</sup> (up-spin) and ...3d<sup>3</sup>4s<sup>1</sup> (down-spin) and Ni2 is in the opposite configuration. After several cycles of the self-consistent iteration processes, the gap between the occupied and unoccupied states disappears and then the spin polarization on Ni site decreases rapidly. Therefore, the antiferromagnetic ground state is considered to be unstable within the conventional LSD approximation. To stabilize the antiferromagnetic state, we modify the exchange correlation potential in such a way that the exchange splitting is 1.5 times as large as the original one proposed by Gunnarsson and Lundqvist. Then we obtain the antiferromagnetic state with the sublattice magnetization of 1.1 Bohr magneton/Ni.

The calculated band structure for up-spin band is shown in Fig. 3. In this case, the Brillouin zone is a half of tetragonal BZ. Then the antiferromagnetic band structure is made by the paramagnetic band which is folded back into the orthorhombic BZ. Due to the antiferromagnetic spin density, the folded antibonding Ni  $d(x^2-y^2)$  - O p and Ni  $d(3z^2-r^2)$  - O p bands have the gap. Note that, to eliminate confusion, we use the definition of state in tetragonal structure. The top of valence band, the  $Z_{3+}$  state, is the lower folded antibonding Ni1  $d(x^2-y^2)$  - O1 p state. The bottom of conduction band, the  $Z_{2-}$  state, is the upper folded antibonding Ni2  $d(3z^2-r^2)$  - O3 p state. In order to show the character of wave function, the total and partial densities of states are shown in Fig. 4. The energy gap is 0.027 Ry.

In summary, we failed to obtain the stable antiferromagnetic ground state within the conventional LSD approximation. This is due to the inadequate exchange correlation potential and especially due to the inadequate treatment of the self-interaction correction. This situation is exactly the same as that in  $\text{La}_2\text{CuO}_4$  but is better quantitatively because of the larger ordered moment in Ni in which two kinds of orbital states,  $d(x^2-y^2)$  and  $d(3z^2-r^2)$ , are equally contributing to the magnetic order.

#### References

- [1] J. Choisnet, J.M. Bassat, H. Pilliere, P. Odier and M. Leblanc: Solid State Commun. 66, 1245 (1988).
- [2] G. Aeppli and D.J. Buttrey: Phys. Rev. Lett. 61, 203 (1988).
- [3] T. Kasuya and K. Takegahara: JJAP Series 1, Superconducting Materials (1988), p. 251.

- [4] T.C.Leung, X.W.Wang and B.N.Harmon: Phys. Rev. B37, 384 (1988).  
 [5] K.Shiraishi, A.Oshiyama, N.Shima, T.Nakayama and H.Kamimura: Solid State Commun. 66, 629 (1988).  
 [6] Y.Hatsugai and T.Fujiwara: Solid State Commun. 65, 1271 (1988).  
 [7] O.Gunnarsson and B.I.Lundqvist: Phys. Rev. B13, 4274 (1976).  
 [8] K.Takegahara, H.Harima and A.Yanase: Jpn. J. Appl. Phys. 26, L352 (1987).

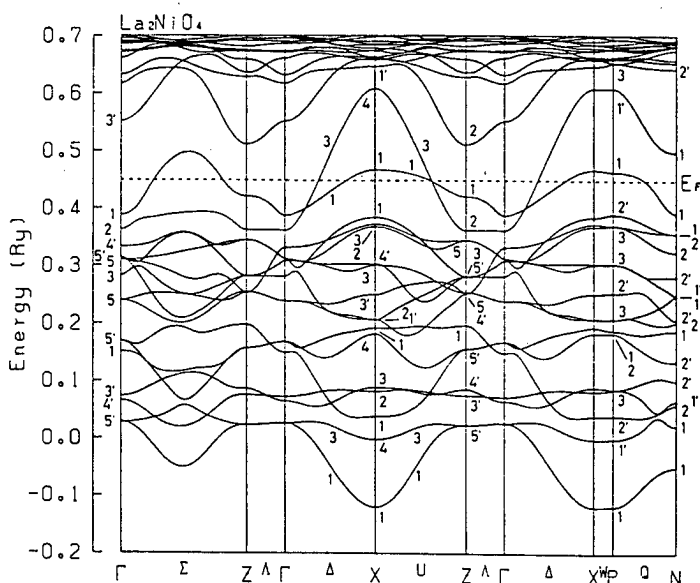


Fig. 1. Energy band structure for paramagnetic  $\text{La}_2\text{NiO}_4$ .

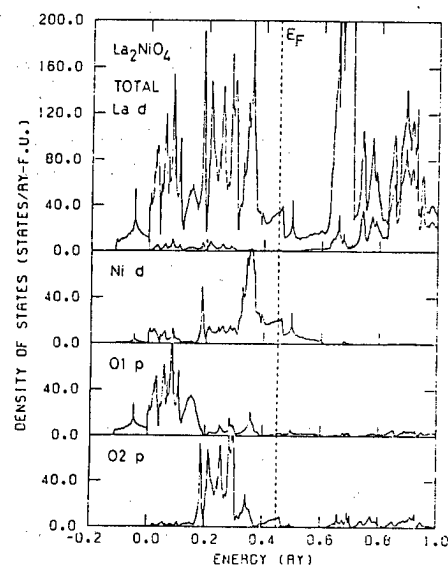


Fig. 2. Total and partial densities of states for paramagnetic  $\text{La}_2\text{NiO}_4$ .

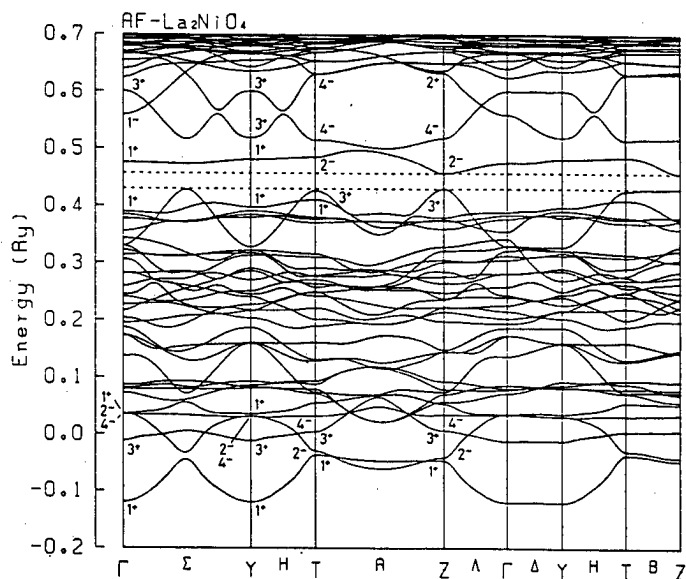


Fig. 3. Energy band structure for the up-spin band of antiferromagnetic  $\text{La}_2\text{NiO}_4$ . The dashed lines show the energy gap.

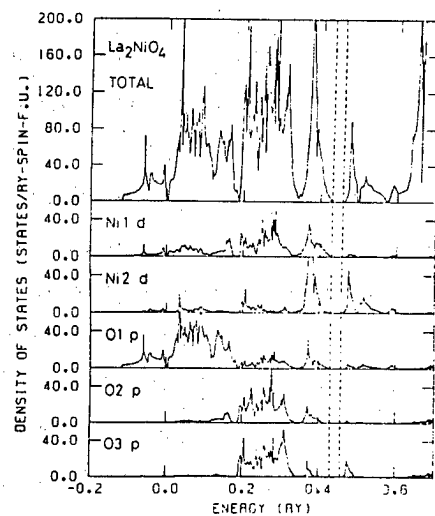


Fig. 4. Total and partial densities of states for the up-spin band of antiferromagnetic  $\text{La}_2\text{NiO}_4$ . The dashed lines show the energy gap.

K. T. Park and K. Terakura

Institute for Solid State Physics, University of Tokyo, Roppongi, Minato-ku, Tokyo 106.

We have performed band calculations for the high- $T_c$  related oxides,  $\text{La}_2\text{CuO}_4$ ,  $\text{YBa}_2\text{Cu}_3\text{O}_y$  ( $y=6$  or  $7$ ),  $\text{La}_2\text{CaCu}_2\text{O}_6$ ,  $\text{CuO}$ , and also  $\text{NiO}$  with the full-potential linear augmented plane wave method in order to derive information about the characteristic aspects of these materials. In this report, we mostly discuss  $\text{YBa}_2\text{Cu}_3\text{O}_y$ , paying particular attention to the role of the Cu-O linear chain in the extra hole doping.

The state-of-the-art band calculation based on the local density approximation (LDA) in the density functional theory is one of the best mean field calculations which takes account of all the details of the real systems. It has been playing important roles as a powerful method to obtain information about the basic properties of a given material, provided that the system belongs to a weak correlation regime. However, some experimental observations suggest that the newly found high- $T_c$  related oxides may be categorized into strongly correlated systems [1-7]. Therefore, we cannot assign high credibility to the results of the LDA band-structure calculations in an absolute scale. On the other hand, detailed study on the electron correlation can be done only for some simplified model systems, whose connection to real systems is not always clear. In this sense, the band-structure calculations will provide us with information complimentary to those model calculations.

We have performed band-structure calculations for the high- $T_c$  related oxides,  $\text{La}_2\text{CuO}_4$  (abbreviated as LCO),  $\text{YBa}_2\text{Cu}_3\text{O}_y$  (abbreviated as YBCO $_y$ ,  $y=6$  or  $7$ ), and  $\text{La}_2\text{CaCu}_2\text{O}_6$  (abbreviated as LCCO) and  $\text{CuO}$  as well as  $\text{NiO}$ , with the full-potential linear augmented plane wave (FLAPW) method. Nonmagnetic state is assumed for all materials. The results of the calculations and their detailed analyses were presented in Ref.8. Some of the important outputs of this work are the followings:

- 1) The electronic structure of LCCO is very similar to those of LCO and YBCO $_y$ , so that LCCO would show superconductivity if holes are doped in a proper way.
- 2) The energy separation  $\Delta$  between the oxygen  $p$  state and the copper  $d$  state in the Cu-O plane is very small for the high- $T_c$  related oxides compared with  $\text{NiO}$  and  $\text{CuO}$ . We argued, by using the concept of Slater's transition state, that the  $\Delta$  estimated from the centers of gravity of partial density of states may be a good measure of the  $\Delta$  used in the photoemission analyses. Small values of  $\Delta$  suggest that LCO, LCCO and YBCO $_6$  are located near the boundary of metal-insulator transition.
- 3) The direct hopping integrals between oxygen  $p$  orbitals are significantly large to make the oxygen  $p$  band width of about 5 eV without  $p$ - $d$  hybridizations.

Reference 8 should be referred to for more details of the above statements. In this report, we present some of our new results for YBCO<sub>y</sub> with regard to the extra hole doping.

There are several experimental evidences that the extra holes introduced by increasing  $y$  from 6 to 7 in YBCO<sub>y</sub> enter mostly the oxygen  $p$  orbitals. Identification of the specific  $p$  orbital for this extra hole doping is an important step toward elucidation of the mechanism of the superconductivity. Although experimental efforts have been extensively made recently for this purpose [9,10], the existence of many inequivalent oxygens makes it difficult to derive a definite conclusion. Some theoretical works have also been made in this context by using cluster models [11,12]. While these works treat the electron correlation carefully, seemingly important ingredients, such as Cu-Cu interaction and Cu-O linear chain, are lacking. As the hole doping in YBCO<sub>y</sub> is realized through increasing O1 concentration in the Cu-O chain, one cannot be confident whether a model without the Cu-O chain can give a reasonable answer to the character of extra holes. On the other hand, the LDA band calculation, though it is not capable of treating the electron correlation properly, takes proper account of the hybridization between the Cu-O chain and plane.

Figures 1 to 4 show symmetry decomposed local densities of states (SDLDOS) for oxygens and coppers in YBCO6 and YBCO7, each of which is defined within a spherical region about a given atom. For O4, O2, Cu1 and Cu2, solid lines are for YBCO6 and broken ones for YBCO7. For O1 in Fig.1, the solid line is for the  $p_z$ , the broken one for the  $p_y$  and the dotted one for the  $p_x$ . Clearly, the extra holes produced by the O1 doping, which is defined as the increase of the unoccupied states in YBCO7 with reference to YBCO6, mostly reside in the orbitals associated with the  $pd\sigma$  bond of the Cu-O chain. These holes are then transferred to the states in the Cu-O plane through the chain-plane hybridization via  $p_z$  orbital of O4. Therefore, Cu2 has certain amount of holes in the  $3z^2-r^2$  orbital. It should also be noted that SDLDOS's of the orbitals pertaining to the  $pd\pi$  antibonding states,  $p_y(O4)-d_{yz}(Cu1)-p_z(O1)$ , are also significantly enhanced at the Fermi level for YBCO7. These states have amplitude at  $p_z$  of O2 through the direct interaction between  $p_y(O4)$  and  $p_z(O2)$  or the indirect one via  $d_{yz}$  of Cu2. SDLDOS's for the orbitals pertaining to the  $pd\sigma$  bond in the Cu-O plane are also enhanced near the Fermi level but only slightly. This is not inconsistent with a picture that super current flows in the Cu-O plane but is rather consistent with the small carrier concentration observed experimentally. In reality, YBCO6 is an antiferromagnetic insulator, whereas our LDA band calculation predicts it to be a nonmagnetic metal. Therefore, the details of the the above results should not be taken seriously. Nevertheless, we believe that the hybridization between Cu-O chain and plane must be a crucial factor for elucidating the character of the extra holes and that the results of the LDA band calculation will give hints on this aspect. Correspondingly in the LCO system, the presence of divalent elements, Ca, Sr and Ba, and the associated strong electrostatic field must be taken into account for the extra hole problem.

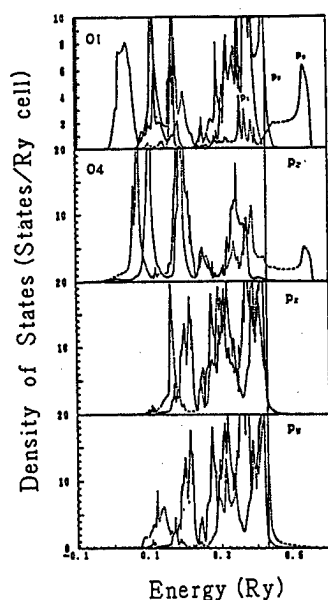


Fig.1

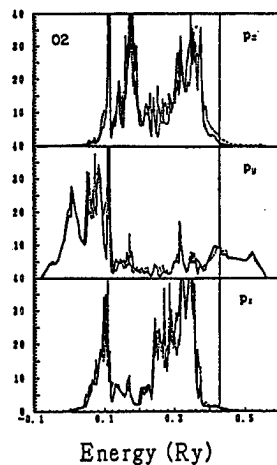


Fig.2

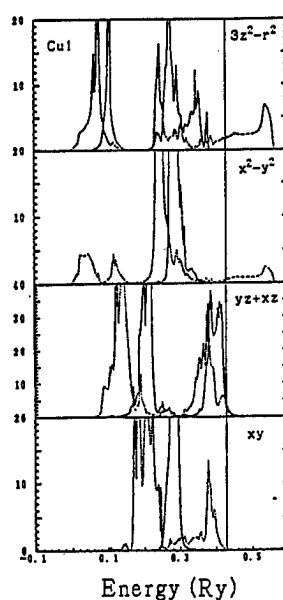


Fig.3

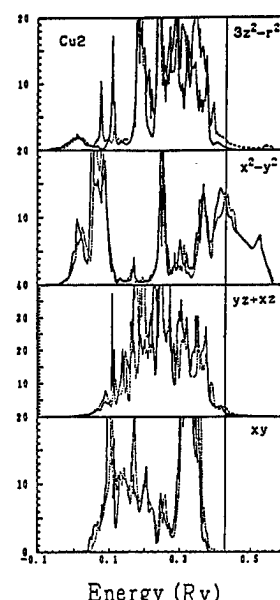


Fig.4

## References

- 1) A. Fujimori, E. Takayama-Muromachi, Y. Uchida and B. Okai: *Phys. Rev. B* **35** (1987) 8814.
- 2) T. Takahashi, F. Maeda, H. Arai, H. Katayama-Yoshida, Y. Okabe, T. Suzuki, S. Hosoya, A. Fujimori, T. Shidara, T. Koide, T. Miyahara, M. Onoda, S. Shamoto and M. Sato: *Phys. Rev. B* **36** (1987) 5686.
- 3) D. van der Marel, J. van Elp, G. A. Savatzky and D. Heitmann: *Phys. Rev. B* **37** (1988) 5136.
- 4) Z. A. Wang, J. Clayhold, N. P. Ong, J. M. Tarascon, and L. H. Greene, W. R. McKinnon and G. W. Hull: *Phys. Rev. B* **36** (1987) 7222.
- 5) S. Uchida, S. Tajima, H. Takagi, K. Kishio, T. Hasegawa, K. Kitazawa, K. Fueki and S. Tanaka: *Proc. 18th Int. Conf. on Low Temp. Phys., Kyoto 1987*, *Jpn. J. Appl. Phys.* **26** (1987) Suppl. 26-3, p.1105.
- 6) D. Vaknin, S. K. Sinha, D. E. Moncton, D. C. Johnston, J. M. Newsam, C. R. Safinya and H. E. King, Jr.: *Phys. Rev. Lett.* **58** (1987) 2802.
- 7) J.M.Tranquada, D.E.Cox, W.Kunmann, H.Moudden, G.Shirane, M.Suenaga, P.Zolliker, D.Vaknin, S.K.Sinha, M.S.Alvarez, A.J.Jacobson and D.C.Johnston: *Phys. Rev. Lett.* **60** (1988) 156.
- 8) K. T. Park, K. Terakura, T. Oguchi, A. Yanase and M. Ikeda: *J. Phys. Soc. Jpn.* **57** (1988) 3445.
- 9) A. Bianconi, M. De Santis, A. Di Cicco, A. M. Flank, A. Fontaine, P. Lagarde, H. Katayama-Yoshida, A. Kotani, and A. Marcelli: *Phys. Rev. B* **38** (1988) 7196.
- 10) N.Nücker, H.Romberg, X.X.Xi, J.Fink, B.Gegenheimer and Z.X.Zhao: to appear in *Phys. Rev. B*.
- 11) H. Eskes and G. A. Savatzky: *Phys. Rev. Lett.* **61** (1988) 1415.
- 12) A. Fujimori: preprint.

# Multiplet Structure of Cu 2p-XPS in $\text{La}_2\text{CuO}_4$ and $\text{CuO}$

K. Okada and A. Kotani

Department of Physics, Faculty of Science, Tohoku University  
Sendai 980, Japan

We have analyzed the Cu 2p-XPS in  $\text{La}_2\text{CuO}_4$  and  $\text{CuO}$  by using the single site Anderson model with five filled valence bands. We take account of the multiplet coupling between a Cu 3d hole and a core hole and of the anisotropic hybridization between the 3d hole and the O 2p valence band holes. We show that the multiplet structure of Cu  $(2p)^5(3d)^9$  electron configuration is affected by the hybridization.

## §1. Introduction

In the study on the mechanism of high- $T_c$  superconductivity in La-Sr-Cu-O, Y-BaCu-O and Bi-Sr-Ca-Cu-O, high energy spectroscopy has been playing an important role to clarify the electronic structure of these materials. In the previous paper[1], we analyzed the Cu 2p-XPS, 3d-XPS, 3p resonant XPS and  $L_3$ -XAS and showed that the anisotropic coupling between the Cu 3d orbitals and the neighboring O 2p orbitals and the strong Coulomb repulsion between the 3d electrons are important in understanding the electronic structure around Cu ions. However, we have not analyzed the observed multiplet structures in various spectra. In this paper, we calculate the multiplet structure in the Cu 2p-XPS to investigate the effect of the hybridization on the multiplet structures in detail. In particular, we concentrate on the Cu 2p-XPS of  $\text{La}_2\text{CuO}_4$ [2-4].

The Cu 2p-XPS spectrum of  $\text{La}_2\text{CuO}_4$  is often compared with those of  $\text{CuO}$  and  $\text{CuCl}_2$  [2,4], and their rough similarity is an evidence that  $\text{La}_2\text{CuO}_4$  belongs to the charge-transfer type insulators. In Fig 1, we show that the observed Cu  $2p_{3/2}$ -XPS spectra in  $\text{CuCl}_2$ ,  $\text{CuO}$  and  $\text{La}_2\text{CuO}_4$ . The line shape of the spectrum consists of the main peak of  $\text{Cu}(2p)^5(3d)^{10}\underline{L}$  and the satellite of  $\text{Cu}(2p)^5(3d)^9$  in origin, where  $\underline{L}$  denotes a hole in the ligand O 2p orbitals. In the study of Cu halides, van der Laan et al.[5] pointed out that the line shape of the satellite structure is similar to that due to the atomic  $\text{Cu}(2p)^5(3d)^9$  electron configuration. Furthermore, they concluded that the

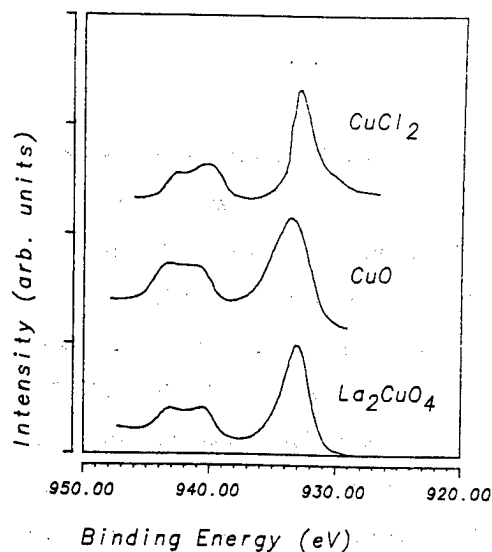


Fig.1: Observed Cu  $2p_{3/2}$ -XPS in  $\text{CuCl}_2$ ,  $\text{CuO}$  and  $\text{La}_2\text{CuO}_4$ . (See ref.[4,5].)



crystal field due to the electrostatic potential energy does not affect the multiplet structure in  $\text{CuCl}_2$ . However, when we compare the Cu 2p-XPS of  $\text{CuCl}_2$  with those of  $\text{CuO}$  and  $\text{La}_2\text{CuO}_4$  in detail, we find that the multiplet structure in  $\text{CuCl}_2$  differs from these in  $\text{CuO}$  and  $\text{La}_2\text{CuO}_4$ . The satellite of 2p-XPS in  $\text{CuCl}_2$  consists of two peaks with different intensities: a peak at 942eV and a weaker one at 944eV. In  $\text{CuO}$  and  $\text{La}_2\text{CuO}_4$ , on the other hand, their intensities are almost the same, and the line shape becomes squarish. Here, we note that van der Laan et al. did not take account of the hybridization between the Cu 3d electrons and the ligand O 2p electrons. Although it has already been discussed that the intensity ratio of the main and satellite peaks depends strongly on the hybridization strength between the  $\text{Cu}(3d)^9$  and  $\text{Cu}(3d)^{10}\underline{L}$  configurations, the effect of the hybridization on the multiplet structure has not been analyzed yet. The purpose of this paper is to study systematically the interplay between the atomic multiplet coupling and the solid state hybridization in the Cu 2p-XPS line shape on the basis of the impurity Anderson model. In §2, we present our model. We show the calculated results in §3 and give some discussion in §4.

## §2. Model

We adopt the single site impurity Anderson model[1]. Since the nominal valence number of Cu ion is 2+ in  $\text{La}_2\text{CuO}_4$ ,  $\text{CuO}$  and  $\text{CuCl}_2$ , a Cu 3d shell has nominally  $d^9$  electron configuration and has 1 hole/Cu. However, the 3d hole can move to the neighboring O 2p orbitals through the overlapping of their wave functions so that the 3d shell does not have an integral number of electrons. We describe the ground state of the system by a linear combination of  $d^9$  and  $d^{10}\underline{L}$  electron configurations. As is well-known, the Cu ion is surrounded by six O ions and is in the local symmetry of  $D_{4h}$  point group. We describe the hole state in the d orbitals and the valence band by the irreducible representations of  $D_{4h}$  ( $a_{1g}$ ,  $b_{1g}$ ,  $b_{2g}$  and  $e_g$ ), where we take account of the valence bands which have a local symmetry of  $D_{4h}$  around the Cu ion. In the final state of the Cu 2p-XPS, there is the multiplet coupling between the Cu 2p and 3d holes which is caused by the Coulomb and spin-orbit interactions. The Hamiltonian is given as

$$H = H_{VB} + H_{\text{atom}} + H_{\text{mix}}, \quad (2.1)$$

where

$$H_{VB} = \sum_{k=1}^N \sum_{\Gamma, \sigma} \varepsilon_{k\Gamma} a_{k\Gamma\sigma}^\dagger a_{k\Gamma\sigma}, \quad (2.2)$$

$$H_{\text{atom}} = \sum_{\nu} \varepsilon_d d_{\nu}^\dagger d_{\nu} + \sum_{\nu} \varepsilon_p p_{\nu}^\dagger p_{\nu} + \frac{1}{2} \sum_{\nu_1, \nu_2, \nu_3, \nu_4} g_{pd}(\nu_1, \nu_2, \nu_3, \nu_4) d_{\nu_1}^\dagger d_{\nu_2} p_{\nu_3}^\dagger p_{\nu_4} \\ + \xi_d \sum_{\nu_1, \nu_2} (\vec{s}_d \cdot \vec{l}_d)_{\nu_1 \nu_2} d_{\nu_1}^\dagger d_{\nu_2} + \xi_p \sum_{\nu_1, \nu_2} (\vec{s}_p \cdot \vec{l}_p)_{\nu_1 \nu_2} p_{\nu_1}^\dagger p_{\nu_2}, \quad (2.3)$$

and

$$H_{\text{mix}} = \sum_{k=1}^N \sum_{\Gamma, \sigma} V(\Gamma, k) / \sqrt{N} (d_{\Gamma\sigma}^\dagger p_{k\Gamma\sigma} + p_{k\Gamma\sigma}^\dagger d_{\Gamma\sigma}), \quad (2.4)$$

where  $\nu_i$ 's denote the combined indices representing the spin and orbital states, and  $\Gamma$ 's are  $b_{1g}$ ,  $a_{1g}$ ,  $b_{2g}$  and  $e_g$ . The Hamiltonian  $H_{VB}$  describes the valence band states,

where the index  $k$  describes the energy distribution of the valence band states which couple to the 3d orbitals through the hybridization  $H_{\text{mix}}$ . In the Hamiltonian  $H_{\text{atom}}$ , the atomic Cu 3d and 2p electron states are described. In  $H_{\text{atom}}$ ,  $g_{\text{pd}}$ 's include the Slater integrals  $F^0$ ,  $F^2$ ,  $G^1$  and  $G^3$  in their explicit forms, and  $\zeta_d$  and  $\zeta_p$  are the spin-orbit interactions. In particular,  $F^0$  is the 2p core-hole potential acting on 3d electrons usually written as  $-U_{\text{dc}}$ . In our calculation, we take  $F^2=7.47\text{eV}$ ,  $G^1=5.62\text{eV}$ ,  $G^3=10.95\text{eV}$ ,  $\zeta_d=0.13\text{eV}$  and  $\zeta_p=11.3\text{eV}$  which are calculated by using the Hartree-Fock and the LSD programs for atomic systems. As is well known, the solid state effects such as the dielectric screening etc. reduce considerably the value of  $U_{\text{dc}}$ , and we treat  $U_{\text{dc}}$  as a free parameter. However, the other parameters are reduced very slightly, so that their reduction does not bring about any essential change in our results given below. As long as we take account of only the  $d^9$  and  $d^{10}_L$  electron configurations, the d-d Coulomb interaction is not necessary, and it is omitted in  $H_{\text{atom}}$ .

The basis wave functions for the ground state are

$$|d^9(\Gamma\sigma)\rangle = d_{\Gamma\sigma}|d^{10}\rangle \quad \text{and} \quad |d^{10}_L(k\Gamma\sigma)\rangle = a_{k\Gamma\sigma}|d^{10}\rangle, \quad (2.5)$$

where  $|d^{10}\rangle$  describes the completely filled 3d and valence band states. The basis wave functions for the final states are obtained by annihilating a Cu 2p electron in the eqs. (2.5). Using the charge transfer energy from the center of the valence band to the d state  $\Delta(\Gamma)$ , we describe the energy difference between the  $d^9$  and  $d^{10}_L$  configurations in the initial state as

$$E[d^{10}_L(k\Gamma\sigma)] - E[d^9(\Gamma\sigma)] = \Delta(\Gamma) - \frac{W(\Gamma)}{2} + \frac{W(\Gamma)}{N} \left( k - \frac{1}{2} \right), \quad (2.6)$$

where  $k = 1 \sim N$  and  $W(\Gamma)$  is the band width. In eq.(2.6), the valence band is approximated by  $N$  discrete levels. The energy dependence of the hybridization  $V(\Gamma, k)$  is assumed to be semi-elliptical as follows.

$$V(\Gamma, k)^2 = V(\Gamma)^2 \frac{8}{\pi W(\Gamma)} \left\{ \left[ \frac{W(\Gamma)}{2} \right]^2 - [\varepsilon_k(\Gamma) - \varepsilon_{N/2}(\Gamma)]^2 \right\}. \quad (2.7)$$

Thus, we describe the Hamiltonians with a finite number of basis wave functions, and diagonalize them numerically without any further approximation. As for the energy dependence of the hybridization, we may use  $V(\Gamma, k)$  obtained by the band structure calculations[6]. We note that the case of  $N=1$  is equivalent to the limiting case of vanishing  $W$ , corresponding to a cluster model.

### §3 Results

#### Atomic Cu 2p-XPS

Firstly, in Figs.2(a) and (b), we show the Cu 2p-XPS spectra of the atomic system with and without the spin-orbit interaction of the d electron  $\zeta_d$ . The continuous spectra are calculated from the line spectra with a Gaussian broadening of 1eV (HWHM). In the case of  $\zeta_d \neq 0$ , the spectrum shows the double-peak feature. For  $\zeta_d = 0$ , the separation of the two peaks decreases and becomes somewhat similar to that of  $\text{CuCl}_2$  shown in Fig. 1. In these transition metal compounds, it is well-known that the 3d level splitting is so large that the orbital angular momentum is quenched, and the effect of the spin-orbit interaction disappears. However, the line shapes of these spectra do not coincide so much with the multiplet observed in the  $\text{La}_2\text{CuO}_4$  and  $\text{CuO}$

quantitatively.

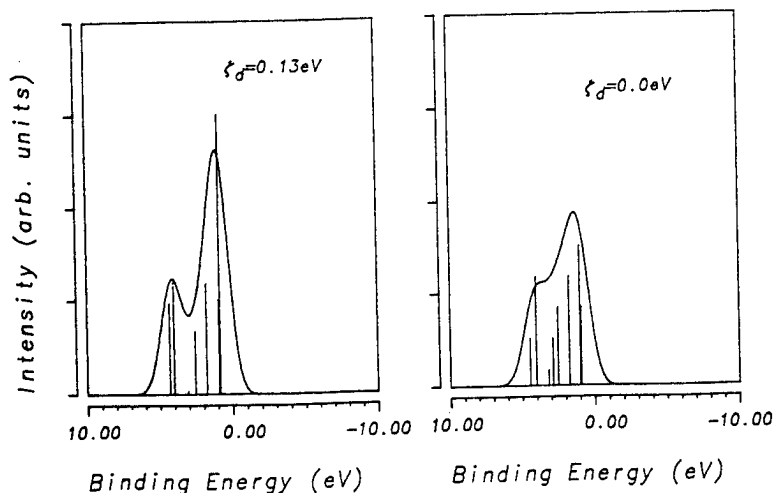


Fig.2(a) and (b): Multiplet Structures of the Cu  $(2p)^5(3d)^9$  final state in the atomic system with and without the spin-orbit interaction of the 3d electron.

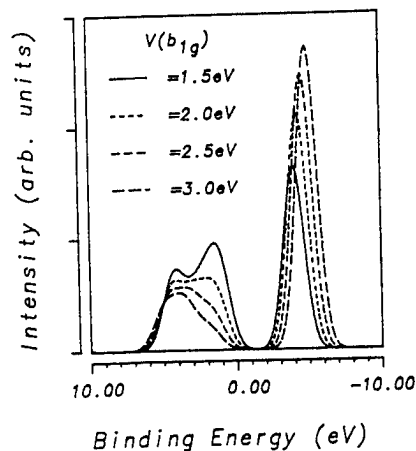


Fig.3: Cu 2p-XPS in the  $D_{4h}$  local symmetry as a function of the hybridization interaction  $V(b_{1g})$ . The hybridization interaction ratios,  $V(a_{1g})=V(b_{1g})/\sqrt{3}$ ,  $V(e_g)=V(b_{2g})/\sqrt{2}$  and  $V(b_{2g})=V(b_{1g})/2$  are assumed.

### Strength of Hybridization

In order to discuss the multiplet structures in the solids, we must take account of the hybridization of the wave functions of 3d and ligand orbitals. In Fig 3, we show the Cu 2p-XPS under the  $D_{4h}$  local symmetry. We assume that the charge transfer energies  $\Delta$ 's are the same for all  $\Gamma$ 's, and we take  $N=1$ . For simplicity, we assume the square planer cluster  $CuO_4$ , where the relations  $V(a_{1g})=V(b_{1g})/\sqrt{3}$  and  $V(b_{2g})=V(e_g)/\sqrt{2}$  are derived from the geometrical condition, and we also use the empirical relation  $V(b_{2g})=V(b_{1g})/2$  [7,8]. In Fig.3, we can see that both the intensity ratio of the satellite to the main peak and the multiplet structure depend strongly on the strength of  $V$ . As for the intensity ratio, the hybridization effect in the initial state is more important than that in the final state. In the initial state,  $\Delta$  is comparable to  $V$ , so that the hybridization between the  $d^9$  and  $d^{10}\bar{L}$  configurations is considerable and these parameters are crucial to determine the valence of the initial state. As  $\Delta$  becomes large or  $V$  becomes small, the amount of the  $d^9$  configuration in the initial state increases, and the satellite peak in the Cu 2p-XPS grows up. In the final state, on the other hand, the two configurations are separated by the core-hole potential  $U_{dc}$  which is much larger than  $\Delta$ , so that the effect of changing  $\Delta$  is not very important in the final state. In contrast, the hybridization in the final states is important in the multiplet structure because the hybridization of about 2eV is large enough to mix the  $(2p)^5(3d)^9$  and  $(2p)^5(3d)^{10}\bar{L}$  configurations. As a result, the multiplet structure in the Cu 2p-XPS changes considerably when we change the strength of the hybridization. In particular, the anisotropy of the hybridizations is important in discussing the multiplet structure, as is shown below.

### Anisotropy of Hybridization

To investigate the role of the anisotropic hybridization, we show the dependence of the 2p-XPS on the hybridization strength ratio  $V(b_{2g})/V(b_{1g})$  in Fig.4. We can see that the deformation of the satellite has a close relation to  $V(b_{2g})/V(b_{1g})$ , in other words, the coupling strength ratio between the  $\sigma$  and  $\pi$  bondings. When the ratio  $V(b_{2g})/V(b_{1g})=1$ , the line shape of the satellite is almost the same as the atomic case. The deformation becomes remarkable as  $V(b_{2g})/V(b_{1g})$  decreases. Therefore, this anisotropy is important in explaining the observed spectra.

### Band Effect

In Fig.5, we show the 2p-XPS spectrum calculated using the valence band with a finite band width. We assume that  $W(\Gamma)=3\text{eV}$ ,  $\Delta(\Gamma)=2\text{eV}$  for all  $\Gamma$ 's,  $N=6$  and the anisotropic hybridization in the square planer case. The line shape is almost the same as those in Fig. 3, except that the main peak is broadened by the band effect. This width of the main peak is narrower than the experimental results of CuO and  $\text{La}_2\text{CuO}_4$ . As for the band width  $W(\Gamma)$ , we can refer to the band structure calculations. We show the Cu 2p-XPS in Fig.6, using the energy dependence of  $V(\Gamma)$  calculated for  $\text{La}_2\text{CuO}_4$  by McMahan et al.[6] on the basis of the LMTO method. Although  $W(\Gamma)$  amounts to 6.5eV in their results, the calculated main peak is still narrow. This problem is an open question. Moreover, in Fig.6, the intensity ratio between the main and satellite peaks is much larger than the observed results, and the multiplet structure differs fairly from the experiment. These are caused by the too strong hybridization and the too large anisotropy. The values estimated by McMahan correspond to  $V(a_{1g})=1.6\text{eV}$ ,  $V(b_{1g})=3.2\text{eV}$ ,  $V(b_{2g})=1.5\text{eV}$  and  $V(e_g)=1.2\text{eV}$ .

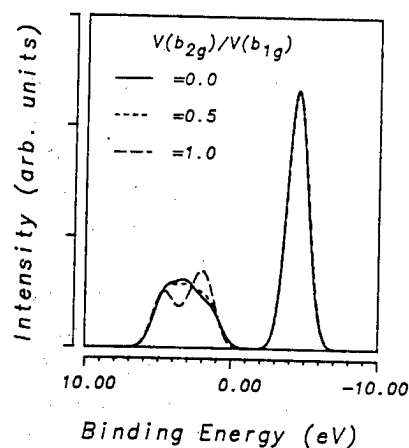


Fig.4: Cu 2p-XPS in the  $D_{4h}$  ligand symmetry as a function of the ratio  $V(b_{2g})/V(b_{1g})$ .

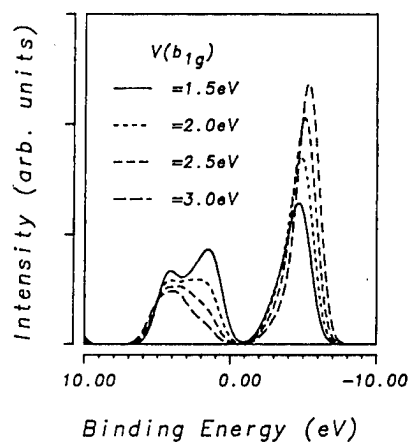


Fig.5: Cu 2p-XPS in the  $D_{4h}$  local symmetry. The valence band width  $W(\Gamma)$  is 3eV and  $N=6$  for all  $\Gamma$ . The hybridization interaction ratios are assumed as  $V(a_{1g})=V(b_{1g})/\sqrt{3}$ ,  $V(e_g)=V(b_{2g})/\sqrt{2}$  and  $V(b_{2g})=V(b_{1g})/2$ .

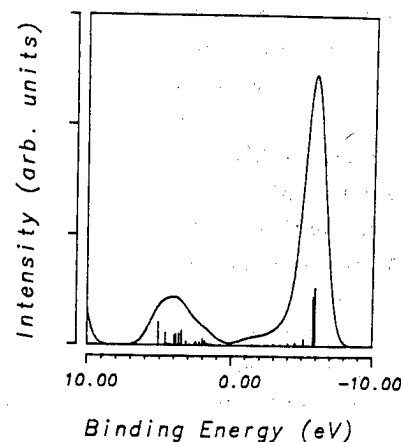


Fig.6: Cu 2p-XPS in the  $D_{4h}$  local symmetry, using the energy dependence of the hybridization  $V(\Gamma, k)$  calculated by McMahan et al.

## §4 Discussion

We have shown that the hybridization between the Cu 3d and O 2p holes affects both the intensity ratio of the satellite to the main peak and the multiplet structure in the Cu 2p-XPS. In particular, we emphasize the effect of the anisotropic hybridization on the multiplet structure. When we compare the multiplet structures observed in  $\text{CuCl}_2$  and  $\text{CuO}$ , the deviation from the atomic multiplet is somewhat significant in  $\text{CuO}$ . It suggests that the hybridization should be stronger in  $\text{CuO}$ . In other words, the ionisity is stronger in  $\text{CuCl}_2$  than in  $\text{CuO}$ . The spectrum of  $\text{La}_2\text{CuO}_4$  is very similar to that of  $\text{CuO}$  as long as the multiplet structure is concerned, which suggests that the hybridization would be almost the same as that of  $\text{CuO}$ . On the other hand, the intensity ratio of the satellite to the main peak is somewhat larger in  $\text{CuO}$  than in  $\text{La}_2\text{CuO}_4$ , so that the  $\Delta$  should be larger in  $\text{CuO}$ . These trends in parameter values are consistent with our previous analysis of  $\text{CuO}$  and  $\text{La}_2\text{CuO}_4$ .

To analyze the spectra quantitatively, we have used the energy dependence of the hybridization calculated by McMahan et al. But the result is unsatisfactory. Their values of  $V$ 's are too large. To avoid this difficulty, we may choose smaller  $V(\Gamma)$ 's than McMahan's. In principle, the hybridization strength may be different between the initial and final states because of the core-hole potential. To get the observed line shape, however, we must reduce the hybridization  $V$  in the final state by about 50%, assuming the McMahan's  $V$  in the initial state. For the Mn 1s core hole in the Cd-Mn-Te system, Gunnarsson et al.[9] have estimated this reduction ratio to be about 10%. The reduction of 50% in the present case seems to be too large. It seems that McMahan et al. overestimated the hybridization.

Thus, we have shown the multiplet structure observed in the core electron XPS is affected by the hybridization. Analyzing the detailed line shape, we can discuss the anisotropy of the hybridization. Since, in the present Cu 2p-XPS case, the multiplet due to the  $p^5d^9$  electron configuration is well separated from the  $p^5d^{10}\underline{L}$  configuration by the large  $U_{dc}$ , the effect of the hybridization interaction is rather small. We showed the importance of the coupling-strength ratio between the  $\sigma$  and  $\pi$  bondings in understanding the Cu 2p-XPS. In the Cu 3p-XPS, the hybridization effect must be more remarkable, because the extension of  $(3p)^5(3d)^9$  multiplet is wider than the 2p-XPS case, and because  $U_{dc}(3p)$  is smaller than  $U_{dc}(2p)$ . The analysis of the multiplet structure observed in various spectra should provide us with much information on the solid state hybridization.

## References

- 1) K. Okada and A. Kotani: to be published in J. Phys. Soc. Jpn. 58, No.3, (1989).
- 2) A. Fujimori et al.: Phys. Rev. B35, 8814 (1987).
- 3) T. Takahashi et al: Phys. Rev. B37, 9788 (1988).
- 4) N. Nucker et al.: Z. Phys. B67, 9 (1987).
- 5) G. van der Laan et al: Phys. Rev. 23, 4369 (1981).
- 6) A. K. McMahan et al.: Phys. Rev. B38, 6650 (1988).
- 7) L. F. Mattheis: Phys. Rev. B5, 290 (1972).
- 8) H. Eskes and G. A. Sawatzky: Phys. Rev. Lett. 61, 1415 (1988).
- 9) O. Gunnarsson et al.: in Core-Level Spectroscopy in Condensed Systems, eds. J. Kanamori and A. Kotani (Springer-Verlag 1988), p.82.

# Dispersive Electronic States near the Fermi Level in High $T_c$ Superconductors

Y. Kuramoto and T. Watanabe

Department of Applied Physics, Tohoku University, Sendai 980, Japan

An effective Hamiltonian for high  $T_c$  superconductors is derived from a tight-binding model by a projection method. Special attention is paid to the effect of direct hopping between adjacent oxygen 2p states. A single-band model emerges after eliminating high-energy states, and the bandwidth of single-particle excitations is several eV in a ferromagnetic background of 3d spins. A hole therefore substantially disrupts the otherwise antiferromagnetic background. The model also has a spin-assisted hopping term which is not suppressed by the Néel order. Discussion is given on the origin of low-energy features observed in photoemission spectrum of  $\text{Bi}_2\text{Sr}_2\text{CaCu}_2\text{O}_8$ .

The electronic structure of copper-oxide high  $T_c$  superconductors is complicated and spans a large energy range. It is therefore desirable for investigation of superconductivity to extract a simpler effective Hamiltonian where high-energy states enter only implicitly as renormalization of parameters in the Hamiltonian. This report derives such a Hamiltonian. It has been pointed out by Zhang and Rice [1] that a 2p hole in a  $B_{1g}$  type molecular orbital on the square of oxygens makes a very stable singlet state with a 3d hole surrounded by them. According to [1] low-energy excitations are described by the single-band Hubbard model. We pay attention to the effect of direct transfer between adjacent 2p orbitals which was not considered in [1]. Band-theoretical calculations [2] show that the transfer is so significant that the 2p bands are several eV wide even without the 3d-2p hybridization.

Experimentally, angle-resolved photoemission studies on  $\text{Bi}_2\text{Sr}_2\text{CaCu}_2\text{O}_8$  have probed 2p-like dispersive electronic states near the Fermi level [3]. On the basis of the effective Hamiltonian we discuss the origin of these states and their relation to the 3d-2p singlet. The weak intensity of the observed spectrum is explained without recourse to complex many-body effects such as the Kondo resonance.

We start with the p-d mixing model on a square lattice with lattice constant unity. Each  $3d(x^2-y^2)$  hole orbital of energy  $\varepsilon_d$  at lattice point  $\mathbf{R}_j = (n, m)$  hybridizes with surrounding  $2p_x$  orbitals at  $(n \pm 1/2, m)$  and  $2p_y$  at  $(n, m \pm 1/2)$  with energy  $\varepsilon_p$ . The difference of two energies is  $\Delta = \varepsilon_p - \varepsilon_d$ . The strength of hybridization  $V$  can be taken to be positive provided that the center of the Brillouin zone is shifted to  $(\pi, \pi)$ . We include the direct transfer  $t_p$  ( $>0$ ) between nearest-neighbor 2p orbitals. The 3d electrons have a large on-site Coulomb repulsion  $U_d$ . If charge fluctuation of 3d states is negligible, a canonical transformation which eliminates the  $3d^{10}$  and  $3d^8$  states leads to the Hamiltonian

$$H = \sum_i H_i + J \sum_{\langle ij \rangle} \mathbf{S}_i \cdot \mathbf{S}_j, \quad (1)$$

$$H_i = -2t_p \sum_{\sigma} (x_{i\sigma}^\dagger y_{i\sigma} + y_{i\sigma}^\dagger x_{i\sigma}) + 2t_s \sum_{\sigma} a_{i\sigma}^\dagger a_{i\sigma} + 4J_s \sum_{\alpha, \beta} \mathbf{S}_i \cdot \mathbf{a}_{i\alpha}^\dagger \boldsymbol{\sigma}_{\alpha\beta} a_{i\beta} - 4V^2/\Delta, \quad (2)$$

where the origin of energy is taken to be the 2p hole level  $\varepsilon_p$ . Here  $J$  is the

superexchange interaction,  $S_i$  denotes the 3d spin at  $R_i$ ,  $\langle ij \rangle$  is the nearest-neighbor pair, and other operators for each molecular orbital are defined in terms of the annihilation operator  $c_{j\sigma}$  of a hole with atomic 2p orbitals by

$$x_{i\sigma} = \frac{1}{\sqrt{2}}(c_{i-x/2,\sigma} + c_{i+x/2,\sigma}), \quad y_{i\sigma} = \frac{1}{\sqrt{2}}(c_{i-y/2,\sigma} + c_{i+y/2,\sigma}), \quad a_{i\sigma} = \frac{1}{\sqrt{2}}(x_{i\sigma} + y_{i\sigma}), \quad (3)$$

where  $x$  and  $y$  in the suffices are unit vectors along each axis. We introduced the notation

$$J_s, t_s = v^2 \left( \frac{1}{\Delta} \pm \frac{1}{U_d - \Delta} \right). \quad (4)$$

Note that  $a_{i\sigma}$  annihilates a bonding state with respect to the transfer  $t_p$ . (In the electron picture with the original Brillouin zone, the state corresponds to an antibonding state.) Thus the state described by  $a_{i\sigma}$  is favorable not only by the  $J_s$  term in eq.(2) but by the transfer  $t_p$ .

It is convenient to work with orthogonal Wannier orbitals whose annihilation operator  $b_{j\sigma}$  is related to nonorthogonal one  $a_{i\sigma}$  by

$$a_{i\sigma} = \sum_j \lambda(R_i - R_j) b_{j\sigma}, \quad (5)$$

$$\lambda(R) = \int \frac{d^2 k}{(2\pi)^2} [1 + \frac{1}{2}(\cos k_x + \cos k_y)]^{1/2} \exp(ik \cdot R), \quad (6)$$

where integration is over the Brillouin zone. The value of  $\lambda(R)$  for the same site is  $\lambda_0 = 0.96$ , for nearest neighbor  $\lambda_1 = 0.14$ , and for next-nearest neighbor  $\lambda_2 = -0.02$ . It should be noticed that the largest energy in eqs.(1) and (2) is the binding energy  $8J_s$  of the d-p singlet relative to the triplet where  $J_s$  is of the order of half eV. The p-p transfer  $t_p$  is about 0.5 eV according to band-theoretical estimates [2]. Thus it is a good first approximation to regard low-energy holes as moving from one d-p singlet site to another, and to neglect the local triplet state. We introduce a projection operator to the singlet state at  $R_i$

$$P_i = \frac{1}{4} - \frac{1}{2} \sum_{\alpha, \beta} S_i \cdot b_{i\alpha}^\dagger \sigma_{\alpha\beta} b_{i\beta}, \quad (7)$$

using the orthogonal orbital. Then the electronic state at each site consists of the spin doublet  $|^2B_{1g}(R_i); \sigma\rangle$  and the d-p singlet  $|^1A_{1g}(R_i)\rangle$ . To describe the transition between these states we introduce the operator  $X_{0\sigma}^{(i)} = |^1A_{1g}(R_i)\rangle \langle ^2B_{1g}(R_i); \sigma|$  and its hermitian conjugate  $X_{\sigma 0}^{(i)}$ . We perform the projection for all sites having a 2p hole. Then we obtain after some algebra

$$H = \sum_{i,j,\sigma} \varepsilon_{ij} X_{0\sigma}^{(i)} X_{\sigma 0}^{(j)} + J \sum_{\langle ij \rangle} S_i \cdot S_j + 2\lambda_1^2 J_s \sum_{\langle ij \rangle} \sum_{\langle i\ell \rangle} \sum_{\mu, \nu} S_i \cdot X_{0\mu}^{(j)} \sigma_{\mu\nu} X_{\nu 0}^{(\ell)}, \quad (8)$$

where terms with factor  $\lambda_2^2$  and even smaller ones were neglected. The Fourier transform  $\varepsilon_k$  of the transfer energy  $\varepsilon_{ij}$  is given by

$$\varepsilon_k = -(6\lambda_0^2 + 2)J_s - 2\mu_0 t_p - 2(6\lambda_0\lambda_1 J_s + \mu_1 t_p - \frac{1}{4}t_s)(\cos k_x + \cos k_y) - 4(6\lambda_0\lambda_2 J_s + \mu_2 t_p) \cos k_x \cos k_y. \quad (9)$$

Here  $\mu_0 = 0.73$ ,  $\mu_1 = 0.55$  and  $\mu_2 = 0.24$ . It turns out that the next-nearest neighbor transfer is negligibly small because of cancellation of  $J_s$  and  $t_p$  terms in eq.(9).

The model given by eq.(8) constitutes a generalization of the result in [1] which does not contain  $t_p$ ,  $t_s$  and the last three-site term. The term represents the motion of a hole without interrupting the antiferromagnetic order. With  $t_p$  included, we can now discuss relative position of electronic states given by eq.(8) and the oxygen 2p bands without d-p hybridization. The bottom of the 2p hole band relative to  $\varepsilon_p$  is  $-4t_p$  which

is higher than the local singlet state with the energy  $-8J_s - 2t_p$ . The center of  $\epsilon_{\mathbf{k}}$  is higher than the local singlet due to the orthogonalization. The range of  $\epsilon_{\mathbf{k}}$  is several eV since the nearest-neighbor transfer is of the order of half eV. Thus the kinetic energy of effective single-particle state is much larger than the superexchange  $J$  which is about 0.1 eV. This means that ferromagnetic polarization around a hole occurs according to the Nagaoka theorem [4].

Let us discuss how the electronic states seen in photoemission experiments are related to the model we obtained. It is then necessary to make a connection to the electron picture in the original Brillouin zone. The energy  $E_{\mathbf{k}}$  for electrons is obtained from  $\epsilon_{\mathbf{k}}$  by first reversing the sign and then shifting  $\mathbf{k}$  by  $(\pi, \pi)$ . In the case of nearest-neighbor transfer alone, the result of the conversion makes  $E_{\mathbf{k}}$  have the same  $\mathbf{k}$  dependence as  $\epsilon_{\mathbf{k}}$ . Thus if a small number of holes are doped, they polarize the spin background ferromagnetically and go to the states near  $\mathbf{k} = (\pi, \pi)$ . The spatial extent of the polarization is determined by the balance between the gain of the kinetic energy and the loss of the exchange interaction, and is estimated to be several lattice spacings. The motion of a hole accompanies the polarization cloud and the effective mass should be larger than the one given by  $\epsilon_{\mathbf{k}}$ . On the other hand, the states near the zone center are very different from eq.(9) because they are less stable than the local singlet. We suggest that in the photoemission experiment the feature near the Fermi level and with little dispersion [3] is related to the local singlet state. The weakness of the spectrum as compared to the main 2p emission is due to the much smaller number of the oxygen states involved in the d-p singlets than in the main bands: The normalization factor 1/2 enters for making  $a_{i\sigma}$  from  $c_{j\sigma}$  and a further factor of  $1/\sqrt{2}$  for making a singlet. Thus the intensity ratio in the case of  $\text{Bi}_2\text{Sr}_2\text{CaCu}_2\text{O}_8$  is  $(1/2\sqrt{2})^2 \cdot 4/(6 \cdot 8) = 1/96$ . Here the factors 4 and 8 refer to the number of oxygens in  $\text{CuO}_2$  layers and in the total unit cell, respectively, and 6 is the number of 2p states per oxygen. It should be noticed that the d-p singlet is possible even in insulating  $\text{CuO}_2$  sheets as the final state of the photoemission. Fujimori [5] indeed observed a corresponding spectral feature in insulating Cu oxides.

In summary we have derived an effective Hamiltonian for low energy electronic states in high  $T_c$  superconductors and have shown that the single-band model is justified for a limited range of the hole states. The dispersion relation in a ferromagnetic background of 3d spins has a similarity to the band theoretical results in that the lowest-energy hole appears in the corner of the square Brillouin zone.

#### References

- [1] F.C. Zhang and T.M. Rice, Phys. Rev. **B37**, 3759 (1988).
- [2] A.K. McMahan et al., Phys. Rev. **B38**, 6650 (1988); K.T. Park et al., J. Phys. Soc. Jpn. **57**, 3445 (1988).
- [3] T. Takahashi et al., Nature **334**, 691 (1988); F. Minami et al., Phys. Rev. B (in press).
- [4] Y. Nagaoka, Phys. Rev. **147**, 392 (1966).
- [5] A. Fujimori, private communication.



# The Madelung Energy in Oxide Superconductors

J. Kondo and S. Nagai<sup>†</sup>

Electrotechnical Laboratory, Tsukuba, Ibaraki 305

<sup>†</sup>Nihon University at Narashino, Funabashi, Chiba 274

The Madelung energy in the  $\text{TlBa}_2\text{Ca}_{n-1}\text{Cu}_n\text{O}_{2n+3}$  system has been calculated and the hole distribution which makes the Madelung energy the smallest has been determined under the assumption that the holes occupy oxygen sites. It is found that the holes enter the outermost  $\text{CuO}_2$  planes (or plane for  $n=1$ ) and do not enter either the inner  $\text{CuO}_2$  planes (or plane for  $n=3$ ) nor the oxygen ions in apical positions of the copper ions. It is also shown that it is much easier to dope  $\text{Nd}_2\text{CuO}_4$  with electrons than to dope  $\text{La}_2\text{CuO}_4$  with electrons.

## 1. The Madelung energy in the YBCO system

For understanding the mechanism of superconductivity in copper-oxide-based ceramics, it is important to know the sites which the holes in these conductors occupy. We take the stand point that these substances are essentially ionic crystals and that the Madelung energy is the most important energy to determine the hole distribution. We have calculated the Madelung energy of YBCO and related compounds, and determined the hole distribution of each compound which makes the Madelung energy the smallest.<sup>1)</sup> Our interest has been focused on whether the distribution is such that holes occupy sites in the  $\text{CuO}_2$  planes or not, and we have divided all the compounds into two classes according to this criterion. We have found a close correlation between the occurrence of superconductivity found by Tokura et al.<sup>2)</sup> and this classification. The conclusion was that the superconductivity of YBCO and related compounds is due to holes in the  $\text{CuO}_2$  planes.

One point which emerged from our calculation is that the nominal hole concentration does not necessarily represent the actual one. An example is  $(\text{Y}_{0.75}\text{Ca}_{0.25})\text{Ba}_2\text{Cu}_3\text{O}_{6.25}$ , whose nominal hole concentration is  $p=-1/12$ . (The definition of  $p$  is given in reference 1) and is the same as that of reference 2).) Although a negative hole concentration might imply electron doping, we have shown that this substance should contain holes in the  $\text{CuO}_2$  planes. Recently, Jirák, Hejtmánek, Pollert, Tríska and Vašek have found that the substance  $(\text{Y}_{0.8}\text{Ca}_{0.2})\text{Ba}_2\text{Cu}_3\text{O}_{6.2}$ , which has a composition close to the above example and has  $p=-0.133$ , is a superconductor with  $T_c=84\text{K}$ .<sup>3)</sup> We believe that this example indicates the validity of our consideration based on the Madelung energy.

## 2. The Madelung energy in $\text{TlBa}_2\text{Ca}_{n-1}\text{Cu}_n\text{O}_{2n+3}$

We next consider the compound  $\text{TlBa}_2\text{Ca}_{n-1}\text{Cu}_n\text{O}_{2n+3}$  ( $n=1, \dots, 4$ ). They are found to be high- $T_c$  superconductors except the case of  $n=1$ .<sup>4)5)</sup> If one assigns nominal charges to each ion (i.e., +3 for Tl; +2 for Ba, Ca and Cu; -2 for O), one is left with one hole

per unit formula of this compound. The fact that the holes are introduced without doping makes this compound suitable for theoretical consideration. Then, the question is which site this hole will occupy. Following the results obtained by several spectroscopic measurements, we assume that the holes enter oxygen sites. Then, we will have two choices; one where the holes enter oxygen ions in the  $\text{CuO}_2$  planes, and the other where they enter those at apical positions of the copper ions. In Fig. 1, we show the unit cell for the compound of  $n=2$ . The former oxygens are denoted by open circles and the latter by circles with dots inside. For  $n=3$  and 4, there are two kinds of the  $\text{CuO}_2$  planes; the outermost planes and the inner planes (or plane for  $n=3$ ). (see Fig. 2)

We have calculated the total Madelung energy for various kinds of hole distribution. Let  $E_1$  be the Madelung energy per unit cell when the hole is placed in the outermost  $\text{CuO}_2$  planes (or plane for  $n=1$ ). Let  $E_2$  be that when it is placed in the inner  $\text{CuO}_2$  planes (or plane for  $n=3$ ), and finally let  $E_3$  be that when it is placed on the apical oxygens. Since there is only one hole per unit cell, only some of the oxygens are occupied by the holes.

We first assume a strong correlation among the holes. This means that they are distributed avoiding each other. In order to achieve such a correlation, we consider a larger unit cell as was done in reference 1) and place holes in it in such a way they form a superlattice. Then, we calculate the total Madelung energy using the Ewald method. The results are shown in the table in units of eV:

n	1	2	3	4
$E_2-E_1$			4.80(4.37)	6.73(6.85)
$E_3-E_1$	4.03(3.46)	3.02(1.89)	2.93(1.92)	2.90(1.89)

We next assume a random distribution of the holes for each case. Thus for  $E_1$ , e.g., the holes are distributed randomly on the oxygen ions in the outermost  $\text{CuO}_2$  planes. The results are shown in the parentheses of the table, which are qualitatively similar to those for the strong correlation.

Our calculation is based on the lattice parameters reported in reference 4). Since the authors showed only the lattice parameters for  $n=3$ , those for other  $n$ 's have been guessed in this calculation. We expect this does not involve a significant error. However, some oxygen positions reported in reference 4) are based on knowledge in related crystal structures. Thus, the distance between the copper ion and the apical oxygen was taken to be 2.7Å, which is somewhat larger than 2.4Å found in the YBCO system. We have repeated calculation using 2.5Å for this distance to see reliability of our result. The results of such a calculation are shown in the next table:

n	1	2	3	4
$E_2-E_1$			4.78(4.35)	6.71(6.83)
$E_3-E_1$	5.10(4.52)	4.03(2.88)	3.94(2.91)	3.92(2.90)

We see that both parameter values give qualitatively identical results. We also see that  $E_1$  is the smallest in all the cases, and that the energy differences are rather large. We conclude that the holes mainly occupy the oxygens in the outermost  $\text{CuO}_2$  planes, i.e., the basal oxygens of  $\text{CuO}_5$  pyramids and that they will not enter the  $\text{CuO}_2$  planes where the copper ions are in the square-planar coordination. The apical oxygens tend to attract holes to the basal oxygens.

### 3. The Madelung energy in $\text{Nd}_2\text{CuO}_4$

Recently, a superconductivity with  $T_c=25\text{K}$  has been reported for the electron-doped

(Nd,Ce)<sub>2</sub>CuO<sub>4</sub>,<sup>6)</sup> which has a crystal structure related to but different from the K<sub>2</sub>NiF<sub>4</sub> structure. We will show that this substance is more suitable for electron doping than the La<sub>2</sub>CuO<sub>4</sub> crystal. The tables show the Madelung potentials (in eV) for the electron at each atomic site for the two substances:

La <sub>2</sub> CuO <sub>4</sub>				Nd <sub>2</sub> CuO <sub>4</sub>			
Cu	La	O(sheet)	O(apex)	Cu	Nd	O(sheet)	O
28.54	27.92	-21.03	-20.13	23.88	29.32	-21.51	-20.18

Except the copper sites, both values are very close to each other. In order to introduce an electron to the copper site, one needs an energy equal to 28.54-I<sub>2</sub> or 23.88-I<sub>2</sub>. With the second ionization energy I<sub>2</sub> of 20eV, one finds that much smaller energy is needed for doping Nd<sub>2</sub>CuO<sub>4</sub> with electrons than doping La<sub>2</sub>CuO<sub>4</sub>. The lower Madelung potential at the copper site in Nd<sub>2</sub>CuO<sub>4</sub> implies that the covalency in the Cu-O bond in the plane is larger than that in La<sub>2</sub>CuO<sub>4</sub> (or Δ is smaller). It is interesting to see whether the moment of copper ions exists in this substance.

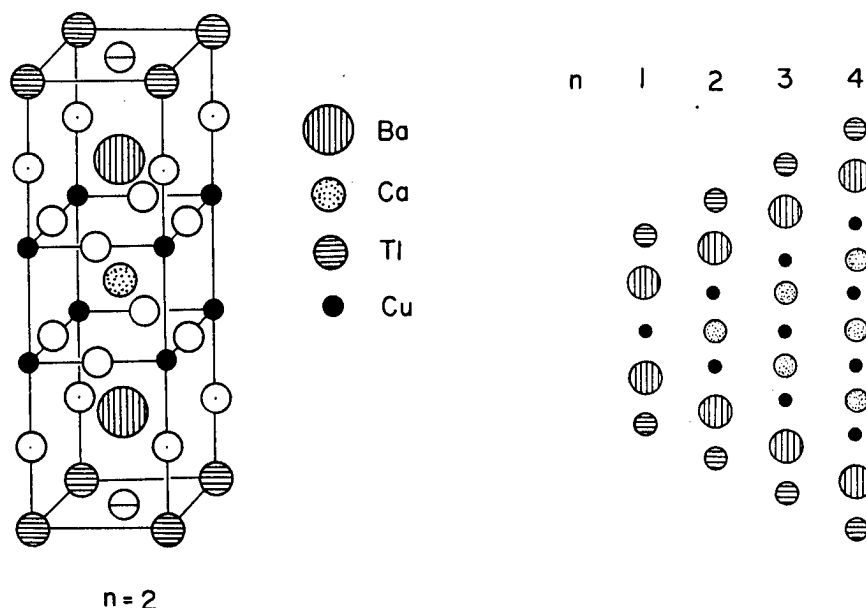


Fig. 1 The unit cell of TlBa<sub>2</sub>CaCu<sub>2</sub>O<sub>7</sub>

Fig. 2

#### References

- 1) J. Kondo, Y. Asai and S. Nagai, J. Phys. Soc. Japan 57 (1988) 4334.
- 2) Y. Tokura, J. B. Torrance, T. C. Huang and A.I. Nazzari, Phys. Rev. B38 (1988) 7156.
- 3) Z. Jirák, J. Hejtmánek, E. Pollert, A. Trřiska and P.Vařek, Physica C155 (1988) 750.
- 4) S. S. P. Parkin, V. Y. Lee, A. I. Nazzari, R. Savoy, R. Beyers and S. J. LaPlaca, Phys. Rev. Letters 61 (1988) 750.
- 5) H. Ihara, R. Sugie, M. Hirabayashi, N. Terada, M. Jo, K. Hayashi, A. Negishi, M. Tokumoto, Y. Kimura and T. Shimomura, Nature 334 (1988) 510.
- 6) Y. Tokura, H. Takagi and S. Uchida, at Symposium on superconductivity (at Univ. of Tokyo, Jan. 1989) and Nature (Jan. 1989).

# Superconductivity in $\text{BaPb}_{1-x}\text{Bi}_x\text{O}_3$ and $\text{Ba}_x\text{K}_{1-x}\text{BiO}_3$

Masafumi SHIRAI, Naoshi SUZUKI and Kazuko MOTIZUKI

Department of Material Physics, Faculty of Engineering Science  
Osaka University, Toyonaka 560, Japan

The superconducting transition temperature of  $\text{BaPb}_{1-x}\text{Bi}_x\text{O}_3$  (BPB) and  $\text{Ba}_x\text{K}_{1-x}\text{BiO}_3$  (BKB) is evaluated on the basis of the strong coupling theory. The electron-lattice interaction is calculated microscopically by using the realistic electronic band structure. It is shown that the superconducting properties in BKB such as a high transition temperature ( $\sim 30$  K) and rather small isotope effect can be understood within the phonon mechanism.

The oxide superconductor  $\text{BaPb}_{1-x}\text{Bi}_x\text{O}_3$  (BPB) has attracted much attention because of its interesting properties of superconductivity. Superconductivity in BPB has been observed in the composition range  $0 < x < 0.35$  and the maximum transition temperature  $T_c$  is about 13 K ( $x=0.25$ ).<sup>1,2)</sup> Recently  $\text{Ba}_x\text{K}_{1-x}\text{BiO}_3$  (BKB) has turned out to have the highest  $T_c$  ( $\sim 30$  K at  $x=0.7$ ) among oxide superconductors not containing Cu ions.<sup>3-5)</sup> Both BPB and BKB have a simple perovskite-type structure and do not contain any transition-metal element. Thus the magnetic mechanism may not be expected for the superconductivity in these compounds. Therefore it is meaningful to investigate the electron-lattice interaction microscopically in order to clarify the mechanism of the superconductivity in BPB and BKB.

We have developed<sup>6)</sup> a microscopic theory of the electron-lattice interaction and the lattice dynamics of BPB in the range  $0 < x < 0.35$  by using the realistic electronic bands of BPB.<sup>7)</sup> We have calculated also the spectral function  $\alpha^2F(\omega)$ <sup>6)</sup> in order to give a basis for discussing quantitatively the superconducting properties of BPB in the framework of a strong coupling theory of the phonon mechanism. The purpose of this report is first to extend our investigation to wider composition range ( $0 < x < 1$ ) which covers the superconducting composition of BKB as well as BPB, and secondly to give an accurate evaluation of  $T_c$  by solving the Eliashberg equations at finite temperatures with use of the calculated spectral function  $\alpha^2F(\omega)$ . We also present a theoretical estimation of the isotope effect on  $T_c$  due to replacing  $^{16}\text{O}$  with  $^{18}\text{O}$ .

The electronic band structure of BPB has been calculated by Mattheiss and Hamann using the LAPW method.<sup>7)</sup> According to their results the conduction band which crosses the Fermi level is a hybridized band consisting of O 2p and Bi (or Pb) 6s and 6p orbitals. This conduction band is well reproduced by the tight-binding (TB) model with three Slater-Koster transfer integrals between nearest neighbouring O and Bi (or Pb) atoms. By using this TB conduction band we have calculated the electron-lattice coupling coefficient  $g_\mu^\alpha(\mathbf{k}, \mathbf{k}')$ , which represents the strength of the coupling between two conduction band states  $\mathbf{k}$  and  $\mathbf{k}'$  caused by displacement of the  $\mu$ -th atom along the  $\alpha$ -direction ( $\alpha=x, y, z$ ). In actual calculation it is necessary to evaluate the derivatives of transfer integrals  $t'$ . By taking into consideration the electronic band structures in the distorted phase of  $\text{BaBiO}_3$  we have estimated the value of  $t'$  as  $t' = 4\sim 5$  eV/Å. Recently Mattheiss and Hamann calculated the band structure for ordered

alloy  $\text{Ba}_{0.5}\text{K}_{0.5}\text{BiO}_3$ ,<sup>8)</sup> and it is confirmed that the conduction band is little affected by substitutional K doping. Therefore we adopt the rigid-band approximation for the doping effects, i.e. we assume that as  $x$  increases the TB conduction band is filled gradually without change of its dispersion.

Next we investigate the lattice dynamics in this system including the effect of the electron-lattice interaction. The dynamical matrix is divided into two parts: the generalized electronic susceptibility  $\chi$ , which is the Fourier transform of the effective long range forces caused by the electron-lattice interaction, and the remaining part  $D_0$ . Usually  $D_0$  is expressed by the Fourier transform of inter-atomic short range forces. For  $D_0$  we consider seven kinds of short range forces. They have been determined so as to fit seven phonon frequencies observed in  $\text{BaPb}_{0.75}\text{Bi}_{0.25}\text{O}_3$ ,<sup>9)</sup> which seem to be insensitive to the effect of the electron-lattice interaction. Calculation of  $\chi$  has been done by taking into account the wave-vector and mode dependences of  $g_\mu^\alpha(\mathbf{k}, \mathbf{k}')$ , and the phonon dispersion curves have been obtained by diagonalizing the dynamical matrix  $\chi + D_0$ . The electron-lattice interaction have turned out to lower the frequencies and to broaden the line-width of the longitudinal (L) O-stretching and/or breathing mode vibration, which is originally located around 60 meV. The phonon frequency renormalization shows remarkable wave-vector and  $x$  dependences. For instance, in case of  $x=0.3$  large renormalization is seen especially around the X-point in the first Brillouin zone while for  $x>0.4$  the phonon branch becomes soft also around the M-point besides the X point. The wave-vector and mode dependences of the phonon renormalization are originated from the wave-vector and mode dependences of  $g_\mu^\alpha(\mathbf{k}, \mathbf{k}')$ .

Now we discuss the superconductivity of BPB and BKB in the framework of the strong coupling theory of the phonon mechanism. For this purpose we have calculated the spectral function  $\alpha^2 F(\omega)$  making use of the renormalized phonons obtained above.

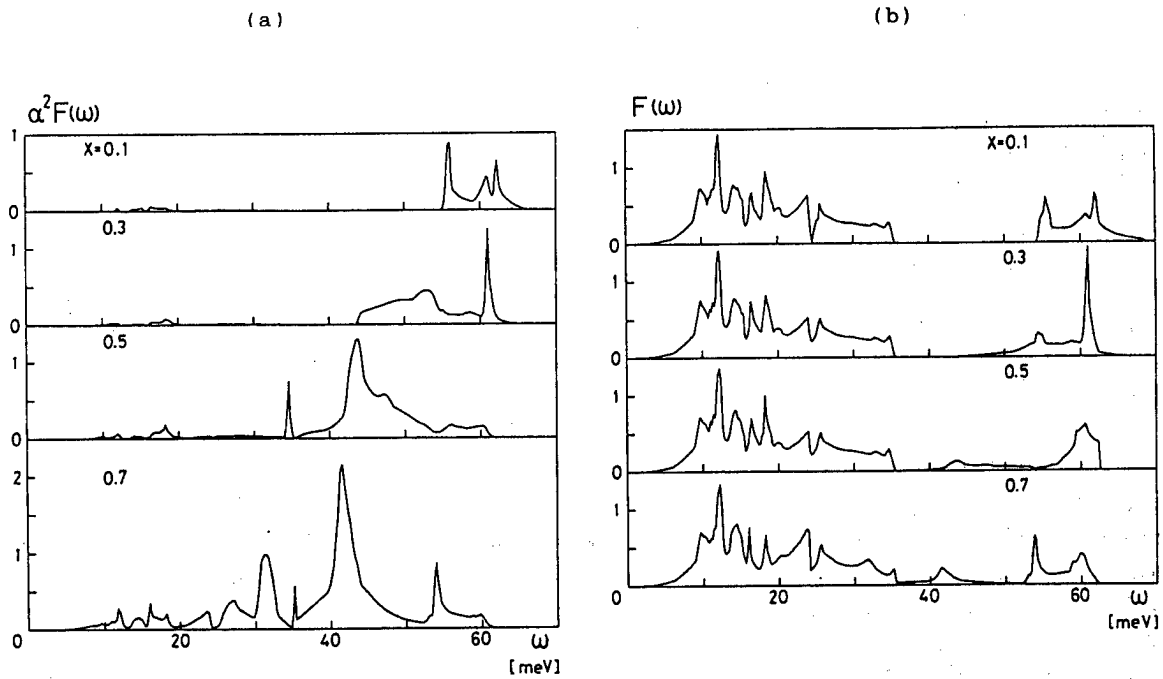


Fig. 1. (a) Spectral function  $\alpha^2 F(\omega)$  and (b) phonon density of states calculated for  $x=0.1, 0.3, 0.5$  and  $0.7$  in case of  $t'=4 \text{ eV}/\text{\AA}$ .

In Fig.1 we show the spectral function  $\alpha^2F(\omega)$  and the phonon density of states  $F(\omega)$  calculated for several values of  $x$  in case of  $t' = 4\text{eV}/\text{\AA}$ . It is found that  $\alpha^2F(\omega)$  has a frequency dependence entirely different from that of  $F(\omega)$ . It should be noted that  $\alpha^2F(\omega)$  has some prominent structures in the frequency range of O-stretching/breathing mode. Thus this O-stretching/breathing mode is expected to contribute dominantly to the superconductivity. As  $x$  increases, some main peaks in  $\alpha^2F(\omega)$  shift to lower frequency side, reflecting the phonon frequency renormalization, and the magnitude of  $\alpha^2F(\omega)$  increases strikingly in the whole frequency range up to 60 meV. This considerable change in  $\alpha^2F(\omega)$  is expected to bring a remarkable  $x$  dependence of  $T_c$ .

The transition temperature  $T_c$  has been evaluated by solving the linearized Eliashberg equations with use of the calculated  $\alpha^2F(\omega)$ . The obtained  $x$ -dependences of  $T_c$  are shown in Fig.2. For each  $x$  we have calculated  $T_c$  with four different values of  $\mu^*$ , 0.0, 0.05, 0.1 and 0.15. Here  $\mu^*$  denotes the effective screened Coulomb repulsion constant. In most superconductors  $\mu^*$  has been taken to be between 0.1 and 0.15 empirically. The calculated  $T_c$  increases rapidly with increasing  $x$ , and reaches 28 K at  $x=0.7$  in case of  $\mu^*=0.1$ .

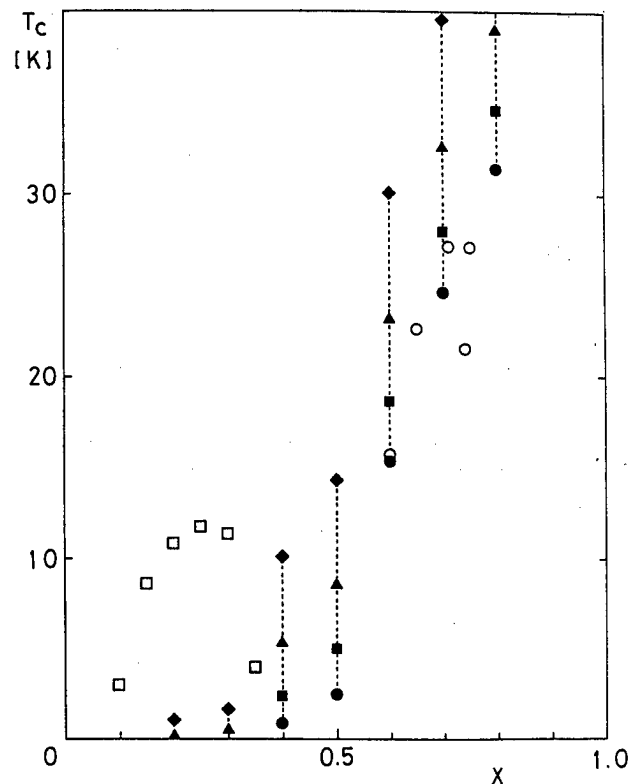


Fig. 2.  
Superconducting transition temperature  $T_c$  as a function of  $x$ . The calculation of  $T_c$  is made for  $\mu^*=0.0$  ( $\blacklozenge$ ), 0.05 ( $\blacktriangle$ ), 0.10 ( $\blacksquare$ ) and 0.15 ( $\bullet$ ), respectively. The experimental data for BPB<sup>2)</sup> ( $\square$ ) and BKB<sup>5)</sup> ( $\circ$ ) are also shown.

The dimensionless coupling constant  $\lambda$  has been evaluated to be 0.98 for  $\mu^*=0.1$  and  $x=0.7$  ( $T_c=28$  K). It should be noted here that we must be careful in using the McMillan's equation for  $T_c$ ,  $T_c=(\Theta_D/1.45)\exp\{-1.04(1+\lambda)/[\lambda-\mu^*(1+0.62\lambda)]\}$ , where  $\Theta_D$  denotes the Debye temperature. For BPB  $\Theta_D$  is estimated to be  $\sim 190$  K. Then, if we use the above McMillan's equation to estimate  $T_c$  for  $\lambda=0.98$  ( $\mu^*$  is fixed at 0.1), we have  $T_c=10.5$  K. On the other hand, if we determine the value of  $\lambda$  from this McMillan's equation so as to get  $T_c=28$  K, we obtain a very large value of  $\lambda$  such as 3.0. Therefore it is not justified to utilize the McMillan's equation with  $\omega_D$  for the evaluation of  $T_c$  in such a complex system as BPB or BKB. Our results for  $T_c$  agree well with observed  $T_c$  in BKB, but disagree with those in BPB. One of reasons for

this discrepancy may be that the rigid-band model is insufficient to BPB because in BPB the Pb atom, which is one of constitutive elements of the conduction band, is substituted randomly by the Bi atom.

Finally we have estimated the isotope effect on  $T_c$  by evaluating  $T_c$  when  $^{16}\text{O}$  is replaced with  $^{18}\text{O}$ . The results for  $t'=4$  eV/Å and  $x=0.7$  are listed in Table I. A characteristic exponent  $\alpha$ , defined as  $T_c \propto M_O^{-\alpha}$ , is found to be sensitive to the value of  $\mu^*$ :  $\alpha=0.33$  for  $\mu^*=0.0$  and  $\alpha=0.24$  for  $\mu^*=0.15$ . Experimentally the value of  $\alpha$  is evaluated to be 0.21 by Batlogg et al.<sup>10)</sup> and 0.3 by Sato et al.<sup>11)</sup> The principal reason why  $\alpha$  differs from the so-called BCS value ( $\alpha=0.5$ ) is that the vibration of atoms other than oxygens, such as Bi atoms, contribute appreciably to the superconductivity, particularly in case large phonon frequency renormalization is caused by the electron-lattice interaction.

Table I.  
Isotope effect on  $T_c$  due  
to replacing  $^{16}\text{O}$  with  $^{18}\text{O}$   
in case of  $t'=4$  eV/Å and  
 $x=0.7$  ( $\text{Ba}_{0.7}\text{K}_{0.3}\text{BiO}_3$ ).

$M_O$	16	18	
$\lambda$	0.978	0.992	
$T_c$ ( $\mu^*=0.0$ )	39.61	37.99	$\alpha = 0.33$
( 0.05)	32.56	31.35	0.30
( 0.10)	27.93	27.00	0.27
( 0.15)	24.61	23.87	0.24

In summary, we have investigated the lattice dynamics and the superconductivity of BPB and BKB in the framework of the strong coupling theory of the phonon mechanism. Our results suggest that the superconducting properties in BKB, such as the magnitude of  $T_c$  and the isotope effect on  $T_c$ , can be understood within the phonon mechanism. It is particularly emphasized that the significant renormalization of the L O-stretching/breathing mode phonons plays an important role for the high  $T_c$  in BKB. On the other hand, it is a further problem whether the superconductivity in BPB can be explained within the phonon mechanism. It seems that effects of random substitution of Bi for Pb have to be taken into account suitably.

#### References

- 1) A.W. Sleight, J.L. Gilson and P.E. Biersteadt: Solid State Commun. 17 (1975) 27.
- 2) T.D. Thanh, A. Koma and S. Tanaka: Appl. Phys. 22 (1980) 205.
- 3) L.F. Mattheiss, E.M. Gyorgy and D.W. Johnson, Jr.: Phys. Rev. B37 (1988) 3745.
- 4) R.J. Cava, B. Batlogg, J.J. Krajewski, R.C. Farrow, L.W. Rupp, Jr., A.E. White, K.T. Short, W.F. Peck, Jr. and T.Y. Kometani: Nature (London) 332 (1988) 814.
- 5) D.G. Hinks, B. Dabrowski, J.D. Jorgensen, A.W. Mitchell, D.R. Richards, S. Pei and D. Shi: Nature (London) 333 (1988) 836.
- 6) M. Shirai, N. Suzuki and K. Motizuki: Solid State Commun. 60 (1986) 489.; JJAP Series 1 "Superconducting Materials" (1988) 255.; Ferroelectricity (1989) in press.
- 7) L.F. Mattheiss and D.R. Hamann: Phys. Rev. B28 (1983) 4227.
- 8) L.F. Mattheiss and D.R. Hamann: Phys. Rev. Lett. 60 (1988) 2681.
- 9) W. Reichardt and W. Weber: JJAP 26, Suppl. 26-3 (1987) 1121.
- 10) B. Batlogg, R.J. Cava, L.W. Rupp, Jr., A.M. Muzsca, J.J. Krajewski, J.P. Remeika, W.F. Peck, Jr., A.S. Cooper and G.P. Espinoza: Phys. Rev. Lett. 61 (1988) 1670.
- 11) M. Sato et al.: Private communications.

# Researches on High $T_c$ Superconductivity in Our Group

M. Tachiki

Institute for Materials Research, Tohoku University  
2-1-1 Katahira, Sendai 980, Japan

I would like to report the research works on high  $T_c$  superconductivity which have been made in our group in the 1988 fiscal year.

Since the discovery of the high  $T_c$  oxide superconductors[1], world-wide extensive studies have been made for the superconductivity in the oxides[2]. From the basic point of view the important problem is to clarify the mechanism of the high  $T_c$  superconductivity. On the other hand from the practical point of view the problem is to find materials with higher  $T_c$  and higher critical current. Taking the above points into consideration, we made the studies on the electronic state in the high  $T_c$  oxide superconductors, a possible mechanism of the high  $T_c$  superconductivity, and a mechanism of the strong pinning intrinsic in the oxide superconductors. The names which are shown below the subject titles are the names of collaborators.

## I. Electronic State in Oxide Superconductors

H.Matsumoto, T.Koyama, M.Sasaki

Recently, Suzuki at NTT Optoelectronic Laboratories made optical transmission experiments using single crystal thin films of  $\text{La}_{2-x}\text{Sr}_x\text{CuO}_4$ [3]. The transmission spectra show an anomalous absorption band in addition to the fundamental absorption band corresponding to the charge transfer gap. This new band develops with Sr doping. These features imply that an electronic band appears inside the gap and develops with Sr doping. A similar character of the electronic state has been observed by photo-emission experiments using  $\text{YBa}_2\text{Cu}_3\text{O}_{7-y}$ [4], and the character of the band has been determined to be mainly of the p-electron of oxygen. The particles in this band may be responsible for the superconductivity.

To describe the electronic structure in the oxide superconductors, we take into account the following p-d mixing model. In the Cu-O plane, d-electrons at Cu-sites receive a strong intra-atomic Coulomb repulsion  $U$  each other. The p-electrons at O-sites form a very narrow band and mix with d-electrons through the charge transfer interaction. The large repulsion  $U$  opens the Hubbard gap in the d band. Since  $U \sim 7\text{eV}$  and the charge transfer gap is about  $2\text{eV}$ , it is natural to assume that the p-electron level is situated in the middle of the Hubbard gap and mixes mainly with the upper Hubbard band, forming a new electronic band.

Since a Cu-site is favorably occupied by one electron, the hopping of electrons from a Cu-site to an O-site causes large deviations of spin and charge at the Cu- and O-site and induces simultaneously spin and charge fluctuations. The electronic state near the Fermi level is largely affected by the fluctuations. Specially around the metal-insulator transition, these fluctuations yield certain drastic change associated with the shift from localized behaviors to itinerant ones. Actually, according to a self-consistent many body calculation, we obtained the electronic structure observed by



the experiments mentioned above.

## II. A Possible Mechanism of High $T_c$ Superconductivity[5-7]

S.Takahashi

The theory mentioned above shows that the Fermi-liquid state appears near the Fermi levels. Also, recent experiments of angular resolved photoemission using single crystals of Bi-Sr-Ca-Cu-O[8,9] and  $\text{YBa}_2\text{Cu}_3\text{O}_7$ [10] show a clear Fermi edge and dispersion in the excitation spectra. Therefore, it seems natural to consider that the superconducting current is carried by this Fermi liquid. The experimental fact that the carrier unit of superconducting current in the oxides is twice the electronic charge[11-14] implies that the superconductivity is generated by the pairs of the particles constituting the Fermi liquid.

The problem is the origin of the large binding energy for the pairing. The phonon-mediated pairing is too weak to account for the high  $T_c$  superconductivity in the oxides. We, therefore, should seek a nonphonon mechanism accountable for the high  $T_c$  superconductivity in the oxides. Since the large spin and charge fluctuations are in the copper oxides, the interactions mediated by these fluctuations are candidates for the pairing interaction. Many experimental results shows that the pairing is of S-wave pairing symmetry[15-17]. The spin fluctuations work destructively on the S-wave pairs. Therefore we consider a charge fluctuation mechanism for the pairing.

When the charge fluctuations are large in a highly correlated electron system such as the oxide superconductors, the electron dielectric constant can be negative. In the system, the charge fluctuations strongly couple with longitudinal optical phonons. The effective interaction between two electrons is given by  $V(q)/\epsilon(q, \omega)$  where  $V(q)$  is the Fourier component of the Coulomb interaction and  $\epsilon(q, \omega)$  is the total dielectric constant given by the sum of the electronic and ionic dielectric constants. Using the effective interaction, we set up the Eliashberg equation and calculate  $T_c$  by solving it. We find that  $T_c$  is very much enhanced, and also that the isotope effect is weakened in consistence with the experimental result that the decrease of  $T_c$ , when  $^{16}\text{O}$ 's in the sample are replaced by  $^{18}\text{O}$ 's, is weakened as  $T_c$  increases[18-23].

## III. Theory of Nuclear Relaxation in Superconducting High $T_c$ Oxides[24]

T.Kayama

The nuclear resonance experiments show the anomalous temperature dependence of the nuclear relaxation rate  $1/T_1$  of Cu(II) in the  $\text{YBa}_2\text{Cu}_3\text{O}_{7-y}$ [25-28]. The nuclear relaxation rate is very much enhanced in the normal state and drastically suppressed in the superconducting state. The hump of  $1/T_1$  which is usually observed just below  $T_c$  in BCS superconductors has not been observed. These anomalous behavior of the nuclear relaxation is found to be explained on the basis of the BCS pairing, if the strong correlation effect of the electrons is properly taking into account. The spin fluctuation makes the superconducting state gapless near  $T_c$  and erase the hump of  $1/T_1$ . The spin fluctuation vertex is strongly renormalized in the superconducting state and thus  $1/T_1$  which is enhanced by the spin fluctuations in the normal state is drastically suppressed in the superconducting state. The above two effects combining give a sharp decrease of  $1/T_1$  below  $T_c$  mentioned above.

#### IV. Strong Vortex Pinning Intrinsic in High $T_c$ Oxide Superconductors[29]

S.Takahashi

Since the coherence length is short[30-31] and the London penetration depth is long[16-17] in the oxide superconductors, usual pinning mechanism due to impurities, defects, precipitates, and grain boundaries do not work in the oxides. Nevertheless, experiments show that high quality films of  $\text{YBa}_2\text{Cu}_3\text{O}_7$  fabricated by sputtering and chemical vapor deposition can carry the large critical current density of the order of  $10^6 \text{ A/cm}^2$ [32-34]. This fact implies that some strong pinning force acts on the vortices in the oxide superconductors. To explain this fact, we consider the following mechanism.

Let us consider a single crystal of  $\text{YBa}_2\text{Cu}_3\text{O}_7$ . In this crystal the  $\text{CuO}_2$  layers and their vicinities are strongly superconductive, and the layers with  $\text{CuO}$  chains and their vicinities are weakly superconductive. In other words the superconducting order parameter is modulated along the  $c$  axis of the crystal with the period of the lattice constant  $a_c$ . The value of the  $a_c$  of  $\text{YBa}_2\text{Cu}_3\text{O}_7$  is  $11.6 \text{ \AA}$ . We inject a vortex whose direction is parallel to the  $ab$  plane of the crystal. The coherence length along the  $c$  axis is shorter than  $a_c$  except in the vicinity of  $T_c$ , and the radius of the vortex core along the  $c$  axis is smaller than  $a_c$ . The superconducting order parameter inside the core almost vanishes. As a result, the loss of the superconducting cohesive energy due to the creation of a vortex is the least when the vortex is placed around the layers with  $\text{CuO}$  chains where the superconducting order parameter is smallest. Since the vortex is stabilized the most in these layers, the modulation of the order parameter works as a natural pinning center. The critical current density estimated from this pinning mechanism is very high, and found to be comparable to the critical current density measured in the single crystal films of high quality[32-34].

#### References

- 1 J.G.Bednorz and K.A.Müller, Z.Phys.B65,189(1986).
- 2 See, for example, the proceedings published in Physica C153-155.
- 3 M.Suzuki, private communications.
- 4 N.Nücker, private communications.
- 5 M.Tachiki, S.Takahashi, Y.Namba, Y.Fukuda, M.Nagoshi, and Y.Syono, Physica C153-155,239(1988).
- 6 M.Tachiki and S.Takahashi, Phys.Rev.B38,218(1988).
- 7 M.Tachiki and S.Takahashi, Phys.Rev.B39,293(1989)
- 8 T.Takahashi, H.Matsuyama, H.Katayama-Yoshida, Y.Okabe, H.Hosoya, K.Seki, H. Fujimoto, M.Sato, and H.Inokuchi, Nature 334,691(1988).
- 9 F.Minami, private communications.
- 10 Y.Sakisaka, private communications.
- 11 C.E.Gough, M.S.Colclough, E.M.Forgan, R.G.Jordan, M.Keene, C.M.Muirhead, A.I.M. Rae, N.Thomas, J.S.Abell, and S.Sutton, Nature 326,855(1987).
- 12 P.L.Gammel, D.J.Bishop, G.J.Dolan, J.R.Kwo, C.A.Murray, L.F.Schneemeyer, and J.V. Waszczak, Phys.Rev.Lett.59,2592(1987).
- 13 J.S.Tsai, Y.Kubo, and J.Tabuchi, Phys.Rev.Lett.58,1979(1987).
- 14 T.Yamashita, A.Kawasaki, T.Nishihara, Y.Hirotsu, and M.Takata, Jpn.J.Appl.Phys.26, L635(1987).
- 15 P.J.M.van Bentum, H.F.C.Hoovers, H.van Kempen, L.E.C.van de Leemput, M.J.M.F.de

- Nivelle, L.W.M.Scheurs, R.T.M.Smokers, and P.A.A.Teunissen, Physica C153-155, 1719(1988).
- 16 Y.J.Uemura, V.J.Emery, A.R.Moodenbaugh, M.Suenaga, D.C.Johnston, A.J.Jacobson, J.T.Lewandowski, J.H.Brewer, R.F.Kiefl, S.K.Kreitmann, G.M.Luke, T.Riseman, S.K.Stronach, W.J.Kossler, J.R.Kempton, X.H.Yu, D.Opie, and H.E.Schone, Phys.Rev.B38, 909 (1988).
  - 17 A.T.Fiory, A.F.Hebard, P.M.Mankiewich, and R.E.Howard, Phys.Rev.Lett.61,1419 (1988).
  - 18 B.Batlogg, G.Kourouklis, W.Weber, R.J.Cava, A.Jayaramann, A.E.White, K.T.Short, L.W.Rupp, and E.A.Reitman, Phys.Rev.Lett.59,912(1987)
  - 19 T.A.Faltens, K.K.Ham, S.W.Keller, K.J.Leary, J.N.Michaels, A.M.Stacy, H.-C.zur Loye, D.E.Morris, T.W.Borbee,III, L.C.Bourne, M.L.Cohen, S.Hoen, and A.Zettl, Phys.Rev.Lett.59, 915(1987).
  - 20 B.Batlogg, R.J.Cava, A.Jayanaman, R.B.van Dover, G.A.Kourouklis, S.Sunshine, D.M.Murphy, L.W.Rupp, H.S.Chen, A.White, K.T. Short, A.M.Mujisce and E.A.Reitman, Phys.Rev.Lett.58,2333(1987).
  - 21 L.C.Bourne, M.F.Crommie, A.Zettl, H.-C.zur Loye, S.W.Keller, K.J.Leary, A.M.Stacy, K.I.Chang, M.L.Cohen, and D.E.Morris, Phys.Rev.Lett.58,2337(1987).
  - 22 K.J.Leary, H.-C.zur Loye, S.W.Keller, T.A.Faltens, W.K.Ham, J.N.Michaels, and A.M.Stacy, Phys.Rev.Lett.59,1236(1987).
  - 23 H.Katayama-Yoshida, T.Hirooka, A.Oyamada, Y.Okabe, T.Takahashi, A.Ochiai, Sasaki, T.Suzuki, A.J.Mascarehas, J.I.Pankove, T.Ciszek, S.K.Deb, R.B.Goldfarb, and Y.Li, Physica C156, 481(1988).
  - 24 T.Koyama and M.Tachiki, Phys.Rev.B(1989).
  - 25 W.W.Warren,Jr, R.E.Walstedt, G.F.Brennert, G.P.Espinosa, and J.P.Remeika, Phys.Rev.Lett.59,1860(1987).
  - 26 M.Mali, D.Brinkmann, L.Pauli, J.Roos, H.Zimmermann, and J.Hulliger, Phys. Lett.A124,112(1987).
  - 27 Y.Kitaoka, S.Hiramatsu, T.Kondo, and K.Asayama, J.Phys.Soc.Jpn. 57,31(1988).
  - 28 T.Imai, T.Shimizu, T.Tsuda, H.Yasuoka, T.Takabatake, Y.Nakazawa, and M.Ishikawa, J.Phys.Soc.Jpn. 57,1771(1988).
  - 29 M.Tachiki and S.Takahashi, Solid State Commun.(1989).
  - 30 Y.Iye, T.Tamegai, T.Sakakibara, T.Goto, N.Miura, H.Takeya, and H.Takei, Physica C153-155, 26(1988).
  - 31 T.K.Worthington, W.J.Gallagher, D.L.Kaiser, F.H.Holtzberg, and T.R.Dinger, Physica C153-155, 32(1988).
  - 32 T.Terashima, K.Iijima, K.Yamamoto, Y.Bando, and H.Mazaki, Jpn.J.Appl.Phys.27, L92(1988).
  - 33 H.Itozaki, S.Tanaka, K.Higaki, and S.Yazu, Physica C153-155, 1155(1988).
  - 34 K.Watanabe, private communications.

To Understand Electronic Properties of High Temperature Superconductors  
 — On the Basis of Fermi Liquid Theory —

Kosaku Yamada and Hiroshi Kohno

Department of Physics, Kyoto University, Kyoto 606

Electronic properties in the normal state are studied on the basis of the Fermi liquid theory. The general expressions for the resistivity, Hall coefficient and Seebeck coefficient are derived. These results, in principle, can be applied to the normal state of the oxide superconductors, as far as they remain in the Fermi liquid state at low temperatures. For the hybridized model with d-orbital of copper and p-orbital of oxygen, which is studied by Imada and Ogata-Shiba, we point out that in order to realize the attractive interaction between p-holes, an attractive interaction should be realized also between d-holes. This result means that p-holes are not indispensable to explain the superconductivity.

A general expression of conductivity at low temperatures is derived on the basis of the Fermi liquid theory. This expression can be applied to the high temperature superconductors in the metallic phase, which should show the  $T^2$ -dependence of resistivity at low temperatures [1]. Conductivity  $\sigma_{\mu\nu}$  is given by

$$\sigma_{\mu\nu} = e^2 \sum_k \sigma - \frac{\partial f}{\partial \epsilon} \Big|_{\epsilon=E_k^*} v_{k\mu}^* \frac{1}{2\Gamma_k^*} J_{k\nu}^* \quad (1)$$

$$J_{k\nu}^* = v_{k\nu}^* - \sum_{k'} \frac{z_k^T z_{k'}^T}{4i\Gamma_k^*} v_{k'\nu}^* \quad (2)$$

Here,  $E_k^*$ ,  $v_k^*$  and  $\hbar/2\Gamma_k^*$  are the energy, velocity and life-time of quasi-particle  $k$ , respectively. The second term of Eq.(2) arises from the vertex correction due to the electron-electron scattering, which is necessary to conserve the current in the absence of Umklapp process. In the presence of Umklapp process Eq.(1) can be rewritten as

$$\sigma_{\mu\nu} = e^2 \sum_k \sigma - \frac{\partial f}{\partial \epsilon} \Big|_{\epsilon=E_k^*} v_{k\mu}^* \frac{C}{2\Gamma_k^*} v_{k\nu}^* , \quad (3)$$

where  $C$  is a factor of order of unity determined by the Umklapp process in the electron scattering.  $\Gamma_k^*$  is proportional to  $T^2$ ,  $T$  being the absolute temperature.

As known well, the positive sign of the observed Hall coefficient cannot be explained in a simple Fermi liquid picture, because the doped system with electron number less than half-filled value is expected to show the electron-like behaviors. In order to treat the electron interaction correctly, we derived a general expression for the Hall coefficient in the metallic phase. The expression is given by

[2]

$$R_H = \frac{\sigma_{xy}}{\sigma_{xx}} \cdot \frac{1}{H} \quad (H \parallel z) \quad (4)$$

$$\sigma_{xy} = \sum_{k\sigma} H \frac{e^3}{c} \left( -\frac{\partial f}{\partial \epsilon} \right)_{\epsilon=E_k} \left( J_{kx} \frac{\partial J_{ky}}{\partial k_y} - J_{ky} \frac{\partial J_{kx}}{\partial k_y} \right) v_{kx} \frac{1}{(2\Gamma_k)^2} \quad (5)$$

Our result, Eqs.(4) and (5), is too complicated to make a realistic estimation and to answer the question whether electron interactions can change the sign of the Hall coefficient. It might be necessary to include the spin-orbit coupling and/or details of crystal structure in order to obtain the correct sign for it.

The Seebeck coefficient of thermoelectric power is also derived along the same line [3], as

$$S_{\mu\nu} = \frac{1}{T} \sigma_{\mu\lambda}^{-1} \alpha_{\lambda\nu} \quad (6)$$

where  $\sigma_{\mu\nu}^{-1}$  is the inverse tensor of Eq.(1) and

$$\alpha_{\mu\nu} = e \sum_{k\sigma} \left( -\frac{\partial f}{\partial \epsilon} \right)_{\epsilon=E_k} (E_k - \mu) v_{k\mu} \frac{C}{2\Gamma_k} v_{k\nu} \quad (7)$$

When  $\sigma_{\mu\nu}$  and  $\alpha_{\mu\nu}$  are diagonal matrices, usual procedure leads to the so called Mott formula [4].

$$S_{\mu\mu} = \frac{\pi^2 k_B^2 T}{3e} \left[ \frac{\partial}{\partial \epsilon} \ln \sigma_{\mu\mu}(\epsilon) \right]_{\epsilon=\mu} \quad (8)$$

where  $\sigma_{\mu\nu}(\epsilon)$  is defined by

$$\sigma_{\mu\nu}(\epsilon) = e^2 \sum_{k\sigma} \delta(\epsilon - E_k) v_{k\mu} \frac{C}{2\Gamma_k} v_{k\nu} \quad (9)$$

Eq.(8) is the lowest order term in the expansion with respect to  $T/\epsilon_0$ ,  $\epsilon_0$  being the characteristic energy scale over which  $\sigma(\epsilon)$  changes appreciably.

Lastly, we add a comment on the attractive interaction in the extended Hubbard Hamiltonian. It is widely accepted that holes created by doping exist in the p-orbitals of oxygens in the  $\text{CuO}_2$  plane. Imada and Ogata-Shiba discussed the origin of the attractive interaction on the basis of the Hamiltonian called the extended Hubbard Hamiltonian [5,6], which is written as

$$H = \sum_{i\sigma} \epsilon_d d_{i\sigma}^\dagger d_{i\sigma} + \sum_{j\sigma} \epsilon_p p_{j\sigma}^\dagger p_{j\sigma} + \sum_{ij\sigma} t (p_{j\sigma}^\dagger d_{i\sigma} + d_{i\sigma}^\dagger p_{j\sigma}) + U \sum_i d_{i\uparrow}^\dagger d_{i\uparrow} d_{i\downarrow}^\dagger d_{i\downarrow} \quad (10)$$

Here,  $d_{i\sigma}^\dagger$  ( $p_{i\sigma}^\dagger$ ) is a creation operator of d(p)-electron with spin  $\sigma$  and energy  $\epsilon_d$  ( $\epsilon_p$ ) at site  $i$ . These p- and d- orbitals hybridize by matrix element  $t$ . In this note we include the Coulomb repulsion  $U$  only between d-electrons, neglecting interactions between p-electrons and between p- and d-electrons. This Hamiltonian is reduced to the spin model studied by those authors in a strong correlation limit. They pointed out that an attractive interaction between p-holes can be realized with appropriate parameters. Here, we point out that as far as we are basing on the Fermi liquid theory and include the electron

interaction only in d-orbitals of copper atoms, neglecting all interactions at oxygen sites, there must be an attractive interaction between d-holes in order to realize the attractive interaction between p-holes. The reason is as follows;

As far as our discussion is based on the Fermi liquid theory, the quasi-particles composed of p- and d-electrons play essential roles. In the Fermi liquid, the interaction between quasi-particles,  $\tilde{\Gamma}$ , is related to the vertex between d-electrons,  $\Gamma_{dd}$ , as

$$\tilde{\Gamma}(k-k; -k' k') = \sqrt{z_k^d z_{-k}^d} \Gamma_{dd}(k-k; -k' k') \sqrt{z_{k'}^d z_{-k'}^d} \quad (11)$$

where  $z_k^d$  is a wave-function renormalization factor. This relation means that to obtain attractive interaction  $\tilde{\Gamma}$ ,  $\Gamma_{dd}$  must have the same nature as  $\tilde{\Gamma}$ . If the results obtained by Imada and Ogata-Shiba mean the existence of the attractive interaction between p-holes, d-holes also should have an attractive interaction between themselves. Thus, we have only to study the interaction between d-holes on the basis of the Fermi liquid theory even in the extended Hamiltonian.

$\text{Nd}_{2-x}\text{Ce}_x\text{CuO}_{4-y}$  system, which seems to be electron-doped system without p-holes, shows also superconductivity [7]. This result seems to be consistent with our statement that there must be always attractive interaction between d-holes(electrons).

#### References

- 1] K. Yamada, M. Nakano, H. Kohno, K. Yosida and K. Hanzawa: in preparation.
- 2] H. Kohno and K. Yamada: Prog. Theor. Phys. 80(1988)623.
- 3] H. Kohno: in preparation.
- 4] J. M. Ziman: "Principles of the Theory of Solids" Chap. 7.
- 5] M. Imada: J. Phys. Soc. Jpn. 56(1987)3793.
- 6] M. Ogata and H. Shiba: J. Phys. Soc. Jpn. 57(1988)3074.
- 7] Y. Tokura, H. Takagi and S. Uchida: to be published in Nature.

Superconductivity by Intra-layer and Inter-layer Cooper Pairing and  
Investigation of Plasmon Mechanism For A Two-Dimensional Superconductors

M.Inoue, T.Takemori and K.Ohtaka+

Institute of Applied Physics, University of Tsukuba, Tsukuba Ibaraki 305 Japan

+Department of Applied Physics, University of Tokyo, Bunkyo-ku, Tokyo 113 Japan

Inter-layer band overlap effect is investigated for the Cooper pairs in layered superconductors. The two Cooper pairs of bonding states and antibonding states couple with each other and as a result, two energy gaps, one for bonding state and the other for antibonding state coexist. This spatial dependence of the gap function should be reflected on experiments which monitor local information of the superconducting states such as NMR relaxation rate. Investigation of the plasmon mechanism of superconductivity for a two-dimensional system is now under way. Motivation of this work is briefly discussed.

Recently discovered oxide superconductors have Cu-O layers in common and it is widely accepted that the carriers in the quasi two-dimensional(2D) system realizes high critical temperature( $T_c$ ). Based upon the crystal structure analysis of  $YBa_2Cu_3O_7$ , whose unit cell consists of a Cu-O chain sandwiched between two 2D layers, possibility of inter-layer Cooper-pairing has been proposed. In a 2D system, effects of the Coulomb repulsion is enhanced compared to a 3D system and this might suppress  $T_c$ . However, if the paired electrons lie in neighboring layers, the repulsion can be substantially reduced. This might result in an enhancement of  $T_c$  if the attractive force between electrons in different layers are large enough. Proposed candidates of the elementary excitation which bring about attraction include charge fluctuation by plasmon, charge density wave, exciton, phonon and magnetic fluctuation. In this report, we consider a model system which consists of two 2D layers with a highly polarizable sheet between them and investigate the effect of the band overlap between the two 2D layers.

For a pair of electrons in the same layer, any excitation of quasi-particles on the polarizable sheet in the middle gives rise to attraction. On the other hand, for electrons in the different layer, excitation of symmetric mode with respect to the middle layer contribute to attraction, while antisymmetric mode gives rise to repulsion. For example, charge density fluctuation in the direction parallel to the layer( plasmon or exciton with polarization parallel to the layer) gives attraction, while charge fluctuation in the perpendicular direction gives repulsion. Therefore, the attractive interaction for inter-layer pairing is in general weak compared to the intra-layer pairing. Though the attraction is reduced, the inter-layer pairing can have higher  $T_c$  than that of the intra-layer pairing due to the reduced Coulomb repulsion. When the band overlap is absent, the superconducting phase with lower  $T_c$  does not appear, because the density of states at the Fermi level is already used by the phase which has higher  $T_c$ . That is, the two phases (i.e., intra- and inter-layer pairing phases) compete with each other.

On the other hand, when the binding energy of the Cooper-pair, which is of the order of  $T_c$ , is smaller than the hopping energy between layers, we should first take into account the effect of the inter-layer hopping and then the Cooper-pairing. In

this case, electronic states are classified into bonding and antibonding states. Then there are four types of possible pairings, which are classified into two symmetric and two antisymmetric pairings. The antisymmetric pairs formed by bonding and antibonding states are discarded because the mismatch of the Fermi wavevector is unfavorable to superconductivity. The other type of pairing, which consists of bonding-bonding pair and the antibonding-antibonding pair have even symmetry with respect to the middle layer and they are coupled to each other. In this case, the origin of the coupling is quite different from the one discussed above and there is no competition between the two. The difference of the nature of the coupling becomes clear if bonding and antibonding pairs are interpreted in terms of the intra-layer and the inter-layer pairs. When the intra-layer pairing is formed, for instance, the inter-layer pair is also formed simultaneously by the hopping of one of the paired

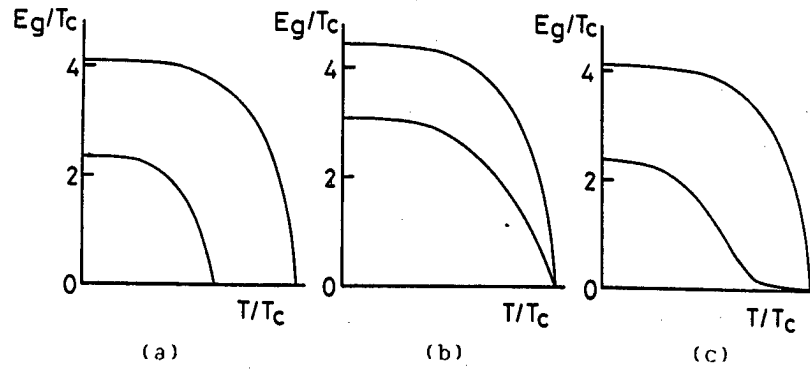


Fig.1

Temperature dependence of the gap energy. (a) without coupling. (b)  $T_c$ 's of the intra- and the inter-layer pairs are different. (c) two  $T_c$ 's are close to each other.

electrons into the other layer. When the transition temperatures of the two types of pairings (intra- and inter-layer) are different, two gap energies, one large (higher  $T_c$  phase) and the other small (lower  $T_c$  phase) appear simultaneously at temperatures below  $T_c$ . When the two  $T_c$ 's are close to each other, only one gap energy due to the bonding states grows as temperature is decreased below  $T_c$ , while the other gap due to the antibonding states remains small. The antibonding gap starts to grow at lower temperatures only as a result of nonlinearity of gap equation as shown in Fig.1. As the amplitude of the bonding state and the antibonding state is different in the middle layer, the two gap structure should be reflected on experiments which is sensitive to the local structure of the superconducting state.

The Eliashberg equation for the bonding states reads as follows.

$$\omega(1-Z_B) = \int_0^\infty d\omega' \{ (W_S + U_S)^2 R_e \left( \frac{\omega'}{\sqrt{\omega'^2 - \Delta_B^2}} \right) + W_A^2 R_e \left( \frac{\omega'}{\sqrt{\omega'^2 - \Delta_A^2}} \right) \} \times \int d\Omega \alpha^2 F(\Omega) I(\omega, \omega', \Omega)$$

$$Z_B(\omega) \Delta_B(\omega) = \int_0^\omega d\omega' \{ (W_S + U_S)^2 R_e \left( \frac{\Delta_B}{\sqrt{\omega'^2 - \Delta_B^2}} \right) + W_A^2 R_e \left( \frac{\Delta_A}{\sqrt{\omega'^2 - \Delta_A^2}} \right) \} \times \int d\Omega \alpha^2 F(\Omega) I_0(\omega, \omega', \Omega)$$

$$- U \int_0^\omega d\omega' \tanh\left(\frac{\omega'}{2T}\right) \times \{ (S_e + \bar{S})^2 R_e \left( \frac{\Delta_B}{\sqrt{\omega'^2 - \Delta_B^2}} \right) + S_0^2 R_e \left( \frac{\Delta_A}{\sqrt{\omega'^2 - \Delta_A^2}} \right) \}$$

For the pairing of the antibonding states, the sign of  $U_S$ ,  $\bar{S}$  and  $S_0^2$  are reversed.  $U_S$  and  $W_S$  are pairing interaction due to the exchange of symmetric modes with or without hopping and  $W_A$  describes interaction with antisymmetric modes. The Coulomb repulsion



is described by the parameters  $\bar{S}$ ,  $S_e$  and  $S_0$  and  $\bar{S}$  is proportional to the band overlap.  $W_S \pm U_S$  and  $UX(S_e \pm S)$  gives the attraction and the Coulomb repulsion for bonding (antibonding) states and the parameters  $W_A$  and  $S_0$  describe the coupling between two types of pairings.

It has long been an issue whether electron gas becomes superconducting solely by Coulomb repulsive interaction. As for the bosonic quasi-particles, whose virtual exchange gives rise to attraction between electrons in the Cooper pair, plasmon and electron-hole pair have been considered. However, the energies of the quasi-particles are much larger than those of phonons and consequently, energy dependence of the self-energy and the vertex function becomes important. Furthermore, as the quasi-particles which give rise to attraction originate from electrons, their group velocity is of the same order of magnitudes with that of the Fermi velocity. This is another difference from the BCS superconductivity by phonons whose velocity is negligible compared to the Fermi velocity. By this fact, momentum dependence of the potential in the gap equation becomes also important. In a 2D system, effects of Coulomb repulsion becomes more important and the possibility of plasmon mediated superconductivity has been explored so far. However, since the energy and the momentum dependences are important in this system, we cannot rely heavily upon a simple-minded approach which treats plasmons like phonons.

Our purpose is to obtain  $T_c$  and the energy-momentum dependence of the gap function quantitatively for a 2D system. A self-consistent calculation of the Eliashberg equation is now under way using the RPA expression for the dielectric function as a first step. The singular square root momentum dependence of the plasmon in 2D system makes the calculation very difficult. As the accuracy of the numerical calculation is crucial to obtain reliable results, we are now trying to reproduce the normal state properties of the self-energy function.

#### References

- 1) Exciton mechanism for the inter-layer pairing is proposed by S. Nakajima; J. Phys. Soc. Jpn. 56 (1987) 871, W. Y. Liang; J. Phys. C20 (1987) L571, J. Bardeen, D. M. Ginsberg and M. Salamon; in Novel Superconductivity, ed. by S. A. Wolf, V. Z. Jrezin (Plenum, New York, 1987), p.333, W. A. Harrison; Phys. Rev. B38 (1988) 270. Using charge fluctuation and phonons, the properties of the intra-layer and the inter-layer pairing states are discussed by M. Inoue, T. Takemori, K. Ohtaka, R. Yoshizaki and T. Sakudo; Solid State Commun. 63 (1987) 201, J. Phys. Soc. Jpn. 56 (1987) 3622. Physica 148B (1987) 396. Preliminary results on the effect of the inter-layer band overlap is published by M. Inoue, S. Matsuda, T. Takemori and T. Sakudo; Nuclear Phys. B(Proc. Suppl.) 5A(1988) 139.
- 2) Plasmon mechanism is first proposed by W. Kohn and J. M. Luttinger; Phys. Rev. Lett., 15 (1965) 525 and the importance of the self-energy and the vertex correction is demonstrated by H. Rietschel and L. J. Sham; Phys. Rev. B28 (1983) 5100, M. Grabowski and L. J. Sham; Phys. Rev. B29 (1984) 6132, Y. Takada; Phys. Rev. B37 (1988) 155. In relation to the high  $T_c$  superconductivity a large number of papers are published. To quote a few, D. H. Lee and J. Ihm; Solid State Commun. 62 (1987) 811, V. Z. Kresin; Phys. Rev. B35 (1987) 8716, J. Ruvalds; Phys. Rev. B35 (1987) 8869, J. I. Gersten; Phys. Rev. B37 (1988) 1616, A. Griffin; Phys. Rev. B37 (1988) 5943, V. Z. Kresin and H. Morawitz; Phys. Rev. B37 (1988) 7854, G. Vignale; Phys. Rev. B38 (1988) 811.

# Theory of Strongly Correlated Electrons

Y. Nagaoka

Department of Physics, Nagoya University  
Chikusa-ku, Nagoya 464-01, Japan

Theoretical treatments of strongly correlated electrons performed at our group are reviewed. The Brueckner approximation, the  $1/N$  expansion method and the numerical diagonalization are carried out for the Hubbard model or the periodic Anderson model.

As discussed by many authors, in order to understand the high  $T_c$  superconductivity from a theoretical point of view, it is crucial to clarify how electrons behave in the normal phase. Now it is believed that electrons on the two-dimensional  $\text{CuO}_2$  plane are responsible to superconductivity, and that the correlation between electrons due to the strong repulsion on Cu sites plays an important role in their behavior. The electron correlation has long been investigated by various method. Then it is interesting to apply these methods to the present problem, and to see what comes out from it.

In this report, I briefly review some of the works in this direction performed in our group of solid state theory at Department of Physics, Nagoya University.

## 1. Brueckner Approximation [1]

The t-matrix approximation was first applied by Brueckner [2] to the nuclear matter, and then by Kanamori [3] to the metallic ferromagnetism. It is applied here to the Hubbard model on the two-dimensional square lattice.

In this approximation, the effective interaction between electrons is obtained by summing up the particle-particle ladder diagrams to infinite order, as

$$K(k, k') = U \left[ 1 + \frac{U}{N} \sum_q \frac{(1-f_{k+q})(1-f_{k'-q})}{E_{k+q} + E_{k'-q} - E_k - E_{k'}} \right]^{-1}, \quad (1)$$

where  $E_k$  is the renormalized energy of an electron and  $f_k$  is the Fermi distribution function. Then  $E_k$  is expressed as

$$E_k = E_{k0} + \frac{1}{N} \sum_{k'} K(k, k') f_{k'}, \quad (2)$$

where  $E_{k0}$  is the bare energy of an electron.

Eqs. (1) and (2) are solved self-consistently. Since it is difficult to solve them for an infinite lattice, they are solved numerically for finite lattices of the sizes  $8 \times 8 \sim 12 \times 12$ . As an example, the calculated equi-energy lines are shown in Fig. 1 for a nearly half-filling case  $n = 0.99$ , where  $n$  is the number of electrons per site. In this case, since the number of electrons is less than half,

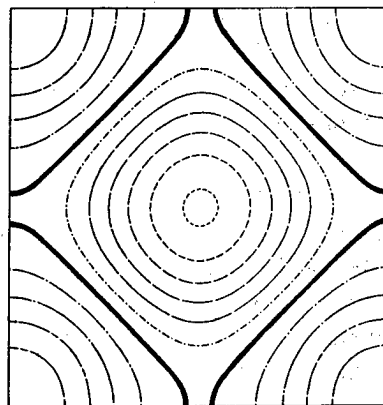


Fig. 1

the Fermi surface of non-interacting electrons is electron-like. As seen in Fig. 1, it becomes hole-like due to the interaction. It means that the Hall coefficient is positive. This result suggests that the sign of the Hall coefficient can be reversed by the interaction.

## 2. $1/N$ Expansion of the Degenerate Anderson Lattice [4]

If one takes the d-p model for electrons on the  $\text{CuO}_2$  plane, it is equivalent to the periodic Anderson model. To study it, the  $1/N$  expansion method of the degenerate Anderson model [5] was employed. Lower order terms of the expansion were calculated exactly by diagrammatical method.

The repulsive interaction on the Cu sites is assumed to be infinite. Then, by introducing slave bosons, the original Anderson Hamiltonian is transformed to

$$H = \sum_k \sum_{m=1}^N E_k C_{km}^\dagger C_{km} + \sum_i \sum_{m=1}^N E_f f_{im}^\dagger f_{im} + \frac{V}{\sqrt{N_L}} \sum_i \sum_k \sum_{m=1}^N (C_{km}^\dagger f_{im} b_i^\dagger e^{-ikRi} + \text{h.c.}) \quad (3)$$

with the condition

$$\hat{Q}_j = \sum_{m=1}^N f_{jm}^\dagger f_{jm} + b_j^\dagger b_j = 1. \quad (4)$$

Here  $b_j^\dagger$  ( $b_j$ ) is the creation (annihilation) operator of the slave boson at the  $j$ -site.

In order to take account of the condition (4), a chemical potential  $\lambda_j$  is introduced, and the limit  $\lambda_j \rightarrow \infty$  is taken. Then the expectation value of the operator  $\hat{O}$  is calculated by

$$\langle \hat{O} \rangle = \lim_{\lambda \rightarrow \infty} [\langle \hat{O} \prod_j \hat{Q}_j \rangle_\lambda / \langle \prod_j \hat{Q}_j \rangle_\lambda], \quad (5)$$

where  $\langle \rangle_\lambda$  is the statistical average with the Hamiltonian

$$H_\lambda = H + \sum_j \lambda_j \hat{Q}_j. \quad (6)$$

The life time  $\tau$  of an electron of the periodic Anderson lattice is calculated to the order  $N^{-3}$ . The result is given as follows;

$$\frac{1}{2\tau} \propto \begin{cases} \frac{1}{N} \log \left( \frac{T_k}{T} \right) & (T \gg T_k) \\ \frac{1}{N^3} \left( \frac{T}{T_k} \right)^2, & (T \ll T_k) \end{cases} \quad (7)$$

and  $1/2\tau$  takes the maximum value in the intermediate temperature region. Precisely speaking, the low temperature region is given by  $T \ll T_0$ , where  $T_0 = T_k / \log N$ . However, in the actual case  $T_0$  may not be distinguished from  $T_k$ .

As shown in Eq. (7), the system behaves as a metal with Kondo impurities at high temperatures, and as a Fermi liquid at low temperature. In this treatment, it was shown that two limiting cases are connected continuously.

### 3. Numerical Diagonalization of Finite System [6]

To clarify the behavior of strongly correlated electrons, numerical diagonalization of a Hubbard-type model was performed. The lattice is a two-dimensional square lattice of the size  $3 \times 3$ . Here the second neighbor transfer as well as the first neighbor one is introduced. Assuming the repulsive interaction  $U$  is large, the model is transformed to the so-called  $t$ - $J$  model. Then the model has four parameters: the first and the second neighbor transfers  $t$  and  $t'$ , and the first and the second neighbor exchange interactions  $J$  and  $J'$ , where the relation  $J' = J(t'/t)^2$  holds. The number of electrons is taken as 8, so that there is one vacant site (or holon).

The ground states of the system are obtained by the numerical diagonalization. They are classified by the total spin  $s$  ( $0 \leq s \leq 4$ ). Among them singlet ground states ( $s = 0$ ) are most interesting. To study their behavior, the projection  $p$  of the singlet ground states onto the short-singlet-pair subspace is calculated. Here the short-singlet-pair subspace is defined as the subspace spanned by the singlet states which are the products of first and/or second neighbor singlet pairs. Then it is found that there appear three types of the singlet ground states with different values of  $p$ . In Fig. 2 they are shown in the parameter plane of  $t'/t$  and  $J/t$ .

Among various singlet states, the state (called as type I RVB), which appears in the region where  $J/t$  is small and  $t'/t \sim 1$ , is most interesting. In this region, the motion of the vacant site plays an important role. Its motion along a triangle closed path results in the antiferromagnetic coupling between first and second neighbor spins. It also causes the motion of short singlet pairs without breaking them. These effects stabilize short singlet pairs, and the type I RVB state.

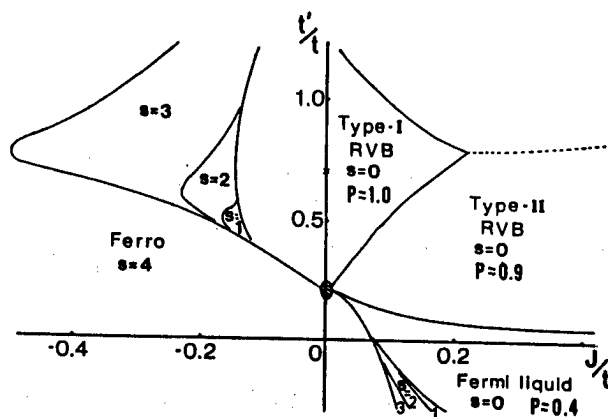


Fig. 2

### References

- [1] Y. Ōno and T. Matsuura, unpublished (Preliminary report was given at the meeting of Phys. Soc. Jpn. (1988)).
- [2] K.A. Brueckner, Phys. Rev. 97, 1353 (1955).
- [3] J. Kanamori, Prog. Theor. Phys. 30, 275 (1963).
- [4] B. Jin and Y. Kuroda, J. Phys. Soc. Jpn. 57, 1687 (1988).
- [5] P. Coleman, Phys. Rev. B29, 3035 (1984).
- [6] K. Sano and K. Takano, J. Phys. Soc. Jpn. 56, 4229 (1987).  
; K. Takano and K. Sano, Phys. Rev. B (in press).

## Magnetic Correlations in Strongly Correlated Electron Systems

T. Saso

Department of Physics, Tohoku University, Sendai, 980 Japan

It is argued that the formation of the Fermi liquid states in strongly correlated electron systems is inevitably accompanied by the short range antiferromagnetic correlation. To understand such systems, a two impurity Kondo problem is investigated by extending the NCA scheme for the single impurity Anderson model. The ground state of the coupled two Anderson impurities proves to be a mixture of RKKY-quenched singlet and the Kondo singlet of the RKKY-triplet states. Properties of the periodic system is discussed based on this picture.

There are several experimental implications that the carriers in the high  $T_c$  oxides behave like Fermi liquid in spite that the Coulomb correlation is very strong at least on Cu sites. Recent photoemission spectroscopy experiment[1] suggested that Bi-Sr-Ca-Cu-O has definite Fermi edge and quasi-particle energy dispersion in the vicinity of the Fermi energy. Weak temperature dependence of magnetic susceptibility above  $T_c$  also supports the formation of the singlet Fermi liquid states. On the other hand, Cu remains almost divalent with a spin half, and the neutron scattering experiments[2] observed a short range antiferromagnetic correlations among these spins. Hall coefficient measurements yielded a small carrier density of  $\sim 10^{21} \text{ cm}^{-3}$ , although several points are still to be explained[3]. These carriers are thought to be placed mainly on the oxygen p orbitals[4] where Coulomb correlation may not be so strong. However, they substantially mix with the d orbitals on Cu sites. It is therefore surprising that such small carrier systems with strong Coulomb correlation form a Fermi liquid state overcoming the tendency towards magnetic ordering and even yield the high transition temperature to superconductivity. Understanding the formation and the characters of such Fermi liquid states seems to be a key to access the mechanism of the high  $T_c$  superconductivity.

A single ion with a magnetic moment forms a singlet Kondo state when coupled with conduction electrons. Finite number of magnetic impurities couple each other above the Kondo temperature  $T_K$  through the oscillatory RKKY interaction, and the competition occurs between the magnetic coupling of the moments and the local singlet formation below  $T_K$ . In the strong coupling limit ( $J_K \rightarrow \infty$ , where  $J_K$  denotes the Kondo coupling), the correlation between near-neighbor local moments becomes always antiparallel irrespective of the sign of the RKKY interaction in the weak coupling limit[5]. If these magnetic ions form a periodic lattice, local Kondo singlet formation is possible only when there are sufficient number of itinerant carriers[6]. In the present case of oxide superconductors, the number of carriers is about  $10^{21} \text{ cm}^{-3}$  and much less than that of Cu spins. Hence the Cu spins have to be accompanied by short range antiferromagnetic correlation with the neighboring spins in order to form a singlet Fermi liquid states as a whole. Thus the situation seems to be that the singlet Kondo state formation occurs on the cluster of spins, which have short range antiferromagnetic correlation among them. Electronic structure of the periodic Kondo lattice may well be described by the superposition of the cluster Kondo singlet states. These features are partly in common with the heavy electron systems found in rare-earth and actinide compounds[7]. A difference is that the number of carriers is

not small in most heavy electron systems.

Numerical renormalization group[7] and quantum Monte Carlo calculation[5] were performed to investigate the ground state and the thermodynamics of the two-impurity Kondo systems. In the following we investigate the properties of the two Anderson impurities embedded in a metal. Extending the NCA scheme, which has been successfully applied to the single impurity Anderson model[8], the partition function of the two impurity system is expressed in the following form

$$Z_2 = \int \frac{dz}{2\pi i} e^{-\beta z} [ R_0(z) + 2R_1^B(z) + 2R_1^A(z) + 3R_2^S(z) + R_2^T(z) ], \quad (1)$$

where  $R_0$  denotes the resolvent for the state with the both sites empty,  $R_1^{B,A}$  the states with one site empty and the other site occupied (B and A denote bonding and anti-bonding states, respectively) and  $R_2^{S,T}$  the states with both sites occupied (S and T denote singlet and triplet spin configurations, respectively). Each resolvent is expressed by the self-energy as  $R_0(z) = [ z - \Sigma_0(z) ]^{-1}$ ,  $R_1^{B,A}(z) = [ z - E_f - \Sigma_1^{B,A}(z) ]^{-1}$  and  $R_2^{S,T}(z) = [ z - 2E_f - \Sigma_2^{S,T}(z) ]^{-1}$ .

We apply the Brillouin-Wigner expansion to eq.(1) in terms of the mixing matrix element  $V$  with the help of the linked cluster theorem. Besides the single site processes which appear in the ordinary NCA, it is necessary to include the processes which couple two sites. Most important one among such processes in order to discuss the competition between local Kondo singlet formation and the tendency towards magnetic ordering is the following contribution to  $\Sigma_2^{S,T}$ :

$$\pm V^4 \sum_{k,k'} f_k(1-f_{k'}) e^{i\langle k-k' \rangle \cdot R} R_1(z - \epsilon_{k'}) R_2^T(z + \epsilon_{k'} - \epsilon_{k'}) R_1(z - \epsilon_{k'}) \quad (2)$$

( $R_1 = R_1^B + R_1^A$ ). Since this term is written as

$$\pm V^4 \sum_{k,k'} R_1(z - \epsilon_{k'}) \frac{f_k(1-f_{k'}) e^{i\langle k-k' \rangle \cdot R}}{z + \epsilon_{k'} - \epsilon_{k'} - 2E_f - \Sigma_2^T(z + \epsilon_{k'} - \epsilon_{k'})} R_1(z - \epsilon_{k'}), \quad (3)$$

it reduces to the ordinary RKKY coupling between moments in the limit of small  $V$  (small  $T_K$ ). As temperature decreases below  $T_K$ , the spectrum of  $R_1(E)$  yields structure with two peaks at  $E \sim E_f$  and  $E \sim T_K$  with the intensity  $1 - (T_K/E_F)$  and  $T_K/E_F$ , respectively. Thus the effective RKKY interaction in the low energy range is substantially reduced at the temperatures below  $T_K$  due to the factor  $R_1(z - \epsilon_{k'})$ [9]. In addition, self-energy  $\Sigma_2$  for the intermediate state may have a large effect when  $T_K$  becomes large, and modify the form of RKKY interaction.

When the RKKY interaction is large enough and antiferromagnetic, the two moments are quenched into singlet as temperature decreases. However, it can be inferred from the present formulation that in the ground state the spin triplet state with the Kondo cloud is always mixed up with the RKKY-quenched singlet when the above scheme is solved self-consistently. Thus the transition from the weak to strong intersite coupling will be smooth as the RKKY interaction at high energy is changed[5].

The above argument may be extended to the larger clusters of spins and the the periodic lattice. Thus in the lattice case the ground state will be a mixture of the antiferromagnetically ordered state and the spin wave states accompanied by the Kondo cloud (electron-hole excitations). However, most features will be understood from the two-impurity cluster calculations.

## References

- [1] T. Takahashi, H. Matsuyama, H. Katayama-Yoshida, Y. Okabe, S. Hoyoya, K. Seki, H. Fujimoto, M. Sato and H. Inokuchi, to appear in Nature.
- [2] Y. Endoh, K. Yamada, R.J. Birgeneau, D.R. Gabbe, H.P. Jensen, M.A. Kastner, C.J. Peters, P.J. Picone, T.R. Thurston, J.M. Tranquada, G. Shirane, Y. Hidaka, M. Oda,

- Y. Enomoto, M. Suzuki and T. Murakami, Phys. Rev. **B37** (1988) 7443.
- [3] N.P. Ong, Z.Z. Wang, J. Clayhold, J.M. Tarascon, L.H. Greene and W.R. McKinnon, Phys. Rev. **B35** (1987) 8807.
  - [4] A. Fujimori, E. Takayama-Muromachi, Y. Uchada and B. Okai, Phys. Rev. **B35** (1987) 8814.
  - [5] R.M. Fye, J.E. Hirsch and D.J. Scalapino, Phys. Rev. **B35** (1987) 4901; J. E. Hirsch and H.Q. Lin, Phys. Rev. **B35** (1987) 4943; R.M. Fye and J.E. Hirsch, preprint(1989).
  - [6] P. Nozieres, Ann. Phys. (France) **10** (1985) 19.
  - [7] B.A. Jones and C.M. Varma, Phys. Rev. Lett. **58** (1987) 843; C.M. Varma, "Fermi Surface Effects" (J. Kondo and A. Yoshimori, eds., Springer, 1987) 117; B.A. Jones, C.M. Varma and J.W. Wilkins, Phys. Rev. Lett. **61** (1988) 125.
  - [8] Y. Kuramoto, Z. Phys. **53** (1983) 37.
  - [9] N. Grewe, Z. Phys. **67** (1987) 323; N. Grewe, T. Pruschke and H. Keiter, Z. Phys. **71** (1988) 75; N. Grewe, Solid State Commun. **66** (1988) 1053.

# Anisotropic Superconductivity in Strongly Correlated Systems: Auxiliary-Particle Formulation

Fusayoshi J. Ohkawa

Department of Physics, Hokkaido University, Sapporo 060, Japan

The Hubbard model with strong correlation is investigated in an auxiliary boson-fermion Hamiltonian. Auxiliary particles must be localized because of a local gauge symmetry. Therefore the Bose condensation of auxiliary bosons is never realized, and auxiliary fermions have no Fermi surfaces. Electrons are described by fermionic pair-excitations of auxiliary particles. The density of states of electrons has a double-peak structure in nearly-half filled cases. The main band is broad and deep, and it is consistent with the prediction by the alloy analogy of the Hubbard model. On the other hand, the shallow and sharp peak can be explained by the formation of heavy quasiparticles or heavy electrons. The mass enhancement factor of heavy electrons is consistent with the prediction by the Gutzwiller variational treatment of the Hubbard model. It is argued that anisotropic Cooper pairs between heavy electrons realized by the superexchange interaction should be responsible for recently discovered high- $T_c$  superconductivity.

It is generally believed that newly discovered high- $T_c$  superconductivity should be realized in strongly correlated electron systems on  $\text{CuO}_2$  planes.[1] However it is not settled at the present stage what model is the right one to describe such Cu-oxide superconductors. Following refs.[1,2], we take a single-band Hubbard model.

The Hubbard Hamiltonian with strong correlation is replaced by an effective Hamiltonian with auxiliary bosons and fermions. Because the auxiliary-particle Hamiltonian is equivalent to the Hubbard Hamiltonian only when the Hilbert space is restricted to  $\{Q_i: Q_i=1 \text{ at any sites}\}$ ,  $Q_i$  being the total number of auxiliary particles, the Lagrangian multipliers are introduced in order to exclude any subspaces besides  $\{Q_i: Q_i=1 \text{ at any sites}\}$ . The Lagrangian multipliers are replaced by a uniform chemical potential in the global approximation. The conservation of  $Q_i$  still holds even in the global approximation, or there is a local gauge symmetry with respect to bosons and fermions. However the local gauge symmetry is broken in the mean field approximation of the RVB theory. Auxiliary particles become itinerant because of the broken symmetry, and they turn out to be real particles in the RVB theory; bosons represent holons, and fermions do spinons.

The local gauge symmetry is not broken in the present treatment.[3,4] Unless the local gauge symmetry is broken, subspaces with different  $\{Q_i\}$  are disjoint to each other. Because the rigorous treatment of the Lagrangian multipliers excludes any subspaces besides  $\{Q_i: Q_i=1 \text{ at any sites}\}$ , it also excludes any probabilities that the local gauge symmetry is broken. In the global approximation symmetry-broken states may have lower energy than the lowest symmetrical state. However we should exclude any symmetry-broken states, because the rigorous treatment of the Lagrangian multipliers excludes them.



Unless the local gauge symmetry is broken, it can be easily proved that the expectation value of any operators that do not conserve  $Q_i$  should identically vanish because subspaces with different  $\{Q_i\}$  are disjoint to each other. For example, Green functions of auxiliary particles should be site-diagonal. This means that auxiliary particles are localized. Therefore it is straightforward to conclude that the Bose condensation of auxiliary bosons is never realized in the present system, and that auxiliary fermions have no Fermi surfaces.

First let us examine the case of the vanishing superexchange interaction,  $J=0$ . The effect of finite  $J$  can be treated in a perturbational manner. Electrons can be described by pair-excitations of auxiliary bosons and fermions, which are called c-particles. Figure 1 shows the density of states of c-particles or electrons for  $n_b=0.1$ ,  $n_b$  being the concentration of auxiliary bosons or holes per unit cell; any vertex corrections are ignored in the present investigation. It should be noted that the density of states has a double-peak structure in nearly-half filled cases. The main band

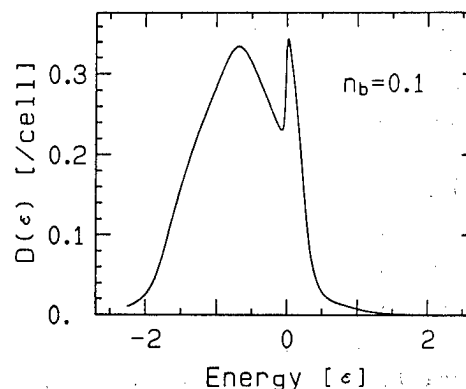


Fig.1

is broad and deep. It is consistent with the alloy analogy of the Hubbard model. The sharp peak is realized at the top of the main band. This implies the formation of heavy quasiparticle, or heavy electrons. The mass enhancement factor is approximately given by  $\chi_m \approx 1/n_b$ , which is consistent with the Gutzwiller variational treatment of the Hubbard model. The chemical potential lies at the top of the main band, or in the sharp peak: the chemical potential is renormalized by strong correlation. The renormalization can explain the discrepancy between band calculation and photo-electron spectroscopy.[5]

However the Fermi liquid relations are only approximately satisfied in the present results. For example, the life-time of quasiparticles at the chemical potential is finite even at 0K. This is partly due to the global approximation. In the global approximation, sites with  $Q_i \neq 1$  play a role as scatterers; the translational symmetry is recovered by the statistical average over discrete degenerate ground states, which are due to the broken translational symmetry.

If the formation of heavy electrons is the case, a characteristic energy scale in low-energy excitations should not be the bare band width,  $W$ , but the quasiparticle band width,  $W^*$ , which is of the order of  $n_b W$ . Therefore one can not yet exclude from the Monte-Carlo results[6] a probability of superconductivity in the single-band Hubbard model, because temperatures are not decreased enough below the quasiparticle band-width. Actually the variational Monte-Carlo studies at the zero temperature imply that the ground state is superconducting in certain regions.[7,8]

When finite  $J$  is treated as a perturbation, a coupling constant is  $\lambda = J/n_b W$ . The system can be classified into three cases: Weak-coupling superconductivity is realized for  $\lambda \ll 1$ . The order parameter of superconductivity is proportional to  $\langle c_{i\sigma}^\dagger c_{j-\sigma}^\dagger \rangle$ ,  $c_{i\sigma}^\dagger$  being a creation operator of the pair c-particles: the condensation of Cooper pairs of c-particles is nothing but the condensation of Cooper pairs of electrons. Strong-coupling superconductivity is realized for  $\lambda \approx 1$  but  $\lambda < 1$ . However the system is unstable against antiferromagnetism for  $\lambda > 1$ . The maximum  $T_c$  is given by the stable condition against antiferromagnetism.

In actual Cu-oxides,  $\lambda \approx 0.5$  or a little smaller than that;  $J = 0.1 \text{ eV}$ ,  $n_b = 0.1$ , and  $W = 4 \text{ eV}$ . Therefore the high- $T_c$  superconductivity can be explained in terms of strong-coupling anisotropic superconductivity realized by the superexchange interactions. By including the vertex corrections to pair-interaction and by assuming square lattices, calculated  $T_c$  for  $d\gamma$ -symmetry Cooper pairs are shown in Fig.2 as a function of the concentration of electrons per unit cell for various values of a parameter,  $-4J_s^* = JW^2$ ;  $W$  is the vertex correction, and it is approximately given by the Wilson ratio. In the present model,  $T_c$  for other symmetry is much lower than that for  $d\gamma$ -symmetry. Instability against antiferromagnetism is ignored in Fig.2. It is reasonable that superconductivity is very close to antiferromagnetism in the present model. It should be noted that the present treatment is consistent with that based on the Fermi liquid theory of the Hubbard Hamiltonian.[9-12]

In summary, auxiliary particles are localized; they are never real particles. The density of states of electrons is examined. The high-energy regime can be explained by the alloy analogy of the Hubbard model. On the other hand, the low-energy regime can be interpreted by the formation of heavy electrons. The mass enhancement factor of heavy electrons is consistent with the prediction by the Gutzwiller variational treatment of the Hubbard model. Therefore it is argued that anisotropic Cooper pairs, in particular,  $d\gamma$ -symmetry in square lattices, between heavy electrons should be responsible for recently discovered high- $T_c$  superconductivity.

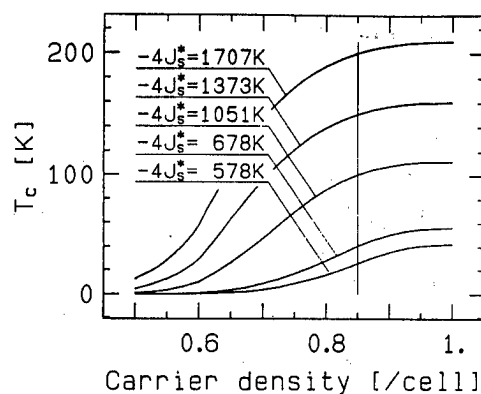


Fig.2

## References

- [1] P. W. Anderson, *Frontiers and Borders in Many Particles Physics*, International School of Physics "Enrico Fermi", edited by J. R. Schrieffer and R. A. Broglia, Course 104, Amsterdam, North-Holland.
- [2] F. C. Zhang and T. M. Rice, *Phys. Rev. B* **37**, 3759 (1988).
- [3] F. J. Ohkawa, *J. Phys. Soc. Jpn.* **57**, 3920, (1988).
- [4] F. J. Ohkawa, submitted to *Phys. Rev. B*.
- [5] A. Fujimori, E. Takayama-Muromachi, Y. Uchida and B. Okai, *Phys. Rev. B* **35**, 8814 (1987).
- [6] J. E. Hirsch and H. Q. Lin, *Phys. Rev. B* **37**, 5070 (1988).
- [7] C. Gros, R. Joynt and T. M. Rice, *Z. Phys. B* **68**, 425 (1987).
- [8] H. Yokoyama and H. Shiba, *J. Phys. Soc. Jpn.* **57**, 2482 (1988).
- [9] F. J. Ohkawa, *J. Phys. Soc. Jpn.* **56**, 2615 (1987).
- [10] F. J. Ohkawa, *Jpn. J. Appl. Phys.* **26**, L652 (1987).
- [11] F. J. Ohkawa, *J. Phys. Soc. Jpn.* **56**, 2267 (1987).
- [12] F. J. Ohkawa, *J. Phys. Soc. Jpn.* **56**, 3017 (1987).

# Small-Cluster Studies on Holes in Two-Dimensional CuO<sub>2</sub> Systems

H. Shiba and M. Ogata

Institute for Solid State Physics, University of Tokyo  
Roppongi, Tokyo 106, Japan

An extensive investigation has been made on small clusters of various two-dimensional CuO<sub>2</sub> systems, by paying particular attention to the interaction between doped holes and Cu spins.

## 1. Introduction

Recent experiments<sup>1)</sup> on various high- $T_c$  cuprates suggest the importance of CuO<sub>2</sub> layers. In addition, holes responsible for superconductivity appear to be mainly doped on in-plane oxygen  $p$  orbitals. Therefore it is essential to study theoretically properties of holes doped in two-dimensional (2D) CuO<sub>2</sub> systems. Keeping this point in mind, we have carried out a series of studies.<sup>2~5)</sup> The purpose of this report is to describe briefly some of our results.

Our strategy is to study with the exact diagonalization method the ground state of small clusters of 2D CuO<sub>2</sub> models by introducing one or two extra holes.<sup>2~5)</sup> This method is expected to be useful especially for strongly correlated electrons, which are elusive in other approximate treatments. As for the orbital of doped holes there are two major proposals: in-plane  $p\sigma$ <sup>6~8)</sup> and in-plane  $p\pi$ .<sup>9,10)</sup> Our results on these two cases will be described below separately.

## 2. Holes on In-Plane $p\sigma$ Orbitals

For this case we start from the following 2D model<sup>6,11)</sup>

$$\begin{aligned} H_A = & -t \sum_{(ij)\sigma} (a_{di\sigma}^+ a_{pj\sigma} + h.c.) - t' \sum_{(jj')\sigma} (a_{pj\sigma}^+ a_{pj'\sigma} + h.c.) \\ & + \epsilon_d \sum_{i\sigma} n_{di\sigma} + \epsilon_p \sum_{j\sigma} n_{pj\sigma} + U_d \sum_i n_{di\uparrow} n_{di\downarrow} + U_p \sum_j n_{pj\uparrow} n_{pj\downarrow} \\ & + V \sum_{(ij)\sigma\sigma'} n_{di\sigma} n_{pj\sigma'}, \end{aligned} \quad (1)$$

where  $a_{di\sigma}^+$  and  $a_{pj\sigma}^+$  are the creation operators of holes with spin  $\sigma$  on the  $i$ -th Cu  $d_{x^2-y^2}$  and  $j$ -th oxygen  $p\sigma$  orbitals, respectively. The summation of  $(ij)$  or  $(ij')$  is taken over the nearest neighbor pairs. We ignore  $t'$ ,  $V$  and  $U_p$  for simplicity<sup>12)</sup> and take  $t = 1$  (unit of energy),  $\Delta = 3$  and  $U_d = 8$  as a typical set for high- $T_c$  cuprates.

In order to extract the essence from (1) we have also studied an effective Hamiltonian, which can be derived for a small  $t$  by assuming together with  $\Delta > 0$  and  $U_d > \Delta$  that each Cu site is singly occupied. It consists of two terms:

$$H_B = H_{eff}^{(2)} + H_{ex}^{(4)} \quad (2)$$

where  $H_{eff}^{(2)}$  is the term proportional to  $t^2$  and  $H_{ex}^{(4)}$  is the Cu-Cu superexchange interaction  $H_{ex}^{(4)} = 2J_{Cu} \sum_{(i,i')} (\vec{S}_i \cdot \vec{S}_{i'} - \frac{1}{4})$  with  $J_{Cu} = 2(t^2/\Delta)^2(1/\Delta + 1/U_d)$ .

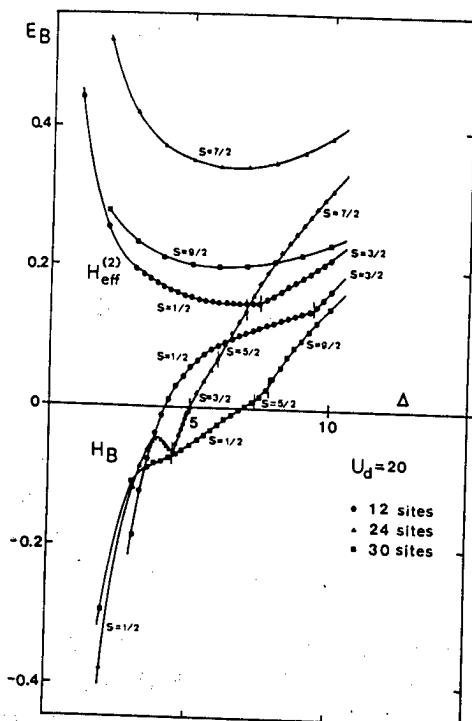
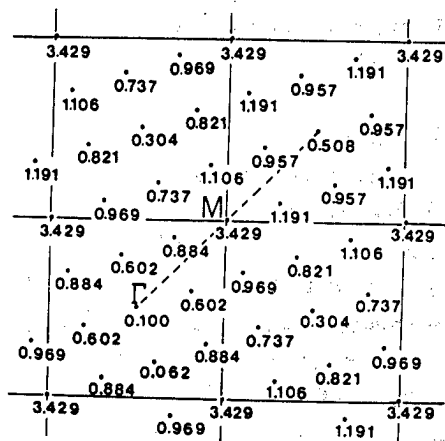


Fig.1  $E_B$  as a function of  $\Delta$  for 12-, 24- and 30-site clusters of  $H_B$ .  $U_d/t$  is fixed at 20. See ref.2 for details.

Fig.2  $4S^{zz}(q)$  calculated for one extra hole in the 30-site cluster, which is equivalent to the hole density of 10%.<sup>4)</sup>



Our clusters consist of  $3n$  atoms in total ( $n$  Cu and  $2n$  O atoms), on which the periodic boundary condition is imposed. We have studied the systems with  $n = 4, 8, 10$  for the effective Hamiltonian  $H_B$ , while the cluster with  $n=4$  has also been examined with  $H_A$  for a comparison.

Let us describe some of our results obtained so far.

[1] The ground state and its energy  $E_\nu$  were determined for each cluster by changing the number of doped extra holes  $\nu$  as 0, 1 and 2. A comparison among  $\nu = 0, 1$ , and 2 gives us much information on the interaction between doped holes and Cu spins.  $E_B$ , which is defined as  $E_B = E_2 + E_0 - 2E_1$ , represents "interaction energy" of 2 doped holes.

Figure 1 shows  $E_B$  as a function of  $\Delta$ . In case  $H_{ex}^{(4)}$  is switched off,  $E_B$  stays always positive, around  $\Delta \sim 3$ , which we are interested in. The one hole state is ferromagnetic with the total spin  $S = (N - 1)/2$  ( $N$ : total number of atoms in the cluster). The realization of this ferromagnetic state is consistent with Zhang and Rice's argument<sup>7)</sup> and Nagaoka's theorem. This ferromagnetic state was studied analytically by Emery and Reiter.<sup>13)</sup>

When  $H_{ex}^{(4)}$  is included, the total spin in the ground state of the one hole state becomes  $1/2$  around  $\Delta \sim 3$  and  $E_B$  turns to be negative. The latter fact suggests a binding of 2 doped holes, which can be confirmed in fact by examining the density-density correlation of doped holes. This binding is due to a constructive interference of magnetic distortions caused by 2 doped holes.<sup>2)</sup>

[2] One important ingredient of  $H_A$  and  $H_B$  is a strong antiferromagnetic coupling between the doped hole on oxygen and surrounding Cu spins. This shows up in a characteristic way, which has not been noticed before.<sup>4)</sup> Since spins are present on oxygen sites as well as on Cu sites, the total spin structure factor consists of Cu-Cu, Cu-O and O-O spin correlations as  $S^{zz}(q) = S_{Cu-Cu}^{zz}(q) + S_{Cu-O}^{zz}(q) + S_{O-O}^{zz}(q)$ . The  $q$  dependence of  $S_{Cu-O}^{zz}(q)$  has a unique feature because of the structure, in which O atoms are located on the bridge sites between 2 Cu atoms, and an antiferromagnetic spin correlation between the nearest neighbor Cu and O spins. We can show

that the periodicity of  $S^{zz}(q)$  is doubled in  $q$  space; consequently  $S^{zz}(q)$  is asymmetric with respect to the M point  $(=\pi, \pi)$  in the scan from  $\Gamma = (0, 0)$  to  $\Gamma = (2\pi, 2\pi)$  through M.

Figure 2 shows an example of  $S^{zz}(q)$ , which has the feature mentioned above. Two recent independent experiments<sup>14,15)</sup> on  $(\text{La,Sr})_2\text{CuO}_4$  seem to show this asymmetry of intensity, which is at least qualitatively consistent with the present calculation. Although more experiments are certainly needed, we wish to emphasize that  $S(q)$  contains useful information to identify the orbital of doped holes and their interaction with Cu spins.

More about the interaction of doped hole and Cu spins will be reported separately.<sup>5)</sup>

### 3. Holes on In-Plane $p\pi$ Orbitals

Let us turn to the case of in-plane  $p\pi$  orbitals.<sup>9,10)</sup> This problem can be studied with the following model:

$$H = -t \sum_{(ij)\sigma} (a_{pj\sigma}^+ a_{pj'\sigma} + h.c.) + 2J \sum_{(ij)} \vec{S}_i \cdot a_{pj\sigma}^+ \vec{S}_{\sigma\sigma'} a_{pj'\sigma'} + 2J_{Cu} \sum_{(jj')} \vec{S}_i \cdot \vec{S}_{i'}, \quad (3)$$

where  $a_{pj\sigma}^+$  is the creation operator of a hole on the in-plane  $p\pi$  orbital of the  $j$ -th oxygen. It is assumed here again that each Cu atom is singly occupied by a hole on the  $d_{x^2-y^2}$  orbital, which is represented by  $\vec{S}_i$ . Because of the orthogonality between  $d_{x^2-y^2}$  and  $p\pi$ ,  $J$  in (3) is expected to be ferromagnetic ( $J < 0$ ).<sup>9,10)</sup>

We have made small-cluster studies on (3).  $E_B$  as well as the density-density correlation of 2 doped holes has been examined to check the binding.<sup>3~5)</sup> For  $t$  much smaller than  $J$  the binding has been found in fact; however it is likely that such a case is not related to superconductivity, but rather to a phase separation.

### References

- 1) See for instance Proceeding of 2nd NEC Symposium "Mechanisms of High Temperature Superconductivity" (Springer, 1988).
- 2) M. Ogata and H. Shiba: J. Phys. Soc. Jpn. **57**, 3074 (1988).
- 3) H. Shiba and M. Ogata: J. Mag. Mag. Mater. **76-77** (1988), in press.
- 4) H. Shiba and M. Ogata: Proceedings of 2nd NEC Symposium "Mechanisms of High Temperature Superconductivity" (Springer, 1988), in press.
- 5) M. Ogata and H. Shiba: in preparation.
- 6) V. Emery: Phys. Rev. Lett. **58**, 2794 (1987).
- 7) F.C. Zhang and T.M. Rice: Phys. Rev. B **37**, 3759 (1988).
- 8) A. Aharony *et al.*: Phys. Rev. Lett. **60**, 1330 (1988).
- 9) Y. Guo, J.M. Langlois and W.A. Goddard III: Science **239**, 896 (1988).
- 10) R.J. Birgeneau, M.A. Kastner and A. Aharony: Z. Phys. B **71**, 57 (1988).
- 11) C.M. Varma, S. Schmitt-Rink and E. Abrahams: Solid State Commun. **62**, 681 (1987).
- 12) Many researchers conclude that  $U_d = 5 - 10\text{eV}$ ,  $U_p = 3 - 6\text{eV}$ ,  $t = 1 - 1.5\text{eV}$ ,  $t' \sim 0.5\text{eV}$  and  $V \sim 1.5\text{eV}$  (by assuming  $\epsilon \sim 5$ ). For charge-transfer-type Mott insulators  $\Delta$  should satisfy  $U_d > \Delta > t, t'$ . The effect of  $U_p$  is reduced in the low-hole-density region.
- 13) V. Emery and G. Reiter: preprint.
- 14) H. Yoshizawa *et al.*: J. Phys. Soc. Jpn. **57**, 3686 (1988).
- 15) R.J. Birgeneau *et al.*: preprint.

# NUMERICAL ANALYSIS ON MAGNETIC MECHANISM OF SUPERCONDUCTIVITY IN TWO-BAND MODELS

Masatoshi IMADA, Yasuhiro HATSUGAI <sup>†</sup> and Naoto NAGAOSA <sup>†</sup>

Department of Physics, College of Liberal Arts,  
University of Saitama, Shimo-Okubo, Urawa 338

<sup>†</sup> Department of Applied Physics, Faculty of Engineering,  
University of Tokyo, Hongo, Bunkyo-ku, Tokyo 113

Various models of high- $T_c$  superconductors and their interrelationship are discussed. Among them, numerical analyses on two-band d-p model for the  $CuO_2$  layers and the coupled spin-fermion model are reported. Results of a quantum Monte Carlo study on the d-p model are briefly summarized, which shows not remarkable but quantitative enhancement of the superconducting susceptibilities. A coupled spin-fermion model is investigated by the exact diagonalization of finite lattices. An extended cloud of singlet liquid around the mobile fermion is characteristic in the strong coupling region characterized by a strong Kondo coupling and large transfer. The bound state of two fermions seems to exist. The origin of the bound state may be ascribed to the distortion of the antiferromagnetic correlation around the singlet cloud. The relevance of its Cooper pairing to high- $T_c$  superconductivity is discussed.

## §1. Introduction

Since the discovery of high- $T_c$  superconductors, various models have been proposed to investigate the mechanism of high- $T_c$  superconductivity. It seems to be widely accepted that the main mechanism lies in the  $CuO_2$  plane. A general starting point is to take account of various electronic orbitals near the plane. The electronic orbital (or hole orbital) responsible for the conduction and the superconductivity has a key to understand the physical picture of the mechanism. At the present stage, the minimum essence needed to realize the superconductivity is not clear enough. Therefore the role of the theoretical approach is to extract the physical picture by examining models as generally as possible and judge the plausibility of the electron (hole) orbitals as the candidate for the superconducting conduction. To study in such an inductive way, we employ numerical analysis of various models. Among several basic numerical techniques, quantum simulation and exact diagonalization of finite systems provide useful information. They provide data free from biased approximations and is useful to judge the reliability of various approximations. In this report, we summarize our recent results of quantum simulation and the exact diagonalization study done for models of the  $CuO_2$  network. In §2, several models for the high- $T_c$  oxides are derived with the discussion on their interrelation and experimental relevance. In §3, the singlet cloud mechanism obtained from the numerical results is explained.

## §2. Models

In most high- $T_c$  superconductors, the holes occupy Cu-3d orbitals as  $3d^9$  states in the half-filled band, where the antiferromagnetic long range order is realized. Many experimental evidences show that the doped holes beyond the half-filling go into oxygen p-orbitals<sup>1,2</sup>. If we assume that the holes are located in the  $p_\sigma$  orbital in the  $CuO_2$  plane the hamiltonian is reduced to a two-band

$d - p_\sigma$  model<sup>3-6</sup>):

$$\begin{aligned}
H = & -t_1 \sum_{\langle ij \rangle, \sigma} (d_{i\sigma}^\dagger p_{j\sigma} + d_{i\sigma}^\dagger q_{j\sigma} + h.c.) \\
& -t_2 \sum_{\langle ij \rangle, \sigma} (p_{i\sigma}^\dagger q_{j\sigma} + h.c.) \\
& + U_d \sum_i n_{di\uparrow} n_{di\downarrow} + U_p \sum_j (n_{pj\uparrow} n_{pj\downarrow} + n_{qj\uparrow} n_{qj\downarrow}) \\
& + V \sum_{\langle ij \rangle} n_{di} (n_{pj} + n_{qj}) \\
& + \epsilon_d \sum_i n_{di} + \epsilon_p \sum_j (n_{pj} + n_{qj}). \tag{1}
\end{aligned}$$

The fermion operators  $d$ ,  $p$  and  $q$  represent holes in  $\text{Cu-}3d_{x^2-y^2}$ ,  $p_x$  and  $p_y$  orbitals, respectively.

If  $U_d > \delta \equiv \epsilon_p - \epsilon_d$  is satisfied, it is classified as the charge transfer type. It has been clarified<sup>1)</sup> that the high- $T_c$  oxides have this character. The Mott-Hubbard type region is characterized by  $U_d < \delta \equiv \epsilon_p - \epsilon_d$ , where the single-band Hubbard model provides an appropriate description. In the charge transfer type region, two regions of the parameter space should further be distinguished. The Kondo region is characterized by the limit of  $\delta \gg t_1, t_2$ , where the local magnetic moment on the Cu-site is preserved even in the doped material. The  $\text{Cu-}3d$  band is reduced to spin-1/2 localized spins and the charge fluctuation at the Cu-sites is suppressed. Then the effective hamiltonian may be derived from eq.(2) by using the perturbational expansion with respect to  $t/U_d$ ,  $t/\delta$  and the hole concentration. The relevant effective hamiltonian is given as  $H_0 + H_1 + H_2$  from

$$H_0 = -t \sum_{\langle lm \rangle} (c_l^\dagger c_m + h.c.)$$

and

$$\begin{aligned}
H_1 &= -2J_K^{(1)} \sum_i \tilde{S}_i \cdot \tilde{\sigma}_i^{(1)}, \\
H_2 &= -2J_K^{(2)} \sum_i \tilde{S}_i \cdot \tilde{\sigma}_i^{(2)} \tag{2}
\end{aligned}$$

up to the second order, where  $\tilde{S}_i$  is the spin -1/2 operator at the  $i$ -th Cu-site. The fermion creation operator  $c_i^\dagger$  is defined at the oxygen sites. The summation with respect to  $\langle lm \rangle$  is over the nearest neighbor pairs. The parameters are given by  $t = t_2$ ,  $J_K^{(1)} = t_1^2(1/(U_d - \delta - V) + 1/(\delta + U_p - V))$  and  $J_K^{(2)} = t_1^2(1/(U_d - \delta - V) + 1/(\delta - V))$  for the  $p_\sigma$  holes. The operators are defined by

$$\tilde{\sigma}_i^{(1)} = \frac{1}{2} \sum_{\tilde{\delta}} c_{i+\tilde{\delta},\sigma}^\dagger (\vec{\sigma})_{\sigma\sigma'} c_{i+\tilde{\delta},\sigma'} \tag{3}$$

and

$$\tilde{\sigma}_i^{(2)} = \frac{1}{2} \left( \sum_{\tilde{\delta}} c_{i+\tilde{\delta},\sigma} (\vec{\sigma})_{\sigma\sigma'} \left( \sum_{\tilde{\delta}'} c_{i+\tilde{\delta}',\sigma'} \right) - \tilde{\sigma}_i^{(1)} \right), \tag{4}$$

where the summation over  $\tilde{\delta}$  and  $\tilde{\delta}'$  denotes that over the nearest neighbor oxygens of the  $i$ -th copper site. If we assume the  $p_x$  orbitals as the location of the doped hole, similar effective hamiltonian is obtained with  $J_K^{(2)} = 0$  and ferromagnetic  $J_K^{(1)}$ .

The fourth order term has the form

$$H_3 = -2J_S \sum_{\langle ij \rangle} \tilde{S}_i \cdot \tilde{S}_j$$

up to the lowest order of the hole concentration. In the case of the  $p_\sigma$  orbital, the superexchange coupling constant  $J_S$  is given by

$$J_S = \frac{2t^4}{(\delta + V)^2} \left[ \frac{1}{U_d} + \frac{2}{U_p + 2\delta} \right]. \quad (5)$$

In this model a doped hole has a strong tendency to form a singlet with one of the localized spins, when  $J_K$  is antiferromagnetic as pointed out in refs.<sup>4,5</sup>) in the argument of the two-band  $d-p_\sigma$  model. To discuss the essence of superconductivity, we have simplified eq.(4) by neglecting the site-off-diagonal hopping term, which corresponds to neglect the term proportional to  $J_K^{(2)}$ <sup>7-10</sup>). The extended character of the singlet cloud is a common feature before and after this simplification, if  $t \sim |J_K|$ . Then the coupled spin-fermion hamiltonian is obtained as

$$\begin{aligned} H = & -t \sum_{\langle i,j \rangle \sigma} (c_{i\sigma}^\dagger c_{j\sigma} + c_{j\sigma}^\dagger c_{i\sigma}) + U_h \sum_i n_{i\uparrow} n_{i\downarrow} \\ & - 2J_K \sum_{\langle i,l \rangle} \tilde{S}_l \cdot \tilde{\sigma}_i - 2J_S \sum_{\langle l,m \rangle} \tilde{S}_l \cdot \tilde{S}_m \quad (J_S < 0) \\ & \tilde{\sigma}_i = \frac{1}{2} c_{i\sigma}^\dagger (\vec{\sigma})_{\sigma\sigma'} c_{i\sigma'} \\ & n_{i\sigma} = c_{i\sigma}^\dagger c_{i\sigma} \end{aligned} \quad (6)$$

To investigate the role of specific lattice structure of the oxygen conduction band, we have also examined a more simplified lattice structure by taking the fermion lattice of the same structure as the square lattice of the localized spins. In this case, the summation over  $\tilde{\delta}$  in eq.(3) is not necessary. The fermions and the spins are coupled at the same site through  $J_K$ . This case is referred to as the  $z_K = 1$  case and the case of more realistic copper and oxygen lattice is referred to as  $z_K = 2$  case. The  $z_K = 1$  class is also related to a possibility of holes doped in  $d_{3z^2-r^2}$  orbital hybridized with the  $p_z$  orbital out of the  $\text{CuO}_2$  plane, when we take ferromagnetic  $J_K$ . Another important limiting case of the  $z_K = 1$  class is seen in the  $t-J$  model<sup>11</sup>):

$$\begin{aligned} H = & -t \sum_{\langle ij \rangle} (1 - n_{i,-\sigma}) c_{i\sigma}^\dagger c_{j\sigma} (1 - n_{j,-\sigma}) + h.c. \\ & - 2J_S \sum_{\langle ij \rangle} \tilde{S}_i \cdot \tilde{S}_j, \end{aligned} \quad (7)$$

which is originally derived as an effective hamiltonian of the single band Hubbard model. This  $t-J$  model is equivalent to the  $z_K = 1$  class of the coupled spin-fermion model in the limit  $J_K \rightarrow -\infty$ <sup>7,8</sup>). In this limit, the singlet cloud shrinks to the on-site local singlet state. The on-site singlet is surrounded by a domain of enhanced quantum mechanical fluctuation of the antiferromagnetic correlation. The common feature seen in the coupled spin-fermion system with



a finite  $J_K$  and the  $t - J$  model is that the distortion of the antiferromagnetic correlation is extended around the singlet. Therefore, we expect that the formation of the quantum cloud is seen even in the  $t - J$  model. Because we are interested in the region  $|J_S| \ll t$ , significant retardation effect is expected in the localized spin system when a fermion moves. For large transfer, the antiferromagnetic correlation is disturbed in an extended area both in the  $t - J$  and the coupled spin-fermion model.

### §3. Numerical Results

In the quantum simulation<sup>3,4)</sup> of the two-band  $d - p_\sigma$  model in the case of  $t_2 = U_p = V = 0$ , the superconducting pairing susceptibilities for the pairing of two oxygen holes in a certain range of distance have shown small but finite enhancement as compared to the noninteracting system when we compare them by keeping each of the oxygen and the copper hole concentrations at the same values as the interacting system. The interacting and noninteracting cases show almost the same amplitude of pairing susceptibilities in the temperature range of the transfer  $t_1$  in eq.(2) and the enhancement gradually increases with the decrease of temperature. Although the results are not conclusive as for the possibility of the superconductivity because of the limited temperature range, the results are in contrast with the case of the single band Hubbard model. The enhancement is seen in an extended zone of the oxygen-oxygen pairing. It suggests that the pairing has an extended character. The nearest neighbor pairing seems to have relatively small amplitude. The parameter region mainly investigated in ref.4 is in the mixed valence region, where the level difference  $\delta$  is comparable to  $t_1$ .

In the Kondo regime, the coupled spin-fermion model has been investigated by the exact diagonalization technique<sup>7-10)</sup>. Spin and charge correlation functions have been calculated in the systems with one hole. The spin correlation shows that the cloud of extended magnetic distortion develops in the region  $t \sim |J_K| \gg |J_S|$  as seen in Tables 1 and 2. In the cloud, the nearest neighbor spin-spin correlation in the substrate spin system is reduced as compared to the pure Heisenberg system. The spin-spin correlations between the hole's spin and localized spins in the cloud are always antiferromagnetic. This shows that the fermion's spin and the extended spin polarization in the cloud form the totally singlet state. Due to the dynamical exchange of spins in the time scale of  $J_K^{-1}$ , the itinerant fermion is represented by the singlet-type linear combination of up fermion's spin with down polarization and down fermion's spin with up polarization.

The interaction of two fermions has been calculated from the ground state energy of the systems with zero, one and two fermions. Two singlet clouds seem to have attractive interaction in the sea of stronger antiferromagnetic correlation. The attractive interaction exists even in the one-dimensional system.

It is likely that the spin symmetry of the pairing is singlet. The order parameter has the form of

$$\Delta = \sum_k f(k) \langle c_{k\sigma}^\dagger c_{-k-\sigma}^\dagger \rangle. \quad (8)$$

The bound state of two holes is seen not only in the region  $t \sim |J_K| \gg |J_S|$  but also in a wide range of parameter space. This suggests a continuous relationship to other regions and may provide a possibility for a unified understanding of the superconductivity induced by the magnetic mechanism. In the small transfer region, the existence of the bound state is rather obvious, because the doped fermion forms a local defect with the nearest neighbor Cu spins. The attractive interaction is derived from the count of wrong antiferromagnetic bonds. Roughly speaking, this mechanism is valid for  $t < |J_K| + |J_S|$ . The binding energy may well be reproduced from the

spin wave analysis at  $t = 0^{12}$ ). However, the relevance of this local defect mechanism to the superconductivity is questionable, because the condensation in real space (segregation) occurs for sufficiently small  $t$  in the coupled spin-fermion model.

The singlet cloud is not found for the ferromagnetic Kondo coupling as seen in Table 3. The interaction of two fermions also shows that the ferromagnetic Kondo coupling is unfavorable for the pairing. These are in sharp contrast with the case of the antiferromagnetic Kondo coupling.

## References

- 1) A. Fujimori, E. Takayama-Muromachi, Y. Uchida and B. Okai: Phys. Rev. B **35**, 8814 (1987).  
T. Takahashi, H. Matsuyama, H. Katayama-Yoshida, Y. Okabe, S. Hosoya, K. Seki, H. Fujimoto, M. Sato and H. Inokuchi: Nature **334**, 691 (1988).
- 2) G. Shirane et al.: Phys. Rev. Lett. **59**, 1613 (1987).  
Y. Endoh et al.: Phys. Rev. B **37**, 7443 (1988).  
R.J. Birgeneau et al.: preprint.  
J.M. Tranquada et al.: Phys. Rev. Lett. **60**, 156 (1988).  
M. Sato et al.: preprint.
- 3) V.J. Emery: Phys. Rev. Lett. **58**, 2794 (1987).
- 4) M. Imada: J. Phys. Soc. Jpn. **56**, 3793 (1987).
- 5) M. Imada: J. Phys. Soc. Jpn. **57**, 3128 (1988).
- 6) M. Ogata and H. Shiba: J. Phys. Soc. Jpn. **57**, 3074 (1988).
- 7) M. Imada, N. Nagaosa and Y. Hatsugai: J. Phys. Soc. Jpn. **57**, 2901 (1988).
- 8) M. Imada, Y. Hatsugai and N. Nagaosa: Proceedings of the Adriatic Research Conference "Towards the Theoretical Understanding of High -  $T_c$  Superconductors" ed. by S. Lundquist et al. (World Scientific, Singapore, 1988) p423.
- 9) Y. Hatsugai, M. Imada and N. Nagaosa: submitted to J. Phys. Soc. Jpn.
- 10) M. Imada: Proceedings of the 2nd.NEC Symposium "Mechanism of High- $T_c$  Superconductivity" (Springer Verlag, 1989).
- 11) P.W. Anderson: Science **235**, 1196 (1987).  
G. Baskaran, Z. Zou and P.W. Anderson: Solid State Commn. **63**, 973 (1987).
- 12) N. Nagaosa, Y. Hatsugai and M. Imada: submitted to J. Phys. Soc. Jpn.

Table 1. The correlation between fermion's spin and the Heisenberg spin at the distance  $j$  for  $t = 8.0$ ,  $J_K = -8.0$  and  $J_S = -1.0$  on a  $4 \times 4$  lattice with the periodic boundary condition.

$j_y$	$j_x$	0	1	2
0		-0.254	-0.033	-0.074
1		-0.033	-0.074	-0.024
2		-0.074	-0.024	-0.064

Table 2. The distortion of the nearest neighbor spin-spin correlation of the Heisenberg spin around the fermion.

$j_y$	$j_x$	0	1	2
0			0.079	0.011
1		0.079	0.011	0.014
2		0.011	0.014	0.010

Table 3. The correlation between fermion's spin and the Heisenberg spin at the distance  $\mathbf{j}$  for  $t = 8.0$ ,  $J_K = 8.0$  and  $J_S = -1.0$  on a  $4 \times 4$  lattice with the periodic boundary condition.

$j_y$	$j_x$	0	1	2
0		0.101	-0.035	0.019
1		-0.035	0.019	-0.027
2		0.019	-0.027	0.015

# Pseudospin Formalism of Superconductivity in Strong Correlation

S. Nakajima, M. Hasegawa and N. Baba

Department of Physics, Tokai University  
Hiratsuka, Kanagawa 259-12

The pseudospin formalism invented to deal with the hard core correlation in superfluid  $^4\text{He}$  is extended to the single band Hubbard model of high- $T_c$  cuprates in the mean field theoretical form proposed by Suzumura, Hasegawa and Fukuyama.

The short coherence distance observed in high- $T_c$  cuprates is an almost inevitable consequence of the high critical temperature itself. It implies theoretically that one needs to deal with strong charge carrier correlation in real space, as is done in one way or another in all the theoretical models presently available. In this respect, our situation is similar to the case of superfluid  $^4\text{He}$  rather than  $^3\text{He}$ . The coherence distance in the former is comparable to the hard core radius of the constituent boson, whereas it is three orders of magnitude bigger than the average fermion spacing in the latter.

To describe the hard core correlation in  $^4\text{He}$ , Matsubara and Matsuda [1] proposed the quantum lattice model, in which each site is either vacant or singly occupied by the boson. These two states are represented respectively by up and down eigenstates of the  $1/2$  pseudospin operator  $\tau_z$ , whereas the quantum tunneling of the boson from one site to another is described by an XY-exchange coupling proportional to  $\tau_i^+ \tau_j$  in terms of pseudospin operators  $\tau_i = \tau_{ix} - i\tau_{iy}$  and their conjugates. Note that the strong hard core correlation is automatically taken into account through  $\tau_i \tau_i = 0$ .

The same formalism can be applied also to the so-called real space pairing model of superconductivity [2] suggested by the short coherence distance, including the bipolaronic model [3] and spin-polaronic model [4]. In the case of high- $T_c$  cuprates, however, there remain physical spins on  $\text{Cu}^{2+}$  sites and they are suppressed from antiferromagnetic to weakly paramagnetic states by doping charge carriers. The argument to show how this suppression takes place is missing in usual bipolaronic models except for the spin bag model of Schrieffer et al. [5] and the field theoretical model of Khveschenko et al. [6] based on the Hubbard model.

In the present paper, we will try to extend the pseudospin formalism to the single band Hubbard Hamiltonian as a simple model of the n-type cuprates discovered quite recently [7]. We thus have both singly and doubly occupied sites, which are represented respectively by up and down eigenstates of  $\tau_z$ . Obviously we obtain the model for the p-type cuprate if we take the down eigenstate as representing the vacant site in the p-type cuprate.

The problem is how to describe the physical spin degree of freedom at the singly occupied site. One possible way is to start with the effective Hubbard Hamiltonian in the large  $U$  limit adopted by Suzumura et al. [8] in their mean field theory of superconductivity in strong correlation. There the ordinary electron destruction operator is replaced by the product of the slave boson operator  $b_i$  and the slave fermion operator  $f_{i\sigma}$ , which are supposed to describe charge and spin fluctuations at each site respectively in accordance with the spirit of Anderson [9].

In our formalism, we further replace their boson operator  $b_i$  by our operator  $\tau_i^\dagger$ , simply because more than two electrons cannot occupy the same site in the single band model. On the other hand, like all other slave particle models, we have introduced one redundant degree of freedom per site by the use of the fermion operator  $f_{i\sigma}$  to describe the physical spin. We have to eliminate them by imposing the local constraints upon the state vector  $\Psi$ :

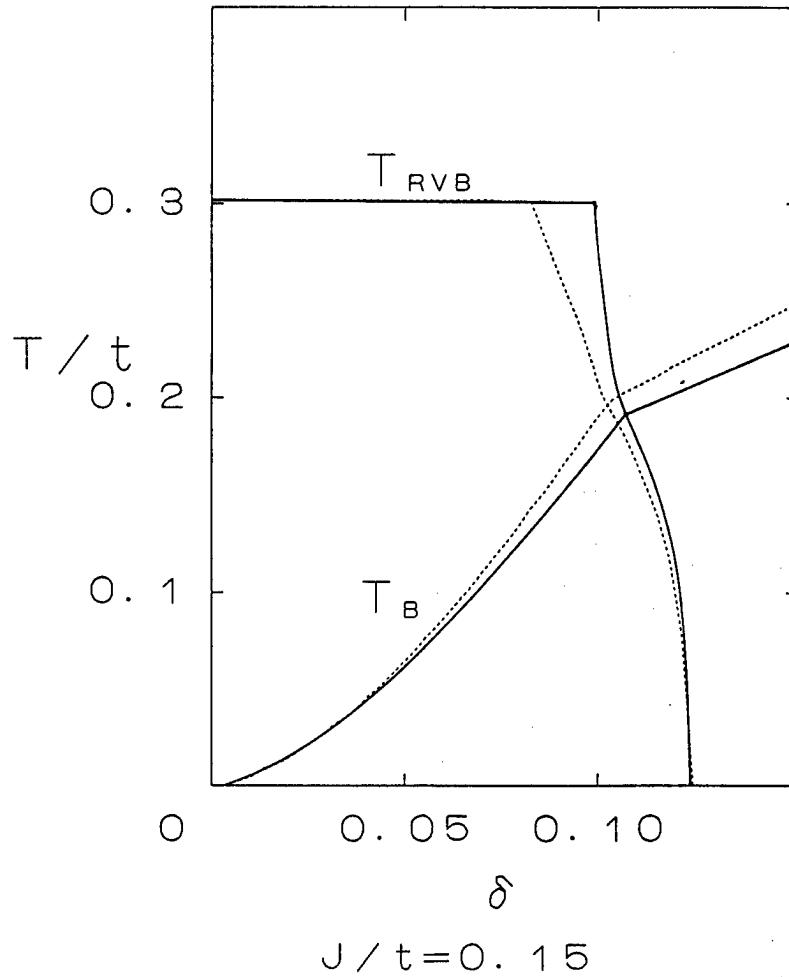
$$(\sum_{\sigma} f_{i\sigma}^\dagger f_{i\sigma} - \tau_i^\dagger \tau_i) \Psi = 0 \quad (1)$$

In order to apply the mean field approximation in ref. [8], however, we need to allow for deviations from (1) to occur and therefore demand that the constraints are satisfied only on the average:

$$\langle \sum_{\sigma} f_{i\sigma}^\dagger f_{i\sigma} - \tau_i^\dagger \tau_i \rangle = 0 \quad (2)$$

The mean field theoretical Hamiltonian takes the same form as in ref. [8], except that their  $b_i$  operators are replaced by our  $\tau_i$  operators. Because of the difference in commutation relations, there appears in our  $\tau$ -spin Green's function the frequency renormalization factor  $Z^{-1} = 1 - 2\delta$ , where  $\delta$  is the concentration of the doubly occupied sites.

For small  $\delta$ , therefore, numerical results obtained by boson and  $\tau$ -spin methods are not so much different from each other. As an example, RVB transition temperature  $T_{RVB}$  and Bose condensation temperature  $T_B$ , below which we have non-vanishing  $\langle f_i^\uparrow f_i^\downarrow \rangle$  and  $\langle \tau_i \rangle$ , respectively, are shown in the following figure. Full lines and dashed lines are obtained respectively by the  $\tau$ -spin method and by the boson method for the same superexchange energy  $J = 0.15t$ , where  $t$  is the nearest neighbor hopping energy.



#### References.

1. T. Matsubara and H. Matsuda: Prog. Theor. Phys. 16 (1956) 569
2. B.K. Chakraverty: Phil. Mag. B42 (1980) 473
3. See the review given by L. J. de Jongh in Proc. ISS'88, Nagoya(Springer Verlag) and references cited there.
4. For instance, H. Kamimura: Int. J. Mod. Phys. B1 (1988) 699
5. J.R. Schrieffer, X.G. Wen and S.C. Zhang: Phys. Rev. Lett. 60 (1988) 944
6. D.V. Khveschenko, V.I. Pokrovsky and G.V. Uimin: Int. J. Mod. Phys. B1 (1988) 593
7. Y. Tokura, H. Takagi and S. Uchida: to be published in Nature
8. Y. Suzumura, Y. Hasegawa and H. Fukuyama: J. Phys. Soc. Jpn 57 (1988) 401
9. P.W. Anderson: Science 235 (1987) 1196

Hidetoshi FUKUYAMA and Hiroshi MATSUKAWA

Institute for Solid State Physics, University of Tokyo  
Roppongi, Minato-ku, Tokyo 106, Japan

The effective Hamiltonian is derived from Cu and O orbitals of high  $T_c$  Cu oxides for both cases of hole and electron doping. In comparison with the recent discovery by Tokura et al. of electron-superconductivity in Nd-Ce-Cu-O, it is indicated that the relevant theoretical model to describe the essence of high  $T_c$  Cu oxides is the t-J model. This conclusion is the same as has been originally proposed by Anderson.

Recent discovery of superconductivity in Ln-Ce-Cu-O (Ln=Nd,Sm,Pr) by Tokura, Takagi and Uchida<sup>1)</sup> is the first demonstration of high  $T_c$  superconductivity on Cu-based oxides with the electron doping. The fact that this system is doped with electrons is expected from the valence of Ce (and the reduction process to realize superconductivity) and is verified by the negative Hall coefficient. Moreover the lattice structure (so-called T') of this series is simple since there are no oxygen atoms above and below Cu atoms. The uSR experiment by Luke et al.<sup>2)</sup> demonstrated that the parent system  $Nd_2CuO_{4-y}$  and the non-superconducting material have a magnetic ordering but that the superconducting sample does not. Moreover it is indicated in this experiment that this magnetic ordering is due to spins on Cu atoms. These features share common characteristics with the well-known cases of hole-doped superconductors.<sup>3)</sup>

These new findings verifying electron-superconductors in Cu-based oxides are very important in sorting a proper theoretical model out of various proposals<sup>4,5)</sup> to describe the essence of the low-lying electronic excitations. As we will discuss in the following, the t-J model will be the model for high  $T_c$  Cu oxides in accordance with the claim by Anderson.<sup>4)</sup>

In view of the simplicity of the T'-structure we start with the Cu:  $d_{x^2-y^2}$  and O:  $p_\sigma$  orbitals to examine the case of electron doping in Ln-Ce-Cu-O systems. We introduce parameters as shown in Fig.1;  $U_d$ ,  $U_p$ ,  $V$  are Coulomb interaction constants on Cu and O sites, and between Cu and O sites, respectively,  $t$ , the mixing, and  $\Delta = \epsilon_p - \epsilon_d$ , the difference of the energy levels of the d and p holes. We take it granted that the parent system is the charge transfer type insulator having spin 1/2 on each Cu-site (atomically  $Cu^{++}$ ).<sup>6)</sup> The electron-doping will leads to as many  $Cu^+$  states as the number of electrons. For such a case the effective Hamiltonian derived from the second order perturbation with respect to  $t$  is expressed in terms of the d-hole operator,  $d_{is}$ , as follows.<sup>7)</sup>

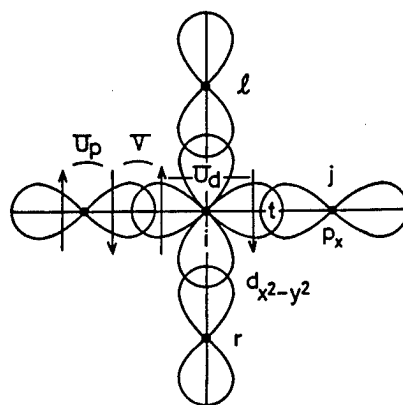


Fig.1 Parameters involved in the present model;  $U_d$ ,  $U_p$ ,  $V$  are Coulomb interaction constants on Cu and O sites, and between Cu and O sites, respectively, and  $t$ , the mixing.

$$H'_e = -\frac{t^2}{\Delta} \sum_i (1-n_{j,-s}) d_{js}^\dagger d_{is} (1-n_{i,-s}) + \left(\frac{t^2}{\Delta} - \frac{t^2}{\Delta+V}\right) \sum_i n_i n_j \quad (1)$$

where  $i$  and  $j$  refer to Cu-sites and the summations are over the nearest neighbor pairs, and  $n_{is} = d_{is}^\dagger d_{is}$ ,  $n_i = n_{i\uparrow} + n_{i\downarrow}$ . Together with this  $H'_e$ , there exists the effective energy present even in the case without doping, i.e. the spin Hamiltonian,  $H_s$ ;

$$H_s = J_s \sum_i S_i \cdot S_j \quad ; \quad J_s = \frac{2t^4}{(\Delta+V)^2} \left( \frac{1}{U_d} + \frac{2}{U_p+2\Delta} \right) \quad (2)$$

If  $V=0$  the sum of  $H_s$  and  $H'_e$  has the same form as the  $t$ - $J$  model,<sup>4)</sup>

$$H_{t-J} = -\tilde{t} \sum_i (1-n_{j,-s}) d_{js}^\dagger d_{is} (1-n_{i,-s}) + \tilde{J} \sum_i S_i \cdot S_j \quad (3)$$

The value of  $V$  is difficult to deduce, though it is sometimes argued to be relatively small.<sup>5)</sup> Even if  $V$  is appreciable, the spin dependent interaction, which should be important, is incorporated in eq.(3) and then the low-lying excitations in the case of electron-doping will be described by the  $t$ - $J$  model. In eq.(3) a doped electron is represented as to quench the Cu spin leading to local (on-site) singlet and induce an electronic charge.

In contrast the case of hole-doping is more involved. We have recently derived the effective Hamiltonian in this case.<sup>8)</sup> First in the case where we start with  $\text{Cu}:d_{x^2-y^2}$  and  $\text{O}:P_z$  in the Cu-O plane and with the assumption that  $\text{Cu}^{++}$  is stable in the presence of doping, we obtained

$$\begin{aligned} H'_h = & J_d \sum_i \left\{ \sum_j \left\{ \vec{S}_i \cdot \vec{p}_{js}^\dagger \vec{\sigma}_{ss}^\dagger p_{js} \cdot (A_1 + A_2 \sum_{r \neq j} n_r) + A_3 n_j + A_4 n_{j\downarrow} n_{j\uparrow} + A_5 n_j \sum_{r \neq j} n_r \right\} \right. \\ & + \sum_{j \neq l} \left\{ \vec{S}_i \cdot \vec{p}_{js}^\dagger \vec{\sigma}_{ss}^\dagger p_{ls} \cdot (A_6 + A_7 \sum_{r \neq j, l} n_r + A_8 (n_j + n_l)) \right. \\ & \left. \left. + (p_{j\uparrow}^\dagger p_{l\uparrow} + p_{j\downarrow}^\dagger p_{l\downarrow}) (A_9 + A_{10} \sum_{r \neq j, l} n_r + A_{11} (n_j + n_l)) \right\} \right\} + J_s \sum_i S_i \cdot S_k + H_0 \quad (4) \end{aligned}$$

Here  $p_j(p_j^\dagger)$  is the annihilation (creation) operator of the hole,  $n_{js} = p_{js}^\dagger p_{js}$ ,  $S_i$  and  $\sigma$  are the Cu-spin at the  $i$ -th site and the Pauli matrix, respectively. The summation over  $j, l$  and  $r$  is over all oxygen sites around the  $i$ -th Cu-site. The parameters,  $A_\alpha$  ( $\alpha=1 \sim 11$ ), are given in terms of  $U_d$ ,  $U_p$ ,  $V$  and  $\Delta$  but their explicit forms are not given here. The effects of  $\text{Cu}:d_{3z^2-r^2}$  and  $\text{O}:P_z$  orbitals have also been examined and it is shown that they are represented just as a modification of the parameters,  $A_\alpha$ .<sup>7)</sup> Equation (4) indicates that there are various interaction processes from the hole doping due to existence of both spins on Cu and carriers on O sites; e.g. for  $V \neq 0$  the existence of attractive interaction between two holes on the adjacent two O-sites around the same Cu leading to the enhancement between a Cu-spin and the adjacent hole. However the essence will be extracted by focusing ourselves to the case of  $U_p=V=0$ , where  $A_1=A_6 \equiv U_d \left( \frac{1}{\Delta} + \frac{1}{U_d-\Delta} \right)$ ;  $A_3=A_9 = \frac{1}{2} U_d \left( \frac{1}{\Delta} - \frac{1}{U_d-\Delta} \right)$  and  $A_\alpha=0$  otherwise. Even in this simpler case the solution is not known. In order to see what is contained in this case, we first considered the case of a single Cu spin and a hole as Eskes and Sawatzky<sup>9)</sup> did for the Anderson model. It is seen that eq.(4) in this case leads to the singlet bound state. The special case with the vanishing kinetic energy of holes in this context has been examined by Zhang and Rice,<sup>10)</sup> leading to the local singlet with hole amplitudes on four O-sites around the Cu spin. The existence of the finite kinetic energy results in the singlet state more extended in space. The existence of such singlet states will persist even for the periodic array of Cu spins and for a finite, but small, concentration



of holes<sup>10)</sup> and in the presence of  $U_p$  and  $V$ . Since the formation of singlet states is the essence the low-lying excitation in this case will also be described by the  $t$ - $J$  model, though the parameters  $t$  and  $J$  should reflect the fact that the singlet states in this case is not completely local, which may be important in quantitative discussions. Actually the numerical simulations by Imada et al.<sup>11)</sup> indicate that the binding energy appears to be enhanced when the singlet state is extended. We think, however, that this is a quantitative but not qualitative question.

These theoretical discussions comparing two distinct cases of hole and electron doping on one hand and the recent experimental findings by Tokura, Takagi and Uchida<sup>1)</sup> on the other hand will lead to a conclusion that the essence of the high  $T_c$  oxides will properly be described by the  $t$ - $J$  model. This is precisely the scenario proposed by Anderson<sup>4)</sup> even before the discovery of YBCO.

We are thankful to the authors of refs.1 and 2 for sending us their preprints prior to the publications. The present research is financially supported by Priority Areas, Mechanisms of Superconductivity (63631007) and New Functionally Materials-Design, Preparation and Control (63604014) of Grant-in-Aid for Scientific Research from the Ministry of Education, Science and Culture.

<sup>†</sup>Fellowship of the Japan Society for the Promotion of Science for Japanese Junior Scientists.

#### References

- 1) Y. Tokura, H. Takagi and S. Uchida, *Nature*, Jan. 26 (1989).
- 2) G.M. Luke, B.J. Sternlieb, Y.J. Uemura, J.H. Brewer, R. Kadono, R.F. Kiefl, S.R. Kreitman, T.M. Riseman, J. Gopalakrishnan, A.W. Sleight, M.A. Subramanian, S. Uchida, H. Takagi and Y. Tokura, submitted to *Nature*.
- 3) e.g. papers in Proc. of Intern. Conf. on High Temperature Superconductors and Materials and Mechanisms of Superconductivity (1988, Interlaken), *Physica* 153-155 ed. by J. Müller and J.L. Olsen (North-Holland, 1988).
- 4) P.W. Anderson: *Science* 235 (1987) 1196.
- 5) Various papers in Proc. of the Adriatico Research Conf. Towards the Theoretical Understanding of High  $T_c$  Superconductors (World Scientific, Singapore 1988).
- 6) J.M. Tranquada, S.M. Heald, A.R. Moodenbaugh and M. Suenaga, *Phys. Rev.* B35 (1987) 7187; A. Fujimori, E. Takayama-Muromachi, Y. Uchida and B. Okai, *Phys. Rev.* B35 (1987) 8814.
- 7) H. Matsukawa and H. Fukuyama, to be submitted to *J. Phys. Soc. Jpn.*
- 8) H. Fukuyama, H. Matsukawa and Y. Hasegawa, *J. Phys. Soc. Jpn.* 58 (1989) #2.
- 9) H. Eskes and G.A. Sawatzkey, *Phys. Rev. Lett.* 61 (1988) 1415.
- 10) F.C. Zhang and T.M. Rice, *Phys. Rev.* B37 (1988) 3759.
- 11) M. Imada, Y. Hatsugai and N. Nagaosa, in ref.5 p.959; Y. Hatsugai, M. Imada and N. Nagaosa, submitted to *J. Phys. Soc. Jpn.*

THEORETICAL STUDY OF HOLES IN  
QUANTUM MAGNETIC INSULATORS

S. Maekawa

Department of Applied Physics  
Nagoya University, Nagoya 464-01

We identify Cu oxide superconductors with strongly correlated electron systems, and consider that the electronic properties are described by holes introduced in the Mott-Hubbard insulators. To clarify the electronic properties, we have examined motion of the holes in the moment expansion method and the high temperature expansion method.

Since the discovery of Cu oxide superconductors, much study of the electronic states has been done. We identify the superconductors with strongly correlated electron systems, and consider that the electronic properties are described by holes introduced in the Mott-Hubbard insulators. Based on this view point, we studied the electronic states in Cu oxides in detail and examined the perturbative approach of the normal and superconducting properties starting from the insulators in the last fiscal year.<sup>1)</sup> In this fiscal year, we have studied motion of the holes introduced in the insulators in the moment expansion method and the high temperature expansion method.

(i) Holes introduced in quantum magnetic insulators

At half filling in the Hubbard model with strong electron correlation in two-dimensional square lattice, the ground state is insulating. Its magnetic state is an antiferromagnetic one with large quantum spin fluctuation or the resonating valence bond (RVB) state because of the low dimensionality and the low spin value ( $S=1/2$ ).<sup>2)</sup> For holes introduced in such magnetic insulators, the propagation is caused by interchange of the position with electrons.<sup>3,4)</sup> Therefore, it is expected that motion of the holes is strongly dependent on the exchange interaction acting on spins.

We have studied the Green's function of holes in various magnetic insulators using the moment expansion method.<sup>5)</sup> We found that long-range spin interactions appear due to the motion of holes and that the low energy states of holes are largely affected by the magnetic states.

When the reasonable values of the exchange interaction ( $J$ ) and the hopping parameter ( $t$ ) of holes for the oxides are introduced, we obtain that holes are stabilized in the RVB state more than in the antiferromagnetic state. This is because the magnetic coherence is weaker in the RVB state. Since holes disturb the magnetic coherence when they propagate, the RVB state without long range order is favorable for holes. Several authors<sup>6,7)</sup> have studied the kinetic energy of holes in the magnetic states in the limit of  $J \rightarrow 0$ . Our conclusion with  $J \neq 0$  is in contrast with the case with  $J \rightarrow 0$ .

When the Green's function of holes is expressed in the continued fraction representation, it can be exactly solved in the Bethe lattice with Ising antiferromagnetic spins.<sup>8)</sup> We have examined effects of the quantum spin fluctuation on the Green's function and obtained that there exists a sharp peak of the density of states of holes in the low energy region. The width of this peak is found to be of the order of  $J$ . We consider that this peak corresponds to the mobile magnetic polaron states.<sup>9-12)</sup> The more detailed calculation of the states is now in progress.

#### (ii) Transport properties in strongly correlated electron systems

As discussed above, a small number of holes carry the transport current in the oxides. Since they propagate by interchanging the position with electrons, the transport properties may be quite different from those in the usual metals.<sup>4,13)</sup> Ohata and Kubo<sup>14)</sup> have studied the resistivity due to holes introduced in the Mott-Hubbard insulators in the limit of strong correlation ( $U \rightarrow \infty$ ), and obtained that the leading term in the resistivity is proportional to  $(T/t)$  with  $T$  being temperature at high temperatures.

We have calculated the resistivity and the thermopower in such a system.<sup>15)</sup> We found that the resistivity is proportional to temperature in the whole temperature range except very low temperatures. It seems interesting to examine the  $T$ -linear resistivity in the oxides in the light of the present theory.

The high temperature limit for the thermopower in the Hubbard model with  $U \rightarrow \infty$  is given by the entropy per hole. Following Chaikin and Beni,<sup>16)</sup> we have at

$$S(T \rightarrow \infty) = (k_B/e) \ln[(1-a)/2a], \quad (1)$$

where  $a$  is the concentration of holes, and  $e > 0$ . Therefore,  $S(T \rightarrow \infty)$  is positive for  $a > 1/3$  and changes the sign at  $a = 1/3$ . We have calculated the leading correction to eq.(1) in the high temperature expansion method, and obtained<sup>16)</sup>

$$S(T) = (k_B/e) \ln[(1-a)/2a] + 5.1(k_B/e)(t/T)^2, \quad (2)$$

in the two-dimensional square lattice. We note that  $S(T)$  increases with decreasing temperature. It is also interesting to see that for a  $\geq 1/3$ ,  $S(T)$  is negative at high temperatures and becomes positive with decreasing temperature. We are now analysing the experimental data in various oxides by using the theory.

#### Acknowledgements

This work described in (i) and (ii) have been done in collaboration with J. Inoue and M. Miyazaki, and A. Oguri, and supported by the Grant-in-Aid for Scientific Research on Priority Areas "Mechanism and Superconductivity".

#### References

- 1) S. Maekawa, Y. Isawa, and H. Ebisawa : Jpn. J. Appl. Phys. Series 1, Superconducting Materials (1988), 235.
- 2) P.W. Anderson : Science 235 (1987) 1196.
- 3) Y. Nagaoka : Phys. Rev. 127 (1987) 392.
- 4) W. F. Brinkman and T. M. Rice : Phys. Rev. B2 (1970) 1324.
- 5) J. Inoue, M. Miyazaki, and S. Maekawa : Physica C 157 (1989) No. 2.
- 6) R. Joynt : Phys. Rev. B37 (1988) 7979.
- 7) P. Lederer and Y. Takahashi : preprint.
- 8) S. Maekawa, J. Inoue and M. Miyazaki : to be published.
- 9) S. A. Trugman : Phys. Rev. B37 (1988) 1598.
- 10) B. I. Shraiman and E. D. Siggia : Phys. Rev. Lett. 60 (1988) 740
- 11) S. Schmitt-Rink, C. M. Varma, and A. E. Ruckenstein : Phys. Rev. Lett. 60 (1988) 2793.
- 12) C. L. Kane, P. A. Lee, and N. Read : to be published.
- 13) A. Oguri and S. Maekawa : Physica C 156 (1988) 679.
- 14) N. Ohta and R. Kubo : J. Phys. Soc. Jpn. 28 (1970) 1402.
- 15) A. Oguri and S. Maekawa : to be published.
- 16) P. M. Chaikin and G. Beni : Phys. Rev. B13 (1976) 647.

# Superexchange Interaction Constant in p-d Mixing Model

Yoshimasa Isawa

Research Institute of Electrical Communication, Tohoku

University, Sendai 980 Japan

We study the anti-ferro magnetic superexchange constant  $J$  in the p-d mixing model as a function of doped p-hole. By use of the atomic operator transformation of d-hole and the double time Green's function,  $J$  is evaluated up to the lowest order of the p-hole concentration which is sensitive to the location of the p-hole in momentum space. The effective coupling constant for the spinon-spinon interaction, which is different from  $J$  in the presence of doped p-hole, is also given.

The single band Hubbard model has been discussed as a model for high  $T_c$  superconductivity in strongly correlated electron systems[1],[2]. In this model, the anti-ferro magnetic superexchange interaction is indispensable in order to obtain the superconducting pairing. This interaction has also played an essential role in the discussion of RVB(resonating valence bond) state proposed by Anderson[2].

In this paper we study the superexchange constant  $J$  in the two band p-d mixing model[3],[4] which is more realistic as a model for high  $T_c$  oxides than the Hubbard model. Its model hamiltonian is written as

$$H = \sum_{p-d} \sum_{\sigma i} \varepsilon_d d_{\sigma i}^{\dagger} d_{\sigma i} + \sum_{\sigma \ell} \varepsilon_p p_{\sigma \ell}^{\dagger} p_{\sigma \ell} + \frac{1}{2} U \sum_{\sigma i} n_{\sigma i} n_{\sigma i - \sigma i} + \sum_{\sigma i \ell} V_{i\ell} (d_{\sigma i}^{\dagger} p_{\sigma \ell} + p_{\sigma \ell}^{\dagger} d_{\sigma i}), \quad (1)$$

where  $\varepsilon_d$  and  $\varepsilon_p$  are the site energies of the Cu d-hole and the oxygen p-hole measured from the chemical potential.  $d_{\sigma i}$  and  $p_{\sigma \ell}$  are the annihilation operators of i-th Cu d-hole and the  $\ell$ -th oxygen p-hole with spin  $\sigma$ , respectively.  $U$  is the on-site Coulomb interaction.  $V_{i\ell}$  is the p-d mixing matrix element, which is chosen as follows[4]:  $V_{i\ell} = V_0$  if  $\ell = i + a(x)/2$  or  $\ell = i + a(y)/2$ ,  $V_{i\ell} = -V_0$  if  $\ell = i - a(x)/2$  or  $\ell = i - a(y)/2$  and  $V_{i\ell} = 0$  otherwise, where  $\vec{a} = (a(x), a(y))$  is the vector connecting the nearest copper sites.

Let us transform the creation and the annihilation operators of d-hole into the atomic operators[5]:

$$\begin{aligned} d_{\sigma i}^{\dagger} &= a_{\sigma i}^{\dagger} a_{0i} + \sigma a_{2i}^{\dagger} a_{-\sigma i}^{\dagger}, \\ d_{\sigma i} &= a_{\sigma i}^{\dagger} a_{0i} + \sigma a_{-\sigma i}^{\dagger} a_{2i}^{\dagger}, \end{aligned} \quad (2)$$

with the local constraint in each site:  $C_i \equiv \sum_{\sigma} a_i^{\dagger} a_{\sigma i}^{\dagger} a_{\sigma i}^{\dagger} a_{0i}^{\dagger} a_{0i}^{\dagger} a_{2i}^{\dagger} a_{2i}^{\dagger} = 1$ . This implies that each i-site should be in a state among four atomic ones. The operator  $a_{\sigma i}$  is a fermion (spinon) annihilation operator and  $a_{0i}$  and  $a_{2i}$  are charged boson annihilation operators defined on the subspace of  $C_i = 1$ . Then we have the transformed hamiltonian  $H = H_0 + H'$ , where the atomic hamiltonian  $H_0$  is given by

$$H_0 = \sum_{\sigma i} (\varepsilon_d - \lambda) a_{\sigma i}^{\dagger} a_{\sigma i} + \sum_i (\varepsilon_2 - \lambda) a_{2i}^{\dagger} a_{2i} - \lambda \sum_i a_i^{\dagger} a_{0i} + \sum_{\ell \sigma} \varepsilon_p p_{\ell \sigma}^{\dagger} p_{\ell \sigma}, \quad (3)$$

and the mixing term  $H'$  is given by

$$H' = \sum_{i \ell \sigma} \{ V_{i \ell} (a_{\sigma i}^{\dagger} a_{\sigma i} + \sigma a_{\sigma i}^{\dagger} a_{\sigma i}) p_{\ell \sigma} + V_{\ell i} p_{\ell \sigma}^{\dagger} (a_{\sigma i}^{\dagger} a_{\sigma i} + \sigma a_{\sigma i}^{\dagger} a_{\sigma i}) \}. \quad (4)$$

Here we introduced the lagrange multiplier  $\lambda$  in order to take into account the local constraint on the average sense. By use of the atomic operator transformation, the effect of on-site Coulomb interaction is completely taken into account in the one particle hamiltonian. However the actual analysis is not so easy since a consistent approximation, in which the local constraint is satisfied, is necessary. One of the methods appropriate to develop a consistent approximation is the double time Green's function method. The local constraint can be taken into account in each stage of the approximation when we deal with it in site representation.

We suppose that Cu d-hole is half-filled even in the presence of the doped holes in the oxygen p-orbit when the p-hole is dilute. In order to realize this situation, the relative position of energy levels should satisfy the conditions: (i)  $\varepsilon_d - \lambda < -\lambda$  and  $\varepsilon_2 - \lambda$ , (ii)  $\varepsilon_d < \varepsilon_p$ . Here  $x \langle y \rangle$  means  $y \cdot x \rangle V^2 / \Delta$  ( $\Delta = (\varepsilon_p - \varepsilon_d)$ ) and  $V^2 / (U - \Delta)$ .

The double time Green's function for the spin operator is defined by [6],  $G_{ik}^{\pm}(E) = \langle S_{\sigma i}^{\pm}; S_{\sigma k}^{\pm} \rangle$ , where  $S_{\sigma i}^+ = a_{\sigma i}^{\dagger} a_{\sigma i - \sigma i}$  and  $S_{\sigma k}^- = (S_{\sigma k}^+)^{\dagger}$ . The equation of motion is given by

$$E G_{ik}^{\pm}(E) = 2\delta_{ik} \langle S_{\sigma i}^{\pm} \rangle + A \{ (a_{\sigma i}^{\dagger} a_{\sigma i} + \sigma a_{\sigma i}^{\dagger} a_{\sigma i}) p_{\sigma i}^{\pm}; S_{\sigma k}^{\pm} \} - A \{ p_{\sigma i}^{\dagger} (a_{\sigma i}^{\dagger} a_{\sigma i} - \sigma a_{\sigma i}^{\dagger} a_{\sigma i}); S_{\sigma k}^{\pm} \}, \quad (5)$$

where  $p_{\sigma i}$  is the p-hole operator defined on the i-th Cu site:  $p_{\sigma i} = \sum_{\ell} V_{i \ell} p_{\ell \sigma} / A$  with  $A^2 = \langle i | V^2 | i \rangle = 4V_0^2$ . We repeat this procedure twice. The 5-th order Green's functions  $G_5$  appear on the r.h.s of the equation of motion, which is given by  $G_5 = \langle ABCDE; S^{\pm} \rangle$  where A, B, C, D, and E are the linear combinations of  $a_{\sigma 1}, a_{\sigma 0}, a_{\sigma 2}, p_{\sigma 2}, a_{\sigma 3}, a_{\sigma 0}, a_{\sigma 2}, p_{\sigma 4}$ . Since the d-hole is half-filled and the p-hole is dilute, a large number of  $G_5$  vanish. Finally we obtain the spin Green's function as follows, in the low energy region,

$$E \langle S_{\sigma i}^{\pm}; S_{\sigma k}^{\pm} \rangle = 2\delta_{ik} \langle S_{\sigma i}^{\pm} \rangle (1 - n_{pi} / 2) + \sum_{j \neq i} J_{ij} \langle S_{\sigma zi}^{\pm} S_{\sigma j}^{\pm} - S_{\sigma i}^{\pm} S_{\sigma zj}^{\pm}; S_{\sigma k}^{\pm} \rangle, \quad (6)$$

where  $n_{pi} = \sum_{\sigma} \langle p_{\sigma i}^{\dagger} p_{\sigma i} \rangle$ , and the effective superexchange constant  $J_{ij}$  is given by [7]

$$J_{ij} = \frac{4}{\Delta^2} \left( \frac{1}{\Delta} + \frac{1}{U} \right) V_{ij}^2 V_{ji}^2 - \frac{A^2}{\Delta^2} \left( \frac{1}{\Delta} + \frac{1}{U\Delta} + \frac{1}{(U-\Delta)^2} \right) V_{ij}^2 \langle p_{\sigma i}^{\dagger} p_{\sigma j} \rangle. \quad (7)$$

The first term in  $J_{ij}$  is the wellknown formula for the super-exchange coupling constant in the half-filled d-hole and in the absence of the p-hole. The second term describes the effect of p-hole. Whether  $J$  increases or not as a function of the concentration of p-hole depends on the sign

of the correlation function of p-hole. In order to obtain J, only the part of the correlation function with i and j being the nearest Cu sites is necessary since  $V_{ij}^2$  in eq.(7) is nonzero for that case. By use of  $p = \frac{1}{\sqrt{N}} \sum \exp(-ik\ell) p_{\ell}$ , the correlation function is given by  $\langle p_{\sigma i}^+ p_{\sigma j} \rangle = \frac{1}{2N} \sum_k \cos(k a(x)) \langle 1 - \frac{1}{2} (\cos(k a(x)) + \cos(k a(y))) \rangle \langle p_{\sigma k}^+ p_{\sigma k} \rangle$ , where  $i=j+a(x)$  and N is the number of Cu sites in the lattice. Let us estimate the correlation function of p-hole on the assumptions that the system is normal and p-holes can move freely in the 2-dimensional square lattice. We evaluate the correlation function in three cases(Fig.1): the band minimum of p-hole is located at (a)  $\Gamma$  point,  $k=(0,0)$  (b) X point,  $k=(\pi/a, 0)$  and (c) M point,  $k=(\pi/a, \pi/a)$ . In the case (a), J increases as a function of doped p-hole while in the cases (b) and (c) J decreases with increasing the doped p-hole concentration. Since the transition temperature for anti-ferromagnetism is a decreasing function of p-hole density in the actual high  $T_c$  oxides, the effective coupling constant J will also decrease with increasing the p-hole. In order to be consistent with the above result, the doped p-hole in these oxides will not be around the  $\Gamma$  point.

The p-hole density dependence of J can not be obtained by the naive effective hamiltonian approach since some of fourth order processes which should lead to the effective superexchange interaction diverge because of the intermediate states being degenerate with the initial one. The reason why our approach is successful to overcome this difficulty is attributed to the self-consistent structure of our theory which is similar to the degenerate perturbation theory.

We also calculated the effective spinon-spinon interaction constant K relevant to the spin degrees of freedom from the equations of motion of one particle spinon Green's function. The expression for K is given by, in low energy region,

$$K = -\left( \frac{4}{\Delta^2 U} + \frac{1}{\Delta} \right) V^2 - 4A^2 \left( \frac{1}{\Delta^3} + \frac{1}{\Delta^2(U-\Delta)} - \frac{1}{(U-\Delta)^3} \right) V^2 \langle p_{\sigma j}^+ p_{\sigma i} \rangle, \quad (8)$$

It is clear that K is equal to J when there is no doping of p-hole. In the presence of p-hole, however, two effective interaction constants are no longer equal which implies that the effective hamiltonian for describing the RVB state should differ from that for the anti-ferromagnetism in p-d mixing model. Since K is larger than J when the p-hole is doped into X or M, it is possible that the RVB condensed state is stabilized compared to the anti-ferromagnetic state in this doping condition. That the two effective interaction constants are unequal means that the spinon is not completely reduced to spin but is an independent degrees of freedom.

The present author would like to thank Prof.H.Ebisawa for useful discussions.

#### References

- [1] J.E.Hirsch: Phys.Rev.Lett.54(1985)1317.
- [2] P.W.Anderson: Science 235(1987)1196.
- [3] V.J.Enery: Phys.Rev.Lett.58(1987)2794.
- [4] F.C.Zhang and T.M.Rice: Phys.Rev.B37(1988)3759.
- [5] Y.Isawa, S.Maekawa and H.Ebisawa: Physica B148(1987)391.
- [6] D.N.Zubarev: Soviet Physics Uspekhi.3(1960)320.
- [7] Y.Isawa: Submitted to J.Phys.Soc.Jpn.

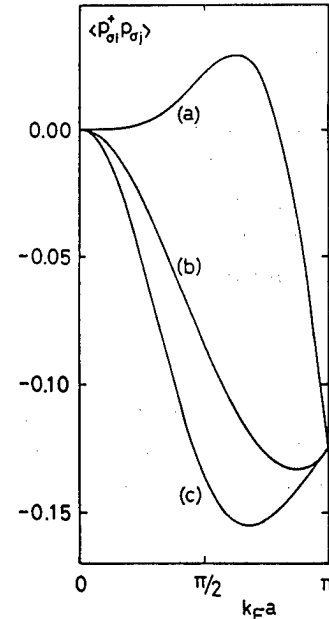


Fig. 1

# Holon Local Density of States of 2D RVB Quantum Spin Liquid

Y. Takahashi and P. Lederer<sup>†</sup>

The Institute for Solid State Physics, the University of Tokyo  
Roppongi, Minato-ku, Tokyo 106, Japan

<sup>†</sup>Physique des Solides, Bat 510, Université Paris Sud, 91405 Orsay Cedex

Holon local densities of states are evaluated from the lower order moments of the Green's function up to 8-th order for a Resonating Valence Bond liquid and quantum anti-ferromagnet. We find almost no energy difference between the undistorted wave functions in the infinite correlation limit. A local defect model shows that large variations in kinetic energy may result from local distortions of the wave function around the hole.

A large part of the current theoretical activity dealing with high  $T_c$  superconductors focuses on the properties of the Hubbard Hamiltonian in the strong correlation limit. The nature of its ground state, and the competition between an Antiferromagnetic (AF) state and a Quantum Spin Liquid (QSL) of the Resonating Valence Bond (RVB) type are crucial, since high  $T_c$  superconductivity may be a result of doping an RVB state.<sup>1)</sup> The different ground states for the undoped case are now found to be very close in energy, their difference being  $\leq 10^{-2}J$  per bond, where  $J = 4t^2/U$ ;  $t$  and  $U$  are the interatomic transfer energy and the intraatomic Coulomb repulsion. A number of authors argue that under doping, hole motion results in a QSL (with no long range AF order) within which singlet pairing due to quantum fluctuations results in superconductivity as originally proposed by Anderson.<sup>1)</sup> Hole motion is a candidate to provide a large energy gain in favour of one ground state or another, since its scale is of order  $t$ . In this report we review a number of results we have obtained<sup>2-6)</sup> about the kinetic energy of holes in the strong correlation limit of the Hubbard model with nearly one electron per site. This includes the construction of an RVB wave function for a spin  $S = 0$  hole (holon)<sup>4)</sup>, the discussion of the kinetic energy of the holon,<sup>5)</sup> that of a hole in a quantum AF,<sup>3)</sup> and that of an RVB wave function locally deformed around a holon.<sup>6)</sup> We also present new results about the single hole, or single holon, density of states in various AF or RVB states.

We study the Hubbard Hamiltonian in  $2-D$  on a square lattice, with nearest neighbour transfer only. In the limit  $U/8t \gg 1$ , it is transformed as

$$H = -t \sum_{ij\sigma} c_{i\sigma}^\dagger c_{j\sigma} + 4t^2/U \sum_{\langle ij \rangle} (\mathbf{S}_i \mathbf{S}_j - \rho_i \rho_j / 4). \quad (1)$$

We neglect here a 3-site hopping term. (1) is valid in the truncated Hilbert space introduced by Nagaoka for a single hole in a half-filled band: a state with  $N - 1$  electrons on  $N$  site lattice and the double occupancy is prohibited. The Green's function  $G(\omega) = (\omega - H)^{-1}$  may be expanded in a power series in  $t/\omega$ , for  $\omega/zt > 1$ ;

$$G_{ii}^{\alpha\alpha}(\omega) = 1/\omega + (1/\omega) \sum_{p=2}^{\infty} \frac{A_p^{\alpha\alpha}}{z^p} \left( \frac{zt}{\omega} \right)^p.$$

The expansion coefficients are related to the number  $A_p^{\alpha\alpha}$  of "diagonal walks", i.e. walks which return to the starting point after  $p$  steps with identical final and initial spin configurations  $\alpha_i$ . The moments of the



density of states  $M_p^\alpha$  are related to  $A_p^\alpha$ :  $M_p^\alpha = A_p^\alpha/z^p$ . Now we can compare various states by calculating the coefficients  $A_p^\alpha$ . This method<sup>2)</sup> is well adapted to the evaluation of the kinetic energy in the dilute doping limit of the Hamiltonian (1) and has various advantages.<sup>2)</sup>

In principle, an RVB wave function is a superposition of singlet products (SP) with arbitrary bond lengths.<sup>1)</sup> We restrict our choice of RVB wave functions to nearest neighbour bonds, for which relatively straightforward calculational procedures can be set up.<sup>4,5)</sup> A holon is defined as an empty site in an otherwise low energy singlet liquid where all electrons are paired. From  $2N(N = 12)$  lattice sites, we can form  $N$  singlet pair bonds (dimers) between nearest neighbour sites. A dimer covering is defined when every site except the central site is connected to exactly one of its nearest neighbours by a dimer. We construct a wave function by superposing these SP states  $\psi_\alpha$ , over all the dimer covering  $\alpha$  with equal weight, but with different ( $\pm$ ) phase. This extends a previous proposal by Sutherland<sup>7)</sup> in the case of the fermion representation, which is appropriate to describe the holon wave function.<sup>4)</sup> Our choice of wave function can be shown to be approximately equivalent to the " $s + id$ " symmetry<sup>8)</sup> of the Gutzwiller type wave function. Energy computation of the " $s + id$ " wave function in the case of no doping shows that it is within  $\sim 5\%$  of the lowest exact energy state for a  $4 \times 4$  cluster; the accuracy is somewhat poorer in the thermodynamic limit.

With the model RVB wave function defined above, we can proceed to calculate the kinetic energy by evaluating the moments of the density of states.<sup>5)</sup> If we assume a simple power law behavior of the density of states  $\rho(\omega) = c(\omega_0^2 - (\omega/zt)^2)^\nu$  at the band edge  $\omega_0$ , the ratio of the succeeding moments is given by  $M_{n+2}/M_n = \omega_0^2(n+1)/(n+2\nu+3)$ . This suggests that if we define  $\nu(n) = [n+1 - (n+3)M_{n+2}/M_n]/(2M_{n+2}/M_n)$ , then  $\nu(n) = an + b$  for large  $n$ . From  $\nu(n)$  we evaluated  $a_n, b_n, \nu_n$  and the band edge  $\omega_0(n)$  by

$$a_n = \{\nu(n+2) - \nu(n)\}/2, \quad b_n = \{(n+2)\nu(n) - n\nu(n+2)\}/2, \\ \nu_n = (b_n - 3a_n)/(1 + 2a_n), \quad \omega_0(n)^2 = 1/(1 + 2a_n).$$

We present here results on a  $5 \times 5$  cluster with rigid boundaries (RVB<sub>1</sub>), on 26 (RVB<sub>2</sub>) and 32 (RVB<sub>3</sub>) atom clusters with two holons with periodic boundary conditions. The corresponding results for the Néel state are also displayed for comparison.

Table I Band Edge Values for Various States

	Néel	RVB <sub>1</sub>	RVB <sub>2</sub>	RVB <sub>3</sub>	QAF
$\omega_0(2)$	0.8544	0.8331	0.8163	0.8157	0.8093
$\omega_0(4)$	0.8504	0.8308	0.8233	0.8203	
$\nu_4$	-0.0543	-0.0243	0.0690	0.0360	

One main result is that the effective number of diagonal paths at any given order is reduced compared to that found for the Néel state, because the holon motion around a loop results, in a number of cases, in a change of sign of the wave function, as well as partial overlap of initial and final state. As a result, the lowest energy state for the holon in the limit  $t/U \rightarrow 0$  is not as low as that for the Néel state, by about  $0.16t$ . The various clusters studied show that boundary effects are still important for a  $5 \times 5$  cluster. The most reliable figure for the lowest band edge is  $\omega_0 = 0.82$ . Takahashi<sup>3)</sup> has pointed out that the comparison between RVB and AF should include the quantum fluctuations in the latter state. Within the spin wave approximation he has evaluated the overlap between initial and final state when the hole motion has loops in the quantum AF. His result is also shown in Table I as QAF. Due to quantum fluctuations the band edge is pushed up in energy by  $0.16t$  compared to the Néel state, quite close to the RVB value. Due to the approximations used here (i.e. no local spin relaxation around the hole) we believe the band narrowing effect in the QAF is slightly overestimated, so that the difference with the RVB value is not significant.

The local distortion we consider amounts to suppressing RVB configurations which have one singlet along the smallest closed loops starting at the origin. This is achieved by factoring out the four singlets nearest to the origin along the  $O_x$  and  $O_y$  axes. Other singlets are allowed to resonate, so that the local symmetry of the wave function more than three interatomic distances away from the defect is " $s + id$ ", while the overall symmetry of the defect is  $s$ -type. This defect has zero spin. The loss of exchange energy  $\Delta E_0$  due to freezing out the four singlets is found to be  $\sim 3.3J$ .

Large order moments in this case show significant increase compared to the undistorted RVB case, resulting in the increase of the density of states at the band edge. The reason for this is that a holon is easier to propagate near the origin like the ferromagnetic polaron, so that a lowering of energy is expected. The density of states

corresponding to the local defect (denoted by RVB\*), as well as those corresponding to the undistorted RVB (RVB) and AF (N) cases are plotted in Fig. 1. The local defect exhibits a significant increase of the density of states at the band edge. Because of holon interactions (infinite repulsion at short distance, Coulomb interactions, etc.) only a small fraction will occupy the lowest energy states, so that depending on the density of holons, significant energy gains of order  $t$  may result from a local distortion such as the one considered here, which compensate for the small loss in resonance energy  $\sim 3.3J$ . The steep decrease of the density of states at the band edge will reflect the logarithmic singularity of the Green's function, consistent with the small value of the exponent  $\nu$  in Table I.

Our main conclusions can be summarized as follows: a) within the framework of "rigid" wave functions, i.e. wave functions which do not allow for local distortions around the hole, we find that the single holon wave function has " $s + id$ " character, which confirms mean field results and Monte Carlo calculations at finite doping; b) within the same framework little difference in kinetic energy of holes is found between AF and our model (nearest neighbour singlet) (RVB) state in the limit  $t/U \rightarrow 0$ , so that we expect at most an energy difference between RVB and AF is of order  $J$  per hole when  $t/U$  is finite; c) However we also discuss a locally deformed RVB wave function with mixed  $s$  and  $d$  character,<sup>6)</sup> which exhibits a large density of states enhancement at low energy, at the expense of little exchange energy; this suggests that detailed knowledge of the holon wave function, as well as better investigations of local deformations around a charge carrier are necessary to obtain reliable estimates of ground state energies, and ground state energy differences in the presence of doping.

#### References

- 1) P.W. Anderson: Science **235** (1987) 1196.
- 2) P. Lederer: J. Phys. Soc. Jpn. **57** (1988) 1729.
- 3) Y. Takahashi: Z. Physik B **71** (1988) 425.
- 4) P. Lederer and Y. Takahashi: Z. Physik B **71** (1988) 311.
- 5) P. Lederer and Y. Takahashi: Z. Physik B **71** (1988) 415.
- 6) Y. Takahashi and P. Lederer: J. Phys. Soc. Jpn. **57** (1988) 2624.
- 7) B. Sutherland: Phys. Rev. B **37** (1988) 3786.
- 8) G. Kotliar: Phys. Rev. B **37** (1988) 3664.

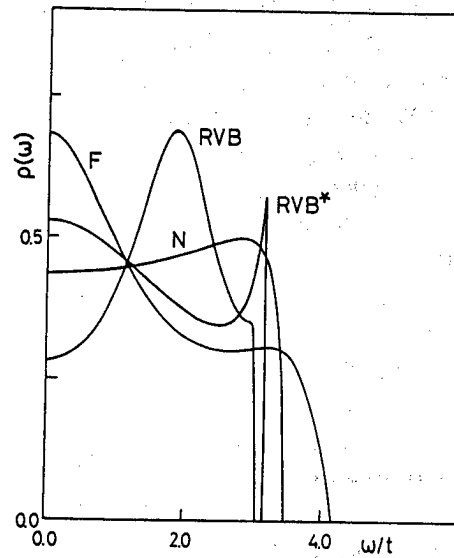


Fig. 1

## On Three Dimensional Gauge Theory

N. Imai, K. Ishikawa, N. Kimura<sup>(a)</sup>, T. Matsuyama<sup>(b)</sup> and I. Tanaka

Department of Physics, Hokkaido University, Sapporo 060

<sup>(a)</sup> Hokkaido Institute of Technology, Sapporo 006

<sup>(b)</sup> Research Institute for Fundamental Physics, Kyoto University, Kyoto 606

Several problems of three dimensional gauge theory which might have connections with high- $T_c$  superconductivity, have been investigated. Unitarity of topologically massive gauge theory in the covariant gauge is shown and classical solutions which carry electric current are obtained. Field theory in strong perpendicular magnetic field is also analyzed, and the universality of quantum Hall effect-regardless of interactions is shown.

Since the discovery of high- $T_c$  superconductivity in several materials, where two dimensional charge carriers play important roles, field theories of two spatial dimensions are getting much attentions. Field theories in two spatial and one temporal dimensions are different from those of four dimensions in many respects. The symmetry property and symmetry breaking mechanism in three dimensions may be different. So it is natural to seek new mechanism of superconductivity in three dimensional gauge theories.

In three dimensions a gauge invariant mass term is allowed<sup>[1]</sup>. This term is topologically non-trivial and is called "topological mass term" or "Chern-Simons term". The theory with C-S term has peculiar properties. The force between charges has short range component and long range one. Polyakov showed that the statistics of charged particles change from the ordinary statistics to the exotic ones (Bose-Fermi transmutation) due to long range self-interaction.<sup>[2]</sup> At the early stage this property was thought to have deep connection with finite T-linear specific heat of some high- $T_c$  superconducting states.<sup>[3]</sup> Unfortunately (or fortunately) new experiments seem to be erasing this T-linearity from specific heat of superconducting materials. None the less, the importance of three dimensional gauge theory in relation to high- $T_c$  superconductivity may not be lost at all.

Since, in the gauge theory with C-S term, the force between charges has two components, it may not clear if the S-matrix is unitary. In a covariant gauge, the photon propagator has massless pole as well as massive pole. Polyakov's Bose-Fermi transmutation is a long range effect of gauge field. This implies that massless mode as well as massive mode, both of which are described by a single gauge field, may propagate. Hence one of them might have a negative norm, as seen in higher derivative theories. Using Nakanishi-Lautrup formalism, we showed that all necessary conditions for a unitary S-matrix to be defined are satisfied.<sup>[4]</sup> We confirmed also that the physical subspace of gauge fields is made of massive state and zero-nor-

massless state, and that no negative norm massless state appears owing to the subsidiary conditions. Hence the theory is consistently interpreted.

The current arising from the topological mass term ( $\sim \mu \epsilon^{ijk} \partial_i A_j A_k$ ), which is bilinear in vector potential but is first order in space-time derivative, is proportional to the field strength. C-S term is known not to exist in real vacuum and is assumed to be generated by a matter which occupies a finite region of space. So a special boundary condition emerges. Hence, new type of classical solutions satisfying these properties are expected. We investigated classical equations of motion in Maxwell theory with C-S term and obtained classical solutions which carry electric current in the presence of constant magnetic field.<sup>[5]</sup> The Meissner effect was expected to occur due to the massiveness of gauge boson and was shown to occur actually.

Field theory of electrons in two dimensional continuum under perpendicular magnetic field was also studied. A connection of average Hall conductance with topological invariant was found first by TKNN in the free electron system in periodic potential.<sup>[6]</sup> In the previous works<sup>[7]</sup> we found a new topological expression of the Hall conductance in quantum field theoretical method. The Hall conductance was identified as anomaly-related topological mass term of three dimensional gauge theory, and agrees with the integer multiple of  $e^2/h$  in the gap regions and in the localized state regions. We developed computational techniques and extended our previous works.<sup>[8]</sup> We expand the field in the localized base functions whose centers correspond to those of classical cyclotron motions and are set on such lattice points that the wave functions satisfy completeness condition. The effective field theory is written on the space of lattice in which lattice translational invariance is preserved. Thus Ward-Takahashi identity is written in a useful manner in the momentum space representation. The explicit computation of physical observables became performable. It was shown that the electrons are localized near the short range impurity. The gauge invariance, which is described by Ward-Takahashi identity, leads that the Hall conductance is written as a topologically invariant form and is stable in the presence of disorders and interactions.

There are many unsolved fundamental problems in three dimensional gauge theory with C-S term. The force caused by the C-S term between static charges is zero because of antisymmetry of  $\epsilon^{ijk}$ . So the bound state problem cannot be solved in the ordinary potential picture. We intend to solve this problem by Bethe-Salpeter type equation. When this problem has been solved the Bose-Fermi transmutation mechanism may be understood more clearly. The strong coupling limit of the half-filled Hubbard Model was shown to have  $U(1)$  gauge symmetry which has subsequently been generalized to an  $SU(2)$  gauge symmetry.<sup>[9]</sup> So the bound state problem in non-abelian gauge theory in three dimensions is also very interesting and possibly have connections with high- $T_c$  superconductivity. We are proceeding in this direction.

To sum up, we have investigated several problems of three dimensional gauge theory and obtained rather firm results. Many problems such as bound state one are under investigation.

# Reference

- [1] S. Deser, R. Jackiw and S. Templeton ; Ann. Phys. 140 (1982) 372, Phys. Rev. Lett. 48 (1982) 975.
- [2] A.M. Polyakov ; Mod. Phys. Lett. A3 (1988) 325.
- [3] I. Dzyaloshinskii, A. Polyakov and P. Wiegmann ; Phys. Lett. A127 (1988) 112. P.B. Wiegmann ; Phys. Rev. Lett. 60 (1988) 821.
- [4] N. Imai, K. Ishikawa and I. Tanaka ; "Unitarity of Topologically Massive Abelian Gauge Theory", Hokkaido University Report EPHOU88 Nov005, to be published in Prog. Theor. Phys. 81 (1989).
- [5] N. Imai, K. Ishikawa and I. Tanaka ; "Current-Carrying Classical Solutions of Generalized Maxwell Theory with Chern-Simons Term", Hokkaido University Report EPHOU88 AUG004, submitted to J. Math. Phys..
- [6] D.J. Thouless, M. Kohmoto, M. Nightingale and M. den Nijs ; Phys. Rev. Lett. 49 (1982) 405.
- [7] K. Ishikawa ; Phys. Rev. Lett. 53 (1984) 1615, Phys. Rev. D31 (1985) 1432. K. Ishikawa and T. Matsuyama ; Z. Phys. C33 (1986) 41, Nucl. Phys. B280 (1987) 523. T. Matsuyama ; Prog. Theor. Phys. 77 (1987) 711.
- [8] N. Imai, K. Ishikawa, T. Matsuyama and I. Tanaka ; "Field Theory in Strong Magnetic Field and Quantum Hall Effect", Hokkaido University Report, 1989.
- [9] G. Baskaran and P.W. Anderson ; Phys. Rev. B37 (1988) 580. I. Affleck, Z. Zou, T. Hsu and P.W. Anderson, Phys. Rev. B (1988).

Possible Relation between the Superstructure and Superconducting Critical Temperatures  
in the Organic Superconductor  $\beta$ -(BEDT-TTF) $_2$ I $_3$

S.Kagoshima, Y.Nogami, M.Hasumi, H.Anzai<sup>+</sup>, M.Tokumoto<sup>+</sup>, G.Saito<sup>++</sup> and N.Mori<sup>++</sup>

Department of Pure and Applied Sciences, University of Tokyo, Komaba 3-8-1, Meguro, Tokyo 153, Japan; <sup>+</sup>Electrotechnical Laboratory, Umezono, Tsukuba, Ibaraki 305, Japan; <sup>++</sup>Institute for Solid State Physics, University of Tokyo, Roppongi 7-22-1, Minato, Tokyo 106, Japan

X-ray diffraction measurements of the superstructure were made under pressure in the title compound. The wave vector of the superstructure was found to become short below about 100K. This change occurs even at ambient pressure when the sample is kept at about 110K for a long time, say, 24hr. Samples thus annealed undergo two superconducting transitions at about 2K and 7K, both of which are higher than that observed in them cooled with a conventional speed.

#### Introduction

The title compound is well-known because of the presence of two superconducting states with different critical temperatures [1,2] and an incommensurate superstructure.[3] One of the states called "high- $T_c$ " state is realized under pressures above about 0.4kbar with the critical temperature  $T_c \sim 8$ K, and the other, "low- $T_c$ " state is formed in the lower pressure range with  $T_c \sim 1.5$ K. It has been believed that the superstructure, which is present in the lower pressure range, brings about the low- $T_c$  state and, therefore, the superstructure provides a clue to investigate possible differences between superconducting mechanisms of the two superconducting states.

By x-ray diffraction studies at various pressures we found, in suitable temperature and pressure ranges, a change of the wave vector describing the superstructure. This change is realized even at ambient pressure when a sufficiently long time is spent to complete the wave-vector change. We found that the state thus made by annealing has two kinds of bulk superconducting temperature  $T_c$  of about 7K and 2K while the sample without annealing remains in the "low- $T_c$ " state with  $T_c \sim 1.5$ K.

These results suggest that some of studies made on this compound should be reexamined because of the change of the superstructure and the annealing effect presumably associated with each other. We report here preliminary experimental results summarized above, and discuss possible origins for this phenomenon in relation to the superconductivity in this compound.

#### Experiments

X-ray diffraction measurements were made by using a conventional x-ray source of Mo-K $\alpha$  rays, a triple axis goniometer and a scintillation detector, and a diamond-anvil pressure cell designed for the present purpose. The pressure cell was cooled down by conduction in a continuous-flow type cryostat. Sample resistance was measured at ambient pressure in the two-dimensional a-b plane of the crystal by four-probe method. Electrical contacts were prepared with gold paint. Measurements of the Meissner effect

were made at ambient pressure by using SQUID magnetometers. Sample crystals were prepared by a conventional electro-chemical method.

## Results and Discussions

Figure 1 shows a part of the phase diagram proposed by Kang et al.[4] and Schegolev et al.[5] It shows also some of lines along which x-ray measurements were made although their position has some ambiguity because of the difficulty of pressure measurements in such low pressure range. The curve X-Y is a second order phase transition curve below which the incommensurate superstructure has been expected to appear. In the present study we verified this expectation directly. The point Y is a critical point from which several first-order phase transition lines have been proposed to emerge.[4,5] Those lines separate the "low- $T_c$ " and "high- $T_c$ " states although their exact position is still uncertain. Generally speaking, however, when the sample is cooled down under pressure close to the ambient pressure, for example along the line C, the sample has been expected to enter the "low- $T_c$ " state.[4,5] When the pressure is high but less than the critical pressure like that of the line A, it is proposed that the cooled sample belongs finally to the "high- $T_c$ " state [5] though the superconducting critical temperature accepted currently is shown by the lines L and H of Fig.1.

Along the lines like A,B and C we measured the intensity, peak profile and the wave vector of the satellite reflection from the incommensurate superstructure as functions of temperature and time.

It is to be noted that precise measurements of pressure is practically impossible for a diamond anvil in such low pressure and low temperature ranges. Therefore we evaluated the pressure by measuring the onset temperature of the superstructure and referring to the curve X-Y which has been almost established. Because of this the

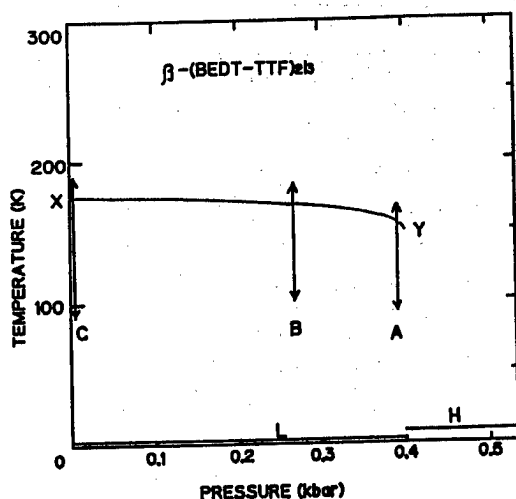


Fig.1 Pressure-temperature phase diagram of  $\beta$ -(BEDT-TTF) $_2$ I $_3$ . The superstructure appears below the curve X-Y. The "low- $T_c$ " and the "high- $T_c$ " superconductivity occurs below the lines L and H, respectively. X-ray measurements were made along the lines A,B and C.

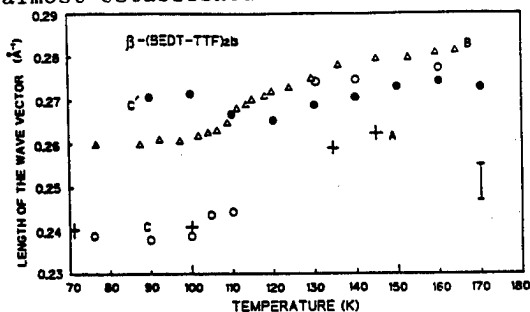


Fig.2 Temperature dependence of the length of the wave vector describing the superstructure. Measurements were made on a satellite reflection accompanying the (311) Bragg reflection. The symbols A,B and C denote results obtained along the lines A,B and C, respectively, of Fig.1 with a very slow temperature variation which allows the structural change occur. The results denoted by C' were obtained with a usual speed of temperature change  $\sim 1$ K/min. Also shown is the probable error of measurements.

position of the lines A, B and C should not be taken too serious.

We found that the wave vector describing the superstructure changes in a temperature range 100-120K. The wave vector is deduced at each temperature from angular conditions of reflection of both the satellite reflections and the ordinary Bragg ones. Figure 2 shows the length of the wave vector of a satellite accompanying the (311) Bragg reflection as functions of temperature. The wave vector becomes short in the lower temperature range. It is to be noted that the change of the reciprocal lattice vector with temperature is found to be negligible compared to the probable error shown in Fig.2. Therefore the change shown in Fig.2 is intrinsic to the superstructure. This change is found to be mostly ascribed to the b-component of the wave vector. We have found, however, no sign of commensurability locking in our preliminary analyses of the data.

The wave vector change needs a long time to be completed when the pressure is close to the ambient one. For example, the result C' near ambient pressure was obtained with the cooling / heating speed of about 1K/min in the range 100-120K. However, with respect to the result C showing the change of the wave vector the sample temperature was kept at about 108K for a time longer than 24 hr. Thus the intensional annealing near 110K is found to be crucial to complete the wave-vector change. Under high pressures, for example along the line A of Fig.1, the change of the wave vector seems to be completed in less than 1 hr, which is the minimum time necessary to obtain each data point.

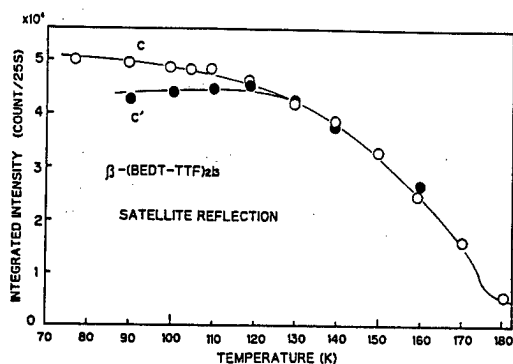


Fig.3 Integrated intensities of the satellite reflection accompanying the (311) Bragg reflection as functions of temperature. The open and closed circles correspond to the results C and C', respectively, of Fig.2.

Figure 3 shows the integrated intensity of the satellite reflection same as that of Fig.2 as functions of temperature. The open circles correspond to the result C in Fig.2 and the closed circles C'. It is evident that the saturation of intensity below about 100K, which has been found by Ravy et al.[6], is caused by an incomplete change of the superstructure. When a sufficiently long time is spent for annealing, the intensity increases smoothly with decreasing temperature as shown by the open circles in Fig.3.

Next, we made resistivity and magnetic susceptibility measurements of samples at ambient pressure in order to investigate possible annealing effect on the superconductivity. By using SQUID magnetometers we measured the susceptibility as functions of annealing time. We kept the sample temperature at 108K for a long time

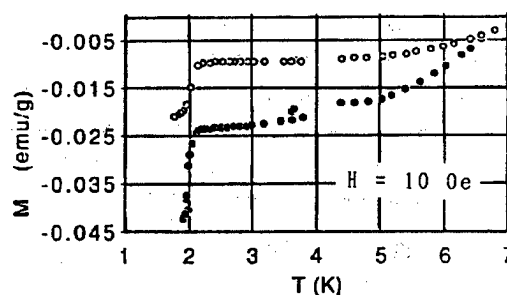


Fig.4 Temperature dependence of the magnetization M of a sample annealed at about 108K for 200 hr. The open and closed circles denote results for the Meissner and the shielding-current signals, respectively.



and then cooled it down with the speed of 1K/min and in the field of 180 or 10 Oe. For the annealing time of 20, 40 and 65 hr we found the onset of the Meissner effect at about 4.5, 6 and 7K, respectively. Figure 4 shows an example of the measured magnetization for the annealing time of 200 hr as a function of temperature. One finds two superconducting states whose critical temperatures are 7K and 2K. The nominal magnitude of the diamagnetic susceptibility reaches 3.3 and 8.3% of the perfect diamagnetism for the 7K- and 2K-states, respectively. It is to be noted that the applied field is more intense than the lower critical field  $H_{C1}$ , and no correction of the demagnetization field is made because of the irregular shape of samples. When these ambiguities are taken into consideration, the result of Fig.4 suggests strongly the presence of two phases of bulk superconductivity.

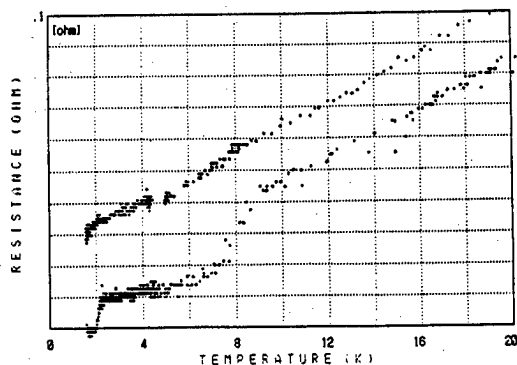


Fig.5 Temperature dependence of the resistivity of a sample cooled without annealing and after the annealing at 108K for 100 hr.

Resistivity of samples was found to decrease with time during the annealing at 108K. The decrement reaches 5% of the resistivity in 30 hr and is found to saturate after this. Figure 5 shows the superconducting transition in resistivity of samples with and without annealing. It is evident that a part of the sample becomes superconducting at about 7K and the remaining at about 2K, both of which are higher than the "low  $T_c$ " of samples cooled by a conventional speed.

We expect that also the sample under pressure, say, the sample cooled down along the line A of Fig.1, will become superconducting near 8K. The reason is that the sample state in this pressure range and below about 100K has been proposed to belong to the "high- $T_c$ " state.[5]

It has been conjectured [7] that the intrinsic critical temperature of this compound is that of the "high- $T_c$ " state and the onset of the superconductivity is suppressed in the "low- $T_c$ " state by some disorder. The possible disorder has been ascribed to the twisting degree of freedom of ethylene groups at both ends of a BEDT-TTF molecule shown in Fig.6. It is known that the twisting makes the so-called "A-type" and "B-type" of molecules. At ambient pressure both of them appear to be present and they are assumed to undergo an ordering incorporated in the incommensurate superstructure formed by translational motion of both BEDT-TTF and  $I_3$  molecules. Presence of disorder in the arrangement of the A- and B-types is inevitable because of the incommensurability of the superstructure. In the pressure range above about 0.4kbar we found actually no superstructure, and all the ethylene groups have been found to be in the A-type at least at 9.5kbar and room temperature, [8] and at 1.5kbar and 4.5K.[9]

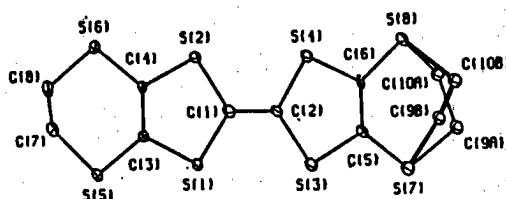


Fig.6 Structure of a BEDT-TTF molecule. The ethylene group at the right end has one of two conformations, A or B.

Our present result provides more direct support to the above conjecture by showing a correlation between the changes of the superstructure and of the superconducting critical temperature. It remains to be investigated, however, what kind of ordering of the ethylene groups is responsible for the two superconducting states created by annealing. Furthermore it is unclear whether or not the 7K-superconducting state has still the superstructure while the 2K-state has, because the x-ray results are dominated by the latter having the much larger fraction of sample volume.

In conclusion we found that the wave vector of the incommensurate superstructure becomes short below about 100K although the changing speed is largely depending on pressure. When this structural changes is completed, the sample is found to have two superconducting states whose critical temperatures are 7K and 2K, both of which are higher than that of samples cooled by an ordinary speed. Present results provide a more direct evidence for the speculation that the "low- $T_c$ " state of this compound is dominated by disorders presumably of ethylene groups.

Details of the present study will be published soon. [10,11]

#### Acknowledgements

We have benefited from useful interactions with T.Yagi, H.Takahashi, W.Utsumi and M.Tanaka of University of Tokyo.

#### REFERENCES

1. K.Murata, M.Tokumoto, H.Anzai, H.Bando, G.Saito, K.Kajimura & T.Ishiguro: J.Phys. Soc.Jpn., 54 (1985) 2084.
2. V.N.Laukhin, E.E.Kostyuchenko, Y.V.Sushko, I.F.Schegolev & E.B.Yagubskii: JETP Lett., 41 (1985) 81.
3. P.C.W.Leung, T.J.Emge, M.A.Beno, H.H.Wang & J.M.Williams: J.Am.Chem.Soc., 106 (1984) 7644.
4. W.Kang, G.Creuzet, D.Jerome & C.Lenoir: J.Physique, 48 (1987) 1035.
5. I.F.Schegolev: Japan.J.Appl.Phys., 26, Suppl. 26-3 (1987) 1972. V.B.Ginodman, A.V.Gudenko, P.A.Kononovich, V.N.Laukhin & I.F.Schegolev: to be published in J.Mol.Elec.
6. S.Ravy, J.P.Pouget, R.Moret & C.Lenoir: to be published in Phys.Rev.B.
7. See for example, A.J.Schultz, M.A.Beno, H.H.Wang & J.M.Williams: Phys.Rev., B33 (1986) 7823.
8. V.N.Molchanov, R.P.Shibaeva, V.F.Kaminskii, E.B.Yagubskii, V.I.Simonov & B.K.Vainshtein: Dokl.Akad.Nauk.USSR, 286 (1986) 637.
9. A.J.Schultz, H.H.Wang & J.M.Williams: J.Am.Chem.Soc., 108 (1986) 7853.
10. S.Kagoshima, Y.Nogami, M.Hasumi, H.Anzai, M.Tokumoto, G.Saito and N.Mori: to be published in Solid State Commun.
11. Y.Nogami, S.Kagoshima, N.Mori, H.Anzai & G.Saito: in preparation.

# CRYSTAL GROWTH AND SUPERCONDUCTIVITY OF MIXED CRYSTALS OF $\beta$ -(BEDT-TTF)<sub>2</sub>TRIHALIDES

Hiroyuki ANZAI, Madoka TOKUMOTO, Kazuhiro TAKAHASHI, Keizo MURATA,  
Nobumori KINOSHITA, Hiroshi BANDO and Takehiko ISHIGURO\*

Electrotechnical Laboratory, 1-1-4 Umezono, Tsukuba, Ibaraki 305, Japan

Mixed crystals of  $\beta$ -(BEDT-TTF)<sub>2</sub>X, where  $X=(I_3)_{1-x}(IBr_2)_x$ ,  $(IBr_2)_{1-x}(I_2Br)_x$  and  $(IBr_2)_{1-x}(I_3)_x$ , with a wide range of anion composition(x) were grown by electrocrystallization. The entire scheme of the phase diagram connecting the two superconductors, one ( $\beta$ -I<sub>3</sub> salt) with high- and low- $T_c$  states and the other ( $\beta$ -IBr<sub>2</sub> salt) with intermediate  $T_c$ , is described. Strong correlation between the superconductivity and the residual resistivity was found, leading to a systematic understanding of the whole scheme in terms of Anderson localization in the weakly localized regime.

## INTRODUCTION

Since the first discovery in 1980, about thirty organic superconductors have been reported so far out of the charge transfer salts. Among them, BEDT-TTF salts are outstanding due to the record-high  $T_c$  among organic superconductors. We carried out growth of mixed crystals of  $\beta$ -(BEDT-TTF)<sub>2</sub>(I<sub>3</sub>)<sub>1-x</sub>(IBr<sub>2</sub>)<sub>x</sub>,  $\beta$ -(BEDT-TTF)<sub>2</sub>(IBr<sub>2</sub>)<sub>1-x</sub>(I<sub>2</sub>Br)<sub>x</sub> and  $\beta$ -(BEDT-TTF)<sub>2</sub>(I<sub>2</sub>Br)<sub>1-x</sub>(I<sub>3</sub>)<sub>x</sub>, for a wide composition range by electrocrystallization. These anions were chosen since I<sub>3</sub>, I<sub>2</sub>Br and IBr<sub>2</sub> anions are chemically similar to each other, and crystals of  $\beta$ -type (BEDT-TTF)<sub>2</sub>trihalides, i.e. (BEDT-TTF)<sub>2</sub>X (X=I<sub>3</sub>, I<sub>2</sub>Br, IBr<sub>2</sub>) are isostructural organic metals and constitute a binary alloy system including the two superconductors, one ( $\beta$ -I<sub>3</sub> salt) with high(8 K) and low(1 K) $T_c$  states and the other ( $\beta$ -IBr<sub>2</sub> salt) with intermediate  $T_c$ , and a non-superconducting metal ( $\beta$ -I<sub>2</sub>Br salt). In this paper, the growth of mixed crystals and the effect of anion size and disorder on the superconductivity is presented.

## CRYSTAL GROWTH AND CHARACTERIZATION

Since BEDT-TTF reacts with Bu<sub>4</sub>NX in some organic solvents, we must select suitable organic solvents for crystal growth that do not promote the reaction of BEDT-TTF with supporting electrolyte before electrolytic oxidation. The crystal growth of (BEDT-TTF)<sub>2</sub>(X<sub>1</sub>)<sub>x</sub>(X<sub>2</sub>)<sub>1-x</sub> was carried out in a solution of 0.52x m mol Bu<sub>4</sub>X<sub>1</sub>, 0.52(1-x) m mol Bu<sub>4</sub>NX<sub>2</sub> and 0.13 m mol BEDT-TTF dissolved in about 60 ml of an organic solvent, where x corresponds 0.01, 0.05, 0.25, 0.50, 0.75, 0.95 or 0.99[1]. The mixed crystals having a wide composition of anions were obtained from only nitrobenzene for X<sub>1</sub>=IBr<sub>2</sub> and X<sub>2</sub>=I<sub>3</sub>, from only chlorobenzene for X<sub>1</sub>=I<sub>2</sub>Br and X<sub>2</sub>=I<sub>3</sub>, and from only THF for X<sub>1</sub>=I<sub>2</sub>Br and X<sub>2</sub>=IBr<sub>2</sub> respectively, and the crystals having such wide composition of anions were not obtained from other organic solvents[1]. Thus organic solvents have been found to show severe selectivity for the growth of mixed crystals between BEDT-TTF and trihalides. The composition of anions in the obtained crystals was evaluated using the atomic ratio of bromine and iodine determined by radioactivation analysis. In the crystal of (BEDT-TTF)<sub>2</sub>X, several structural varieties are known including  $\alpha$ - and  $\beta$ -types for X=I<sub>3</sub>, I<sub>2</sub>Br and IBr<sub>2</sub>. Figure 1 shows the distribution of determined crystal structures. In grown crystals, the structures of I<sub>3</sub> rich crystals were either of  $\alpha$ - or  $\beta$ -types, I<sub>2</sub>Br rich crystals were of  $\beta$ -type, and IBr<sub>2</sub> rich crystals were either of  $\alpha$ - or  $\beta$ -types. The structures of mixed crystals were also determined by utilizing the difference in the ESR linewidth between  $\beta$ -type and other types. The lattice parameters of mixed crystals were determined using an automated 4-circle X-ray diffractometer. Figure 2 shows that the lattice parameters (BEDT-TTF)<sub>2</sub>(X<sub>1</sub>)<sub>x</sub>(X<sub>2</sub>)<sub>1-x</sub>

\* Present Address: Department of Physics, Faculty of Science, Kyoto University, Kyoto 606, Japan

change with  $x$  continuously as we expected. Thus the mixed crystals are useful for studies of lattice parameter dependence of the physical properties of  $\beta$ -(BEDT-TTF) $_2$ X which shows the drastic pressure dependence. Actually, it was found in the compound  $\beta$ -(BEDT-TTF) $_2$ (I $_3$ ) $_x$ (IBr $_2$ ) $_{1-x}$  that the incommensurate superstructure which took place below 175 K and was related to the two superconducting states of  $\beta$ -(BEDT-TTF) $_2$ I $_3$  was suppressed by alloying.[2,3]

### ELECTRICAL AND SUPERCONDUCTING PROPERTIES

Figure 3 shows the temperature dependence of resistance for (a)  $\beta$ -(BEDT-TTF) $_2$ X (X=I $_3$ , I $_2$ Br, IBr $_2$ ) and their 1:1 mixed crystals, and (b) mixed crystals  $\beta$ -(BEDT-TTF) $_2$ (I $_3$ ) $_{1-x}$ (IBr $_2$ ) $_x$ . These temperature dependences indicate that the mixed crystals of (BEDT-TTF)-trihalides constitute a clean alloy system, where the scattering of conduction electrons are predominantly due to phonons at temperatures above 100 K, even in high concentration alloys, and the effect of alloying on the resistivity appears only as a residual resistivity at very low temperatures. Figure 4 shows the residual conductivity ( $\sigma_R$ ) and superconducting transition temperature ( $T_C$ ) for mixed crystals  $\beta$ -(BEDT-TTF) $_2$ (I $_3$ ) $_{1-x}$ (IBr $_2$ ) $_x$ ,  $\beta$ -(BEDT-TTF) $_2$ (IBr $_2$ ) $_{1-x}$ (I $_2$ Br) $_x$  and  $\beta$ -(BEDT-TTF) $_2$ (I $_2$ Br) $_{1-x}$ (I $_3$ ) $_x$ . The residual conductivity( $\sigma_R$ ) of each alloy sample was evaluated from the relation  $\sigma_R = RRR \times \sigma_0(rt)$ , where RRR is the residual resistance ratio and  $\sigma_0(rt) = 20$  S/cm[2]. Samples with composition near the I $_3$  salt have two  $T_C$ 's. Open and closed circles indicate superconducting and nonsuperconducting (i.e.  $T_C < 0.5$  K) samples, respectively. The dashed line corresponds to an empirically found border line between the superconducting and nonsuperconducting samples, indicating that a minimum residual conductivity of  $\sigma_R$  (=6000 S/cm) is necessary for superconducting samples[2,3]. Note that the absence of superconductivity in the pure I $_2$ Br salt is also consistent with this criterion, since the value of  $\sigma_R$  is somewhat less than the critical value, as shown in Fig. 4. Also, the pressure effect on the normal and superconducting properties of these alloys did not violate this criterion as shown in Fig.3(c)[4]. The observed close correlation between residual resistivity and superconductivity opens a possibility that the suppression of  $T_C$  by alloying is related to the effect of Anderson localization. Moreover, the value of critical conductivity given above was found to be in good agreement with the theory by Hasegawa and Fukuyama based on the Anderson localization in the weakly localized regime[5].

### CONCLUSIONS

The mixed crystals of (BEDT-TTF) $_2$ (X $_1$ ) $_x$ (X $_2$ ) $_{1-x}$  (X $_1$  and X $_2$  are I $_3$ , I $_2$ Br or IBr $_2$ , but X $_1 \neq$  X $_2$ ) were grown successfully with a wide composition range of these anions. We found that, in order to obtain the mixed crystals between BEDT-TTF and trihalides, it is very important to select suitable organic solvents. Mixed crystals, or alloying, among organic metals  $\beta$ -(BEDT-TTF) $_2$ -trihalides enabled us to realize a continuous control of lattice parameters. The mixed crystals of (BEDT-TTF)-trihalides constitute a clean alloy system. The potential disorder introduced in the anion sheet by alloying, which manifests as an increased residual resistance at low temperature, strongly suppresses the  $T_C$  in  $\beta$ -(BEDT-TTF) $_2$ X. Close correlation between superconductivity and residual conductivity was found in  $\beta$ -(BEDT-TTF) $_2$ X, leading to a systematic understanding of the whole scheme in terms of Anderson localization.

### REFERENCES

- [1] H. Anzai, M. Tokumoto, K. Takahashi and T. Ishiguro, J. Cryst. Growth. **91** (1988) 225.
- [2] M. Tokumoto, H. Anzai, K. Murata, K. Kajimura and T. Ishiguro, Jpn. J. Appl. Phys. **26** (1987) Suppl. 26-3, 1977.
- [3] M. Tokumoto, H. Anzai, K. Murata, K. Kajimura and T. Ishiguro, Proc. ICSM'88, Santa Fe.
- [4] K. Murata, M. Tokumoto, H. Anzai, Y. Honda, N. Kinoshita, T. Ishiguro, N. Toyota, T. Sasaki and Y. Muto, Proc. ICSM'88, Santa Fe.
- [5] Y. Hasegawa and H. Fukuyama: J. Phys. Soc. Jpn., **55** (1986) 3717.

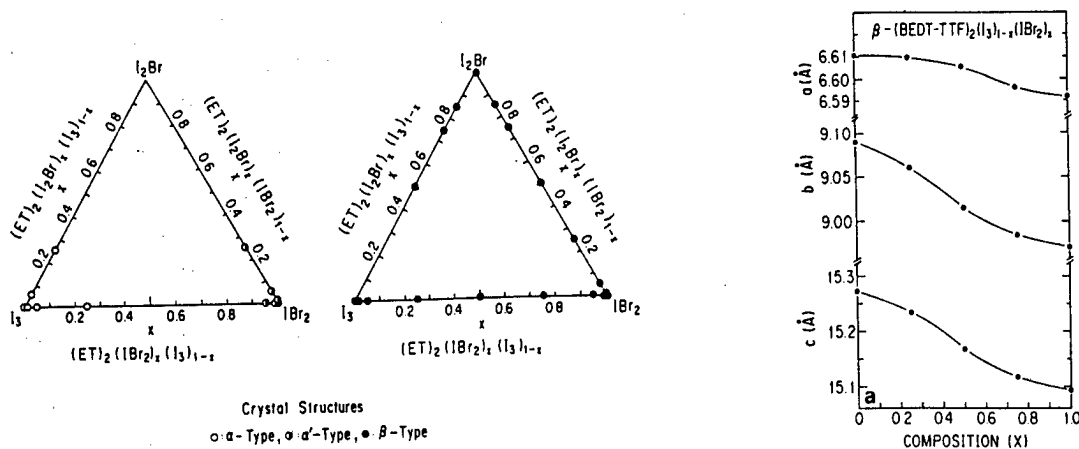


Fig.1.(left) Distribution of crystal structures of grown mixed crystals.  
Fig.2.(right) Lattice parameters of single crystals of  $\beta-(BEDT-TTF)_2(I_3)_{1-x}(I_2Br)_x$ .

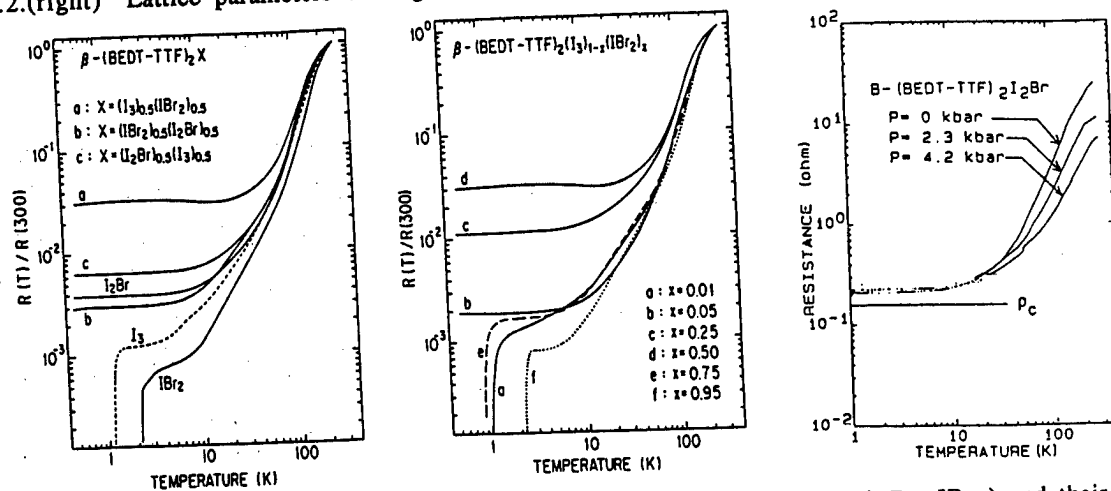


Fig.3. Temperature dependence of resistance. (a)  $\beta-(BEDT-TTF)_2X$  ( $X=I_3, I_2Br, IBr_2$ ) and their 1:1 mixed crystals. (b)  $\beta-(BEDT-TTF)_2(I_3)_{1-x}(IBr_2)_x$ . (c) pressure effect on  $\beta-(BEDT-TTF)_2I_2Br$ .

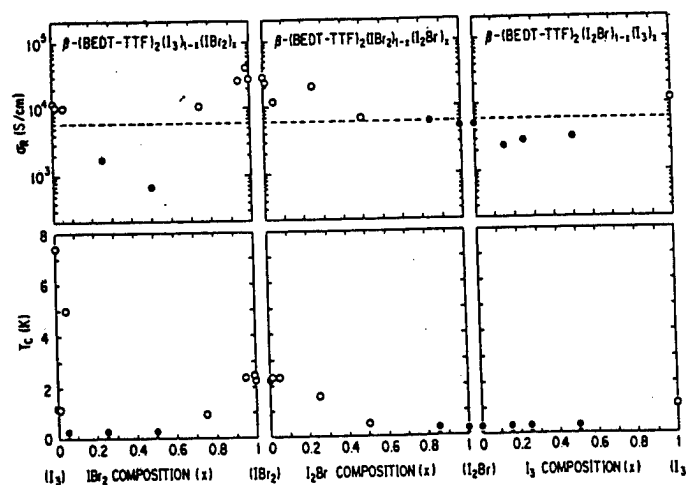


Fig.4. Residual conductivity ( $\sigma_R$ ) and  $T_C$  for mixed crystals  $\beta-(BEDT-TTF)_2(I_3)_{1-x}(IBr_2)_x$ ,  $\beta-(BEDT-TTF)_2(IBr_2)_{1-x}(I_2Br)_x$  and  $\beta-(BEDT-TTF)_2(I_2Br)_{1-x}(I_3)_x$ . Samples with composition near the  $I_3$  salt have two  $T_C$ 's. Closed circles indicate nonsuperconducting (or  $T_C < 0.5$  K) samples.

K. Kajita, Y. Nishio, T. Takahashi, W. Sasaki, R. Kato, H. Kobayashi,  
 Faculty of Science, Toho University,  
 Miyama 2-2-1, Funabashi 274  
 A. Kobayashi,  
 Department of Chemistry, Faculty of Science, The University of Tokyo,  
 and Y. Iye,  
 ISSP, The University of Tokyo

Anomalous magnetotransport phenomena have been observed in  $\theta$ -(BEDT-TTF) $_2$ I $_3$  crystals at temperatures below 15K. The magnetoresistance  $M$  is not affected by the angle between the electric current and the magnetic field, but depends on the magnetic field orientation with respect to the crystal axis. Magnetoresistance at low magnetic field is expressed as  $M = (aH_a^2 + bH_b^2 + cH_c^2)\rho_0^{-3/2}/H$  in terms of  $H = (H_a, H_b, H_c)$ , the zero field resistivity  $\rho_0$ , and parameters  $a, b, c$  ( $b \gg a > c$ ) which are independent of temperature and magnetic field.

In the high magnetic field region, we have found another anomalous magnetoresistance. It appears as an oscillation of the magnetoresistance against the magnetic field direction.

## 1. LOW FIELD MAGNETORESISTANCE

Similarly to other type crystals of (BEDT-TTF) $_2$ I $_3$ , an  $\theta$ -type crystal is composed of two different molecular layers piled up alternatively. On one layer are BEDT-TTF molecules and on the other layer are I $_3$  molecules.

The conductive carriers are holes on BEDT-TTF molecules. A tight binding band calculation gives a cylindrical energy spectrum with the Fermi surface open in two directions[1].

Reflecting the two dimensionality of the crystal, it exhibits neither CDW nor SDW phase transitions. The resistivity decreases monotonically with the decreasing temperature down to 3.6K where some crystals undergo superconducting transition[2].

In this experiment, the magnetic field effect on the resistivity is studied in the temperature region below 15K. The magnetotransport phenomenon in this material is unusual in that the magnetoresistance  $M \equiv \Delta\rho/\rho_0$  is a linear function of the magnetic field and that the crucial parameter which determines  $M$  is not the angle between the magnetic field and the current but it is the orientation of the magnetic field with respect to the crystal axis.

From the measurement of  $M$  for various magnetic field orientation shown in Fig.2,  $M$  is found to be written as,  $M = (AH_a^2 + BH_b^2 + CH_c^2)/H$ . Here,  $H_a, H_b, H_c$  are magnetic field components along the  $a$ -,  $b$ - and  $c$ - crystal axes ( $ab$ -plane is the conductive plane), respectively, and  $A, B$  and  $C$  are parameters which depend on temperature and the sample character. Magnetic field  $H$  in the denominator is put into the equation so that the equation expresses not only the angle dependence of  $M$  but also the fact that  $M$  is a linear function of the magnetic field.

Examining the temperature dependence of  $M$ , we found that it is related to the temperature through the change in the zero field resistivity  $\rho_0$ . Figure 3 gives a relation  $M \propto \rho_0^{-3/2}$  at temperatures below 10K.

Thus, the final form of  $M$  is given as

$$M = (aH_a^2 + bH_b^2 + cH_c^2) \rho_0^{-3/2} / H,$$

where  $a, b, c$  are parameters independent of the temperature and the magnetic field. The ratio of parameters obtained from the experiment in Fig.1 is  $b:a:c=2:0.7:0.5$ .

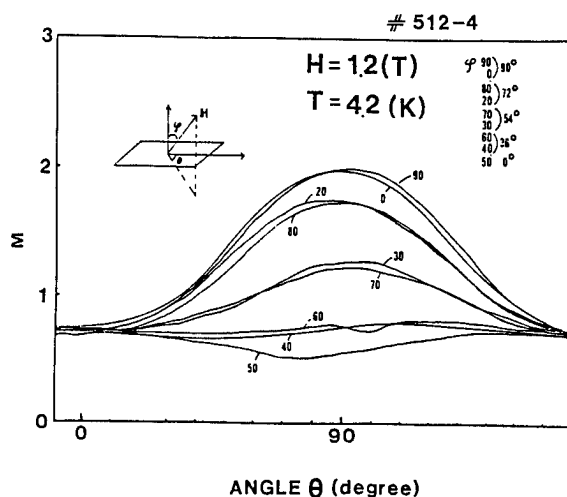


Fig.1 Magnetoresistance against the magnetic field direction.

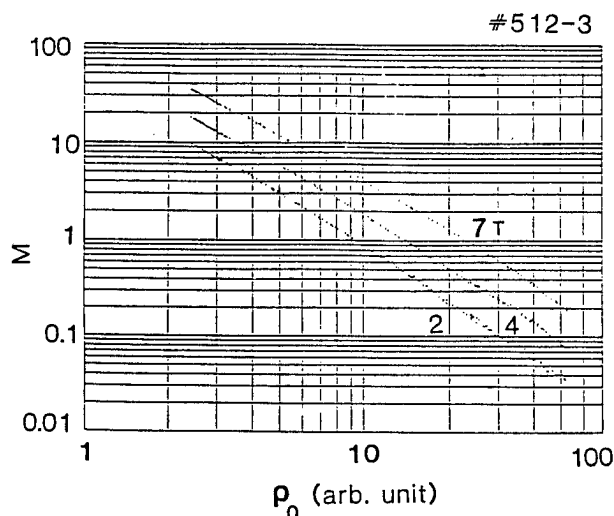


Fig.2 Magnetoresistance in the field parallel to the b-crystal axis is plotted against zero field resistivity.

## 2. HIGH FIELD MAGNETORESISTANCE

In the high magnetic field region above 3T and at low temperatures below 5K, another anomalous magnetoresistance appears. In the orientation dependence of  $M$  shown in Fig.3, a low magnetic field gives a sine curve (for an example, see the curve for  $H=2T$ ), which is represented by the equation obtained in Sec.1, while in the high field region above 3T, a characteristic oscillation appears. This oscillatory phenomenon is quite a new type and has no connection with the well known Schubnikov de Haas oscillation. It is most evidently shown by the fact that  $M$  does not oscillate against the strength of the magnetic field but it does against the magnetic field direction.

It is noted that the positions of the tops and bottoms of oscillation do not move with increasing magnetic field. Thus, it seems that the magnetic field strength does not work in determining the oscillation period.

The oscillatory part of the magnetoresistance is given in Fig.4 in a  $M-\tan(\theta)$  scheme. In this plot, the bottoms of the curve appears with equal spacing of about 0.42, which indicates that the positions of bottoms are given by an equation  $\tan(\theta) = s \times N$  ( $s=0.42, N=0,1,2,\dots$ ).

Although such a  $\tan(\theta)$  dependent magnetotransport phenomenon is not familiar to us, we believe that this analysis indicates the right way to understand the phenomena, because it is consistent with the fact that the period of the oscillation is independent of the magnetic field strength. The period is related to  $\tan(\theta) = H_c/H_a$  which is a parameter indicating the magnetic field orientation.

On the other hand, the amplitude of the oscillation is not a function of  $\tan(\theta)$  but is a function of the magnetic field normal to the conductive plane. The amplitude depends also on the temperature. The temperature seems to affect the amplitude through the zero field resistivity.

Two types of the anomalous magnetoresistance discussed here resembles in two points: The first is that the geometrical configuration of the magnetic field is important and the second is that the amplitude of  $M$  is related to the zero field resistivity. Thus, the origin of these phenomena are likely to be the same. The phenomena can never be explained in a simple scheme in which two dimensional electron energy spectrum is considered and, thus, some three dimensionality should be taken into consideration.

In this crystal, BEDT-TTF molecules are aligned on a plane with their long side being normal to the plane and two different transfer paths of electrons exist between BEDT-TTF molecules. This may give rise to a three dimensionality in this system.

#### References

- [1] A.Kobayashi et. al., Chem. Letters 2017 (1986).
- [2] K.Kajita et. al., Solid State Commun. 64 1279(1987).

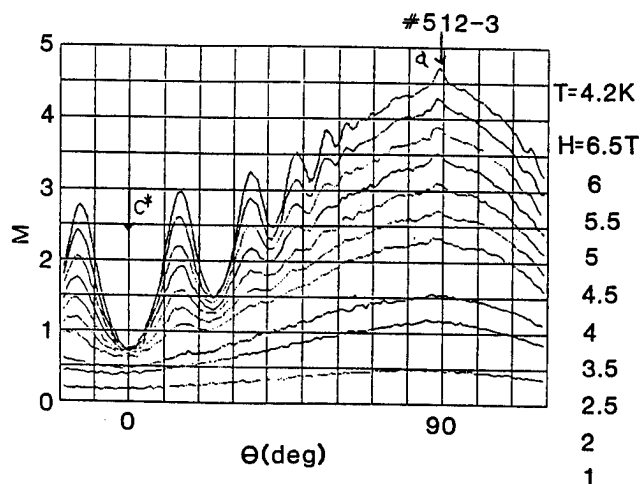


Fig.3 Magnetoresistance against the magnetic field direction which is rotated in the ac-plane

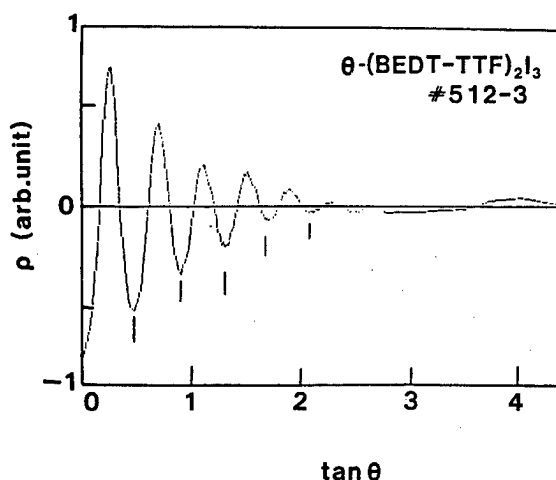


Fig.4 Oscillatory part of the magnetoresistance derived from the data in Fig.3.



G. SAITO, H. URAYAMA, H. YAMACHI

The University of Tokyo, Institute for Solid State Physics, 7-22-1 Roppongi Minato-ku Tokyo, Japan 106

K. OSHIMA

The University of Tokyo, Cryogenic Center, 2-11-16 Yayoi Bunkyo-ku Tokyo, Japan 113

(present address: Okayama University, Department of Physics, 3-1-1 Tsushimanaka, Okayama, Japan 700)

An overview of the chemical and physical properties of a new organic superconductor  $\kappa$ -(BEDT-TTF)<sub>2</sub>Cu(NCS)<sub>2</sub>, of which T<sub>c</sub> (10.4-11.0K) is the highest among those of organic superconductors so far known, is presented. Distorted-hexagon-shaped crystals of the Cu(NCS)<sub>2</sub> salt were prepared by the electrochemical oxidation of BEDT-TTF in 1,1,2-trichloroethane in the presence of CuSCN, KSCN, and 18-crown-6 ether (or K(18-crown-6 ether)Cu(NCS)<sub>2</sub> complex, or CuSCN and TBA·SCN, as a supporting electrolyte) under a constant current of 1-5  $\mu$ A. The black shiny crystals were stable towards air and moisture and start to decompose above 190°C. The crystal structure analyses indicate that both dextro- and levorotatory optical isomers are present and the absolute crystal structures of both isomers were determined. The specific rotatory power is about 230° at 25°C and 632.8nm. T<sub>c</sub> of the BEDT-TTF-h<sub>8</sub> salt is 10.2-10.4K by four-probe dc resistivity measurements and T<sub>c</sub> decreases with increasing pressure. An inverse isotope effect was observed in our samples so far measured (more than seven each samples). By four-probe method T<sub>c</sub> of the deuterated samples was observed at 10.8-11.0K. The inverse isotope effect was confirmed by the RF penetration depth measurements. Magnetic susceptibility indicates that the salt is non-ideal class II superconductor and almost 100% of the perfect diamagnetism was observed below 7K at 0.3 Oe by the ac susceptibility measurements. The estimated anisotropy in the GL coherence length from the critical field near T<sub>c</sub> is  $\xi_{bc}(0) : \xi_{a^*}(0) = 182\text{\AA} : 9.6\text{\AA} = 19:1$ . The Shubnikov-de Haas signal with the period of  $0.0015\text{T}^{-1}$  was observed below 1K and above 8T. The period corresponds to the area of extremal orbit of 18% of the first Brillouin zone. The anisotropic nature of the thermoelectric power of the crystal in the 2D plane can be explained on the basis of the complicated Fermi surface. No EPR signal ascribed to Cu<sup>2+</sup> was observed. The linewidth of the EPR signal of BEDT-TTF<sup>+</sup> increased monotonically with decreasing temperature in contrast to the predictions of the Elliot formula for the spin relaxation in metals. A Korringa relation was observed in <sup>1</sup>H NMR measurements between 77K and 10K. Below 10K a big enhancement of the relaxation rate was observed with a peak at considerably lower temperature than T<sub>c</sub>. Anisotropic superconducting gaps were detected by tunneling spectroscopic work.

#### CRYSTAL GROWTH

Distorted-hexagon-shaped crystals of Cu(NCS)<sub>2</sub> salt (3x2x0.05mm<sup>3</sup>) were prepared by the electrochemical oxidation of BEDT-TTF. BEDT-TTF was purified by recrystallization from chloroform, THF, then monochlorobenzene (mp. 256-258°C). 18-Crown-6 ether was recrystallized from CH<sub>3</sub>CN. KSCN was recrystallized from abs. EtOH. Crude CuSCN showed an EPR signal due to Cu<sup>2+</sup> which was eliminated by treatment with aq. KSCN solution, but the Cu(NCS)<sub>2</sub> salt of BEDT-TTF prepared using either crude or purified CuSCN gave almost the same EPR and conductivity results. TBA·SCN was prepared from TBA·Br and KSCN and dried. K<sup>+</sup>(18-crown-6 ether)Cu(NCS)<sub>2</sub><sup>-</sup> complex (abbreviated to K(crown)Cu(NCS)<sub>2</sub>) was recrystallized from acetone-water, washed with acetone and dried. We used three kinds of supporting electrolytes; 1. K(crown)Cu(NCS)<sub>2</sub>, 2. CuSCN+KSCN+crown, 3. CuSCN+TBA·SCN, to prepare single crystals, and whichever we took the same kind of crystals was obtained so far in our group. The solvents were 1,1,2-trichloroethane, 1,2-dichloroethane, monochlorobenzene, THF, etc. and they gave the same kind of crystals. In the cases of electrolyte 2 or 3, undissolved materials remained on the bottom of the cell during the course of the electrocrystallization but the precipitation did not affect the crystal growth.

The single crystals were harvested within 1-3 weeks, washed with appropriate solvent and dried. The crystals were stable towards light, air and moisture. No change in DSC, TG, and DTG was observed between -130 C-190°C. The crystals decomposed at around 230°C with gas evolution.

#### CRYSTAL AND BAND STRUCTURES

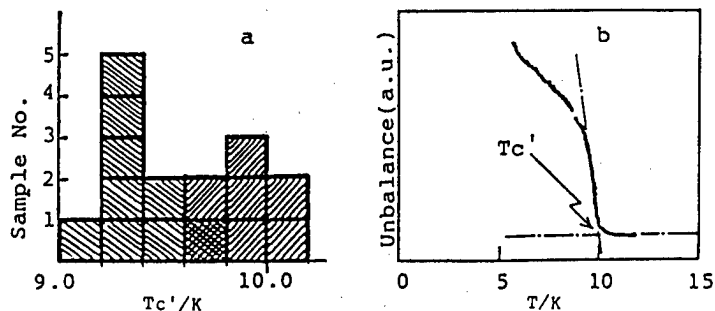
The crystal structures of this salt are very similar to that of  $\kappa$ -I<sub>3</sub> salt. Namely, two BEDT-TTF molecules form a dimerized pair and the pairs are linked one another almost perpendicularly. There are short intra- and interdimer sulfur-sulfur atomic contacts, so the donor molecules construct two-dimensional (2D) conducting sheets in the bc-plane. Every conducting layer is sandwiched by the insulating layers of anion along the a-axis and these different kinds of layers are linked to each other by short C-H(ethylene)...N and C-H(ethylene)...S(anion) atomic contacts. It is not clear the role of these short contacts in the superconductivity though the substitution of hydrogen atoms of BEDT-TTF with deuterium atoms caused T<sub>c</sub> higher by about 0.5-0.6K. The anion Cu(NCS)<sub>2</sub> is neither symmetric nor linear but asymmetrically bent like a boomerang and forms an infinite chain polymer -SCN-Cu-SCN- with a coordination of a pendant -NCS. Every polymers lie in the same direction to form an insulating layer in the bc-plane. Therefore the crystal does not have an inversion center and is optically active. The optical isomerism of this salt was examined. Ten dextrorotatory isomers were found out of 13 single crystals examined and the specific rotatory power of the crystal is about 230° (25 °C, 632.8nm). The absolute crystal structures of the dextro- and levorotatory isomers were determined.

The Fermi surface of the Cu(NCS)<sub>2</sub> salt is composed of two different ones; one is a closed cylindrical 2D surface and the other is a modulated 1D open surface.

#### TRANSPORT PROPERTIES

The dc electrical conductivity along the b-axis at room temperature is 10-40 Scm<sup>-1</sup> by four-probe method and the conductivity ratio is  $\sigma_a:\sigma_b:\sigma_c=1/600:1:1.2$ . T<sub>c</sub> of the salt of BEDT-TTF-h<sub>8</sub> (H salt) is 10.2-10.4K and the T<sub>c</sub> decreases with increasing pressure (-1.3K/kbar). An isotope effect on T<sub>c</sub> was studied by using deuterated BEDT-TTF-d<sub>8</sub> (99.8%). By 4-probe method T<sub>c</sub> of the D-salt was observed at 10.8-11.0K (T<sub>c</sub> of 11.1K was claimed by German group later). Since 4-probe method needs electrical contacts which might cause pressure effect on T<sub>c</sub>, we have compared the superconducting transition of H- and D-salts by RF penetration depth measurements ( Fig.1) where T<sub>c</sub>' is defined by the cross point of the base line and the straight line of the slope. Therefore T<sub>c</sub>' is significantly smaller than T<sub>c</sub> obtained by the resistive transition. The average T<sub>c</sub>' of nine H-salts was 9.3K and that of seven D-salts was 9.9K. As far as our samples concern an inverse isotope effect by 0.5K on T<sub>c</sub> was observed so far measured.

Fig.1. Scatter(a) in T<sub>c</sub>' for the deuterated(▨) and undeuterated (▩) samples of  $\kappa$ -(BEDT-TTF)<sub>2</sub> Cu(NCS)<sub>2</sub> determined by RF penetration depth measurements(b).



Below 1K and above 8 Tesla Shubnikov-de Haas (SdH) oscillation was observed in the transverse magnetoresistance curve. The oscillation of  $\Delta(1/H)=0.0015\text{T}^{-1}$  (for both H and D-salts) corresponds to the area of the extremal orbit of  $S=6.37\times 10^{14}\text{cm}^{-2}$  from  $S=2\pi e/\Delta(1/H)\hbar c$ . Since the area of the first Brillouin zone is  $1/bc=3.56\times 10^{15}\text{cm}^{-2}$ , the area of the extremal orbit corresponds to 18% of the first Brillouin zone, which is quantitatively equal to that of the calculated cylindrical Fermi surface. Moreover, the calculated Fermi surface is in good agreement with the observed thermopower qualitatively. The cylin-

drical Fermi surface is hole-like and the modulated open Fermi surface is electron-like. These complicated nature of the Fermi surface may result in the anisotropic thermopower which is positive along the c-axis and negative along the b-axis just as observed, though a simple consideration of the chemical formula indicates that the carrier is only hole (carrier density  $n=1.18 \times 10^{21} \text{ cm}^{-3}$ ). The temperature dependence of the SdH oscillation gave an effective mass at the Fermi level as  $m^*/m_0=3.5$  in accordance with those derived from optical measurements (4.0 and 3.0 along the b- and c-axes, respectively). A considerably small effective mass of  $m^*/m=2.4$  was obtained at 8 kbar.

#### MAGNETIC AND OTHER PROPERTIES

The dc magnetic susceptibility on polycrystalline sample (30 KOe) showed that almost constant (with slight decrease at ca. 90K) Pauli paramagnetism of  $\chi_p=4.1-4.6 \times 10^{-4} \text{ emu/mol}$  between room temperature and about 10K. From the room temperature value the density of states per formula unit for a single spin is calculated as  $N(E_F)=7.1 \text{ eV}^{-1}$  by the relation  $\chi_p=2\mu_B N_A N(E_F)[1-(1/3)(m/m^*)^2]$  and neglecting the term of the Landau diamagnetism. By using the optical data and the relation  $N(E_F)=(m_b m_c)^{1/2}/(\pi a^2)$ , where  $a$  is the lattice spacing, a comparable value of  $N(E_F)=7.5 \text{ eV}^{-1}$  was obtained and the Fermi energy from the top of the band was estimated as 0.13eV by using  $E_F=\pi a^2/(m_b m_c)^{1/2}$ . The ac susceptibility on polycrystalline sample showed that  $T_c$  is  $10.3 \pm 0.4 \text{ K}$  and almost 100% of the perfect diamagnetism ( $-1/4\pi \text{ emu cm}^{-3}$ ) was observed below 7K at 0.3 Oe. No signal ascribed to  $\text{Cu}^{2+}$  was observed in ESCA at room temperature and EPR down to 4K. A broad Lorentzian signal due to BEDT-TTF<sup>+</sup> was observed in EPR with a cylindrical cavity (TE011). Additional sharp signal ( $\Delta H=10-20 \text{ G}$ ,  $g=2.0075$ ) appeared at the center of the broad signal below 30K. This sharp signal may be due to defect or contamination of another phase of  $\text{Cu}(\text{NCS})_2$  salt. Due to the broadening of the main signal and to the appearance of the sharp signal, accurate estimations of  $g$  values and line width ( $\Delta H$ ) were not possible below 20K. The constant  $g$ -values (2.0078-2.0070) down to 20K where the external magnetic field ( $H_0$ ) is normal to the bc-plane indicate that the molecular orientation of BEDT-TTF does not change substantially with respect to the crystal axis. The line width at room temperature was 61G and increased to about 80G at 110K smoothly. Then  $\Delta H$  increased more pronouncedly to 100G down to 30K followed by a rapid increase to 120G (20K). Since the electrical resistivity increases down to 90K, the increase of the line width can be explained by the increase of the scattering rate of conduction electrons in this region. The pronounced increase of  $\Delta H$  below 90K, especially below 30K, cannot be explained in terms of scattering rate since  $\Delta H$  does not follow the temperature dependence of the resistivity. So the EPR data are in contrast to the predictions of the Elliot formula,  $\Delta H \propto (\Delta g)^2 \times \tau_1^{-1}$  where  $\Delta g=g-2.0023$  and  $\tau_1$  is the interchain tunneling time, for the spin relaxation in metals. The EPR intensity obtained with polycrystals is almost constant ( $3.2 \times 10^{-4} \text{ emu/mol}$  at RT) down to 90K in good agreement with the d.c. susceptibility measurements.

In the  $^1\text{H}$  NMR measurements on polycrystals a Korringa relation was observed between 77K and 10K. The  $T_1 T$  value of this salt (about 1050 secK) is less than 2/3 of that of low  $T_c$   $\beta\text{-I}_3$  salt (1730 secK,  $T_c=1.5 \text{ K}$ ). From a relation of  $N(E_F) \propto (1/T_1 T)^{1/2}$ ,  $N(E_F)$  value of this salt is expected to be 1.28 times than that of the  $\beta\text{-I}_3$  salt. A big enhancement of relaxation rate  $T_1^{-1}$  was noticed with a peak at considerably lower temperature than  $T_c$ . The peak height is about 30 times than that of the normal state at 3.28KOe.

The superconducting gaps have been measured with a tunneling spectroscopic method on  $\text{Cu}(\text{NCS})_2$  salt/ $\text{Al}_2\text{O}_3/\text{Au}$  junctions. No reliable spectra was obtained at temperatures above 4.2K. Well below  $T_c$  the superconducting energy gap somewhat comparable to the BCS theory was detected ( $2\Delta=4 \text{ meV}$ ,  $2\Delta/kT_c=4.5$  vs. 3.52 for BCS ratio) for one sample. The other sample showed much smaller gap less than 1meV. Therefore at this stage we may postulate that the superconducting gaps of this salt are anisotropic.

**ACKNOWLEDGEMENTS** We would like to thank all our colleagues: K.Nozaawa, T.Sugano, M.Kinoshita, S.Sato, Y.Ishida, T.Yajima(ISSP), T.Mori, H.Inokuchi, T.Inabe, Y.Maruyama(IMS), S.Kagoshima(Univ. Tokyo), and T.Takahashi(Gakushuin Univ.).

T. Takahashi

Department of Physics, Gakushuin University  
Mejiro 1-5-1, Toshima-ku, Tokyo 171, Japan

<sup>1</sup>H-NMR relaxation rate  $1/T_1$  in the organic superconductor [bis(ethylenedithio)tetrathiafulvalene]<sub>2</sub>Cu(NCS)<sub>2</sub> was measured in the temperature range between 0.5 K and room temperature.  $1/T_1$  exhibits an enormous enhancement below  $T_c$ , forming a sharp peak around 4 K (at 3.28 kOe), and then decreases rapidly at lower temperatures. The peak value of  $1/T_1$  at the field of 3.28 kOe is 70 times as large as that given by the Korringa relation  $T_1T=1100$  secK above  $T_c$ . The enhancement is strongly field-dependent. Possible mechanisms responsible for this anomaly are discussed.

The nuclear spin-lattice relaxation rate  $1/T_1$  is a useful tool to probe the nature of the superconductivity. The best example is a recent work on (TMTSF)<sub>2</sub>ClO<sub>4</sub>, a typical salt of the first family of organic superconductors, (TMTSF)<sub>2</sub>X [1]: From the temperature dependence of zero field relaxation rate, this salt was found to be a gapless superconductor, where the energy gap vanishes along lines on the Fermi surface [2]. On the contrary, in the high- $T_c$  state of  $\beta$ -(BEDT-TTF)<sub>2</sub>I<sub>3</sub> of the other family of organic superconductors, a curious enhancement of  $1/T_1$  has been observed below the transition temperature  $T_c$ [3,4]. This phenomenon may be indicative of new feature of the superconductivity in this family, but has thus far no reasonable explanation. In this work, we have observed quite similar but much more pronounced enhancement of  $1/T_1$  in a 10K-organic superconductor, (BEDT-TTF)<sub>2</sub>Cu(NCS)<sub>2</sub> [5]. This clearly indicates that a strange relaxation mechanism never seen in conventional superconductors should exist in both compounds. We present the characteristics of the experimental results and some considerations on possible mechanisms.

The temperature dependence of  $1/T_1$  on a polycrystalline sample can be well described by a Korringa relation  $T_1T = 1.1 \times 10^3$  secK in the region between 10 K and 80 K. The value of  $1/(T_1T)$  is larger than that of the  $\beta$ -phase of I<sub>3</sub> salt by a factor of 1.6. Since  $1/(T_1T)$  is proportional to the square of the electronic density of states, we expect a slightly larger density of states (by 30%) in this salt than that of the  $\beta$ -I<sub>3</sub> salt. At higher temperatures, the contribution of ethylene vibrations becomes dominant. The frequency dependence of  $1/T_1$  is consistent with the usual BPP-type behavior.

Below 10 K, the <sup>1</sup>H-NMR relaxation rate  $1/T_1$  is significantly enhanced, as shown in Fig. 1.  $1/T_1$  forms a sharp peak around 4 K, at an applied field of 3.28 kOe, and then decreases rapidly at lower temperatures towards zero at absolute zero. As far as  $1/(T_1T)$  is concerned, the maximum of the enhancement with respect to the Korringa value of  $1/1100$  sec<sup>-1</sup>K<sup>-1</sup> amounts to about 70. Such an enormous enhancement is quite unusual and cannot be explained as a BCS superconductor. At higher fields, the enhancement of  $1/T_1$  is reduced and the peak position shifts slightly towards the lower temperature side (from 4 K at 3.28 kOe to about 3 K at 11.7 kOe). It is evident that the relaxation enhancement appears in the superconducting state. Since our sample is polycrystalline, the transition temperature in a magnetic field should differ from crystal to crystal due to the anisotropy of the critical field. At 3.28 kOe, for example, the maximum and the minimum of the transition temperature are expected as 10 K

and 8 K, respectively, considering the data of Oshima et al. [6]. The superconducting transition in the measured sample was actually monitored by rf penetration measurements in the same run. The maximum of the relaxation enhancement appears well below the transition region of our sample.

A quite similar behavior of NMR relaxation rate has been observed in the high- $T_c$  state of  $\beta$ -(BEDT-TTF) $_2$ I $_3$  [3,4], where  $T_c$  was slightly lower (6 ~ 8 K) and the enhancement of  $1/T_1$  was smaller than in the present salt. Most of the qualitative features described above are common in both compounds. Orsay group has suggested that the relaxation peak appears at  $T_c$  [3], while we found the peak position was much lower than  $T_c$ , as observed in the present salt, by a zero field measurement using a field cycling method [4]. They have discussed the effects of superconducting fluctuations in low dimensional systems, but the divergence of  $1/T_1$  in this model is expected at  $T_c$ , contrary to our observation.

The sharp maximum of  $1/T_1$  well below  $T_c$  may suggest the existence of another phase transition. If it is a real thermodynamic transition successive to the superconductivity, there should remain some other degrees of freedom in the superconducting ordered state. Hasegawa and Fukuyama have pointed out the possibility of superconducting glass transition in triplet superconductivity, where the order parameter should be a vector in spin space [7]. This picture cannot be ruled out at present, but we need more experimental evidence before discussing this possibility. It is also reminiscent of a magnetic transition, as the SDW transition observed in (TMTSF) $_2$ X family [8]. However, we have observed no appreciable change in the shape of the free induction decay signal, which should be sensitive to the magnetic ordering, throughout the measured temperature range. It means that the amplitude of SDW's, if any, should be much smaller than in (TMTSF) $_2$ X family [8].

We point out the possibility of phase transition in the superconducting state, that is, a vortex melting transition expected in two dimensional superconducting films under a perpendicular magnetic field [9]. Considering that the present system is quasi-two-dimensional and that the measurements were carried out in vortex states, the vortex melting might as well occur. For superconducting films, the melting temperature  $T_M$  is given as a function of sheet resistance,  $R$  [10]. If we assume the BEDT-TTF molecular layers as two-dimensional films,  $R$  per BEDT-TTF layer just above  $T_c$  is estimated as about 1.5 k $\Omega$  by reference to the conductivity data [5,6], yielding the melting temperature  $T_M$  of 2.7 K. This value obtained in the two dimensional limit is surprisingly close to the observed temperature giving the  $1/T_1$  anomaly. The difference and the observed field dependence may be caused by the interlayer coupling between BEDT-TTF sheets; the external field suppresses the interlayer coupling, reducing the melting temperature towards the value of the isolated layer, i.e., 2.7 K.

Recently, we have proposed another possible mechanism based on the idea of superconducting glass states, expected in granular superconductors [11]; if the system is composed of many superconducting domains coupled through weak Josephson links, the relative phase of the order parameters in the clusters is "frustrated" in the external magnetic field [12]. There exist numerous competing states with energies nearly equal to the ground state. Because of the energy barriers between these states, the transitions from one state to another are inhibited at low temperatures. But if the cluster is sufficiently heated, the system can "hop" from one state to another. Such "hopping motions" may produce fluctuating fields at the nuclear sites, which would contribute to the NMR  $T_1$ . The temperature and field-dependence of  $T_1^{-1}$  are qualitatively explained by this model. The zero-field measurements using the field-cycling method [4] may prove that the magnetic flux is trapped in the crystal. This is another significant feature of the superconducting glass.

In summary, it was found that in the superconducting state of (BEDT-TTF) $_2$ Cu(NCS) $_2$  the nuclear spin-lattice relaxation rate exhibits a striking enhancement unexpected for usual superconductors to date. Although we cannot specify the origin at present, it is sure that this anomaly implies a special feature of superconductivity never seen in conventional superconductors. In order to pursue the possibilities mentioned above further, one requires measurements on a single crystal, since these mechanisms would

give strong anisotropy of the relaxation depending on the field direction. A preliminary result for an aligned sample is shown in Fig. 2. Surprisingly, the relaxation peak appears at the highest temperature ( $\sim 5$  K) when the external field is parallel to the conductive plane. Systematic studies of the field dependence, including a zero-field measurement, are also in progress.

This work was carried out in collaboration with T. Tokiwa, K. Kanoda (Gakushuin University), H. Urayama, H. Yamochi and G. Saito (ISSP, The University of Tokyo). We thank Dr. Y. Maniwa (Tokyo Metropolitan University), Dr. M. Hasegawa and Prof. H. Fukuyama (ISSP, The University of Tokyo) for valuable discussions.

#### REFERENCES

1. M. Takigawa *et al.*, J. Phys. Soc. Jpn., **56** (1987) 873.
2. Y. Hasegawa and H. Fukuyama, J. Phys. Soc. Jpn., **56** (1987) 877.
3. F. Creuzet *et al.*, Europhys. Lett., **1** (1986) 461.
4. Y. Maniwa *et al.*, Jpn. J. Appl. Phys., **26** (1987) Suppl. 26-3, 1361.
5. H. Urayama *et al.*, Chem. Lett., **1988** (1988) 55.
6. K. Oshima *et al.*, J. Phys. Soc. Jpn., **57** (1988) 730.
7. Y. Hasegawa and H. Fukuyama, J. Phys. Soc. Jpn., **56** (1987) 2619.
8. T. Takahashi *et al.*, Physica **143B** (1986) 417;  
T. Takahashi *et al.*, J. Phys. Soc. Jpn., **55** (1986) 1364.
9. T. Takahashi *et al.*, Physica **C153-155** (1988) 487;  
T. Takahashi *et al.*, Synth. Met. **27** (1988) A319-A324.
10. B.A. Huberman and S. Doniach, Phys. Rev. Lett., **43** (1979) 950;  
D.S. Fisher, Phys. Rev., **B22** (1980) 1190.
11. Y. Maniwa *et al.*, J. Phys. Soc. Jpn. **58** (1989) to be published.
12. C. Ebner and D. Stroud: Phys. Rev. **B31** (1985) 165.

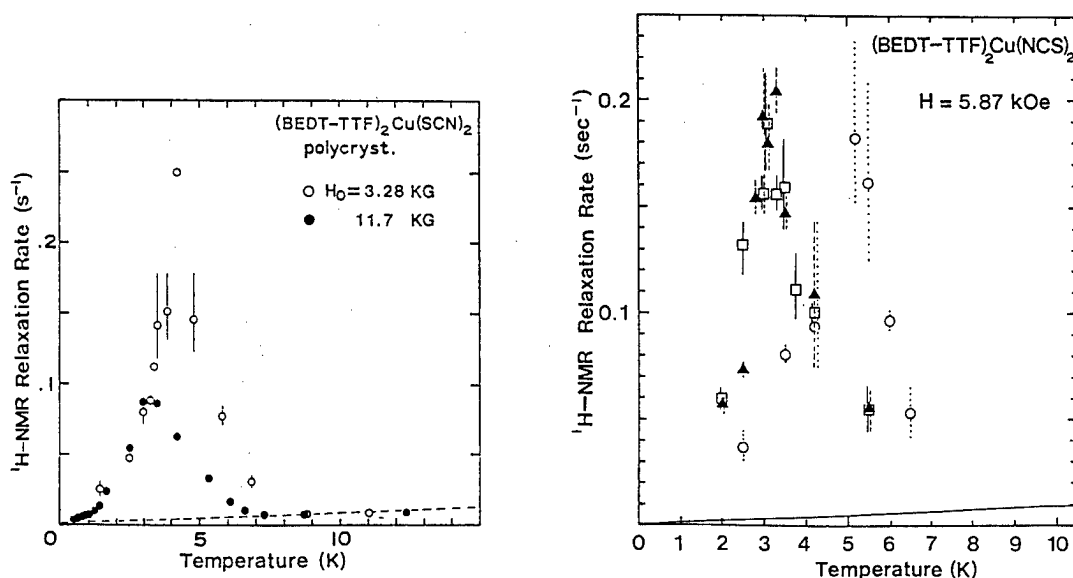


Fig. 1. (left)  $^1\text{H}$ -NMR relaxation rate  $1/T_1$  at low temperatures. The open and closed circles indicate the results at 3.28 kOe and at 11.7 kOe, respectively. The broken line indicates the Korringa behavior  $T_1 T = 1100$  secK, determined at high temperatures.

Fig. 2. (right)  $^1\text{H}$ -NMR relaxation rate  $1/T_1$  for an aligned sample. 15 single crystals are aligned together so as to make the bc-planes parallel. The symbols  $\circ$ ,  $\bullet$ , and  $\triangle$  indicate the results for the angles between the external field and the bc-plane of 0 (parallel), 45 and 90 degree (perpendicular), respectively. The straight line indicates the Korringa behavior,  $T_1 T = 1100$  secK.

Thermoelectric Power of Organic Superconductors.  
Calculation on the Basis of the Tight-Binding Theory

T. Mori and H. Inokuchi

Institute for Molecular Science, Okazaki 444, Japan

Thermoelectric power of organic superconductors,  $\beta$ -(BEDT-TTF) $_2$ I $_3$  and (BEDT-TTF) $_2$ Cu(NCS) $_2$  (BEDT-TTF: bis(ethylenedithio)tetrathiafulvalene) is calculated by the integration of the Boltzmann equation on the basis of the two-dimensional tight-binding band models. This calculation provides the interpretation of the observed complicated temperature dependence and anisotropy of the thermoelectric power and a tool estimating the transfer integrals.

Thermoelectric power  $S$  of organic metals has been frequently used as one of the conventional methods of estimation of the bandwidths. Their temperature dependences are usually linear, and the bandwidths have been extracted from their slopes by assuming a simple band structure, in most cases the one-dimensional tight-binding band. However,  $S$  of recent organic superconductors, especially of BEDT-TTF salts, shows much more complicated temperature dependence and anisotropy. Such a behavior is associated with the two-dimensional band structures of the BEDT-TTF salts. In order to interpret the temperature dependence and the anisotropy, we attempted the theoretical calculation of  $S$ , where the Boltzmann equation is integrated by using the tight-binding band structure. This method was applied to two organic superconductors,  $\beta$ -(BEDT-TTF) $_2$ I $_3$  and (BEDT-TTF) $_2$ Cu(NCS) $_2$  [1].

Figure 1 shows the observed  $S$  of (BEDT-TTF) $_2$ Cu(NCS) $_2$  [2] and the calculated  $S$  where the transfer integrals are optimized so as to reproduce the experimental results. The fairly good agreement indicates that the complicated temperature dependences and anisotropy of  $S$  can be explained on the basis of the rather simple band model.

#### References

- [1] T. Mori and H. Inokuchi: J. Phys. Soc. Jpn. **57** (1988) 3674.
- [2] H. Urayama, H. Yamochi, G. Saito, T. Sugano, M. Kinoshita, T. Inabe, T. Mori, Y. Maruyama, and H. Inokuchi: Chem. Lett. **1988** (1988) 1057.

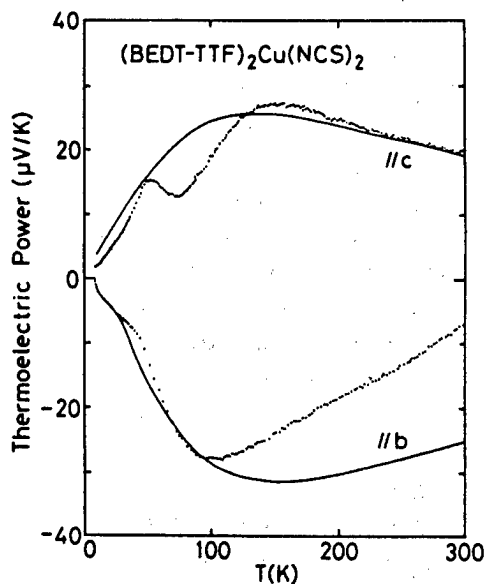


Fig. 1. Temperature dependence of  $S$  of (BEDT-TTF) $_2$ Cu(NCS) $_2$ . The dots from the experiment [2], and the solid curves from the theory.

Structural Characteristics of BEDT-TTF Superconductors and a New Type of Molecular Metal with Coordination Structure

H. Kobayashi, R. Kato and A. Kobayashi\*

Department of Chemistry, Faculty of Science, Toho University, Funabashi, Chiba 274 Japan

\*Department of Chemistry, Faculty of Science, The University of Tokyo,  
Hongo, Bunkyo-ku, Tokyo 113, Japan

Recent our studies on organic metals and superconductors were presented: (1) the possible relation between superconducting transition temperature  $T_c$  and disorder of anion sites and/or stereochemical disorder of BEDT-TTF in  $\beta$ -(BEDT-TTF) $_2$ (I $_3$ ) $_{1-x}$ (AuI $_2$ ) $_x$ , (2) structure refinement of an organic superconductor  $\theta$ -(BEDT-TTF) $_2$ I $_3$  ( $T_c$ =3.6 K), (3) structural characteristics and solid state properties of a new molecular metal (R $_1$ ,R $_2$ -DCNQI) $_2$ Cu with the  $pn$ - $d$  interactions.

Since a possible route to design new types of two-dimensional(2D) molecular metals has been suggested by the structure chemical analyses of the molecular arrangement in (TMTSF) $_2$ X (X=PF $_6$ , ClO $_4$ ,...), we have made intensive studies on the molecular conductors based on multi-sulfur (or selenium)  $\pi$ -molecules such as BEDT-TTF(ET) analogues and M(dmit) $_2$  (M=Ni, Pd, Pt). We have found three new molecular superconductors ( $\theta$ - and  $\kappa$ -ET) $_2$ I $_3$ , [(CH $_3$ ) $_4$ N][Ni(dmit) $_2$ ] $_2$  and proved an existence of almost ideally 2D molecular metals composed of planar  $\pi$ -molecules. Organic molecular metals are constructed from the complex structure units. In other words, molecular metals are metals with substructures. This structural characteristics give us a possibility of preparing a variety of metals. A molecule maintains its individuality in the crystalline state, which possibly influences the solid state properties. An example may be seen in the high- $T_c$  and low- $T_c$  phenomena of  $\beta$ -ET) $_2$ I $_3$ . In this report, our recent studies on two ET superconductors and new molecular metals with coordination structures will be briefly described.

[I]  $\beta$ -ET) $_2$ (I $_3$ ) $_{1-x}$ (AuI $_2$ ) $_x$ <sup>2)</sup>

Since  $\beta$ -ET) $_2$ I $_3$  (ambient pressure) and  $\beta$ -ET) $_2$ AuI $_2$  are in so-called low- $T_c$  and high- $T_c$  states respectively,  $\beta$ -ET) $_2$ (I $_3$ ) $_{1-x}$ (AuI $_2$ ) $_x$  must transform from the low- $T_c$  state to high- $T_c$  one with increasing  $x$  from 0 to 1. At the same time, the conformational disorder of ethylene group of ET observed in  $\beta$ -ET) $_2$ I $_3$  will be vanished when the AuI $_2$  content becomes high because there exists no structural disorder in the pure AuI $_2$  salt. We have made the following experiments: 1) crystal growth 2) examination of the ethylene conformation and  $T_c$  as a function of  $x$  and 3) observation of the IC-lattice distortion wave. The results are: 1) When  $x < 0.2$ ,  $T_c$  is depressed to lower than 1.5 K probably owing to the conformational disorder of ET and randomness of the anion sites. 2) At  $x > 0.2$ , the conformational disorder and the lattice distortion disappear but  $T_c$  is still lower than 1.5 K because of the large random potential of anions. 3) When  $x$  approaches to 1.0,  $T_c$  increases up to 4.5 K with increasing  $x$ .

[III]  $\theta$ -ET) $_2$ I $_3$ <sup>3)</sup>

$\theta$ -ET) $_2$ I $_3$  is an organic superconductor ( $T_c$ =3.6 K) discovered by us (1986). Almost all the crystals are twinned but we have recently found a crystal composed of a single component of the twinned structure. Crystal data are: monoclinic,  $P2_1/c$ ,  $a=9.943$ ,  $b=10.086$ ,  $c=34.262$  Å,  $\beta=98.51^\circ$ . The crystal are composed of metal layers of ET and insulating I $_3^-$  anion layers, which are stacked alternately along  $c$ . Tight-binding band examination based on the HOMO of ET revealed a strong 2D nature of the system. Recently Kajita et al. have found an anomalous magnetoresistance.



[III]  $(R_1, R_2\text{-DCNQI})_2\text{Cu}^{41}$

A series of highly conducting anion radical salts with formula  $(2,5\text{-}R_1, R_2\text{-DCNQI})_2\text{Cu}$  ( $\text{DCNQI}=\text{N},\text{N}'\text{-dicyanoquinonediimine}$ ;  $R_1, R_2 = \text{CH}_3, \text{CH}_3\text{O}, \text{Cl}, \text{Br}$ ) have provided fertile solid state chemistry and physics; a new type of electron-phonon coupling (the coupling of the CDW formation and the Jahn-Teller distortion), the pressure-induced metal-insulator transition, and the interaction between 3d magnetic ions and the  $2p\pi$  conduction electrons. We have performed systematic crystal structure analyses at room temperature and at low temperature (100 K), and have proposed a "multi-Fermi surface" model to understand the exotic physical properties of  $(2,5\text{-}R_1, R_2\text{-DCNQI})_2\text{Cu}$ .

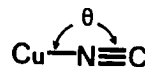
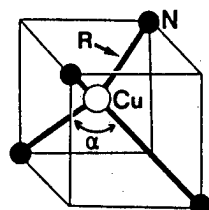
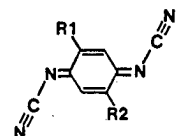
At room temperature, all these Cu salts are isomorphous with space group  $14_1/a$ . The structure consists of face-to-face DCNQI columns running along the crystallographic c axis (Fig. 1). The Cu cation is coordinated in  $D_{2d}$  distorted tetrahedral fashion to the N atoms of DCNQI molecules. The structural feature of the DCNQI column is almost common to all the Cu salts, while there are small but significant differences in the coordination geometry around the Cu cation (Table 1). The X-ray satellite reflections in the low-temperature insulator phase indicate the threefold structure, which suggests the mixed valence state of Cu ( $\text{Cu}^+ : \text{Cu}^{2+} = 2 : 1$ ). Table 1 shows that the  $D_{2d}$  distortion of the coordination tetrahedron is enhanced at low temperature. The  $\Delta\alpha$  ( $\alpha(100\text{K}) - \alpha(\text{R.T.})$ ) values in Table 1 clearly distinguish the metallic  $(\text{DMe-DCNQI})_2\text{Cu}$  from the other insulating salts. Figure 2 clearly exhibits that the metal-insulator transition is associated with the abrupt distortion of the coordination tetrahedron. The existence of  $\text{Cu}^{2+}$  leads us to consider the distortion the second-order Jahn-Teller type. The metal-insulator transition in the  $(2,5\text{-}R_1, R_2\text{-DCNQI})_2\text{Cu}$  system can be described as an cooperative structural phase transition induced by the CDW instability of the DCNQI column and the Jahn-Teller distortion around the Cu cation.

The electronic structure of this system was examined by the simple tight-binding band calculations. The essential point is that the mixed valence state of Cu leads to the mixing of the organic  $2p\pi$  orbitals and 3d orbitals of Cu. This  $p\pi\text{-}d$  interaction generates multiple sheet-like Fermi surface. In such a case, a complete gap formation by the CDW or SDW may be hindered by the frustration effects due to the mismatch among the several Fermi wavevectors. The metallic state will become stable, in spite of the sheet-like Fermi surface. We call such a metallic system "multi-Fermi surface" system. The second-order Jahn-Teller distortion of the coordination tetrahedron decreases the number of the d orbitals participating in the  $p\pi\text{-}d$  mixing and weakens the multi-Fermi surface nature, which leads to the gap formation by the CDW. The electrons associated with the d-origin bands will tend to localize on the Cu cations and give a minor contribution to the electrical conductivity, but play an important role in the magnetic properties.

Table 1. Metal-Insulator Transition Temperature ( $T_{N-1}$ ) and Coordination Geometry of Cu

$R_1$	$R_2$	$T_{N-1}^a / \text{K}$	$R/\text{\AA}$		$\alpha / ^\circ$		$\Delta\alpha^b / ^\circ$	$\theta / ^\circ$	
			R.T.	100K	R.T.	100K		R.T.	100K
Me	Me	metal	1.977	1.969	124.5	126.0	1.5	168.7	169.0
MeO	MeO	metal	1.988		126.0			177.6	
Me	Br	152° 156° <sup>x</sup>	1.979	1.958	125.3	128.2	2.9	168.7	168.2
Br	Br	161° 160° <sup>x</sup>	1.973		125.3			169.2	
Me	Cl	210° 210° <sup>x</sup>	1.968	1.945	126.3	129.1	2.8	169.7	169.4
Br	Cl	213° 210° <sup>x</sup>	1.964	1.958	126.1	129.1	3.0	167.0	166.6
Cl	Cl	230°	1.972		127.1			168.1	

<sup>a</sup> The superscripts C and X indicate  $T_{N-1}$  determined by resistivity measurements and the abrupt lattice distortion detected from X-ray experiments, respectively. <sup>b</sup>  $\alpha(100\text{K}) - \alpha(\text{R.T.})$ .



The static susceptibilities were measured on the powder samples of  $(\text{DMe-DCNQI})_2\text{Cu}$  and  $(\text{DBr-DCNQI})_2\text{Cu}$  (Fig. 3). The results are : [I]  $(\text{DMe-DCNQI})_2\text{Cu}$  (1) Weakly temperature-dependent metallic paramagnetic susceptibility ( $\chi_p$ ) was observed above 100 K. (2) In contrast with the monotonous change of the resistivity ( $\rho \propto T^2$ ) over the temperature range 30-300 K,  $\chi_p$  increases considerably around 70 K, with decreasing T. (3) Except a slight anomaly around 4.5 K,  $\chi_p$  (emu/g) is well described as,  $0.89 \times 10^{-6} + 0.59 \times 10^{-6}/T$  between 1.5 K and 30 K, where  $\rho$  is temperature independent. [II]  $(\text{DBr-DCNQI})_2\text{Cu}$  (1) Weakly temperature dependent  $\chi_p$  was observed above 155 K. Room-temperature value of  $\chi_p$  is smaller than that of  $(\text{DMe-DCNQI})_2\text{Cu}$ , indicating smaller contribution of d electrons to  $N(\epsilon_F)$ . (2)  $\chi_p$  jumps at 153 K (M-I transition temperature), suggesting disappearance of Fermi surface and appearance of local spins of  $\text{Cu}^{2+}$ . (3) An anomaly was observed at 13 K ( $T_N$ ).

The authors thank to Profs. W. Sasaki and K. Kajita and Dr. Y. Nishio for valuable discussions and magnetic susceptibility experiments.

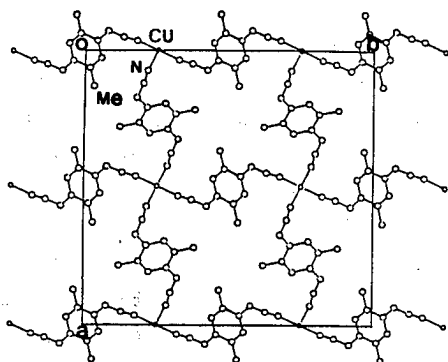


Fig. 1. Crystal structure of  $(\text{DMe-DCNQI})_2\text{Cu}$ .

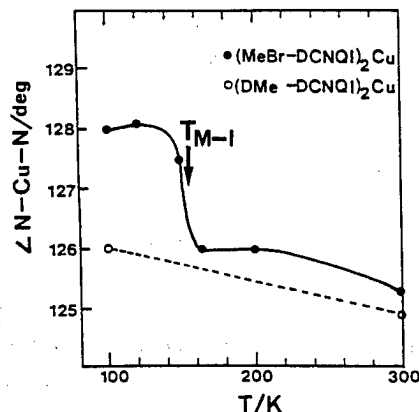


Fig. 2. Temperature dependence of  $\alpha$ .

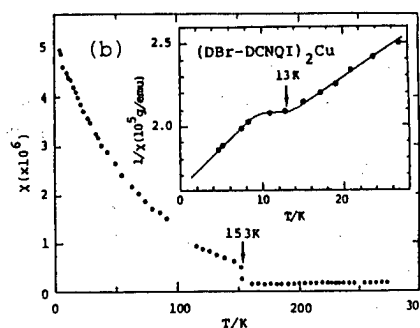
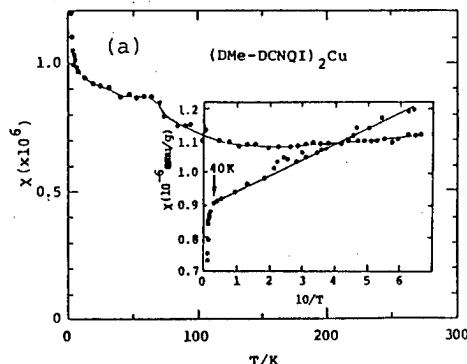


Fig. 3. Magnetic susceptibility. (a)  $(\text{DMe-DCNQI})_2\text{Cu}$  (b)  $(\text{DBr-DCNQI})_2\text{Cu}$

#### References

- 1) H. Kobayashi, Research Report on New Superconducting Materials (1985), pp92-94. Special Project Research No. 106, Ministry of Education, Science and Culture; H. Kobayashi, R. Kato and A. Kobayashi, Israel J. Chem. 27 301-307 (1986).
- 2) T. Ishiguro, H. Anzai, M. Tokumoto, K. Murata, H. Bando, K. Kajimura, N. Kinoshita, " Research Reports on New Superconducting Materials and High Temperature Oxide Superconductors(1984-1987)" edited by S. Nakajima and H. Fukuyama, ppl64-170.
- 3) H. Kobayashi, R. Kato, A. Kobayashi, Y. Nishio, K. Kajita, and W. Sasaki, Chem. Lett., 1986, 789-792, 833-836; H. Kobayashi, R. Kato, A. Kobayashi, S. Moriyama, Y. Nishio, K. Kajita, and W. Sasaki, Synthetic Metals, 27, B339-B346 (1988).
- 4) R. Kato, H. Kobayashi, A. Kobayashi, T. Mori, and H. Inokuchi, Chem. Lett, 1987, 1579-1582; A. Kobayashi, R. Kato, H. Kobayashi, T. Mori, and H. Inokuchi, Solid State Commun., 64, 45-51 (1987); ibid., 65, 1351-1354 (1988).

Coexistence of a Magnetic Order and Metallic Conduction  
in an Organic System, (DMDCNQI)<sub>2</sub>Cu

T. Mori, S. Bandow, K. Imaeda H. Inokuchi,  
A. Kobayashi,\* R. Kato,\*\* and H. Kobayashi\*\*

Institute for Molecular Science, Okazaki 444, Japan

\*Department of Chemistry, Faculty of Science,  
The University of Tokyo, Tokyo 113, Japan

\*\* Department of Chemistry, Faculty of Science,  
Toho University, Funabashi 274, Japan

The transport and magnetic properties of highly-conducting organic charge-transfer salts ( $R_1R_2$ -DCNQI)<sub>2</sub>M ( $R_1, R_2 = \text{CH}_3, \text{CH}_3\text{O}, \text{Cl}, \text{or Br}$ ; DCNQI: *N,N'*-dicyanoquinonediimine;  $M = \text{Cu}, \text{Ag}, \text{Li}, \text{Na}, \text{K}, \text{or NH}_4$ ) are investigated. In (DMDCNQI)<sub>2</sub>Cu ( $R_1, R_2 = \text{CH}_3$ ), no metal-insulator transition occurs, while some kind of magnetic order of the Cu<sup>2+</sup> spins takes place in spite of its metallic conduction.

A new family of organic molecules,  $R_1R_2$ DCNQI, works as a ligand as well as an electron acceptor to form highly-conducting charge-transfer/coordination compounds as ( $R_1R_2$ DCNQI)<sub>2</sub>M. These salts are investigated by the measurements of electrical conductivity, thermoelectric power, electron spin resonance, static susceptibility, and specific heat.

The conducting properties of these salts are appropriately understood by classifying them into three groups [1]. Group I consisting of the salts with cations,  $M$ , other than Cu, undergoes the Peierls transitions at 50 - 100 K. Their thermoelectric power is interpreted by the large- $U$  limit of the Hubbard model. Group II salts, the Cu salts of the halogen-containing DCNQI, also exhibit the metal-insulator transitions between 150 K and 250 K, followed by antiferromagnetic transitions around 10 K. With the one-dimensional tight-binding approximation, the bandwidth is estimated to be 0.4 - 0.5 eV from the thermoelectric power. Group III salts, the Cu salts with  $R_1 = R_2 = \text{CH}_3$  or  $\text{CH}_3\text{O}$  retain metallic conductivity down to 1.5 K. These transport properties as well as their crystal structures indicate the carriers of the metallic conduction are electrons on the organic molecules, DCNQIs. The appearance of the three-fold X-ray satellite reflections in the group-II salts and the XPS measurements show the Cu atoms of the group-II and group-III salts to be mixed-valent, Cu<sup>1.3+</sup> [2]. In the group-III salts, the metallic states are considered to be stabilized by the interchain interaction mediated by the mixed-valent Cu.

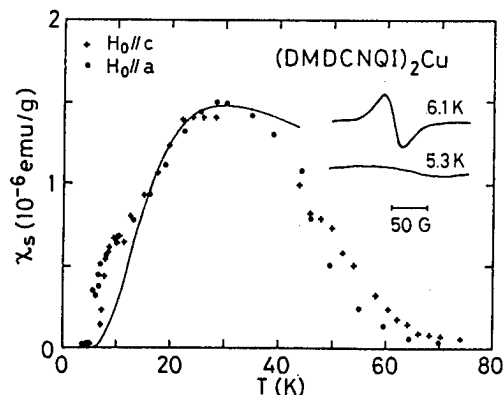


Fig. 1. Temperature dependence of the ESR intensity of (DMDCNQI)<sub>2</sub>Cu.

The group-III salt  $(\text{DMDCNQI})_2\text{Cu}$  shows  $\text{Cu}^{2+}$  ESR signal; the temperature dependence of its intensity is shown in Fig. 1. The decrease of the spin susceptibility below 30 K suggests development of some kind of short-range magnetic order of the  $\text{Cu}^{2+}$  spins. The disappearance or the drastic broadening of the ESR signal at 5.5 K indicates a long-range magnetic order. It is interesting that the conductivity remains metallic and is not affected by the magnetic order. This may be the first organic conductor where metallic conduction and a magnetic order are coexisting.

The anomaly of  $\chi_s$  is also observed in the static susceptibility measurement (Fig. 2) [3]. The susceptibility increases below 70 K, but decreases below ca. 30 K. The contribution of this anomalous  $\text{Cu}^{2+}$  spins is, however, small; that is about one fifth of the Pauli paramagnetism.

In this temperature region, the magnetoresistance showed no anomalous behavior (Fig. 3) [4].

#### References

- [1] T. Mori, H. Inokuchi, A. Kobayashi, R. Kato, and H. Kobayashi: *Phys. Rev.* **B38** (1988) 5913.
- [2] A. Kobayashi, R. Kato, H. Kobayashi, T. Mori, and H. Inokuchi: *Solid State Commun.*, **64** (1987) 45.
- [3] T. Mori, S. Bandow, H. Inokuchi, A. Kobayashi, R. Kato, and H. Kobayashi: *Solid State Commun.*, **67** (1988) 565.
- [4] T. Mori, H. Inokuchi, A. Kobayashi, R. Kato, and H. Kobayashi: *Synth. Metals* **27** (1988) B237.

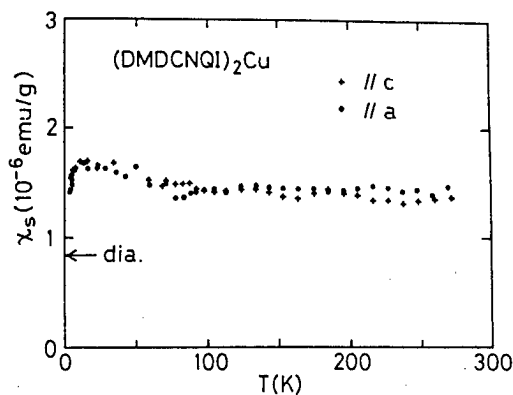


Fig. 2. Temperature dependence of static magnetic susceptibility of  $(\text{DMDCNQI})_2\text{Cu}$ .

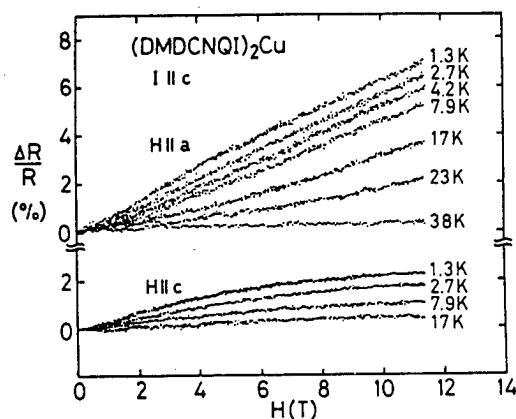


Fig. 3. Transverse and longitudinal magnetoresistance of  $(\text{DMDCNQI})_2\text{Cu}$ .

# Magnetic Behavior and Resonating Valence Bond State in Organic Free Radicals

K. Takeda, H. Deguchi, T. Hoshiko, K. Takahashi, K. Konishi,  
T. Idogaki, N. Uryû and J. Yamauchi<sup>†</sup>

Department of Applied Science, Faculty of Engineering,  
Kyushu University, Fukuoka 812, Japan

<sup>†</sup>Department of Chemistry, College of Liberal Arts,  
Kyoto University, Kyoto 606, Japan

The magnetic behavior in the quantum system where spin-singlet pairs are expected to resonate has been investigated for the organic free radicals, TANOL and triphenylverdazyl (TPV). The magnetic parameters of TANOL are found to be more sensitive to the pressure  $p$  than in the usual systems with the superexchange interaction: the Néel temperature  $T_N(p)$  changes as  $T_N(p) = T_N(p_0)(1 + 0.15p)$  for  $p(\text{kbar})$ . The pressurization up to 6 kbar, however, has not changed the magnetic state into any different phase. TPV is revealed to be a two-dimensional quantum system with  $T_N = 1.7 \text{ K}$ , and to be a candidate which is supposed to show the intrinsic features of the delocalization of unpaired electron in its large molecule.

Among many reports on the high-temperature superconductivity, the resonating valence bond (RVB) state is stressed to play an important role in the  $\text{CuO}_2$  plane with the electronic holes. The RVB state is quite sensitive to the character of the holes, which are supposed to be relevant to  $\text{Cu}^{3+}$  or  $\text{O}^-$ . Anyhow, in this category of mechanism for superconductivity,<sup>1)</sup> the crucial condition is to realize RVB state in a two-dimensional quantum ( $S = 1/2$ ) system.

In the present work, we examine the possibility of RVB state with the use of the crystal of organic free radical which has some remarkable points when compared with inorganic compounds with the 3d electron. In the latter case, the 3-d electron is easily affected by the crystalline field and hence the  $g$ -value is usually different from  $g_e$  for electron. This anisotropy in the  $g$ -value acts to bring the system into the Néel state. While, the  $g$ -value of the unpaired electron in the radicals is almost equal to  $g_e$  because of excellent quenching of orbital momentum of the electron which moves

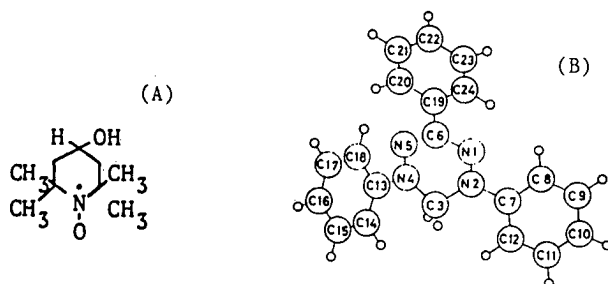


Fig. 1. Molecular structure of TANOL (A) and TPV (B).

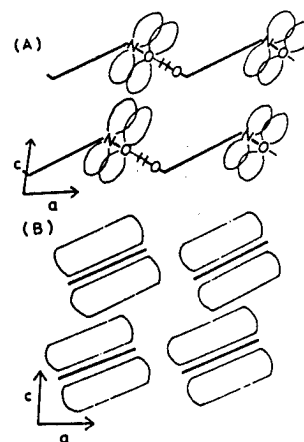


Fig. 2 Schematic model of molecular plane and unpaired electron density between the localized (A) and delocalized (B) systems.

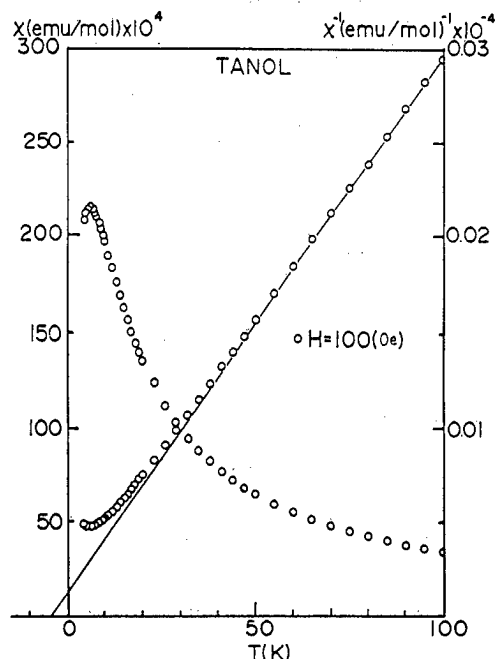


Fig. 3 Magnetic susceptibility and inverse susceptibility of TANOL.

to 1/100 of the intrachain exchange field. These facts indicate that TANOL is one of the typical one-dimensional radicals where RVB state is realized at low temperatures. The pressurization of this radical up to 6 kbar, however, does not change the magnetic state into a different state such as conductive behavior. From the pressure dependence of the heat capacity measurements, we get the information about the softness of radical crystals through the variation of the Néel temperature and exchange interactions. It is found that these parameters could be controlled up to 100 % for  $p < 10$  kbar:  $T_N(p) = T_N(p_0)(1 + 0.15p)$ , for example.<sup>5)</sup>

**TPV** The magnetic susceptibility of TPV is shown in Fig. 4. The broad maximum appears around 5 K which indicates a feature of low-dimensional antiferromagnets. Although the overall behavior resembles to the case for TANOL, the value of  $\chi$  of TPV is suppressed by the external field of 8 kOe. If we take TPV as a quasi-one-dimensional system, the value of 8 kOe is only about  $10^{-2}$  of the exchange field and too small to reduce the value of  $\chi$  as in Fig. 4. While, the heat capacity shows a broad maximum around 5 K (Fig. 5) nearly the same temperature region where the broad maximum of  $\chi$  appears. This is not the case for the one-dimensional system in which the broad maximum must locate at  $k_B T \approx 0.96|J|$  for heat capacity and at  $k_B T \approx 1.28|J|$  for susceptibility.<sup>6)</sup> Taking these results and the crystal structure of TPV into consideration, we think TPV is rather a two-dimensional antiferromagnet. The overall behavior of the magnetic heat capacity, including

on the p-orbitals of O, N or C. In addition to this, the radical crystal is magnetically constructed in low-dimensional system because of the structural feature of constituent plane-like molecules. The isotropy of the g-value and the low-dimensionality of the system are indispensable condition for the RVB state.

Two kinds of the organic free radicals are examined here: one is TANOL in which the unpaired electron localizes almost on the  $p_z$ -orbitals of the -NO bond in the molecule, and the other is 1,3,5-triphenylverdazyl (TPV) where spin delocalizes in the larger space of the molecule as illustrated in Figs. 1 and 2.<sup>2,3)</sup>

**TANOL** The magnetic susceptibility<sup>2)</sup> and heat capacity are well approximated to a quasi-one-dimensional Heisenberg antiferromagnet with the magnetic parameters: intra- and inter-chain exchange constants  $J/k_B \approx -5.0$  K,  $|J'| \approx 10^{-2}|J|$  and  $T_N = 0.5$  K.<sup>4,5)</sup> The g-value is about 2.004 above  $T_N$ . More than 90 % of the magnetic entropy for  $S = 1/2$  is consumed below 20 K. Figure 3 shows the results of susceptibility of TANOL which indicate characteristic broad maximum of the one-dimensional system. The value of  $\chi$  does not change in the field up to 8 kOe which corresponds

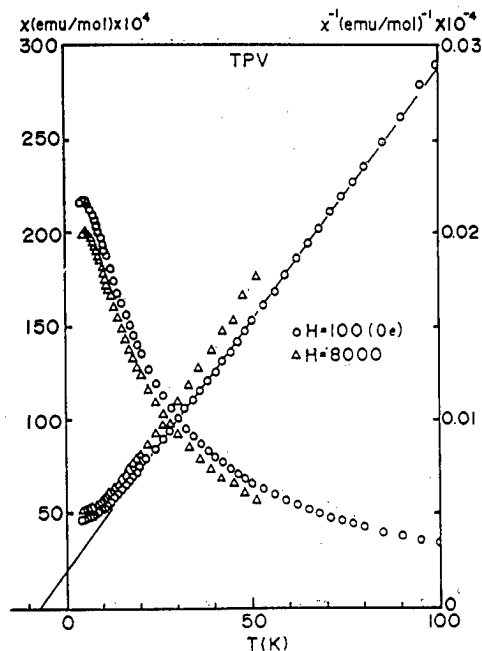


Fig. 4 Magnetic susceptibility and inverse susceptibility of TPV.

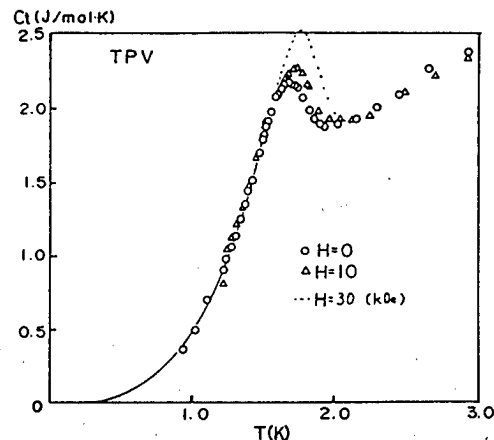
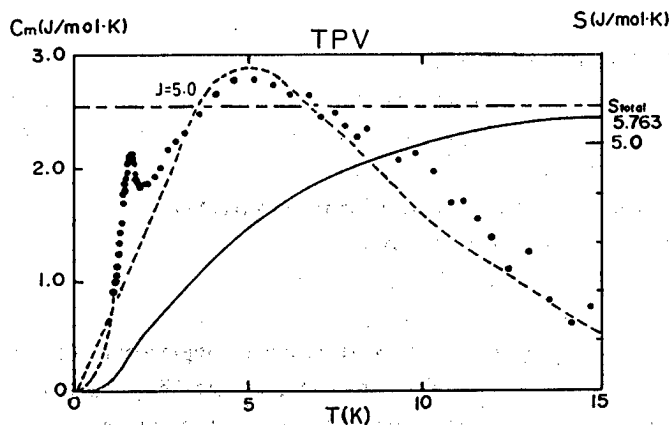


Fig. 5. Magnetic heat capacity and entropy of TPV.

Fig. 6 Heat capacity of TPV in the magnetic field.

the peak at  $T_N = 1.7$  K, is reminiscent of that of two-dimensional magnets such as  $K_2CuF_4$  and  $(C_nH_{2n+1}NH_3)CuCl_4$  which have the ratio of inter- to intra-plane exchange constants  $|J'/J| \leq 10^{-3}$ .<sup>7)</sup> The field 8 kOe applied in the susceptibility measurement may suppress the fluctuations of spins coupled by the weak interaction  $J'$ .

Another feature to be remarked for TPV is that the heat capacity peak at  $T_N$  is not of the diverging type as shown in Fig. 6. This may be intrinsic to the delocalization of the unpaired electron in the large molecule of the radical. It should be also noted that in the stronger field the peak grows and shifts to the higher temperatures, reflecting field-induced crossover of spin symmetry which takes place in low-dimensional Heisenberg antiferromagnets.<sup>8)</sup>

The heat capacity plotted in Fig. 5 can be fit to the theoretical result for the Hubbard model with  $U/t \approx 4 \sim 6$ .<sup>9)</sup> However, the result of susceptibility can not be compared quantitatively to the calculation on the same model. The realization of the low-dimensional Hubbard model is quite instructive.

We conclude that TPV is a first candidate for two-dimensional quantum system with resonating singlet pairs of spin. The experiment under hydrostatic pressure and method to introduce the electronic holes in TPV are to be undertaken.

The measurements of susceptibility was done by the use of the SQUID magnetometer of Low-Temperature Lab. of Kyushu University.

#### References

- 1) See for example, S.Liang, B.Doucot, and P.W.Anderson. Phys. Rev. Lett. **61** (1988) 365.
- 2) J.Yamauchi. Bull. Chem. Soc. Jpn. **44** (1971) 2301.
- 3) N.Azuma, J.Yamauchi, K.Mukai, H.Ohya-Nishiguchi, and Y.Deguchi. Bull. Chem. Soc. Jpn. **46** (1973) 2728.
- 4) J.-P.Boucher, M.Nechtschen, and M.Saint-Paul. Phys. Lett. **42A** (1973) 397.
- 5) K.Takeda, N.Uryû, M.Inoue, and J.Yamauchi. J. Phys. Soc. Jpn. **56** (1987) 736.
- 6) J.C.Bonner and M.E.Fisher. Phys. Rev. **135** (1964) A640.
- 7) See for example, L.J.de Jongh and A.R.Miedema. Adv. Phys. **23** (1971) 1.
- 8) K.Takeda, T.Koike, T.Tonegawa, and I.Harada. J. Phys. Soc. Jpn. **48** (1980) 1115.
- 9) H.Shiba. Prog. Theo. Phys. Jpn. **48** (1972) 2171.

I. Ikemoto, K. Kikuchi and K. Saito

Department of Chemistry, Faculty of Science, Tokyo Metropolitan University,  
Fukazawa, Setagaya-ku, Tokyo 158, Japan

DMET superconductors are classified into three groups from the temperature dependence of resistivities at ambient pressure;  $\text{Au}(\text{CN})_2$ ,  $\text{AuCl}_2$  and  $\text{AuI}_2$  salts (Group 3),  $\text{I}_3$  and  $\text{IBr}_2$  salts (Group 4), and two types of  $\text{AuBr}_2$  salts (Group 5). The crystal structures of these superconductors were determined and compared with each other. The salts in Groups 3 and 4 have columnar structure, but the salts in Group 5 have non-columnar structure. Detailed comparison between the salts in Group 3 and 4 are described.

We have found DMET conductors to be classified into five groups from the temperature dependence of resistivity (Fig. 1). DMET salts which show superconductivity are classified into three groups (Groups 3, 4 and 5).  $(\text{DMET})_2\text{X}$  ( $\text{X} = \text{Au}(\text{CN})_2$ ,  $\text{AuI}_2$ , and  $\text{AuCl}_2$ ) belong to one group (Group 3). They exhibit a resistance upturn at low temperature due to SDW instability at ambient pressure and need some pressure to become superconductors except  $\text{AuCl}_2$  salt. On the other hand, the other DMET superconductors does not show such a upturn at ambient pressure.  $(\text{DMET})_2\text{X}$  ( $\text{X} = \text{I}_3$  and  $\text{IBr}_2$ ) (Group 4) are metallic down to low temperature and undergo a superconducting transition at 0.47 K and 0.58 K, respectively. Two types of crystals of  $(\text{DMET})_2\text{AuBr}_2$  (Group 5) which are rhombus-like exhibit other type of the temperature dependence of resistivity. Their resistivities increase gradually, show the maximum and then turn to decrease as temperature decreases. One type of crystal becomes superconductor at 1.9 K at ambient pressure. Another shows superconductivity only under pressure. It is generally thought that the crystal structure affects the electrical properties. Therefore it is interesting to make it clear whether or not there are some differences in structure among Groups 3, 4 and 5. In this report we present the crystal structures of DMET superconductors.

The crystal structure of  $\text{Au}(\text{CN})_2$  salt is shown in Figs. 2 and 3. As is shown in Fig. 2, DMET molecules form an ordered stack along the b axis. In a column, DMET molecules are stacked with an alternate molecular orientation related by an inversion center, and there are two different types of overlap between the neighboring molecules. One type of overlap has two shorter Se-Se contacts than the sum of the van der Waals radii. The other has four shorter Se-S contacts. It is noted that the ethylenedithio group is not responsible for shorter contacts in both types of overlap of DMET molecules within the column. In other DMET superconductors belonging to Group 3 or 4, the similar stacking

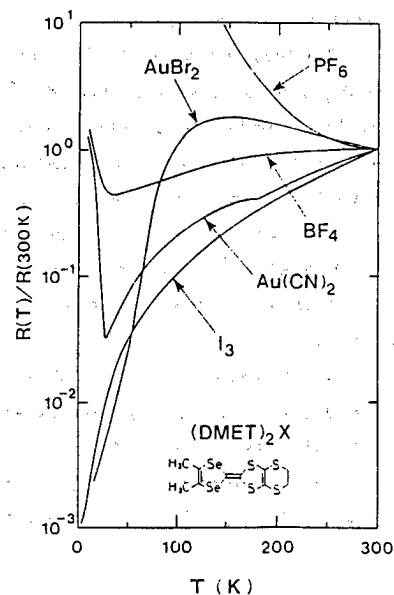


Fig. 1. Temperature dependence of resistivity of  $(\text{DMET})_2\text{X}$ .



pattern of DMET is also observed and shorter contacts are almost the same as those in  $\text{Au}(\text{CN})_2$  salt. Intercolumnar contacts in  $\text{Au}(\text{CN})_2$  salt are shown in Fig. 3. There exist two S-S and one Se-Se contacts shorter than the sum of the van der Waals radii. These contacts lie between the molecules related by a translation of  $a$  along the  $a$  axis, in contrast to TMTSF salts. In the case of the intercolumnar contacts the ethylenedithio group contributes to S-S contacts.

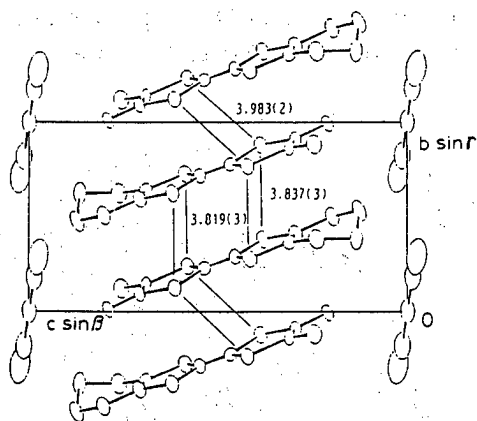


Fig. 2. Crystal structure of  $(\text{DMET})_2\text{Au}(\text{CN})_2$  viewed along the  $a$  axis.

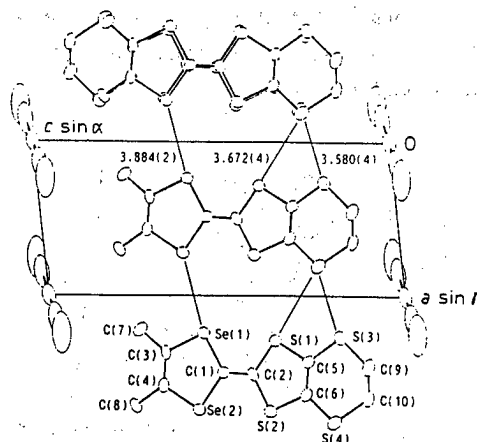


Fig. 3. Crystal structure of  $(\text{DMET})_2\text{Au}(\text{CN})_2$  viewed along the  $b$  axis.

Figure 4 shows shorter intercolumnar contacts than the sum of the van der Waals radii in  $\text{AuCl}_2$  salt. There are two types of short intercolumnar contacts; one consists of two Se-S contacts and another consists of one Se-Se contact. These contacts lie between the molecules related by the inversion center out of the column and do not exist between molecules related by a translation along the  $a$  axis, in contrast to other superconductors in Group 3 or 4.  $\text{AuCl}_2$  anions are located among eight DMET molecules as in the case of  $\text{Au}(\text{CN})_2$  salt.

Figure 5 shows intercolumnar contacts in  $\text{AuI}_2$  salt. The pattern of intercolumnar contacts is similar to that in  $\text{Au}(\text{CN})_2$  salt. These contacts are little shorter than the corresponding contacts in  $\text{Au}(\text{CN})_2$  salt. Moreover, the relative positions of anions to DMET molecules is quite different from those in  $\text{Au}(\text{CN})_2$  and  $\text{AuCl}_2$ . That is,  $\text{AuI}_2$  anion lie nearly in the direction of the long molecular axis of DMET and among four DMET.

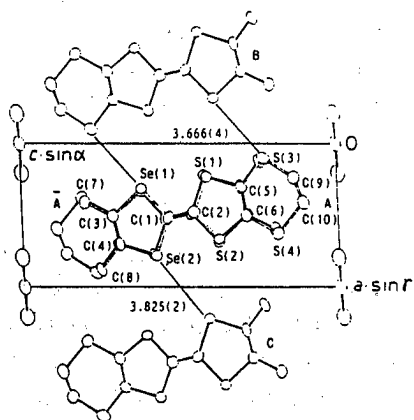


Fig. 4. Crystal structure of  $(\text{DMET})_2\text{AuCl}_2$  viewed along the  $b$  axis.

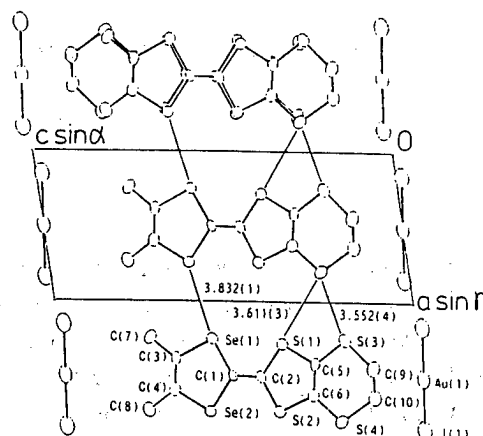


Fig. 5. Crystal structure of  $(\text{DMET})_2\text{AuI}_2$  viewed along the  $b$  axis.

As presented above, even among Group 3, each salt has different characters of crystal structure. On the other hand, the structures are almost the same among Group 4. Figure 6 shows the crystal structure of  $I_3$  salt, which is very similar to that of  $I\text{Br}_2$  salts. The patterns of intra- and intercolumnar contacts are almost the same as those in  $\text{Au}(\text{CN})_2$  and  $\text{AuI}_2$  salts. The intra- and intercolumnar contacts are given in Table. The intracolumnar contacts in the salts in Group 4 are almost the same as those in the salts in Group 3, but intercolumnar contacts are shorter. This indicates that the salts in Group 4 have higher two-dimensionality than the salts in Group 3, which may be related to the absence of SDW phase even at ambient pressure.

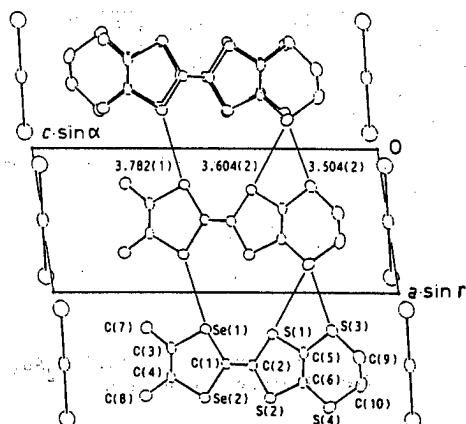


Fig. 6. Crystal structure of  $(\text{DMET})_2\text{I}_3$  viewed along the  $b$  axis.

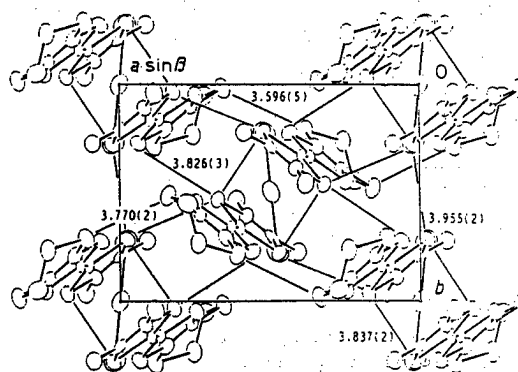


Fig. 7. Crystal structure of  $(\text{DMET})_2\text{AuBr}_2$  viewed along the  $c$  axis.

Table Short Intra- and Intercolumnar Contacts in DMET Superconductors

		$\text{Au}(\text{CN})_2$	$\text{AuCl}_2$	$\text{AuI}_2$	$\text{I}_3$	$\text{I}\text{Br}_2$
Intracolumnar	Se-Se	3.938	3.976	3.965	3.957	3.949
	Se-S	3.819	3.798	3.819	3.845	3.836
		3.837	3.814	3.825	3.837	3.840
Intercolumnar	Se-Se	3.844	3.825	3.832	3.782	3.774
	S-S	3.672		3.611	3.604	3.588
		3.580		3.552	3.504	3.494
	Se-S		3.666			

There are two types of  $\text{AuBr}_2$  salt in Group 5 as mentioned above. The crystal structure of the crystal which shows superconductivity at 1.9 K at ambient pressure is shown in Fig. 7. The structure is quite different from those of the salts in Groups 3 and 4. It is not columnar and consists of sheets of DMET molecules and  $\text{AuBr}_2$  anions. This salt is thought to be a two-dimensional material. The crystal structure of the other type which shows superconductivity at 1.0 K under pressure was determined. No apparent difference was, however, found.

- END -

10

## For Official Use Only

This is a U.S. Government publication. Its contents in no way represent the policies, views, or attitudes of the U.S. Government. Users of this publication may cite FBIS or JPRS provided they do so in a manner clearly identifying them as the secondary source.

Foreign Broadcast Information Service (FBIS) and Joint Publications Research Service (JPRS) publications contain political, economic, military, and sociological news, commentary, and other information, as well as scientific and technical data and reports. All information has been obtained from foreign radio and television broadcasts, news agency transmissions, newspapers, books, and periodicals. Items generally are processed from the first or best available source; it should not be inferred that they have been disseminated only in the medium, in the language, or to the area indicated. Items from foreign language sources are translated; those from English-language sources are transcribed, with personal and place names rendered in accordance with FBIS transliteration style.

Headlines, editorial reports, and material enclosed in brackets [ ] are supplied by FBIS/JPRS. Processing indicators such as [Text] or [Excerpts] in the first line of each item indicate how the information was processed from the original. Unfamiliar names rendered phonetically are enclosed in parentheses. Words or names preceded by a question mark and enclosed in parentheses were not clear from the original source but have been supplied as appropriate to the context. Other unattributed parenthetical notes within the body of an item originate with the source. Times within items are as given by the source. Passages in boldface or italics are as published.

### SUBSCRIPTION/PROCUREMENT INFORMATION

The FBIS DAILY REPORT contains current news and information and is published Monday through Friday in eight volumes: China, East Europe, Soviet Union, East Asia, Near East & South Asia, Sub-Saharan Africa, Latin America, and West Europe. Supplements to the DAILY REPORTs may also be available periodically and will be distributed to regular DAILY REPORT subscribers. JPRS publications, which include approximately 50 regional, worldwide, and topical reports, generally contain less time-sensitive information and are published periodically.

Current DAILY REPORTs and JPRS publications—except those which have restricted dissemination due to copyright or other reasons—are listed in *Government Reports Announcements* issued semimonthly by the National Technical Information Service (NTIS), 5285 Port Royal Road, Springfield, Virginia 22161 and the *Monthly Catalog of U.S. Government Publications* issued by the Superintendent of Documents, U.S. Government Printing Office, Washington, D.C. 20402. Information on the Official Use Only JPRS Reports must be obtained from FBIS at the address or telephone number given below.

U.S. Government offices may obtain subscriptions to the DAILY REPORTs or JPRS publications (hard-cover or microfiche, unrestricted and Official Use Only reports) at no charge through their sponsoring organizations. Department of Defense consumers are required to submit requests through appropriate command validation channels to DIA, RTS-2C, Washington, D. C. 20301. (Telephone: (202) 373-3771, Autovon: 243-3771.) For additional information or assistance, call FBIS, (703) 338-6735, or write to P.O. Box 2604, Washington, D.C. 20013.

Back issues or single copies of the DAILY REPORTs and JPRS publications are not available.

Both the DAILY REPORTs and the JPRS publications are on file for public reference at the Library of Congress and at many Federal Depository Libraries. Reference copies—except the Official Use Only Reports—may also be seen at many public and university libraries throughout the United States.